A CRITICAL EVALUATION AND REFINEMENT OF THE PERFORMANCE PREDICTION OF WET-COOLING TOWERS

by

Johannes Christiaan Kloppers

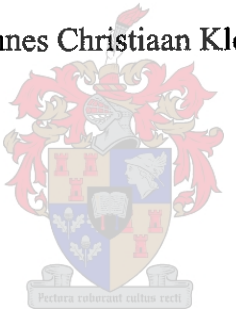

Dissertation presented for the degree
Doctor of Philosophy (Mechanical Engineering)
at the University of Stellenbosch

Promoter: Prof. D.G. Kröger

Department of Mechanical Engineering
University of Stellenbosch
December 2003

DECLARATION

I, the undersigned, declare that the work contained in this dissertation is my own original work, and has not previously in its entirety or in part been submitted at any university for a degree.

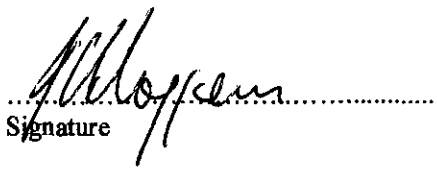

Signature

2003-11-09

Date

ABSTRACT

The thermal performance prediction of wet-cooling towers is critically analyzed and refined. Natural draft counterflow towers and mechanical draft counterflow and crossflow towers are considered. The Merkel, Poppe and *e-NTU* heat and mass transfer methods of analysis are derived from first principles, as these methods form the cornerstone of wet-cooling tower performance evaluation. The critical differences between these methods, when applied to fill performance analyses and cooling tower performance evaluations, are highlighted. The reasons for these differences are discussed with the aid of psychrometric charts. A new extended empirical relation for the loss coefficient of fills is proposed where the viscous and form drag effects are accounted for as well as the buoyancy, momentum and fill height effects. The empirical equation for the transfer characteristic of fills is extended to include the effects of fill height and the inlet water temperature. Empirical equations to predict the temperature inversion profile, height of the temperature inversion and the height from which air is drawn into the cooling tower are developed. The influence of temperature and humidity inversions on the performance of wet-cooling towers is subsequently investigated. A comprehensive analytical computer program is developed to predict and optimize the performance of wet-cooling towers. Computer programs are also developed to generate cooling tower performance curves, analyze fill performance test data and plot psychrometric charts.

Keywords:
Wet-cooling tower, Merkel, Poppe, *e-NTU*, natural draft, mechanical draft, fill, temperature inversion.

SAMEVATTING

Die termiese werksverrigtingvoorspelling van nat koeltorings word krities geanaliseer en verfyn. Natuurlike trek teenvloei koeltorings en meganiese trek teen- en dwarsvloei koeltorings word ondersoek. Die Merkel, Poppe and *e-NTU* warmte- en massaoordrag berekeningsmetodes word afgelei vanuit eerste beginsels omdat hierdie metodes die hoeksteen is van die berekening van die werkverrigting van koeltorings. Die kritiese verskille tussen hierdie metodes, wanneer dit toegepas word op die berekening van die werksverrigting van pakkings en koeltorings, word beklemtoon. Die redes vir hierdie verskille word verduidelik aan die hand van psichrometriese kaarte. 'n Nuwe uitgebreide empiriese vergelyking vir die verlieskoëffisiënt van pakkings word voorgestel waar daar voorsiening gemaak word vir die viskeuse- en vormsleur effekte, asook die vlotkrag, momentum en pakkingshoogte effekte. Die empiriese vergelyking vir die oordragskoëffisiënt van pakkings word uitgebrei om die effekte van die pakkingshoogte en die inlaat watertemperatuur in te sluit. Empiriese vergelykings om die profiel van temperatuuromkerings, die hoogte van temperatuuromkerings en die hoogte waaruit lug in die koeltoring ingesuig word, word ontwikkel. Die invloed van die temperatuur- en humiditeitomkerings op die werkverrigting van koeltorings word vervolgens ondersoek. 'n Omvangryke analitiese rekenaarprogram word ontwikkel om die werkverrigting van nat koeltorings te voorspel en te optimeer. Rekenaarprogramme word ook ontwikkel om koeltoring werksverrigtingskurwes te genereer, pakkingstoetsdata te analiseer en psychrometriese kaarte te genereer.

Sleutelwoorde:
Nat koeltoring, Merkel, Poppe, *e-NTU*, natuurlike trek, meganiese trek, pakking, temperatuuromkering.

Dedicated to

Oupa Chris van der Walt

(1914 – 2000)

ACKNOWLEDGEMENTS

Thank you Lord Jesus Christ, my heavenly Father, for giving me the strength and the will to do everything in Your name.

The author would also like to thank the following persons and institutions for their assistance and contributions during the course of this study:

My promoter Prof. D.G. Kröger for his world class guidance and support and for the countless discussions concerning my research project.

Cobus Zietsman for his friendship, help with the experimental work and knowledge and experience he has shared with me. Calvin Hamerse for his help with the experimental work.

SASOL for their financial support and Hein Botes, my mentor at Sasol.

Dr. P.J. Erens of Industrial Water Cooling for the financial support with the fill tests and for supplying the fill materials.

My wife, Lynette, for her love and support and for being the inspiration in my life and her parents for their support.

My best friend for his calming influence and for always lying at my feet when I am working into the early hours of the morning - my dog Boetie.

My mother for her interest in my work and for being a pillar of strength in my life.

My family and friends for their interest and support.

TABLE OF CONTENTS

LIST OF SYMBOLS

A	Area, m^2
a	Surface area per unit volume, m^{-1}, or coefficient
B	Breadth, m
b	Exponent
C	Coefficient, or heat capacity rate mc_p, W/K, or fluid capacity rate ,C_{min}/C_{max}, or cost, $
c	Concentration, kg/m^3, or constant
c_p	Specific heat at constant pressure, J/kgK
D	Diffusion coefficient, m^2/s
$DALR$	Dry adiabatic lapse rate, K/m
d	Diameter, m
e	Effectiveness
F	Force, N
f	Optimization objective function
G	Mass velocity, kg/m^2s
g	Gravitational acceleration, m/s^2, or inequality constraint function
H	Height, m
h	Heat transfer coefficient, W/m^2K, or equality constraint function
h_D	Mass transfer coefficient, m/s
h_d	Mass transfer coefficient, kg/m^2s
i	Enthalpy, J/kg
i_{fg}	Latent heat, J/kg
J	Momentum flux, kg m/s^2
K	Loss coefficient, or thermal eddy diffusivity, m^2/s, or kinematic momentum flux, m^4/s^2
k	Thermal conductivity, W/mK, or turbulent kinetic energy
L	Length, m
l	Characteristic length
M	Molecular weight, kg/mole
m	Mass flow rate, kg/s
NTU	Number of transfer units
n	Number
P	Power, W
P_e	Perimeter, m
p	Pressure, N/m^2, or Pa
Q	Heat transfer rate, W
q	Heat flux, W/m^2
R	Gas constant, J/kgK
Ry	Characteristic flow parameter, m^{-1}
r	Radius, m, or correlation coefficient

S	Sum of the least squares
T	Temperature, °C or K
t	Time, s, or thickness, m
u	Internal energy, J/kg, or Cartesian velocity component
V	Volume flow rate, m^3/s, or molecular volume, or characteristic velocity, or volume, m^3
v	Velocity, m/s, or Cartesian velocity component
W	Width, m
w	Humidity ratio, kg water vapor/ kg dry air, or Cartesian velocity component
x	Coordinate
Y	Approach velocity factor
y	Coordinate
z	Coordinate, or elevation, m, or exponent

Greek Symbols

α	Thermal diffusivity, $k/\rho c_p$, or m^2/s, or relaxation factor
α_e	Kinetic energy coefficient
δ	Boundary layer thickness
Δ	Differential
ε	Virtual kinematic viscosity, m^2/s, or dissipation rate of turbulent kinetic energy
η	Non-dimensional coordinate
θ	Angle, °
μ	Dynamic viscosity, kg/ms
υ	Kinematic viscosity, m^2/s
ξ	Non-dimensional coordinate
ρ	Density, kg/m^3
σ	Area ratio, or surface tension, N/m
φ	Stream function
τ	Shear stress, N/m^2
ϕ	Relative humidity, or expansion factor

Dimensionless Groups

Fr_D	Desimetric Froude number, $\rho v^2/(\Delta\rho dg)$
Le	Lewis number, $k/(\rho c_p D)$, or Sc/Pr
Le_f	Lewis factor, $h/(c_p h_d)$
Me	Merkel number, $h_d a_{fi} L_{fi}/G_w$
Nu	Nusselt number, hL/k
Pg	Vapor pressure gradient
Pr	Prandtl number, $c_p\mu/k$
Re	Reynolds number, $\rho vL/\mu$

Sc	Schmidt number, $\mu/(\rho D)$
Sh	Sherwood number, $h_D L/D$
St	Stanton number, $h/(\rho v c_p)$, or $Nu/(RePr)$
St_m	Mass transfer Stanton number, $h_d/(\rho v)$, or $Sh/(ReSc)$

Subscripts

a	Air, or above
b	Below
c	Convection heat transfer, or critical
ct	Cooling tower
ctc	Cooling tower contraction
cte	Cooling tower expansion
D	Drag
d	Drop, or discharge, or day
de	Drift eliminator
dif	Diffuser
e	Evaporative, or expansion, or *e-NTU* theory
em	Empirical
ex	Experimental
F	Fan
F/dif	Fan/diffuser
fi	Fill
fr	Frontal
g	Gas
i	Inlet
il	Inlet louver
it	Inversion top
M	Merkel theory
m	Mean, or mass transfer
max	Maximum
min	Minimum
n	Nozzle
o	Outlet
op	Orifice plate
P	Poppe theory
pl	Plenum chamber
r	Reference, or radial coordinate
rz	Rain zone
s	Saturation, or shell
sp	Spray

ss	Supersaturated
t	Total, or top, or turbulent
tr	Trough
ts	Tower support
up	Upstream
v	Vapor
w	Water
wb	Wetbulb
wd	Water distribution system
x	Coordinate
y	Coordinate
z	Coordinate

CHAPTER 1

INTRODUCTION

1.1 OVERVIEW OF WET-COOLING TOWERS

Heat is discharged in power generation, refrigeration, petrochemical, steel, processing and many other industrial plants. In many cases, this heat is discharged into the atmosphere with the aid of a cooling tower. Figure 1.1 shows an example of the application of a cooling tower in a simple steam power plant. Heat is discharged into the atmosphere by the cooling tower via a secondary cycle with water as the process fluid.

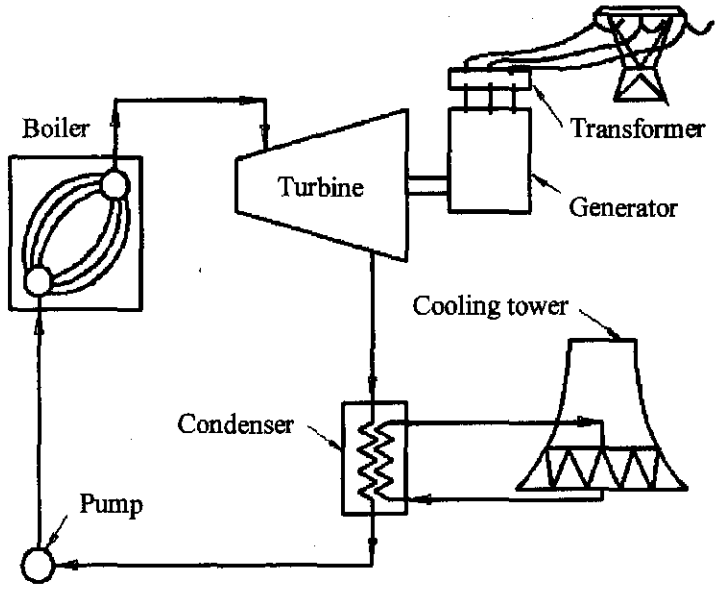

Figure 1.1: Simple steam power plant with cooling tower.

Wet-cooling towers are considered in this study. Wet-cooling takes place when the water is in direct contact with the air. Cooling is the result of sensible and latent heat transfer where the latent heat transfer component generally dominates.

Cooling towers can be classified according to the type of draft through the tower. Figure 1.2 shows an example of a natural draft wet-cooling tower. The draft in natural draft towers is established by the buoyancy of the hotter air inside the tower shell compared to the cooler ambient air on the outside of the tower shell. Although the art of evaporative cooling is quite ancient, the first natural draft cooling tower was only constructed in 1916 at the Emma Pit in the Netherlands by the Dutch State Mines [97BO1]. The worlds tallest cooling tower is 200 m high and is situated at the Niederaussem power plant in Germany [02BU1, 02HA1].

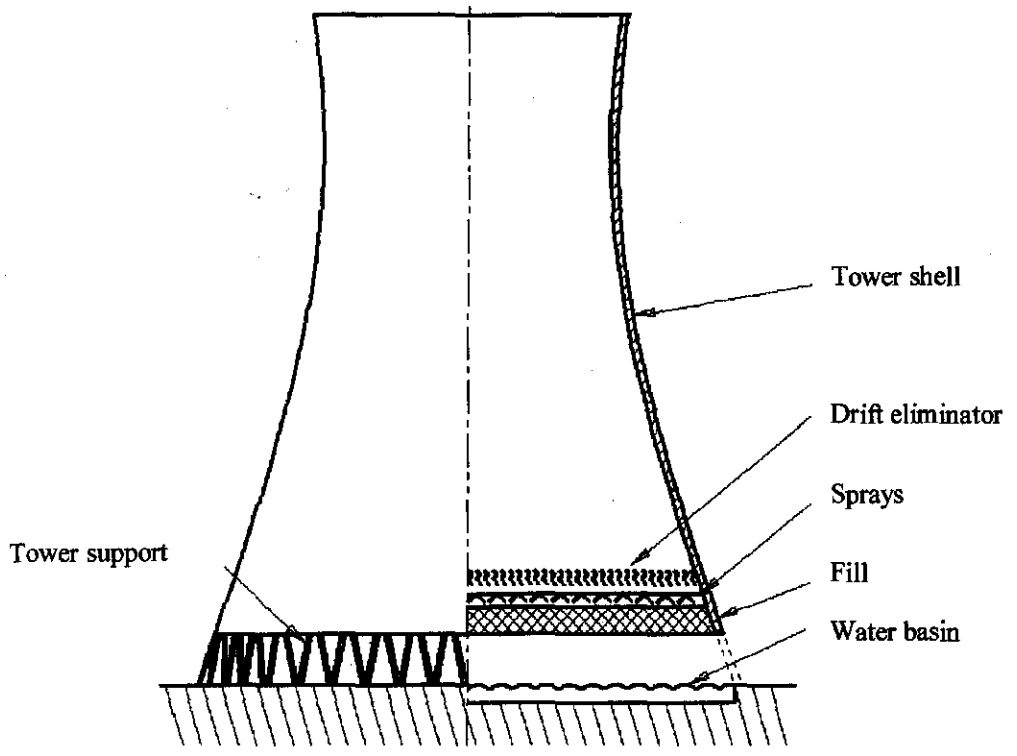

Figure 1.2: Natural draft counterflow wet-cooling tower.

Figure 1.3 shows an example of a mechanical draft wet-cooling tower. Draft in mechanical draft towers is established by fans that force or draw air through the towers, usually referred to as forced draft and induced draft respectively.

A further distinction between cooling towers is whether they are counterflow or crossflow towers. Figures 1.2 and 1.3 show examples of counterflow cooling towers, while figure 1.4 shows an example of a crossflow cooling tower. In a crossflow tower the fill is usually installed at some angle to the vertical to make provision for the inward motion of the droplets due to drag forces caused by the entering cooling air [98KR1]. Less pumping power is needed for modern counterflow towers, as the towers are generally not as high as crossflow cooling towers. Icing and wind effects are more prevalent in crossflow towers than in counterflow towers [95BL1].

When a single cooling tower incorporates a wet and a dry section, this is also sometimes referred to as a hybrid system [98KR1]. Figure 1.5 shows an example of a hybrid cooling tower [98KR1, 98ST1]. Hybrid cooling towers are generally used for plume abatement and in regions where water is relatively scarce.

The operation of a wet-cooling tower relies on relatively simple principles. Hensley [92HE1] and Kröger [98KR1] discuss the operating principles of wet-cooling towers while Willa [92WI1] presents a history of the development of wet-cooling towers during the last century. The rest of this section describes the development, operating principles and limitations of the basic components of wet-cooling towers.

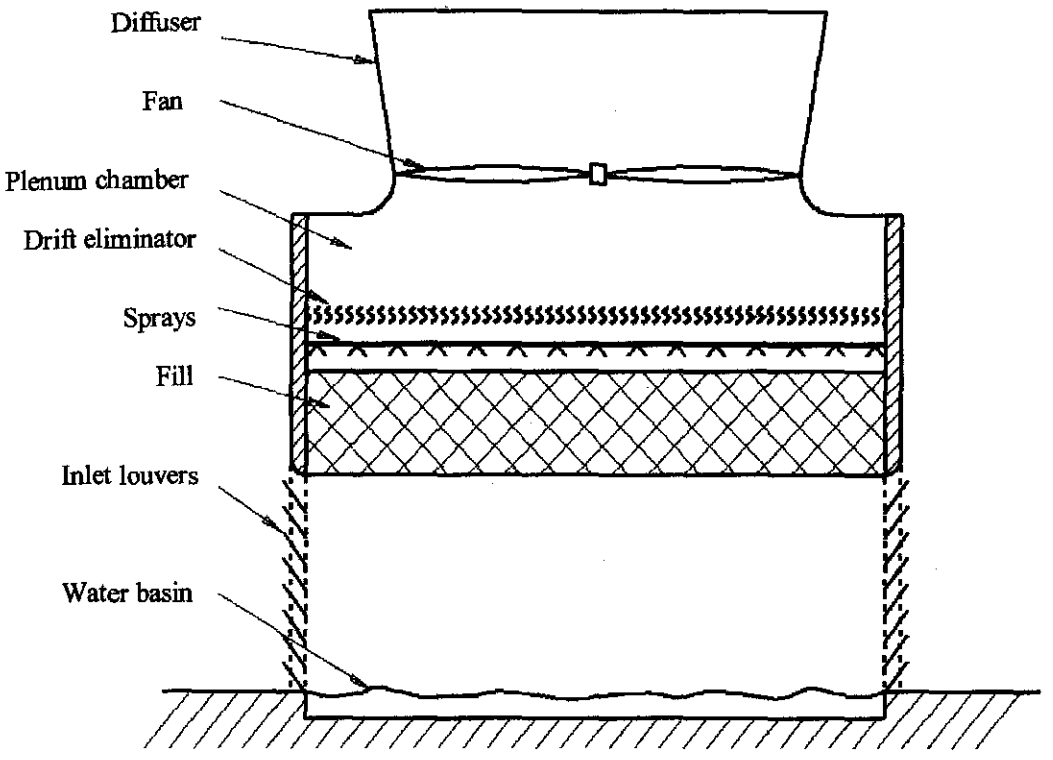

Figure 1.3: Induced draft counterflow wet-cooling tower.

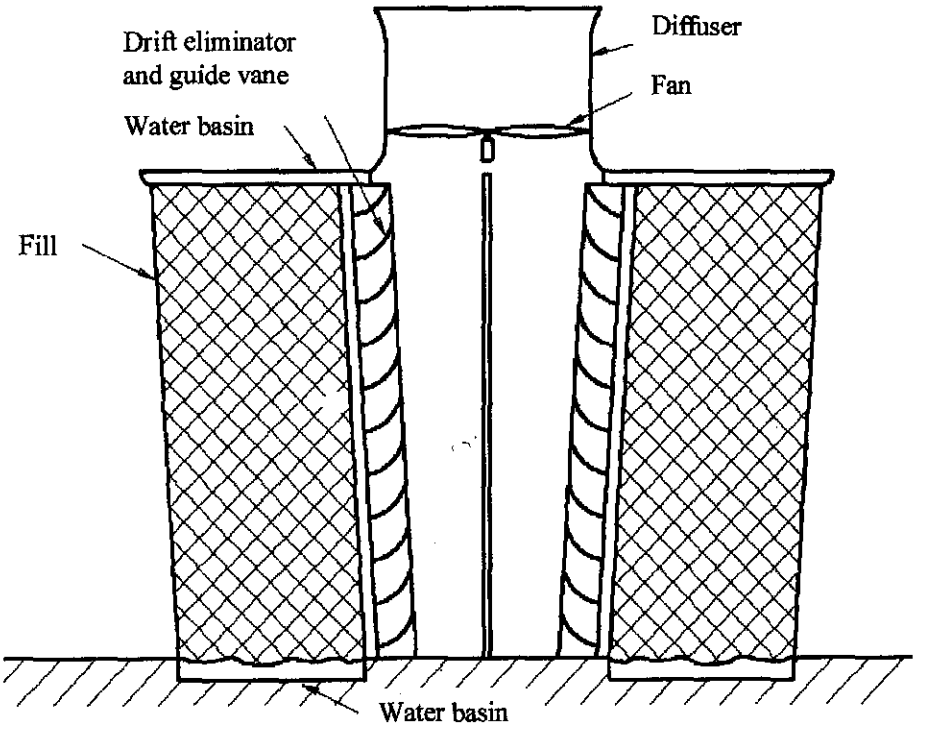

Figure 1.4: Induced draft crossflow wet-cooling tower.

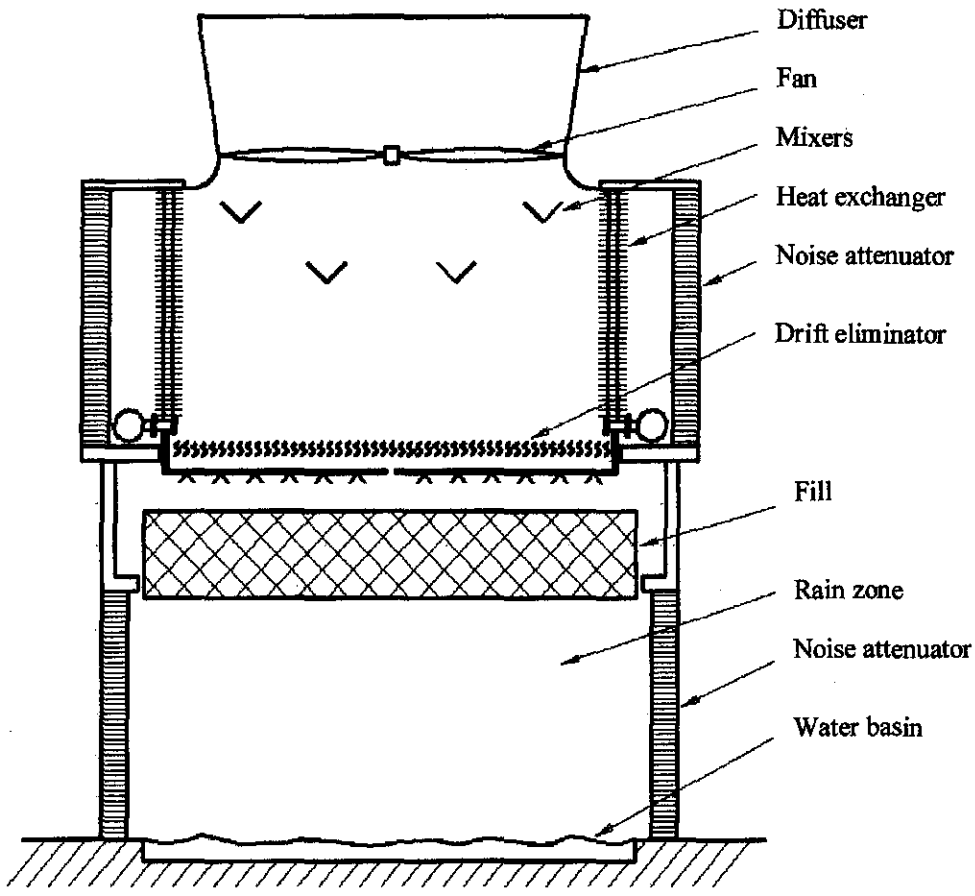

Figure 1.5: Hybrid cooling tower.

Hot water is sprayed over the fill material. The spray zone can account for as much as 25% of the total heat transfer in a tower [01TU1]. It is very important that the water is distributed uniformly over the fill. Maldistribution of liquid flow is often cited as a cause of reduced performance in packed towers [93KR1, 95LI1]. Mohiuddin and Kant [96MO2] present different spray system designs.

A poor water flow distribution over the fill is commonly experienced at water flowrates in excess of around 4.2 kg/m^{2}s [96MO2]. If the flowrate is increased beyond this value, the water cascades in thick streams instead of falling as a spray, so that the effective area is reduced. This condition is called flooding. On the other hand, if the water flowrate drops to about 0.8 kg/m^{2}s or less, surface tension causes the waterflow to channel. This gives a poor water distribution, and hence a marked drop in performance.

The fill increases the transfer area by breaking the water up into smaller droplets or by forming a thin film depending on the type of fill. The fill also increases the contact time between the water and the air [83MA1]. The factors influencing the choice of fill are its heat transfer performance, quality of water, pressure drop, cost and durability [96MO2]. Over the last 30 years, there has been a gradual change in the types of fill used in process cooling towers [99WA1]. The most dramatic change has been the introduction of film fills that provide significantly higher thermal performance through the increase of

water-to-air contact area and a reduction in pressure drop. This results in a reduction in capital expenditures, lower operating costs and smaller tower footprint. However, in many applications, due to poor water quality or potential process contamination, these benefits are forfeited and the older splash fill technology is still used. The film fill designs can be grouped in three broad categories: cross corrugated, vertical offset and vertical flow as can be seen in figure 1.6. Mirsky and Bauthier [93MI1] present a history of the development of wet-cooling tower fills. Aull and Krell [00AU1] investigated the performance of various film fills.

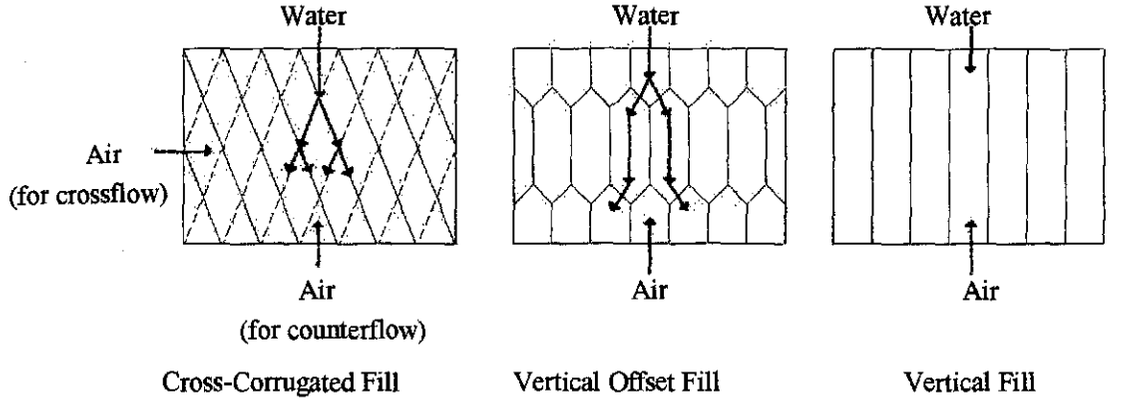

Figure 1.6: Film fill designs [99WA1].

From the fill the water falls unobstructed through the rain zone into the water basin. A significant amount of heat and mass transfer takes place in the rain zone. The drift eliminator is situated on the air downstream side of the fill as shown in figures 1.2 to 1.3. Drift refers to the small droplets of circulating water that are carried out of the cooling tower by the exhaust air. Inertial impaction separators, known as drift eliminators, are used to strip the water droplets from the warm exhaust air. In this type of separator, the two-phase exhaust flow is forced to abruptly change direction. This causes the dense drift droplets to hit the eliminator walls and become trapped inside the cooling tower. Drift eliminators have evolved from early single-pass wood lath to multiple-pass wood and then to sinusoidal-wave shapes. These were followed by combinations of sinusoidal and honeycomb shapes. Currently, various styles of cellular drift eliminator packs are constructed from thermoformed sheets of polyvinylchloride (PVC). The performance of these drift eliminator packs is measured by two criteria: droplet collection efficiency and system pressure loss caused by the eliminator pack. To achieve peak operating efficiency of the overall cooling tower system, it is desirable that the system pressure loss from the eliminators be minimized [93BE1].

1.2 OUTLINE OF THESIS

1.2.1 CHAPTER 1

Chapter 1 presents a broad overview of wet-cooling towers. The basic terminology and operation of natural draft and mechanical draft wet-cooling towers are explained. The outline of the thesis is also presented in chapter 1.

1.2.2 CHAPTER 2

Chapter 2 presents the theoretical heat and mass transfer analyses employed in wet-cooling tower performance evaluation. These analytical models or approaches are the foundation of any theoretical and experimental investigation into cooling tower performance. Three different analytical models, the Merkel [25ME1], Poppe [91PO1] and *e-NTU* [89JA1], are considered. These models are later employed to determine the transfer characteristics of the cooling tower fill materials and subsequently employed to determine cooling tower performance.

1.2.3 CHAPTER 3

The Merkel [25ME1], Poppe [91PO1] and *e-NTU* [89JA1] approaches, discussed in chapter 2, are employed to determine fill performance characteristics including the loss coefficients and the Merkel numbers, or transfer characteristics, according to each method of analysis. A new extended empirical relation for the loss coefficient is proposed where the viscous and form drag effects are accounted for as well as the buoyancy, momentum and fill height effects. It will be shown that the proposed empirical relation gives very accurate correlations for splash, trickle and film fill types, over a wide range of air and water mass flow rates when compared to other forms of empirical relations commonly found in the literature. The dependence of the transfer characteristic on the height of the fill, inlet air drybulb temperature and inlet water temperature is investigated. It is shown that the transfer characteristic per unit height is a function of the water and air flow rates as well as the fill height and the inlet water temperature but not of the air inlet temperature.

1.2.4 CHAPTER 4

The performance of natural and mechanical draft counterflow cooling towers is critically evaluated by respectively employing the Merkel, Poppe and *e-NTU* methods of analysis at different operating and ambient conditions. The WCTPE software program, presented and developed in the appendices, is employed in the investigation. The importance of using a particular method of analysis when evaluating the performance characteristics of a certain fill material and subsequently employing the same analytical approach to predict cooling tower performance, is investigated. Procedures to evaluate and improve the accuracy of the Merkel and *e-NTU* methods, when compared to the more rigorous Poppe method, are discussed.

1.2.5 CHAPTER 5

The effect of temperature and humidity inversions on cooling tower performance is investigated. A very simple empirical relation of the nocturnal temperature inversion profile is developed in the appendices and presented in chapter 5. This empirical relation correlates measured data more accurately than models found in the literature which require more input data. An equation to determine the height of the temperature inversion is also developed. An analytical model to determine the height from which air is drawn into a cooling tower is developed.

1.2.6 CHAPTER 6

Chapter 6 gives a summary of all the main recommendations made and the conclusions drawn during the thesis. Most of the conclusions are repeated from the conclusions drawn at the end of each chapter. It serves as a complete overview of the main results and recommendations. The computer software programs developed to aid in the performance analysis of cooling towers and cooling tower fills are summarized.

1.2.7 APPENDICES

Most of the research, development and presentation of theoretical and analytical models, equations and computer programs are presented in the appendices. Most appendices are self-contained chapters with results and conclusions. The most important results of the appendices are summarized and presented in the main chapters of the thesis while the details of calculations and the methods followed are presented in the appendices.

1.3 COMPUTER SOFTWARE DEVELOPMENT

A program is developed to process and analyze fill performance test data. This program is presented in appendix K and processes the pressure transducer and thermocouple data, determines the transfer and loss coefficients and fits relatively complex curves through the test data with mathematical optimization algorithms. A comprehensive program is developed to predict wet-cooling tower performance. This program is presented in appendix P. Natural draft counterflow and mechanical draft counterflow and crossflow cooling towers can be analyzed by the program. The latest empirical and heat and mass transfer models found in the literature are included in the solution algorithms of the software. The analytical and empirical models, developed in this thesis from theoretical and experimental investigations, are also included in the software. The geometrical dimensions of a natural draft cooling tower can be optimized by the program to obtain the minimum combined capital and operational cost compounded over the economic life of the cooling tower. Furthermore, programs are developed to plot psychrometric charts (chapter 2) and generate cooling tower performance curves (appendix Q).

Comment

In the numerical examples, given in the appendices, values are often given to a large number of decimal places. These numbers are usually as given directly by the computer program output and do not necessarily imply a corresponding degree of accuracy.

CHAPTER 2

WET-COOLING TOWER HEAT AND MASS TRANSFER ANALYSIS

2.1 INTRODUCTION

The analytical models or approaches that predict heat and mass transfer in cooling towers are the foundation of any theoretical and experimental investigation into cooling tower performance. It is thus imperative to understand their limitations and applications. Three different analytical models, referred to as the Merkel, Poppe and *e-NTU* approaches respectively, are employed in this study to evaluate the heat and mass transfer processes in wet-cooling towers. These models are later employed to determine the transfer characteristics of cooling tower fill materials and subsequently to determine cooling tower performance. The heat and mass transfer processes are presented graphically with the aid of psychrometric charts.

2.2 PSYCHROMETRIC CHART

Psychrometric charts are useful and widely accepted tools for the design and analysis of heat and mass exchange involving moist air [82ST1]. Properties of air-water vapor mixtures are presented in graphical form on psychrometric charts. The state of air at a specified pressure is completely specified by two independent intensive properties. The basic features of the psychrometric chart are illustrated in figure 2.1. The drybulb temperatures are shown on the abscissa and the specific humidity or humidity ratio is shown on the vertical axis. On the left end of the chart there is a curve called the saturation curve where the relative humidity is 100%. All the saturated air states are located on this curve. Other constant relative humidity curves have the same general shape. The enthalpy has an inclined coordinate. Although it is not shown in figure 2.1, wetbulb temperature and specific volume can also be presented on a psychrometric chart.

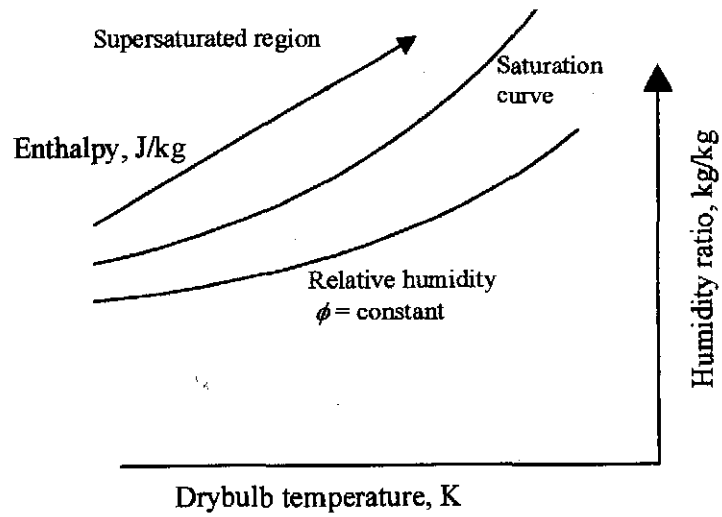

Figure 2.1: Psychrometric chart coordinates.

Figure 2.2 illustrates the various processes of air-vapor mixtures on a psychrometric chart. If only heat transfer is present and no mass transfer, it can be seen that the humidity ratio remains constant, since the moisture content of the air remains constant, and pure heating or cooling of the air occurs.

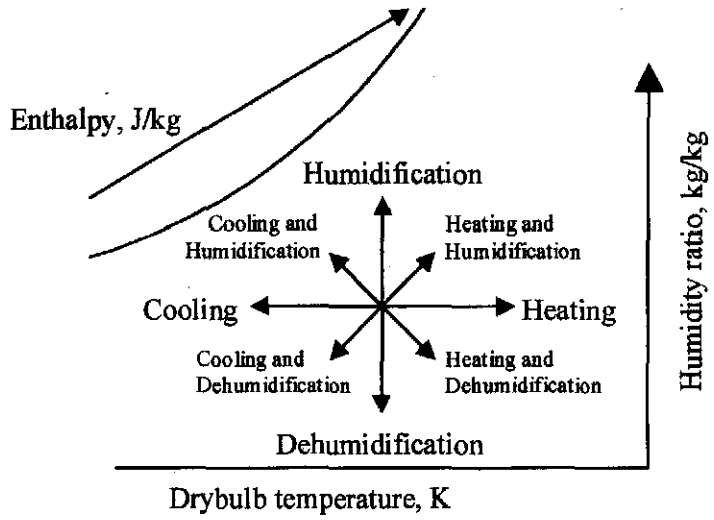

Figure 2.2: Various processes depicted on a psychrometric chart.

Psychrometric charts only describe what happens to the air in wet-cooling processes and the charts can generally not be used in the supersaturated region, illustrated in figure 2.1. The outlet air in practical wet-cooling towers, however, is generally in this latter region. However, the psychrometric chart is an excellent tool to analyze and describe the direction of enthalpy transfer in cooling towers.

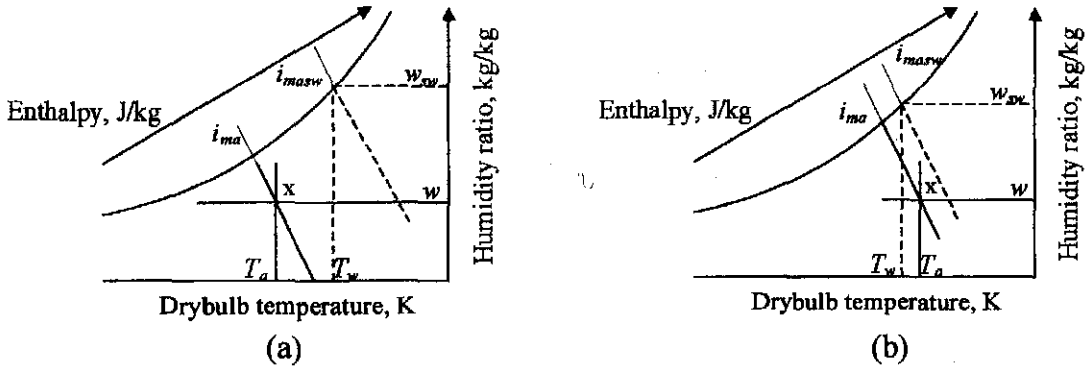

Figure 2.3: Psychrometric charts

The enthalpy potential provides a qualitative indication of the direction of nett heat flow in the fill region of cooling towers. Air at condition x (refer to figure 2.3) is in contact with water at temperature T_w. Figure 2.3 represent two different cases that can occur inside a cooling tower fill. Consider the case in figure 2.3 (a) where $w_{sw} > w$, thus, the latent heat transfer is from the water to the air and $T_w > T_a$, where the sensible heat transfer is from the water to the air. The total enthalpy transfer is from the water to the air since $i_{masw} > i_{ma}$ and since both the latent and sensible heat transfer are from the water to the air. The air is heated and the water is cooled.

However, both the air and the water can be cooled, while the nett enthalpy transfer is still in the direction of the air. Consider the case presented in figure 2.3 (b), where $w_{sw} > w$, thus, the latent heat transfer is from the water to the air and $T_a > T_w$, where the sensible heat transfer is from the air to the water. The nett enthalpy transfer is from the water to the air since $i_{masw} > i_{ma}$. Furthermore, Goyal [00GO2] states that it is a common misconception that cooling towers cannot operate when the inlet air is saturated. Even though the inlet air is saturated there still exists a potential for sensible and latent heat transfer. The excess water vapor transferred to the free stream air will condense as a mist [98KR1].

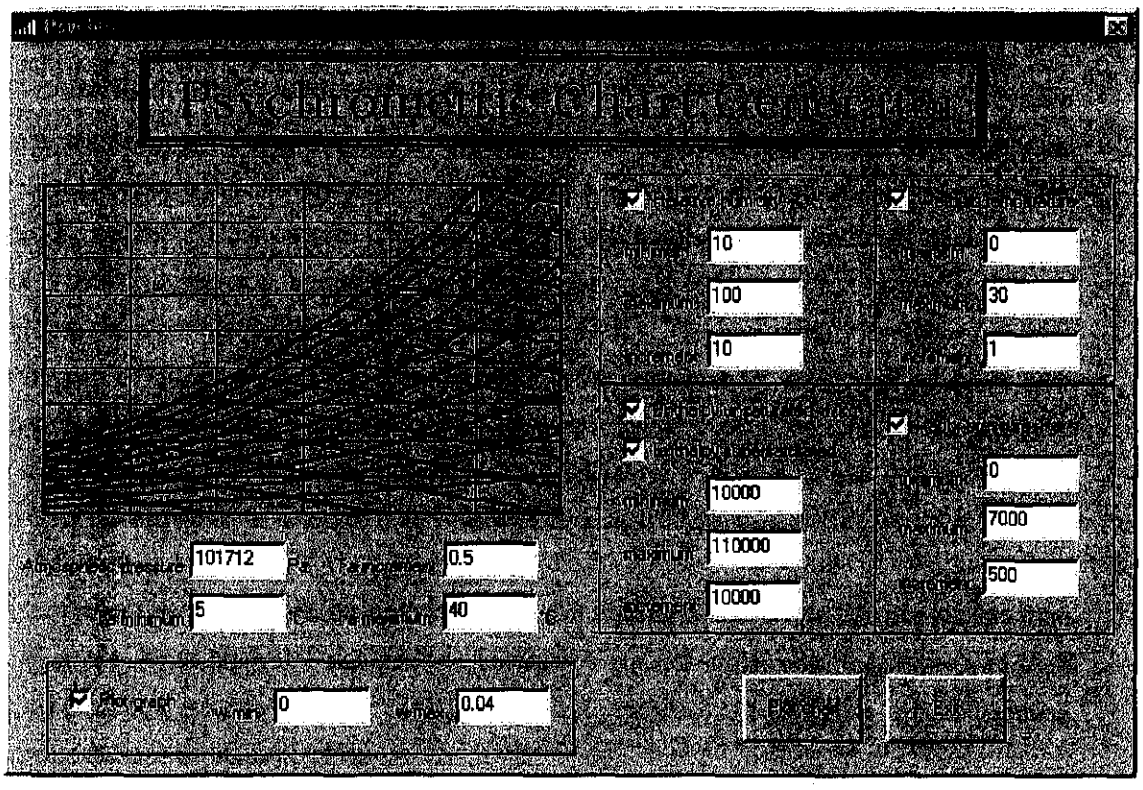

Figure 2.4: Dialog window of the psychrometric chart generator computer program.

Figure 2.4 shows the dialog window of a computer program that is developed to generate psychrometric charts. The psychrometric charts are used in conjunction with the heat and mass transfer models, presented next, to graphically represent the transfer process.

2.3 MERKEL ANALYSIS

Merkel [25ME1] developed the theory for the performance evaluation of cooling towers in 1925. This work was largely neglected until 1941 when the paper was translated into English. Since then, the model has been widely applied [91OS1]. The Merkel model is a very popular model and its employment is recommended by international standards [88BR1, 90CO1, 97CO1]. The Merkel theory relies on several critical assumptions to reduce the solution of heat and mass transfer in wet-cooling towers to a simple hand calculation. Because of these assumptions, however, the Merkel method does not accurately represent the physics of heat and mass transfer process in the cooling tower fill. The critical simplifying

assumptions of the Merkel theory are that the Lewis factor, Le_f, is equal to unity, the exiting air is saturated and the reduction of the water flow rate, due to evaporation, is neglected in the energy balance.

Appendix B gives a detailed derivation, from first principles, of what is commonly referred to as Merkel's equation for a counterflow configuration. Merkel's equation is given by equation (B.21) and is repeated here,

$$Me_M = \frac{h_d A}{m_w} = \frac{h_d a_{fi} A_{fr} L_{fi}}{m_w} = \frac{h_d a_{fi} L_{fi}}{G_w} = \int_{T_{wo}}^{T_{wi}} \frac{c_{pw} dT_w}{(i_{masw} - i_{ma})} \tag{2.1}$$

where Me_M is the Merkel number according to the Merkel theory.

The Merkel number is a non-dimensional coefficient of performance. The right-hand side of equation (2.1) can be solved if the water inlet temperature, water outlet temperature, air inlet drybulb temperature, air inlet wetbulb temperature, water mass flow rate and airflow rate are known. The mass transfer coefficient, h_d, and the surface area per unit volume, a_{fi}, of a particular fill are practically impossible to determine [01RO1]. However, h_d and a_{fi} exist as a product inside the Merkel number, as seen in equation (2.1), and it is therefore not necessary to specify them explicitly. The heat transfer coefficient, h, also does not have to be specified explicitly as it is coupled to the mass transfer coefficient, as can be seen from equation (F.10), through the assumption that the Lewis factor is equal to 1. In the literature the notation frequently used for the Merkel number is KaV/L where $K = h_d$, $a = a_{fi}$ and $L = m_w$. Refer to appendix C for the derivation of the governing equations for a crossflow configuration.

It can be seen from equation (2.1) that the Merkel number, or transfer characteristic, can be obtained from the evaluation of a simple integral. Equation (2.1), however, is not self-sufficient so it does not lend itself to direct mathematical solution [61BA1, 82MI1]. The usual procedure is to integrate it in conjunction with an energy balance expressed by

$$m_w c_{pwm} dT_w = m_a di_{ma} \tag{2.2}$$

Figure 2.5 shows the enthalpy curves of the air in a counterflow wet-cooling tower. The fill test results, from which figure 2.5 is generated, are given in the beginning of appendix G. I. The i_{ma} curve, i.e. the enthalpy of the air as it moves through the fill, shown in figure 2.5, is linear due to the linear nature of equation (2.2). The i_{masw} curve is the saturation curve of the air at the water interface temperature. The potential for heat and mass transfer at a particular water temperature is the difference between i_{masw} and i_{ma}. The Merkel number, Me_M, of equation (2.1), is a function of the area under the $1/(i_{masw} - i_{ma})$ curve as shown in figure 2.5.

The integral in equation (2.1) needs to be evaluated by numerical integration techniques. The British Standard [88BR1] and the Cooling Tower Institute [90CA1, 97CA1] recommends that the four-point Chebyshev integration technique be employed. A discussion of the Chebyshev integration technique can also be found in Oosthuizen [95OO1] and Mohiuddin and Kant [96MO1].

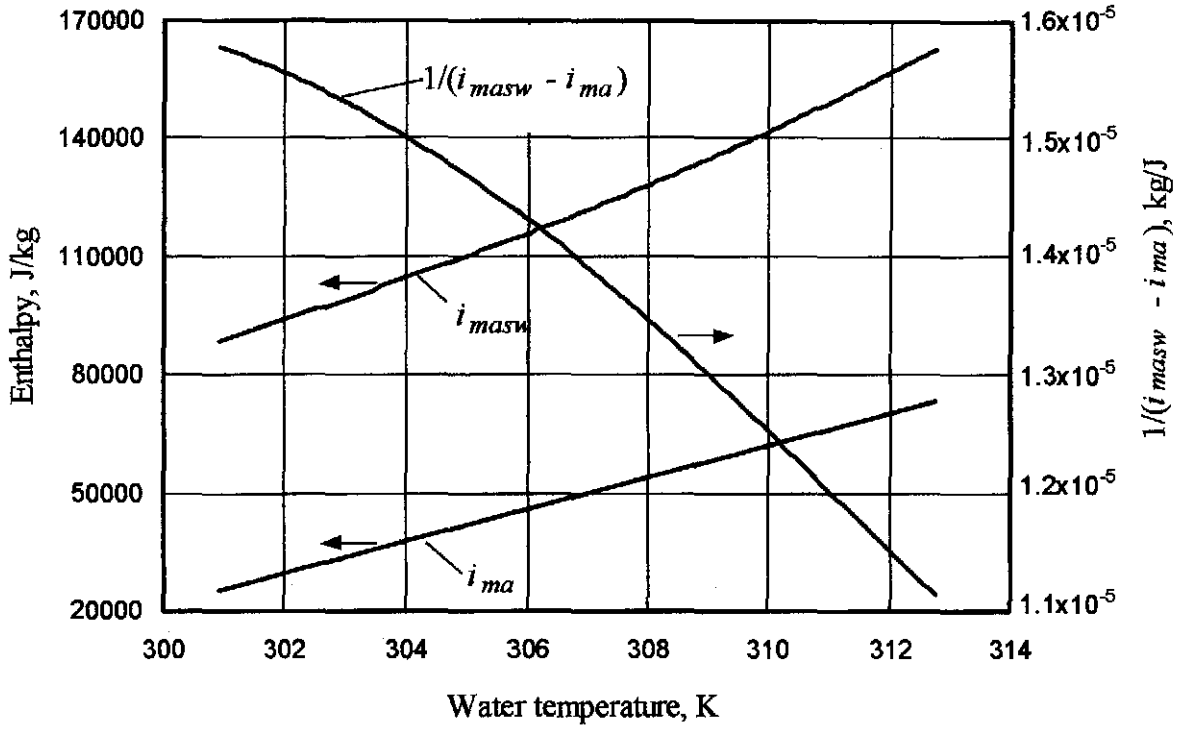

Figure 2.5: Enthalpy diagram of the Merkel approach.

The four-point Chebyshev integration technique essentially uses four intervals for the determination of the integral. Li and Priddy [85LI1] and Mills [95MI1] use thirteen and seven intervals respectively for numerical integration to determine the change of water and air enthalpy through the fill for a cooling range of approximately 14°C. Li and Priddy [85LI1] effectively employ a Riemann sum [90EL1] to determine the integral while Mills [95MI1] employs the composite trapezoidal rule [97BU1].

The composite Simpson rule is employed in this investigation to determine the accuracy of the Chebyshev procedure. The Simpson rule is chosen because of its superior accuracy compared to the trapezoidal rule. The error of the trapezoidal rule is of the second order while that of the Simpson rule is of the fourth order [92MA1]. Any number of intervals can be chosen for the Simpson rule while that of the Chebyshev procedure is fixed.

The integral of the $1/(i_{masw} - i_{ma})$ curve in figure 2.5 multiplied by c_{pw} is 0.68468 while employing the Chebyshev procedure. If the Simpson rule is employed with 150 intervals the integral is 0.684876, which is only a 0.03% change from the value obtained by employing the Chebyshev procedure. If only one interval is used in conjunction with the trapezoidal rule, the integral, or Merkel number is given by

$$Me_M \approx \frac{c_{pwm}(T_{wi} - T_{wo})}{2}\left[\frac{1}{i_{maswi} - i_{mai}} + \frac{1}{i_{maswo} - i_{mao}}\right] \tag{2.3}$$

For two intervals the Merkel equation is

$$Me_M \approx \frac{c_{pwm}(T_{wi} - T_{wo})}{4}\left[\frac{1}{i_{maswi} - i_{mai}} + \frac{2}{i_{maswm} - i_{mam}} + \frac{1}{i_{maswo} - i_{mao}}\right] \tag{2.4}$$

The Merkel numbers are 0.667587 and 0.685014 when equations (2.3) and (2.4) are respectively employed. This is 2.5% and 0.05% change respectively from the value determined by the Chebyshev procedure.

For the case investigated above is it found that the Chebyshev procedure is very accurate if compared to results of the Simpson procedure with many intervals. Kelly [76KE2] states that the Chebyshev procedure lacks accuracy when the approach (i.e. the difference between the water outlet temperature and the air inlet wetbulb temperature) is small (down to 0.56 °C). The accuracy of equations (2.3) and (2.4) depend on the degree of curvature of the $1/(i_{masw} - i_{ma})$ curve as shown in figure 2.5. Any integration technique can be employed to solve equation (2.1) but it is strongly recommended that the same integration technique be employed in the fill performance analysis and the subsequent cooling tower performance analysis. This point will be substantiated in further investigations later in this study.

As already mentioned, the driving potential in wet-cooling towers is the difference between the enthalpies i_{masw} and i_{ma} as shown in figure 2.5. The i_{ma} curve is obtained from equation (2.2) that ignores the change in water flow rate due to evaporation. The effect of evaporation on the energy balance is thus ignored for a second time. It was first ignored when equation (2.1) was derived as seen in appendix B. Baker and Shryock [61BA1] investigated the effect of this second time the effect of evaporation is ignored in the energy balance. They've considered three different cases and found that the Merkel number increases with the more accurate representations of the energy balance. However, the Merkel number increases not as much for the most accurate case investigated as for the second most accurate case. The maximum increase in the Merkel number is 4.4%. Again, it is stressed that the same energy balance be employed in the fill performance analysis and the subsequent cooling tower performance analysis.

Curves are published in the literature to determine the Merkel number in equation (2.1) by graphical means from known air and water temperatures and air and water mass flow rates. Curves to determine the tower characteristic for counterflow towers are given by the CTI [67CT1] and for crossflow towers by Kelly [76KE1]. Figure 2.6 is an example of such a curve for a counterflow tower for a particular cooling range and wetbulb temperature. Since the advent of high speed digital computers, these curves are less frequently used.

The cooling process shown in the enthalpy diagram of figure 2.5 can also be indicated on a psychrometric chart as shown in figure 2.7. The Merkel approach is shown as a broken straight line in figure 2.7. The line for the Merkel approach is presented as a broken line because straight lines can only be used on psychrometric charts if the temperature of the water surface is constant. The line for the Merkel approach is presented as a straight line because no other information is given by the Merkel theory about the humidity of the air, except that it is saturated at the air outlet side. That is why the air at the outlet of the cooling tower is assumed to be on the saturation line as shown in figure 2.7.

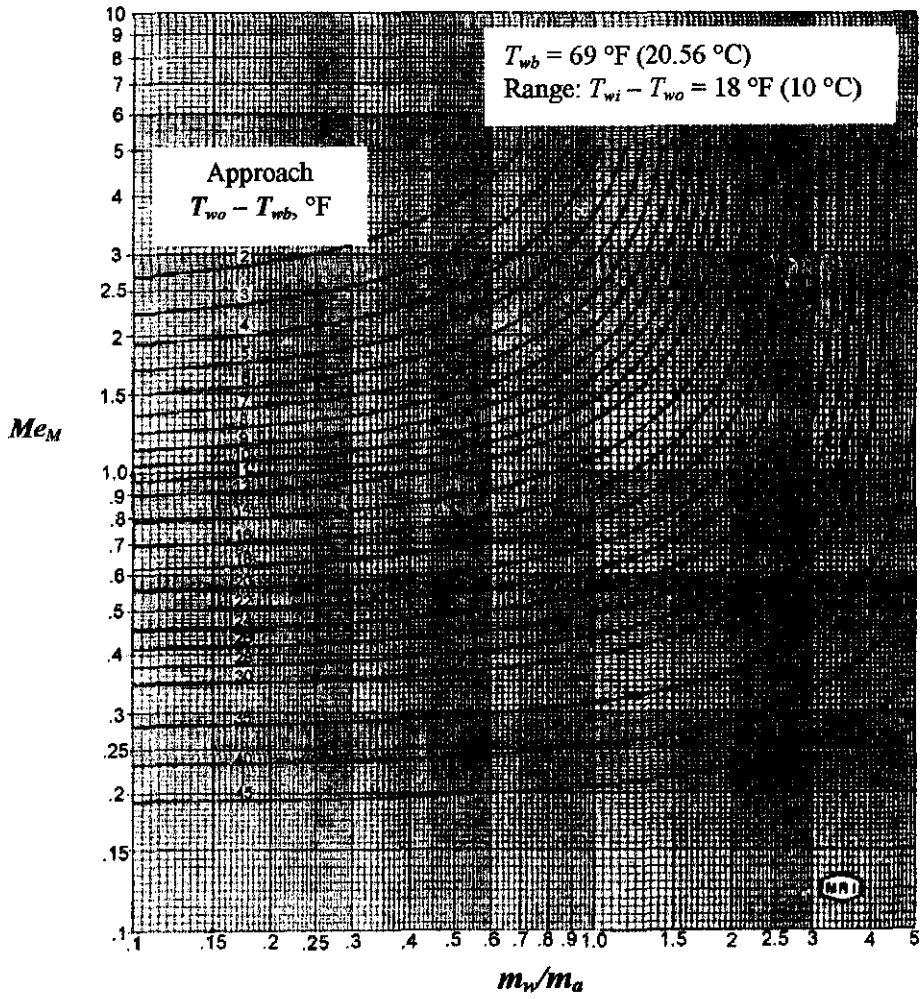

Figure 2.6: Counterflow tower characteristic curves [67CT1].

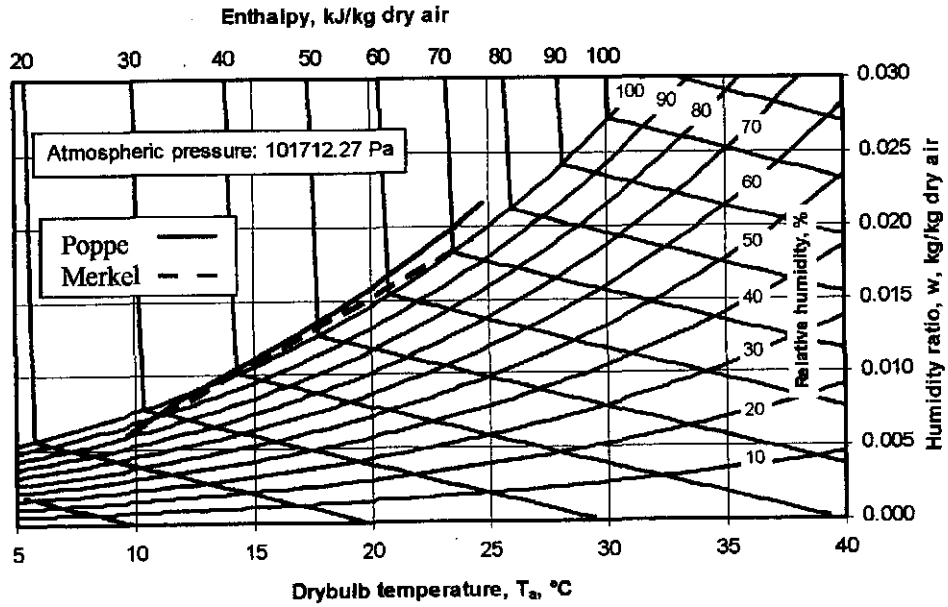

Figure 2.7: Psychrometric chart

2.4 POPPE ANALYSIS

The Poppe model was developed by Poppe and Rögener [84PO1, 91PO1] in the early seventies. The method of Poppe does not make the simplifying assumptions made by Merkel. The derivation of the governing equations of heat and mass transfer, for a counterflow configuration, according to Poppe, is given in appendix B.

Equations (B.24), (B.25) and (B.30) are the governing equations for the counterflow Poppe method when the air is not saturated with water vapor while equations (B.42), (B.43) and (B.47) are the governing equations when the air is supersaturated. For a crossflow configuration, the two-dimensional partial differential equations are given in appendix C.

Again, as in the case with the Merkel method, h_d and a_{fi} appear in the Merkel number. The heat transfer coefficient, h, is obtained from the Lewis factor, Le_f, but this time the Lewis factor is not assumed to be unity. It must be stressed, however, that the heat and mass transfer coefficients are never specified explicitly when the governing equations are solved.

The Lewis factor, Le_f, and its application to evaporative air-water systems is discussed in detail in appendix F. Poppe employs equation (F.16) to express the Lewis factor in his model. Equation (F.16), developed by Bosnjakovic [65BO1], is also the preferred equation to express the Lewis factor in this study. Other equations, given in appendix F, can be employed to express the Lewis factor. It will be shown later in this study that it is very important to employ the same equation or definition for the Lewis factor in the fill performance analysis and in the subsequent cooling tower performance analysis. This consistent usage of definitions, in all aspects of the governing equations, in the fill performance analysis and in the subsequent cooling tower performance analysis, for all the transfer models, is very important to obtain accurate and reliable results.

It is expected that the Poppe approach will lead to more accurate results than that obtained by employing the Merkel approach, as it is the more rigorous approach. The comparison between the Poppe and Merkel approaches is shown on the psychrometric chart in figure 2.7. The humidity of the air through the entire cooling process is predicted by the Poppe approach, unlike the Merkel approach where only the outlet condition of the air is known, i.e. it is saturated.

Figure 2.8 shows the differences in the enthalpy diagrams between the Merkel and Poppe approaches. The i_{masw} curves of the two approaches fall on top of each other. There is a small discrepancy in the i_{ma} curves of the two different approaches, especially at the hot water side. It can be seen that the Poppe approach predicts an appoximately linear variation of the air enthalpy for this specific case, but the gradient is different from that predicted by the Merkel approach. The $1/(i_{masw} - i_{ma})$ curve of the Poppe approach lies above the $1/(i_{masw} - i_{ma})$ curve of the Merkel approach. As the transfer characteristic, or Merkel number, is a function of the area under the $1/(i_{masw} - i_{ma})$ curve, the Merkel number according to the Poppe approach will be greater than the Merkel number predicted by the Merkel approach.

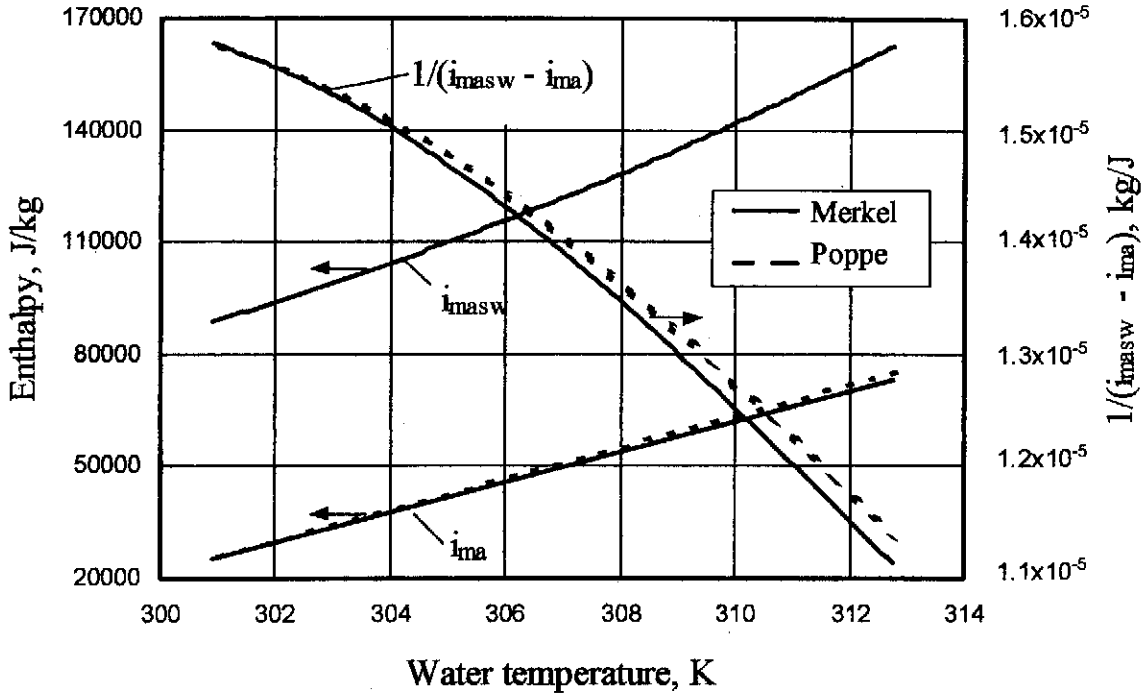

Figure 2.8: Enthalpy diagram of the Merkel and Poppe approaches.

Figure 2.9 shows an example of a psychrometric chart for a water cooling process solved by the Poppe method. The inlet air to the cooling process is very hot and dry. It can be seen that the temperature of the outlet air is cooler than the inlet air. This scenario is explained in section 2.2 with the aid of figure 2.3(b).

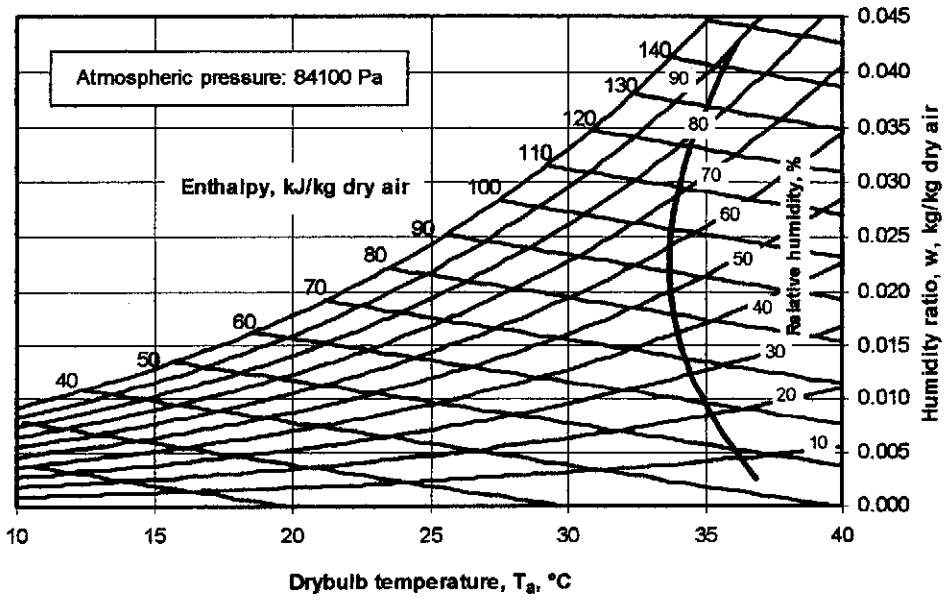

Figure 2.9: Psychrometric chart with a process determined by the Poppe method.

2.5 *e-NTU* ANALYSIS

The *e-NTU* method, developed by Jaber and Webb [89JA1], is based on the assumptions made by Merkel. The results obtained by employing this approach is therefore not very different from that obtained by employing the Merkel approach. The difference between these two models is essentially that a different

integration procedure is employed to obtain the area under the $1/(i_{masw} - i_{ma})$ curve, as shown in figure 2.5. A brief description of the *e-NTU* model is presented in appendix B.5.

The Merkel number according to the *e-NTU* approach, Me_e, is given by

$$Me_e = \frac{c_{pw}}{di_{masw}/dT_w} NTU \tag{2.5}$$

if m_a is greater than $m_w c_{pw}/(di_{masw}/dT_w)$. If m_a is less than $m_w c_{pw}/(di_{masw}/dT_w)$ the Merkel number according to the *e-NTU* approach is given by

$$Me_e = \frac{m_a}{m_w} NTU \tag{2.6}$$

where *NTU* is given by equation (B.73) for counterflow cooling towers. The great advantage of the effectiveness-*NTU* approach is its simplicity in the application of crossflow configurations. For crossflow, however, it must be specified whether the air and water streams are mixed or unmixed or a combination of mixed and unmixed. Thus, there exists a choice of four possible flow geometries for crossflow. The question now is which geometry will yield the most accurate results for a particular fill material.

It is not important which flow geometry is chosen, as long as the same geometry is assumed for both the fill performance analysis and the subsequent cooling tower performance analysis. If used consistently, the four different geometries together with the Merkel approach and Poppe approach will predict practically identical water outlet temperatures if all other variables are assumed to be constant and if the fill test analysis and the subsequent cooling tower performance analysis is conducted at the same operating conditions.

2.6 OTHER ANALYSES FOR EVALUATING COOLING TOWER PERFORMANCE

Papers are regularly published in the literature that present heat and mass transfer models in cooling tower applications. These models differ in complexity and are essentially based on the Merkel or Poppe models. Some of these models are according to Nahavandi et al. [75NA1], Montakhab [78MO1], Bourrilot [83BO1, 83BO2], Sutherland [83SU1], Feltzin and Benton [91FE1], Bernier [95BE1], Ibrahim et al. [95IB1], Sadasivam and Balakrishnan [95SA1], El-Dessouky et al. [97EL1], Al-Nimr [98AL1], Söylemez [99SO1], Makkinejad [01MA1], Milosavljevic and Heikkilä [01MI1] and Fisenko et al. [02FI1].

There are two-dimensional models that calculate the flow field in the cooling towers by finite difference equations. These models can therefore accommodate non-uniform air and water flow distributions. These models are according to Majumdar [83MA1, 83MA2, 83MA3] and Hawlader and Lui [02HA2].

Johnson [89JO1] presents a comprehensive list of assumptions used for some of the models mentioned above. Mohiuddin and Kant [96MO1] present a summary and overview of the some of the models found in the literature.

2.7 CONCLUSION

The consistent employment of the heat and mass transfer model in the fill performance evaluation and then using the same model in the subsequent cooling tower performance analysis is stressed. If used consistently the different models ought to give the same cooling ranges for the water in a particular cooling tower if all the operating conditions are exactly the same for each model. Because the Poppe approach is the more rigorous approach, it will predict the water evaporation rate, the total heat transfer rate and thus the air outlet temperature more accurately than the other approaches. This may lead to situations where the predicted cooling tower operating conditions will not be the same as those predicted by the other approaches, and it may therefore predict cooling ranges different from those predicted by the Merkel or *e-NTU* approaches. For example, the draft through natural draft cooling towers is a function of the air outlet temperature and the Poppe method will thus predict more accurate tower draft and tower performance. The Poppe method also has distinct advantages in the analysis of hybrid cooling towers since the humidity of the outlet air is calculated, even if the air is supersaturated [01RO1]. This information is important to ensure that the correct amount of heated dry air is mixed with the wet plume to ensure no visible plume after mixing of the two streams.

CHAPTER 3

FILL PERFORMANCE EVALUATION

3.1 INTRODUCTION

The Merkel [25ME1], Poppe [91PO1] and *e-NTU* [89JA1] methods to evaluate cooling tower performance were discussed in the previous chapter. In this chapter the different methods of analysis are employed to determine fill performance transfer characteristics. Fill transfer and loss coefficient correlations given in the literature for wet-cooling tower fills are relatively simple and are generally not accurate over a wide range of operational conditions. A new extended empirical relation for the loss coefficient is proposed where the viscous and form drag effects are accounted for as well as the buoyancy, momentum and fill height effects. It is shown that the proposed empirical relation gives very accurate correlations for splash, trickle and film fill types, over a wide range of air and water mass flow rates when compared to other forms of empirical relations commonly found in the literature. The dependence of the transfer characteristic on the height of the fill, inlet air drybulb temperature and inlet water temperature is investigated. It is shown that the transfer characteristic per unit height is a function of the fill height and the inlet water temperature but not of the air inlet temperature. The empirical relations for the loss and transfer coefficients do not include effects of different spray types or ageing effects.

3.2 LOSS COEFFICIENT

The loss coefficient of a cooling tower fill is determined by measuring the pressure drop over the fill during the testing phase. Empirical relations are then obtained for the loss coefficient of the fill as a function of the air and water mass flow rates. These empirical relations are subsequently employed in the design of cooling towers to determine the draft through the cooling towers. Suitable fans for mechanical draft cooling towers are selected based among others, on the loss coefficient of the fill. The draft in a natural draft cooling tower is a function of the fill loss coefficient. It is thus important to represent the fill loss coefficient accurately, as inaccurate representation of the loss coefficients in the form of empirical relations can have financial implications if the cooling tower does not meet design specifications.

The fill loss coefficient is defined as

$$K_{fi} = 2\Delta p_{fi} / (\rho v^2) \tag{3.1}$$

where Δp_{fi} is the measured static pressure drop across the fill.

The static pressure drop across the fill (Δp_{fi}) is due to viscous drag (frictional drag) and form drag resistance in addition to the acceleration of the air due to heating and mass transfer, while the buoyancy

due to the difference in density of the air in the fill and that in the manometer tube external to the test section will tend to counteract these effects in cases of counterflow [98KR1], i.e.

$$\Delta p_{fi} = \Delta p_{fd} + \left(\rho_{avo} v_{avo}^2 - \rho_{avi} v_{avi}^2\right) - \left(\rho_{ava} - \rho_{avm}\right) g L_{fi} \tag{3.2}$$

where the subscript *fd* refers to frictional and drag effects and ρ_{ava} is the density of the ambient air which is essentially equal to the density of the air entering the fill i.e. ρ_{avi}. The density of the air leaving the fill is ρ_{avo} and the mean harmonic density $\rho_{avm} = 2/(1/\rho_{avi} + 1/\rho_{avo})$. The second term on the right-hand side of equation (3.2) represents the momentum change experienced by the air stream while the third term considers buoyancy effects. This equation assumes that the porosity of the particular fill, which is defined as the ratio of the free flow area at a cross-section to the corresponding cross-sectional area of the fill, is unity. In the absence of momentum changes a loss coefficient which is determined by frictional and drag effect can be defined, i.e.

$$K_{fd} = 2\Delta p_{fd} / (\rho v^2) = 2\left[\Delta p_{fi} - \left(\rho_{avo} v_{avo}^2 - \rho_{avi} v_{avi}^2\right) + \left(\rho_{avi} - \rho_{avm}\right) g L_{fi}\right] / (\rho v^2) \tag{3.3}$$

In practice the reference conditions chosen for the denominator in equation (3.3) differ. For example, the loss coefficient for a particular fill can be defined in terms of the mean air-vapor flow rate and its density through the fill i.e.

$$K_{fdm} = 2\left[\Delta p_{fi} - \left(\rho_{avo} v_{avo}^2 - \rho_{avi} v_{avi}^2\right) + \left(\rho_{avi} - \rho_{avm}\right) g L_{fi}\right] \rho_{avm} A_{fr}^2 / m_{avm}^2 \tag{3.4}$$

where $m_{avm} = \rho_{avm} v_{avm} A_f$. Per unit height of the fill it follows from equation (3.4) that $K_{fdm1} = K_{fdm}/L_{fi}$.

The following measurements are generally made during fill tests where the transfer coeffcients and loss coefficients are determined: the air inlet drybulb temperature (T_{ai}), and the air wetbulb temperature (T_{wb}), the water inlet temperature (T_{wi}), the water outlet temperature (T_{wo}), the water mass flow rate (m_w) and the air mass flow rate (m_a). The atmospheric pressure (p_a) is also measured to determine the humidity ratio of the inlet air (w_i). The air outlet drybulb temperature (T_{ao}) is generally not measured since it is relatively difficult to measure accurately because of condensation, drift and supersaturation of the outlet air. The outlet air temperature is not employed in the Merkel [25ME1] or Poppe [91PO1] theories to determine the transfer coefficient. However, the outlet temperature can be predicted by these theories. Merkel assumed that the outlet air is saturated which enabled him to determine the outlet air temperature from a simple energy balance. In the case of the Poppe theory the outlet air temperature is evaluated as Poppe did not make the simplifying assumptions of the Merkel approach.

The loss coefficient as given by equation (3.4) is dependent on the air outlet temperature. Since the Poppe approach generally predicts higher air outlet temperatures than the Merkel method, the loss coefficients will differ. This difference, however, is generally small.

3.2.1 EMPIRICAL EQUATIONS

Lowe and Christie [61LO1] used the following form of equation to represent the loss coefficients of counterflow splash and film type fills.

$$K_{fi} = c_1 \left(\frac{G_w}{G_a}\right) + c_2 \tag{3.5}$$

where c_1 and c_2 are empirical constants that depend on the fill design. The empirical relations of Lowe and Christie [61LO1] are widely applied and cited by other researchers [83MA3, 96MO2, 98KR1]. Majumdar et al. [83MA3] correlated the data in Kelly [76KE1] by employing equation (3.5).

Johnson [89JO1] gives fill loss coefficient test results for counterflow cellular type fills with variable heights as

$$K_{fi} = c_1 G_w^{c_2} G_a^{c_3} L_{fi}^{c_4} \tag{3.6}$$

where L_{fi} is the height of the fill. If the fill height is constant then equation (3.6) becomes

$$K_{fi} = c_1 G_w^{c_2} G_a^{c_3} \tag{3.7}$$

Baard [98BA1] conducted extensive tests on expanded metal type fills in various configurations and employed equation (3.7) to correlate his pressure drop data. The correlation coefficients obtained by Baard [98BA1] indicates that equation (3.7) does not necessarily correlate the measured data accurately for some fill configurations. He obtained correlation coefficients ranging from 0.61 to 0.98.

Milosavljevic and Heikkilä [01MI1] tested seven types of counterflow film type fills and correlated their pressure drop data with

$$\Delta p_{fi} / L_{fi} = c_1 \left(1 + G_w^{c_2}\right) G_a^{c_3} \tag{3.8}$$

Goshayshi and Missenden [00GO1] tested seven types of counterflow film type fills in various arrangements. Their tests were conducted in a 0.15 m × 0.15 m counterflow test section where G_a is varied between 0.2 and 1.5 kg/m^{2}s, and G_w is varied between 0.45 to 2.22 kg/m^{2}s. These mass velocities are very low and are not typical for industrial applications [85LI1]. Their fill test data is correlated by

$$\Delta p_{fi} = c_1 G_w^{c_2} G_a^{c_3} \tag{3.9}$$

where c_2 and c_3 are constant for all the fills tested. Goshayshi and Missenden [00GO1] reported a maximum error of ±3% for equation (3.9) when applied to their tests.

3.2.2 NEW EMPIRICAL EQUATION

The loss coefficient is essentially a drag coefficient. Figure 3.1 shows the drag coefficients of two simple shapes as a function of the Reynolds number. The total drag on a body placed in a stream of fluid consists of skin friction and of form or pressure drag. The sum of the two is called the total drag [60SC1].

It can be seen in figure 3.1 that the drag coefficient at low Reynolds numbers decreases for increasing Reynolds numbers. This is due to the fact that viscous or friction effects predominate. The curve flattens out and remains essentially constant at high Reynolds numbers. Form drag is predominant in this region. The reason for the existence of form drag lies in the fact that the boundary layer displaces the external, potential flow [60SC1].

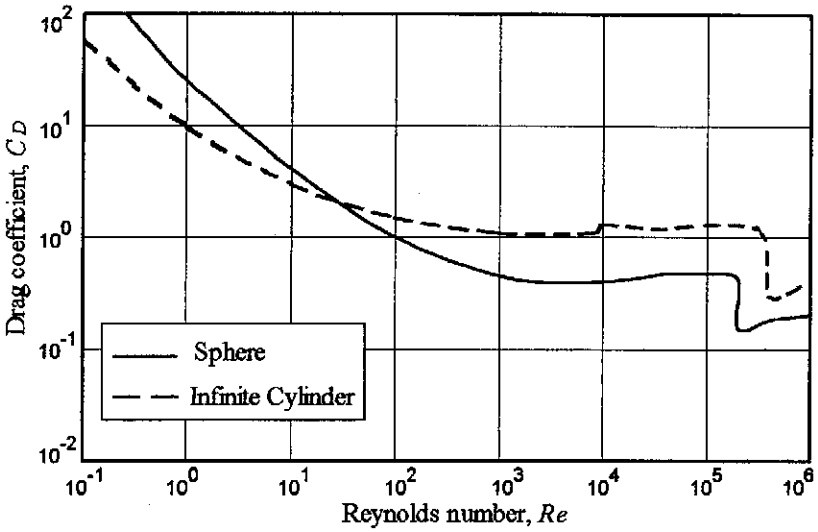

Figure 3.1: Drag coefficient for bodies of revolution (adapted from Daugherty et al. [89DA1]).

The Ergun [52ER1] equation for the pressure drop through packed beds is given by

$$\frac{dp}{dx} = \frac{150\mu V}{l^2} + \frac{1.75\rho V^2}{l} \tag{3.10}$$

where V and l are the characteristic velocity and characteristic length respectively. The first terms accounts for the viscous drag, and the second term accounts for form drag. The characteristic length is constant for a specific packed bed while the characteristic velocity is a function of the air velocity. If a cooling tower fill is approximated by a packed bed, V and l will also be a function of water mass flow rate. Water droplets may be retained in the fill area or be entrained by the air when the drag force acting on the droplets is greater or equal to the weight of the water droplets. This phenomenon is a function of the air velocity and the water droplet size and ultimately on the type and configuration of the fill. Wet-cooling tower fills differ from packed beds as the pebbles (or water droplets in this case) are not static, and of variable shape, quantity and size. The fill, of course, is stationary. However, equation (3.10) gives a basis of what form a generalized correlation for pressure drop in fills must take. The pressure drop is a sum of two terms where each term is a function of the air and water mass flow rates. Thus, a new general empirical relation is proposed which accounts for the form drag and viscous drag effects as well as the effects that are dependent on the water mass flow rate and the configuration of the fill, i.e.

$$K_{fi} = c_1 G_w^{c_2} G_a^{c_3} + c_4 G_w^{c_5} G_a^{c_6} \tag{3.11}$$

3.2.3 ACCURACY OF EMPIRICAL EQUATIONS

Splash, trickle and film type fills are tested to show the accuracy and generality of equation (3.11) compared to that of equation (3.7), that is commonly found in the literature, and the equation,

$$K_{fi} = c_1 (G_w / G_a)^{c_2} \tag{3.12}$$

The form of equation (3.12) is commonly encountered in the literature to represent the Merkel number, but it is applied here to represent the loss coefficient.

The experimental results for the trickle, splash and film type fills are respectively presented in appendix R, appendix S and appendix T. The results in these appendices are obtained by employing the methods and computer program presented in appendix K.

Table R.14 shows the empirical equations of the loss coefficients of three different trickle fill heights obtained from experimental tests presented in appendix R. It can be seen that the correlation coefficient, while employing equation (3.11), is very accurate when compared to that of equations (3.7) and (3.12). Figures R.3, R.5 and R.7 show the comparative curve fits of the three different fill heights. The superiority of equation (3.11) to accurately represent the measured data is evident from these figures.

Table S.18 shows the loss coefficient empirical equations of splash fills for four different splash fill spacings. It is again evident from the correlation coefficients that equation (3.11) is superior to equations (3.7) and (3.12) to represent the measured data accurately. Figures S.3, S.5, S.7 and S.9 show the comparative curve fits for fill spacings of 0.1, 0.2, 0.3 and 0.4 m respectively. It can be seen that equation (3.11) represents the measured data very accurately when compared to equations (3.7) and (3.12).

Table T.14 shows the loss coefficient empirical equations of cross-corrugated film fills for three different fill heights. It is again evident from the correlation coefficients that equation (3.11) is superior to equations (3.7) and (3.12) in representing the measured data accurately. Figures T.3, T.5 and T.7 show the comparative curve fits for fill heights of 0.6, 0.9 and 1.2 m respectively. It can be seen that equation (3.11) represents the measured data accurately when compared to equations (3.7) and (3.12).

Majumdar et al. [83MA3] correlated the data in Kelly for employment in their VERA2D program for the heat and mass transfer analysis of wet-cooling towers. As already mentioned, they employed equation (3.5). Figure 3.2 shows Kelly's [76KE1] data for a type F fill correlated by Majumdar et al. [83MA3] by employing equation (3.5). The air flow range employed in the experiments of Kelly is relatively narrow compared to the experiments conducted in this investigation. Correlations of Kelly's data by employing equation (3.7) and (3.11) are also shown in figure 3.2. In this instance, equation (3.7) and equation (3.11) give virtually identical results with correlation coefficients for both equal to 0.9991.

3.2.4 EFFECT OF FILL HEIGHT AND AIR AND WATER TEMPERATURES ON THE LOSS COEFFICIENT

Equation (3.11) correlates the measured data presented in appendices R, S and T for trickle, splash and film type fills respectively, and the data in the literature, relatively accurately. It is further investigated in appendix R if the loss coefficient is a function of the fill height, water inlet temperature and air inlet temperature. Equation (R.4) and figure R.10 show that the loss coefficient per unit height of fill is a function of the height of the fill. Equation (3.11) must therefore be extended to include the effect of the height of the fill on the loss coefficient per unit height of the fill,

$$K_{fil} = \left(c_1 G_w^{c_2} G_a^{c_3} + c_4 G_w^{c_5} G_a^{c_6}\right) L_{fi}^{c_7} \tag{3.13}$$

It can be seen from equations (R.5) and (R.14) that the loss coefficient is not a strong function of the water inlet temperature, T_{wi}, and air inlet temperature, T_{ai}, respectively as the exponents of T_{wi} and T_{ai} in these equations are very small. Equation (3.13) is thus adequate for correlating loss coefficient data.

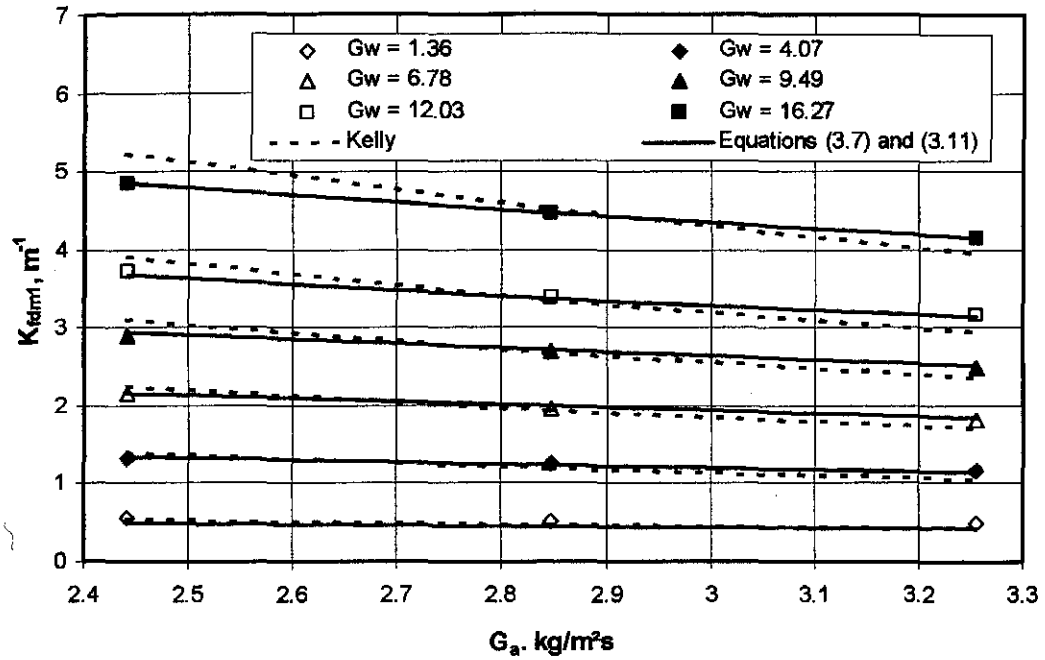

Figure 3.2: Data by Kelly [76KE1] correlated by Majumdar et al. [83MA3] (equation (3.5)) and equations (3.7) and (3.11).

3.3 TRANSFER CHARACTERISTIC

In the fill performance test phase, the water outlet temperature, together with the other variables mentioned in appendix K, are measured under controlled operating conditions. An empirical equation for the transfer characteristic or Merkel number is then determined from these measurements. In the subsequent cooling tower performance analysis, the water outlet temperature is determined from the known transfer characteristic or Merkel number.

3.3.1 EMPIRICAL EQUATIONS

Lowe and Christie [61LO1] used the following form of equation to represent the Merkel numbers of counterflow splash and film type fills.

$$Me/L_{fi} = c_1(G_w/G_a)^{c_2} \tag{3.14}$$

where c_1 and c_2 are constants.

Kröger [98KR1] and Baard [98BA1] use the following form of equation to represent the Merkel number

$$Me/L_{fi} = c_1 G_w^{c_2} G_a^{c_3} \tag{3.15}$$

where L_{fi} is the length of the fill and c_1, c_2 and c_3 are constants.

Johnson [89JO1] expresses the Merkel number for counterflow cellular type fills with the relation

$$Me/L_{fi} = c_1 G_w^{c_2} G_a^{c_3} T_{wi}^{c_4} \quad (3.16)$$

where the Merkel number is a function of the water inlet temperature.

The Merkel numbers in equations (3.14) and (3.15) are only functions of the air and water mass velocities. These empirical equations, to represent the Merkel number or transfer characteristic, are gross simplifications of a very complex heat and mass transfer process. Equation (3.14) assumes that the absolute values of c_2 and c_3 in equation (3.15) are equal. Equation (3.16) makes provision for changes in the inlet water temperature.

3.3.2 ACCURACY OF EMPIRICAL EQUATIONS

A more general equation is proposed for expressing the Merkel number, i.e.,

$$Me/L_{fi} = c_1 G_w^{c_2} G_a^{c_3} + c_4 G_w^{c_5} G_a^{c_6} \quad (3.17)$$

where equation (3.17) is the same form as equation (3.11) that is proposed for the loss coefficient. Splash, trickle and film type fill tests are tested to evaluate the accuracy and generality of equations (3.14), (3.15) and (3.17).

Table R.13 summarizes the empirical equations of the Merkel numbers for the trickle fill for three different fill heights. It can be seen from the correlation coefficients in table R.13 and figures R.2, R.4 and R.6 that equation (3.14) is the least accurate. The accuracy of equations (3.15) and (3.17) is of the same order.

Table S.17 summarizes the empirical equations and correlation coefficients of the Merkel numbers for the splash fill for fill spacings of 0.1, 0.2, 0.3 and 0.4 m. Equation (3.14) is again the least accurate. Equations (3.15) and (3.17) have the same order of accuracy.

Table T.13 summarizes the empirical equations of the Merkel numbers for the cross-corrugated film fill for three different fill heights. It can be seen from the correlation coefficients in table T.13 and figures T.2, T.4 and T.6 that equation (3.14) is the least accurate. The accuracy of equations (3.15) and (3.17) is of the same order.

It is therefore clear that equation (3.14) employed by Lowe and Christie [61LO1] does not always represent the test data accurately. It is only accurate in limited conditions where the exponents c_2 and c_3 in equation (3.15) is close to each other. Equations (3.15) and (3.17) correlates fill performance test data with approximately the same degree of accuracy for all the types of fills tested. Equation (3.15) can be used instead of equation (3.17) as it is the simpler of the two equations.

3.3.3 EFFECT OF FILL HEIGHT ON THE MERKEL NUMBER

Equation (R.1) shows that the Merkel number per unit height of fill is a function of the height of the fill. Figure R.8 graphically compares equation (R.1) and the measured values of the Merkel number for the different fill heights. Equation (3.15) must therefore be extended to include the effect of the height of the fill on the Merkel number per unit height of the fill,

$$Me / L_{fi} = c_1 G_w^{\ c_2} G_a^{\ c_3} L_{fi}^{c_4} \tag{3.18}$$

3.3.4 EFFECT OF INLET WATER TEMPERATURE ON THE MERKEL NUMBER

Fill tests, for a 1.53 m high trickle fill, where the water and air flow rates are varied, are conducted at different inlet water temperatures. These tests are presented in sections R.5 and R.6. Equation (R.6) express the Merkel number as a function of the inlet water temperature for the combined data in sections R.5 and R.6. It is therefore clear that equation (3.15) must be extended to include the effect of the inlet water temperature as Johnson [89JO1] did in equation (3.16). Including the effect of the inlet water temperature, equation (3.18) can be extended to the general form

$$Me / L_{fi} = c_1 G_w^{\ c_2} G_a^{\ c_3} L_{fi}^{c_4} T_{wi}^{c_5} \tag{3.19}$$

Sections R.7 and R.8 show the experimental results of 1.08 and 1.98 m high trickle fills respectively where only the water inlet temperature is varied during the testing periods. Figures R.13 and R.17 shows the variation of the Merkel numbers, according to the Merkel, *e-NTU* and Poppe approaches, as the inlet water temperature varies, for fill heights of 1.08 and 1.98 m respectively. Figure R.17 is repeated here as figure 3.3. It can be seen from figure 3.3 that the Merkel numbers according to the different approaches are relatively strong functions of the water inlet temperature. The exponents of T_{wi} in equations (R.7) and (R.8) for the 1.08 and 1.98 m fill respectively are –0.2471 and –0.2774.

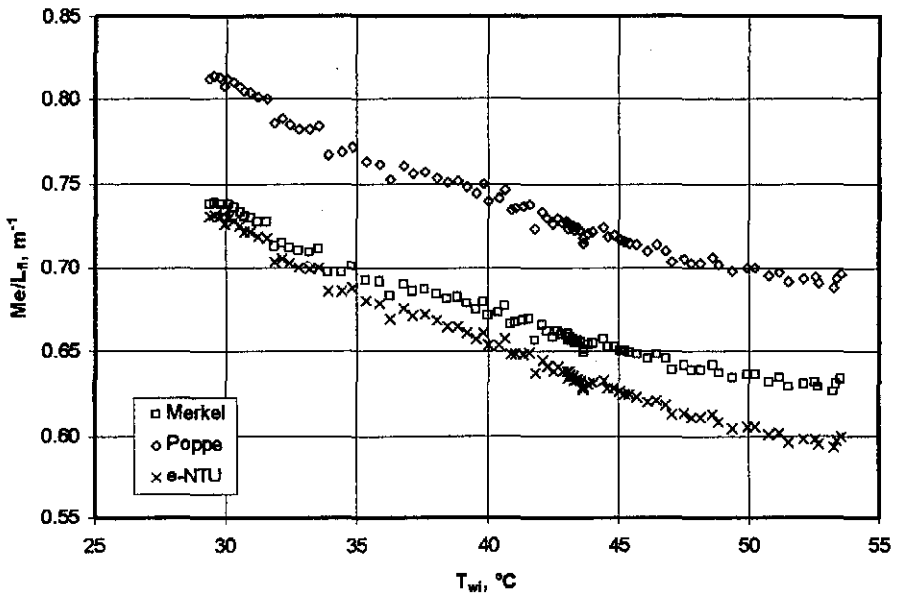

Figure 3.3: Transfer coefficients according the *e-NTU*, Merkel and Poppe approaches where only T_{wi} is varied.

It is interesting to note from figure R.13 and figure R.17 (figure 3.3) that the Merkel numbers, according to the *e-NTU*, Merkel and Poppe theories, decrease for increasing water inlet temperatures. Thus as design loads of cooling towers increase above design specifications, the cooling tower will be less effective.

3.3.5 EFFECT OF INLET AIR TEMPERATURE ON THE MERKEL NUMBER

According to the Merkel theory, the Merkel number is not a function of the inlet air drybulb temperature. This is because the assumed linear increase in the air enthalpy is indeed linear as indicated by equation (2.2). The cooling tower performance curves compiled by the Cooling Tower Institute [67CT1] and Kelly [76KE1], for counterflow and crossflow fills respectively, do not present the Merkel number as a function of air temperature (refer to figure 2.6).

Roth [01RO1], however, found from experiment that the Merkel number appears to be a function of the air inlet drybulb temperature decreasing for increasing air temperatures. Figure 3.4 shows the results of Roth [01RO1] where the Merkel number is a function of the inlet air drybulb temperature. The water inlet temperatures in figure 3.4 are varied until a constant cooling range is obtained. Roth [01RO1] does not give values for the low medium and high air temperatures or states whether the air temperatures are approximately constant or not. It will be shown that the apparent dependence of the Merkel number on the inlet air drybulb temperature, according to Roth [01RO1], is actually the dependence of the Merkel number on the inlet water temperature.

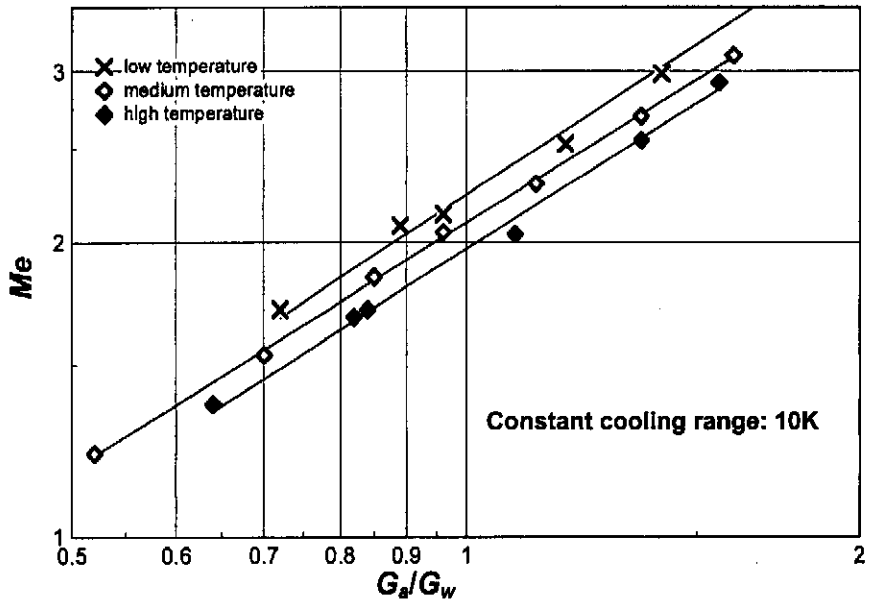

Figure 3.4: Merkel number for a fill according to the Poppe theory (Adapted from Roth [01RO1]).

The effects of the inlet drybulb and wetbulb temperatures, on the Merkel number or transfer coefficient, are investigated experimentally for a trickle fill. The summary of the results of this investigation is presented in section R.11. Figure R.23 is repeated as figure 3.5 and shows the Merkel numbers for three different inlet air drybulb temperatures versus the right hand side of equation (R.10) where the air temperature is omitted. It is evident from figure 3.4 that there is no significant temperature effect on the Merkel number. Refer to section R.11 for a detailed discussion of the fact that the inlet air drybulb and wetbulb temperatures do not influence the empirical equation for the Merkel number significantly.

The cooling range for all the data presented by Roth [01RO1] in figure 3.4 is constant. In order to achieve a constant cooling range, with variable air inlet temperatures, it is necessary to vary the water inlet

temperature. The effect of the inlet water temperature on the Merkel number is therefore hidden in the analysis of Roth [01RO1].

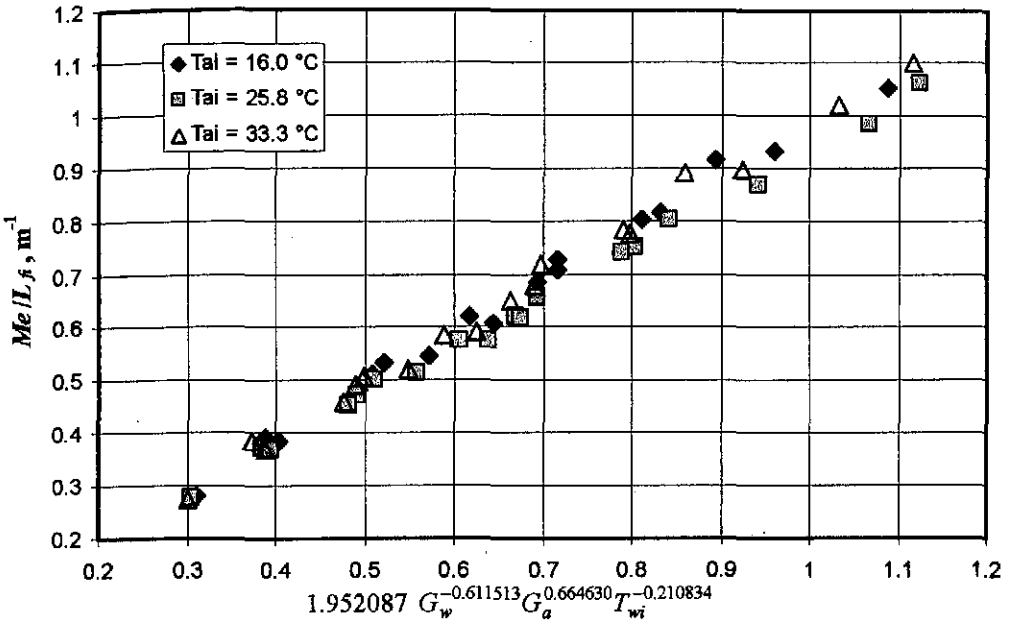

Figure 3.5: The measured Merkel number per unit length of fill versus right hand side of equation (R.10) where the temperature of the air is omitted.

3.4 CONCLUSION

A new empirical relation is developed that correlates measured pressure loss coefficients accurately for all types of fills under all types of operational conditions as it is based on fundamental principles that make provision for forces due to shear and drag. Other types of equations may correlate observed trends accurately, but they generally lack generality and are only applicable for limited ranges of water and air flow rates.

Both the empirical relations for the loss and transfer coefficients per unit height of fill of wet-cooling tower fills are extended to include the effect of the height of the fill. In addition, the empirical relation for the Merkel number is extended to include the effect of the water inlet temperature. The inlet water temperature has no significant effect on the loss coefficient. It is also found that the inlet air drybulb and wetbulb temperatures have no significant effect on the loss or transfer coefficients.

It is recommended that as much information as possible be supplied with the empirical relations of the loss coefficients, such as the ranges of applicability of G_a and G_w. The goodness of fit must also be supplied in the form of a correlation coefficient. This will enable the designer of wet-cooling systems to take the necessary precautions to compensate for any uncertainties. If possible, the same water spray system must be employed in the fill test and the subsequent cooling tower application of the fill. This will eliminate the effects of droplet size and distribution on the loss coefficient. Ageing effects of the fill are not investigated in this study.

CHAPTER 4

WET-COOLING TOWER PERFORMANCE EVALUATION

4.1 INTRODUCTION

The performance of natural and mechanical draft counterflow cooling towers is critically evaluated by respectively employing the Merkel [25ME1], Poppe [91PO1] and *e-NTU* [89JA1] methods of analysis at different operating and ambient conditions. The Wet-Cooling Tower Performance Evaluation (WCTPE) software program, presented in appendix P, is employed in this investigation. The importance of using a particular method of analysis when evaluating the performance characteristics of a certain fill material and subsequently employing the same analytical approach to predict cooling tower performance, is investigated.

By employing the different approaches at different ambient conditions for natural and mechanical draft cooling towers, the resultant predicted performances are compared. The differences in performance of natural draft and mechanical draft towers, for the same ambient conditions, are evaluated. The performance of the natural draft cooling tower, specified in appendix I, is evaluated in the WCTPE program in this investigation. Furthermore, the performance of the mechanical draft tower, presented in appendix J, is employed in this investigation, with the exception that the fill height, L_{fi}, and the water mass velocoty, G_w, are the same as those of the natural draft tower. The fan speed of the mechanical draft tower is also adjusted so that the air mass velocity and cooling range is the same as that of the natural draft cooling tower, at the ambient conditions as specified in appendix I.

Ambient air drybulb temperatures of 280, 290, 300 and 310 K are considered in the analysis. At each of these temperatures, the ambient humidity is varied from dry to saturated conditions. The results of the cooling tower analyses are given in graphical form in appendix O. Most of the graphs in figures O.1 to O.19 are presented in the same general form. Subfigures (a_1) to (a_5) in each figure respectively illustrate the heat rejected, Q, the water outlet temperature, T_{wo}, the air outlet temperature, T_{a5}, the mean air-water vapor mass flow rate, m_{av15}, and the water evaporation rate, $m_{w(evap)}$, at an ambient temperature of 280 K at ground level, where the humidity of the inlet air is varied from dry to saturated conditions. The subfigures (b_1) to (b_5), (c_1) to (c_5) and (d_1) to (d_5) show the same variables as subfigures (a_1) to (a_5), except that they are for ambient temperatures at ground level of 290, 300 and 310 K respectively.

4.2 NATURAL DRAFT COOLING TOWER

The natural draft cooling tower specified in appendix I is taken as the reference tower. Figures O.1(a_1)-O.1(a_5) respectively illustrate the heat rejected, Q, the water outlet temperature, T_{wo}, the air outlet temperature, T_{a5}, the mean air-water vapor mass flow rate, m_{av15}, and the mass flow rate of the water evaporated from the water stream, $m_{w(evap)}$, as the inlet air is varied from dry to saturated conditions where

the ambient temperature is equal to 280 K. The solid line in each of the figures represents the results according to the Merkel approach while the broken lines represent the results according to the more rigorous Poppe approach. The same method of analysis is used for both the fill performance evaluation and the subsequent cooling tower analysis, i.e., for example, the fill performance characteristics, determined by the Poppe approach, are used in the cooling tower performance calculations, while employing the Poppe approach.

4.2.1 HEAT REJECTED

The heat rejected by the cooling tower at ambient temperatures of 280, 290, 300 and 310 K in dry to saturated conditions, can be seen in figures O.1(a_1), O.1(b_1), O.1(c_1) and O.1(d_1). It can be seen that the heat rejection predicted by the Poppe approach is higher than that predicted by the Merkel approach at all the ambient conditions considered in this investigation. The Poppe approach predicts heat rejection rates that are approximately 3% higher at 280 K and 4% higher at 290 K than the values predicted by the Merkel approach at all the inlet humidity conditions. At 300 K, in very dry conditions, the difference between the Poppe and Merkel approaches is approximately 7% and 4% in the case of saturated inlet conditions. The difference is 13% in very dry inlet conditions and 4% in the case of saturated inlet conditions, at an ambient temperature of 310 K. Thus, it is evident that the difference in heat rejection rates between the Merkel and Poppe approaches increases as the inlet air becomes dryer and hotter.

4.2.2 WATER OUTLET TEMPERATURE

The heat rejected by the cooling tower at ambient temperatures of 280, 290, 300 and 310 K in dry to saturated conditions, can be seen in figures O.1(a_2), O.1(b_2), O.1(c_2) and O.1(d_2).It can be seen that the water outlet temperatures predicted by both the Merkel and Poppe approaches are practically identical. The water outlet temperatures determined by the two different approaches are practically identical, because the same approach (i.e., Merkel or Poppe) is used in the fill performance analysis and the subsequent cooling tower performance analysis. Thus, if the same method is used in both the fill and cooling tower analysis, it will result in the same cooling range, if all other variables remain unchanged. In hot, dry conditions, there is however a discrepancy between the water outlet temperatures predicted by the Merkel and Poppe approaches, i.e. the water outlet temperature, predicted by the Poppe approach, is less than that predicted by the Merkel approach. This is because there is a discrepancy between the air outlet temperatures predicted by the Merkel and Poppe approaches.

4.2.3 AIR OUTLET TEMPERATURE

It can be seen in figures O.1(a_3), O.1(b_3), O.1(c_3) and O.1(d_3) that the air outlet temperatures predicted by the Poppe approach are higher than those predicted by the Merkel approach in all the ambient conditions considered. When the ambient temperature is low, the discrepancy between the predicted air outlet temperatures is the smallest. When the temperature of the ambient air increases, the discrepancy between the predicted air outlet temperatures increases in very dry conditions. When the humidity increases at a given temperature, the discrepancy decreases.

The air outlet temperature, according to the Merkel approach, can only be determined after the assumption that the air after the spray zone is saturated. The Poppe approach does not make this simplifying assumption and calculates the outlet humidity directly from the governing equations for heat and mass transfer presented in appendix B. The condition of the outlet air, determined according to the Poppe approach, can therefore be unsaturated, saturated or supersaturated.

For low ambient temperatures (280 K) at any ambient humidity, the outlet air is, according to the Poppe approach, always supersaturated. There is no discrepancy in the air outlet temperature trend, according to the Poppe approach, as the humidity increases at 280 K, compared to the trend of the Merkel approach, as seen in figure O.1(a_3). However, for a very low ambient humidity at higher temperatures, there is a discrepancy between the values predicted by the Merkel and Poppe approaches. This occurs because the outlet air, as predicted by the Poppe approach, is unsaturated. As the outlet air becomes saturated and supersaturated, the trend is the same as that predicted by the Merkel approach for a given ambient humidity ratio. This point of saturation is approximately at w_1 = 0.003 kg/kg in figure O.1(b_3) and w_1 = 0.022 kg/kg in figure O.1(c_3). The reasons for the difference in the air outlet temperatures predicted by the Merkel and Poppe approaches are discussed in section 4.3.3 for the mechanical draft cooling tower. Because the operating processes in mechanical draft towers are not as strongly coupled as in natural draft towers, the differences in the air outlet temperatures between the two approaches can be explained without secondary influences of other variables.

Another interesting phenomena evident in figure O.1(d_3) for dry conditions is that the outlet air is colder than the inlet air. The nett enthalpy transfer is still from the water to the air as explained in section 2.2 with the aid of a psychrometric chart. Notwithstanding the fact that the air outlet temperature is colder than the ambient temperature, there is still a draft through the tower. Draft through the natural draft tower is still possible, because the molar mass of vapor is less than that of air at the same temperature. Thus, a potential for draft still exists because the density of the air-vapor mixture inside the tower is less than that of the hotter less humid air on the outside of the tower.

4.2.4 MEAN AIR-WATER VAPOR MASS FLOW RATE

The mean air-water vapor mass flow rates, determined by the Poppe approach, are higher than those predicted by the Merkel approach at all the ambient conditions considered, as seen in figures O.1(a_4), O.1(b_4), O.1(c_4) and O.1(d_4). The mean air-water vapor mass flow rate is strongly coupled to the air outlet temperature. This is because the density of the air inside the cooling tower is a function of the air temperature. The mass flow rate of air through the tower is, in turn, a function of the density differential of the air internal and external to the cooling tower. Thus, the draft through the natural draft cooling tower is strongly coupled to the air outlet temperature. The draft, in turn, will influence the heat rejection rate in the cooling tower. It is clear that the processes in a natural draft cooling tower are strongly coupled.

If the outlet air is unsaturated, according to the Poppe approach, the mass flow rates are much higher than the mass flow rates predicted by the Merkel approach, than when the air is supersaturated, according to

the Poppe approach. The mass flow rate according to the Poppe approach is higher than that predicted by the Merkel approach, because the air outlet temperature, predicted by the Poppe approach, is higher than that predicted by the Merkel approach.

At temperatures of 280, 290 and 300 K (see figures O.1(a_4), O.1(b_4) and O.1(c_4)) the air-vapor mass flow rates increase as the inlet ambient humidity ratio is increased. It is very interesting to note that this is not the case at an ambient temperature of 310 K. Both the Merkel and Poppe approaches predict this interesting phenomenon. At ambient temperatures of 290 K (figure O.1(b_4)) and 300 K (figure O.1(c_4)) the predicted mass flow rates are decreasing for increasing ambient humidity ratios, according to the Poppe approach, when the air is unsaturated. Figures O.1(e_4), O.1(f_4) and O.1(g_4) illustrate the mass air-vapor mass flow rate at air inlet temperatures of 305, 307.5 and 308.75 K respectively. It can be seen that there is a gradual decrease of the slope of the mass flow rate, predicted by Merkel, as the ambient temperature is increased.

4.2.5 WATER EVAPORATION RATE

The predicted water evaporation rates in natural draft cooling towers are always higher according to the Poppe approach than according to the Merkel approach. This is the case even if the outlet air is unsaturated, according to the Poppe approach. The air can be unsaturated, according to the Poppe approach, but the predicted evaporation rate is still higher than that predicted by the Merkel approach where the outlet air is saturated, because of the strongly coupled draft and energy equations. The outlet air temperatures predicted by the Poppe approach are higher than those predicted by the Merkel approach. The hotter the air, the higher the draft. The higher the draft, the more heat and mass transfer and thus higher evaporation rates.

4.3 MECHANICAL DRAFT COOLING TOWER

The mechanical draft tower employed in this section has the same fill depth as the natural draft tower employed in the previous section. It also has exactly the same water and air mass flow rates per unit area as the natural draft tower at the reference conditions. At the reference point, the heat rejected and evaporation rates per unit area will exactly be the same in the reference mechanical and reference natural draft cooling towers. The ambient conditions of the natural draft cooling tower in the previous section are repeated here with the analysis of the mechanical draft tower. Figure O.2 shows the variation of the heat rejected, water and air outlet temperatures, air-water vapor mass flow rates and evaporation rates for different ambient temperatures and humidities.

4.3.1 HEAT REJECTED

The trends of the heat rejected at the different ambient conditions are the same as those of the natural draft tower discussed in the previous section. The average difference between the heat rejection rates, predicted by the Merkel and Poppe approaches, is approximately 2.8% in the case where T_{a1} = 280 K (figure O.2(a1)). The average difference is approximately 3.2%, 3.7% and 4.6% at ambient temperatures

of 290, 300 and 310 K respectively. Thus, at higher ambient temperatures, the differences between the Merkel and Poppe approaches are the greatest.

The percentages given for the mechanical draft tower, correspond approximately to those obtained for the natural draft cooling tower, where T_{a1} = 280 K and T_{a1} = 290 K. At higher temperatures, in dry conditions, the discrepancy between the Poppe and Merkel approaches is higher for the natural draft tower than that for the mechanical draft tower, because the governing equations are strongly coupled for the natural draft towers, which is not the case for mechanical draft towers.

4.3.2 WATER OUTLET TEMPERATURE

The water outlet temperatures, predicted by the Merkel and Poppe approaches, are practically identical at all the different ambient temperatures and humidities considered. This is not the case with natural draft cooling towers in very dry, relatively warm ambient conditions. This is again because of the strongly coupled energy and draft equations for natural draft towers. The energy and draft equations for mechanical draft towers are not as strongly coupled, and therefore are there essentially no discrepancies between the Merkel and Poppe approaches.

4.3.3 AIR OUTLET TEMPERATURE

It can be seen from figures O.2(a_3), O.2(b_3), O.2(c_3) and O.2(d_3) that the air outlet temperatures, for the mechanical draft tower, follow the same trend as those of the natural draft tower, as discussed in section 4.2.3, for both the Merkel and Poppe approaches. The differences between these two models are explained by the discussion that follows.

Merkel assumes that the air above the transfer areas is saturated with water vapor. The enthalpy of the air at this point, according to the Merkel approach, is known from a simple energy balance with the cooling water stream, where the water loss, due to evaporation, is neglected. By assuming that the air is saturated, with the known air enthalpy, the temperature of the air can be determined. The assumption made by Merkel that the air is saturated leads to greater errors when the air is unsaturated, according to the Poppe approach, than when it is supersaturated. The assumption by made by Merkel that the loss in the water mass flow rate, due to evaporation, could be neglected in the energy balance plays a secondary role, especially during hot and dry ambient conditions. A procedure to minimize the error introduced by neglecting the loss of water due to evaporation in the energy balance is discussed in section 4.8.

Refer to figure 4.1 which is the same as figure O.2(a_3). As already mentioned in section 4.2.3, the Merkel and Poppe approaches predict air outlet temperatures that follow the same trends for variable ambient humidities at low ambient temperatures.

At higher ambient temperatures, as shown in figure 4.2, which is the same as figure O.2(d_3), the respective trends predicted by the Poppe and Merkel approaches are not the same. The outlet air, according to the Poppe approach, in figure 4.1 is supersaturated across the whole range of inlet ambient

humidities. The outlet air, according to the Poppe approach, in figure 4.2 is, however, unsaturated across the whole range of inlet ambient humidities. It is therefore clear that the discrepancy between the Merkel and Poppe approaches is the greatest when the outlet air according to Poppe is unsaturated. If the outlet air is supersaturated, according to the Poppe approach, the discrepency is considerably smaller.

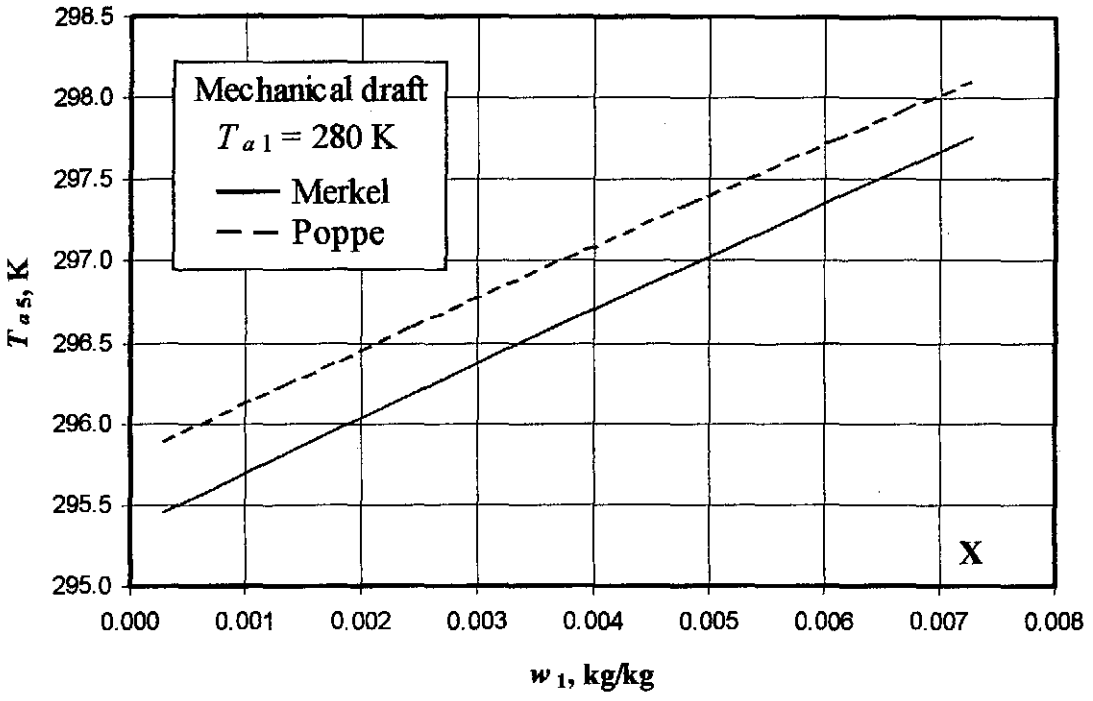

Figure 4.1: Air outlet temperature of a mechanical draft cooling tower for a low air inlet temperature.

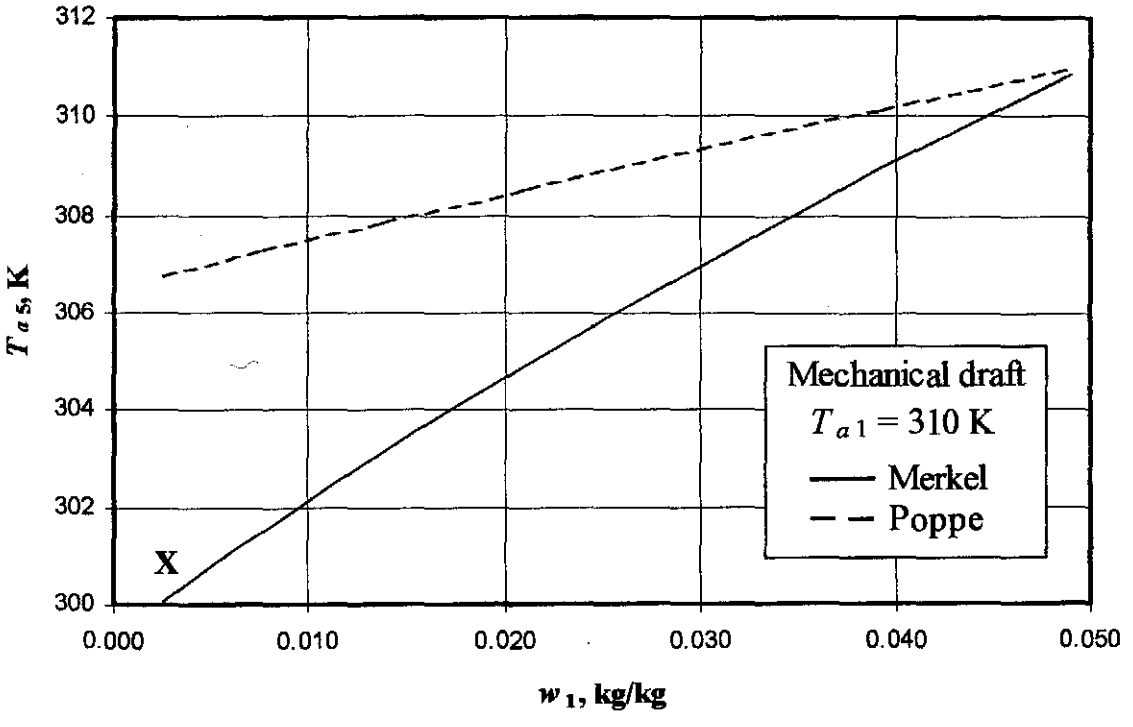

Figure 4.2: Air outlet temperature of a mechanical draft cooling tower for a high air inlet temperature.

Figure 4.3 shows the heating path of the air in the cooling tower for cold inlet air, which is saturated with water vapor. These inlet conditions are indicated with an 'X' in figure 4.1. Since the inlet air is saturated with water vapor, indicated by point 1 in figure 4.3, it immediately becomes supersaturated, according to the Poppe approach, as it enters the fill. As the air is heated and the humidity ratio increases, due to the latent heat transfer from the water, it follows the saturation curve very closely. This is because as the air is heated, it can contain more water vapor before it reaches the point of saturation. Point 2b in figure 4.3 shows the state of the air at the outlet of the fill, according to the Poppe approach. Point 2a in figure 4.3 shows the outlet air state according to the Merkel approach. It can be seen that the air is saturated at the outlet according to Merkel. The outlet air temperatures according to the Merkel and Poppe approaches are relatively close to each other in figure 4.3. The same trends are therefore predicted by the two approaches as shown in figure 4.1 when the outlet air is supersaturated according to the Poppe approach. The assumption of Merkel that the outlet air is saturated, is therefore a very good assumption, if the actual outlet air temperature is supersaturated.

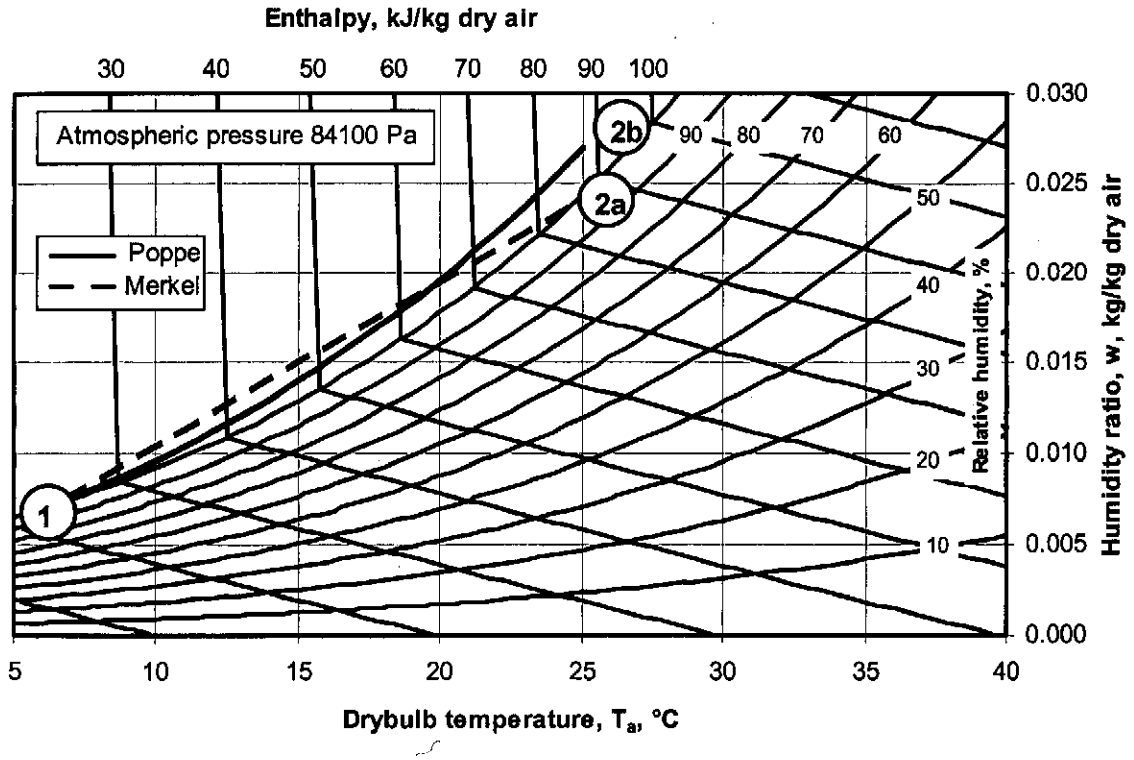

Figure 4.3: Psychrometric chart of cooling process for cold saturated ambient air.

The degree of supersaturation does not have a great influence on the relative difference between the outlet air temperatures predicted by the Merkel and Poppe approaches. This is because the lines of constant air enthalpy, in the supersaturated region, are very close to vertical as seen in figure 4.3. It therefore does not matter how much water vapor and mist are present in the supersaturated air, for a specific air enthalpy, the air temperature will be approximately constant. The difference in the air temperatures at point 2a and 2b in figure 4.3, for the Merkel and Poppe methods respectively, can be reduced by improving the energy balance employed by the Merkel approach where the approximate loss of water, due to evaporation, in the

energy balance is neglected. Refer to section 4.8 where the loss of water, due to evaporation, is accounted for in the energy balance.

Figure 4.4 shows the heating path of the air in the cooling tower for hot inlet air, which is virtually void of water vapor. These inlet conditions are indicated with a 'X' in figure 4.2. Point 1 in figure 4.4 shows the state of the inlet air on a psychrometric chart. Point 2b in figure 4.4 shows the state of the air at the outlet of the fill, according to the Poppe approach. It can be seen that the outlet air is colder than the inlet air. This scenario is described in chapter 2 with the aid of figure 2.3. Point 2a shows the outlet air state according to the Merkel approach.

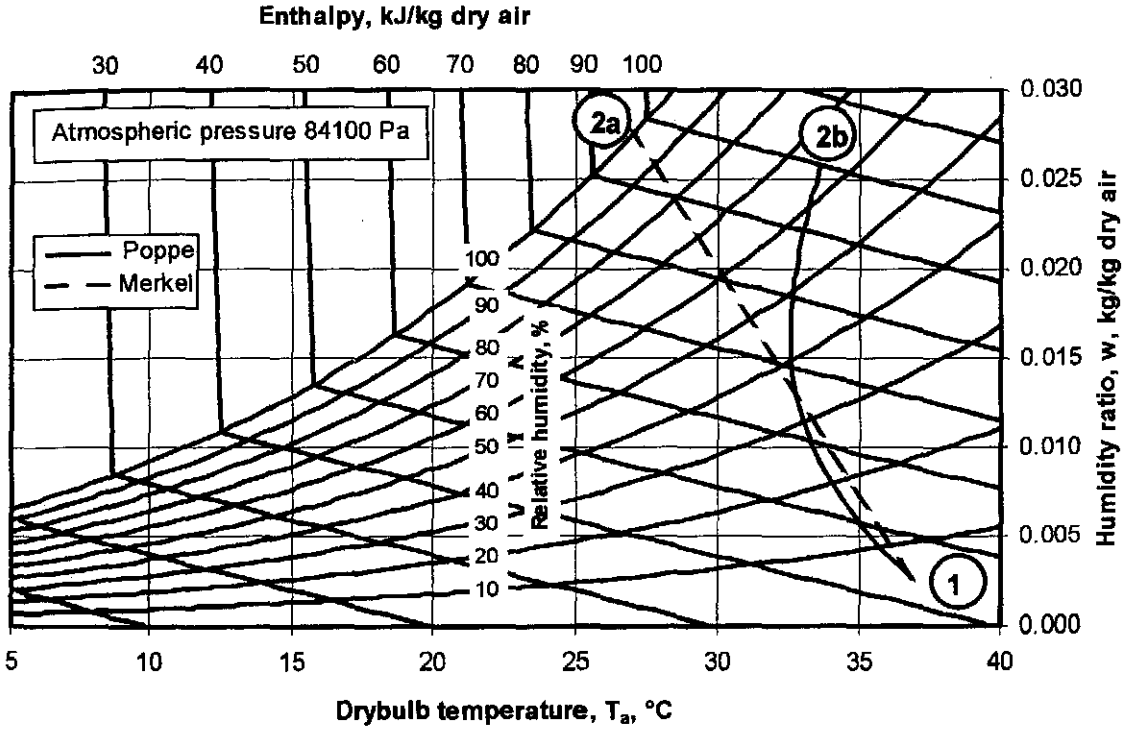

Figure 4.4: Psychrometric chart of cooling process for hot and very dry ambient air.

It can be seen in figure 4.4 that the outlet air is saturated according to the Merkel approach. The outlet air temperatures according to the Merkel and Poppe approaches are not very close to each other. The outlet air temperatures predicted by the Merkel and Poppe approaches lie approximately on the same constant enthalpy line in figure 4.4, as was the case in figure 4.3 when the outlet air was supersaturated according to the Poppe approach. In the unsaturated region, however, the lines of constant enthalpy are far for vertical and therefore the large discrepancy in the temperatures. The assumption of Merkel that the outlet air is saturated with water vapor, is not as accurate if the actual outlet air is unsaturated as when it is supersaturated.

4.3.4 MEAN AIR-WATER VAPOR MASS FLOW RATE

Figures O.2(a_4), O.2(b_4), O.2(c_4) and O.2(d_4) show the air-vapor mass flow rates predicted, by the Merkel and Poppe methods, at ambient temperatures of 280, 290, 300 and 310 K respectively. At each ambient temperature, the differences between the Poppe and Merkel approaches are practically negligible.

However, it is still informative to discuss the respective trends. If the trends in figure O.2, of the air-water vapor mass flow rate, are compared to the natural draft cooling tower in figure O.1, it can be seen that the trends are the inverse of each other. The Poppe approach predicts a smaller air-water vapor mass flow rate through the mechanical draft tower than the Merkel approach. For the natural draft cooling tower it is the opposite. If the inlet air humidity is increased for a given ambient temperature, then the mass flow rate through the mechanical draft tower decreases. Again, the opposite is true in natural draft cooling towers. The reason for this is that a lower air density at the outlet of the fill will increase the draft in natural draft towers, due to the increased pressure differential between the inside and outside of the tower. A lower density of the air, at the outlet of the fill of the mechanical draft tower, means that less air passes through the fan and hence the lower mass flow rate at higher air temperatures.

4.3.5 WATER EVAPORATION RATE

The Poppe approach always predicts higher mass flow rates than the Merkel approach in natural draft towers. For mechanical draft towers it is not always the case. In hot, dry conditions (see figures O.2(c_5) and O.2(d_5)) the outlet air can be unsaturated, according to the Poppe approach and hence the lower evaporation rate than in the Merkel approach where the outlet air is always saturated.

4.4 INVESTIGATION INTO THE DRAFT EQUATION OF NATURAL DRAFT COOLING TOWERS

A detailed draft equation is employed in the performance evaluation of the natural draft cooling tower presented in appendix I. The detailed draft equation is also employed in the analysis of the natural draft tower discussed in the section 4.2. The detailed draft equation accounts for the moist air that is raised in a gravitational field, adiabatic cooling and condensation. In this section the influence that the detailed draft equation has on the performance evaluation of a natural draft cooling tower is investigated and compared to a simplified equation that is commonly employed by other researchers [83BO1, 96MO2].

In its simplest form, the draft equation of a cooling tower can be expressed by

$$\Delta p_o - \Delta p_i = \Sigma K \, \rho v/2^2 \qquad (4.1)$$

where Δp_o is the pressure differential outside the tower and Δp_i is the pressure differential inside the tower while the flow resistances are represented by $\Sigma K \cdot 0.5 \rho v^2$. The right-hand side of equation (4.1) is the same for both the detailed and simplified draft equations. The difference between the detailed and simplified draft equations is thus on the left-hand side of equation (4.1). The simplified draft equation is given by

$$(\rho_{av1} - \rho_{av5}) \, g \, (H_6 - H_3 - L_{fi}/2) = \Sigma K \, \rho v^2/2 \qquad (4.2)$$

Figure O.3 illustrates the heat rejected, water outlet temperature, air outlet temperature, air-water vapor mass flow rate and the evaporation rate for temperatures of 280, 290, 300 and 310 K respectively. If all

the graphs in figure O.3 are compared to the corresponding graphs in figure O.1 it can be seen that the graphs are practically identical. Thus, for this specific cooling tower with the specified ambient conditions the simplified draft equation gives accurate results. Notwithstanding this fact, the detailed draft equation is still employed in all the investigations that follow.

Figures O.4(a) to O.4(b) show the pressure differentials of the detailed and simplified draft equations in the Merkel and Poppe approaches at ambient temperatures of 280 and 290 K respectively. It can be seen from figure O.4(a) that the difference in the pressure differential between the detailed and simplified draft equations, in both the Merkel and Poppe approaches, is approximately only 3 Pa across the entire range of ambient humidities considered. The difference in the pressure differential between the detailed and simplified draft equations decreases to approximately 2 Pa at an ambient temperature of 290 K, as can be seen in figure O.4(b). At 310 K the difference is less than 1 Pa as can be seen in figure O.4(d). Thus, the higher the ambient temperature, the smaller the difference in the pressure differential between the detailed and simplified draft equations for these particular ambient conditions.

4.5 CONSISTENT APPLICATION OF COOLING TOWER PERFORMANCE EVALUATION ANALYSES

It can be seen in figures O.1 and O.2 for the natural draft and mechanical draft towers respectively that the water outlet temperatures, predicted by the Merkel and Poppe approaches, are practically identical. It is concluded that the water temperatures are practically identical, because the same method of analysis is used for the evaluation of the performance characteristics of the fill and then subsequently used for the prediction of the cooling tower performance. This is denoted as the consistent application of a particular approach. It will be investigated what the influence on the accuracy will be if the approaches are applied inconsistently. A common error by cooling tower designers is to apply the approaches inconsistently. Empirical relations for fill performance characteristics, derived by employing the Merkel approach, are commonly available. These fill performance characteristics are then employed incorrectly in cooling tower performance calculations, while employing, for example, the more rigorous Poppe approach.

Figures O.5 and O.6 show the performance graphs of the natural draft and mechanical draft cooling towers respectively for the range of ambient conditions similar to those in figures O.1 and O.2. The fill performance characteristics obtained by the Merkel approach are applied inconsistently to the cooling tower performance evaluation while employing the Poppe approach. The results for the Merkel approach are not included in the graphs. The Poppe approach with consistent application of the fill performance characteristics is compared to the Poppe approach with inconsistent application of the fill performance analysis. The legend denoted 'Merkel' in each of the graphs in figures O.5 and 6 refers to the inconsistent application of the fill performance characteristics in the cooling tower performance evaluation. In this inconsistent application, the fill performance characteristics are determined by employing the Merkel approach while the performance of the cooling tower is evaluated by the Poppe approach. The legend, denoted 'Poppe', refers to the consistent application and is identical to the corresponding plots in figure O.1.

4.5.1 HEAT REJECTED

Although it seems from figures O.5(a_1), O.5(b_1), O.5(c_1) and O.5(d_1) for natural draft towers and from figures O.6(a_1), O.6(b_1), O.6(c_1) and O.6(d_1) for mechanical draft towers, that the discrepancy between the consistent and inconsistent analysis, decreases with increasing ambient temperatures, it is actually not always the case. The discrepancy between the consistent and inconsistent analyses of the heat rejection rate is approximately 2-2.5% at all the ambient temperatures and humidities. The heat rejection rates for the consistent analysis of the Poppe approach are approximately 2-2.5% higher than the inconsistent analysis, where the fill characteristics are obtained by employing the Merkel approach.

4.5.2 WATER OUTLET TEMPERATURE

Figures O.5(a_2), O.5(b_2), O.5(c_2) and O.5(d_2) for natural draft towers and figures O.6(a_2), O.6(b_2), O.6(c_2) and O.6(d_2) for mechanical draft towers present the water outlet temperatures of the consistent and inconsistent application of the Poppe approach to cooling tower performance. The discrepancy between the consistent and inconsistent analyses is approximately 0.4 K for both natural draft and mechanical draft cooling towers. For the mechanical draft tower, at an ambient temperature of 280 K, the discrepancy is less at approximately 0.15 K.

4.5.3 WATER EVAPORATION RATE

The discrepancy in the water evaporation rate between the consistent and inconsistent analyses of both natural and mechanical draft cooling towers is approximately 2.5% in all the ambient conditions considered.

4.6 LEWIS FACTOR

A detailed history and description of the Lewis factor are presented in appendix F. It is assumed in the Merkel approach that the Lewis factor is equal to unity. The Lewis factor, however, is specified explicitly in the Poppe approach. The equation of Bosnjakovic [65BO1] is employed in the Poppe approach to specify the Lewis factor in the investigation in sections 4.2 to 4.5. The value of the Lewis factor, calculated by the equation of Bosnjakovic [65BO1], is approximately 0.92. Häszler [99HA1] found that the Lewis factor could vary from 0.5 to 1.3, depending on the state of the air in the boundary layer of the interface between the air and the water. Three different specifications of the Lewis factor are employed in this section to determine the effect of the Lewis factor on the results of the Poppe approach. The equation of Bosnjakovic [65BO1] is employed as well as arbitrarily chosen Lewis factors of 0.5 and 1.3.

The various Lewis factors are applied consistently to the evaluation of the fill performance characteristic and the subsequent cooling tower performance evaluation, i.e. the same definition of the Lewis factor is employed in the fill performance analysis and the subsequent cooling tower performance analysis. The results achieved by the consistent application of the Lewis factor in the natural draft tower are shown in figure O.7 and those achieved in the mechanical draft tower are shown in figure O.8. The trends of the variables in the graphs in figure O.7 and figure O.8, of the natural draft and mechanical draft towers

respectively, are approximately the same, except for the air-vapor mass flow rate as discussed in section 4.3.4.

4.6.1 HEAT REJECTION RATE

The heat rejection rates for the different specifications of the Lewis factor can be seen in figures O.7(a_1), O.7(b_1), O.7(c_1) and O.7(d_1) for natural draft towers and in figures O.8(a_1), O.8(b_1), O.8(c_1) and O.8(d_1) of mechanical draft towers. The higher the Lewis factor, the more heat is rejected. In the natural draft cooling tower at an ambient temperature of 280 K the differences in heat rejection rates, between the analyses of Lewis factors of 0.5 and 1.3, are approximately 2.4%. The difference is 0.8% at 290 K and approximately zero at 300 K. At 310 K in very dry conditions, the difference is almost 5% where the heat rejected, due to the smaller Lewis factor, is more than that predicted by the higher Lewis factor. The mechanical draft tower follows approximately the same trends.

4.6.2 WATER OUTLET TEMPERATURE

Because more heat is rejected at higher Lewis factors, the corresponding water outlet temperature is lower. In the natural draft cooling tower, the discrepancy between the water outlet temperatures, by applying Lewis factors of 0.5 and 1.3 respectively, is approximately 0.65 K at an ambient temperature of 280 K. This discrepancy is practically zero at 300 K. At 310 K, however, in very dry conditions, the discrepancy is 0.6 K. The mechanical draft tower follows approximately the same trend.

4.6.3 WATER EVAPORATION RATE

The water evaporation rate is higher when applying smaller Lewis factors than with higher ones. Thus, the air becomes saturated more quickly with lower Lewis factors. The discrepancy between the water evaporation rates in natural draft cooling towers with Lewis factors of 0.5 and 1.3, is approximately 15% at 280 K and reduces to 6% at 310 K. The mechanical draft tower follows approximately the same trend.

4.6.4 DISCUSSION ON THE CONSISTENT APPLICATION OF THE LEWIS FACTOR

The Lewis factor has little influence on the water outlet temperature and the heat rejected from the cooling tower in very humid ambient air. In dry conditions, at all ambient temperatures considered, the differences between the results of the different Lewis factors can be quite significant. The rate of water evaporation is strongly dependent on the Lewis factor for both the natural draft and mechanical draft towers. This is because the Lewis factor is an indication of the relative rates of heat and mass transfer in an evaporative process. The Lewis factor can therefore be tuned to represent the physically measured evaporation rates and outlet air temperatures more closely in fill performance analyses. It is therefore important to perform the fill performance tests in conditions that closely represent actual operational conditions, especially if the cooling tower is operated at a very low ambient humidity.

If the fill performance test data is insufficient to accurately predicts the Lewis factor of a particular fill, it is recommended that the equation of Bosnjakovic be used as the numerical value is approximately 0.92, which is approximately the mean between the limiting values of 0.5 and 1.5 given by Häszler [99HA1].

4.6.5 THE INCONSISTENT APPLICATION OF THE LEWIS FACTOR

The analyses of the natural and mechanical draft cooling towers are repeated with an inconsistent application of the Lewis factor specification. The equation of Bosnjakovic is used in the fill performance evaluation, while Lewis factors of 0.5 and 1.3 are used in the cooling tower performance evaluation. Figure O.9 and figure O.10 show the results of the natural draft and mechanical draft towers respectively for the inconsistent application of the Lewis number.

If figures O.9 and O.10 are compared to figures O.7 and O.8, it can be seen that the inconsistent application of the Lewis factor results in larger discrepancies than is the case with the consistent application of the Lewis factor. The discrepancy between the heat rejection rate of both natural and mechanical draft cooling towers, is approximately 8% at an ambient temperature of 280 K. The discrepancy is only 2.4% where the Lewis factors are applied consistently. The discrepancy reduces at higher ambient temperatures to approximately 2% at 310 K. This is consistent with the conclusion reached previously, that the influence of the Lewis factor diminishes at higher ambient temperatures. The discrepancy in the water outlet temperature for the natural draft cooling tower, for the inconsistent analysis of the Lewis factor, is larger than the consistent application. Ironically, the discrepancy between predicted water evaporation rates is smaller during the inconsistent application of the Lewis factor than during the consistent application.

4.7 ATMOSPHERIC PRESSURE

An atmospheric pressure of 84200 Pa has been used in all the cooling tower analyses discussed so far. The atmospheric pressure is increased to 101325 Pa to see what the effect on cooling tower performance is in both the natural and mechanical cooling towers. Figures O.11 and O.12 show the cooling tower performance curves in the natural draft and mechanical draft towers respectively. The Merkel and Poppe approaches are employed in the cooling tower performance evaluation.

If figures O.11 and O.12 are compared to figures O.1 and O.2 respectively for natural and mechanical draft towers, where an atmospheric pressure of 84200 Pa is specified, it can be seen that the trends are practically identical for all the plotted variables.

It is difficult to give exact quantification of the differences between the results at low and high atmospheric pressures. The reason is that the ambient humidity and the draft through the respective towers are functions of the atmospheric pressure. The processes in a cooling tower are strongly coupled and it is therefore difficult to make accurate predictions. However, if all other variables remain unchanged, the cooling towers at higher altitude, and thus lower atmospheric pressure, will perform better than those towers at lower altitudes.

4.8 IMPROVED MERKEL ENERGY EQUATION

The Poppe approach predicts higher heat rejection rates than the Merkel approach. This is because the Merkel approach ignores the loss in the water mass flow rate, due to evaporation, in the energy equation. In a cooling tower analysis, employing the Merkel approach, the heat transfer rate is generally given by

$$Q = m_w c_{pwm} (T_{wi} - T_{wo}) \tag{4.3}$$

The effect of the change in water mass flow rate is not included in the energy balance in equation (4.3). If it is assumed that the air is saturated at the outlet of the fill, then the mass flow rate of the evaporated water can be approximated by the equation,

$$m_{w(evap)} = m_a(w_i - w_o) \tag{4.4}$$

A new improved equation of the heat rejection rate, according to the Merkel approach, is proposed where the water loss, due to evaporation, is included in the energy equation, i.e.,

$$Q = m_{wi} c_{pwm} T_{wi} - (m_{wi} - m_{w(evap)}) c_{pwm} T_{wo} \tag{4.5}$$

Figures O.13 and O.14 show the results of the cooling tower performance analyses for the natural draft and mechanical draft towers respectively, where the improved Merkel equation is employed in the analyses. It can be seen that the results of the improved Merkel approach and the Poppe approach are practically identical for both the natural and mechanical draft cooling towers. At hot, dry conditions there is a discrepancy between the improved Merkel and Poppe approaches. The reason for this discrepancy is discussed in detail in section 4.3.3. In a nutshell it is because of the Merkel assumption that the air is saturated at the outlet when the Poppe approach predicts that the air is unsaturated. At low ambient temperatures, the outlet air is generally supersaturated and the assumption of Merkel is relatively accurate.

Thus, the improved energy equation of the Merkel approach can be employed in the relatively simple Merkel approach to predict heat rejection rates and water outlet temperatures that are within very close tolerance with the predictions by the more rigorous Poppe approach. This is especially the case, as mentioned earlier, when the ambient air is cold or relatively humid.

4.9 *e-NTU* APPROACH

The *e-NTU* approach is employed in both the natural draft and mechanical draft cooling towers. The results of the *e-NTU* approach are compared to those of the Merkel approach. They are compared to the Merkel approach because the governing equations of both approaches are derived while making the same simplifying assumptions, i.e. the Lewis factor is equal to unity and the water evaporation rate is omitted from the energy balance.

The fill performance characteristics are applied consistently in the cooling tower performance evaluation for the comparison between the Merkel and *e-NTU* approaches. It is found that the transfer characteristic, obtained by the *e-NTU* approach, is approximately 1% lower than that derived by employing the Merkel approach.

Figures O.15 and O.16, of natural draft and mechanical draft towers respectively, show the comparison between the Merkel and *e-NTU* approaches. The heat rejected, water and air outlet temperatures and water evaporation rates, predicted by both approaches, are practically identical across the entire range of ambient temperatures and humidities.

Figure O.17 shows the results of the natural draft tower where the fill performance characteristic, obtained by the Merkel approach, is applied inconsistently to the cooling tower performance analysis while employing the *e-NTU* approach. It can be seen that the results are practically identical to those in figure O.15, where the fill performance characteristic is applied consistently. The fill performance characteristics, obtained by the Merkel and *e-NTU* approaches, can therefore be applied inconsistently in cooling tower performance evaluations employing either approach. This is because the transfer characteristic of the *e-NTU* approach is, as mentioned above, only 1% less than the transfer characteristic obtained while employing the Merkel approach.

4.10 CONSTANT HEAT REJECTION

The water inlet temperature is 313.15 K in the investigation in sections 4.2 to 4.9. However, at power stations, the heat to be rejected is known and the inlet water temperature is not known beforehand. This is because the condenser will have to absorb the heat load it receives from the turbine exit stream.

Figures O.18 and O.19 show the results of the natural draft and mechanical draft towers respectively where the heat rejection rate is known and the water outlet temperature is unknown. The plotted trends are approximately the same for both natural draft and mechanical draft cooling towers. The water inlet temperatures, for the natural draft cooling tower, calculated by both approaches, are practically identical at low ambient temperatures. At higher temperatures, in dry conditions, the discrepancies are greater. For mechanical draft towers, the water inlet and outlet temperatures are practically identical for both approaches at all ambient conditions considered.

4.11 CONCLUSION

It is very important that the same model, definitions and assumptions be employed in the fill performance analysis to determine the transfer coefficient and in the subsequent analysis to determine cooling tower performance. This will ensure that the water outlet temperature in cooling tower performance analyses, predicted by the different models, are practically the same when all other variables are assumed constant.

The predicted water evaporation rates in natural draft cooling towers are always higher according to the Poppe approach than according to the Merkel approach. This is not the case for mechanical draft cooling towers at very hot and dry ambient conditions.

The performance prediction of natural draft cooling towers is not as strongly influenced by the accuracy of the left-hand side of the draft equation given by equation (4.1). If the left hand side of the draft

equation accounts for the moist air that is raised in a gravitational field, adiabatic cooling and heating by condensation, the same order of results are obtained when the simplified equation, given by equation (4.2) is employed.

When the Poppe approach is employed during hot ambient conditions, the value of the Lewis factor has little influence on the prediction of the water outlet temperature, if it is employed consistently or inconsistently.

The heat transfer rate, water outlet temperature, draft, air outlet temperature and evaporation rate of the Merkel approach can be brought within closer tolerances of the more rigorous Poppe approach, when the reduction of the water mass flow rate, due to evaporation, is included in the energy balance. The assumption of Merkel that the outlet air is saturated with water vapor, leads to tower performance that are within close tolerance of the tower performance predicted by the Poppe approach, for cold or humid ambient conditions.

The *e-NTU* and Merkel approaches predict virtually the same tower performances when the models are applied consistently or inconsistently.

CHAPTER 5

THE INFLUENCE OF TEMPERATURE AND HUMIDITY INVERSIONS ON WET-COOLING TOWER PERFORMANCE

5.1 INTRODUCTION

The influence of temperature and humidity inversions on the performance of wet-cooling towers is investigated. Hoffman [97HO1] investigated the effect of temperature stratification in the atmospheric boundary layer on the performance of natural draft dry-cooling towers. Hoffman [97HO1] followed a predominantly numerical approach in addressing the problem. A semi-empirical approach is followed in the current analysis with the emphasis on simplicity. Pure theoretical approaches that predict temperature profiles during nocturnal inversions are generally impractical due to the vagaries of nature and the complexity of the models. Relatively simple equations are developed to predict the vertical temperature profile or distribution and the height of the inversion throughout the course of the year. The diurnal and annual variations of atmospheric humidity are investigated.

The buoyancy force that drives the air through a natural draft tower is negatively affected when temperature inversions occur. Cooling tower designs are generally based on the ambient air drybulb temperature, measured at, or near, the ground. The average temperature of the air at the inlet of the tower may deviate significantly from the measured air temperature near the ground due to temperature inversions. The effective inlet humidity ratio of the air may also deviate due to the presence of humidity inversions that occur during the night. The deviation of the effective inlet air temperature and humidity ratios occur because the tower draws in air from high above the ground. A simple equation is recommended to determine this height for a particular tower.

5.2 TEMPERATURE AND HUMIDITY INVERSION PROFILES

Appendix L presents the development of an empirical approach to extrapolate temperature profiles during nocturnal inversions from ground based measurements. Equation (L.5), repeated here as equation (5.1), gives the temperature inversion profile after the first few hours after the inception of an inversion.

$$T = (T_r + 273.15)\left(\frac{z}{z_r}\right)^b \tag{5.1}$$

where T_r and z_r are the reference temperature and reference height respectively. T_r (°C) is measured at z_r which is about 1 m above ground level. The value of the exponent , b, varies throughout the course of the year and is given by equation (L.9), repeated here as equation (5.2).

$$b = 0.0035\sin(0.0177 n_b - 2.32392) + 0.0065 \tag{5.2}$$

where n_b is the number of the day of the year (1 January is the first day of the year). Equation (5.2) is only valid for the specific geographical location, as mentioned in appendix L.

The height of the inversion is of importance in a cooling tower performance analysis, especially when the cooling tower draws in air from above this height. The height of an inversion, during a specific inversion period, is given by equation (L.26), repeated here as equation (5.3).

$$z_{it} = \left[\frac{0.00975}{b(T_r + 273.15)}\right]^{\frac{1}{b-1}} \tag{5.3}$$

Equation (5.3) will predict, in conjunction with equation (5.2), inversion heights of approximately 300 m in the winter months and approximately 90 m in high summer at the specific geographical location, as mentioned in appendix L. Equation (5.3) is only valid after the first few hours of the inception of an inversion.

Equation (5.1) requires less data than that required by equations (L.1), (L.2) and (L.4), which are found in the literature.

Appendix M describes the complexity of determining the vertical vapor profiles in the atmosphere, especially in the atmospheric boundary layer. Empirical relations are given in the literature that predict atmospheric humidity profiles, but these equations are not accurate in the atmospheric boundary layer during humidity inversions. Humidity profiles are very unpredictable and depend on the vegetation and meteorological conditions. Examples of nocturnal humidity inversion profiles are given in figures M.2 and M.3.

5.3 HEIGHT FROM WHICH AIR IS DRAWN INTO A COOLING TOWER

The height from which air is drawn into a natural draft cooling tower, H_r, is investigated analytically in appendix N for windless conditions. Refer to figure N.2 for a graphical description of H_r. It is shown in appendix N that H_r is only a function of the diameter of the cooling tower and is constant some distance away from the cooling tower in the radial direction. For the cooling tower presented in appendix I, H_r is approximately 127 m, according to the results in appendix N. Wilber et al. [85WI1] state that H_r is generally between 50 and 100 m while Lauraine et al. [88LA1] estimate H_r to be between 50 and 150 m. The effect of H_r on cooling tower performance is investigated in appendix V.6. It is shown that tower performance is relatively insensitive to the choice of H_r. It is therefore recommended that H_r be arbitrarily taken as half the height of the cooling tower shell,

$$H_r = H_6/2 \tag{5.4}$$

where H_6 is the height of the tower shell, as shown in figure I.1.

5.4 EFFECT OF TEMPERATURE AND HUMIDITY INVERSIONS ON TOWER DRAFT AND INLET CONDITIONS

Appendix V contains a sample calculation that calculates the effective inlet air temperature and humidity ratio during prescribed ambient temperature and humidity inversions. Since the height of the temperature inversion, z_{it}, throughout the course of the year, as determined by equation (5.3) or (L.26), is generally higher than H_r, it has no effect on the effective inlet air temperature and humidity ratio.

Figure V.5 shows the heat rejected by a particular cooling tower as a function of the exponent, b, of equation (5.1) or (L.5). The particular tower heat rejection is reduced by approximately 20 % when the magnitude of temperature inversions is strongest during winter. Tower performance is 8 % down in summer when temperature inversions are generally not as strong. The reduction in performance due to the temperature inversion is very high when compared to the reduction in performance due to the humidity inversion. The effect of the humidity inversion on tower performance is generally very small (1.5 %).

A sample calculation of the pressure differential between ground level and the top of the tower shell is also presented in appendix V. Approximately 20 % of the reduction in heat rejected is due to the reduction in draft and approximately 80 % is due to the increased effective inlet air temperature and humidity. If z_{it} is less than the height of the cooling tower shell (z_{it} = 90 m from equation (5.3) when b = 0.003), it does not influence the reduction in performance significantly if z_{it} is increased to the same height as the tower shell.

5.5 CONCLUSION

A very simple empirical relation of the nocturnal temperature inversion profile is developed in appendix L that correlates measured data more accurately than more complex equations found in the literature which require more input data. The height of the temperature inversion and the height from which air is drawn into the cooling tower are obtained by relatively simple equations.

It is found that the choice of practical values of the height from which air is drawn into the cooling tower, H_r, does not influence tower performance significantly. The effect of the inversion height, if it is less than the tower shell and higher than H_r, also does not effect tower performance significantly. The influence of the humidity inversion on the reduction of tower performance is relatively small when compared to the effect of the temperature inversion on the reduction of cooling tower performance. Temperature inversions reduce a particular tower heat rejection by approximately 20 % in winter and by approximately 8 % in summer. The reduction in tower performance due to the adversely affected pressure differential (draft equation) on the outside of the tower, during temperature inversions, accounts for approximately 20 % of the total loss and the increased effective inlet temperature (transfer process) for approximately 80 % of the reduction in tower performance.

CHAPTER 6

CONCLUSION

6.1 INTRODUCTION

This chapter presents a summary of all the main recommendations made and the conclusions drawn during the thesis. Most of the conclusions are repeated from the conclusions drawn at the end of each chapter. It serves as a complete overview of the main results and recommendations. The computer software programs developed to aid in the performance analyses of cooling towers are summarized.

6.2 WET-COOLING METHODS OF ANALYSIS

The consistent employment of the heat and mass transfer methods of analysis in the fill performance evaluation and then using the same model in the subsequent cooling tower performance analysis is stressed. If used consistently the different models ought to give the same cooling ranges for the water in a particular cooling tower if all the operating conditions are exactly the same for each model. Because the Poppe approach is the more rigorous approach, it will predict the water evaporation rate, the total heat transfer rate and thus the air outlet temperature more accurately than the other approaches. This may lead to situations where the predicted cooling tower operating conditions will not be the same as those predicted by the other approaches, and it may therefore predict cooling ranges different from those predicted by the Merkel or *e-NTU* approaches. For example, the draft through natural draft cooling towers is a function of the air outlet temperature and the Poppe method will thus predict more accurately tower draft and tower performance. The Poppe method also has distinct advantages in the analysis of hybrid cooling towers since the state of the outlet air is calculated [01RO1]. This information is important to ensure that the correct amount of heated dry air is mixed with the wet plume to ensure no visible plume after mixing of the two streams.

6.3 FILL PERFORMANCE

A new empirical relation is developed that correlates measured pressure loss coefficients accurately for all types of fills under all types of operational conditions as it is based on fundamental principles that make provision for forces due to shear and drag. Other types of empirical equations, found in the literature, may correlate observed trends accurately, but they generally lack generality and are only applicable for limited ranges of water and air flow rates.

Both the empirical relations for the loss and transfer coefficients per unit height of fill of wet-cooling tower fills are extended to include the effect of the height of the fill. In addition, the empirical relation for the transfer coefficient is extended to include the effect of the water inlet temperature. The inlet water temperature has no significant effect on the loss coefficient. It is also found that the inlet air drybulb and wetbulb temperatures have no significant effect on the loss and transfer coefficients.

It is recommended that as much information as possible be supplied with the empirical relations of the loss coefficients, such as the ranges of applicability of G_a and G_w. The goodness of fit must also be supplied in the form of a correlation coefficient. This will enable the designer of wet-cooling systems to take the necessary precautions to compensate for any uncertainties. If possible, the same water spray system must be employed in the fill test and the subsequent cooling tower application of the fill. This will eliminate the effects of droplet size and distribution on the loss coefficient. Ageing effects of the fill are not investigated in this study.

6.4 WET-COOLING TOWER PERFORMANCE EVALUATION

As already mentioned, it is very important that the same model, definitions and assumptions be employed in the fill performance analysis to determine the transfer coefficient and in the subsequent analysis to determine cooling tower performance. This will ensure that the water outlet temperature in cooling tower performance analyses, predicted by the different models, are practically the same when all other variables are assumed constant.

The predicted water evaporation rates in natural draft cooling towers are always higher according to the Poppe approach than according to the Merkel approach. This is not the case for mechanical draft cooling towers at very hot and dry ambient conditions.

The performance prediction of natural draft cooling towers is not as strongly influenced by the accuracy of the left-hand side of the draft equation given by equation (4.1). If the left hand side of the draft equation accounts for the moist air that is raised in a gravitational field, adiabatic cooling and heating by condensation, the same order of results are obtained when the simplified equation, given by equation (4.2) is employed.

When the Poppe approach is employed in hot ambient conditions, the value of the Lewis factor has little influence on the prediction of the water outlet temperature, if it is employed consistently or inconsistently.

The results of the Merkel approach can be brought within close tolerance of the more rigorous Poppe approach, when the reduction of the water mass flow rate, due to evaporation, is included in the energy balance. The assumption of Merkel that the outlet air is saturated with water vapor, leads to tower performances that are within close tolerance of the tower performance predicted by the Poppe approach, for cold or humid ambient conditions. The outlet air is generally supersaturated when the inlet ambient air is cold or relatively humid. The air drybulb temperature at a specific air enthalpy is practically constant for air in the saturated state or air in any degree of supersaturation. This is the reason why the results of the Merkel and Poppe methods are within close tolerance with each other. The Merkel method predicts saturated outlet air while the Poppe method generally predicts supersaturated outlet air when the inlet ambient air is cold or relatively humid. The discrepancy between the performance evaluations according to the Merkel and Poppe methods are greater when the outlet air according to the Poppe method is

unsaturated. This is because the temperature of unsaturated air is a strong function of the humidity of the air at a specific air enthalpy.

The *e-NTU* and Merkel approaches predict virtually the same tower performances when the models are applied consistently or inconsistently.

6.5 THE INFLUENCE OF TEMPERATURE AND HUMIDITY INVERSIONS ON COOLING TOWER PERFORMANCE

A very simple empirical relation of the nocturnal temperature inversion profile is developed in appendix L that correlates measured data more accurately than models found in the literature which require more input data. Drybulb temperature measurements at two heights are sufficient to determine the temperature inversion profile. The one measurement is typically taken at 1 m above ground elevation while the second measurement must be taken as high above ground elevation as possible (typically 10 m). The height of the temperature inversion and the height from which air is drawn into the cooling tower are obtained by relatively simple empirical equations.

It is found that the choice of practical values of the height from which air is drawn into the cooling tower, H_r, does not influence tower performance significantly. The effect of the inversion height, if it is less than the tower shell and higher than H_r, also does not effect tower performance significantly. The influence of the humidity inversion on the reduction of tower performance is relatively small when compared to the effect of the temperature inversion on the reduction of cooling tower performance. Temperature inversions reduce a particular tower heat rejection by approximately 20 % in winter and by approximately 8 % in summer. The reduction in tower performance due to the adversely affected pressure differential (draft equation) on the outside of the tower, during temperature inversions, accounts for approximately 20 % of the total loss and the increased effective inlet temperature (transfer process) for approximately 80 % of the reduction in tower performance.

6.6 SOFTWARE DEVELOPMENT

A program is developed to process and analyze fill performance test data. This program is presented in appendix K and processes the pressure transducer and thermocouple data, determines the transfer and loss coefficients and fits relatively complex curves through the test data with mathematical optimization algorithms. A comprehensive program is developed to predict wet-cooling tower performance. This program is presented in appendix P. Natural draft counterflow and mechanical draft counterflow and crossflow cooling towers can be analyzed by the program. The latest empirical and heat and mass transfer models found in the literature are included in the solution algorithms of the software. The analytical and empirical models, developed in this thesis from theoretical and experimental investigations, are also included in the software. As discussed in appendix U, the geometrical dimensions of a natural draft cooling tower can be optimized by the program to obtain the minimum combined capital and operational cost compounded over the economic life of the cooling tower. It is shown in appendix U that the inlet height of the cooling tower is generally the critical dimension influencing the combined operational and

capital cost of a cooling tower. A comprehensive cooling tower performance evaluation tool, that is very user friendly, is therefore developed that predicts and analyzes the thermal performance of wet-cooling towers. Furthermore, programs are developed to plot psychrometric charts (chapter 2) and generate cooling tower performance curves (appendix Q).

6.7 SCOPE FOR FUTURE WORK

All of the results obtained in this thesis are obtained by essentially employing one-dimensional analytical models. However, some problems can only be solved satisfactorily by three-dimensional numerical modelling when the air or water mass flow rates are non-uniform, or a combination of counterflow and crossflow exists in the fill.

REFERENCES

Each reference is identified by a code in square brackets which consists of two digits for the year of publication, the first two letters of the first authors surname and a sequentially assigned digit to make the reference unique.

[08HA1] Hann, J., Handbuch der Klimatologie, I. Band: Allgemeine Klimalehre, Verlag von J. Engelhorn, Stuttgart, 1908.

[22LE1] Lewis, W.K., The Evaporation of a Liquid into a Gas, Transactions of ASME, Vol. 44, pp. 325-340, May, 1922.

[25ME1] Merkel, F., Verdunstungskühlung, VDI-Zeitchrift, Vol. 70, pp. 123-128, January 1925.

[33LE1] Lewis, W.K., The Evaporation of a Liquid into a Gas – A Correction, Mechanical Engineering, Vol. 55, pp. 567-573, 1933.

[42HU1] Hutchison, W.K. and Spivey, E., Design and Performance of Cooling Towers, Transactions of the Institute of Chemical Engineers, Vol. 20, pp. 14-29, 1942.

[49JO1] Jordan, R.C. and Priester, G.B., Refrigeration and Air Conditioning, Constable and Company, Ltd., London, 1949.

[52ER1] Ergun, S., Fluid Flow through Packed Columns, Chemical Engineering Progress, Vol. 48, pp. 89-94, 1952.

[54MO1] Monin, A.S. and Obukhov, A.M., Basic Regularity in Turbulent Mixing in the Surface Layer of the Atmosphere, Frud. Geofig. Inst. Akkad. Nauk. SSSR, Vol. 24, pp. 151-163, 1954.

[56ZI1] Zivi, S.M. and Brand, B.B., An Analysis of the Crossflow Cooling Tower, Refrigerating Engineering, Vol. 64, pp. 31-34 & 90-92, 1956.

[58ME1] Meteorological Office, Tables of Temperature, Relative Humidity and Precipitation for the World, Part IV, Africa, The Atlantic Ocean South of 35°N and the Indian Ocean, Her Majesty's Stationary Office, London, 1958.

[59MC1] McKelvey, K.K. and Brooke, M., The Industrial Cooling Tower, Elsevier Publishing Company, Amsterdam, 1959.

[60SC1] Schlichting, H., Boundary Layer Theory, Fourth Edition, McGraw-Hill, New York, 1960.

[61BA1] Baker, D.R. and Shryock, H.A., A Comprehensive Approach to the Analysis of Cooling Tower Performance, Transactions of the ASME, Journal of Heat Transfer, pp. 339-350, 1961.

[61BE1] Berman, L.D., Evaporative Cooling of Circulating Water, 2nd Edition, Chapter 2, pp. 94-99, ed. Sawistowski, H., Translated from Russian by R. Hardbottle, Pergamon Press, New York, 1961.

[61LO1] Lowe, H.J. and Christie, D.G., Heat Transfer and Pressure Drop Data on Cooling Tower Packings and Model Studies of the Resistance of Natural Draft Towers to Airflow, Proceedings of the International Heat Transfer Conference, Colorado, Part V, pp. 933-950,

1961.

[65BO1] Bosnjacovic, F., Technische Thermodinmik, Theodor Steinkopf, Dresden, 1965.

[65GE1] Geiger, R., The Climate Near the Ground, Harvard University Press, Cambridge, 1965.

[67CT1] CTI, Cooling Tower Performance Curves, The Cooling Tower Institute, Houston, 1967.

[72MC1] McGee, O.S., The Content of Water Vapor in the Atmosphere Over Southern Africa, S.A. Geographer, Vol. 4, No. 1, pp. 25-32, 1972.

[74LA1] Launder, B.E. and Spalding, D.B., The Numerical Computation of Turbulent Flows, Computer Methods in Applied Mechanics and Engineering, Vol. 3, pp. 269-289, 1974.

[75NA1] Nahavandi, A. N., Kershah, R.M. and Serico, B.J., The Effect of Evaporation Losses in the Analysis of Counterflow Cooling Towers, Journal of Nuclear Engineering and Design, Vol. 32, pp. 29-36, 1975.

[75YO1] Yoshino, M.M., Climate in a Small Area, An Introduction to Local Meteorology, University of Tokyo Press, Tokyo, 1975.

[76AN1] Anfossi, D., Bacci, P. and Longhetto, A., Forcasting of Vertical Temperature Profiles in the Atmosphere during Nocturnal Radiation Inversion from Air Temperature Trend at Screen Height, Quarterly Journal of the Royal Meteorological Society, Vol. 102, pp. 173-180, 1976.

[76KE1] Kelly, N.W., Kelly's Handbook of Crossflow Cooling Tower Performance, Kansas City, Missouri, Neil W. Kelly and Associates, 1976.

[76KE2] Kelly, N.W., A Blueprint for the Preparation of Crossflow Cooling Tower Characteristic Curves, Paper Presented before the Cooling Tower Institute Annual Meeting, January, 1976.

[77MI1] Miller, D.H., Water at the Surface of the Earth, An Introduction to Ecosystem Hydrodynamics, Academic Press, New York, 1977.

[78MO1] Montakhab, A., Waste Heat Disposal to Air with Mechanical and Draft – Some Analytical Considerations, Heat Transfer Division of the ASME, Winter Annual Meeting, San Francisco, 1978.

[78OK1] Oke, T.R., Boundary Layer Climates, Methuen & Co Ltd, London, 1978.

[80PA1] Patankar, S.V., Numerical Heat Transfer and Fluid Flow, Hemisphere Publishing Co., New York, 1980.

[81BR1] British Standard 1042, Measurement of Fluid Flow in Closed Conduits, Part 1, Section 1.1, 1981.

[81GO1] Gorchakov, G.I., Kostko, O.K. and Krikunov, G.A., Statistical Properties of Humidity Profiles and the Backscattering Coefficient in the Lower Troposphere, Atmospheric and Oceanic Physics, Vol. 17, No. 10, pp. 777-781, 1981.

[82CA1] Cale, S.A., Development of Evaporative Cooling Packing, Commission of European Communities, Report EUR 7709 EN, Luxembourg, 1982.

[82MI1] Missimer, J. and Wilber, K., Examination and Comparison of Cooling Tower Component Heat Transfer Characteristics, IAHR Cooling Tower Workshop, Hungary, October 12-15, 1982.

[82SN1] Snyman, J. A., A New and Dynamic Method for Unconstrained Minimization, Appl. Math. Modelling, Vol. 6, pp. 449-462, 1982.

[82ST1] Stoecker, W.F. and Jones, J.W., Refrigeration and Air Conditioning, McGraw-Hill Book Co., Singapore, 1982.

[83BO1] Bourillot, C., TEFERI, Numerical Model for Calculating the Performance of an Evaporative Cooling Tower, EPRI Report CS-3212-SR, August 1983.

[83BO2] Bourillot, C., On the Hypothesis of Calculating the Water Flowrate Evaporated in a Wet Cooling Tower, EPRI Report CS-3144-SR, August 1983.

[83MA1] Majumdar, A.K., Singhal, A.K. and Spalding, D.B., Numerical Modeling of Wet Cooling Towers – Part 1: Mathematical and Physical Models, Transactions of the ASME, Journal of Heat Transfer, Vol. 105, pp. 728-735, November 1983.

[83MA2] Majumdar, A.K., Singhal, A.K., Reilly, H.E. and Bartz, J.A., Numerical Modeling of Wet Cooling Towers – Part 2: Application to Natural and Mechanical Draft Towers, Transactions of the ASME, Journal of Heat Transfer, Vol. 105, pp. 736-743, November 1983.

[83MA3] Majumdar, A.K., Singhal, A.K. and Spalding., D.B., VERA2D: Program for 2-D Analysis of Flow, Heat, and Mass Transfer in Evaporative Cooling Towers, EPRI Report CS 2923, Volume 1 and 2, March 1983.

[83SN1] Snyman, J. A., An Improved Version of the Original Leap-Frog Dynamic Method for Unconstrained Minimization LFOP1(b), Appl. Math. Modelling, Vol. 7, pp. 216-218, 1983.

[83SU1] Sutherland, J.W., Analysis of Mechanical-Draught Counterflow Air/Water Cooling Towers, Transactions of the ASME, Journal of Heat Transfer, Vol. 105, pp. 576-583, August 1983.

[84BR1] British Standard 1042, Measurement of Fluid Flow in Closed Conduits, Part 1, Section 1.2 and Section 1.4, 1984.

[84PO1] Poppe, M. and Rögener, H., Berechnung von Rückkühlwerken, VDI-Wärmeatlas, pp. Mh1-Mh15, 1984.

[85LI1] Li, K.W. and Priddy, A.P., Power Plant System Design, John Wiley & Sons, 1985.

[85SN1] Snyman, J. A., Unconstrained Minimization by Combining the Dynamic and Conjugate Gradient Methods, Quaestiones Mathematicae, Vol. 8, pp. 33-42, 1985.

[85WI1] Wilber, K.R., Yost, J.G. and Wheeler, D.E, An Examination of the Uncertainties in the Determination of Natural Draft Cooling Tower Performances, Joint AMSE/IEEE Power Generation Conference, Milwaukee, Wisconsin, October 20-24, 1985.

[86SU1] Surridge, A.D., Extrapolation of the Nocturnal Temperature Inversion from Ground-Based Measurements, Atmospheric Environment, Vol. 20, No. 4, pp. 803-806, 1986.

[87HO1] Hoffmann, J.E., Bedryfspunt Voorspelling vir Nat Koeltorings, M.Eng Thesis, University of Stellenbosch, Stellenbosch, South Africa, 1987.

[87SU1] Surridge, A.D., On the Evolution of the Height and Temperature Difference Across the Nocturnal Stable Boundary Layer, Boundary-Layer Meteorology, Vol. 40, pp. 87-98, 1987.

[88BR1] British Standard 4485, Water Cooling Towers, Part 2: Methods for Performance Testing, 1988.

[88DR1] Dreyer, A.A., Analysis of Evaporative Coolers and Condensers, M.Eng Thesis, University of Stellenbosch, Stellenbosch, South Africa, 1988.

[88LA1] Lauraine, H., Lemmens, P. and Monoie, M., Experimental Data Coupling Atmospheric

Temperature Inversions and Cooling Tower Performances, Proceedings of the 6th IAHR Cooling Tower Workshop, Pisa, Italy, 1988.

[88PR1] Preston-Whyte, R.A. and Tyson, P.D., The Atmosphere and Weather of Southern Africa, Oxford University Press, Cape Town, 1988.

[89DA1] Duagherty, R.L., Franzini, J.B. and Finnemore, E.J., Fluid Mechanics with Engineering Applications, SI Metric Edition, McGraw-Hill, Singapore, 1989.

[89JA1] Jaber, H. and Webb, R.L., Design of Cooling Towers by the Effectiveness-NTU Method, Journal of Heat Transfer, Vol. 111, pp. 837-843, November 1989.

[89JO1] Johnson, B.M. (ed.), Cooling Tower Performance Prediction and Improvement, Volume 1, Applications Guide, EPRI Report GS-6370, Volume 2, Knowledge Base, EPRI Report GS-6370, EPRI, Palo Alto, 1989.

[90CO1] Cooling Tower Institute, CTI Code Tower, Standard Specifications, Acceptance Test Code for Water-Cooling Towers, Part I, Part II and Part III, CTI Code ATC-105, Revised, February 1990.

[90EL1] Ellis, R. and Gulick, D., Calculus with Analytic Geometry, Fourth Edition, Harcourt Brace Jovanovic College Publishers, Fort Worth, 1990.

[90SU1] Surridge, A.D., Swanepoel, D.J.deV., Held, G., Research on Thermal Feedback Caused by Dry-Cooling Power Generating Stations, Confidential Report, EMA-C 9086, CSIR, Pretoria, 1990.

[91FE1] Feltzin, A.E. and Benton D., A More Exact Representation of Cooling Tower Theory, Cooling Tower Institute Journal, Vol. 12, No. 2, pp. 8-26, 1991.

[91OS1] Osterle, F., On the Analysis of Counter-Flow Cooling Towers, International Journal of Heat and Mass Transfer, Vol. 34, No. 4/5, pp. 1313-1316, 1991.

[91PO1] Poppe, M. and Rögener, H., Berechnung von Rückkühlwerken, VDI-Wärmeatlas, pp. Mi 1-Mi 15, 1991.

[91WH1] White, F.M., Viscous Fluid Flow, Second Edition, McGraw-Hill, New York, 1991.

[92HE1] Hensley, J., Maximize Tower Power, Chemical Engineering, pp. 74-82, February, 1992.

[92MA1] Mathews, J.H., Numerical Methods for Mathematics, Science, and Engineering, Second Edition, Prentice-Hall International, Inc, 1992.

[92WI1] Willa, J.L., Evolution of the Cooling Tower, CTI Journal, Vol. 13, No. 1, pp. 40-49, 1992.

[93BE1] Becker, B.R. and Burdick, L.F., Drift Eliminators and Cooling Tower Performance, ASHRAE Journal, pp. 28-36, June 1993.

[93BE2] Beckwith, T.G., Marangoni, R.D. and Lienhard, J.H., Mechanical Mearurements, Fifth Edition, Addison-Wesley Publishing Company, 1993.

[93KR1] Kranc, SC, Performance of Counterflow Cooling Towers with Structured Packings and Maldistributed Water Flow, Numerical Heat Transfer, Part A, Vol. 23, pp. 115-127, 1993.

[93MI1] Mirsky, G.R. and Bauthier, J., Evolution of Cooling Tower Fill, CTI Journal, Vol. 14, No. 1, pp. 12-19, 1993.

[94DU1] Du Preez, A.F. and Kröger, D.G., The Influence of a Buoyant Plume on the Performance of a Natural Draft Cooling Tower, 9th IAHR Cooling Tower and Spraying Pond Symposium,

Brussels, 1994.

[94GR1] Grange, J.L., Calculating the Evaporated Water Flow in a Wet Cooling Tower, Paper presented at the 9th IAHR Cooling Tower and Spraying Pond Symposium, von Karman Institute, Brussels, Belgium, September 1994.

[94SN1] Snyman, J. A., Stander, N. and Roux, W. J., A Dynamic Penalty Function Method for the Solution of Structural Optimization Problems, Appl Math Modelling, Vol. 18, pp. 453-460, 1994.

[94WH1] White, F.M., Fluid Mechanics, Third Edition, McGraw-Hill, New York, 1998.

[95AN1] Anderson, Jr., J.D., Computational Fluid Dynamics, The Basics with Applications, McGraw –Hill, New York, 1995.

[95BE1] Bernier, M.A., Thermal Performance of Cooling Towers, ASHRAE Journal, pp. 56-61, April 1995.

[95BL1] Bland, C., A Cool Solution to a Hot Problem, Process Engineering, pp. 33, June, 1995.

[95CO1] Conradie, A.E., Performance Optimization of Engineering Systems with Particular Reference to Dry-Cooled Power Plants, Ph.D. Thesis, University of Stellenbosch, South Africa, 1995.

[95IB1] Ibrahim, G.A., Nabhan, M.B.W. and Anabtawi M.Z., An Investigation into a Falling Film Type Cooling Tower, International Journal of Refrigeration, Vol. 18, No. 8, pp. 557-564, 1995.

[95KI1] Kintner-Meyer, M. and Emery, A.F., Cost-Optimal Design for Cooling Towers, ASHRAE Journal, pp. 46-55, April 1995.

[95MI1] Mills, A.F., Basic Heat and Mass Transfer, Irwin, Chicago, 1995.

[95LI1] Liffick, G.W. and Cooper, Jr, J.W., Thermal Performance Upgrade of the Arkansas Nuclear One Cooling Tower: A "Root Cause" Analysis Approach, Proceedings of the American Power Conference, Vol. 57, No. 2, pp. 1357-1362, 1995.

[95OO1] Oosthuizen, P.C., Performance Characteristics of Hybrid Cooling Towers, M.Eng. Thesis, University of Stellenbosch, Stellenbosch, South Africa, 1995.

[95SA1] Sadasivam, M. and Balakrishnan, A.R., On the Effective Driving Force for Transport in Cooling Towers, Transactions of the ASME, Journal of Heat Transfer, Vol. 117, pp. 512-515, May 1995.

[96HA1] Hardy, R., Weather, Teach Yourself Books, Hodder & Stoughton, London, 1996.

[96MO1] Mohiuddin, A.K.M. and Kant, K., Knowledge Base for the Systematic Design of Wet Cooling Towers. Part I: Selection and Tower Characteristics, International Journal of Refrigeration, Vol. 19, No. 1, pp. 43-51, 1996.

[96MO2] Mohiuddin, A.K.M. and Kant, K., Knowledge Base for the Systematic Design of Wet Cooling Towers. Part II: Fill and other Design Parameters, International Journal of Refrigeration, Vol. 19, No. 1, pp. 52-60, 1996.

[97BO1] Bowman, C.F. and Benton, D.J., Oriented Spray-Assisted Cooling Tower, CTI Journal, Vol. 18, No. 1, 1997.

[97BU1] Burden, R.L. and Faires, J.D., Numerical Analysis, Sixth Edition, Brooks/Cole Publishing

Company, 1997.

[97CO1] Cooling Tower Institute, CTI Code Tower, Standard Specifications, Acceptance Test Code for Water-Cooling Towers, Vol. 1, CTI Code ATC-105(97), Revised, February 1997.

[97DE1] De Villiers, E. and Kröger, D.G., Analysis of Heat, Mass and Momentum Transfer in the Rain Zone of Counterflow Cooling Towers, Proceedings of the 1997 IJPGC, Vol.2, PWR-Vol. 32, pp. 141-149, Denver, November 1997.

[97EL1] El-Dessouky, H.T.A., Al-Haddad, A. and Al-Juwayhel, F., A Modified Analysis of Counter Flow Wet Cooling Towers, Journal of Heat Transfer, Vol. 119, No. 3, pp. 617-626, 1997.

[97HO1] Hoffmann, J.E., The Influence of Temperature Stratification in the Lower Atmospheric Boundary Layer on the Operating Point of a Natural Draft Dry-Cooling Tower, Ph.D Thesis, University of Stellenbosch, Stellenbosch, South Africa, 1997.

[97HU1] Huser, A., Nilsen, P.J. and Skatun, H., Application of k-ε Model to the Stable ABL: Pollution in Complex Terrain, Journal of Wind Engineering and Industrial Aerodynamics, Vol. 67 and 68, pp. 425-436, 1997.

[98AL1] Al-Nimr, M.A., Dynamic Thermal Behaviour of Cooling Towers, Energy Conversion Management, Vol. 39. No. 7, pp. 631-636, 1998.

[98BA1] Baard, T.W., Performance Characteristics of Expanded Metal Cooling Tower Fill, M.Eng Thesis, University of Stellenbosch, Stellenbosch, South Africa, 1998.

[98CO1] Conradie, A.E., Buys, J.D. and Kroger, D.G., Performance Optimization of Dry-Cooling Systems for Power Plants through SQP Methods, Applied Thermal Engineering, Vol. 18, Nos. 1-2, pp. 25-40, 1998.

[98KR1] Kröger, D.G., Air-Cooled Heat Exchangers and Cooling Towers Thermal-Flow Performance, Evaluation and Design, Begell House, Inc., New York, 1998.

[98SE1] Seinfeld, J.H. and Pandis, S.N., Atmospheric Chemistry and Physics, From Air Pollution to Climate Change, John Wiley & Sons, Inc., New York, 1998.

[98SN1] Snyman, J. A., ETOPC: A Fortran Program for Solving General Constrained Minimization Problems by the Conjugate Gradient Method without Explicit Line Searches, Research Report, Department of Mechanical Engineering, University of Pretoria, 1998.

[98ST1] Streng, A., Combined Wet/Dry Cooling Towers of Cell-Type Construction, Journal of Energy Engineering, Vol. 124, No. 3, pp. 104-121, December 1998.

[99DE1] De Villiers, E. and Kröger, D.G., Inlet Losses in Counterflow Wet-Cooling Towers, Joint Power Generation Conference, Vol.2, PWR-Vol. 34, ASME, 1999.

[99HA1] Häszler, R., Einflusz von Kondensation in der Grenzschicht auf die Wärme- und Stoffübertragung an einem Rieselfilm, Fortschritt-Berichte VDI, Reihe 3, Nr. 615, 1999.

[99SO1] Söylemez, M.S., Theoretical and Experimental Analysis of Cooling Towers, ASHRAE Transactions: Research, Vol. 105, No. 1, pp. 330-337, 1999.

[99WA1] Wallis, J.S. and Aull, R.J., Improving Cooling Tower Performance, Hydrocarbon Engineering, pp. 92-95, May, 1999.

[99WI1] Williams, T. and Kelly, C., Gnuplot, MS-Windows 32 bit Version 3.7, Patchlevel 0, 1999.

[00AU1] Aull, R.J., and Krell, T., Design Features of Cross-Fluted Film Fill and Their Effect on

Thermal Performance, CTI Journal, Vol. 21, No. 2, pp. 12-33, 2000.

[00CA1] Castro, M.M., Song, T.W. and Pinto, J.M., Minimization of Operational Costs in Cooling Water Systems, Transactions of the Institution of Chemical Engineers, Vol. 78, Part A, pp. 192-201, March, 2000.

[00GO1] Goshayshi, H.R. and Missenden, J.F., The Investigation of Cooling Tower Packing in Various Arrangements, Applied Thermal Engineering, Vol. 20, pp. 69-80, 2000.

[00GO2] Goyal, O.P., Maintenance and Retrofitting, Guidelines and Troubleshooting, Hydrocarbon Processing, Vol. 79, No. 1, p. 69, 2000.

[00SN1] Snyman, J. A., The LFOPC Leap-Frog Method for Constrained Optimization, Computers Math. Applic., Vol. 40, No. 8/9, pp. 1085-1096, 2000.

[00SN2] Snyman, J. A. and Hay, A. M., The Dynamic-Q Optimization Method: An Alternative to SQP?, Proceedings of the International Workshop on Multidisciplinary Design Optimization, University of Pretoria, Pretoria, South Africa, pp. 163-172, August, 2000.

[01MA1] Makkinejad, N., Temperature Profile in Countercurrent/Cocurrent Spray Towers, International Journal of Heat and Mass Transfer, Vol. 44, pp. 429-442, 2001.

[01MI1] Milosavljevic, N. and Heikkilä, P., A Comprehensive Approach to Cooling Tower Design, Applied Thermal Engineering, Vol. 21, pp. 899-915, 2001.

[01RO1] Roth, M., Fundamentals of Heat and Mass Transfer in Wet Cooling Towers. All Well Known or are Further Developments Necessary? 12th IAHR Symposium in Cooling Towers and Heat Exchangers, UTS, Sydney, Australia, pp. 100-107, November, 2001.

[01TU1] Turpin, J.R. (ed.), Want to Save Energy? Look at your Cooling Tower, Engineered Systems, Vol. 18, No. 10, p. 48, 2001.

[02BU1] Busch, D., Harte, R., Krätzig, W.B. and Montag, U., New Natural Draft Cooling Tower of 200 m of Height, Engineering Structures, Vol. 24, pp. 1509-1521, 2002.

[02FI1] Fisenko, S.P., Petruchik, A.I. and Solodukhin, A.D., Evaporative Cooling of Water in a Natural Draft Cooling Tower, International Journal of Heat and Mass Transfer, Vol. 45, pp. 4683-4694, 2002.

[02HA1] Harte, R. and Krätzig, W.B., Large-Scale Cooling Towers as Part of an Efficient and Cleaner Energy Generating Technology, Thin-Walled Structures, Vol. 40, pp. 651-664, 2002.

[02HA2] Hawlader, M.N.A. and Lui, B.M., Numerical Study of the Thermal-Hydraulic Performance of Evaporative Natural Draft Cooling Towers, Applied Thermal Engineering, Vol. 22, pp. 41-59, 2002.

[02TH1] Thiart, G.D., Preliminary CFD Analysis of a Solar Chimney, HEFAT2002, 1st International Conference on Heat Transfer, Fluid Mechanics and Thermodynamics, Kruger Park, South Africa, pp. 449-452, 2002.

APPENDIX A

PROPERTIES OF FLUIDS

AS SUMMURISED BY KRÖGER [98KR1]

A.1 THE THERMOPHYSICAL PROPERTIES OF DRY AIR FROM 220K TO 380K AT STANDARD ATMOSPHERIC PRESSURE (101325N/m^2).

Density:

$$\rho_a = p_a/(287.08\ T),\ \text{kg/m}^3 \tag{A.1.1}$$

Specific heat:

$$c_{pa} = 1.045356 \times 10^3 - 3.161783 \times 10^{-1}\ T + 7.083814 \times 10^{-4}\ T^2 - 2.705209 \times 10^{-7}\ T^3,\ \text{J/kgK} \tag{A.1.2}$$

Dynamic viscosity:

$$\mu_a = 2.287973 \times 10^{-6} + 6.259793 \times 10^{-8}\ T - 3.131956 \times 10^{-11}\ T^2 + 8.15038 \times 10^{-15}\ T^3,\ \text{kg/sm} \tag{A.1.3}$$

Thermal conductivity:

$$k_a = -4.937787 \times 10^{-4} + 1.018087 \times 10^{-4}\ T - 4.627937 \times 10^{-8}\ T^2 + 1.250603 \times 10^{-11}\ T^3,\ \text{W/mK} \tag{A.1.4}$$

A.2 THE THERMOPHYSICAL PROPERTIES OF SATURATED WATER VAPOR FROM 273.15K TO 380K.

Vapor pressure:

$$p_v = 10^z, \text{ N/m}^2 \tag{A.2.1}$$

$$z = 10.79586(1 - 273.16/T) + 5.02808 \log_{10}(273.16/T) + 1.50474 \times 10^{-4}[1 - 10^{-8.29692\{(T/273.16)-1\}}] + 4.2873 \times 10^{-4}[10^{4.76955(1-273.16/T)} - 1] + 2.786118312$$

Specific heat:

$$c_{pv} = 1.3605 \times 10^3 + 2.31334\,T - 2.46784 \times 10^{-10}\,T^5 + 5.91332 \times 10^{-13}\,T^6, \text{ J/kgK} \tag{A.2.2}$$

Dynamic viscosity:

$$\mu_v = 2.562435 \times 10^{-6} + 1.816683 \times 10^{-8}\,T + 2.579066 \times 10^{-11}\,T^2 - 1.067299 \times 10^{-14}\,T^3, \text{ kg/sm} \tag{A.2.3}$$

Thermal conductivity:

$$k_v = 1.3046 \times 10^{-2} - 3.756191 \times 10^{-5}\,T + 2.217964 \times 10^{-7}\,T^2 - 1.111562 \times 10^{-10}\,T^3, \text{ W/mK} \tag{A.2.4}$$

Vapor density:

$$\rho_v = -4.062329056 + 0.10277044T - 9.76300388 \times 10^{-4}\,T^2 + 4.475240795 \times 10^{-6}T^3 - 1.004596894 \times 10^{-8}T^4 + 8.9154895 \times 10^{-12}T^5, \text{ kg/m}^3 \tag{A.2.5}$$

Temperature:

$$T = 164.630366 + 1.832295 \times 10^{-3}p_v + 4.27215 \times 10^{-10}p_v^2 + 3.738954 \times 10^3 p_v^{-1} - 7.01204 \times 10^5 p_v^{-2} + 16.161488 \ln p_v - 1.437169 \times 10^{-4}\,p_v \ln p_v, \text{ K} \tag{A.2.6}$$

A.3 THE THERMOPHYSICAL PROPERTIES OF MIXTURES OF AIR AND WATER VAPOR.

Density:

$\rho_{av} = (1 + w)\,[1 - w/(w + 0.62198)]\,p_{abs}/(287.08T)$, kg air-vapor/m^3 (A.3.1)

Specific heat:

$c_{pav} = (c_{pa} + wc_{pv})/(1 + w)$, J/K kg air-vapor (A.3.2a)

or the specific heat of the air-vapor mixture per unit mass of dry air:

$c_{pma} = (c_{pa} + wc_{pv})$, J/K kg dry air (A.3.2b)

Dynamic viscosity:

$\mu_{av} = (X_a\mu_a M_a^{0.5} + X_v\mu_v M_v^{0.5})/\,(X_a M_a^{0.5} + X_v M_v^{0.5})$, kg/ms (A.3.3)

where $M_a = 28.97$ kg/mole, $M_v = 18.016$ kg/mole, $X_a = 1/(1 + 1.608\,w)$ and $X_v = w/(w + 0.622)$

Thermal conductivity:

$k_{av} = (X_a k_a M_a^{0.33} + X_v k_v M_v^{0.33})/\,(X_a M_a^{0.33} + X_v M_v^{0.33})$, W/mK (A.3.4)

Humidity ratio:

$$w = \left(\frac{2501.6 - 2.3263(T_{wb} - 273.15)}{2501.6 + 1.8577(T - 273.15) - 4.184(T_{wb} - 273.15)}\right)\left(\frac{0.62509\,p_{vwb}}{p_{abs} - 1.005\,p_{vwb}}\right) - \left(\frac{1.00416(T - T_{wb})}{2501.6 + 1.8577(T - 273.15) - 4.184(T_{wb} - 273.15)}\right) \quad \text{(A.3.5)}$$

Enthalpy:

$i_{av} = [c_{pa}(T - 273.15) + w\{i_{fgwo} + c_{pv}(T - 273.15)\}]/(1 + w)$, J/kg air vapor (A.3.6a)

or the enthalpy of the air-vapor mixture per unit mass of dry air:

$i_{ma} = c_{pa}(T - 273.15) + w[i_{fgwo} + c_{pv}(T - 273.15)]$, J/kg air vapor (A.3.6b)

where the specific heats are evaluated at $(T + 273.15)/2$ and the latent heat i_{fgwo}, is evaluated at 273.15K according to equation (A.4.5).

A.4 THE THERMOPHYSICAL PROPERTIES OF SATURATED WATER LIQUID FROM 273.15K TO 380K.

Density:

$$\rho_w = (1.49343 \times 10^{-3} - 3.7164 \times 10^{-6}T + 7.09782 \times 10^{-9}T^2 - 1.90321 \times 10^{-20}T^6)^{-1}, \text{kg/m}^3 \quad \text{(A.4.1)}$$

Specific heat:

$$c_{pw} = 8.15599 \times 10^3 - 2.80627 \times 10\,T + 5.11283 \times 10^{-2}\,T^2 - 2.17582 \times 10^{-13}\,T^6, \text{J/kgK} \quad \text{(A.4.2)}$$

Dynamic viscosity:

$$\mu_w = 2.414 \times 10^{-5} \times 10^{\,247.8/(T-140)}, \text{kg/sm} \quad \text{(A.4.3)}$$

Thermal conductivity:

$$k_w = -6.14255 \times 10^{-1} + 6.9962 \times 10^{-3}\,T - 1.01075 \times 10^{-5}\,T^2 + 4.74737 \times 10^{-12}\,T^4, \text{W/mK} \quad \text{(A.4.4)}$$

Latent heat of vaporation:

$$i_{fgw} = 3.4831814 \times 10^6 - 5.8627703 \times 10^3\,T + 12.139568\,T^2 - 1.40290431 \times 10^{-2}\,T^3, \text{J/K} \quad \text{(A.4.5)}$$

Critical pressure:

$$p_{wc} = 22.09 \times 10^6, \text{N/m}^2 \quad \text{(A.4.6)}$$

Surface tension:

$$\sigma_w = 5.148103 \times 10^{-2} + 3.998714 \times 10^{-4}\,T - 1.4721869 \times 10^{-6}\,T^2 + 1.21405335 \times 10^{-9}\,T^3 \quad \text{(A.4.7)}$$

APPENDIX B

HEAT AND MASS TRANSFER IN COUNTERFLOW WET-COOLING TOWERS

B.1 INTRODUCTION

The governing equations for heat and mass transfer in the fill of a counterflow cooling tower are derived in this appendix. The governing equations for Merkel's and Poppe's models are presented. The Merkel theory relies on several critical assumptions to reduce the solution to a simple hand calculation. Because of these assumptions, however, the Merkel method does not accurately represent the physics of heat and mass transfer process in the cooling tower fill.

The critical simplifying assumptions of the Merkel theory are [83BO2]:

- The Lewis factor relating heat and mass transfer is equal to 1. This assumption has a small influence but affects results at low ambient temperatures.
- The air exiting the tower is saturated with water vapor and it is characterized only by its enthalpy. This assumption regarding saturation has a negligible influence above an ambient temperature of 20°C but is of importance at lower temperatures.
- The reduction of water flow rate by evaporation is neglected in the energy balance. This energy balance simplification has a greater influence at elevated ambient temperatures.

Bourillot [83BO2] stated that the Merkel theory is simple to use and can correctly predict cold water temperature when an appropriate value of the coefficient of evaporation is used. In contrast, it is insufficient for the estimation of the characteristics of the warm air leaving the fill and for the calculation of changes in the water flow rate due to evaporation. These quantities are important to estimate water consumption and to predict the behavior of plumes exiting the cooling tower.

The method of Poppe does not make the simplifying assumptions of Merkel. Predictions from the Poppe formulation result in values of evaporated water flow rate that are in good agreement with full scale cooling tower test results. In addition, the Poppe method predicts the water content of the exit air accurately [83BO1, 83BO2].

Sections B.1 and B.2 are adapted from Bourillot [83BO1], Poppe and Rögener [91PO1], Kröger [98KR1] and Baard [98BA1].

B.2 GOVERNING EQUATIONS FOR HEAT AND MASS TRANSFER IN FILL FOR UNSATURATED AIR

Figure B.1 shows a control volume in the fill of a counterflow wet-cooling tower. Figure B.2 shows an airside control volume of the fill illustrated in figure B.1.

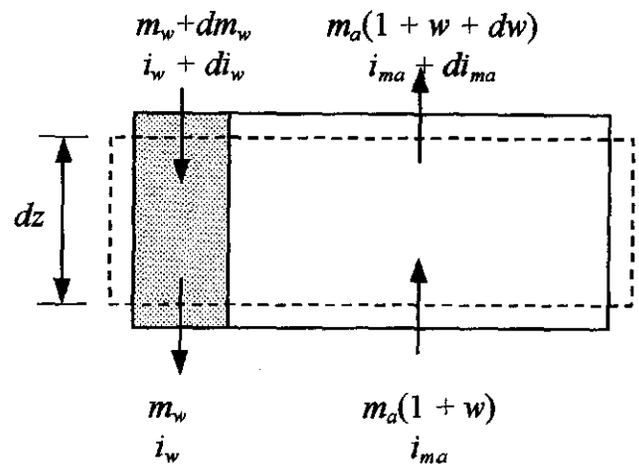

Figure B.1: Control volume of counterflow fill

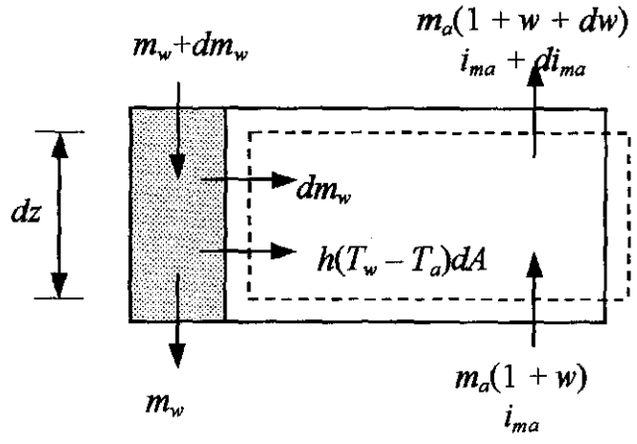

Figure B.2: Air side control volume of the fill

A mass balance for the control volume in figure B.1 yields,

$$dm_w = m_a dw \tag{B.1}$$

The energy balance for the control volume of the fill in figure B.1 is as follows:

$$m_a di_{ma} - m_w di_w - i_w dm_w = 0 \tag{B.2}$$

where i_{ma} is the enthalpy of the air-vapor mixture, expressed by equation (A.3.6b).

Substitute equation (B.1) into equation (B.2) to find upon rearrangement,

$$dT_w = \frac{m_a}{m_w}\left(\frac{1}{c_{pw}} di_{ma} - T_w dw\right) \tag{B.3}$$

Consider the interface between the water and the air in figure B.2. An energy balance at the interface yields,

$$dQ = dQ_m + dQ_c \tag{B.4}$$

where dQ_m is the enthalpy transfer due to difference in vapor concentration between the saturated air at the interface and the mean stream air and dQ_c is the sensible heat transfer due to the difference in temperature. The mass transfer at the interface is expressed by,

$$dm_w = h_d(w_{sw} - w)dA \tag{B.5}$$

The corresponding enthalpy transfer for the mass transfer in equation (B.5) is

$$dQ_m = i_v\, dm_w = i_v\, h_d(w_{sw} - w)dA \tag{B.6}$$

The enthalpy of the water vapor, i_v, at the bulk water temperature, T_w, is given by

$$i_v = i_{fgwo} + c_{pv}\, T_w \tag{B.7}$$

The convective heat transfer from figure B.2 is given by

$$dQ_c = h(T_w - T_a)dA \tag{B.8}$$

The temperature differential in equation (B.8) can be substituted by an enthalpy differential. The enthalpy of saturated air evaluated at the local bulk water temperature is given by

$$i_{masw} = c_{pa}\, T_w + w_{sw}(i_{fgwo} + c_{pv}\, T_w) \tag{B.9}$$

Substitute equation (B.7) into equation (B.9) and find upon rearrangement

$$i_{masw} = c_{pa}\, T_w + w\, i_v + (w_{sw} - w)i_v \tag{B.10}$$

The enthalpy of the air-water vapor mixture per unit mass of dry air, which according to equation (A.3.6b) is expressed by

$$i_{ma} = c_{pa}\, T_a + w(i_{fgwo} + c_{pv}\, T_a) \tag{B.11}$$

The specific heat of the air-water vapor mixture for unsaturated air is defined by

$$c_{pma} = c_{pa} + w\, c_{pv} \tag{B.12}$$

Subtract equation (B.11) from (B.10). The resultant equation can be simplified if the small differences in specific heats, which are evaluated at different temperatures, are ignored.

$$T_w - T_a = \frac{(i_{masw} - i_{ma}) - (w_{sw} - w)i_v}{c_{pma}} \tag{B.13}$$

where c_{pma} is given by equation (B.12).

Substitute equation (B.13) into equation (B.8). Substitute the resultant equation and equation (B.6) into equation (B.4) to find upon rearrangement,

$$dQ = h_d\left[\frac{h}{c_{pma}h_d}(i_{masw} - i_{ma}) + \left(1 - \frac{h}{c_{pma}h_d}\right)i_v(w_{sw} - w)\right]dA \tag{B.14}$$

$\dfrac{h}{c_{pma}h_d}$ is known as the Lewis factor, Le_f, and is an indication of the relative rates of heat and mass transfer in an evaporative process. Bosnjakovic [65BO1] developed an empirical relation for the Lewis factor, Le_f, for air-water vapor systems. The Lewis factor for unsaturated air, according to Bosnjakovic [65BO1] is given by

$$Le_f = 0.865^{0.667}\,\frac{\left(\dfrac{w_{sw} + 0.622}{w + 0.622} - 1\right)}{\ln\left(\dfrac{w_{sw} + 0.622}{w + 0.622}\right)} \tag{B.15}$$

Refer to appendix F for a discussion on the derivation of equation (B.15). Alternative approaches for the determination of the Lewis factor are also given in appendix F.

The enthalpy transfer to the air stream from equation (B.14) is

$$di_{ma} = \frac{1}{m_a} dQ = \frac{h_d dA}{m_a}\left[Le_f (i_{masw} - i_{ma}) + (1 - Le_f) i_v (w_{sw} - w)\right] \tag{B.16}$$

For a one-dimensional model of the cooling tower fill, where the available area for heat and mass transfer is the same at any horizontal section through the fill, the transfer area for a section dz is usually expressed as

$$dA = a_{fi} A_{fr} dz \tag{B.17}$$

where a_{fi} is the area density of the fill, i.e. the wetted area divided by the corresponding volume of the fill and A_{fr} is the corresponding frontal area or face area.

Substitute equation (B.17) into equation (B.16) and find

$$\frac{di_{ma}}{dz} = \frac{h_d a_{fi} A_{fr}}{m_a}\left[Le_f (i_{masw} - i_{ma}) + (1 - Le_f) i_v (w_{sw} - w)\right] \tag{B.18}$$

To simplify the analysis of an evaporative process Merkel [25ME1] assumed that the evaporative loss is negligible, i.e. $dw = 0$ from equation (B.3), and that the Lewis factor is equal to unity. The governing equations (B.18) and (B.3) of the counterflow evaporative process simplify respectively to

$$\frac{di_{ma}}{dz} = \frac{h_d a_{fi} A_{fr}}{m_a}(i_{masw} - i_{ma}) \tag{B.19}$$

and by dividing equation (B.3) by dz on both sides of equation (B.3) to

$$\frac{dT_w}{dz} = \frac{m_a}{m_w}\frac{1}{c_{pw}}\frac{di_{ma}}{dz} \tag{B.20}$$

Equations (B.19) and (B.20) describe respectively the change in the enthalpy of the air-water vapor mixture and the change in water temperature as the air travel distance changes. Equations (B.19) and (B.20) can be combined to yield upon integration the Merkel equation,

$$Me_M = \frac{h_d A}{m_w} = \frac{h_d a_{fi} A_{fr} L_{fi}}{m_w} = \frac{h_d a_{fi} L_{fi}}{G_w} = \int_{T_{wo}}^{T_{wi}} \frac{c_{pw} dT_w}{(i_{masw} - i_{ma})} \tag{B.21}$$

where Me_M is the Merkel number according to the Merkel approach. It is not possible to calculate the state of the air leaving the fill according to equation (B.21). Merkel assumed that the air leaving the fill is saturated with water vapor. This assumption enables the air temperature leaving the fill to be calculated.

Poppe and Rögener [91PO1] did not make the simplifying assumptions Merkel made. They derived the governing equation through the fill by following a different strategy than Merkel [25ME1]. Whereas the governing equations (B.19) and (B.20) according to the Merkel theory describe the changes of the enthalpy of the air-water vapor mixture and of water temperature to the change of air travel distance (i.e. di_{ma}/dz and dT_w/dz), Poppe and Rögener [91PO1] describe the change of the humidity ratio and the enthalpy of the air-water vapor mixture to the change of water temperature (i.e. dw/dT_w and di_{ma}/dT_w). Bourillot [83BO1] presented the governing Poppe equations as three equations describing the change of water temperature (dT_w), air enthalpy (di_{ma}) and humidity ratio (dw) to the change of air travel distance (dz). The method of Poppe and Rögener [91PO1] is employed in the derivation of the governing equations in this study.

Substitute equations (B.5) and (B.16) into equation (B.2) to find upon rearrangement,

$$m_w di_w = h_d dA\left[i_{masw} - i_{ma} + \left(Le_f - 1\right)\left[i_{masw} - i_{ma} - \left(w_{sw} - w\right)i_v\right] - \left(w_{sw} - w\right)c_{pw}T_w\right] \tag{B.22}$$

Find upon rearrangement of equation (B.3),

$$\frac{dw}{dT_w} = \frac{1}{c_{pw}T_w}\frac{di_{ma}}{dT_w} - \frac{1}{T_w}\frac{m_w}{m_a} \quad \text{or} \quad \frac{dw}{dT_w} = \frac{di_{ma}}{T_w di_w} - \frac{1}{T_w}\frac{m_w}{m_a} \tag{B.23}$$

Substitute equations (B.16) and (B.22) into equation (B.23) and find upon rearrangement,

$$\frac{dw}{dT_w} = \frac{c_{pw}\dfrac{m_w}{m_a}\left(w_{sw} - w\right)}{i_{masw} - i_{ma} + \left(Le_f - 1\right)\left[i_{masw} - i_{ma} - \left(w_{sw} - w\right)i_v\right] - \left(w_{sw} - w\right)c_{pw}T_w} \tag{B.24}$$

Substitute equation (B.24) into equation (B.23) and find upon rearrangement,

$$\frac{di_{ma}}{dT_w} = \frac{m_w c_{pw}}{m_a}\left(1 + \frac{\left(w_{sw} - w\right)c_{pw}T_w}{i_{masw} - i_{ma} + \left(Le_f - 1\right)\left[i_{masw} - i_{ma} - \left(w_{sw} - w\right)i_v\right] - \left(w_{sw} - w\right)c_{pw}T_w}\right) \tag{B.25}$$

From equations (B.1) and (B.5) find

$$h_d dA = \frac{m_a dw}{w_{sw} - w} \tag{B.26}$$

Divide both sides by m_w and introduce dT_w/dT_w to the right hand side of equation (B.26) and integrate to find

$$\int \frac{h_d}{m_w} dA = \int \frac{m_a}{m_w}\frac{dw/dT_w}{w_{sw} - w} dT_w \tag{B.27}$$

From equation (B.27) find

$$\frac{h_d A}{m_w} = \int \frac{m_a}{m_w}\frac{dw/dT_w}{w_{sw} - w} dT_w \tag{B.28}$$

Equation (B.28) is defined as the Merkel number according to the Poppe approach i.e.,

$$Me_P = \int \frac{m_a}{m_w}\frac{dw/dT_w}{w_{sw} - w} dT_w \tag{B.29}$$

Upon substitution of equation (B.24) into equation (B.29) and differentiation of the latter with respect to the water temperature, find

$$\frac{dMe_P}{dT_w} = \frac{c_{pw}}{i_{masw} - i_{ma} + \left(Le_f - 1\right)\left[i_{masw} - i_{ma} - \left(w_{sw} - w\right)i_v\right] - \left(w_{sw} - w\right)c_{pw}T_w} \tag{B.30}$$

The ratio of the mass flow rates, m_w/m_a, changes as the air moves towards the top of the fill. The change in the mass flow rate is determined by considering the control volume of a portion of the fill illustrated in figure B.3.

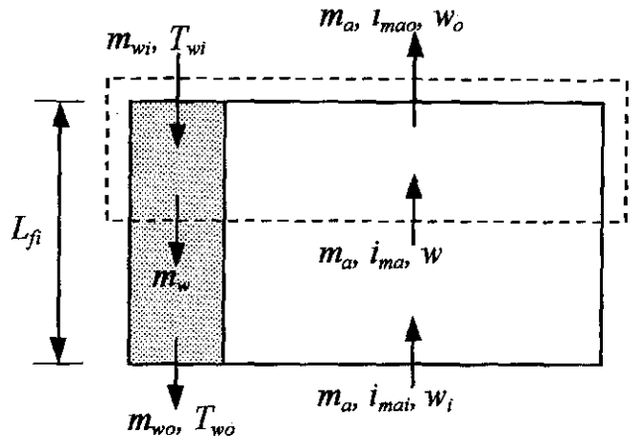

Figure B.3: Control volume of the fill.

The varying water mass flow rate can be determined from the known inlet water mass flow rate, m_{wi}. From the control volume in figure B.3 a mass balance will yield,

$$m_{wi} = m_w + m_a(w_o - w) \tag{B.31}$$

Upon rearrangement of equation (B.31) find,

$$\frac{m_w}{m_a} = \frac{m_{wi}}{m_a}\left(1 - \frac{m_a}{m_{wi}}(w_o - w)\right) \tag{B.32}$$

From equations (B.15), (B.24), (B.25) and (B.32) the air outlet conditions in terms of enthalpy and humidity ratio can be calculated.

The preceding system of equations is only applicable for unsaturated air. In some cases, the air can become saturated before it leaves the fill [98KR1]. Because the water temperature is still higher than the temperature of the air, the potential for heat and mass transfer still exists. Under these conditions, the excess water vapor will condense as a mist.

B.3 GOVERNING EQUATIONS FOR HEAT AND MASS TRANSFER IN FILL FOR SUPERSATURATED AIR

The control volumes in figures B.1 and B.2 are also applicable for supersaturated air. Since the excess water vapor will condense as a mist, the enthalpy of supersaturated air is expressed by

$$i_{ss} = c_{pa} T_a + w_{sa}(i_{fgwo} + c_{pv} T_a) + (w - w_{sa})c_{pw}T_a \tag{B.33}$$

where w_{sa} is the humidity ratio of saturated air at temperature T_a.

Assume that the heat and mass transfer coefficients for supersaturated and unsaturated air are the same, as proposed by Bourillot [83BO1] and Poppe and Rögener [91PO1]. The driving potential for mass transfer is the humidity ratio difference between the saturated air at the air-water interface and the saturated free stream air, thus

$$dm_w = h_d (w_{sw} - w_{sa})\, dA \tag{B.34}$$

The enthalpy driving potential for supersaturated air can be obtained by subtracting equation (B.33) from equation (B.10). By introducing,

$(w - w_{sa})\, c_{pw}\, T_w - (w - w_{sa})\, c_{pw}\, T_w + w_{sa}\, c_{pv}\, T_w - w_{sa}\, c_{pv}\, T_w$

which add up to zero, into the resultant enthalpy differential, the temperature differential can be obtained by manipulation.

$$T_w - T_a = \frac{i_{masw} - i_{ss} - (w_{sw} - w_{sa})i_v + (w - w_{sa})c_{pw}T_w}{c_{pmas}} \tag{B.35}$$

where c_{pmas} is the specific heat of supersaturated air per unit mass and defined as

$$c_{pmas} = c_{pa} + w_{sa}c_{pv} + (w - w_{sa})c_{pw} \tag{B.36}$$

Proceeding along the same lines as in the case of unsaturated air, using equations (B.34) and (B.35) instead of equations (B.5) and (B.13), find for supersaturated air,

$$di_{ma} = \frac{h_d dA}{m_a}\left[Le_f\left\{i_{masw} - i_{ss} - (w_{sw} - w_{sa})i_v + (w - w_{sa})c_{pw}T_w\right\} + (w_{sw} - w_{sa})i_v\right] \tag{B.37}$$

where the Lewis factor, Le_f, is equal to $h/h_d c_{pmas}$. The empirical relation of Bosnjakovic [65BO1] can be used to calculate the Lewis factor, which for supersaturated air is given by

$$Le_f = 0.865^{0.667}\,\frac{\left(\frac{w_{sw} + 0.622}{w_{sa} + 0.622} - 1\right)}{\ln\left(\frac{w_{sw} + 0.622}{w_{sa} + 0.622}\right)} \tag{B.38}$$

Substitute equations (B.34) and (B.37) into equation (B.2) to find upon rearrangement,

$$m_w di_w = m_w c_{pw} dT_w = h_d dA\left[\begin{matrix} Le_f\left\{i_{masw} - i_{ss} - (w_{sw} - w_{sa})i_v + (w - w_{sa})c_{pw}T_w\right\} \\ + (w_{sw} - w_{sa})i_v - (w_{sw} - w_{sa})c_{pw}T_w \end{matrix}\right] \tag{B.39}$$

By introducing,

$$\left[i_{masw} - i_{ss} - (w_{sw} - w_{sa})i_v + (w - w_{sa})c_{pw}T_w\right] - \left[i_{masw} - i_{ss} - (w_{sw} - w_{sa})i_v + (w - w_{sa})c_{pw}T_w\right]$$

into the main parenthesis on right hand side of equation (B.39) the following equation yields after rearrangement.

$$m_w di_w = m_w c_{pw} dT_w = h_d dA\left[\begin{matrix} i_{masw} - i_{ss} + (Le_f - 1)\left(\begin{matrix} i_{masw} - i_{ss} - (w_{sw} - w_{sa})i_v \\ + (w - w_{sa})c_{pw}T_w \end{matrix}\right) \\ + (w - w_{sw})c_{pw}T_w \end{matrix}\right] \tag{B.40}$$

Substitute equation (B.34) into equation (B.1) and find upon rearrangement,

$$h_d dA = \frac{m_a dw}{(w_{sw} - w_{sa})} \tag{B.41}$$

Substitute equation (B.41) into equation (B.40) to find upon rearrangement,

$$\frac{dw}{dT_w} = \frac{c_{pw}\dfrac{m_w}{m_a}\left(w_{sw} - w_{sa}\right)}{i_{masw} - i_{ss} + \left(Le_f - 1\right)\left[\begin{matrix} i_{masw} - i_{ss} - \left(w_{sw} - w_{sa}\right)i_v \\ + \left(w - w_{sa}\right)c_{pw}T_w \end{matrix}\right] + \left(w - w_{sw}\right)c_{pw}T_w} \tag{B.42}$$

Substitute equation (B.42) into equation (B.23) and find upon rearrangement,

$$\frac{di_{ma}}{dT_w} = c_{pw}\frac{m_w}{m_a}\left(1 + \frac{c_{pw}T_w\left(w_{sw} - w_{sa}\right)}{i_{masw} - i_{ss} + \left(Le_f - 1\right)\left[\begin{matrix} i_{masw} - i_{ss} - \left(w_{sw} - w_{sa}\right)i_v \\ + \left(w - w_{sa}\right)c_{pw}T_w \end{matrix}\right] + \left(w - w_{sw}\right)c_{pw}T_w}\right) \tag{B.43}$$

From equations (B.1) and (B.34) find

$$h_d dA = \frac{m_a dw}{w_{sw} - w_{sa}} \tag{B.44}$$

Divide both sides of equation (B.44) by m_w, introduce dT_w/dT_w to the right hand side of equation (B.44) and integrate to find

$$\int \frac{h_d}{m_w} dA = \int \frac{m_a}{m_w}\frac{dw/dT_w}{w_{sw} - w_{sa}} dT_w \tag{B.45}$$

Equation (B.45) is defined as the Merkel number according to the Poppe approach i.e.,

$$Me_P = \frac{h_d A}{m_w} = \int \frac{m_a}{m_w}\frac{dw/dT_w}{w_{sw} - w_{sa}} dT_w \tag{B.46}$$

Upon substitution of equation (B.42) into equation (B.46) and differentiation of the latter with respect to water temperature, find

$$\frac{dMe_P}{dT_w} = \frac{c_{pw}}{i_{masw} - i_{ss} + \left(Le_f - 1\right)\left[\begin{matrix} i_{masw} - i_{ss} - \left(w_{sw} - w_{sa}\right)i_v \\ + \left(w - w_{sa}\right)c_{pw}T_w \end{matrix}\right] + \left(w - w_{sw}\right)c_{pw}T_w} \tag{B.47}$$

From equations (B.32), (B.38), (B.42) and (B.43) the air outlet conditions in terms of enthalpy and humidity ratio can be calculated.

B.4. SOLVING THE SYSTEM OF DIFFERENTIAL EQUATIONS

The fourth order Runge-Kutta method [83BO1, 92MA1, 97BU1] is used to solve the system of differential equations for unsaturated and supersaturated air. The system of equations for unsaturated air (including saturated air) is represented by equations (B.24), (B.25) and (B.30). The system of equations for supersaturated air is represented by equations (B.42), (B.43) and (B.47). In the equations that follow, i_{ma} must be replaced by i_{ss} for supersaturated air. Refer to the example problems in appendices G and I for a description of the conventions that is used, i.e. the conventions of the variable subscripts, fill intervals and fill levels.

Equations (B.24), (B.25) and (B.30) for unsaturated and saturated air or equations (B.42), (B.43) and (B.47) for supersaturated air can be respectively written as.

$$\frac{dw}{dT_w} = f(w, i_{ma}, T_w) \tag{B.48}$$

$$\frac{di_{ma}}{dT_w} = g(w, i_{ma}, T_w) \tag{B.49}$$

$$\frac{dMe_P}{dT_w} = h(w, i_{ma}, T_w) \tag{B.50}$$

The fill is divided into one or more intervals with the same water temperature difference across each interval. In addition to the intervals, levels are specified (a level is an imaginary horizontal plane through the fill at the top and bottom of the fill and between two fill intervals). Initial values of the variables, w, i_{ma} and T_w, are required on a particular level, say level (n). The values of the variables can then be determined at level (n + 1) with the aid of equations (B.51) to (B.53).

$$w_{(n+1)} = w_{(n)} + \left(j_{(n+1,1)} + 2j_{(n+1,2)} + 2j_{(n+1,3)} + j_{(n+1,4)}\right)/6 \tag{B.51}$$

$$i_{ma(n+1)} = i_{ma(n)} + \left(k_{(n+1,1)} + 2k_{(n+1,2)} + 2k_{(n+1,3)} + k_{(n+1,4)}\right)/6 \tag{B.52}$$

$$Me_{P(n+1)} = Me_{P(n)} + \left(l_{(n+1,1)} + 2l_{(n+1,2)} + 2l_{(n+1,3)} + l_{(n+1,4)}\right)/6 \tag{B.53}$$

where

$$j_{(n+1,1)} = \Delta T_w \cdot f\left(T_{w(n)}, i_{ma(n)}, w_{(n)}\right) \tag{B.54}$$

$$k_{(n+1,1)} = \Delta T_w \cdot g\left(T_{w(n)}, i_{ma(n)}, w_{(n)}\right) \tag{B.55}$$

$$l_{(n+1,1)} = \Delta T_w \cdot h\left(T_{w(n)}, i_{ma(n)}, w_{(n)}\right) \tag{B.56}$$

$$j_{(n+1,2)} = \Delta T_w \cdot f\left(T_{w(n)} + \frac{\Delta T_w}{2}, i_{ma(n)} + \frac{k_{(n+1,1)}}{2}, w_{(n)} + \frac{j_{(n+1,1)}}{2}\right) \tag{B.57}$$

$$k_{(n+1,2)} = \Delta T_w \cdot g\left(T_{w(n)} + \frac{\Delta T_w}{2}, i_{ma(n)} + \frac{k_{(n+1,1)}}{2}, w_{(n)} + \frac{j_{(n+1,1)}}{2}\right) \tag{B.58}$$

$$l_{(n+1,2)} = \Delta T_w \cdot h\left(T_{w(n)} + \frac{\Delta T_w}{2}, i_{ma(n)} + \frac{k_{(n+1,1)}}{2}, w_{(n)} + \frac{j_{(n+1,1)}}{2}\right) \tag{B.59}$$

$$j_{(n+1,3)} = \Delta T_w \cdot f\left(T_{w(n)} + \frac{\Delta T_w}{2}, i_{ma(n)} + \frac{k_{(n+1,2)}}{2}, w_{(n)} + \frac{j_{(n+1,2)}}{2}\right) \tag{B.60}$$

$$k_{(n+1,3)} = \Delta T_w \cdot g\left(T_{w(n)} + \frac{\Delta T_w}{2}, i_{ma(n)} + \frac{k_{(n+1,2)}}{2}, w_{(n)} + \frac{j_{(n+1,2)}}{2}\right) \tag{B.61}$$

$$l_{(n+1,3)} = \Delta T_w \cdot h\left(T_{w(n)} + \frac{\Delta T_w}{2}, i_{ma(n)} + \frac{k_{(n+1,2)}}{2}, w_{(n)} + \frac{j_{(n+1,2)}}{2}\right) \tag{B.62}$$

$$j_{(n+1,4)} = \Delta T_w \cdot f\left(T_{w(n)} + \Delta T_w, i_{ma(n)} + k_{(n+1,3)}, w_{(n)} + j_{(n+1,3)}\right) \tag{B.63}$$

$$k_{(n+1,4)} = \Delta T_w \cdot g\left(T_{w(n)} + \Delta T_w, i_{ma(n)} + k_{(n+1,3)}, w_{(n)} + j_{(n+1,3)}\right) \tag{B.64}$$

$$l_{(n+1,4)} = \Delta T_w \cdot h\left(T_{w(n)} + \Delta T_w, i_{ma(n)} + k_{(n+1,3)}, w_{(n)} + j_{(n+1,3)}\right) \tag{B.65}$$

where

$$\Delta T_w = (T_{wi} - T_{wo})/(\textit{Number of intervals}) \tag{B.66}$$

The four variables in the Runge-Kutta method are T_w, w, i_{ma} or i_{ss} and Me_P from the left-hand side of equations (B.24), (B.25) and (B.30) for unsaturated air and equations (B.42), (B.43) and (B.47) for supersaturated air. For this reason equations (B.48) to (B.50) are functions of only w, i_{ma} or i_{ss} and T_w. Most of the other variables are functions of these variables. Equations (B.48) to (B.50) are not functions of Me_P because dMe_P/dT_w is a function of dw/dT_w as can be seen from equation (B.46). Thus, equations (B.24) and (B.25) for unsaturated air, or equations (B.42) and (B.43) for supersaturated air can be solved without equation (B.30) or equation (B.47) respectively.

B.5 *e-NTU* METHOD

Jaber and Webb [89JA1] developed the equations necessary to apply the *e-NTU* method directly to counterflow or crossflow cooling towers. The approach is particularly useful in the latter case and simplifies the method of solution when compared to a more conventional numerical procedure as discussed in appendix C. Kröger [98KR1] gives a detailed derivation and implementation of the *e-NTU* method applied to evaporative air-water systems.

It can be shown according to Jaber and Webb [89JA1] that

$$\frac{d\left(i_{masw} - i_{ma}\right)}{\left(i_{masw} - i_{ma}\right)} = h_d \left(\frac{di_{masw} / dT_w}{m_w c_{pw}} - \frac{1}{m_a} \right) dA \tag{B.67}$$

Equation (B.67) corresponds to the heat exchanger *e-NTU* equation

$$\frac{d\left(T_h - T_c\right)}{\left(T_h - T_c\right)} = -U \left(\frac{1}{m_h c_{ph}} + \frac{1}{m_c c_{pc}} \right) dA \tag{B.68}$$

Two possible cases of equation (B.67) can be considered where m_a is greater or less than $m_w c_{pw}/(di_{masw}/dT_w)$. The maximum of m_a and $m_w c_{pw}/(di_{masw}/dT_w)$ is denoted by C_{max} and the minimum by C_{min}. The gradient of the saturated air enthalpy-temperature curve is

$$\frac{di_{masw}}{dT_w} = \frac{i_{maswi} - i_{maswo}}{T_{wi} - T_{wo}} \tag{B.69}$$

The fluid capacity rate ratio is defined as

$$C = C_{\min} / C_{\max} \tag{B.70}$$

The effectiveness is given by

$$e = \frac{Q}{Q_{\max}} = \frac{m_w c_{pw}(T_{wi} - T_{wo})}{C_{\min}(i_{maswi} - \lambda - i_{mai})} \tag{B.71}$$

where λ is a correction factor, according to Berman [61BE1], to improve the approximation of the i_{masw} versus T_w curve as a straight line. The correction factor, λ, is given by

$$\lambda = (i_{maswo} + i_{maswi} - 2i_{maswm})/4 \tag{B.72}$$

where i_{maswm} donates the enthalpy of saturated air at the mean water temperature. The number of transfer units for counterflow cooling towers is given by

$$NTU = \frac{1}{1-C} \ln \frac{1-eC}{1-e} \tag{B.73}$$

If m_a is greater than $m_w c_{pw}/(di_{masw}/dT_w)$ the Merkel number according to the *e-NTU* approach is given by

$$Me_e = \frac{c_{pw}}{di_{masw}/dT_w} NTU \tag{B.74}$$

If m_a is less than $m_w c_{pw}/(di_{masw}/dT_w)$ the Merkel number according to the *e-NTU* approach is given by

$$Me_e = \frac{m_a}{m_w} NTU \tag{B.75}$$

APPENDIX C

HEAT AND MASS TRANSFER IN CROSSFLOW WET-COOLING TOWERS

C.1 INTRODUCTION

In 1956, Zivi and Brand [56ZI1] extended the analysis of Merkel to the fill of crossflow cooling towers. In 1976, Kelly [76KE1] used the model of Zivi and Brand [56ZI1] along with laboratory data to produce a volume of crossflow cooling tower characteristic curves to be used in graphical solutions of cooling tower performance.

The present analysis does not make the simplifying assumptions of Merkel and is also known, as in the case with counterflow towers, as the Poppe approach. A different approach is followed in the derivation of the governing equations for crossflow cooling towers than was the case in appendix B for counterflow cooling towers. A more fundamental approach is followed to prevent confusion with sign conventions and partial derivatives because of the two dimensional nature of the problem.

C.2 GOVERNING EQUATIONS FOR HEAT AND MASS TRANSFER IN FILL FOR UNSATURATED AIR

Figure C.1 shows a control volume in the fill of a crossflow wet-cooling tower.

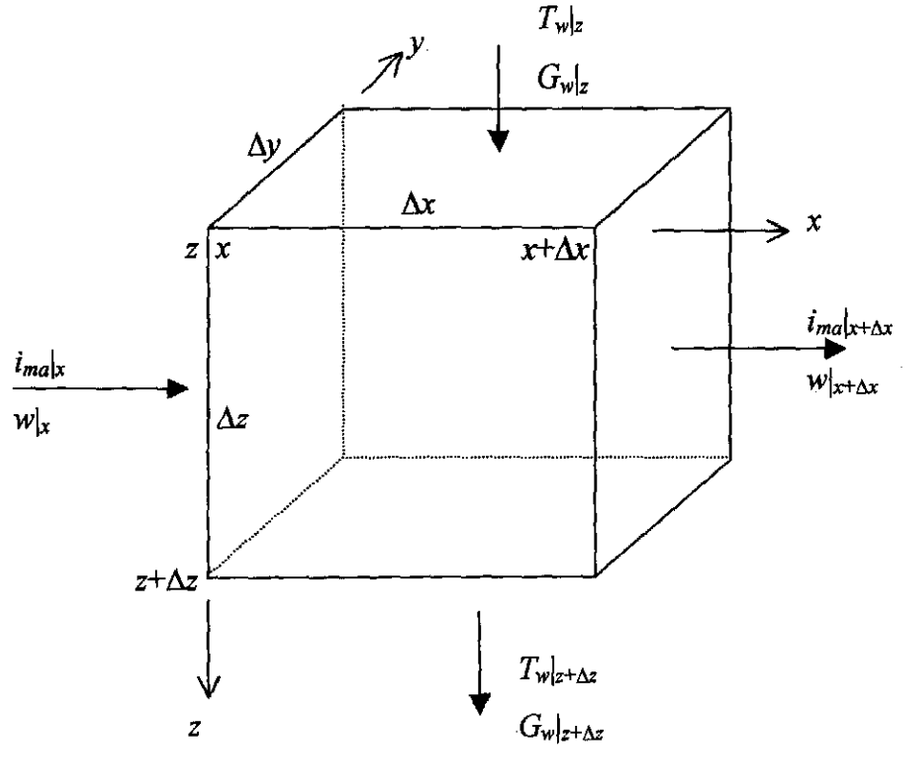

Figure C.1: Control volume of crossflow fill

A mass balance for the control volume in figure C.1 yields,

$G_w|_z\ \Delta x\Delta y - G_w|_{z+\Delta z}\ \Delta x\Delta y + G_a\ \Delta y\Delta z\ w|_x - G_a\ \Delta y\Delta z\ w|_{x+\Delta x} = 0$ (C.1)

Divide equation (C.1) by $\Delta x\Delta y\Delta z$ and let $\Delta x, \Delta z \rightarrow 0$

$$\frac{\partial G_w}{\partial z} = -G_a \frac{\partial w}{\partial x} \tag{C.2}$$

The energy balance for the control volume of the fill in figure C.1 is as follows:

$c_{pw}(T_w\ G_w)|_z\ \Delta x\Delta y - c_{pw}(T_w\ G_w)|_{z+\Delta z}\ \Delta x\Delta y + G_a\ \Delta y\Delta z\ i_{ma}|_x - G_a\ \Delta y\Delta z\ i_{ma}|_{x+\Delta x} = 0$ (C.3)

Divide equation (C.3) by $\Delta x\Delta y\Delta z$ and let $\Delta x, \Delta z \rightarrow 0$ and find after using the chain rule of differentiation,

$$c_{pw}T_w \frac{\partial G_w}{\partial z} + c_{pw}G_w \frac{\partial T_w}{\partial z} + G_a \frac{\partial i_{ma}}{\partial x} = 0 \tag{C.4}$$

Substitute equation (C.2) into equation (C.4) to find upon rearrangement,

$$\frac{\partial T_w}{\partial z} = \frac{G_a}{G_w}\left(T_w \frac{\partial w}{\partial x} - \frac{1}{c_{pw}} \frac{\partial i_{ma}}{\partial x}\right) \tag{C.5}$$

The mass balance for the water stream in the control volume is expressed by

$G_w|_z\ \Delta x\Delta y - G_w|_{z+\Delta z}\ \Delta x\Delta y - h_d\ a_{fi}\ (w_{sw}-w)\Delta x\Delta y\Delta z = 0$ (C.6)

where $h_d\ a_{fi}\ (w_{sw}-w)\Delta x\Delta y\Delta z$ is the amount of water evaporated in the control volume in figure C.1.

Divide equation (C.6) by $\Delta x\Delta y\Delta z$ and let $\Delta x, \Delta z \rightarrow 0$

$$\frac{\partial G_w}{\partial z} = -G_a \frac{h_d a_{fi}}{G_a}(w_{sw} - w) \tag{C.7}$$

Substitute equation (C.7) into equation (C.2) rearrange and find,

$$\frac{\partial w}{\partial x} = \frac{h_d a_{fi}}{G_a}(w_{sw} - w) \tag{C.8}$$

The sensible heat transfer to the air stream in the control volume is expressed by

$q_c|_x\ \Delta y\Delta z - q_c|_{x+\Delta x}\ \Delta y\Delta z + h\ a_{fi}\ (T_w-T_a)\Delta x\Delta y\Delta z = 0$ (C.9)

where $h\ a_{fi}\ (T_w-T_a)\Delta x\Delta y\Delta z$ is the amount of sensible heat transferred to the air stream in the control volume in figure C.1. Divide equation (C.9) by $\Delta x\Delta y\Delta z$ and let $\Delta x, \Delta z \rightarrow 0$

$$\frac{\partial q_c}{\partial x} = h a_{fi}(T_w - T_a) \tag{C.10}$$

The latent heat transfer to the air stream in the control volume is expressed by

$q_m|_x\ \Delta y\Delta z - q_m|_{x+\Delta x}\ \Delta y\Delta z + i_v G_w|_z\ \Delta x\Delta y - i_v G_w|_{z+\Delta z}\ \Delta x\Delta y = 0$ (C.11)

Divide equation (C.11) by $\Delta x\Delta y\Delta z$, let $\Delta x, \Delta z \rightarrow 0$ and substitute equation (C.8) into the resultant equation

$$\frac{\partial q_m}{\partial x} = -i_v \frac{\partial G_w}{\partial z} = i_v h_d a_{fi}(w_{sw} - w) \tag{C.12}$$

An energy balance at the air/water interface inside the control volume yields,

$$\frac{\partial q}{\partial x} = \frac{\partial q_c}{\partial x} + \frac{\partial q_m}{\partial x} \tag{C.13}$$

Substitute equation (B.13) into equation (C.10). Substitute the resultant equation and equation (C.12) into equation (C.13) to find upon rearrangement,

$$\frac{\partial q}{\partial x} = h_d a_{fi}\left[\frac{h}{c_{pma}h_d}(i_{masw} - i_{ma}) + \left(1 - \frac{h}{c_{pma}h_d}\right) i_v (w_{sw} - w)\right] \tag{C.14}$$

$\frac{h}{c_{pma}h_d}$ is the Lewis factor, Le_f. The Lewis factor for unsaturated air, according to Bosnjakovic [65BO1] is given by equation (B.15).

The enthalpy transfer to the air stream from equation (C.14) is

$$\frac{\partial i_{ma}}{\partial x} = \frac{1}{G_a}\frac{\partial q}{\partial x} = \frac{h_d a_{fi}}{G_a}\left[i_{masw} - i_{ma} + (Le_f - 1)\{i_{masw} - i_{ma} - i_v(w_{sw} - w)\}\right] \tag{C.15}$$

Substitute equations (C.8) and (C.15) into equation (C.5) to find upon rearrangement,

$$\frac{\partial T_w}{\partial z} = \frac{1}{c_{pw}}\frac{G_a}{G_w}\frac{h_d a_{fi}}{G_a}\left[\begin{matrix}(w_{sw} - w)c_{pw}T_w - (i_{masw} - i_{ma}) - \\ (Le_f - 1)[i_{masw} - i_{ma} - (w_{sw} - w)i_v]\end{matrix}\right] \tag{C.16}$$

Thus, the system of equations to be solved for unsaturated air for the crossflow fill are equations (C.7), (C.8), (C.15) and (C.16).

C.3 GOVERNING EQUATIONS FOR HEAT AND MASS TRANSFER IN FILL FOR SUPERSATURATED AIR

The governing equations for supersaturated air can be manipulated as was done for the unsaturated case using the same arguments as in the counterflow case to obtain the following equations for supersaturated air in crossflow,

$$\frac{\partial G_w}{\partial z} = -h_d a_{fi}(w_{sw} - w_{sa}) \tag{C.17}$$

$$\frac{\partial w}{\partial x} = \frac{h_d a_{fi}}{G_a}(w_{sw} - w_{sa}) \tag{C.18}$$

$$\frac{\partial i_{ss}}{\partial x} = \frac{1}{G_a}\frac{\partial q}{\partial x} = \frac{h_d a_{fi}}{G_a}\left[\begin{matrix}i_{masw} - i_{ss} + (Le_f - 1)\{i_{masw} - i_{ss} - i_v(w_{sw} - w_{sa})\} + \\ Le_f c_{pw}T_w(w - w_{sa})\end{matrix}\right] \tag{C.19}$$

$$\frac{\partial T_w}{\partial z} = \frac{1}{c_{pw}}\frac{G_a}{G_w}\frac{h_d a_{fi}}{G_a}\left[\begin{matrix}(w_{sw} - w_{sa})c_{pw}T_w - (i_{masw} - i_{ss}) - Le_f c_{pw}T_w(w - w_{sa}) \\ (Le_f - 1)[i_{masw} - i_{ss} - (w_{sw} - w_{sa})i_v]\end{matrix}\right] \tag{C.20}$$

C.4 SOLVING THE SYSTEM OF PARTIAL DIFFERENTIAL EQUATIONS

Figure C.2 illustrates an example of a grid of a crossflow fill that is divided into four intervals in both the vertical and horizontal directions.

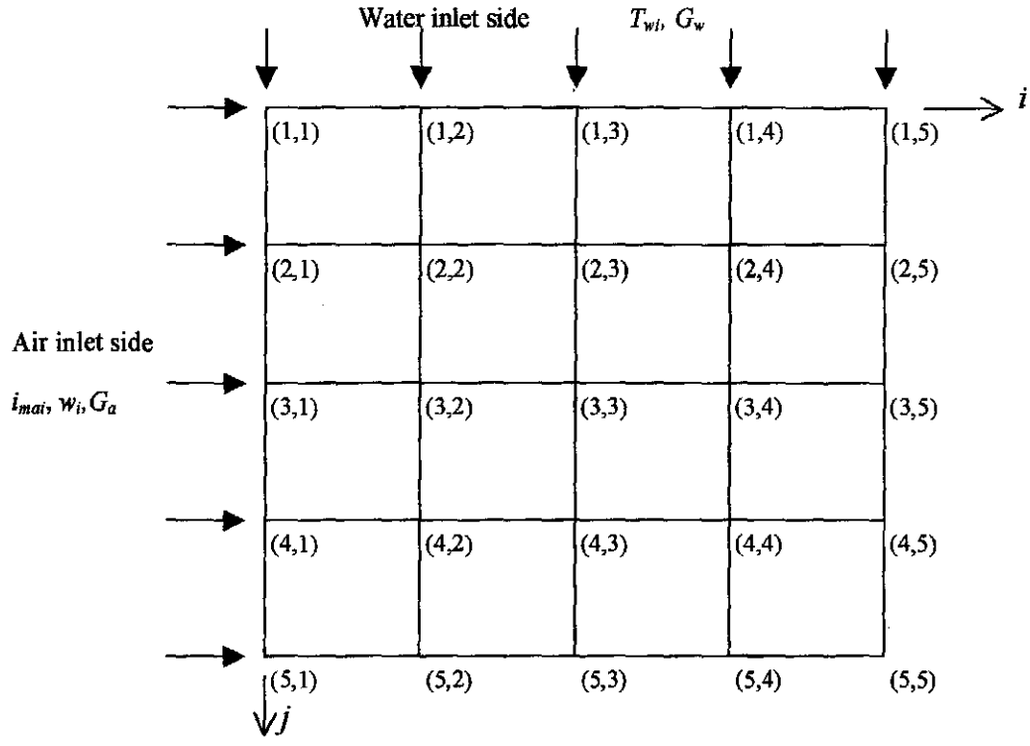

Figure C.2: Example of a crossflow fill that is divided into four intervals in each direction.

To simplify the solution process of the governing equations the fill dimensions can be non-dimensionalized. Poppe and Rögener [91PO1] presented the governing equations for crossflow fills in non-dimensional form. Thus, in non-dimensional form the fill can be analyzed without any reference to fill dimensions.

All the governing equations are of the first order. These first derivatives can be approximated by first-order rearward finite difference expressions. An example of the application of this finite difference technique to first derivatives can be seen in figure C.3.

First-order rearward difference with respect to x

$$\left(\frac{\partial u}{\partial x}\right)_{i,j} = \frac{u_{i,j} - u_{i-1,j}}{\Delta x}$$

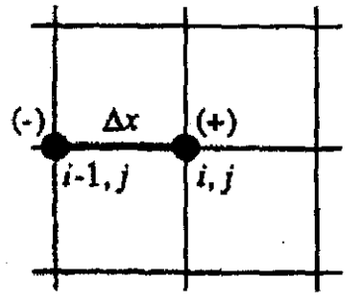

Figure C.3: An example of a first derivative approximated as a first-order rearward finite difference with respect to x for an arbitrary variable u [95AN1].

Where the fill dimensions are non-dimensional, equations (C.7), (C.8), (C.15) and (C.16) respectively become

$$\frac{\partial G_w}{\partial \eta} = -G_a \frac{h_d a_{fi}}{G_a}(w_{sw} - w) \tag{C.21}$$

$$\frac{\partial w}{\partial \xi} = \frac{h_d a_{fi}}{G_a}(w_{sw} - w) \tag{C.22}$$

$$\frac{\partial i_{ma}}{\partial \xi} = \frac{h_d a_{fi}}{G_a}\left[i_{masw} - i_{ma} + \left(Le_f - 1\right)\left\{i_{masw} - i_{ma} - i_v\left(w_{sw} - w\right)\right\}\right] \tag{C.23}$$

$$\frac{\partial T_w}{\partial \eta} = \frac{1}{c_{pw}}\frac{G_a}{G_w}\frac{h_d a_{fi}}{G_a}\left[\begin{array}{l}\left(w_{sw} - w\right)c_{pw}T_w - \left(i_{masw} - i_{ma}\right) - \\ \left(Le_f - 1\right)\left[i_{masw} - i_{ma} - \left(w_{sw} - w\right)i_v\right]\end{array}\right] \tag{C.24}$$

where $\xi = x/L_x$ and $\eta = z/L_z$ with L_x and L_z the fill lengths in the x and z directions respectively.

Figure C.4 illustrates an excerpt of four grid points from the conputational grid in figure C.2 for generalized non-dimentional coordinates. It is essential that the fill is divided into equal intervals in both the horizontal and vertical directions for the non-dimensional fill analysis and thus is $\Delta\eta = \Delta\xi$.

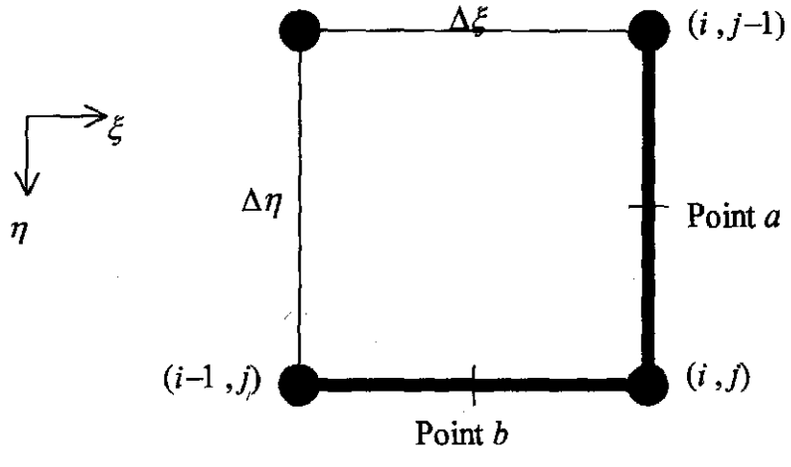

Figure C.4: Four generalized grid points of one cell of a crossflow fill.

By applying first-order rearward differences and letting $Me_\xi = h_d a_{fi}\Delta\xi/G_a \quad = h_d a_{fi}\Delta\eta/G_a$, equations (C.7), (C.8), (C.15) and (C.16) respectively become

$$G_{w(i,j)} = G_{w(i,j-1)} - G_a Me_\xi (w_{sw} - w)\Big|_a \tag{C.25}$$

$$w_{(i,j)} = w_{(i-1,j)} + Me_\xi (w_{sw} - w)\Big|_b \tag{C.26}$$

$$i_{ma(i,j)} = i_{ma(i-1,j)} + Me_\xi\left[i_{masw} - i_{ma} + \left(Le_f - 1\right)\left\{i_{masw} - i_{ma} - i_v\left(w_{sw} - w\right)\right\}\right]_b \tag{C.27}$$

$$T_{w(i,j)} = T_{w(i,j-1)} + \frac{1}{c_{pw}}\frac{G_a}{G_w}Me_\xi\left[\begin{array}{l}\left(w_{sw} - w\right)c_{pw}T_w - \left(i_{masw} - i_{ma}\right) - \\ \left(Le_f - 1\right)\left[i_{masw} - i_{ma} - \left(w_{sw} - w\right)i_v\right]\end{array}\right]\Bigg|_a \tag{C.28}$$

The $|_a$ and $|_b$ symbols in the last terms in equations (C.25) to (C.28) refer to point a and b respectively in figure C.4. Point a refers to the average value of the last term of equation (C.25) or (C.28) between points (i, j) and $(i, j-1)$ while point b refers to the average value of the last term of equation (C.26) or (C.27) between points (i, j) and $(i-1, j)$. Take for example the average value of the last term of equation (C.28) between points (i, j) and $(i, j-1)$, i.e.,

$$\frac{1}{c_{pw}}\frac{G_a}{G_w}Me_\xi\left[(w_{sw}-w)c_{pw}T_w-(i_{masw}-i_{ma})-(Le_f-1)\left[i_{masw}-i_{ma}-(w_{sw}-w)i_v\right]\right]_a =$$

$$\frac{Me_\xi G_a}{2}\left[\frac{1}{c_{pw(i,j)}G_{w(i,j)}}\left[(w_{sw(i,j)}-w_{(i,j)})c_{pw(i,j)}T_{w(i,j)}-(i_{masw(i,j)}-i_{ma(i,j)})-(Le_{f(i,j)}-1)\left[i_{masw(i,j)}-i_{ma(i,j)}-(w_{sw(i,j)}-w_{(i,j)})i_{v(i,j)}\right]\right]+\frac{1}{c_{pw(i,j-1)}G_{w(i,j-1)}}\left[(w_{sw(i,j-1)}-w_{(i,j-1)})c_{pw(i,j-1)}T_{w(i,j-1)}-(i_{masw(i,j-1)}-i_{ma(i,j-1)})-(Le_{f(i,j-1)}-1)\left[i_{masw(i,j-1)}-i_{ma(i,j-1)}-(w_{sw(i,j-1)}-w_{(i,j-1)})i_{v(i,j-1)}\right]\right]\right] \quad \text{(C.29)}$$

where G_a and Me_ξ are constant throughout the solution domain. Equation (C.29) can be substituted into equation (C.28) to obtain the value of $T_{w(i,j)}$. Equations (C.25) to (C.27) are treated in a similar manner to obtain average values for the last terms of these equations.

The governing partial differential equations are solved by an iterative technique. G_w and T_w are known at the water inlet side. i_{ma} and w are known at the air inlet side. G_a is constant throughout the solution domain. Equations (C.25) and (C.28) are used to solve respectively for G_w and T_w at the air inlet side while equations (C.26) and (C.27) are used to solve for w and i_{ma} at the water inlet side. Equations (C.25) to (C.28) can be solved simultaneously throughout the rest of the domain. All of the other variables in equations (C.25) to (C.28) are functions of T_w, G_w, i_{ma} and w.

If the air is supersaturated at a point in the fill, the governing equations for supersaturated air must be solved instead of the equations for unsaturated air.

The mean water outlet temperature can be obtained by integrating the water temperature values at the water outlet side of the fill, i.e.,

$$T_{wom}=\frac{1}{n_\xi}\int_0^{n_\xi}T_{wo}\,d\xi \quad \text{(C.30)}$$

where n_ξ is the number of fill intervals in the ξ or x direction

The mean outlet air enthalpy and humidity can be obtained by integrating these values at the air outlet side of the fill, i.e.,

$$i_{maom}=\frac{1}{n_\eta}\int_0^{n_\eta}i_{mao}\,d\eta \quad \text{(C.31)}$$

$$w_{om} = \frac{1}{n_\eta} \int_0^{n_\eta} w_o d\eta \tag{C.32}$$

where n_η is the number of fill intervals in the η or z direction

Me_ξ in equations (C.25) to (C.28) can be referred to as the local Merkel number according to the air stream in the horizontal direction where

$$Me_\xi = h_d a_{fi} \Delta\xi / G_a = h_d a_{fi} \Delta\eta / G_a \tag{C.33}$$

At every point in the solution domain the local Merkel number according to the water stream is determined by

$$Me_{\eta(i,j)} = \frac{G_a}{G_{w(i,j)}} Me_\xi \tag{C.34}$$

The Merkel number for the fill, *Me*, is obtained by integrating $Me_{\eta(i,j)}$ across the entire fill. Firstly, determine the average of the $Me_{\eta(i,j)}$ quantities at the center of each cell of the entire fill.

The mean Merkel number, $Me_{\eta m(i,j)}$, at the cell center is calculated from figure C.5 as follows,

$$Me_{\eta m(i,j)} = \left(Me_{\eta(i,j)} + Me_{\eta(i+1,j)} + Me_{\eta(i,j+1)} + Me_{\eta(i+1,j+1)}\right)/4 \tag{C.35}$$

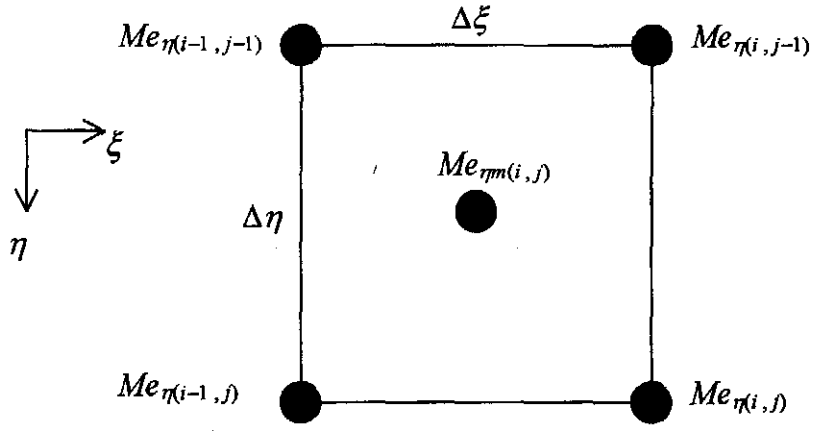

Figure C.5: Average value of $Me_{\eta(i,j)}$ at the cell center.

The mean quantity of all the $Me_{\eta m(i,j)}$ values is donated by Me_m where

$$Me_m = \frac{\sum Me_{\eta m(i,j)}}{n_\xi n_\eta} \tag{C.36}$$

The Merkel number of the fill is given by

$$Me = \frac{h_d a_{fi} L_z}{G_w} = \frac{h_d a_{fi} n_\eta \Delta\eta}{G_w} = n_\eta Me_m \tag{C.37}$$

where $L_z = n_\eta \Delta\eta$

The Merkel number for a crossflow fill is determined from experimental data by the following approach. A value for Me_ξ is guessed. This value is constant throughout the computational domain. The water outlet temperature is determined by equation (C.30) after the governing equations have converged. Me_ξ is varied until the water outlet temperature from equation (C.30) matches the known water outlet temperature. The Merkel number is then determined by equation (C.37).

APPENDIX D

LOSS COEFFICIENTS AND TRANSFER CHARACTERISTICS

D.1 INTRODUCTION

The loss coefficients and transfer characteristics that are employed in the performance evaluation of wet-cooling towers are presented. Most of this section is abridged from Kröger [98KR1] where a detailed derivation and presentation of the information presented in this section can be found.

D.2 LOSS COEFFICIENTS

Frictional resistance, abrupt changes in cross section, inlets and outlets, amongst others, reduce the "mechanical energy" between any two sections of a duct. The mechanical energy is converted to thermal energy. The "mechanical energy" refers to the $p/\rho + \alpha_e v^2/2$ terms in the equation of the first law of thermodynamics, i.e.,

$$P+Q=m\left[\left(u_2+\frac{p_2}{\rho_2}+\frac{\alpha_{e2}v_2^2}{2}+gz_2\right)-\left(u_1+\frac{p_1}{\rho_1}+\frac{\alpha_{e1}v_1^2}{2}+gz_1\right)\right] \tag{D.1}$$

The subscripts 1 and 2 refer to a control volume between sections 1 and 2 respectively. P and Q respectively represent the power and the rate of heat input into the fluid.

A dimensionless loss coefficient, also referred to as the total pressure loss coefficient, can in general be defined between two cross-sections in a horizontal duct as

$$K=\frac{\left(\frac{p_1}{\rho_1}+\frac{\alpha_{e1}v_1^2}{2}\right)-\left(\frac{p_2}{\rho_2}+\frac{\alpha_{e2}v_2^2}{2}\right)}{v^2/2} \tag{D.2}$$

where v is usually based on conditions at either section 1 or 2. For incompressible and uniforms flow with $\alpha_e \approx 1$, equation (D.2) can be written as

$$K=\frac{p_{t1}-p_{t2}}{\rho v^2/2}=\frac{p_{t1}-p_{t2}}{\left(\frac{m}{A}\right)^2/(2\rho)} \tag{D.3}$$

where p_{t1} and p_{t2} are the total pressures at sections 1 and 2 respectively.

To simplify the solution process the loss coefficients are usually referred to the mean fill conditions by using the principle of the conservation of mass. Referred to the same conditions, the values of the loss coefficients can then be added. The relative magnitudes of the loss coefficients can then be observed. For example, refer the loss coefficient, at one set of conditions, to another set of conditions. These conditions are denoted by subscripts 1 and 2 in the following discussion. If the pressure drop is equal at both sets of conditions, find from equation (D.3),

$$\Delta p = K_1 \frac{\left(\frac{m_1}{A_1}\right)^2}{2\rho_1} = K_2 \frac{\left(\frac{m_2}{A_2}\right)^2}{2\rho_2} \tag{D.4}$$

It follows from equation (D.4) that the loss coefficient K_2 referred to the conditions at 1, is equal to

$$K_2 = K_1 \left(\frac{\rho_2}{\rho_1}\right)\left(\frac{m_1}{m_2}\right)^2\left(\frac{A_2}{A_1}\right)^2 \tag{D.5}$$

Loss coefficients are usually expressed by, empirical relations that are obtained from numerical or experimental work, or, directly as a value.

D.2.1 SPRAY REGION

Data presented by Cale [82CA1] suggests that the loss coefficient in the spray zone may be expressed approximately as

$$K_{sp} \approx L_{sp}\left[0.4\left(G_w / G_a\right)+1\right] \tag{D.6}$$

D.2.2 DRIFT ELIMINATOR, INLET LOUVERS

The loss coefficient of a drift eliminator is determined experimentally for each eliminator. A typical empirical relation for a drift eliminator loss coefficient is

$$K_{de} = a_{de} Ry_{de}^{b_{de}} \tag{D.7}$$

D.2.3 WATER DISTRIBUTION

Kröger [98KR1] gives an approximate for a water distribution system loss coefficient as $K_{wd} = 0.5$.

D.2.4 RAIN ZONE

According to De Villiers and Kröger [99DE1], the loss coefficient for a circular rain zone is given by

$$K_{rz} = 3a_v v_w \left(H_i / d_d\right) \left[\begin{array}{l} 0.2246 - 0.31467\, a_\rho \rho_a + 5263.04 a_\mu \mu_a \\ + 0.775526\left\{1.4824163 \exp\left(71.52 a_L d_d\right) - 0.91\right\} \\ \times \left\{0.39064 \exp\left(0.010912\, a_L d_i\right) - 0.17\right\} \\ \times \left\{2.0892\left(a_v v_{azo}\right)^{-1.3944} + 0.14\right\} \\ \times \exp\left[\begin{array}{l} \left\{0.8449 \ln\left(a_L d_i / 2\right) - 2.312\right\} \\ \times \left\{0.3724 \ln\left(a_v v_{azo}\right) + 0.7263\right\} \\ \times \ln\left\{206.757\left(a_L H_i\right)^{-2.8344} + 0.43\right\} \end{array}\right] \end{array}\right] \tag{D.8}$$

where

$$a_\mu = 3.061 \times 10^{-6}\left(\rho^4 g^9 / \sigma_w\right)^{0.25}$$

$$a_\rho = 998/\rho_w$$

$$a_v = 73.298\left(g^5\sigma_w^3/\rho_w^3\right)^{0.25}$$

$$a_L = 6.122\left(g\sigma_w/\rho_w\right)^{0.25}$$

The equation is valid under the following conditions:

$0°C \le T_a \le 40°C$; $10°C \le T_w \le 40°C$; $0.927\ kg/m^3 \le \rho_a \le 1.289\ kg/m^3$

$992.3\ kg/m^3 \le \rho_w \le 1000\ kg/m^3$; $1.717\times10^{-5}\ kg/ms \le \mu_a \le 1.92\times10^{-5}\ kg/ms$

$0.0696\ N/m \le \sigma_w \le 0.0742\ N/m$; $0.002\ m \le d_d \le 0.008\ m$; $9.7m/s^2 \le g \le 10\ m/s^2$

$30\ m \le d_i/2 \le 70\ m$; $4\ m \le H_i \le 12\ m$; $0.00075\ m/s \le v_w \le 0.003\ m/s$; $1\ m/s \le v_{azo} \le 3\ m/s$

The loss coefficient for a rectangular rain zone is given by

$$K_{rz} = 1.5a_v v_w\left(H_i/d_d\right)\times\left[\begin{array}{l}0.219164 - 0.30487a_\rho\rho_a + 8278.7a_\mu\mu_a \\ +0.954153\left\{0.328467\exp\left(135.7638a_L d_d\right)+0.47\right\} \\ \times\left\{26.28482\left(a_L H_i\right)^{-2.95729}+0.56\right\} \\ \times\exp\left\{\begin{array}{l}\ln\left(0.204814\exp\left(0.066518a_L W_i\right)+0.21\right) \\ \times\left(3.9186\exp\left(-0.3a_L H_i\right)\right) \\ \times\left(0.31095\ln\left(a_L d_d\right)+2.63745\right)\end{array}\right\} \\ \times\left\{2.177546\left(a_v v_{azo}\right)^{-1.46541}+0.21\right\}\end{array}\right] \quad (D.9)$$

where the range of applicability is the same as for the circular tower except that

$1\ m/s \le v_{azo} \le 5\ m/s$; $2\ m \le H_i \le 8\ m$; $4\ m \le W_i \le 40\ m$

D.2.5 TOWER INLET

For a round counterflow cooling tower with an isotropic fill (e.g. splash or trickle type fill) operating in the absence of a rain zone, the loss coefficient is according to De Villiers and Kröger [99DE1].

$$\begin{aligned}K_{ct(norz)} &= 0.011266\exp\left(0.093d_i/H_i\right)K_{fi}^2 - 0.3105\exp\left(0.1085d_i/H_i\right)K_{fi} \\ &\quad -1.7522 + 4.5614\exp\left(0.131d_i/H_i\right) \\ &\quad +\sin^{-1}\left[\begin{array}{l}\left\{\left(10970.2\exp\left(-0.2442K_{fi}\right)+1391.3\right)/\left(d_i/H_i-15.7258\right)\right\} \\ +1205.54\exp\left(-0.23K_{fi}\right)+109.314 \\ \times\left\{2r_i/d_i - 0.01942/\left(d_i/H_i-27.929\right)-0.016866\right\}\end{array}\right]\end{aligned} \quad (D.10)$$

which is valid for $7.5 \le d_i/H_i \le 15$, $5 \le K_{fi} \le 25$ and $0 \le r_i/d_i \le 0.02$. K_{fi} in this case is the sum of the loss coefficients in the vicinity of the fill.

This value must be multiplied by the correction factor C_{rz} as given by equation (D.11) to obtain the correct inlet loss coefficient in the presence of a rain zone.

$$C_{rz} = \begin{bmatrix} 0.2394 + 80.1\{0.0954/(d_i/H_i) + d_d\}\exp(0.395G_w/G_a) \\ -0.3195(G_w/G_a) - 966\{d_d/(d_i/H_i)\}\exp(0.686G_w/G_a) \end{bmatrix} \times (1 - 0.06825G_w)K_{fi}^{0.09667}\exp\{8.7434(1/d_i - 0.01)\} \quad (D.11)$$

This correction factor is valid in the range $7.5 \le d_i/H_i \le 20$, $5 \le K_{fi} \le 25$, $3 \le d_d \le 6$ mm, $1 \le G_w \le 3$ kg/m^{2}s, $1.2 \le G_a \le 3.6$ kg/m^{2}s and $80 \le d_i \le 120$ m.

The tower inlet loss coefficient in the presence of a rain zone is given by

$$K_{ct} = C_{rz}K_{ct(norz)} \quad (D.12)$$

The inlet loss coefficient in isotropically packed induced draft rectangular towers is according to De Villiers and Kröger [99DE1],

$$K_{ct(norz)} = 0.2339 + \left(3.919\times10^{-3}K_{fi}^2 - 6.840\times10^{-2}K_{fi} + 2.5267\right) \times \exp\left\{\frac{W_i}{H_i}\left(0.5143 - 0.1803\times\exp\{0.0163K_{fi}\}\right)\right\} - \sinh^{-1}\left[2.77\times\exp\left\{0.958\frac{W_i}{H_i}\right\}\times\exp\left\{K_{fi}\left(2.457 - 1.015\frac{W_i}{H_i}\right)\times10^{-2}\right\}\times\left(\frac{r_i}{W_i} - 0.013028\right)\right] \quad (D.13)$$

De Villiers and Kröger [99DE1] states that it becomes acceptable to ignore the inlet loss correction factor for the rain zone in cases where $W_i/H_i \le 3$. In this case, $W_i/H_i = 3$, which means that $K_{ct} = K_{ct(norz)}$. Where the correction factor for a rectangular tower is needed, the following empirical correlation provides the required value,

$$C_{rz} = 1 - G_w\left[0.123 - 12.1d_d - 272.26d_d^2 + 5.04\times10^{-4}\times\exp\left\{0.466\frac{W_i}{H_i}\right\}\right] \times \left(1 - 1.16\times10^{-3}\times\exp\{G_a\}\right) \quad (D.14)$$

and is valid for $3 \le W_i/H_i \le 7.5$ m, $3 \le d_d \le 6$ mm, $1 \le G_w \le 3$ kg/m^{2}s and $2 \le G_a \le 6$ kg/m^{2}s. This equation can only be used with any degree of confidence at high W_i/H_i values and since this is not normally the case, it becomes prudent to take the conservative approach by ignoring the influence of the rain zone loss on the inlet loss.

D.2.6 TOWER SUPPORTS

The loss coefficient due to the tower supports, based on the drag coefficient of the particular support geometry is given approximately as

$$K_{tsfi} = \frac{C_{dts}L_{ts}d_{ts}n_{ts}A_{fr}^2}{(\pi d_i H_i)^3} \quad (D.15)$$

D.2.7 EXPANSION LOSSES

The expansion loss coefficient after the fill, referred to the mean conditions through the fill, is given by

$$K_{cte} = (1-\sigma_e)^2 \tag{D.16}$$

where $\sigma_e = A_{fr}/A_i$ is the expansion area ratio.

D.2.8 FILL LOSSES

The losses through the fill are usually expressed as an empirical relation of one of the following forms.

$$K_{fdm} = a_p L_{fi} G_w^{\ b_p} G_a^{\ c_p} \tag{D.17}$$

$$K_{fdm} = L_{fi}\left(a_p\left[\frac{G_w}{G_a}\right]+b_p\right) \tag{D.18}$$

where a_p, b_d and c_d are coefficients specified for each fill.

The actual fill loss coefficient applicable to the cooling tower is then given by

$$K_{fi} = K_{fdm} + \left(\frac{G_{avo}^2}{\rho_{avo}} - \frac{G_{avi}^2}{\rho_{avi}}\right) \Big/ \frac{G_{avm}^2}{\rho_{avm}} \tag{D.19}$$

where $1/\rho_{avm} = 0.5(1/\rho_{avi}+1/\rho_{avo})$ and $G_{avm} = (G_{avi}+G_{avo})/2$

D.2.9 OTHER LOSS COEFFICIENTS

In addition to the above mentioned losses are there also other losses, for example, contraction losses and losses due to the fill supports. In mechanical draft cooling towers there are also fan upstream and downstream losses, plenum losses and diffuser losses. The loss coefficients for these cases can either be specified or obtained from empirical relations in the literature.

D.3 TRANSFER CHARACTERISTICS

The total transfer characteristic of a wet-cooling tower consists of the transfer characteristics for the fill, spray zone and rain zone.

D.3.1 RAIN ZONE

The transfer characteristic or Merkel number in the rain zone of a circular cooling tower is given by [97DE1],

$$\frac{h_{drz}a_{rz}H_i}{G_w} = 12\left(\frac{D}{v_{azo}d_d}\right)\left(\frac{H_i}{d_d}\right)\left(\frac{p_a}{\rho_w R_v T_a}\right)Sc^{0.33}\left[\ln\left(\frac{w_s+0.622}{w+0.622}\right)/(w_s+0.622)\right]\times$$

$$\left[0.90757a_\rho\rho_a - 30341.04a_\mu\mu_a - 0.37564 + 4.04016\left[\begin{array}{l}\{0.55+41.7215(a_L d_d)^{0.80043}\}\{0.713+3.741(a_L H_i)^{-1.23456}\} \\ \times\{3.11\exp(0.15a_v v_{azo})-3.13\} \\ \times\exp\left[\begin{array}{l}\{5.3759\exp(-0.2092a_L H_i)\} \\ \times\ln\{0.3719\exp(0.0019055a_L d_i)+0.55\}\end{array}\right]\end{array}\right]\right] \tag{D.20}$$

where the range of applicability is the same as for K_{rz} in equation (D.8). D is given by equation (D.21) where $M_a = 28.97$ and $V_a = 29.9$ for air, while for water vapor $V_v = 18.8$ and $M_v = 18.016$.

$$D = 0.04357T^{1.5}\frac{(1/M_a + 1/M_v)^{0.5}}{p\left[V_a^{0.333} + V_v^{0.333}\right]^2} \tag{D.21}$$

The equation for the rain zone Merkel number in a rectangular tower is,

$$\frac{h_{drz}a_{rz}H_i}{G_w} = 3.6\left(\frac{D}{v_{azo}d_d}\right)\left(\frac{H_i}{d_d}\right)\left(\frac{p_a}{\rho_w R_v T_a}\right)Sc^{0.33}\left[\ln\left(\frac{w_s + 0.622}{w + 0.622}\right)/(w_s - w)\right]$$

$$\times\left[\begin{array}{l} 4.68851a_p\rho_a - 187128.7a_\mu\mu_a - 2.29322 \\ + 22.4121\left\{0.350396(a_v v_{azo})^{1.38046} + 0.09\right\}\left\{1.60934(a_L H_i)^{-1.12083} + 0.66\right\} \\ \times\left\{34.6765(a_L d_d)^{0.732448} + 0.45\right\} \\ \times\exp\left\{7.7389\exp(-0.399827a_L H_i)\ln\left\{\begin{array}{l}0.087498\exp(0.026619a_L W_i)\\ +0.85\end{array}\right\}\right\} \end{array}\right] \tag{D.22}$$

The range of applicability for equation (D.22) is the same as that for equation (D.9).

D.3.3 SPRAY ZONE

The data of Lowe and Christie [61LO1] can be correlated to give

$$\frac{h_{dsp}a_{sp}L_{sp}}{G_w} = 0.2L_{sp}\left(\frac{G_a}{G_w}\right)^{0.5} \tag{D.23}$$

D.3.4 FILL

The transfer characteristic of the fill is usually expressed as an empirical relation of one of the following forms.

$$\frac{h_{dfi}a_{fi}L_{fi}}{G_w} = a_d L_{fi} G_w{}^{b_d} G_a{}^{c_d} \tag{D.24}$$

$$\frac{h_{dfi}a_{fi}L_{fi}}{G_w} = a_d L_{fi}(G_w/G_a)^{b_d} \tag{D.25}$$

where a_d, b_d and c_d are coefficients specified for each fill.

APPENDIX E

EFFECT OF ATMOSPHERIC CONDITIONS ON THE OPERATION OF COOLING TOWERS

E.1 INTRODUCTION

The atmospheric conditions prevailing in the region of a cooling tower affect the operation and performance of a cooling tower. An atmospheric temperature inversion, for example, reduces the performance of cooling towers. This is because the effective temperature of the air entering the cooling tower is higher than during conditions where the adiabatic lapse rate prevails, and the potential driving force or pressure differential is less. The formulas for calculating the pressure differential and the approximate effective air inlet temperature are derived in this appendix for various atmospheric temperature and humidity profiles.

E.2 EFFECT ON TOWER DRAFT

In it's simplest form the draft equation of a cooling tower can be expressed as

$$\Delta p_o - \Delta p_i = \Sigma K \, \rho v^2/2 \tag{E.1}$$

where Δp_o is the pressure differential outside the tower and Δp_i is the corresponding pressure differential inside the tower. The effect of the atmosphere on the draft equation will be evident from the pressure difference external to the tower, Δp_o , where Δp_o is equal to

$$\Delta p_o = p_1 - p_7 \tag{E.2}$$

where p_1 and p_7 refer to the atmospheric pressure at points 1 and 7 respectively shown in figure E.1. Point 6 is on the inside of the tower shell at the same elevation as point 7.

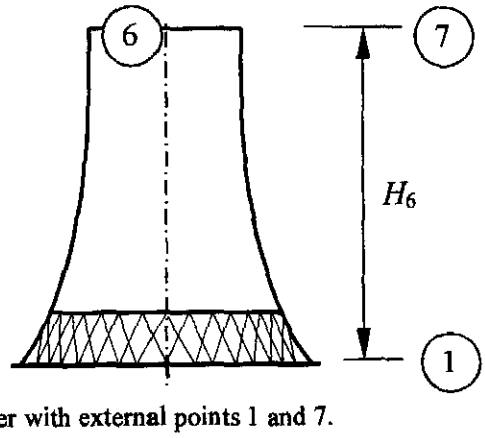

Figure E.1: Natural draft cooling tower with external points 1 and 7.

The pressure gradient in a gravity field is given by

$$\frac{dp}{dz} = -\rho_{av} g \tag{E.3}$$

The density of mixtures of air and water vapor is given by equation (A.3.1),

$$\rho_{av} = (1+w)\left(1-\frac{w}{w+0.62198}\right)\frac{p}{RT} \quad \approx 0.622\frac{(w+1)}{(w+0.622)}\frac{p}{RT} \tag{E.4}$$

Substitute equation (E.4) into equation (E.3) and find after rearrangement

$$\frac{dp}{p} = -\frac{0.622(w+1)}{(w+0.622)}\frac{g}{R}\frac{dz}{T} \tag{E.5}$$

The pressure difference between ground level and an arbitrary elevation z can be obtained by integrating equation (E.5) between these two points. After rearrangement find

$$p = p_1 \exp\left(-\frac{0.622 \cdot g}{R}\int_0^z \frac{(w+1)}{(w+0.622)}\frac{dz}{T}\right) \tag{E.6}$$

Equation (E.6) can be solved if the humidity and temperature profiles as a function of the altitude, z, are known. Refer to appendix M for a detailed discussion on atmospheric humidity. Refer to appendix L for a detailed discussion on the temperature profile during nocturnal inversions.

Kröger [98KR1] shows that temperature distribution for moist air of constant humidity is,

$$T = T_1 - \frac{0.00975(1+w)}{(1+1.9w)}z \tag{E.7}$$

Assume that the humidity ratio is constant at w_1 and substitute equation (E.7) into equation (E.6) to find upon integration between ground level and H_6 with $g = 9.8$ m/s^2 and $R = 287.08$ J/kg K that

$$p_7 = p_1\left(1-\frac{0.00975(1+w_1)H_6}{(1+1.9w_1)T_1}\right)^{\frac{2.1778(1+1.9w_1)}{w_1+0.62198}} \tag{E.8}$$

The pressure difference between points 1 and 7 from equation (E.8) is,

$$p_1 - p_7 = p_1\left[1-\left(1-\frac{0.00975(1+w_1)H_6}{(1+1.9w_1)T_1}\right)^{\frac{2.1778(1+1.9w_1)}{w_1+0.62198}}\right] \tag{E.9}$$

If it is assumed that the air is dry, with respect to both the temperature and the humidity profiles, i.e. $w_1 = 0$, equation (E.8) can be simplified to give

$$p_7 = p_1\left(1-0.00975\ H_6/T_1\right)^{3.5} \tag{E.10}$$

The corresponding pressure difference between points 1 and 7 from equation (E.10) is,

$$p_1 - p_7 = p_1\left[1-\left(1-0.00975\ H_6/T_1\right)^{3.5}\right] \tag{E.11}$$

The pressure difference between points 1 and 7 in figure E.1 can also be derived if it is assumed that the air temperature profile corresponds to a dry adiabatic lapse rate and that the atmospheric humidity is constant at w_1. The temperature profile for a dry adiabatic lapse rate is given by

$$T = T_1 - 0.00975z \tag{E.12}$$

Substitute w_1 and equation (E.12) into equation (E.6). After integration between ground level and H_6, and after rearrangement find

$$p_7 = p_1\left(1 - 0.00975\ H_6 / T_1\right)^{\frac{2.1778(1+w_1)}{w_1+0.62198}} \tag{E.13}$$

The corresponding pressure difference external to the tower is,

$$p_1 - p_7 = p_1\left[1 - \left(1 - 0.00975\ H_6 / T_1\right)^{\frac{2.1778(1+w_1)}{w_1+0.62198}}\right] \tag{E.14}$$

The temperature profile in a temperature inversion, discussed in appendix L, can be expressed as

$$T = (T_r + 273.15)\left(\frac{z}{z_r}\right)^b \tag{E.15}$$

where T_r is in °C and the exponent, b, is given by

$$b = 0.0035\sin(0.0177 \cdot n_d - 2.32392) + 0.0065 \tag{E.16}$$

where n_d is the number of the day of the year (n_d = 1 on the first of January). Equation (E.16) is developed in appendix L from experimental measurements.

If it is assumed that the humidity ratio is constant, substitute w_1 and equation (E.15) into equation (E.6). After integration between ground level and H_6 find,

$$p_7 = p_1 \exp\left[-0.021232\frac{(w_1+1)z_r^b H_6^{1-b}}{(w_1+0.622)(T_r+273.15)(1-b)}\right] \tag{E.17}$$

If the height of the inversion, z_{it}, is higher than the tower height, H_6, then the pressure difference between points 1 and 7 in figure E.1 is

$$p_1 - p_7 = p_1\left(1 - \exp\left[-0.021232\frac{(w_1+1)z_r^b H_6^{1-b}}{(w_1+0.622)(T_r+273.15)(1-b)}\right]\right) \tag{E.18}$$

If the top of the inversion is lower than the tower height then the pressure at the inversion top is given by

$$p_{it} = p_1 \exp\left[-0.021232\frac{(w_1+1)z_r^b z_{it}^{1-b}}{(w_1+0.622)(T_r+273.15)(1-b)}\right] \tag{E.19}$$

where p_{it} is the pressure at the inversion top at elevation z_{it}.

Assuming a constant humidity ratio w_1 for both the temperature and the humidity profiles from the top of the inversion to an elevation corresponding to the top of the cooling tower, find the pressure at this latter elevation

$$p_7 = p_{it}\left(1 - \frac{0.00975(1+w_1)(H_6 - z_{it})}{(1+1.9w_1)T_{it}}\right)^{\frac{2.1778(1+1.9w_1)}{w_1+0.62198}} \tag{E.20}$$

where p_{it} is given by equation (E.19) and T_{it} is given from equation (E.15) by

$$T_{it} = (T_r + 273.15)\left(\frac{z_{it}}{z_r}\right)^b \tag{E.21}$$

where T_r is in °C.

z_{it} in the equations above is still unknown and can be determined by referring to appendix L. If the humidity is not assumed to be constant or zero, but expressed as a function of the height above ground level, then equation (E.6) has generally to be solved by numerical integration techniques.

E.3 EFFECT ON THE EFFECTIVE AIR INLET TEMPERATURE

The height of the air drawn into a cooling tower, H_r, is constant at radial distances not close to the cooling tower, as shown in figure E.2. Refer to appendix N for a discussion on this statement.

The temperature of the air flowing from below the inversion top, z_{it}, into the cooling tower taking into consideration adiabatic compression is given by

$$T_{bit} = (T_r + 273.15)\left(\frac{z}{z_r}\right)^b + 0.00975z\left(1 - \frac{H_3}{H_r}\right) \tag{E.22}$$

where H_3 and H_r are shown in figure E.2.

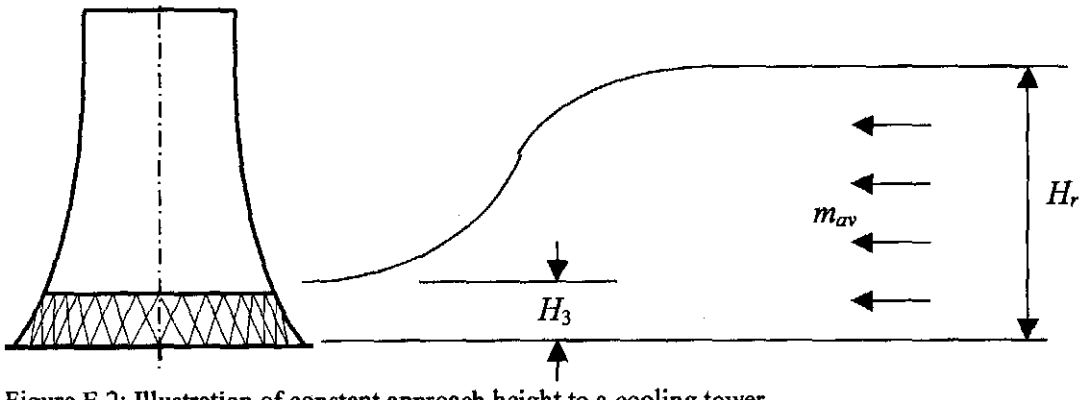

Figure E.2: Illustration of constant approach height to a cooling tower.

The air originally from a region above the inversion top enters the cooling tower at

$$T_{ait} = T_{it} - 0.00975(z - z_{it}) + 0.00975z\left(1 - \frac{H_3}{H_r}\right) \tag{E.23}$$

The last term in equation (E.22) and (E.23) accounts for the heating of the air due to adiabatic compression.

The mean effective inlet temperature to the cooling tower is thus the integral of equation (E.22) and equation (E.23) up to a height of H_r if $z_{it} < H_r$.

$$T_{aim} = \int_0^{H_r} \frac{(T_{bit} - T_{ait})}{H_r} dz = \int_0^{z_{it}} \left[(T_r + 273.15)\left(\frac{z}{z_r}\right)^b + 0.00975z\left(1 - \frac{H_3}{H_r}\right)\right]\frac{dz}{H_r}$$
$$+ \int_{z_{it}}^{H_r} \left[T_{it} - 0.00975(z - z_{it}) + 0.00975z\left(1 - \frac{H_3}{H_r}\right)\right]\frac{dz}{H_r} \tag{E.24}$$

Substitute equation (E.21) into equation (E.24) and find after integration and rearrangement,

$$T_{aim} = (T_r + 273.15)\left(\frac{z_{it}}{z_r}\right)^b \left[\frac{1}{b+1}\left(\frac{z_{it}}{H_r}\right) + \frac{H_r - z_{it}}{H_r}\right] + 0.00975\left[z_{it} - \frac{z_{it}^2}{2H_r} - \frac{H_3}{2}\right] \quad \text{(E.25)}$$

If $z_{it} > H_r$ then equation (E.24) reduces to

$$T_{aim} = \int_0^{H_r} \frac{T_{bit}}{H_r} dz = \int_0^{H_r} \left[(T_r + 273.15)\left(\frac{z}{z_r}\right)^b + 0.00975z\left(1 - \frac{H_3}{H_r}\right)\right] \frac{dz}{H_r} \quad \text{(E.26)}$$

After integration of equation (E.26), find

$$T_{aim} = (T_r + 273.15)\left(\frac{H_r}{z_r}\right)^b \left(\frac{1}{b+1}\right) + 0.00975\left(\frac{H_r}{2}\right)\left(1 - \frac{H_3}{H_r}\right) \quad \text{(E.27)}$$

E.4 CONCLUSION

Equations are derived that predict the effects of atmospheric temperature and humidity on the draft through natural draft cooling towers. Equations are also derived that determine the temperature at the inlet of cooling towers during nocturnal temperature inversions.

APPENDIX F

LEWIS FACTOR

F.1 INTRODUCTION

It can be seen in appendix B that the Lewis factor, Le_f, appears in the governing equations of the heat and mass transfer processes in a wet-cooling tower. Merkel assumed that the Lewis factor is equal to 1 to simplify the governing equations while Poppe used the equation of Bosnjakovic [65BO1] to express the Lewis factor in his more rigorous approach. The Lewis factor and its relation to the Lewis number are investigated in this appendix.

F.2 LEWIS NUMBER

The rate equation for momentum transfer is given by Newton's law of viscosity, i.e.,

$$\frac{F}{A} = -\mu\frac{\partial v}{\partial y} = -\upsilon\frac{\partial(\rho v)}{\partial y} \tag{F.1}$$

The rate equation for heat or energy transfer is given by Fourier's law of heat conduction,

$$\frac{Q}{A} = -k\frac{\partial T}{\partial y} = -\alpha\frac{\partial(\rho c_p T)}{\partial y} \tag{F.2}$$

The rate equation for mass transfer is given by Fick's law of diffusion, i.e.,

$$\frac{m}{A} = -D\frac{\partial c}{\partial y} \tag{F.3}$$

The coefficients υ, α and D in equations (F.1), (F.2) and (F.3) respectively have dimensions of $[L^2/T]$. Any ratio of two of these coefficients will result in a dimensionless number. In systems undergoing simultaneous convective heat and momentum transfer, the ratio of υ to α would be of importance and is defined as the Prandtl number, i.e.,

$$Pr = \frac{\upsilon}{\alpha} = \frac{c_p\mu}{k} \tag{F.4}$$

In processes involving simultaneous momentum and mass transfer the Schmidt number is defined as the ratio of υ to D, i.e.,

$$Sc = \frac{\upsilon}{\alpha} = \frac{c_p\mu}{k} \tag{F.5}$$

In processes involving simultaneous convective heat and mass transfer, the ratio of α to D is defined as the Lewis number, i.e.,

$$Le = \frac{\alpha}{D} = \frac{k}{\rho c_p D} = \frac{Sc}{Pr} \tag{F.6}$$

From equation (F.6) can it be seen that the Lewis number is equal to the ratio of the Schmidt to the Prandtl number and is relevant to simultaneous convective heat and mass transfer. The relative rate of

growth of the thermal and concentration boundary layers are determined by the Lewis number. The temperature and concentration profiles will coincide when Le = 1. Mills [95MI1] states that other definitions of the Lewis number are found in the literature, for example, the ratio of the Prandtl to the Schmidt number and the ratio of the heat to mass transfer conductance.

The values of k, ρ and c_p in equation (F.6) can be determined by the equations in appendix A. According to Mills [95MI1] the diffusion coefficient, D, for air-water vapor mixtures can be given by

$$D = 1.97 \times 10^{-5} \left(\frac{p_0}{p} \right) \left(\frac{T}{T_0} \right)^{1.685} \tag{F.7}$$

where p_0 = 101325 Pa and T_0 = 256 K. Equation (F.7) is valid under the following condition, 273 K < T < 373 K.

F.3 LEWIS FACTOR

In addition to the Lewis number the Lewis factor can be defined. In some references the Lewis factor is referred to as the Lewis relation [91FE1, 95MI1, 99HA1]. The Lewis factor is an indication of the relative rates of heat and mass transfer in an evaporative process. In some of the literature encountered there seems to be confusion about the definitions of these dimensionless numbers and the Lewis factor is often incorrectly referred to as the Lewis number.

The Lewis factor, Le_f, is equal to the ratio of the heat transfer Stanton number, St, to the mass transfer Stanton number, St_m where

$$St = \frac{Nu}{RePr} = \frac{h}{\rho v c_p} \tag{F.8}$$

$$St_m = \frac{Sh}{ReSc} = \frac{h_d}{\rho v} \tag{F.9}$$

The Lewis factor can be obtained by dividing equation (F.8) by equation (F.9), i.e.,

$$Le_f = \frac{St}{St_m} = \frac{h}{\rho v c_p} \cdot \frac{\rho v}{h_d} = \frac{h}{c_p h_d} \tag{F.10}$$

Lewis [22LE1] tried to prove analytically that Le_f = 1 for gas/liquid systems. In a later article Lewis [33LE1] stated that the relation, Le_f = 1, holds approximately for air/water mixtures but not for all mixtures of liquid and gas. Although the proof given by Lewis was incorrect [88DR1] the ratio $h/c_p h_d$ is today known as the Lewis factor.

In chemical engineering practice, the analogy between convective heat and mass transfer is widely used in a form recommended by Chilton and Colburn in 1934, namely,

$$\frac{St}{St_m} = \left(\frac{Pr}{Sc}\right)^{-\frac{2}{3}} \tag{F.11}$$

The Chilton-Colburn relation is of adequate accuracy for most external forced flows [95MI1].

Equation (F.11) is obtained for laminar forced flow from the Chilton-Colburn analogy power law relations, i.e.,

$$St = C \cdot Re^{-\frac{1}{2}} Pr^{-\frac{2}{3}} = \frac{h}{\rho v c_p} \tag{F.12}$$

$$St_m = C \cdot Re^{-\frac{1}{2}} Sc^{-\frac{2}{3}} = \frac{h_d}{\rho v} \tag{F.13}$$

Thus,

$$Le_f = \left(\frac{Pr}{Sc}\right)^{-\frac{2}{3}} = Le^{\frac{2}{3}} \tag{F.14}$$

Bourillot [83BO2] states that the Lewis number is not constant and is tied to the nature of the vapor-gas mixture. It also depends on the nature of the boundary layer near the exchange surfaces and the thermodynamic state of the mixture [83BO2, 94GR1]. Bosnjakovic pointed out that the mass transfer is not proportional to the difference ($w_{sw} - w$). A corrector term, $F(\xi)$, is applied to equation (F.14) and the expression for Le_f in the Bosnjakovic form is obtained.

$$Le_f = Le^{\frac{2}{3}} \frac{1}{F(\xi)} \tag{F.15}$$

where

$$F(\xi) = \frac{\ln \xi}{\xi - 1} \text{ and } \xi = \frac{w_{sw} + 0.622}{w + 0.622}$$

Poppe and Rögener cited that the Lewis factor, Le_f, is according to the Bosnjakivic form,

$$Le_f = 0.865^{\frac{2}{3}} \frac{\frac{w_{sw} + 0.622}{w + 0.622} - 1}{\ln\left(\frac{w_{sw} + 0.622}{w + 0.622}\right)} \tag{F.16}$$

where the Lewis number, Le, is taken constant at 0.865. Bourillot [83BO1] and Grange [94GR1] state that the Lewis factor for a wet-cooling tower, using equation (F.16), is approximately 0.92.

Merkel [25ME1] assumed in his classical work on evaporation that $Le_f = 1$. Häszler [99HA1] cited that other researchers showed that the assumption of Merkel is not correct and that all of the researchers find Lewis factors in the range from 0.6 to 1.3. An analysis of both splash and film packings by Feltzin and Benton [91FE1] indicates that for counterflow towers a Lewis factor of 1.25 is more appropriate. According to Feltzin and Benton [91FE1] the Lewis number does not appear to be dependent on whether the packing is splash type or film type, but only on the configuration (i.e. counterflow or crossflow). Sutherland [83SU1] used a Lewis factor of 0.9 in his "accurate" tower analysis. Osterle [91OS1]

developed a wet-cooling tower model that corrects the Merkel [25ME1] assumption so that the mass of water lost by evaporation is accounted for. However, he still assumes that the Lewis factor is equal to unity.

Häszler [99HA1] states that when the humidity potential ($w_{sw} - w$) is large, equation (F.14) is not valid any more. Figure F.1 illustrates the Lewis factor as a function of the dimensionless vapor pressure gradient, Pg, defined by equation (F.17). The dimensionless vapor pressure gradient is a measure of the degree of supersaturation in the boundary layer. If $Pg < 1$ then there is no mist in the boundary layer. If $Pg > 1$ then mist is present in the boundary layer. Häszler [99HA1] gives a detailed account for the derivation of the dimensionless vapor pressure gradient, i.e.,

$$Pg = \left(\frac{dp_s}{T_a}\right)_0 \frac{(1+0.622w_0)}{0.622p_a} \frac{T_{a0} - T_a}{w_0 - w} \tag{F.17}$$

where the subscript 0 refers to the water film surface.

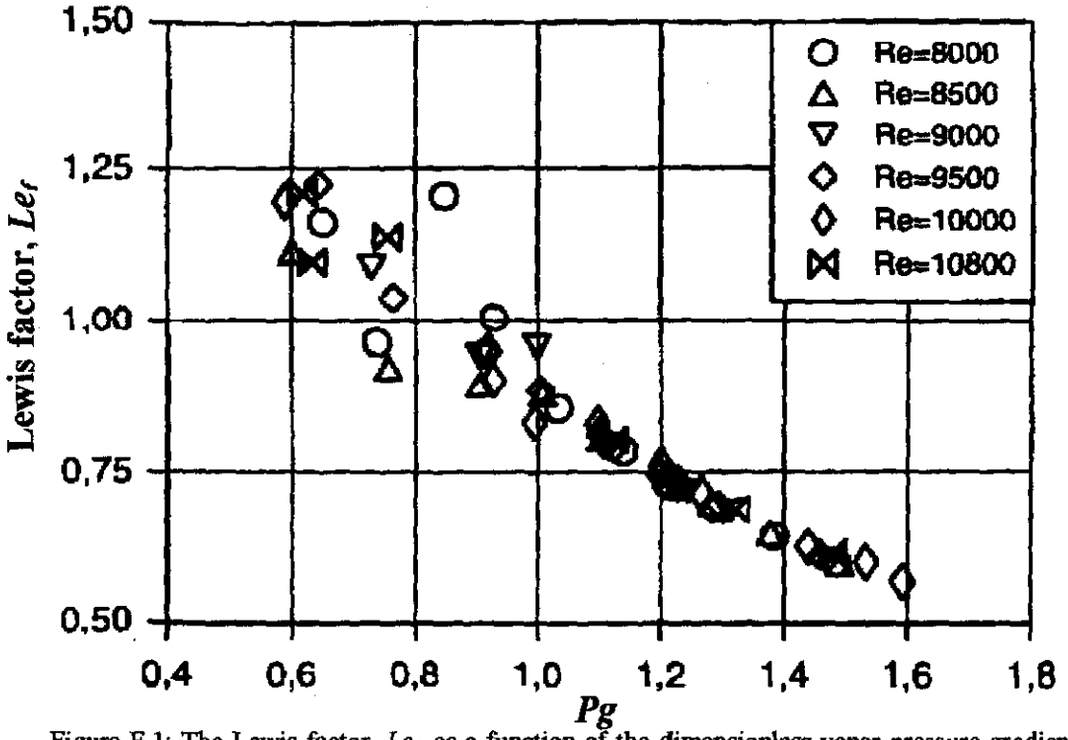

Figure F.1: The Lewis factor, Le_f, as a function of the dimensionless vapor pressure gradient, Pg. Le = 0.82, T_{wm} = 40°C [99HA1].

The average water temperature for the data in figure F.1 is 40°C with Le = 0.82. With Le = 0.82 in equation (F.14) Le_f = 0.88. The discrepancy between equation (F.14) and the data in figure F.1 is an indication that equation (F.14) is not valid for all conditions.

APPENDIX G

COUNTERFLOW FILL ANALYSIS ACCORDING TO THE POPPE APPROACH

Oosthuizen [95OO1] and Kröger [98KR1] present a sample calculation where the transfer coefficient of an expanded metal fill is evaluated while employing the Merkel method with Chebyshev numerical integration. Baard [98BA1] presents a sample calculation for the same experimental data while employing the Poppe approach. The method Baard [98BA1] employed to calculate the Merkel number is improved in the sample calculation presented here.

During a test of an expanded metal fill of height, L_{fi} = 1.878 m, the following measurements are made [95OO1, 98KR1],

Atmospheric pressure	p_a	= 101712.27 Pa
Air inlet temperature	T_{ai}	= 9.7 °C (282.85 K)
Air inlet temperature (wetbulb)	T_{wb}	= 8.23 °C (281.38 K)
Dry air mass flow rate	m_a	= 4.134 kg/s
Static pressure drop across fill	Δp_{fi}	= 4.5 Pa
Water inlet temperature	T_{wi}	= 39.67 °C (312.82 K)
Water outlet temperature	T_{wo}	= 27.77 °C (300.92 K)
Inlet water mass flow rate	m_w	= 3.999 kg/s

Refer to section B.4 for a discussion on the Runge-Kutta method applied to the governing equations.

The Runge-Kutta method requires four intermediate calculation steps per fill interval. Variables for the four intermediate calculation steps for the different intervals are denoted with the subscript (n,m), where n is the fill interval number and the second subscript, m, refers to the intermediate calculation step. It must be stressed that the single value subscripts between brackets refer to the level numbers as shown in figure G.1. For this evaluation consider a fill that is divided into two intervals as shown in figure G.1.

According to Kröger [98KR1] the initial values at level (0) are $w_{(0)} = w_i$ = 0.00616336 kg/kg dry air and $i_{ma(0)} = i_{mai}$ = 25291.87496 J/kg dry air

By following an iterative procedure find that a humidity ratio $w_o = w_{(2)}$ at the outlet of the fill is 0.02226 kg/kg dry air. The outlet humidity ratio is required in equation (B.32), which is used in all the intermediate calculation steps of the Runge-Kutta method for all the fill intervals.

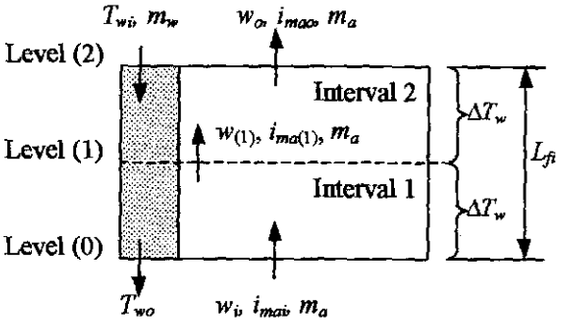

Figure G.1: Counterflow fill divided into two intervals

Since the fill is divided into two intervals find from equation (B.66)

$\Delta T_w = (T_{wi} - T_{wo})/(\text{number of intervals}) = (312.82 - 300.92)/2 = 5.95$ K.

From equations (B.51) to (B.53) find for level (1) at the top of the first interval of the Runge-Kutta method,

$w_{(1)} = w_{(0)} + (j_{(1,1)} + 2j_{(1,2)} + 2j_{(1,3)} + j_{(1,4)})/6$

$i_{ma(1)} = i_{ma(0)} + (k_{(1,1)} + 2k_{(1,2)} + 2k_{(1,3)} + k_{(1,4)})/6$

$Me_{P(1)} = Me_{P(0)} + (l_{(1,1)} + 2l_{(1,2)} + 2l_{(1,3)} + l_{(1,4)})/6$

where $Me_{P(0)} = 0$ is equal to zero at the air inlet side of the fill or at level (0).

Commence with the first intermediate calculation step of the Runge-Kutta method for the first fill interval. It can be seen from equations (B.54) to (B.56) that $j_{(1,1)}$, $k_{(1,1)}$ and $l_{(1,1)}$ are functions of $T_{w(0)}$, $i_{ma(0)}$ and $w_{(0)}$. Define that

$T_{w(1,1)} = T_{w(0)} = T_{wo} = 300.92$K

$w_{(1,1)} = w_{(0)} = w_i = 0.00616336$ kg/kg dry air

$i_{ma(1,1)} = i_{ma(0)} = i_{mai} = 25291.87496$ J/kg dry air.

To calculate $j_{(1,1)}$, $k_{(1,1)}$ and $l_{(1,1)}$ in equations (B.51) to (B.53) respectively, the specific heats have to be evaluated at $(T_{w(1,1)} + 273.15)/2 = (300.92 + 273.15)/2 = 287.035$K.

Specific heat of dry air from equation (A.1.2)

$$c_{pa(1,1)} = 1.045356 \times 10^3 - 3.161783 \times 10^{-1} \times 287.035 + 7.083814 \times 10^{-4} (287.035)^2 - 2.705209 \times 10^{-7} (287.035)^3 = 1006.567 \text{ J/kgK}$$

Specific heat of water vapor from equation (A.2.2)

$$c_{pv(1,1)} = 1.3605 \times 10^3 + 2.31334 \times 287.035 - 2.46784 \times 10^{-10} (287.035)^5 + 5.91332 \times 10^{-13} (287.035)^6 = 1874.385 \text{ J/kgK}$$

Specific heat of water from equation (A.4.2)

$$c_{pw(1,1)} = 8.15599 \times 10^3 - 2.80627 \times 10 \times 287.035 + 5.11283 \times 10^{-2}(287.035)^2$$
$$- 2.17582 \times 10^{-13}(287.035)^6 = 4191.744 \text{ J/kgK}$$

Pressure of water vapor from equation (A.2.1) evaluated at $T_{(1,1)} = 300.92$K.

$$z_{(1,1)} = 10.79586(1 - 273.16/300.92) + 5.02808 \log_{10}(273.16/300.92) + 1.50474$$
$$\times 10^{-4}[1 - 10^{-8.29692\{(300.92/273.16)-1\}}] + 4.2873 \times 10^{-4}[10^{4.76955(1-273.16/300.92)} - 1] + 2.786118312 = 3.57157$$

$$p_{v(1,1)} = 10^{3.57157} = 3729 \text{ Pa}$$

Humidity ratio for saturated air at $T_{(1,1)} = 300.92$K from equation (A.3.5)

$$w_{ws(1,1)} = \left(\frac{0.62509(3729)}{101712.3 - 1.005(3729)}\right) = 0.02379 \text{ kg/kg dry air}$$

Latent heat at 273.15K follows from equation (A.4.5)

$$i_{fgw(1,1)} = 2.5016 \times 10^6 \text{ J/kg}$$

The enthalpy of water vapor at the local bulk water temperature, $T_{w(1,1)}$, relative to water at 0°C,

$$i_{v(1,1)} = i_{fgw(1,1)} + c_{pv(1,1)}\, T_{w(1,1)} = 2.5016 \times 10^6 + 1874.385(300.92 - 273.15) = 2553650 \text{ J/kg}$$

The enthalpy of saturated air at the local bulk water temperature from equation (A.3.6b)

$$i_{masw(1,1)} = 1006.567(300.92 - 273.15) + (0.02379)(2553650) = 88711 \text{ J/kg}$$

The Lewis factor from equation (B.15)

$$Le_{f(1,1)} = 0.865^{0.667} \frac{\left(\frac{0.662 + 0.02379}{0.662 + 0.00616336} - 1\right)}{\ln\left(\frac{0.662 + 0.02379}{0.662 + 0.00616336}\right)} = 0.9205$$

The mass balance from equation (B.32),

$$\left(\frac{m_w}{m_a}\right)_{(1,1)} = \frac{3.999}{4.134}\left[1 - \frac{4.134}{3.999}(0.02226 - 0.00616336)\right] = 0.9512$$

From equation (B.54) find

$$j_{(1,1)} = \Delta T_w \cdot f\left(T_{w(0)}, i_{ma(0)}, w_{(0)}\right) = \Delta T_w \cdot f\left(T_{w(1,1)}, i_{ma(1,1)}, w_{(1,1)}\right)$$

From equation (B.48) find

$$\frac{dw}{dT_w} = f\left(T_{w(0)}, i_{ma(0)}, w_{(0)}\right) = f\left(T_{w(1,1)}, i_{ma(1,1)}, w_{(1,1)}\right)$$

but from equation (B.24),

$$\frac{dw}{dT_w} = \frac{c_{pw(1,1)}\left(\frac{m_w}{m_a}\right)_{(1,1)}\left(w_{sw(1,1)} - w_{(1,1)}\right)}{i_{masw(1,1)} - i_{ma(1,1)} + \left(Le_{f(1,1)} - 1\right)\left[i_{masw(1,1)} - i_{ma(1,1)} - \left(w_{sw(1,1)} - w_{(1,1)}\right)i_{v(1,1)}\right] - \left(w_{sw(1,1)} - w_{(1,1)}\right)c_{pw(1,1)}T_{w(1,1)}}$$

Combine equations (B.24), (B.48) and (B.54) to find

$$j_{(1,1)} = \frac{\Delta T_w c_{pw(1,1)}\left(\frac{m_w}{m_a}\right)_{(1,1)}\left(w_{sw(1,1)} - w_{(1,1)}\right)}{i_{masw(1,1)} - i_{ma(1,1)} + \left(Le_{f(1,1)} - 1\right)\left[i_{masw(1,1)} - i_{ma(1,1)} - \left(w_{sw(1,1)} - w_{(1,1)}\right)i_{v(1,1)}\right] - \left(w_{sw(1,1)} - w_{(1,1)}\right)c_{pw(1,1)}T_{w(1,1)}}$$

$$= \frac{(5.95)(4191.744)(0.9512)(0.02379 - 0.00616336)}{\left[\begin{array}{l} 88711 - 25291.87496 \\ +(0.9205-1)[88711 - 25291.87496 - (0.02379 - 0.00616336)(2553650)] \\ -(0.02379 - 0.00616336)(4191.744)(300.92 - 273.15) \end{array}\right]}$$

$$= 0.006982$$

Combine equations (B.25), (B.49) and (B.55) to find.

$$k_{(1,1)} = \Delta T_w c_{pw(1,1)}\left(\frac{m_w}{m_a}\right)_{(1,1)}$$

$$\times\left(1 + \frac{\left(w_{sw(1,1)} - w_{(1,1)}\right)c_{pw(1,1)}T_{w(1,1)}}{i_{masw(1,1)} - i_{ma(1,1)} + \left(Le_{f(1,1)} - 1\right)\left[i_{masw(1,1)} - i_{ma(1,1)} - \left(w_{sw(1,1)} - w_{(1,1)}\right)i_{v(1,1)}\right] - \left(w_{sw(1,1)} - w_{(1,1)}\right)c_{pw(1,1)}T_{w(1,1)}}\right)$$

$$= (5.95)(4191.744)(0.9512)$$

$$\times\left(1 + \frac{(0.02379 - 0.00616336)(4191.744)(300.92 - 273.15)}{\left[\begin{array}{l} 88711 - 25291.87496 + (0.9205-1)\times[88711 - 25291.87496 - (0.02379 - \\ 0.00616336)(2553650)] - (0.02379 - 0.00616336)(4191.744)(300.92 - 273.15) \end{array}\right]}\right)$$

$$= 24537.63$$

Combine equations (B.30), (B.50) and (B.56) to find

$$l_{(1,1)} = \frac{\Delta T_w c_{pw(1,1)}}{i_{masw(1,1)} - i_{ma(1,1)} + \left(Le_{f(1,1)} - 1\right)\left[i_{masw(1,1)} - i_{ma(1,1)} - \left(w_{sw(1,1)} - w_{(1,1)}\right)i_{v(1,1)}\right] - \left(w_{sw(1,1)} - w_{(1,1)}\right)c_{pw(1,1)}T_{w(1,1)}}$$

$$= \frac{(5.95)(4191.744)}{\left[\begin{array}{l} 88711 - 25291.87496 \\ +(0.9205-1)[88711 - 25291.87496 - (0.02379 - 0.00616336)(2553650)] \\ -(0.02379 - 0.00616336)(4191.744)(300.92 - 273.15) \end{array}\right]}$$

$$= 0.41635$$

By proceeding along the same lines $j_{(1,2)}$, $k_{(1,2)}$ and $l_{(1,2)}$ are determined for the second intermediate calculation step of the Runge-Kutta method for the first fill interval:

From equations (B.57) to (B.59) can be seen that $j_{(1,2)}$, $k_{(1,2)}$ and $l_{(1,2)}$ are functions of

$T_{w(0)} + \frac{\Delta T_w}{2}, i_{ma(0)} + \frac{k_{(1,1)}}{2}$ and $w_{(0)} + \frac{j_{(1,1)}}{2}$ thus define

$T_{w(1,2)} = T_{w(0)} + \Delta T_w/2 = 300.92 + 5.95/2 = 303.895\text{K}$

$w_{(1,2)} = w_{(1)} + j_{(1,1)}/2 = 0.00616336 + 0.006982/2 = 0.0096544$ kg/kg dry air

$i_{ma(1,2)} = i_{ma(1)} + k_{(1,1)}/2 = 25291.88 + 24537.63/2 = 37560.67$ J/kg

The specific heats have to be evaluated at $(T_{w(1,2)} + 273.15)/2 = 288.5225\text{K}$

Specific heat of dry air from equation (A.1.2)

$c_{pa(1,2)} = 1.045356\times10^{3} - 3.161783\times10^{-1} \times 288.5225 + 7.083814\times10^{-4}(288.5225)^2$
$- 2.705209\times10^{-7}(288.5225)^3 = 1006.603$ J/kgK

Specific heat of water vapor from equation (A.2.2)

$c_{pv(1,2)} = 1.3605 \times 10^{3} + 2.31334 \times 288.5225 - 2.46784 \times 10^{-10}(287.035)^5$
$+ 5.91332 \times 10^{-13}(288.5225)^6 = 1875.654$ J/kgK

Specific heat of water from equation (A.4.2)

$c_{pw(1,2)} = 8.15599 \times 10^{3} - 2.80627 \times 10 \times 288.5225 + 5.11283 \times 10^{-2}(288.5225)^2$
$- 2.17582 \times 10^{-13}(288.5225)^6 = 4189.941$ J/kgK

The vapor pressure and humidity ratio of saturated air are calculated at the local water temperature $T_{w(1,2)}$ = 303.895K

Vapor pressure from equation (A.2.1): $p_{v(1,2)} = 4427.4$ Pa

Humidity ratio for saturated air from equation (A.3.5): $w_{sw(1,2)} = 0.028454$ kg/kg dry air

The enthalpy of water vapor at the local bulk water temperature, $T_{w(1,2)}$, relative to water at 0°C,

$i_{v(1,2)} = i_{fgw(1,2)} + c_{pv(1,2)} T_{w(1,2)} = 2.5016 \times 10^{6} + 1875.654(303.895-273.15) = 2553650$ J/kg

The entalpy of saturated air at the local bulk water temperature from equation (A.3.6b)

$i_{masw(1,2)} = 1006.603(303.8950 - 273.15) + (0.028454)(2553650) = 103770$ J/kg

The Lewis factor from equation (B.15)

$$Le_{f(1,2)} = 0.865^{0.667} \frac{\left(\frac{0.662 + 0.028454}{0.662 + 0.0096582} - 1\right)}{\ln\left(\frac{0.662 + 0.028454}{0.662 + 0.0096582}\right)} = 0.9212$$

The mass balance from equation (B.32)

$$\left(\frac{m_w}{m_a}\right)_{(1,2)} = \frac{3.999}{4.134}\left(1 - \frac{4.134}{3.999}(0.02226 - 0.0096544)\right) = 0.9547$$

From equation (B.57) find

$$j_{(1,2)} = \Delta T_w \cdot f\left(T_{w(1,2)}, i_{ma(1,2)}, w_{(1,2)}\right)$$

From equation (B.48) find

$$\frac{dw}{dT_w} = f\left(T_{w(1,2)}, i_{ma(1,2)}, w_{(1,2)}\right)$$

From equation (B.24) find

$$\frac{dw}{dT_w} = \frac{c_{pw(1,2)}\left(\frac{m_w}{m_a}\right)_{(1,2)}\left(w_{sw(1,2)} - w_{(1,2)}\right)}{i_{masw(1,2)} - i_{ma(1,2)} + \left(Le_{f(1,2)} - 1\right)\left[i_{masw(1,2)} - i_{ma(1,2)} - \left(w_{sw(1,2)} - w_{(1,2)}\right)i_{v(1,2)}\right] - \left(w_{sw(1,2)} - w_{(1,2)}\right)c_{pw(1,2)}T_{w(1,2)}}$$

Combine equations (B.24), (B.48) and (B.57) to find

$$j_{(1,2)} = \frac{\Delta T_w c_{pw(1,2)}\left(\frac{m_w}{m_a}\right)_{(1,2)}\left(w_{sw(1,2)} - w_{(1,2)}\right)}{i_{masw(1,2)} - i_{ma(1,2)} + \left(Le_{f(1,2)} - 1\right)\left[i_{masw(1,2)} - i_{ma(1,2)} - \left(w_{sw(1,2)} - w_{(1,2)}\right)i_{v(1,2)}\right] - \left(w_{sw(1,2)} - w_{(1,2)}\right)c_{pw(1,2)}T_{w(1,2)}}$$

$$= \frac{(5.95)(4189.941)(0.9547)(0.028454 - 0.0096544)}{\left[\begin{array}{l}103770 - 37560.67 \\ +(0.9212 - 1)[103770 - 37560.67 - (0.028454 - 0.0096544)(2559265)] \\ -(0.028454 - 0.0096544)(4189.941)(303.895 - 273.15)\end{array}\right]}$$

$$= 0.00717527$$

A relation for $k_{(1,2)}$ is obtained by combining (B.25), (B.49) and (B.58) i.e.

$$k_{(1,2)} = \Delta T_w c_{pw(1,2)}\left(\frac{m_w}{m_a}\right)_{(1,2)}$$

$$\times\left(1 + \frac{\left(w_{sw(1,2)} - w_{(1,2)}\right)c_{pw(1,2)}T_{w(1,2)}}{i_{masw(1,2)} - i_{ma(1,2)} + \left(Le_{f(1,2)} - 1\right)\left[i_{masw(1,2)} - i_{ma(1,2)} - \left(w_{sw(1,2)} - w_{(1,2)}\right)i_{v(1,2)}\right] - \left(w_{sw(1,2)} - w_{(1,2)}\right)c_{pw(1,2)}T_{w(1,2)}}\right)$$

$$= (5.95)(4189.941)(0.9547)$$

$$\times\left(1 + \frac{(0.028454 - 0.0096544)(4189.941)(303.985 - 273.15)}{\left[\begin{array}{l}103770 - 37560.67 + (0.9212 - 1) \times [103770 - 37560.67 - (0.028454 - 0.0096544)] \\ \times (2559265)] - (0.028454 - 0.0096544)(4189.941)(303.895 - 273.15)\end{array}\right]}\right)$$

$$= 24726$$

$l_{(1,2)}$ is obtained by combining equation (B.30), (B.50) and (B.59)

$$l_{(1,2)} = \frac{\Delta T_w c_{pw(1,2)}}{i_{masw(1,2)} - i_{ma(1,2)} + \left(Le_{f(1,2)} - 1\right)\left[i_{masw(1,2)} - i_{ma(1,2)} - \left(w_{sw(1,2)} - w_{(1,2)}\right)i_{v(1,2)}\right] - \left(w_{sw(1,2)} - w_{(1,2)}\right)c_{pw(1,2)}T_{w(1,2)}}$$

$$= \frac{(5.95)(4189.941)}{\left[\begin{array}{l} 103770 - 37560.67 + (0.9212 - 1)[103770 - 37560.67 \\ -(0.028454 - 0.0096544)(2559265)] \\ -(0.028454 - 0.0096544)(4189.941)(303.895 - 273.15) \end{array}\right]} = 0.3997$$

Proceeding along the same lines, the following values are calculated to complete the Runge-Kutta numerical integration for the first interval of the fill.

$j_{(1,3)} = 0.007150$; $k_{(1,3)} = 24725$; $l_{(1,3)} = 0.4004$; $j_{(1,4)} = 0.0073899$; $k_{(1,4)} = 24927$; $l_{(1,4)} = 0.3738$

The humidity ratio at level (1) follows from equation (B.51),

$w_{(1)} = w_{(0)} + (j_{(1,1)} + 2j_{(1,2)} + 2j_{(1,3)} + j_{(1,4)})/6$

$= 0.00616336 + [0.006982 + (2)0.00717527 + (2)0.007150 + 0.0073899] / 6 = 0.0133338$ kg/kg dry air

The enthalpy of the air at level (1) follows from equation (B.52),

$i_{ma(1)} = i_{ma(0)} + (k_{(1,1)} + 2k_{(1,2)} + 2k_{(1,3)} + k_{(1,4)})/6$

$= 25291.89 + [24537.63 + (2)24726 + (2)24725.12 + 24927] / 6 = 50019.67$ J/kg

The transfer characteristic or Merkel number at level (1) follows from equation (B.53),

$Me_{P(1)} = Me_{P(0)} + (l_{(1,1)} + 2l_{(1,2)} + 2l_{(1,3)} + l_{(1,4)})/6$

$= [0.41635 + (2)0.3997 + (2)0.4004 + 0.3738] = 0.3984$

The dry bulb temperature $T_{a(1)}$ and wet bulb temperature $T_{wb(1)}$ at level (1) are determined by assuming that the air is unsaturated. If $T_{wb(1)} > T_{a(1)}$ the air is supersaturated and the assumption of unsaturated air must be corrected. The assumption is then corrected by assuming supersaturated air with $T_{wb(1)} = T_{a(1)}$.

Find the dry bulb temperature at level (1), $T_{a(1)}$:

The enthalpy of the air at level (1) is, $i_{ma(1)} = 50019.67$ J/kg.

Assume that the air is unsaturated and that the drybulb temperature, $T_{a(1)} = 289.307$ K.

The specific heats are evaluated at $(T_{a(1)}+273.15)/2 = (289.307+273.15)/2 = 281.2258$ K

Specific heat of dry air from equation (A.1.2) $c_{pa(1)} = 1006.446$ J/kgK

Specific heat of water vapor from equation (A.2.2) $c_{pv(1)} = 1869.495$ J/kgK

Equation (A.3.6b) gives an expression for the enthalpy of an air vapor mixture per unit mass of dry air.

$i_{ma(1)} = 1006.446(289.307 - 273.15) + 0.0133338 \times [2501598 + 1869.495(289.307 - 273.15)] = 50020$ J/kg

The value of $i_{ma(1)}$ determined by equation (A.3.6b) is within close tolerance of the value determined by equation (B.52). The assumption of the value of the dry bulb temperature is therefore correct if the air is unsaturated at level (1).

Find the wetbulb temperature at level (1), $T_{wb(1)}$:

The humidity ratio at level (1), $w_{(1)} = 0.0133338$ kg/kg dry air.

Assume that the wetbulb temperature at level (1) is $T_{wb(1)} = 291.617$ K and find from equations (A.2.1) and (A.3.5) respectively the corresponding vapor pressure and the humidity ratio.

Vapor pressure from equation (A.2.1): $p_{v(1)} = 2124.092$Pa

Humidity ratio from equation (A.3.5): $w_{(1)} = 0.0133338$ kg/kg dry air

The value of $w_{(1)}$, determined according to (A.3.5) is the same as the value determined earlier. The assumed value of the wetbulb temperature is therefore correct if the air is unsaturated at level (1).

Test if air is unsaturated or supersaturated:

Since $T_{wb(1)} > T_{a(1)}$ the air is actually supersaturated at level (1). The assumption that the air is unsaturated for the determination of $T_{a(1)}$ and $T_{wb(1)}$ is therefore incorrect. For supersaturated air at level (1) $T_{a(1)} = T_{wb(1)}$. Assume a value for $T_{a(1)} = T_{wb(1)} = 290.8448$ K and find at this temperature

Vapor pressure from equation (A.2.1): $p_{vsa(1)} = 2023.427$ Pa

Humidity ratio from equation (A.3.5): $w_{sa(1)} = 0.012689$ kg/kg dry air

The following specific heats are determined at $(T_{a(1)} + 273.15)/2 = (290.8448 + 273.15)/2 = 281.99$ K

Specific heat of dry air from equation (A.1.2): $c_{pa(1)} = 1006.460$ J/kgK

Specific heat of water vapor from equation (A.2.2): $c_{pv(1)} = 1870.138$ J/kgK

Specific heat of water from equation (A.4.2): $c_{pw(1)} = 4198.815$ J/kgK

From equation (B.33) it follows that

$$i_{ss(1)} = c_{pa(1)}(T_{a(1)} - 273.15) + w_{sa(1)}[i_{fgwo} + c_{pv(1)}(T_{a(1)} - 273.15)] + (w_{(1)} - w_{sa(1)})c_{pw(1)}(T_{a(1)} - 273.15) = 1006.460(290.8448 - 273.15) + 0.012689[2501598 + 1870.138(290.8448 - 273.15)] + (0.0133338 - 0.012689)(4198.815)(290.8448 - 273.15) = 50020 \text{ J/kg}$$

$i_{ss(1)}$, determined by equation (B.33), is within close tolerance of $i_{ma(1)}$, determined by equation (B.52), thus, the assumption of the value of the dry bulb temperature at level (1) is therefore correct. The air temperature at level (1), $T_{a(1)}$, is therefore equal to 290.8448 K.

Apply Runge-Kutta numerical integration to the second fill interval. Find from equations (B.51) to (B.53) at level (2),

$$w_{(2)} = w_{(1)} + (j_{(2,1)} + 2j_{(2,2)} + 2j_{(2,3)} + j_{(2,4)})/6$$

$$i_{ss(2)} = i_{ss(1)} + (k_{(2,1)} + 2k_{(2,2)} + 2k_{(2,3)} + k_{(2,4)})/6$$

$Me_{P(2)} = Me_{P(1)} + (l_{(2,1)} + 2l_{(2,2)} + 2l_{(2,3)} + l_{(2,4)})/6$

Because the air is supersaturated $i_{ss(1)} = i_{ma(1)}$. The water temperature at level (1) is $T_{w(1)} = T_{wo} + \Delta T_w$ = 300.92 + 5.95 = 306.87K. For the first intermediate calculation step of the second fill interval, $i_{ss(2,1)} = i_{ss(1)}$, $T_{w(2,1)} = T_{w(1)}$ and $w_{sa(2,1)} = w_{sa(1)}$.

To calculate $j_{(2,1)}$, $k_{(2,1)}$ and $l_{(2,1)}$ for the first intermediate calculation step for the second fill interval certain thermophysical properties have to be evaluated at $(T_{w(2,1)} + 273.15)/2 = (306.87 + 273.15)/2 = 290.01$ K

Specific heat of dry air from equation (A.1.2)

$c_{pa(2,1)} = 1.045356 \times 10^3 - 3.161783 \times 10^{-1} \times 290.01 + 7.083814 \times 10^{-4} (290.01)^2$
$- 2.705209 \times 10^{-7} (290.01)^3 = 1006.642$ J/kgK

Specific heat of water vapor from equation (A.2.2)

$c_{pv(2,1)} = 1.3605 \times 10^3 + 2.31334 \times 290.01 - 2.46784 \times 10^{-10} (290.01)^5$
$+ 5.91332 \times 10^{-13} (290.01)^6 = 1876.933$ J/kgK

Specific heat of water from equation (A.4.2)

$c_{pw(2,1)} = 8.15599 \times 10^3 - 2.80627 \times 10 \times 290.01 + 5.11283 \times 10^{-2} (290.01)^2$
$- 2.17582 \times 10^{-13} (290.01)^6 = 4188.264$ J/kgK

Vapor pressure from equation (A.2.1) evaluated at $T_{w(2,1)} = 306.87$K

$z_{(2,1)} = 10.79586(1 - 273.16/306.87) + 5.02808 \log_{10}(273.16/306.87)$
$+ 1.50474 \times 10^{-4}[1 - 10^{-8.29692\{(306.87/273.16)-1\}}]$
$+ 4.2873 \times 10^{-4}[10^{4.76955(1-273.16/306.87)} - 1] + 2.786118312 = 3.71909$

$p_{v(2,1)} = 10^{3.71909} = 5237$ Pa

Humidity ratio for saturated air evaluated at $T_{w(2,1)} = 306.87$K from equation (A.3.5),

$$w_{sw(2,1)} = \left(\frac{0.62509(5237)}{101712.3 - 1.005(5237)} \right) = 0.0339417 \text{ kg/kg dry air}$$

The enthalpy of water vapor at the local bulk water temperature, $T_{w(2,1)}$, relative to water at 0°C,

$i_{v(2,1)} = i_{fgw(2,1)} + c_{pv(2,1)} T_{w(2,1)} = 2.5016 \times 10^6 + 1876.933(306.87 - 273.15) = 2564889$ J/kg

The entalpy of saturated air at the local bulk water temperature from equation (A.3.6b)

$i_{masw(2,1)} = 1006.642(306.87 - 273.15) + (0.0339417)(2564889) = 121001$ J/kg

The Lewis factor from equation (B.38)

$$Le_{f(2,1)} = 0.865^{0.667} \frac{\left(\frac{0.662+0.0339417}{0.662+0.012689}-1\right)}{\ln\left(\frac{0.662+0.0339417}{0.662+0.012689}\right)} = 0.9229$$

The mass balance from equation (B.32)

$$\left(\frac{m_w}{m_a}\right)_{(2,1)} = \frac{3.999}{4.134}\left(1-\frac{4.134}{3.999}(0.02226-0.0133338)\right) = 0.9584$$

From equation (B.54) find

$$j_{(2,1)} = \Delta T_w \cdot f\left(T_{w(1)}, i_{ss(1)}, w_{(1)}\right) = \Delta T_w \cdot f\left(T_{w(2,1)}, i_{ss(2,1)}, w_{(2,1)}\right)$$

From equation (B.48) find

$$\frac{dw}{dT_w} = f\left(T_{w(1)}, i_{ss(1)}, w_{(1)}\right) = f\left(T_{w(2,1)}, i_{ss(2,1)}, w_{(2,1)}\right)$$

but from equation (B.42)

$$\frac{dw}{dT_w} = \frac{c_{pw(2,1)}\left(\frac{m_w}{m_a}\right)_{(2,1)}\left(w_{sw(2,1)}-w_{sa(2,1)}\right)}{\begin{matrix} i_{masw(2,1)}-i_{ss(2,1)}+\left(Le_{f(2,1)}-1\right)\left[i_{masw(2,1)}-i_{ss(2,1)}-\left(w_{sw(2,1)}-w_{sa(2,1)}\right)i_{v(2,1)}+\left(w_{(2,1)}-w_{sa(2,1)}\right)c_{pw(2,1)}T_{w(2,1)}\right] \\ +\left(w_{(2,1)}-w_{sw(2,1)}\right)c_{pw(2,1)}T_{w(2,1)}\end{matrix}}$$

Combine equations (B.42), (B.48) and (B.54) to find

$$j_{(2,1)} = \frac{\Delta T_w c_{pw(2,1)}\left(\frac{m_w}{m_a}\right)_{(2,1)}\left(w_{sw(2,1)}-w_{sa(2,1)}\right)}{\begin{matrix} i_{masw(2,1)}-i_{ss(2,1)}+\left(Le_{f(2,1)}-1\right)\left[i_{masw(2,1)}-i_{ss(2,1)}-\left(w_{sw(2,1)}-w_{sa(2,1)}\right)i_{v(2,1)}+\left(w_{(2,1)}-w_{sa(2,1)}\right)c_{pw(2,1)}T_{w(2,1)}\right] \\ +\left(w_{(2,1)}-w_{sw(2,1)}\right)c_{pw(2,1)}T_{w(2,1)}\end{matrix}}$$

$$= \frac{(5.95)(4188.264)(0.9584)(0.0339417-0.012689)}{\begin{bmatrix} 121001-50019.67 \\ +(0.9229-1)[121001-50019.67-(0.0339417-0.012689)(2564889) \\ +(0.0133338-0.012689)(4188.264)(306.87-273.15)] \\ +(0.0133338-0.0339417)(4188.264)(306.87-273.15)\end{bmatrix}}$$

$$= 0.007599$$

Combine equations (B.43), (B.49) and (B.55) to find,

$$k_{(2,1)} = \Delta T_w c_{pw[1]}\left(\frac{m_w}{m_a}\right)_{(2,1)}$$

$$\times\left[1+\frac{\left(w_{sw(2,1)}-w_{sa(2,1)}\right)}{\begin{matrix}i_{masw(2,1)}-i_{ss(2,1)}+\left(Le_{f(2,1)}-1\right)\left[i_{masw(2,1)}-i_{ss(2,1)}-\left(w_{sw(2,1)}-w_{sa(2,1)}\right)i_{v(2,1)}+\left(w_{(2,1)}-w_{sa(2,1)}\right)c_{pw(2,1)}T_{w(2,1)}\right]\\+\left(w_{(2,1)}-w_{sw(2,1)}\right)c_{pw(2,1)}T_{w(2,1)}\end{matrix}}\right]$$

$$=(5.95)(4188.264)(0.9548)$$

$$\times\left[1+\frac{(0.0339417-0.012689)(4188.264)(306.87-273.15)}{\begin{matrix}\left[121001-50019.67+(0.9229-1)\right.\\\times[121001-50019.67-(0.0339417-0.012689)(2564889)\\+(0.0133338-0.012689)(4188.264)(306.87-273.15)]\\\left.+(0.0133338-0.0339417)(4188.264)(306.87-273.15)\right]\end{matrix}}\right]=24957$$

Combine equations (B.47), (B.50) and (B.56) to find,

$$l_{(2,1)}=\frac{\Delta T_w c_{pw(2,1)}}{\begin{matrix}i_{masw(2,1)}-i_{ss(2,1)}+\left(Le_{f(2,1)}-1\right)\left[i_{masw(2,1)}-i_{ss(2,1)}-\left(w_{sw(2,1)}-w_{sa(2,1)}\right)i_{v(2,1)}+\left(w_{(2,1)}-w_{sa(2,1)}\right)c_{pw(2,1)}T_{w(2,1)}\right]\\+\left(w_{(2,1)}-w_{sw(2,1)}\right)c_{pw(2,1)}T_{w(2,1)}\end{matrix}}$$

$$=\frac{(5.95)(4188.264)}{\begin{matrix}\left[121001-50019.67+(0.9229-1)\right.\\\times[121001-50019.67-(0.0339417-0.012689)(2564889)\\+(0.0133338-0.012689)(4188.264)(306.87-273.15)]\\\left.+(0.0133338-0.0339417)(4188.264)(306.87-273.15)\right]\end{matrix}}$$

$$=0.3731$$

By proceeding along the same lines, the following values are calculated for the second to fourth intermediate calculation steps to finish the Runge-Kutta numerical integration for the second interval of the fill.

$j_{(2,2)}=0.008957$; $k_{(2,2)}=25346$; $l_{(2,2)}=0.33598$

$j_{(2,3)}=0.008973$; $k_{(2,3)}=25365$; $l_{(2,3)}=0.03364$

$j_{(2,4)}=0.010124$; $k_{(2,4)}=25771$; $l_{(2,4)}=0.2965$

The humidity ratio at level (2) follows from equation (B.51),

$w_{(2)}=w_{(1)}+(j_{(2,1)}+2j_{(2,2)}+2j_{(2,3)}+j_{(2,4)})/6$

$=0.0133338+[0.007599+(2)0.008957+(2)0.008973+0.010124]/6=0.02226$ kg/kg dry air

Since $w_{(2)}$ is equal to w_o, which is assumed to be 0.02226 kg/kg dry air in the beginning of this example, the system of equations has converged.

The air enthalpy at level (2) follows from equation (B.52),

$i_{ss(2)}=i_{ss(1)}+(k_{(2,1)}+2k_{(2,2)}+2k_{(2,3)}+k_{(2,4)})/6$

$=50019.67+[24957+(2)25346+(2)25635+25771]/6=75378$ J/kg

The transfer characteristic or Merkel number at level (2) follows from equation (B.53),

$Me_{P(2)} = Me_{P(1)} + (l_{(2,1)} + 2l_{(2,2)} + 2l_{(2,3)} + l_{(2,4)})/6$

$= 0.3984 + [0.3731 + (2)0.33598 + (2)0.3364 + 0.2965] = 0.7341$

The air was already supersaturated at level (1). Therefore assume that the temperature of the supersaturated air at level (2) is $T_{a(2)} = T_{wb(2)} = 297.8508$ K

The partial pressure and humidity ratio of saturated air, from equations (A.2.1) and (A.3.5), evaluated at $T_{a(2)}$ are respectively

$p_{vsa(2)} = 3110.68$ Pa

$w_{sa(2)} = 0.01972$ kg/kg dry air

The specific heat of dry air, water liquid and vapor are evaluated at $(T_{a(2)} + 273.15)/2 = (297.8508 + 273.15)/2 = 285.5$ K

Specific heat of dry air from equation (A.1.2): $c_{pa(2)} = 1006.532$ J/kgK

Specific heat of water vapor equation (A.2.2): $c_{pv(2)} = 1873.084$ J/kgK

Specific heat of water equation (A.4.2): $c_{pw(2)} = 4193.739$ J/kgK

It follows from equation (B.33) that

$i_{ss(2)} = c_{pa(2)}(T_{a(2)} - 273.15) + w_{sa(2)}[i_{fgw[1]} + c_{pv(2)}(T_{a(2)} - 273.15)]$

$+ (w_{(2)} - w_{sa(2)})c_{pw(2)}(T_{a(2)} - 273.15) = 1006.532(297.8508 - 273.15)$

$+ 0.01972[2501598 + 1873.084(297.8508 - 273.15)] + (0.02226$

$- 0.01972)(4193.739)(297.8508 - 273.15) = 75378.4$ K

$i_{ss(2)}$, determined by equation (B.33), is within close tolerance of $i_{ss(2)}$, determined by equation (B.52), thus the value of the air temperature assumed at level (2) is therefore correct.

Therefore the conditions at the outlet of the fill are:

$i_{mao} = i_{ss(2)} = 75378$ J/kg; $w_o = w_{(2)} = 0.02226$ kg/kg dry air; $T_{ao} = T_{a(2)} = 297.8508$K

where the Merkel number for the fill is $Me_P = Me_{P(2)} = 0.7341$. This is 7.2% greater than the Merkel number obtained by the Merkel approach in Kröger [98KR1].

APPENDIX H

CROSSFLOW FILL ANALYSIS ACCORDING TO THE *e-NTU*, MERKEL AND POPPE APPROACHES

H.1 INTRODUCTION

Experimental test measurements of a counterflow expanded metal fill are presented in appendix G. Kröger [98KR1] obtained the Merkel number, for the experimental values given in appendix G, according to the Merkel approach. The Merkel number, according to the counterflow Poppe approach, is presented in appendix G.

The same values of the experimental values are used in this crossflow fill performance analysis as in the counterflow case presented in appendix G. This is done to evaluate the differences between the Merkel numbers obtained for the counterflow and crossflow fill configurations.

A sample calculation for the crossflow configuration for the Merkel and Poppe approaches can not be presented in the same form as for the counterflow configuration presented in appendix G. The governing partial differential equations for the crossflow configuration are solved by a point-by-point Gauss-Seidel [80PA1, 92MA1] iterative procedure across a two-dimensional domain using the principle of finite differences. It is therefore very cumbersome to present a sample calculation and only the results are therefore presented. The results can be presented graphically for the Merkel and Poppe approaches due to the two-dimensional nature of the crossflow configuration.

H.2 POPPE APPROACH

The governing equations of the Poppe approach for crossflow fills are solved by an iterative technique as discussed in appendix C. The governing equations must be satisfied on each vertex in the computational domain before convergence can be obtained. Figure H.1 shows the solution domain of a counterflow fill for non-dimensional fill dimensions. The solution domain is divided in 50 intervals in both directions. It can be seen from figure H.1 in which parts of the fill the air is unsaturated and supersaturated, for the experimental measurements specified in appendix G. The dividing line between the unsaturated and supersaturated regions will be smooth if the solution domain is divided in much more intervals. It can be seen that the air becomes saturated soon after entering the fill, especially in the top parts of the fill. The governing equations for unsaturated and supersaturated air are thus solved in the respective regions shown in figure H.1.

Figures H.2(a) to H.2(f) show the distribution of the water temperature, water mass velocity, Lewis factor, air enthalpy, air temperature and the humidity ratio of the air respectively across the non-dimensional solution domain of the crossflow fill. Refer to figure H.1 for the coordinate system

convention used in figure H.2. The water and air inlet sides of the various plots in figure H.2 are the same as those illustrated in figure H.1.

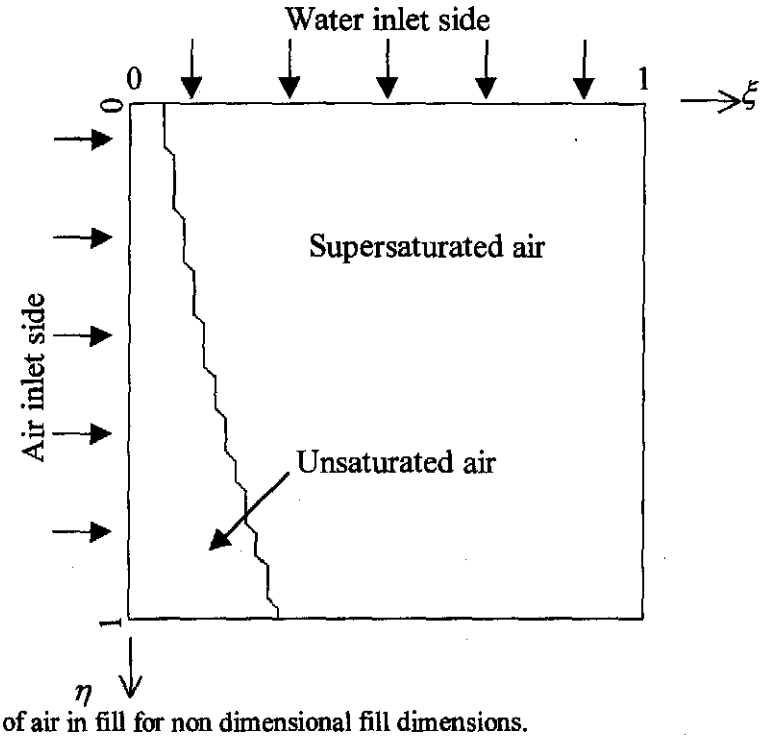

Figure H.1: State of air in fill for non dimensional fill dimensions.

The distribution of the water temperature across a vertical section of the fill is illustrated in figure H.2(a). The mean water outlet temperature is determined by equation (C.30) and is equal to 300.92K. It can be seen that water cooling is more effective near the air inlet side. This is because the water near the air inlet side is in contact with the cool inlet air all the time it falls through the fill. The mass velocity of the water, as it passes through the fill, can be seen in figure H.2(b). Approximately the same trends can be observed as the water temperature in figure H.2(a). The water mass velocity is reduced as it passes through the fill because of evaporation. The evaporation loss is larger near the air inlet side because the inlet air is relatively dry compared to the air deeper into the fill. Thus, a greater potential for evaporation loss exists where the air is the driest. Figure H.2(c) shows how the value of the Lewis factor, according to the equation of Bosnjakovic [65BO1], is distributed across the fill. Figures H.2(d) to H.2(f) show the enthalpy, temperature and humidity ratio of the air as it passes through the fill. It can be seen that the plotted contours of these three variables follow approximately the same trends. The air enthalpy increases more rapidly in the top of the fill because the air is in contact with the hot inlet water stream the entire time as it moves through the fill.

H.3 MERKEL APPROACH

Figures H.3(a) and H.3(b) show the distribution of the water temperature and air enthalpy according to the Merkel approach. The results of the Merkel approach can be compared to the results of the more rigorous Poppe approach presented in figure H.2. The mean water outlet temperature of both approaches is equal to 300.92K. The mean outlet air enthalpy and temperature of the Merkel approach is less than that predicted by the Poppe approach.

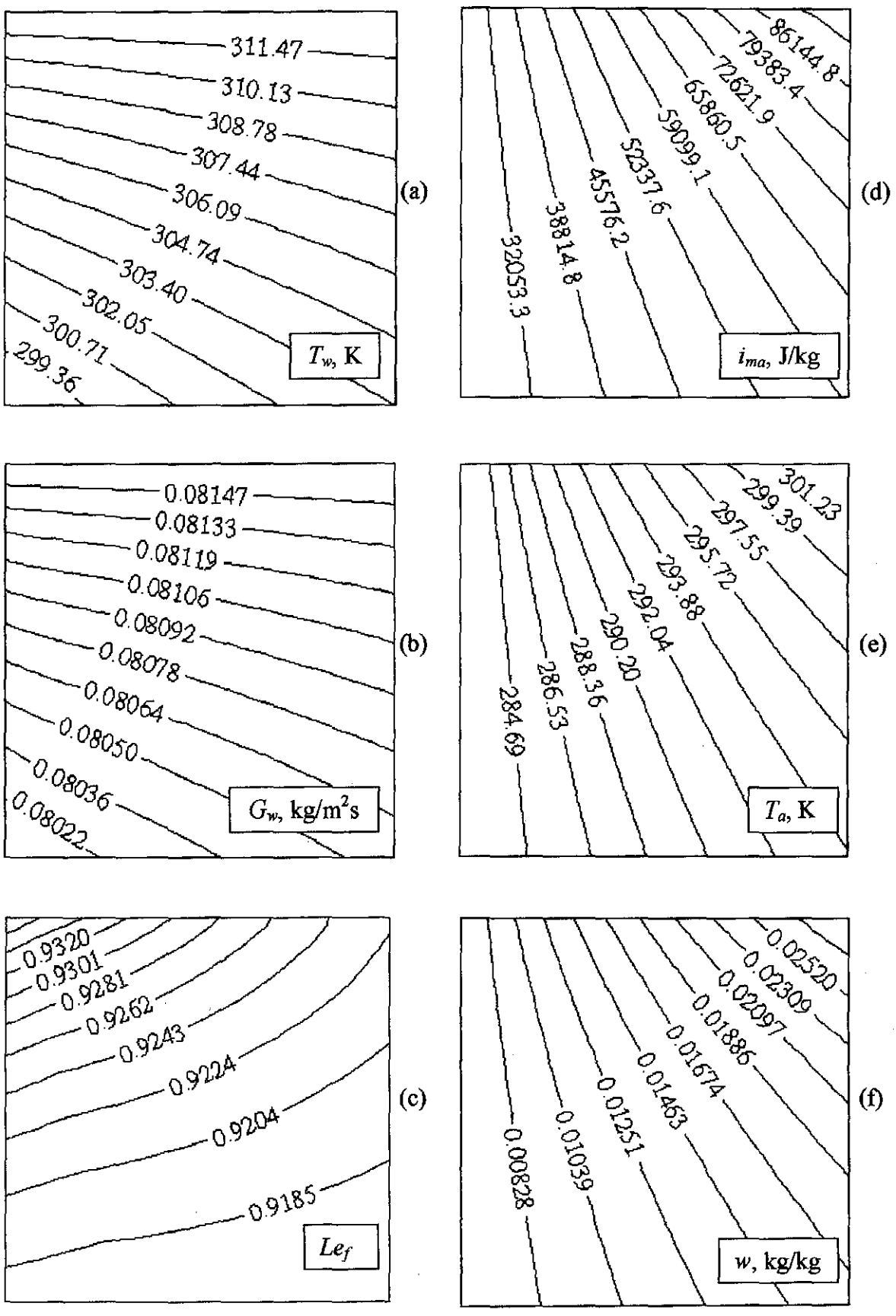

Figure H.2: Distribution of water temperature, water mass velocity, Lewis factor, air enthalpy, air temperature and humidity across a crossflow fill, determined according to the Poppe approach.

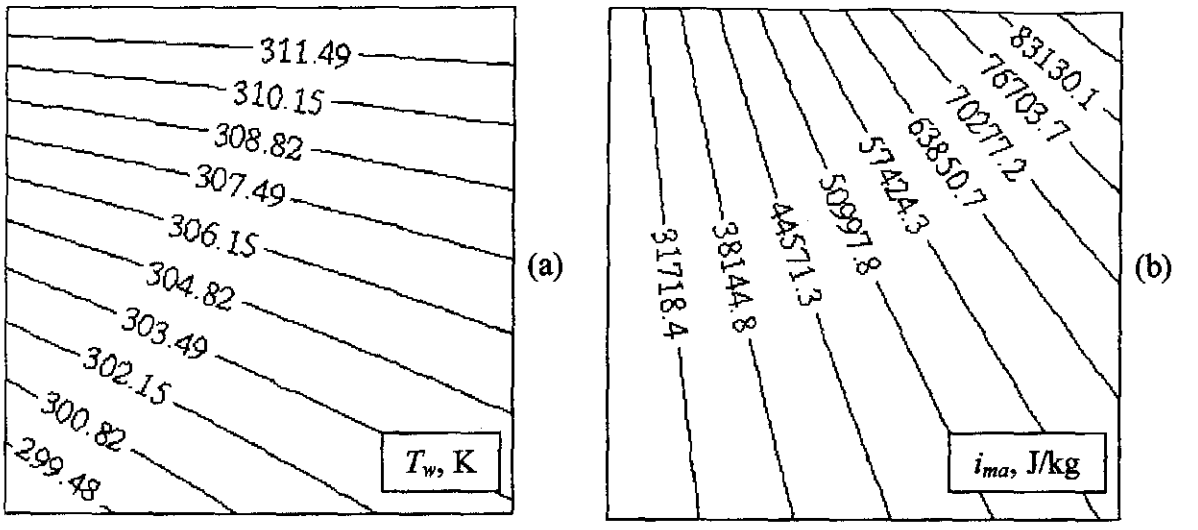

Figure H.3: Water temperature and air enthalpy distribution in a crossflow fill according to the Merkel approach.

H.4 *e-NTU* APPROACH

The crossflow Merkel number according to the *e-NTU* approach is not solved by two-dimensional finite differences. Four variants of the *e-NTU* approach are employed. *e-NTU*$_1$ and *e-NTU*$_2$ refer respectively to the crossflow cases where both the water and air streams are unmixed and both the air and water streams are mixed. *e-NTU*$_3$ refers to the crossflow case where C_{max}, which is generally the water stream, is mixed, and C_{min}, which is generally the air stream, is unmixed. C_{max} is unmixed and C_{min} is mixed for the *e-NTU*$_4$ case. The comparison of the four different e-NTU approaches and the comparison to the Merkel and Poppe approaches are presented in the next section.

H.5 COMPARATIVE RESULTS OF THE *e-NTU*, MERKEL AND POPPE APPROACHES

The heat rejected, air outlet temperature, water evaporation rate and the Merkel number for the fill test conditions given above, obtained by employing the Merkel, Poppe and the four *e-NTU* approaches, are given in table H.1. The 2-d computational domain is divided in 50 intervals in both the horizontal and vertical directions for the Merkel and Poppe analyses.

Q, T_{ao} and $m_{w(evap)}$ determined by all four variants of the *e-NTU* approach are identical. These variables are also identical to the values obtained by the Merkel approach. This is because it is assumed, for both approaches, that the outlet air is saturated with water vapor. The heat rejection rate is calculated by exactly the same manner for all the variants of the *e-NTU* approach and the Merkel approach, i.e., $Q = m_w c_{pwm}(T_{wi} - T_{wo})$.

The Merkel numbers obtained by the Merkel approach and the *e-NTU*$_1$ approach are practically identical. Where both streams are mixed, i.e., the *e-NTU*$_2$ approach, the Merkel number is approximately 5% higher than that predicted by the Merkel approach. The Merkel numbers for the other two cases, *e-NTU*$_3$ and *e-NTU*$_4$ respectively, are in between the limiting, *e-NTU*$_1$ and *e-NTU*$_2$, cases.

Table H.1: Fill performance characteristics of a crossflow fill according to the Merkel, *e-NTU* and Poppe approaches.

	Merkel	**Poppe**	***e-NTU*$_1$**	***e-NTU*$_2$**	***e-NTU*$_3$**	***e-NTU*$_4$**
Q, **MW**	0.1987946	0.2064673	0.1987946	0.1987946	0.1987946	0.1987946
T_{ao}, **K**	297.4277	297.8390	297.4277	297.4277	297.4277	297.4277
$m_{w(evap)}$, **kg/s**	0.05395610	0.06277423	0.05395610	0.05395610	0.05395610	0.05395610
Me	0.7395232	0.7976296	0.7404729	0.7750973	0.7588670	0.7486152

Thus, only the Merkel numbers differ for the respective *e-NTU* approach variants and the Merkel approach. The fill outlet conditions, predicted by all the variants of the *e-NTU* approach and the Merkel approach are identical. Thus, any variant of the *e-NTU* approach or the Merkel approach can be used consistently in the fill performance analysis and in the subsequent cooling tower performance analysis. Cooling tower performance, predicted by the all the variant of the *e-NTU* approach and Merkel approach, will therefore be practically identical. It is recommended that the fill performance evaluation be carried out at approximately the same conditions where the cooling tower will operate.

The Merkel numbers according to the Merkel approach and the *e-NTU*$_1$ approach are practically identical for the fill performance analysis. However, this is only true for the operational conditions specified above. Therefore, the empirical relations obtained from fill performance analyses, by employing the one approach, cannot be used interchangeably in cooling tower performance calculations while employing the other approach. For other water temperatures and practical water to air mass flow ratios the differences between the Merkel numbers of the two approaches can be quite significant.

It can be seen from table H.1 that the more rigorous Poppe approach predicts higher heat rejection rates, water evaporation rates and Merkel numbers than the Merkel approach. The Merkel number according to the Poppe approach is approximately 8 % higher than that predicted by the Merkel approach. The predicted heat rejection rate according to the Poppe approach is approximately 4% higher than that predicted by the Merkel approach.

It is important to realize that the comparisons between the different approaches are only for the ambient and operational conditions specified above. The differences between the approaches can vary quite significantly at extreme ambient conditions.

The mean outlet air temperature and humidity ratio, according to the Merkel approach, are obtained by integrating the outlet air enthalpy, at the air outlet side of the fill, and by assuming that the air is saturated at this mean enthalpy. The air outlet temperature and humidity ratio can also be obtained, at each grid point at the air outlet side of the fill, by assuming that the air is saturated at each grid point. The mean air temperature and humidity ratio can then be obtained by integration. Therefore, it does not matter if the

assumption of saturated air is applied to each air outlet grid point, or to the mean outlet air enthalpy, the same results are obtained.

H.6 COMPARISON BETWEEN THE PERFORMANCE OF COUNTERFLOW AND CROSSFLOW FILLS

The results of the crossflow fill performance analysis are compared to the results of a counterflow fill performance analysis. The same operational and ambient conditions are used in both the crossflow and counterflow fill performance analyses. Thus, the cooling range is identical for both the counterflow and crossflow fill tests. The heat rejection rates, air outlet temperatures, evaporation rates and the Merkel numbers, according to the Merkel, Poppe and *e-NTU* approaches for the counterflow fill analysis, are shown in table H.2.

If the values in table H.2 are compared to the corresponding values in table H.1, it can be seen that the heat rejection rate, Q, the air outlet temperature, T_{ao}, and the water evaporation rate, $m_{w(evap)}$, for the Merkel and *e-NTU* approaches are identical for both the crossflow and counterflow fills. The heat rejection rates are the same because of the equal cooling ranges for the crossflow and counterflow fills. The outlet air enthalpy can be calculated from a simple energy balance. Subsequently, the outlet air temperature can be calculated after the assumption that the outlet air is saturated with water vapor. The Merkel number for the counterflow case, however, is equal to 0.68468, which is approximately 7% smaller than that predicted for the crossflow fill.

Table H.2: Fill performance characteristics of a counterflow fill according to the Merkel, *e-NTU* and Poppe approaches.

	Merkel	**Poppe**	***e-NTU***
Q, **MW**	0.1987946	0.211380	0.1987946
T_{ao}, **K**	297.428	298.1192	297.428
$m_{w(evap)}$, **kg/s**	0.05395610	0.0649723	0.05395610
Me	0.68468	0.741356	0.6770926

The heat rejection rates, air outlet temperatures and water evaporation rates for the fill performance analyses, for the crossflow and counterflow fills, according to the Poppe approach, are not equal as was the case with the Merkel and *e-NTU* approaches. The heat rejection rate according to the Poppe approach for the counterflow fill is approximately 2.5% higher than that predicted for the crossflow fill. The air outlet temperature is also approximately 0.3K higher for the counterflow fill compared to the crossflow fill. Approximately 3.5% more water is evaporated in the counterflow fill compared to the crossflow fill.

It is evident that the Merkel numbers for the crossflow fill, for the Merkel and Poppe approaches, are higher than those for the counterflow fill. A larger wetted area is needed in the crossflow fill to obtain the same cooling load as in the counterflow fill. Thus, a larger volume of fill is needed in crossflow towers than in counterflow towers to obtain the same cooling load.

APPENDIX I

ANALYSIS OF A NATURAL DRAFT WET-COOLING TOWER EMPLOYING THE POPPE APPROACH

I.1 INTRODUCTION

The heat rejection rate and the loss in cooling water, due to evaporation, in a hyperbolic natural draft counterflow wet-cooling tower, as shown in figure I.1, are determined while employing the Poppe approach for heat and mass transfer in the fill. Kröger [98KR1] employed the Merkel approach to calculate the heat rejection rate and evaporation rate while employing the same cooling tower and operational specifications. It is assumed that the water and the airflow through the fill are uniform and that the inside diameter of the upper section of the tower is constant.

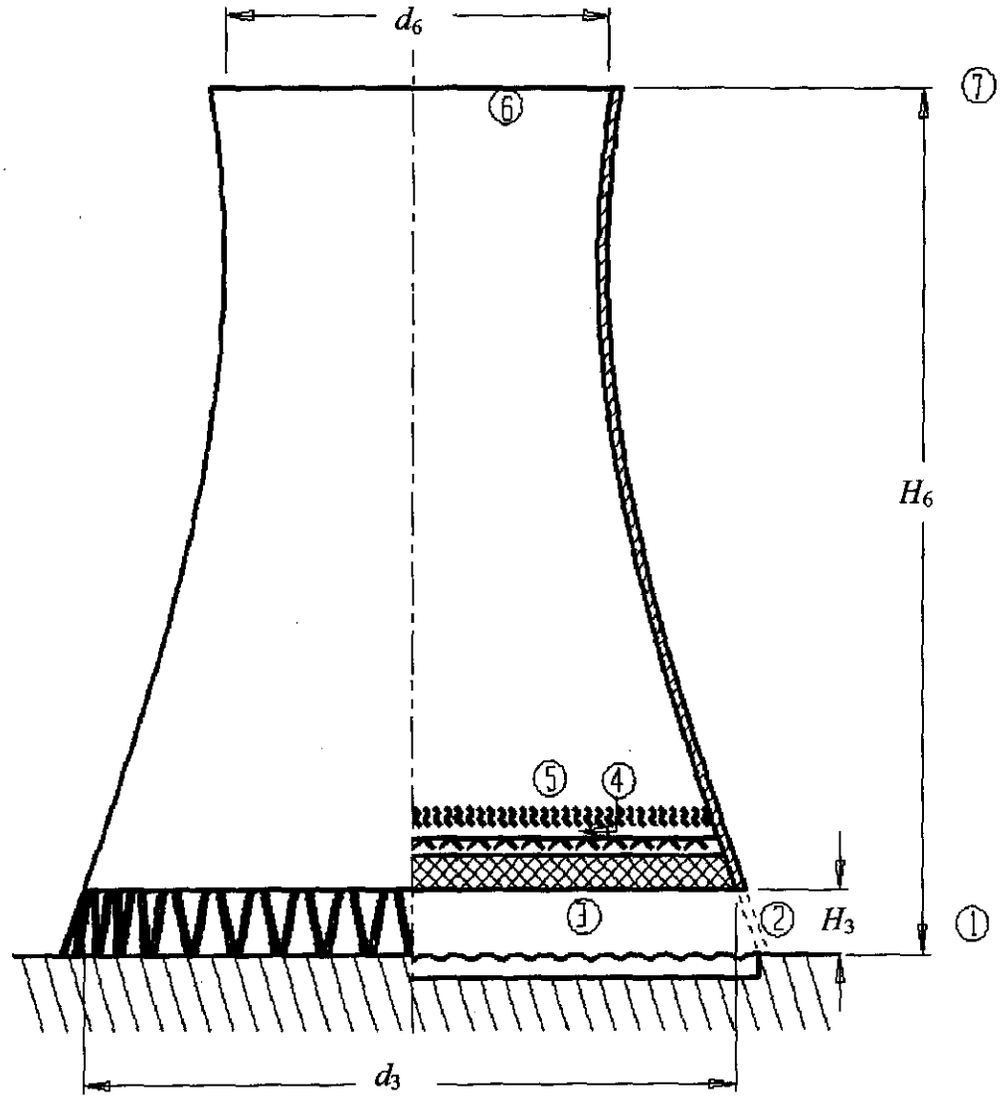

Figure I.1: Natural draft cooling tower with horizontal fill.

Ambient conditions:

Air temperature at ground level	T_{a1}	= 15.45°C (288.6K)
Wetbulb temperature at ground level	T_{wb}	= 11.05°C (284.2K)
Atmospheric pressure	p_{a1}	= 84100 N/m^2
Ambient temperature gradient	dT_a/dz	= –0.00975 K/m from ground level

Cooling tower and operational specifications:

Water mass flow rate	m_w	= 12500 kg/s
Water inlet temperature	T_{wi}	= T_{w5} = 40°C
Rounded tower shell inlet	r_i/d_3	= 0.02
Tower height	H_6	= 147 m
Tower inlet height	H_3	= 10 m
Tower inlet diameter	d_3	= 104.5 m
Tower outlet diameter	d_6	= 60.85 m
Number of tower supports	n_{ts}	= 72
Length of tower supports	L_{ts}	= 11.6 m
Diameter of support	d_{ts}	= 0.8 m
Drag coefficient of round tower supports	C_{Dts}	= 1.0
Shell thickness at air inlet	t_s	= 1.0 m

Fill specifications:

The cooling tower is fitted with an expanded metal fill (L_{fi} = 2.504 m) for which the performance characteristics are respectively:

Transfer coefficient	$Me_{Pfi} = \dfrac{h_{dfi} a_{fi}}{G_w} = 0.27928 G_w^{-0.094} G_a^{0.6023}$
Loss coefficient	$K_{fdm1} = 1.851 G_w^{1.2752} G_a^{-1.0356}$
Frontal area of the fill	A_{fr} = 8300 m^2

Other specifications:

Depth of spray zone above fill	L_{sp}	= 0.5 m
Mean drop diameter in rain zone	d_d	= 0.0035 m
Loss coefficient for contraction and fill supports based on Afr	$K_{fs} + K_{ctc}$	= 0.5
Loss coefficient for distribution system	K_{wd}	= 0.5
Kinetic energy coefficient at tower outlet	α_{e6}	= 1.01

The transfer area, i.e., the fill, rain zone and spray zone, is divided into five intervals, with an equal temperature difference across each interval, for the numerical integration of the governing equations of the Poppe approach.

I.2 AIR INLET CONDITIONS

The enthalpy of the inlet air, i_{ma1}, is found according to equation (A.3.6b). At the specified air inlet drybulb temperature of T_{a1} = 288.6K and wetbulb temperature of T_{wb} = 284.2K find the following:

Pressure of water vapor from equation (A.2.1) evaluated at T_{wb}, where T_{wb} = 284.2K.

$z_1 = 10.79586(1 - 273.16/284.2) + 5.02808 \log_{10}(273.16/284.2) + 1.50474$

$\times 10^{-4}[1 - 10^{-8.29692\{(284.2/273.16)-1\}}] + 4.2873 \times 10^{-4}[10^{4.76955(1-273.16/284.2)} - 1] + 2.786118312 = 3.119284$

$p_{v1} = 10^{3.119284} = 1316.086$ Pa

Humidity ratio for saturated air from equation (A.3.5)

$$w_1 = \left(\frac{2501.6 - 2.3263(T_{wb} - 273.15)}{2501.6 + 1.8577(T - 273.15) - 4.184(T_{wb} - 273.15)}\right)\left(\frac{0.62509 p_{vwb}}{p_{abs} - 1.005 p_{vwb}}\right)$$

$$- \left(\frac{1.00416(T - T_{wb})}{2501.6 + 1.8577(T - 273.15) - 4.184(T_{wb} - 273.15)}\right)$$

$$= \left(\frac{2501.6 - 2.3263(284.2 - 273.15)}{2501.6 + 1.8577(288.6 - 273.15) - 4.184(284.2 - 273.15)}\right)\left(\frac{0.62509 \cdot 1316.086}{84100 - 1.005 \cdot 1316.086}\right)$$

$$- \left(\frac{1.00416(288.6 - 284.2)}{2501.6 + 1.8577(288.6 - 273.15) - 4.184(284.2 - 273.15)}\right)$$

= 0.008127 kg/kg dry air

The enthalpy of the inlet air, i_{ma1}, is found according to equation (A.3.6b) with c_{pa1} = 1006.44 J/kgK and c_{pv1} = 1869.2 J/kgK being evaluated at $(T_{a1} + 273.15)/2 = (288.6 + 273.15)/2 = 280.875$K according to equations (A.1.2) and (A.2.2) respectively. The latent heat is found to be $i_{fgwo} = 2.5016 \times 10^6$ J/kgK according to equation (A.4.5) at 273.15K. With these values find i_{ma1} = 36114.71 J/kg dry air.

I.3 INITIAL APPROXIMATION OF VARIABLES

Six cooling tower design variables are chosen and solved through an iterative procedure. These variables are m_{av15}, p_{a5}, p_{a6}, T_{a5}, T_{wo} and w_5. Initial approximations for the variables must be supplied for the first iteration of the cooling tower analysis. A preliminary estimate can be made on the evidence of empirical results and simple physical models. The initial approximations of the water outlet temperature, T_{wo}, and the outlet air temperature, T_{a5}, are determined from empirical relations found in the literature. The initial approximations of the pressures p_{a5} and p_{a6} are found from a pressure distribution derived for a constant atmospheric humidity and a dry adiabatic lapse rate. The initial approximation for the mass flow rate, m_{av15}, is found from a simple heat balance of the cooling tower. The air outlet humidity, w_5, is determined by assuming that the air is saturated at the air outlet of the fill.

An empirical formula to determine the approximate water outlet temperature is according to Johnson and Priester [49JO1],

$$T_{wo} = \frac{T_{wi} + 2T_{wb} + T_{a1}}{4} = \frac{313.15 + (2)(284.2) + 288.6}{4} = 292.5375\,\text{K}$$

Where the temperature of the saturated air leaving the tower, T_{ao}, is not known to the designer can it be approximated by the average of the inlet and outlet temperatures as can be seen in figure I.2. The data in figure I.2 are obtained from Mohiuddin and Kant [96MO1], Hutchison and Spivey [42HU1] and McKelvey and Brook [59MC1].

$$T_{a5} = \frac{T_{wi} + T_{wo}}{2} = \frac{313.15 + 292.5375}{2} = 302.8437\,\text{K}$$

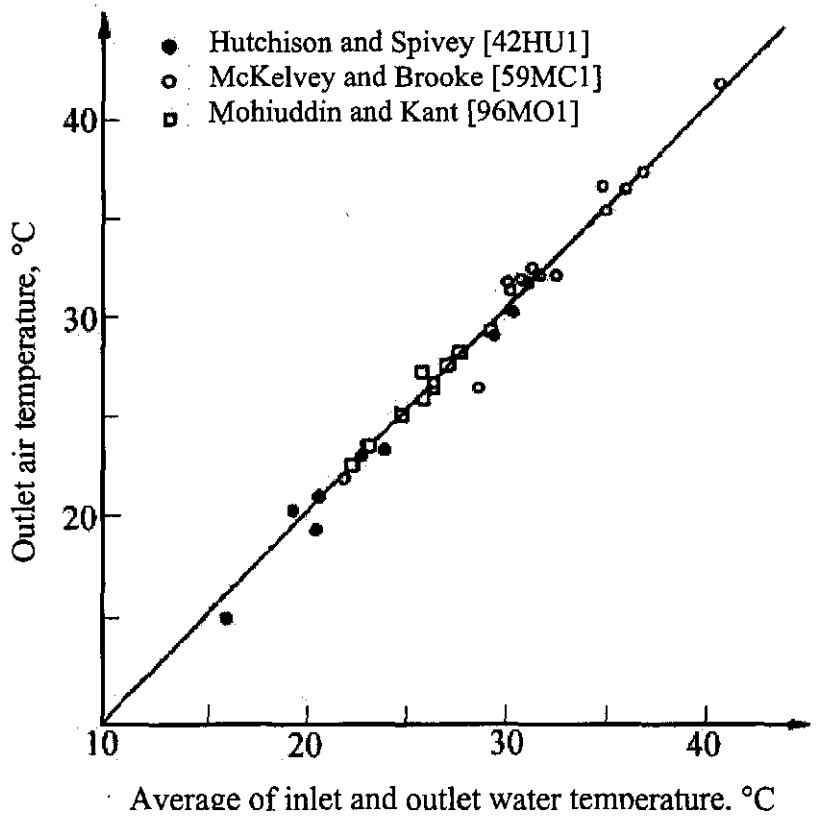

Figure I.2: Variation of outlet air temperature with average water temperature.

The air pressures inside the cooling tower at elevation 6 and 7 can be approximated by using the are pressure distribution relation derived for a constant atmospheric humidity, w_1, and a dry adiabatic lapse rate, i.e.,

$$p_{a5} = p_{a1}\left[1 - \frac{0.00975\left(H_3 + L_{fl} + L_{sp}\right)}{T_{a1}}\right]^{3.5(1+w_1)\left(1-\frac{w_1}{w_1+0.62198}\right)}$$

$$= 84100\left[1 - \frac{0.00975(10 + 2.504 + 0.5)}{288.6}\right]^{3.5(1+0.008127)\left(1-\frac{0.008127}{0.008127+0.62198}\right)} = 83971.38\ \text{Pa}$$

$$p_{a6} = p_{a1}\left[1 - \frac{0.00975H_6}{T_{a1}}\right]^{3.5(1+w_1)\left(1-\frac{w_1}{w_1+0.62198}\right)}$$

$$= 84100\left[1-\frac{0.00975(147)}{288.6}\right]^{3.5(1+0.008127)\left(1-\frac{0.008127}{0.008127+0.62198}\right)} = 82654.27 \text{ Pa}$$

The initial approximated air mass flow rate can be obtained by a simple heat balance for the cooling tower,

$$m_a\left(i_{mas5}-i_{ma1}\right)=m_w c_{pwm}\left(T_{wi}-T_{wo}\right)$$

After rearrangement and assuming that $m_{av15} = m_a$ find,

$$m_{av15}=\frac{m_w c_{pwm}\left(T_{wi}-T_{wo}\right)}{\left(i_{mas5}-i_{ma1}\right)}$$

where c_{pwm} is evaluated at $(T_{wi} + T_{wo})/2 = (313.15 + 292.5375)/2 = 302.8437$ K. From equation (A.4.2) find

$c_{pwm} = 8.15599 \times 10^3 - 2.80627 \times 10\,(302.8437) + 5.11283 \times 10^{-2}\,(302.8437)^2 - 2.17582 \times 10^{-13}$ $(302.8437)^6 = 4178.721$ J/kgK

The enthalpy of the saturated outlet air, i_{mas5}, is found according to equation (A.3.6b) at the approximated air outlet temperature, $T_{a5} = 288.6$ K,

Pressure of water vapor from equation (A.2.1) evaluated at T_{a5}, where $T_{a5} = 302.8437$K.

$z_5 = 10.79586(1 - 273.16/302.8437) + 5.02808 \log_{10}(273.16/302.8437) + 1.50474$ $\times 10^{-4}[1 - 10^{-8.29692\{(302.8437/273.16)-1\}}] + 4.2873 \times 10^{-4}[10^{4.76955(1-273.16/302.8437)} - 1] + 2.786118312 = 3.61998$

$p_{v5} = 10^{3.61998} = 4168.581$ Pa

Humidity ratio for saturated air from equation (A.3.5)

$$w_5=\frac{0.62509p_{vwb}}{p_{abs}-1.005p_{vwb}}=\frac{0.62509\cdot 4168.581}{83971.38-1.005\cdot 4168.581}=0.0326607 \text{ kg/kg dry air}$$

The enthalpy of the inlet air, i_{ma5}, is found according to equation (A.3.6b) with $c_{pa5} = 1006.59$ J/kgK and $c_{pv5} = 1875.204$ J/kgK being evaluated at $(T_{a5} + 273.15)/2 = (302.8437 + 273.15)/2 = 287.9969$K according to equations (A.1.2) and (A.2.2) respectively. The latent heat is found to be $i_{fgwo} = 2.5016 \times 10^6$ J/kgK according to equation (A.4.5) at 273.15K. With these values find $i_{mas5} = 113412.1$ J/kg dry air.

The air vapor mass flow rate is

$$m_{av15}=\frac{m_w c_{pwm}\left(T_{wi}-T_{wo}\right)}{\left(i_{mas5}-i_{ma1}\right)}=\frac{(12500)(4178.721)(313.15-292.5375)}{113412.1-36114.76}=13928.97 \text{ kg/s}$$

I.4 THE ENERGY EQUATION

The values for T_{wo}, T_{a5}, m_{av15}, p_{a5}, p_{a6} and w_5, determined in the previous section, are only initial approximations. This problem can only be solved by following an iterative procedure to obtain a solution

that will satisfy both the energy and draft equations. The choice of an air-vapor mass flow rate of m_{av15} = 16966.47 kg/s through the fill will satisfy these equations, giving corresponding pressures of p_{a5} = 83937.04 Pa and p_{a6} = 82650.57 Pa, and an air temperature of T_{a5} = 299.85626K. The mean temperature of the recooled water in the basin is T_{wo} = 294.5572K. The humidity of the supersaturated air above the spray zone is w_5 = 0.027888 kg/kg dry air with w_{sa5} = 0.027176 kg/kg dry air.

At the specified air inlet drybulb temperature of T_{a1} = 288.6K, wetbulb temperature of T_{wb} = 284.2K, find the following thermophysical properties employing the equations given in appendix A.

Density of air-vapor	ρ_{av1} = 1.0101 kg/m3	(A.3.1)
Viscosity of the air vapor mixture	$\mu_{av1} = 1.7857 \times 10^{-5}$ kg/ms	(A.3.3)

If the air is assumed to be supersaturated immediately after the drift eliminator, the wetbulb temperature at 5 will be equal to the given drybulb temperature T_{a5} = 299.8563K at this elevation. The corresponding thermophysical properties at 5 can be determined according to the equations given in appendix A.

Saturated vapor pressure	p_{v5} = 3503.482 N/m^2	(A.2.1)
Density of air-vapor	ρ_{av5} = 0.95964 kg/m^3	(A.3.1)
Dynamic viscosity of air	$\mu_{a5} = 1.8462\times10^{-5}$ kg/ms	(A.1.3)
Dynamic viscosity of vapor	$\mu_{v5} = 1.0041\times10^{-5}$ kg/ms	(A.2.3)
Dynamic viscosity of air-vapor	$\mu_{av5} = 1.8182 \times10^{-5}$ kg/ms	(A.3.3)

The enthalpy of the supersaturated outlet air, i_{ss5}, is found according to equation (B.33) with c_{pa5} = 1006.5548 J/kgK and c_{pv5} = 1873.9329 J/kgK being evaluated at $(T_{a5} + 273.15)/2 = (299.8563 + 273.15)/2$ = 286.50315K according to equations (A.1.2) and (A.2.2) respectively. The latent heat is found to be i_{fgwo} = 2.5016×10^6 J/kgK according to equation (A.4.5) at 273.15K. With these values find i_{ss5} = 96303.4766 J/kg dry air.

The approximate harmonic mean density of the air-vapor in the fill is given by

$$\rho_{av15} = \frac{2}{\frac{1}{\rho_{av1}} + \frac{1}{\rho_{av5}}} = \frac{2}{\frac{1}{1.01012} + \frac{1}{0.95964}} = 0.98424 \text{ kg/m}^3$$

The dry air mass flow rate can be determined from the following relation:

$$m_{av15} = [m_a(1 + w_1) + m_a(1 + w_{sa5})]$$

or

$$m_a = 2m_{av15}/(2 + w_1 + w_{sa5}) = 2(16966.47)/(2 + 0.008127 + 0.027176) = 16672.19 \text{ kg/s}$$

The respective air-vapor mass flow rates upstream and downstream of the fill are thus

$$m_{av1} = m_a(1 + w_1) = 16672.19(1 + 0.008127) = 16807.68 \text{ kg/s}$$

and

$m_{av5} = m_a(1 + w_{sa5}) = (1 + 0.027176) = 17125.27$ kg/s

The corresponding mass velocities are

$G_{av15} = m_{av15} / A_{fr}$ = 16966.47/8300 = 2.04415 kg/m^{2}s

$G_a = m_a / A_{fr}$ = 16672.19/8300 = 2.00870 kg/m^{2}s

$G_{av1} = m_{av1} / A_{fr}$ = 16807.68/8300 = 2.02502 kg/m^{2}s

$G_{av5} = m_{av5} / A_{fr}$ = 17125.27/8300 = 2.06329 kg/m^{2}s

According to equation (A.4.2) the specific heat of water c_{pwm} = 4178.32 J/kg at the mean water temperature of $(T_{wi} + T_{wo})/2 = (313.15 + 294.5573)/2 = 303.8536$K.

At the mean outlet temperature of the water T_{wo} = 294.5573K find

Density of water	ρ_{wo} = 997.8629 kg/m3	(A.4.1)
Surface tension	σ_{wo} = 0.07256 N/m	(A.4.7)

The mass velocity for the water based on the frontal area of the fill is

$G_w = m_w / A_{fr}$ = 12500/8300 = 1.50602 kg/m^{2}s

The transfer coefficients can be determined with the above values. To find the transfer coefficient in the rain zone, use equation (D.20). The "a" coefficients appearing in the equation for the rain zone transfer and pressure drop coefficients are as follows:

$$a_\mu = 3.061\times10^{-6}\left(\rho_{wo}^4 g^9 / \sigma_{wo}\right)^{0.25} = 3.061\times10^{-6}\left(997.8629^4 9.8^9 / 0.07256\right)^{0.25} = 1.00004$$

$$a_\rho = 998 / \rho_{wo} = 998/997.8629 = 1.00014$$

$$a_v = 73.298\left(g^5\sigma_{wo}^3 / \rho_{wo}^3\right)^{0.25} = 73.298\left(9.8^5 \times 0.07256^3 / 997.8629\right)^{0.25} = 1.0008$$

$$a_L = 6.122\left(g\sigma_{wo} / \rho_{wo}\right)^{0.25} = 6.122\left(9.8\times 0.07256 / 997.8629\right)^{0.25} = 1.00025$$

Other quantities required to evaluate the rain zone transfer coefficient are:

The humidity ratio of saturated air at T_{wo}	w_{s1} = 0.019539 kg/kg	(A.3.5)
Diffusion coefficient at inlet conditions	$D_1 = 2.29972\times10^{-5}$ m^2/s	(D.21)

Furthermore, the Schmidt number is

$S_{c1} = \mu_{av1} / \left(\rho_{av1} D_1\right) = 1.7857\times10^{-5}/(1.01012 \times 2.29972\times10^{-5}) = 0.76865$

and the air-vapor velocity before the fill

$v_{av3} = m_{av1} / \left(\rho_{av1} A_{fr}\right) = 16807.68/(1.01012\times8300) = 2.00473$ m/s

With these values find

$$Me_{rz} = \frac{h_{drz} a_{rz} H_3}{G_w} = 12\left(\frac{D_1}{v_{av3} d_d}\right)\left(\frac{H_3}{d_d}\right)\left(\frac{p_{a1}}{\rho_{wo} R_v T_{a1}}\right) Sc_1^{0.33}\left[\ln\left(\frac{w_{s1}+0.622}{w_1+0.622}\right)/\left(w_{s1}-w_1\right)\right]$$

$$\times\left[\begin{array}{l} 0.90757 a_\rho \rho_{av1} - 30341.04 a_\mu \mu_{av1} - 0.37564 \\ +4.04016\left[\begin{array}{l} \left\{0.55+41.7215\left(a_L d_d\right)^{0.80043}\right\}\left\{0.713+3.741\left(a_L H_3\right)^{-1.23456}\right\} \\ \times\left\{3.11\exp\left(0.15 a_v v_{av3}\right)-3.13\right\} \\ \times\exp\left\{5.3759\exp\left(-0.2092 a_L H_3\right)\ln\left\{\begin{array}{l}0.3719\exp\left(0.0019055 a_L d_3\right) \\ +0.55\end{array}\right\}\right\} \end{array}\right] \end{array}\right]$$

$$=12\left(\frac{2.29972\times10^5}{2.00473\times0.0035}\right)\left(\frac{10}{0.0035}\right)\left(\frac{84100}{997.8629\times461.52\times288.6}\right)0.76865^{0.33}\left[\frac{\ln\left(\frac{0.019539+0.622}{0.008127+0.622}\right)}{(0.019539-0.008127)}\right]$$

$$\times\left[\begin{array}{l} 0.90757\times1.00014\times1.01012 - 30341.04\times1.00004\times1.7857\times10^{-5} - 0.37564 \\ +4.04016\left[\begin{array}{l} \left\{0.55+41.7215\left(1.00025\times0.0035\right)^{0.80043}\right\}\left\{0.713+3.741\left(1.00025\times10\right)^{-1.23456}\right\} \\ \times\left\{3.11\exp\left(0.15\times1.0008\times2.00473\right)-3.13\right\} \\ \times\exp\left\{\begin{array}{l}5.3759\exp\left(-0.2092\times1.00025\times10\right) \\ \times\ln\left\{\begin{array}{l}0.3719\exp\left(0.0019055\times1.00025\times104.5\right) \\ +0.55\end{array}\right\}\end{array}\right\} \end{array}\right] \end{array}\right]$$

$= 0.4150354$

The Merkel number applicable to the fill is specified in the form of equation (D.24)

$$Me_{Pfi} = \frac{h_{dfi} a_{fi}}{G_w} = 0.27928 G_w^{-0.094} G_a^{0.6023}$$

$$= 0.27928 \times 1.878 \times (1.50602)^{-0.094} \times (2.00870)^{0.6023} = 1.024240$$

The transfer coefficient in the spray zone is given by (D.23)

$$Me_{sp} = \frac{h_{dsp} a_{sp} L_{sp}}{G_w} = 0.2 L_{sp}\left(\frac{G_a}{G_w}\right)^{0.5} = 0.2\times0.5\left(\frac{2.00870}{1.50602}\right)^{0.5} = 0.11549$$

The total transfer characteristic of the cooling tower is

$$Me = Me_{rz} + Me_{Pfi} + Me_{sp} = \frac{h_{drz} a_{rz} H_3}{G_w} + \frac{h_{dfi} a_{fi} L_{fi}}{G_w} + \frac{h_{dsp} a_{sp} L_{sp}}{G_w}$$

$$= 0.4150354 + 1.024240 + 0.11549 = 1.55476$$

The empirical relations for the transfer characteristics of the rain zone and spray zone were derived by employing the Merkel approach. However, the Poppe approach is used to evaluate cooling tower performance. The transfer characteristic of this particular fill, determined by the Poppe approach, is approximately 7% larger than that determined by the Merkel approach. Thus, the transfer characteristics of the spray zone and rain zone were increased by 7% in another investigation by the author. This was done to determine the influence of the inconsistent application of the fill performance characteristics to the cooling tower performance evaluation. The fill performance characteristics according to the Poppe approach were employed in that investigation.

It is found that cooling tower performance, determined by the Poppe approach, where the transfer characteristics of the spray zone and rain zone are increased by 7 %, is practically identical to the cooling tower performance where the transfer characteristic of the spray and rain zones are not increased by 7 %. The results are practically identical across a broad range of ambient temperatures and humidities. Thus, the transfer characteristics of the rain zone and spray zone, obtained by the Merkel approach, can be employed in cooling tower performance evaluations while employing the Poppe approach. The transfer characteristics of the fill, however, must be obtained from the Poppe approach, if the Poppe approach is employed in the cooling tower performance evaluation. The inconsistent application of the transfer characteristics of the rain and spray zones is possible because these characteristics are respectively approximately only 27 % and 7 % of the total transfer characteristic.

Thus, due to the uncertainties associated in converting the transfer characteristics of the rain zone and spray zone, obtained from the Merkel approach, to that of the Poppe approach, by increasing it by 7 % and the fact that the Merkel approach gives conservative results, can the empirical relations of the transfer characteristics of the rain zone and spray zone be used inconsistently without compromising solution accuracy.

I.5 TRANSFER AREA ANALYSIS ACCORDING TO THE POPPE APPROACH

The fourth order Runge-Kutta method is used to solve the governing equations. As already mentioned, the fill is divided into five intervals with an equal water temperature difference across each interval. Refer to figure I.3 for a layout of the transfer area, i.e., the fill rain zone and spray zone, that is divided into five intervals.

Refer to appendix B.4 for a detailed discussion on the application of the Runge-Kutta method to the governing equations of the Poppe approach. Refer to appendix G for the convention used for the subscripts.

The Runge-Kutta method is an initial value problem; therefore, the initial values at level (0) are as obtained previously

$w_{(0)} = w_1 = 0.008127$ kg/kg dry air

$i_{ma(0)} = i_{ma1} = 36114.71$ J/kg dry air

Since the transfer area is divided into two intervals find from equation (B.66)

$\Delta T_w = (T_{wi} - T_{wo})/(\text{Number of intervals}) = (313.15 - 294.5572)/5 = 3.719\text{K}$

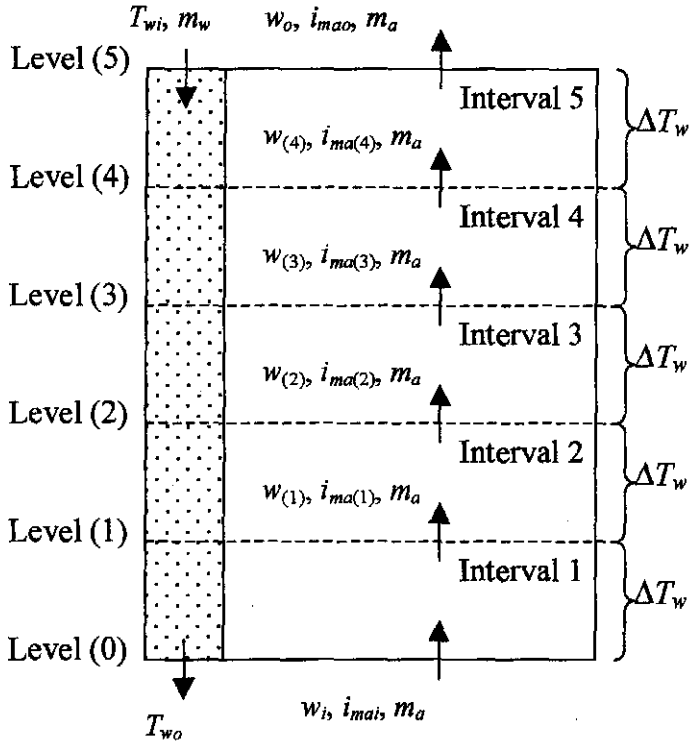

Figure I.3: Total transfer area of a counterflow tower, divided into five intervals.

From equations (B.51) to (B.53) find for the first interval of the Runge-Kutta method,

$w_{(1)} = w_{(0)} + (j_{(1,1)} + 2j_{(1,2)} + 2j_{(1,3)} + j_{(1,4)})/6$

$i_{ma(1)} = i_{ma(0)} + (k_{(1,1)} + 2k_{(1,2)} + 2k_{(1,3)} + k_{(1,4)})/6$

$Me_{P(1)} = Me_{P(0)} + (l_{(1,1)} + 2l_{(1,2)} + 2l_{(1,3)} + l_{(1,4)})/6$

where $Me_{P(0)}$ is equal to zero at the air inlet side or at level (0).

Commence with the first intermediate calculation step of the Runge-Kutta method for the first interval. It can be seen from equations (B.54) to (B.56) that $j_{(1,1)}$, $k_{(1,1)}$ and $l_{(1,1)}$ are functions of $T_{w(0)}$, $i_{ma(0)}$ and $w_{(0)}$. Define that

$T_{w(1,1)} = T_{w(0)} = T_{wo} = 294.5572\text{K}$

$w_{(1,1)} = w_{(0)} = w_i = 0.008127$ kg/kg dry air

$i_{ma(1,1)} = i_{ma(0)} = i_{mai} = 36114..71$ J/kg dry air.

To calculate $j_{(1,1)}$, $k_{(1,1)}$ and $l_{(1,1)}$ in equations (B.51) to (B.53) respectively, the specific heats have to be evaluated at $(T_{w(1,1)} + 273.15)/2 = (294.5572 + 273.15)/2 = 283.8536\text{K}$

Specific heat of dry air from equation (A.1.2)

$c_{pa(1,1)} = 1.045356 \times 10^3 - 3.161783 \times 10^{-1}(283.8536) + 7.083814 \times 10^{-4}(283.8536)^2$

$$- 2.705209 \times 10^{-7} (283.8536)^3 = 1006.497 \text{ J/kgK}$$

Specific heat of water vapor from equation (A.2.2)

$$c_{pv(1,1)} = 1.3605 \times 10^3 + 2.31334 (283.8536) - 2.46784 \times 10^{-10} (283.8536)^5$$
$$+ 5.91332 \times 10^{-13} (283.8536)^6 = 1871.695 \text{ J/kgK}$$

Specific heat of water from equation (A.4.2)

$$c_{pw(1,1)} = 8.15599 \times 10^3 - 2.80627 \times 10 (283.8536) + 5.11283 \times 10^{-2} (283.8536)^2$$
$$- 2.17582 \times 10^{-13} (283.8536)^6 = 4196.035 \text{ J/kgK}$$

Pressure of water vapor from equation (A.2.1) evaluated at $T_{(1,1)} = 294.5572$K.

$$z_{(1,1)} = 10.79586(1 - 273.16/294.5572) + 5.02808 \log_{10}(273.16/294.5572) + 1.50474$$
$$\times 10^{-4}[1 - 10^{-8.29692\{(294.5572/273.16)-1\}}] + 4.2873 \times 10^{-4}[10^{4.76955(1-273.16/294.5572)} - 1] + 2.786118312 = 3.40626$$

$$p_{v(1,1)} = 10^{3.57157} = 2548.33 \text{ Pa}$$

Humidity ratio for saturated air at $T_{(1,1)} = 294.5572$K from equation (A.3.5)

$$w_{ws(1,1)} = \left(\frac{0.62509(2548.33)}{84100 - 1.005(2548.33)} \right) = 0.019536 \text{ kg/kg dry air}$$

Latent heat at 273.15K follows from equation (A.4.5)

$$i_{fgw(1,1)} = 2.5016 \times 10^6 \text{ J/kg}$$

The enthalpy of water vapor at the local bulk water temperature, $T_{w(1,1)}$, relative to water at 0°C,

$$i_{v(1,1)} = i_{fgw(1,1)} + c_{pv(1,1)} T_{w(1,1)}$$
$$= 2.5016 \times 10^6 + 1871.695 (294.5572 - 273.15) = 2541662 \text{ J/kg}$$

The enthalpy of saturated air at the local bulk water temperature from equation (A.3.6b)

$$i_{masw(1,1)} = 1006.497(294.5572 - 273.15) + (0.019536)(2541662) = 71198 \text{ J/kg}$$

The Lewis factor from equation (B.15)

$$Le_{f(1,1)} = 0.865^{0.667} \frac{\left(\frac{0.662 + 0.019536}{0.662 + 0.008127} - 1 \right)}{\ln\left(\frac{0.662 + 0.019536}{0.662 + 0.008127} \right)} = 0.9160$$

The mass balance from equation (B.32),

$$\left(\frac{m_w}{m_a} \right)_{(1,1)} = \frac{12500}{16672.19} \left[1 - \frac{16672.19}{12500} (0.027889 - 0.008127) \right] = 0.730$$

From equation (B.54) find

$$j_{(1,1)} = \Delta T_w \cdot f\left(T_{w(0)}, i_{ma(0)}, w_{(0)}\right) = \Delta T_w \cdot f\left(T_{w(1,1)}, i_{ma(1,1)}, w_{(1,1)}\right)$$

From equation (B.48) find

$$\frac{dw}{dT_w} = f\left(T_{w(0)}, i_{ma(0)}, w_{(0)}\right) = f\left(T_{w(1,1)}, i_{ma(1,1)}, w_{(1,1)}\right)$$

but from equation (B.24),

$$\frac{dw}{dT_w} = \frac{c_{pw(1,1)}\left(\frac{m_w}{m_a}\right)_{(1,1)}\left(w_{sw(1,1)} - w_{(1,1)}\right)}{\begin{array}{l} i_{masw(1,1)} - i_{ma(1,1)} + \left(Le_{f(1,1)} - 1\right)\left[i_{masw(1,1)} - i_{ma(1,1)} - \left(w_{sw(1,1)} - w_{(1,1)}\right)i_{v(1,1)}\right] \\ -\left(w_{sw(1,1)} - w_{(1,1)}\right)c_{pw(1,1)}T_{w(1,1)} \end{array}}$$

Combine equations (B.24), (B.48) and (B.54) to find

$$j_{(1,1)} = \frac{\Delta T_w c_{pw(1,1)}\left(\frac{m_w}{m_a}\right)_{(1,1)}\left(w_{sw(1,1)} - w_{(1,1)}\right)}{\begin{array}{l} i_{masw(1,1)} - i_{ma(1,1)} + \left(Le_{f(1,1)} - 1\right)\left[i_{masw(1,1)} - i_{ma(1,1)} - \left(w_{sw(1,1)} - w_{(1,1)}\right)i_{v(1,1)}\right] \\ -\left(w_{sw(1,1)} - w_{(1,1)}\right)c_{pw(1,1)}T_{w(1,1)} \end{array}}$$

$$= \frac{(3.719)(4196.035)(0.730)(0.019536 - 0.008127)}{\begin{bmatrix} 71198 - 36114.71 \\ +(0.9160-1)[71198 - 36114.71 - (0.019536 - 0.008127)(2541662)] \\ -(0.019536 - 0.008127)(4196.035)(294.5572 - 273.15) \end{bmatrix}} = 0.003874$$

Combine equations (B.25), (B.49) and (B.55) to find.

$$k_{(1,1)} = \Delta T_w c_{pw(1,1)}\left(\frac{m_w}{m_a}\right)_{(1,1)} \times \left(1 + \frac{\left(w_{sw(1,1)} - w_{(1,1)}\right)c_{pw(1,1)}T_{w(1,1)}}{\begin{array}{l} i_{masw(1,1)} - i_{ma(1,1)} + \left(Le_{f(1,1)} - 1\right)\left[i_{masw(1,1)} - i_{ma(1,1)} - \left(w_{sw(1,1)} - w_{(1,1)}\right)i_{v(1,1)}\right] \\ -\left(w_{sw(1,1)} - w_{(1,1)}\right)c_{pw(1,1)}T_{w(1,1)} \end{array}} \right)$$

$$= (3.719)(4196.035)(0.730) \times \left(1 + \frac{(0.019536 - 0.008127)(4196.035)(294.5572 - 273.15)}{\begin{bmatrix} 71198 - 36114.71 + (0.9160-1)\times \\ [71198 - 36114.71 - (0.019536 - 0.008127)(2541662)] \\ -(0.019536 - 0.008127)(4196.035)(294.5572 - 273.15) \end{bmatrix}} \right) = 11739.34$$

Combine equations (B.30), (B.50) and (B.56) to find

$$l_{(1,1)} = \frac{\Delta T_w c_{pw(1,1)}}{i_{masw(1,1)} - i_{ma(1,1)} + \left(Le_{f(1,1)} - 1\right)\left[i_{masw(1,1)} - i_{ma(1,1)} - \left(w_{sw(1,1)} - w_{(1,1)}\right)i_{v(1,1)}\right] - \left(w_{sw(1,1)} - w_{(1,1)}\right)c_{pw(1,1)}T_{w(1,1)}}$$

$$= \frac{(3.719)(4196.035)}{\left[\begin{array}{l} 71198 - 36114.71 \\ +(0.9160-1)[71198 - 36114.71 - (0.019536 - 0.008127)(2541662)] \\ -(0.019536 - 0.008127)(4196.035)(294.5572 - 273.15) \end{array}\right]} = 0.4651566$$

By proceeding along the same lines $j_{(1,2)}$, $k_{(1,2)}$ and $l_{(1,2)}$ are determined for the second intermediate calculation step of the Runge-Kutta method for the first interval:

From equations (B.57) to (B.59) can be seen that $j_{(1,2)}$, $k_{(1,2)}$ and $l_{(1,2)}$ are functions of

$T_{w(0)} + \frac{\Delta T_w}{2}, i_{ma(0)} + \frac{k_{(1,1)}}{2}$ and $w_{(0)} + \frac{j_{(1,1)}}{2}$ thus define

$T_{w(1,2)} = T_{w(0)} + \Delta T_w/2 = 294.5572 + 3.719/2 = 296.4147\text{K}$

$w_{(1,2)} = w_{(1)} + j_{(1,1)}/2 = 0.008127 + 0.003874/2 = 0.010064$ kg/kg dry air

$i_{ma(1,2)} = i_{ma(1)} + k_{(1,1)}/2 = 36114.71 + 11739.34/2 = 41984.43$ J/kg

The specific heats have to be evaluated at $(T_{w(1,2)} + 273.15)/2 = 284.7823\text{K}$

Specific heat of dry air from equation (A.1.2)

$c_{pa(1,2)} = 1.045356\times10^{3} - 3.161783\times10^{-1}(284.7823) + 7.083814\times10^{-4}(284.7823)^2$
$- 2.705209\times10^{-7}(284.7823)^3 = 1006.516$ J/kgK

Specific heat of water vapor from equation (A.2.2)

$c_{pv(1,2)} = 1.3605 \times 10^{3} + 2.31334(284.7823) - 2.46784 \times 10^{-10}(284.7823)^5$
$+ 5.91332 \times 10^{-13}(284.7823)^6 = 1872.478$ J/kgK

Specific heat of water from equation (A.4.2)

$c_{pw(1,2)} = 8.15599 \times 10^{3} - 2.80627 \times 10(284.7823) + 5.11283 \times 10^{-2}(284.7823)^2$
$- 2.17582 \times 10^{-13}(284.7823)^6 = 4194.72$ J/kgK

The vapor pressure and humidity ratio of saturated air are calculated at the local water temperature $T_{w(1,2)}$ = 296.4147K

Vapor pressure from equation (A.2.1): $p_{v(1,2)} = 2853.55$ Pa

Humidity ratio for saturated air from equation (A.3.5): $w_{sw(1,2)} = 0.021958$ kg/kg dry air

The enthalpy of water vapor at the local bulk water temperature, $T_{w(1,2)}$, relative to water at 0°C,

$i_{v(1,2)} = i_{fgw(1,2)} + c_{pv(1,2)}\,T_{w(1,2)} = 2.5016 \times 10^{6} + 1872.478(296.4147 - 273.15) = 2545161$ J/kg

The entalpy of saturated air at the local bulk water temperature from equation (A.3.6b)

$i_{masw(1,2)} = 1006.516(296.4147 - 273.15) + (0.021958)(2545161) = 79304$ J/kg

The Lewis factor from equation (B.15)

$$Le_{f(1,2)} = 0.865^{0.667} \frac{\left(\frac{0.662+0.021958}{0.662+0.010064} - 1\right)}{\ln\left(\frac{0.662+0.021958}{0.662+0.010064}\right)} = 0.9164$$

The mass balance from equation (B.32)

$$\left(\frac{m_w}{m_a}\right)_{(1,2)} = \frac{12500}{16672.19}\left(1 - \frac{16672.19}{12500}(0.027889 - 0.010064)\right) = 0.7319$$

From equation (B.57) find

$$j_{(1,2)} = \Delta T_w \cdot f\left(T_{w(1,2)}, i_{ma(1,2)}, w_{(1,2)}\right)$$

From equation (B.48) find

$$\frac{dw}{dT_w} = f\left(T_{w(1,2)}, i_{ma(1,2)}, w_{(1,2)}\right)$$

From equation (B.24) find

$$\frac{dw}{dT_w} = \frac{c_{pw(1,2)}\left(\frac{m_w}{m_a}\right)_{(1,2)}\left(w_{sw(1,2)} - w_{(1,2)}\right)}{\begin{aligned} & i_{masw(1,2)} - i_{ma(1,2)} + \left(Le_{f(1,2)} - 1\right)\left[i_{masw(1,2)} - i_{ma(1,2)} - \left(w_{sw(1,2)} - w_{(1,2)}\right)i_{v(1,2)}\right] \\ & - \left(w_{sw(1,2)} - w_{(1,2)}\right)c_{pw(1,2)}T_{w(1,2)} \end{aligned}}$$

Combine equations (B.24), (B.48) and (B.57) to find

$$j_{(1,2)} = \frac{\Delta T_w c_{pw(1,2)}\left(\frac{m_w}{m_a}\right)_{(1,2)}\left(w_{sw(1,2)} - w_{(1,2)}\right)}{\begin{aligned} & i_{masw(1,2)} - i_{ma(1,2)} + \left(Le_{f(1,2)} - 1\right)\left[i_{masw(1,2)} - i_{ma(1,2)} - \left(w_{sw(1,2)} - w_{(1,2)}\right)i_{v(1,2)}\right] \\ & - \left(w_{sw(1,2)} - w_{(1,2)}\right)c_{pw(1,2)}T_{w(1,2)} \end{aligned}}$$

$$= \frac{(3.719)(4194.72)(0.7319)(0.021958 - 0.010064)}{\begin{bmatrix} 79304 - 41984.43 \\ +(0.9164-1)[79304 - 41984.43 - (0.021958 - 0.010064)(2545161)] \\ -(0.021958 - 0.010064)(4194.72)(296.4147 - 273.15) \end{bmatrix}} = 0.00381818$$

A relation for $k_{(1,2)}$ is obtained by combining (B.25), (B.49) and (B.58) i.e.

$$k_{(1,2)} = \Delta T_w c_{pw(1,2)} \left(\frac{m_w}{m_a}\right)_{(1,2)} \times \left(1 + \frac{\left(w_{sw(1,2)} - w_{(1,2)}\right) c_{pw(1,2)} T_{w(1,2)}}{\begin{matrix} i_{masw(1,2)} - i_{ma(1,2)} + \left(Le_{f(1,2)} - 1\right)\left[i_{masw(1,2)} - i_{ma(1,2)} - \left(w_{sw(1,2)} - w_{(1,2)}\right) i_{v(1,2)}\right] \\ - \left(w_{sw(1,2)} - w_{(1,2)}\right) c_{pw(1,2)} T_{w(1,2)} \end{matrix}} \right)$$

$$= (3.719)(4194.72)(0.7319) \times \left(1 + \frac{(0.021958 - 0.010064)(4194.72)(296.4147 - 273.15)}{\begin{bmatrix} 79304 - 41984.43 + (0.9164 - 1) \times \\ [79304 - 41984.43 - (0.021958 - 0.010064)(2545161)] \\ - (0.021958 - 0.010064)(4194.72)(296.4147 - 273.15) \end{bmatrix}} \right) = 11790.64$$

$l_{(1,2)}$ is obtained by combining equation (B.30), (B.50) and (B.59)

$$l_{(1,2)} = \frac{\Delta T_w c_{pw(1,2)}}{\begin{matrix} i_{masw(1,2)} - i_{ma(1,2)} + \left(Le_{f(1,2)} - 1\right)\left[i_{masw(1,2)} - i_{ma(1,2)} - \left(w_{sw(1,2)} - w_{(1,2)}\right) i_{v(1,2)}\right] \\ - \left(w_{sw(1,2)} - w_{(1,2)}\right) c_{pw(1,2)} T_{w(1,2)} \end{matrix}}$$

$$= \frac{(3.719)(4194.72)}{\begin{bmatrix} 79304 - 41984.43 \\ + (0.9164 - 1)[79304 - 41984.43 - (0.021958 - 0.010064)(2545161)] \\ - (0.021958 - 0.010064)(4194.72)(296.4147 - 273.15) \end{bmatrix}} = 0.438578$$

Proceeding along the same lines, the following values are calculated to finish the Runge-Kutta numerical integration for the first interval.

$j_{(1,3)} = 0.00382916$; $k_{(1,3)} = 11791.28$; $l_{(1,3)} = 0.4388265$

$j_{(1,4)} = 0.00380129$; $k_{(1,4)} = 11844.59$; $l_{(1,4)} = 0.4080234$

The humidity ratio at level (1) follows from equation (B.51),

$w_{(1)} = w_{(0)} + (j_{(1,1)} + 2j_{(1,2)} + 2j_{(1,3)} + j_{(1,4)})/6$

$= 0.008127 + [0.003874 + (2)0.00381818 + (2)0.00382916 + 0.00380129] / 6 = 0.011955$ kg/kg dry air

The enthalpy of the air at level (1) follows from equation (B.52),

$i_{ma(1)} = i_{ma(0)} + (k_{(1,1)} + 2k_{(1,2)} + 2k_{(1,3)} + k_{(1,4)})/6$

$= 36114.71 + [11739.34 + (2)11790.64 + (2)11791.28 + 11844.59] / 6 = 47906.31$ J/kg

The transfer characteristic or Merkel number at level (1) follows from equation (B.53),

$Me_{P(1)} = Me_{P(0)} + (l_{(1,1)} + 2l_{(1,2)} + 2l_{(1,3)} + l_{(1,4)})/6$

$= 0 + [0.4651566 + (2)0.438578 + (2)0.4388265 + 0.4080234] = 0.4380259$

The dry bulb temperature, $T_{a(1)}$, and wet bulb temperature, $T_{wb(1)}$, at level (1) are determined by assuming that the air is unsaturated. If $T_{wb(1)}>T_{a(1)}$ the air is supersaturated and the assumption of unsaturated air must be corrected. The assumption is then corrected by assuming supersaturated air with $T_{wb(1)} = T_{a(1)}$.

Find the dry bulb temperature at level (1), $T_{a(1)}$:

The enthalpy of the air at level (1) is, $i_{ma(1)} = 47906.31$ J/kg.

Assume that the air is unsaturated and that the drybulb temperature, $T_{a(1)} = 290.6444$K. The specific heats are evaluated at $(T_{a(1)}+273.15)/2 = (290.6444+273.15)/2 = 281.8972$K

Specific heat of dry air from equation (A.1.2) $c_{pa(1)} = 1006.458$ J/kgK

Specific heat of water vapor from equation (A.2.2) $c_{pv(1)} = 1870.054$ J/kgK

Equation (A.3.6b) gives an expression for the enthalpy of an air vapor mixture per unit mass of dry air.

$i_{ma(1)} = 1006.458(290.6444 - 273.15) + 0.011955$

$\times[2501598 + 1870.054(290.6444 - 273.15)] = 47906.31$ J/kg dry air

The value of $i_{ma(1)}$ determined by equation (A.3.6b) is equal to the value determined by equation (B.52). The assumption of the value of the dry bulb temperature is therefore correct.

Find the wet bulb temperature at level (1), $T_{wb(1)}$:

The humidity ratio at level (1), $w_{(1)} = 0.011955$ kg/kg dry air.

Assume that the wet bulb temperature at level (1) is $T_{wb(1)} = 286.9630$K.

From equations (A.2.1) and (A.3.5) find at $T_{wb(1)} = 286.9630$ K respectively the vapor pressure and the humidity ratio.

Vapor pressure from equation (A.2.1): $p_{v(1)} = 1578.146$ Pa

Humidity ratio from equation (A.3.5): $w_{(1)} = 0.011955$ kg/kg dry air

The value of $w_{(1)}$, determined by equation (A.3.5) is equal to the value determined earlier. The assumption of the value of the wet bulb temperature is therefore correct.

$T_{wb(1)} < T_{a(1)}$ and hence the air is still unsaturated.

By following the same procedure as above find the following the values for the relative humidity, air enthalpy, Merkel number and air temperatures on the next three levels in figure I.3,

$w_{(2)} = 0.015760627$ kg/kg dry air; $i_{ma(2)} = 59806.97$ J/kg

$Me_{(2)} = 0.8126387$; $T_{a(2)} = 292.8226$K; $T_{wb(2)} = 291.1911$K

$T_{wb(2)} < T_{a(2)}$ and hence the air is still unsaturated.

$w_{(3)} = 0.019614896$ kg/kg dry air; $i_{ma(3)} = 71826.70$ J/kg

$Me_{(3)} = 1.119698$; $T_{a(3)} = 294.9653$K; $T_{wb(3)} = 294.6191$K

$T_{wb(3)} < T_{a(3)}$ and hence the air is still unsaturated.

$w_{(4)} = 0.0235572$ kg/kg dry air; $i_{ma4(4)} = 83973.91$ J/kg

$Me_{(4)} = 1.364207$; $T_{a(4)} = 296.9861$K; $T_{wb(4)} = 297.5420$K

$T_{wb(4)} > T_{a(4)}$ and hence the air is supersaturated. The assumption that the air is unsaturated for the determination of $T_{a(4)}$ and $T_{wb(4)}$ is therefore incorrect. This can be corrected by assuming that the air is supersaturated where $T_{a(4)} = T_{wb(4)} = 297.4155$K

From equation (B.52) the enthalpy at level (4) is equal to $i_{ma(4)} = 83973.91$ J/kg

The partial pressure and humidity ratio of saturated air evaluated at $T_{a(4)}$,

Partial pressure from equation (A.2.1): $p_{vsa(4)} = 3030.684$ Pa

Humidity ratio from equation (A.3.5): $w_{sa(4)} = 0.0133173$ kg/kg dry air

The following specific heats are determined at $(T_{a(4)} + 273.15)/2 = (297.4155 + 273.15)/2 = 285.28275$K

Specific heat of dry air from equation (A.1.2): $c_{pa(4)} = 1006.527$ J/kgK

Specific heat of water vapor from equation (A.2.2): $c_{pv(4)} = 1872.9$ J/kgK

Specific heat of water from equation (A.4.2): $c_{pw(4)} = 4194.033$ J/kgK

From equation (B.33) it follows that

$$i_{ss(4)} = c_{pa(4)}(T_{a(4)} - 273.15) + w_{sa(4)}[i_{fgwo} + c_{pv(4)}(T_{a(4)} - 273.15)] + (w_{(4)} - w_{sa(4)})c_{pw(4)}(T_{a(4)} - 273.15)$$

$$= 1006.527(297.4155 - 273.15) + 0.0133173[2501598 + 1872.9(297.4155-273.15)]$$

$$+ (0.0235572 - 0.0133173)(4194.033)(297.4155 - 273.15) = 83974 \text{ J/kg}$$

$i_{ss(4)}$, determined by equation (B.33), is within close tolerance of $i_{ma(4)}$, determined by equation (B.52), thus, the assumption of the value of the dry bulb temperature at level (1) is therefore correct. The air temperature at level (4), $T_{a(4)}$, is therefore equal to 297.4155K.

Apply Runge-Kutta numerical integration to the fifth interval. Find from equations (B.51) to (B.53) for the fifth interval,

$w_{(5)} = w_{(4)} + (j_{(5,1)} + 2j_{(5,2)} + 2j_{(5,3)} + j_{(5,4)})/6$

$i_{ss(5)} = i_{ss(4)} + (k_{(5,1)} + 2k_{(5,2)} + 2k_{(5,3)} + k_{(5,4)})/6$

$Me_{P(5)} = Me_{P(5)} + (l_{(5,1)} + 2l_{(5,2)} + 2l_{(5,3)} + l_{(5,4)})/6$

Because the air is supersaturated $i_{ss(4)} = i_{ma(4)}$. The water temperature at level (1) is $T_{w(4)} = T_{w(3)} + \Delta T_w = 305.712 + 3.719 = 309.4311$K. For the first intermediate calculation step of the fifth interval, $i_{ss(5,1)} = i_{ss(4)}$, $T_{w(5,1)} = T_{w(4)}$ and $w_{sa(5,1)} = w_{sa(4)}$.

To calculate $j_{(5,1)}$, $k_{(5,1)}$ and $l_{(5,1)}$ for the first intermediate calculation step for the fifth interval certain thermophysical properties have to be evaluated at $(T_{w(5,1)} + 273.15)/2 = (309.4311 + 273.15)/2 = 291.2905$K

Specific heat of dry air from equation (A.1.2)

$c_{pa(5,1)} = 1.045356 \times 10^3 - 3.161783 \times 10^{-1}(291.2905) + 7.083814 \times 10^{-4}(291.2905)^2$
$- 2.705209 \times 10^{-7}(291.2905)^3 = 1006.676$ J/kgK

Specific heat of water vapor from equation (A.2.2)

$c_{pv(5,1)} = 1.3605 \times 10^3 + 2.31334(291.2905) - 2.46784 \times 10^{-10}(291.2905)^5$
$+ 5.91332 \times 10^{-13}(291.2905)^6 = 1878.043$ J/kgK

Specific heat of water from equation (A.4.2)

$c_{pw(5,1)} = 8.15599 \times 10^3 - 2.80627 \times 10(291.2905) + 5.11283 \times 10^{-2}(291.2905)^2$
$- 2.17582 \times 10^{-13}(291.2905)^6 = 4186.92$ J/kgK

Vapor pressure from equation (A.2.1) evaluated at $T_{w(5,1)} = 309.4311$K

$z_{(5,1)} = 10.79586(1 - 273.16/309.4311) + 5.02808 \log_{10}(273.16/309.4311)$
$+ 1.50474 \times 10^{-4}[1 - 10^{-8.29692\{(309.4311/273.16)-1\}}]$
$+ 4.2873 \times 10^{-4}[10^{4.76955(1-273.16/309.4311)} - 1] + 2.786118312 = 3.780603$

$p_{v(5,1)} = 10^{3.780603} = 6033.964$ Pa

Humidity ratio for saturated air evaluated at $T_{w(5,1)} = 309.4311$K from equation (A.3.5),

$$w_{sw(5,1)} = \left(\frac{0.62509(6033.964)}{84100 - 1.005(6033.964)}\right) = 0.0483338 \text{ kg/kg dry air}$$

The enthalpy of water vapor at the local bulk water temperature, $T_{w(5,1)}$, relative to water at 0°C,

$i_{v(5,1)} = i_{fgw(5,1)} + c_{pv(5,1)} T_{w(5,1)} = 2.5016 \times 10^6 + 1878.043(309.4311 - 273.15) = 2569736$ J/kg

The entalpy of saturated air at the local bulk water temperature from equation (A.3.6b)

$i_{masw(5,1)} = 1006.676(309.4311 - 273.15) + (0.0483338)(2569736) = 160728.4$ J/kg

The Lewis factor from equation (B.38)

$$Le_{f(5,1)} = 0.865^{0.667} \frac{\left(\frac{0.662 + 0.0483338}{0.662 + 0.0133173} - 1\right)}{\ln\left(\frac{0.662 + 0.0483338}{0.662 + 0.0133173}\right)} = 0.92529$$

The mass balance from equation (B.32)

$$\left(\frac{m_w}{m_a}\right)_{(5,1)} = \frac{12500}{16672.19}\left(1-\frac{16672.19}{12500}(0.027889-0.0235572)\right) = 0.74542$$

From equation (B.54) find

$$j_{(5,1)} = \Delta T_w \cdot f\left(T_{w(4)}, i_{ss(4)}, w_{(4)}\right) = \Delta T_w \cdot f\left(T_{w(5,1)}, i_{ss(5,1)}, w_{(5,1)}\right)$$

From equation (B.48) find

$$\frac{dw}{dT_w} = f\left(T_{w(4)}, i_{ss(4)}, w_{(4)}\right) = f\left(T_{w(5,1)}, i_{ss(5,1)}, w_{(5,1)}\right)$$

but from equation (B.42)

$$\frac{dw}{dT_w} = \frac{c_{pw(5,1)}\left(\frac{m_w}{m_a}\right)_{(5,1)}\left(w_{sw(5,1)} - w_{sa(5,1)}\right)}{\begin{aligned} & i_{masw(5,1)} - i_{ss(5,1)} + \left(Le_{f(5,1)} - 1\right)\left[\begin{aligned} & i_{masw(5,1)} - i_{ss(5,1)} - \left(w_{sw(5,1)} - w_{sa(5,1)}\right) i_{v(5,1)} \\ & + \left(w_{(5,1)} - w_{sa(5,1)}\right) c_{pw(5,1)} T_{w(5,1)} \end{aligned}\right] \\ & + \left(w_{(5,1)} - w_{sw(5,1)}\right) c_{pw(5,1)} T_{w(5,1)} \end{aligned}}$$

Combine equations (B.42), (B.48) and (B.54) to find

$$j_{(5,1)} = \frac{\Delta T_w c_{pw(5,1)}\left(\frac{m_w}{m_a}\right)_{(5,1)}\left(w_{sw(5,1)} - w_{sa(5,1)}\right)}{\begin{aligned} & i_{masw(5,1)} - i_{ss(5,1)} + \left(Le_{f(5,1)} - 1\right)\left[\begin{aligned} & i_{masw(5,1)} - i_{ss(5,1)} - \left(w_{sw(5,1)} - w_{sa(5,1)}\right) i_{v(5,1)} \\ & + \left(w_{(5,1)} - w_{sa(5,1)}\right) c_{pw(5,1)} T_{w(5,1)} \end{aligned}\right] \\ & + \left(w_{(5,1)} - w_{sw(5,1)}\right) c_{pw(5,1)} T_{w(5,1)} \end{aligned}}$$

$$= \frac{(3.719)(4186.92)(0.74542)(0.0483338-0.0133173)}{\left[\begin{aligned} & 160728.4 - 83973.91 \\ & + (0.92529-1)[160728.4 - 83973.91 - (0.0483338-0.0133173)(2569736) \\ & + (0.0235572-0.0133173)(4186.92)(309.4311-273.15)] \\ & + (0.0235572-0.0483338)(4186.92)(309.4311-273.15) \end{aligned}\right]}$$

$$= 0.00402131$$

Combine equations (B.43), (B.49) and (B.55) to find,

$$= \Delta T_w c_{pw(5,1)}\left(\frac{m_w}{m_a}\right)_{(5,1)}$$

$$\times\left(1+\frac{\left(w_{sw(5,1)}-w_{sa(5,1)}\right)}{\begin{matrix}i_{masw(5,1)}-i_{ss(5,1)}+\left(Le_{f(5,1)}-1\right)\left[\begin{matrix}i_{masw(5,1)}-i_{ss(5,1)}-\left(w_{sw(5,1)}-w_{sa(5,1)}\right)i_{v(5,1)}\\+\left(w_{(5,1)}-w_{sa(5,1)}\right)c_{pw(5,1)}T_{w(5,1)}\end{matrix}\right]\\+\left(w_{(5,1)}-w_{sw(5,1)}\right)c_{pw(5,1)}T_{w(5,1)}\end{matrix}}\right)$$

$$=(3.719)(4186.92)(0.74542)$$

$$\times\left(1+\frac{(0.0483338-0.0133173)(4186.92)(309.4311-273.15)}{\left[\begin{matrix}160728.4-83973.91\\+(0.92529-1)[160728.4-83973.91-(0.0483338-0.0133173)(2569736)\\+(0.0235572-0.0133173)(4186.92)(309.4311-273.15)]\\+(0.00.0235572-0.0483338)(4186.92)(309.4311-273.15)\end{matrix}\right]}\right)$$

$$=12217.76$$

Combine equations (B.47), (B.50) and (B.56) to find,

$$l_{(5,1)}=\frac{\Delta T_w c_{pw(5,1)}}{\begin{matrix}i_{masw(5,1)}-i_{ss(5,1)}+\left(Le_{f(5,1)}-1\right)\left[\begin{matrix}i_{masw(5,1)}-i_{ss(5,1)}-\left(w_{sw(5,1)}-w_{sa(5,1)}\right)i_{v(5,1)}\\+\left(w_{(5,1)}-w_{sa(5,1)}\right)c_{pw(5,1)}T_{w(5,1)}\end{matrix}\right]\\+\left(w_{(5,1)}-w_{sw(5,1)}\right)c_{pw(5,1)}T_{w(5,1)}\end{matrix}}$$

$$=\frac{(3.719)(4186.92)}{\left[\begin{matrix}160728.4-83973.91\\+(0.92529-1)[160728.4-83973.91-(0.0483338-0.0133173)(2569736)\\+(0.0235572-0.0133173)(4186.92)(309.4311-273.15)]\\+(0.0235572-0.0483338)(4186.92)(309.4311-273.15)\end{matrix}\right]}$$

$$=0.2161235$$

By proceeding along the same lines, the following values are calculated for the second to fourth intermediate calculation steps to finish the Runge-Kutta numerical integration for the fifth interval.

$j_{(5,2)} = 0.00433930$; $k_{(5,2)} = 12328.45$; $l_{(5,2)} = 0.01900152$

$j_{(5,3)} = 0.00434170$; $k_{(5,3)} = 12331.31$; $l_{(5,3)} = 0.1900797$

$j_{(5,4)} = 0.00460331$; $k_{(5,4)} = 12440.13$; $l_{(5,4)} = 0.1670177$

The humidity ratio at level (5) follows from equation (B.51),

$w_{(5)} = w_{(4)} + (j_{(5,1)} + 2j_{(5,2)} + 2j_{(5,3)} + j_{(5,4)})/6$

$= 0.023557229 + [0.004020131 + (2)0.00433930 + (2)0.00434170 + 0.00460331] / 6$

$= 0.027888$ kg/kg dry air $= w_5$.

The value of w_5 is equal to the value given initially in the example.

The air enthalpy at level (5) follows from equation (B.52),

$i_{ss(5)} = i_{ss(4)} + (k_{(5,1)} + 2k_{(5,2)} + 2k_{(5,3)} + k_{(5,4)})/6$

$= 83973.91 + [12217.76 + (2)12328.45 + (2)12331.31 + 12440.13] / 6 = 96303.48$ J/kg

The transfer characteristic or Merkel number at level (5) follows from equation (B.53),

$Me_{P(5)} = Me_{P(4)} + (l_{(5,1)} + 2l_{(5,2)} + 2l_{(5,3)} + l_{(5,4)})/6$

$= 1.364207 + [0.2161235 + (2)0.01900152 + (2)0.01900797 + 0.1670177] = 1.554762$

This value is almost identical to the value obtained by adding the transfer coefficients in the three wet zones which means that the water outlet temperature, $T_{wo} = 294.5572$K is correct.

The air was already supersaturated at level (4). Therefore assume that the air is still supersaturated and that $T_{a(5)} = T_{wb(5)} = 299.855$K

The partial pressure and humidity ratio of saturated air, from equations (A.2.1) and (A.3.5), evaluated at $T_{a(5)}$ are respectively

$p_{vsa(5)} = 3503.218$ Pa

$w_{sa(5)} = 0.027176$ kg/kg dry air

The value of $w_{sa(5)}$ is equal to the value of w_{sa5} given initially in the example.

The specific heat of dry air, water liquid and vapor are evaluated at $(T_{a(5)} + 273.15)/2 = (299.855 + 273.15)/2 = 286.5025$K

Specific heat of dry air from equation (A.1.2): $c_{pa(5)} = 1006.555$ J/kgK

Specific heat of water vapor from equation (A.2.2): $c_{pv(5)} = 1873.932$ J/kgK

Specific heat of water from equation (A.4.2): $c_{pw(5)} = 4192.421$ J/kgK

It follows from equation (B.33) that

$i_{ss(5)} = c_{pa(5)}(T_{a(5)} - 273.15) + w_{sa(5)}[i_{fgw(5)} + c_{pv(5)}(T_{a(5)} - 273.15)] + (w_{(5)} - w_{sa(5)})c_{pw(5)}(T_{a(5)} - 273.15)$

$= 1006.555(299.855 - 273.15) + 0.027176[2501598 + 1873.932(299.855 - 273.15)]$

$+ (0.027888 - 0.027176)(4192.421)(299.855 - 273.15) = 96303$ J/kg

$i_{ss(5)}$, determined by equation (B.33), is within close tolerance of $i_{ss(5)}$, determined by equation (B.52), thus the value of the air temperature assumed at level (5) is therefore correct. $T_{a(5)} = T_{a5} = 299.85$K is also within close tolerance of the temperature given initially in the example.

Therefore the conditions at the outlet of the fill according to the Poppe approach are:

$i_{ma5} = i_{ss(5)} = 96303.48$ J/kg

$w_5 = w_{(5)} = 0.027888$ kg/kg dry air

$w_{sa5} = w_{sa(5)} = 0.027176$ kg/kg dry air

$T_{a5} = T_{a(5)} = 299.8563$K

where the Merkel number is $Me_P = Me_{P(5)} = 1.554762$.

The heat rejected by the cooling tower is given by

$$Q = m_a\left(i_{ma5} - i_{ma1}\right) = 16672.19(96303.48 - 36114.71) = 1003.4775 \text{ MW}$$

The path of the air through the cooling tower, predicted by the Poppe approach, is shown in figure L.4.

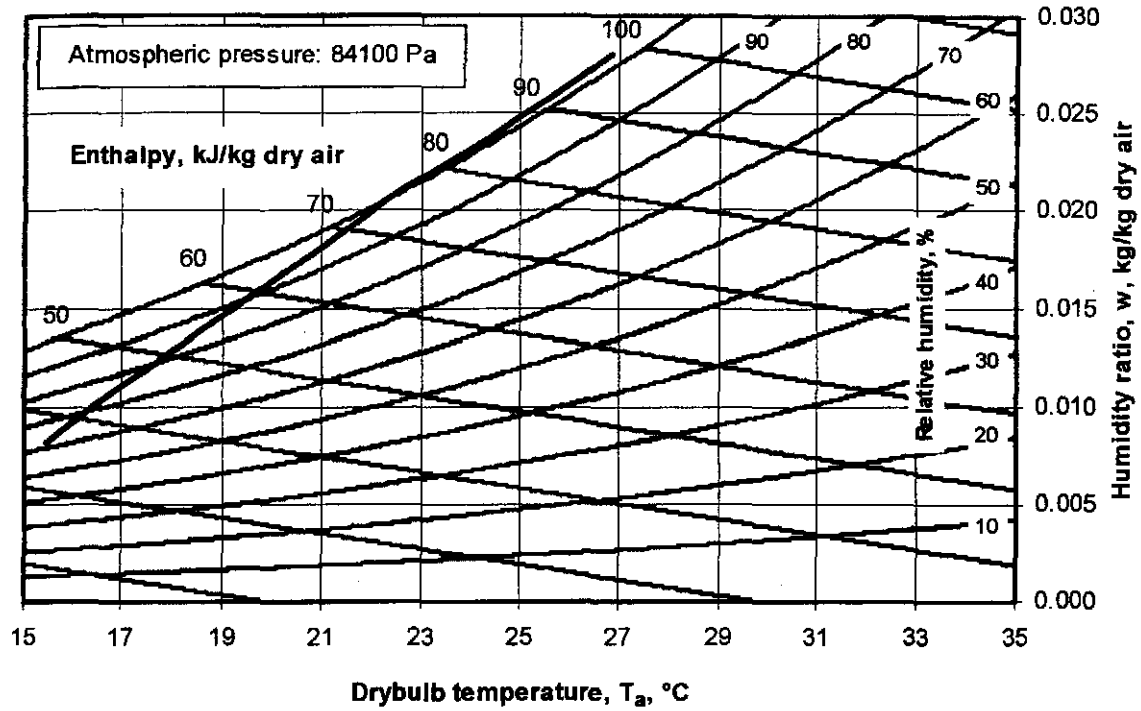

Figure I.4: Airside heating process indicated on a psychrometric chart.

I.6 THE DRAFT EQUATION

The specified loss coefficient due to the support structure of the fill is referred to the mean conditions through the fill i.e.

$$K_{fsfi} + K_{ctcfi} = 0.5\left(\frac{\rho_{av15}}{\rho_{av1}}\right)\left(\frac{m_{av1}}{m_{av15}}\right)^2 = 0.5\left(\frac{0.98424}{1.01012}\right)\left(\frac{16807.68}{16966.47}\right)^2 = 0.4781096$$

According to the specified fill loss coefficient find

$$K_{fdm} = 1.851 L_{fi} G_w^{1.2752} G_a^{-1.0356} = 1.851 \times 2.504 \times (1.50602)^{1.2752} (2.00870)^{-1.0356} = 3.79414$$

It follows that the actual fill loss coefficient applicable to the cooling tower is given by

$$K_{fi} = K_{fdm} + \left(\frac{G_{av5}^2}{\rho_{av5}} - \frac{G_{av1}^2}{\rho_{av1}}\right) / \left(\frac{G_{av15}^2}{\rho_{av15}}\right) = 3.79414 + \left(\frac{2.06329^2}{0.95964} - \frac{2.02502^2}{1.01012}\right) / \left(\frac{2.04415^2}{0.98424}\right) = 3.88284$$

The expansion loss coefficient after the fill, referred to the mean conditions through the fill, follows from equation (D.16).

$$K_{ctefi} = \left(1 - \frac{A_{fr}}{A_3}\right)^2 \left(\frac{\rho_{av15}}{\rho_{av5}}\right)\left(\frac{m_{av5}}{m_{av15}}\right)^2 = \left(1 - \frac{8300 \times 4}{\pi \times 104.5^2}\right)^2 \left(\frac{0.98424}{0.95964}\right)\left(\frac{17125.27}{0.95964}\right)^2 = 0.001088$$

The loss through the spray zone above the fill referred to the mean conditions through the fill is given by equation (D.6)

$$K_{spfi} = L_{sp}\left[0.4\left(\frac{G_w}{G_a}\right)+1\right]\left(\frac{\rho_{av15}}{\rho_{av5}}\right)\left(\frac{m_{av5}}{m_{av15}}\right)^2 = 0.5\left[0.4\left(\frac{1.50602}{2.00870}\right)+1\right]\left(\frac{0.98424}{0.95964}\right)\left(\frac{17125.27}{16966.47}\right)^2$$

$$= 0.679143$$

The specified loss coefficient due to the water distribution system is referred to the mean conditions through the fill i.e.

$$K_{wdfi} = K_{wd}\left(\frac{\rho_{av15}}{\rho_{av5}}\right)\left(\frac{m_{av5}}{m_{av15}}\right)^2 = 0.5\left(\frac{0.98424}{0.95964}\right)\left(\frac{17125.27}{16966.47}\right)^2 = 0.522458$$

The loss coefficient for the specified type c drift eliminator [98KR1] based on fill conditions is

$$K_{defi} = 27.4892Ry^{-0.14247}\left(\frac{\rho_{av15}}{\rho_{av5}}\right)\left(\frac{m_{av5}}{m_{av15}}\right)^2$$

$$= 27.4892\left(\frac{17125.27}{1.81816\times10^{-5}\times8300}\right)^{-0.14247}\left(\frac{0.98424}{0.95964}\right)\left(\frac{17125.27}{16966.47}\right)^2 = 5.47101$$

The sum of these loss coefficients in the vicinity of the fill is

$$K_{HE} = K_{fsfi} + K_{ctc} + K_{fi} + K_{cte} + K_{spfi} + K_{wdfi} + K_{defi}$$

$$= 0.4781096 + 3.88284 + 0.001088 + 0.679143 + 0.522458 + 5.47101 = 11.03465$$

The inlet loss coefficient for a circular cooling tower with isentropic fill operating in the absence of a rain zone can be determined according to equation (D.10) which is applicable if the inlet is rounded with $r_i/d_3 = 0.02$ and $10 \le d_3/H_3 = \le 15$. The sum of the loss coefficients in the vicinity of the fill (effective fill loss coefficient = K_{HE} = 11.03465) also falls within the range of the applicability of the equation, i.e. $5 \le K_{fi} \le 25$.

$$K_{ct(norz)} = 0.011266\exp(0.093d_3/H_3)K_{HE}^2 - 0.3105\exp(0.1085d_3/H_3)K_{HE}$$
$$-1.7522 + 4.5614\exp(0.131d_3/H_3)$$
$$+\sin^{-1}\left[\begin{Bmatrix}(10970.2\exp(-0.2442K_{HE})+1391.3)/(d_3/H_3-15.7258)\\+1205.54\exp(-0.23K_{HE})+109.314\\\times\{2r_i/d_3-0.01942/(d_3/H_3-27.929)-0.016866\}\end{Bmatrix}\right]$$

$$K_{ct(norz)} = 0.011266\exp(0.093\times104.5/10)11.03465^2 - 0.3105\exp(0.1085\times104.5/10)$$
$$\times11.03465 - 1.7522 + 4.5614\exp(0.131\times104.5/10)$$
$$+\sin^{-1}\left[\begin{Bmatrix}(10970.2\exp(-0.2442\times11.03465)+1391.3)/(104.5/10-15.7258)\\+1205.54\exp(-0.23\times11.03465)+109.314\\\times\{2\times0.02-0.01942/(104.5/10-27.929)-0.016866\}\end{Bmatrix}\right] = 6.15873$$

This value must be multiplied by the correction factor C_{rz} as given by equation (D.15) to obtain the correct inlet loss coefficient in the presence of a rain zone. Present values fall in the range of applicability of equation (D.15).

$$C_{rz} = \begin{bmatrix} 0.2394 + 80.1\{0.0954/(d_3/H_3) + d_d\}\exp(0.395 G_w/G_a) \\ -0.3195(G_w/G_a) - 966\{d_d/(d_3/H_3)\}\exp(0.686 G_w/G_a) \end{bmatrix}$$

$$\times(1 - 0.06825 G_w) K_{HE}^{0.09667} \exp\{8.7434(1/d_3 - 0.01)\}$$

$$= \begin{bmatrix} 0.2394 + 80.1\{0.0954/(104.5/10) + 0.0035\}\exp(0.395 \times 1.50602/2.00870) \\ -0.3195(1.50602/2.00870) - 966\{0.0035/(104.5/10)\}\exp(0.686 \times 1.50602/2.00870) \end{bmatrix}$$

$$\times(1 - 0.06825 \times 1.50602) 1.03465^{0.09667} \exp\{8.7434(1/104.5 - 0.01)\} = 0.9233078$$

Referred to the mean conditions through the fill, the inlet loss coefficient from equation (D.12) becomes,

$$K_{ctfi} = C_{rz} K_{ct} \left(\frac{\rho_{av15}}{\rho_{av1}}\right)\left(\frac{m_{av1}}{m_{av15}}\right)^2 \left(\frac{A_{fr}}{A_3}\right)^2$$

$$= 0.9233078 \times 6.15873 \left(\frac{0.98424}{1.01012}\right)\left(\frac{16807.68}{16966.47}\right)^2 \left(\frac{4 \times 8300}{\pi \times 104.5^2}\right)^2 = 5.686403$$

With equation (D.8) find the loss coefficient for the rain zone.

$$K_{rzfi} = 3 a_v v_{w3} (H_3/d_d) \begin{bmatrix} 0.2246 - 0.31467 a_\rho \rho_{av1} + 5263.04 a_\mu \mu_{av1} + \\ 0.775526\{1.4824163\exp(71.52 a_L d_d) - 0.91\} \\ \times \{0.39064\exp(0.010912 a_L d_3) - 0.17\}\{2.0892(a_v v_{av3})^{-1.3944} + 0.14\} \\ \times \exp\begin{Bmatrix} (0.8449\ln(a_L d_3/2) - 2.312) \\ \times (0.3724\ln(a_v v_{av3}) + 0.7263) \\ \times \ln(0.206.757\exp(0.066518 a_L H_3)^{-2.8344} + 0.43) \end{Bmatrix} \end{bmatrix}$$

$$\times \left(\frac{\rho_{av15}}{\rho_{av1}}\right)\left(\frac{m_{av1}}{m_{av15}}\right)^2 \left(\frac{4 A_{fr}}{\pi d_3^2}\right)^2$$

where the values of the "a" coefficients are identical to those employed in the mass transfer coefficient equation with $v_{w3} = G_w/\rho_{wo}$ = 1.50602 / 997.8629 = 1.5092 $\times 10^3$ m/s, the value of the coefficient is found to be

$$K_{rzfi} = 3 \times 1.0008 \times 1.5092 \times 10^{-3} (10/0.0035)$$

$$\left[\begin{array}{l} 0.2246-0.31467\times1.00014\times1.01012+5263.04\times1.00014\times1.7857\times10^{-5}+ \\ 0.775526\left\{1.4824163\exp(71.52\times1.00025\times0.0035)-0.91\right\}\times \\ \left\{0.39064\exp(0.010912\times1.00025\times0.0035)-0.17\right\}\times\left\{2.0892(1.0008\times2.00473)^{-1.3944}+0.14\right\}\times \\ \exp\left\{\begin{array}{l}(0.8449\ln(1.00025\times104.5/2)-2.312)\times(0.3724\ln(1.0008\times2.00473)+0.7263) \\ \times\ln\left(0.206.757\exp(0.066518\times1.00025\times10)^{-2.8344}+0.43\right)\end{array}\right\} \end{array}\right]$$

$$\times\left(\frac{0.98424}{1.01012}\right)\left(\frac{16807.68}{16966.47}\right)^2\left(\frac{4\times8300}{\pi\times104.5^2}\right)^2=6.39225$$

The loss coefficient due to the tower supports referred to the fill follows from equation (D.15)

$$K_{tsfi}=\left[\frac{C_{dts}L_{ts}d_{ts}n_{ts}A_{fr}^2}{(\pi d_3H_3)^3}\right]\left(\frac{\rho_{av15}}{\rho_{av1}}\right)\left(\frac{m_{av1}}{m_{av15}}\right)^2$$

$$=\left[\frac{1\times11.6\times0.8\times72\times8300^2}{(\pi\times104.5\times10)^3}\right]\left(\frac{0.98424}{1.01012}\right)\left(\frac{16807.68}{16966.47}\right)^2=1.24393$$

At this stage it is possible to confirm the value of p_{a5} where

$$p_{a5}=p_{a1}\left[1-\frac{0.00975(H_3+L_{fl}/2)}{T_{a1}}\right]^{3.5(1+w_1)\left(1-\frac{w_1}{w_1+0.622}\right)}$$

$$-\left(K_{tsfi}+K_{ctfi}+K_{rzfi}+K_{fsfi}+K_{ctcfi}+K_{fi}+K_{ctefi}+K_{spfi}+K_{wdfi}+K_{defi}\right)\frac{\left(\frac{m_{av15}}{Afr}\right)^2}{2\rho_{av15}}$$

$$=101325\left[1-\frac{0.00975(10+2.504/2)}{288.6}\right]^{3.5(1+0.008127)\left(1-\frac{0.008127}{0.008127+0.622}\right)}$$

$$-\left(\begin{array}{l}1.24393+5.686403+6.39225+0.4781096+3.88284 \\ +0.001088+0.679143+0.522458+5.47101\end{array}\right)\frac{\left(\frac{16966.47}{8300}\right)^2}{2\times0.98424}=83937.04\text{ Pa}$$

This value is in agreement with that used previously in calculations in this example.

To find the temperature lapse rate inside the tower, the specific heat of water is evaluated at (299.8563 + 273.15)/2 = 286.5032 K. According to equation (A.4.2) find c_{pw} = 4192.42 J/kgK. Using the previously obtained values for the specific heat of dry air and water vapor at this temperature and $c_{pma} = c_{pa5} + w_{sa5}\times c_{pv5}$ = 1006.5548 + 0.027176×1873.9329 = 1057.481, find

$$\xi_{T_{a5}}=-(1+w_{sa5})g\left[\begin{array}{l}1+0.42216\times10^{-11}w_{sa5}^2p_{a5}\exp(5406.1915/T_{a5}) \\ \times\left\{i_{fgwo}-(c_{pw}-c_{pv})(T_{a5}-273.15)\right\}/\left\{(w_{sa5}+0.622)RT_{a5}\right\}\end{array}\right]$$

$$/\left[c_{pma}+3.6696\times10^{-8}w_{sa5}^2p_{a5}\exp(5406.1915/T_{a5})\left\{i_{fgwo}-(c_{pw}-c_{pv})(T_{a5}-273.15)\right\}/T_{a5}^2\right]$$

$$= -(1+0.027176)9.8\left[\begin{array}{l}1+0.42216\times10^{-11}\times0.027176^2\times\exp(5406.1915/299.8563)\\ \times\{2.5016\times10^6-(4192.43-1873.932)(299.8563-273.15)\}\\ /\{(0.027176+0.622)287.08\times299.8563\}\end{array}\right]$$

$$/\left[\begin{array}{l}1057.481+3.6696\times10^{-8}\times0.027176^2\times\exp(5406.1915/299.8563)\\ \{2.5016\times10^6-(4192.42-1873.9329)(299.8563-273.15)\}^{/2}\end{array}\right] = -0.0034113\text{K/m}$$

According to du Preez and Kröger [94DU1] the difference in the mean pressure at the tower outlet and the ambient pressure at the same elevation is given by

$$p_{a6} - p_{a7} = \left[0.02Fr_D^{-1.5} - 0.14/Fr_D\right](m_{av5}/A_6)^2/\rho_{av6}$$

To find the pressure difference $(p_{a6} - p_{a7})$ given by equation above the air properties and corresponding desimetric Froude number must be determined at the outlet of the tower. Using the lapse rate obtained above, and assuming it essentially constant over the height of the cooling tower, the air temperature at 6 may be determined.

$$T_{a6} = T_{a5} + \xi_{T_{a5}}\left(H_6 - H_3 - L_{fl} - L_{sp}\right) = 299.8563 - 0.0034113\ (147 - 10 - 2.504 - 0.5) = 299.399\text{K}$$

The corresponding density of the air-vapor mixture at this temperature is according to equation (A.3.1)

$$\rho_{av6} = (1+w_{sa5})\left[1-\frac{w_{sa5}}{w_{sa5}+0.62198}\right]\frac{p_{a6}}{RT_{a6}}$$

$$= (1+0.027176)\left[1-\frac{0.027176}{0.027176+0.62198}\right]\frac{82650.57}{287.08\times299.399} = 0.9464\ \text{kg/m}^3$$

The ambient temperature at elevation 7 follows from equation (E.12) with $H_7 = H_6$.

$T_{a7} = T_{a1} - 0.00975H_6 = 288.6 - 0.00975\times147 = 287.167$K

The pressure at 7 may be determined from equation (E.13).

$$p_{a7} = p_{a1}\left(1-0.00975\ H_6/T_{a1}\right)^{\frac{2.1778(1+w_1)}{w_1+0.62198}} = 84100\left(1-0.00975\times147/288.6\right)^{\frac{2.1778(1+0.008127)}{0.008127+0.62198}}$$

$$= 82654.27\ \text{Pa}$$

The corresponding density of the ambient air at elevation 7 assuming a uniform ambient humidity ratio w_1, is according to equation (A.3.1)

$$\rho_{av7} = (1+w_1)\left[1-\frac{w_1}{w_1+0.62198}\right]\frac{p_{a7}}{RT_{a7}} = (1+0.008127)\left[1-\frac{0.008127}{0.008127+0.62198}\right]\frac{82654.27}{287.08\times287.167}$$

$$= 0.9977\ \text{kg/m}^3$$

With no cold inflow these values yield

$$Fr_D = (m_{av5}/A_6)^2/[\rho_{av6}(\rho_{av7}-\rho_{av6})gd_6]$$

$$= (17125.27/\{0.25\times\pi\times 60.85^2\})^2/[0.9464(0.9977-0.9464)9.8\times 60.85] = 1.19697$$

Substitute this expression for Fr_D into the equation of Du Preez and Kröger [94DU1] presented above and find p_{a6}.

$$p_{a6} = p_{a7} + [0.02Fr_D^{-1.5} - 0.14/Fr_D](m_{av5}/A_6)^2/\rho_{av6}$$

$$= 82654.27 + [0.02\times 1.19697^{-1.5} - 0.14/1.19697][17125.27/(0.25\times\pi\times 60.85^2)]^2/0.9464$$

$= 82650.57$ N/m^2 which is in good agreement with the value given initially.

The draft equation from equation (E.1) may now be solved using the above values

$$(p_{a1}-p_{a7})-(p_{a1}-p_{a34})-(p_{a34}-p_{a6})-(p_{a6}-p_{a7}) =$$

$$(K_{tsfi}+K_{ctfi}+K_{rzfi}+K_{fsfi}+K_{ctcfi}+K_{fi}+K_{ctefi}+K_{spfi}+K_{wdfi}+K_{defi})\frac{\left(\frac{m_{av15}}{Afr}\right)^2}{2\rho_{av15}}+\alpha_{e6}\frac{\left(\frac{m_{av6}}{A_6}\right)^2}{2\rho_{av6}}$$

where $(p_{a1}-p_{a7})$ and $(p_{a1}-p_{a34})$ is given by equation (E.14)

$$(p_{a1}-p_{a7}) = p_{a1}\left[1-\left(1-0.00975\ H_6/T_{a1}\right)^{\frac{2.1778(1+w_1)}{w_1+0.62198}}\right]$$

$$= 84100\left[1-(1-0.00975\times 147/288.6)^{\frac{2.1778(1+0.008127)}{0.008127+0.62198}}\right] = 1445.732 \text{ Pa}$$

$$(p_{a1}-p_{a34}) = p_{a1}\left[1-\left\{1-0.00975(H_6+L_{fi}/2)/T_{a1}\right\}^{\frac{2.1778(1+w_1)}{w_1+0.62198}}\right]$$

$$= 84100\left[1-\left\{1-0.00975(147+2.504/2)/288.6\right\}^{\frac{2.1778(1+0.008127)}{0.008127+0.62198}}\right] = 111.2947 \text{ Pa}$$

$$(p_{a34}-p_{a6}) = p_{a5}\left[1-\left\{1+\xi_{T_{a5}}(H_6-H_3-L_{fi}/2)/T_{a5}\right\}^{-(1+w_{sa5})\left\{1-\frac{w_{sa5}}{w_{sa5}+0.62198}\right\}\frac{g}{R\xi_{T_{a5}}}}\right]$$

$$= \left[1-\left\{1+0.0034113\frac{147-10-2.504/2}{299.8563}\right\}^{-(1+0.027176)\left\{1-\frac{0.027176}{0.027176+0.62198}\right\}\frac{9.8}{287.08\times(-0.0034113)}}\right] = 1267.954 \text{ Pa}$$

$$(p_{a6}-p_{a7}) = [0.02Fr_D^{-1.5} - 0.14/Fr_D](m_{av5}/A_6)^2/\rho_{av6}$$

$$= [0.02\times 1.19697^{-1.5} - 0.14/1.19697][17125.27/(0.25\times\pi\times 60.86^2)]^2/0.9464 = -3.726184 \text{ Pa}$$

Upon substitution the left-hand side of the draft equation yields,

$$(p_{a1}-p_{a7})-(p_{a1}-p_{a34})-(p_{a34}-p_{a6})-(p_{a6}-p_{a7})$$

$$= 1445.732 - 111.2947 - 1267.954 + 3.726184 = 70.20883 \text{ Pa}$$

The value on the right-hand side of the draft-equation is

$$\left(K_{tsfi}+K_{ctfi}+K_{rxfi}+K_{fsfi}+K_{ctcfi}+K_{fi}+K_{ctefi}+K_{spfi}+K_{wdfi}+K_{defi}\right)\frac{\left(\frac{m_{av15}}{Afr}\right)^2}{2\rho_{av15}}+\alpha_{e6}\frac{\left(\frac{m_{av6}}{A_6}\right)^2}{2\rho_{av6}}$$

$$=\begin{pmatrix}1.24393+5.686403+6.39225+0.4781096+3.88284\\+0.001088+0.67914+0.522458+5.47101\end{pmatrix}\frac{\left(\frac{16966.47}{8300}\right)^2}{2\times 0.98424}$$

$$+1.01\frac{\left(\frac{17125.27}{0.25\times\pi\times 60.86^2}\right)^2}{2\times 0.9464} = 70.20879 \text{ Pa}$$

Since the value of the right-hand side of the draft equation is essentially the same as the left-hand side, the chosen air-vapor mass flow rate is correct.

The amount of water lost due to evaporation is given by

$$m_{w(evap)} = m_a(w_5 - w_1) = (0.027888 - 0.008127) = 329.464 \text{ kg/s}$$

APPENDIX J

ANALYSIS OF AN INDUCED DRAFT WET-COOLING TOWER EMPLOYING THE MERKEL APPROACH

J.1 INTRODUCTION

A sample calculation is presented for the performance evaluation of an induced draft wet-cooling tower while the Merkel method of analysis is employed. The main dimensions of the tower are shown in figure J.1.

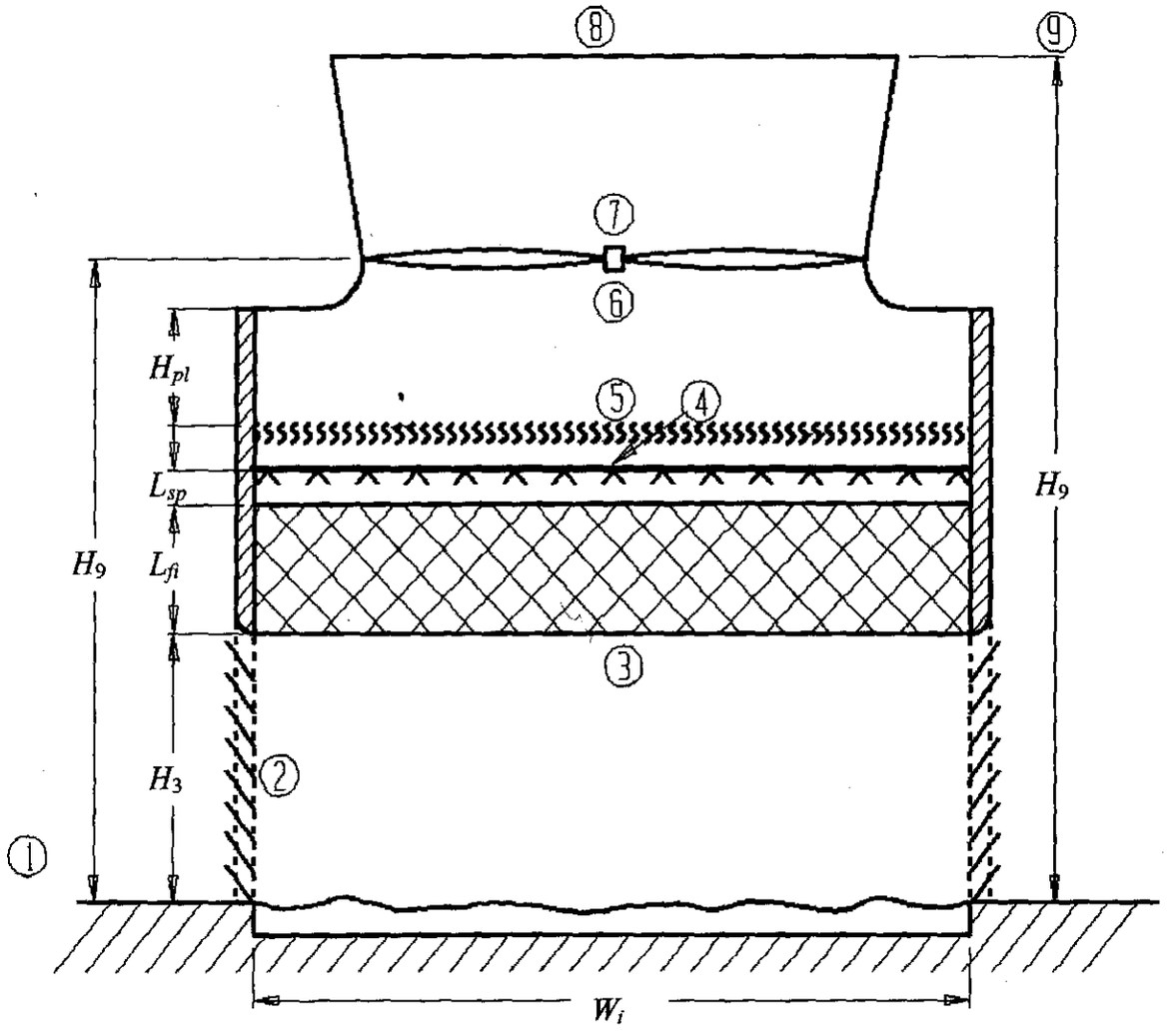

Figure J.1: Induced draft wet-cooling tower

Ambient conditions:

Atmospheric pressure at ground level	p_{a1} = 101325 Pa
Air temperature at ground level	T_{a1} = 306.65 K (33.5 °C)
Wetbulb temperature at ground level	T_{wb} = 298.15 K (25 °C)

Cooling tower and operational specifications:

Tower height	H_9 = 12.5 m
Fan height	H_6 = 9.5 m
Tower inlet height	H_3 = 4 m
Tower inlet width	W_i = 12 m
Tower breadth	B_i = 12m
Fill height	L_{fi} = 1.878 m
Height of spray zone	L_{sp} = 0.5m
Inlet rounding	r_i = 0.025Wi
Plenum chamber height	H_{pl} = 2.4 m
Inlet water temperature	T_{wi} = 314.65K (41.5 °C)
Water mass flow rate	m_w = 412 kg/s

Fill specifications:

Transfer coefficient

$$\frac{h_{dfi}a_{fi}}{G_w} = 0.2692G_w^{-0.094}G_a^{0.6023}$$

Loss coefficient

$$K_{fdm1} = 1.9277G_w^{1.2752}G_a^{-1.0356}$$

The frontal area of the fill $A_{fr} = B_i \times W_i = 144\ m^2$

Other specifications:

Mean drop diameter in rain zone	d_d = 0.0035 m
Loss coefficient for inlet louvers	K_{il} = 2.5
Loss coefficient for fill support system	K_{fs} = 0.5
Loss coefficient for water distribution system	K_{wd} = 0.5
Fan upstream losses	K_{up} = 0.52

The loss coefficient for the drift eliminator (type c) is given by equation (D.7).

Fan/diffuser with rounded inlet dimensions and performance characteristics:

Fan diameter	d_F = 8 m
Fan rotational speed	N_F = 120 rpm
Fan model diameter	d_{Fr} = 1.536 m
Reference rotational speed	N_{Fr} = 750 rpm
Reference air density	ρ_r = 1.2 kg/m^3

Fan/diffuser static pressure:

$$\Delta p_{F/dif} = 320.85 - 6.9604V_{F/dif} + 0.31373V_{F/dif}^2 - 0.021393V_{F/dif}^3 \text{ Pa}$$

Fan shaft power:

$$P_{F/dif} = 4245.1 - 64.134V_{F/dif} + 17.586V_{F/dif}^2 - 0.71079V_{F/dif}^3 \quad \text{W}$$

J.2 SOLUTION

It is assumed in this problem that the atmospheric pressure and humidity fields have no influence on the draft equation. This problem is solved by following an iterative procedure to find a solution that will satisfy both the energy and draft equations. The choice of an air-vapor mass flow rate of m_{av15} = 442.1426 kg/s through the fill will satisfy these equations, giving a corresponding pressure of p_{a5} = 101170.6 Pa, an air temperature T_{a5} = 306.7645 K and an exit water temperature T_{wo} = 303.4677 K.

At the specified air inlet drybulb temperature of T_{a1} = 306.65 K, wetbulb temperature of T_{wb} = 298.15 K and atmospheric pressure at ground level p_{a1} = 101325 Pa, find the following thermophysical properties employing the equations given in appendix A.

Density of air-vapor	ρ_{av1} = 1.1397 kg/m3	(A.3.1)
Humidity ratio of inlet air	w_1 = 0.016569kg/kg	(A.3.5)
Viscosity of the air vapor mixture	μ_{av1} = 1.85928 × 10^{-5} kg/ms	(A.3.3)

The enthalpy of the inlet air, i_{ma1}, is found according to equation (A.3.6b) with c_{pa1} = 1006.64 J/kgK and c_{pv1} = 1876.84 J/kgK being evaluated at (T_{a1} + 273.15)/2 = (306.65 + 273.15)/2 = 289.9 K according to equations (A.1.2) and (A.2.2) respectively. The latent heat is found to be i_{fgwo} = 2.5016 × 10^6 J/kgK according to equation (A.4.5) at 273.15K. With these values find i_{ma1} = 76213.73 J/kg dry air.

If the air is assumed to be saturated immediately after the drift eliminator, the wetbulb temperature at 5 will be equal to the given drybulb temperature T_{a5} = 306.7645 K at this elevation. The corresponding thermophysical properties at 5 can be determined according to the equations given in appendix A.

Saturated vapor pressure	p_{v5} = 5206.305 N/m^2	(A.2.1)
Humidity ratio	w_5 = 0.033922 kg/kg	(A.3.5)
Density of air-vapor	ρ_{av5} = 1.12634 kg/m^3	(A.3.1)
Dynamic viscosity of air	μ_{a5} = 1.8779×10^{-5} kg/ms	(A.1.3)
Dynamic viscosity of vapor	μ_{v5} = 1.0254×10^{-5} kg/ms	(A.2.3)
Dynamic viscosity of air-vapor	μ_{av5} = 1.84273×10^{-5} kg/ms	(A.3.3)

The enthalpy of the inlet air, i_{mas5}, is found according to equation (A.3.6b) with c_{pa5} = 1006.640 J/kgK and c_{pv5} = 1876.887 J/kgK being evaluated at (T_{a5} + 273.15)/2 = (306.7645 + 273.15)/2 = 289.9573 K according to equations (A.1.2) and (A.2.2) respectively. The latent heat is found to be i_{fgwo} = 2.5016 × 10^6 J/kgK according to equation (A.4.5) at 273.15K. With these values find i_{mas5} = 120836.9 J/kg dry air.

The approximate harmonic mean density of the air-vapor in the fill is given by

$$\rho_{av15} = \frac{2}{\frac{1}{\rho_{av1}} + \frac{1}{\rho_{av5}}} = \frac{2}{\frac{1}{1.1397} + \frac{1}{1.12634}} = 1.132982 \text{ kg/m}^3$$

The dry air mass flow rate can be determined from the following relation:

$m_{av15} = [m_a(1+w_1) + m_a(1+w_5)]$, or

$m_a = 2m_{av15}/(2+w_1+w_5)$ = 2(442.1426)/(2 + 0.016569 + 0.033922) = 431.2545 kg/s

The respective air-vapor mass flow rates upstream and downstream of the fill are thus

$m_{av1} = m_a(1+w_1)$ = 431.2545(1 + 0.016569) = 438.4000 kg/s, and

$m_{av5} = m_a(1+w_5)$ = 431.2545(1 + 0.033922) = 445.8834 kg/s

The corresponding mass velocities are

$G_{av15} = m_{av15} / A_{fr}$ = 442.1426/144 = 3.070429 kg/m^{2}s

$G_a = m_a / A_{fr}$ = 431.2545/144 = 2.994823 kg/m^{2}s

$G_{av1} = m_{av1} / A_{fr}$ = 438.4000/144 = 3.044444 kg/m^{2}s

$G_{av5} = m_{av5} / A_{fr}$ = 445.8834/144 = 3.096413 kg/m^{2}s

According to equation (A.4.2) the specific heat of water c_{pwm} = 4176.992 J/kg at the mean water temperature off$(T_{wi} + T_{wo})/2$ = (314.65 + 303.4677)/2 = 309.0589 K.

At the mean outlet temperature of the water T_{wo} = 303.4677 K find

Density of water	ρ_{wo} = 995.6046 kg/m3	(A.4.1)
Surface tension	σ_{wo} = 0.0711808 N/m	(A.4.7)

The mass velocity for the water based on the frontal area of the fill is

$G_w = m_w / A_{fr}$ = 412/144 = 2.86111 kg/m^{2}s

The transfer coefficients can be determined with the above values. To find the transfer coefficient in the rain zone, use equation (D.22). The "a" coefficients appearing in the equation for the rain zone transfer and pressure drop coefficients are as follows:

$a_\mu = 3.061\times10^{-6}(\rho_{wo}^4 g^9 / \sigma_{wo})^{0.25} = 3.061\times10^{-6}(995.6046^4 9.8^9 / 0.0711808)^{0.25}$ =1.0026

$a_\rho = 998/\rho_{wo}$ = 998/995.6046 = 1.0024

$a_v = 73.298(g^5\sigma_{wo}^3 / \rho_{wo}^3)^{0.25} = 73.298(9.8^5 \times 0.0711808^3 / 995.6046)^{0.25}$ = 0.9882

$a_L = 6.122(g\sigma_{wo}/\rho_{wo})^{0.25} = 6.122(9.8\times0.0711808/995.6046)^{0.25}$ = 0.9960

Other quantities required to evaluate the rain zone transfer coefficient are:

The humidity ratio of saturated air at T_{wo} $w_{s1} = 0.027848$ kg/kg (A.3.5)

Diffusion coefficient at inlet conditions $D_1 = 2.09061\times10^{-5}$ m^2/s (D.21)

Furthermore, the Schmidt number is

$$Sc_1 = \mu_{av1}/(\rho_{av1}D_1) = 1.85928\times10^{-5}/(1.1397\times2.09061\times10^{-5}) = 0.7803$$

and the air-vapor velocity before the fill

$$v_{av3} = m_{av1}/(\rho_{av1}A_{fr}) = 438.4000/(1.1397\times144) = 2.67127 \text{ m/s}$$

With these values find from equation (D.22)

$$\frac{h_{drz}a_{rz}H_3}{G_w} = 3.6\left(\frac{D_1}{v_{av3}d_d}\right)\left(\frac{H_3}{d_d}\right)\left(\frac{p_{a1}}{\rho_{wo}R_vT_{a1}}\right)Sc_1^{0.33}\left[\ln\left(\frac{w_{s1}+0.622}{w_1+0.622}\right)/(w_{s1}-w_1)\right]$$

$$\times\left[\begin{array}{l}4.68851a_\rho\rho_{av1} - 187128.7a_\mu\mu_{av1} - 2.29322\\ +22.4121\{0.350396(a_vv_{av3})^{1.38046}+0.09\}\{1.60934(a_LH_3)^{-1.12083}+0.66\}\\ \times\{34.6765(a_Ld_d)^{0.732448}+0.45\}\\ \times\exp\left\{7.7389\exp(-0.399827a_LH_3)\ln\left\{\begin{array}{l}0.087498\exp(0.026619a_LW_t)\\ +0.85\end{array}\right\}\right\}\end{array}\right]$$

$$=3.6\left(\frac{2.09061\times10^{-5}}{2.67127\times0.0035}\right)\left(\frac{12}{0.0035}\right)\left(\frac{101325}{995.6046\times461.52\times306.65}\right)$$

$$\times0.78033^{0.33}\left[\ln\left(\frac{0.027848+0.622}{0.016569+0.622}\right)/(0.027848-0.016569)\right]$$

$$\times\left[\begin{array}{l}4.68851\times1.0024\times1.1397-187128.7\times1.0026\times1.85928\times10^{-5}-2.29322\\ +22.4121\{0.350396(0.9882\times2.67127)^{1.38046}+0.09\}\\ \times\{1.60934(0.9960\times4)^{-1.12083}+0.66\}\\ \times\{34.6765(0.9960\times0.0035)^{0.732448}+0.45\}\\ \times\exp\left\{\begin{array}{l}7.7389\exp(-0.399827\times0.9960\times4)\\ \times\ln\left\{\begin{array}{l}0.087498\exp(0.026619\times0.9960\times12)\\ +0.85\end{array}\right\}\end{array}\right\}\end{array}\right] = 0.2851664$$

The Merkel number applicable to the fill is specified i.e.

$$\frac{h_{dfi}a_{fi}L_{fi}}{G_w} = 0.2692L_{fi}G_w^{-0.094}G_a^{0.6023} = 0.2692\times1.878\times(2.86111)^{-0.094}\times(2.994823)^{0.6023} = 0.8866959$$

The transfer coefficient in the spray zone is given by Lowe and Christie [61LO1]

$$\frac{h_{dsp}a_{sp}L_{sp}}{G_w} = 0.2L_{sp}\left(\frac{G_a}{G_w}\right)^{0.5} = 0.2\times 0.5\left(\frac{2.994823}{2.86111}\right)^{0.5} = 0.102310$$

The total transfer characteristic of the cooling tower is

$$Me_M = \frac{h_{drz}a_{rz}H_3}{G_w} + \frac{h_{dfi}a_{fi}L_{fi}}{G_w} + \frac{h_{dsp}a_{sp}L_{sp}}{G_w} = 0.2851664+0.8866959 + 0.102310 = 1.274172$$

According to equation (B.21) the Merkel number, Me_M, is

$$Me_M = \int_{T_{wo}}^{T_{wi}} \frac{c_{pw}dT_w}{(i_{masw} - i_{ma})}$$

It the four point Chebyshev integral is applied to this relation, the integral on the can be expressed as

$$Me_M = \int_{T_{wo}}^{T_{wi}} \frac{c_{pw}dT_w}{(i_{masw} - i_{ma})} \approx \frac{c_{pwm}(T_{wi} - T_{wo})}{4}\left(\frac{1}{\Delta i_{(1)}} + \frac{1}{\Delta i_{(2)}} + \frac{1}{\Delta i_{(3)}} + \frac{1}{\Delta i_{(4)}}\right)$$

A detailed discussion of the Chebyshev integration method applied to equation (B.21) is given in the literature [88BR1, 90CO1, 95OO1, 96MO1, 97CO1].

The enthalpy differentials are dependent on the following intermediate temperatures:

$T_{w(1)} = T_{wo} + 0.1(314.65 - T_{wo}) =$ 303.4677 + 0.1(314.65 – 303.4677) = 304.5859 K

$T_{w(2)} = T_{wo} + 0.4(314.65 - T_{wo}) =$ 303.4677 + 0.4(314.65 – 303.4677) = 307.9406 K

$T_{w(3)} = T_{wo} + 0.6(314.65 - T_{wo}) =$ 303.4677 + 0.6(314.65 – 303.4677) = 310.1711 K

$T_{w(4)} = T_{wo} + 0.9(314.65 - T_{wo}) =$ 303.4677 + 0.9(314.65 – 303.4677) = 313.5318 K

The bracketed subscript numbers refer to the intervals in the Chebyshev integral and should not be confused with the numbers indicating various positions in the cooling tower.

To find the corresponding increments in enthalpy, determine the enthalpy of saturated air at $T_{w(1)}$ = 304.5859 K. The relevant specific heats of air and water vapor respectively are evaluated at ($T_{w(1)}$ + 273.15)/2 = (304.5859 + 273.15)/2 = 288.868 K.

Specific heat of air	$c_{pa(1)}$ = 1006.612 J/Kg K	(A.1.2)
Specific heat of water vapor	$c_{pv(1)}$ = 1875.950 J/kg K	(A.2.2)

The pressure of saturated water at $T_{w(1)}$ follows from equation (A.2.1) and the corresponding humidity ratio evaluated at p_{a15} follows from equation (A.3.5). Where $p_{a15} = (p_{a1} + p_{a5})/2$ = (101325 + 101170.6)/2 = 101247.8 Pa.

Pressure of the water vapor	$p_{vs(1)}$ = 4605.056 J/Kg K	(A.2.1)
Humidity ratio	$w_{s(1)}$ = 0.02979283 J/kg K	(A.3.5)

With these values determine the enthalpy of saturated air at $T_{w(1)}$ according to equation (A.3.6b)

$i_{masw(1)} = c_{pa(1)}(T_{w(1)} - 273.15) + w_{s(1)}[i_{fgwo} + c_{pv(1)}(T_{w(1)} - 273.15)]$

$= 1006.612\ (304.5859 - 273.15) + 0.02979283$

$\times [2.5016\times10^6 + 1875.950\ (304.5859 - 273.15)] = 107930.4$ J/kg

The enthalpy of the air at $T_{w(1)}$ can be determined by applying equation (B.21) i.e.

$i_{ma(1)} = m_w c_{pwm}(T_{w(1)} - T_{wo})/m_a + i_{ma1}$

$= 412 \times 4176.992(\ 304.5859 - 303.4677)/431.2545 + 76213.73 = 80676.0$ J/kg

With these values find the difference in enthalpy

$\Delta i_{(1)} = i_{masw(1)} - i_{ma(1)} = 107930.4 - 80676.0 = 27254.42$ J/kg dry air

Repeat the above procedure in the case of the other three intermediate temperatures and find

$\Delta i_{(2)} = 34190.49$ J/kg dry air; $\Delta i_{(3)} = 40692.23$ J/kg dry air; $\Delta i_{(4)} = 53759.63$ J/kg dry air

Substitute these values into the approximate expression for the integral and find

$$Me_M = \int_{T_{wo}}^{T_{wi}} \frac{c_{pw}\,dT_w}{(i_{masw} - i_{ma})} \approx \frac{c_{pwm}(T_{wi} - T_{wo})}{4}\left(\frac{1}{\Delta i_{(1)}} + \frac{1}{\Delta i_{(2)}} + \frac{1}{\Delta i_{(3)}} + \frac{1}{\Delta i_{(4)}}\right)$$

$$= \frac{4176.992(314.65 - 303.4677)}{4}\left(\frac{1}{27254.42} + \frac{1}{34190.49} + \frac{1}{40692.23} + \frac{1}{53759.63}\right) = 1.274150$$

This value is almost identical to the value obtained by adding the transfer coefficients in the three wet zones which means that the water outlet temperature, $T_{wo} = 303.4677$ K is correct.

The heat rejected by the cooling tower is given by

$Q = m_w c_{pwm}(T_{wi} - T_{wo}) = 412 \times 4176.992\ (314.65 - 303.4677) = 19.243874$ MW

The correctness of the temperature of the saturated air leaving the spray zone, T_{a5}, can thus be confirmed from the relation

$Q = m_a(i_{mas5} - i_{ma1})$

The enthalpies i_{mas5} and i_{ma1} are already known, thus

$Q = 431.2545\ (120.836.9 - 76213.73) = 19.243942$ MW

The values of Q are in agreement which means that the value for T_{a5} is correct.

The specified loss coefficient due to the louvers is referred to the mean conditions through the fill i.e.

$$K_{ilfi} = K_{il}\left(\frac{\rho_{av15}}{\rho_{av1}}\right)\left(\frac{W_l B_l}{2H_3 W_i}\right)\left(\frac{m_{av1}}{m_{av15}}\right)^2 = 2.5\left(\frac{1.132982}{1.1397}\right)\left(\frac{144}{2\times4\times12}\right)\left(\frac{438.4000}{442.1426}\right)^2 = 5.497609$$

With equation (D.9) find the loss coefficient for the rain zone with

$$v_{w3} = \frac{G_w}{\rho_{wo}} = \frac{2.86111}{995.6046} = 2.873743\times10^{-3}\ \text{m/s}$$

$$K_{rz} = 1.5a_v v_{w3}(H_3/d_d)\begin{bmatrix} 0.219164 - 0.30487a_\rho\rho_{av1} + 8278.7a_\mu\mu_{av1} \\ +0.954153\{0.328467\exp(135.7638a_L d_d)+0.47\} \\ \times\{26.28482(a_L H_3)^{-2.95729}+0.56\}\exp\begin{Bmatrix}\ln(0.204814\exp(0.066518a_L W_i)+0.21)\\ \times(3.9186\exp(-0.3a_L H_3))\\ \times(0.31095\ln(a_L d_d)+2.63745)\end{Bmatrix} \\ \times\{2.177546(a_v v_{av3})^{-1.46541}+0.21\}\end{bmatrix}$$

$$= 1.5\times0.9882\times2.873743\times10^{-3}(4/0.0035)$$
$$\times\begin{bmatrix} 0.219164 - 0.30487\times1.0024\times1.1397 + 8278.7\times1.0026\times1.85928\times10^{-5} \\ +0.954153\{0.328467\exp(135.7638\times0.9960\times0.0035)+0.47\} \\ \times\{26.28482(0.9960\times4)^{-2.95729}+0.56\}\exp\begin{Bmatrix}\ln(0.204814\exp(0.066518\times0.9960\times12)+0.21)\\ \times(3.9186\exp(-0.3\times0.9960\times4))\\ \times(0.31095\ln(0.9960\times0.0035)+2.63745)\end{Bmatrix} \\ \times\{2.177546(0.9882\times2.67127)^{-1.46541}+0.21\}\end{bmatrix}$$
$$= 2.072855$$

The rain zone loss coefficient referred to fill conditions is

$$K_{rzfi} = K_{rz}\left(\frac{\rho_{av15}}{\rho_{av1}}\right)\left(\frac{m_{av1}}{m_{av15}}\right)^2 = 2.072855\left(\frac{1.132982}{1.1397}\right)\left(\frac{438.4000}{442.1426}\right)^2 = 2.025911$$

The specified loss coefficient due to the support structure of the fill is referred to the mean conditions through the fill i.e.

$$K_{fsfi} = K_{fs}\left(\frac{\rho_{av15}}{\rho_{av1}}\right)\left(\frac{m_{av1}}{m_{av15}}\right)^2 = 0.5\left(\frac{1.132982}{1.1397}\right)\left(\frac{438.4000}{442.1426}\right)^2 = 0.4886764$$

According to the specified fill loss coefficient

$$K_{fdm} = 1.9277L_{fi}G_w^{\ 1.2752}G_a^{\ -1.0356} = 1.9277\times1.878\times(2.86111)^{1.2752}(2.994823)^{-1.0356} = 4.441997$$

From the note at the end of example 4.3.1, it follows that the actual fill loss coefficient applicable to the cooling tower is given by

$$K_{fi} = K_{fdm} + \left(\frac{G_{av5}^2}{\rho_{av5}} - \frac{G_{av1}^2}{\rho_{av1}}\right)\Big/\left(\frac{G_{av15}^2}{\rho_{av15}}\right) = 4.441997 + \left(\frac{3.096413^2}{1.12634} - \frac{3.044444^2}{1.1397}\right)\Big/\left(\frac{3.070429^2}{1.132982}\right)$$
$$= 4.487634$$

The loss through the spray zone above the fill referred to the mean conditions through the fill is given by equation (D.6)

$$K_{spfi} = L_{sp}\left[0.4\left(\frac{G_w}{G_a}\right)+1\right]\left(\frac{\rho_{av15}}{\rho_{av5}}\right)\left(\frac{m_{av5}}{m_{av15}}\right)^2 = 0.5\left[0.4\left(\frac{2.86111}{2.994823}\right)+1\right]\left(\frac{1.132982}{1.12634}\right)\left(\frac{445.8834}{442.1426}\right)^2$$

$$= 0.7069580$$

The specified loss coefficient due to the water distribution system is referred to the mean conditions through the fill i.e.

$$K_{wdfi} = K_{wd}\left(\frac{\rho_{av15}}{\rho_{av5}}\right)\left(\frac{m_{av5}}{m_{av15}}\right)^2 = 0.5\left(\frac{1.132982}{1.12634}\right)\left(\frac{445.8834}{442.1426}\right)^2 = 0.5114949$$

From equation (D.7) the loss coefficient for the specified type c drift eliminator based on fill conditions is

$$K_{defi} = 27.4892Ry^{-0.14247}\left(\frac{\rho_{av15}}{\rho_{av5}}\right)\left(\frac{m_{av5}}{m_{av15}}\right)^2$$

$$= 27.4892\left(\frac{445.8834}{1.84273\times10^{-5}\times144}\right)^{-0.14247}\left(\frac{1.132982}{1.12634}\right)\left(\frac{445.8834}{442.1426}\right)^2 = 5.06490$$

The inlet loss coefficient in isotropically packed induced draft rectangular towers is according to equation (D.13),

$$K_{ct(norz)} = 0.2339+\left(3.919\times10^{-3}K_{fie}^2 - 6.840\times10^{-2}K_{fie} + 2.5267\right)$$
$$\times\exp\left\{\frac{W_i}{H_3}\left(0.5143-0.1803\exp\left\{0.0163K_{fie}\right\}\right)\right\}$$
$$-\sinh^{-1}\left[2.77\exp\left\{0.958\frac{W_i}{H_3}\right\}\times\exp\left\{K_{fie}\left(2.457-1.015\frac{W_i}{H_3}\right)\times10^{-2}\right\}\times\left(\frac{r_i}{W_i}-0.013028\right)\right]$$

$$= 0.2339+\left(3.919\times10^{-3}\times11.25966^2 - 6.840\times10^{-2}\times11.25966+2.5267\right)$$
$$\times\exp\left\{\frac{12}{4}\left(0.5143-0.1803\exp\left[0.0163\times11.25966\right]\right)\right\}$$
$$-\sinh^{-1}\left[2.77\exp\left\{0.958\frac{12}{4}\right\}\times\exp\left\{11.25966\left(2.457-1.015\frac{12}{4}\right)\times10^{-2}\right\}\times\left(\frac{0.3}{12}-0.013028\right)\right]$$

$$= 5.212728$$

where K_{fie} is the loss coefficient in the vicinity of the fill i.e.

$$K_{fie} = K_{fsfi} + K_{fi} + K_{spfi} + K_{wdfi} + K_{defi}$$

$$= 0.4886764 + 4.487634 + 0.7069580 + 0.5114949 + 5.06490 = 11.25966$$

De Villiers and Kröger [99DE1] state that it becomes acceptable to ignore the inlet loss correction factor in cases where $W_i / H_3 \leq 3$. In this case, $W_i / H_3 = 3$, which means that $K_{ct} = K_{ct(norz)}$

Referred to the mean conditions through the fill, the inlet loss coefficient becomes,

$$K_{ctfi} = K_{ct}\left(\frac{\rho_{av15}}{\rho_{av1}}\right)\left(\frac{m_{av1}}{m_{av15}}\right)^2 = 5.212728\left(\frac{1.132982}{1.1397}\right)\left(\frac{438.4000}{442.1426}\right)^2 = 5.094674$$

The specified fan upstream loss coefficient is referred to the mean conditions through the fill i.e.

$$K_{upfi} = K_{up}\left(\frac{\rho_{av15}}{\rho_{av5}}\right)\left(\frac{m_{av5}}{m_{av15}}\right)^2\left(\frac{A_{fr}}{A_c}\right)^2 = 0.5\left(\frac{1.132982}{1.12634}\right)\left(\frac{445.8834}{442.1426}\right)^2\left(\frac{144\times 4}{\pi\times 8^2}\right)^2 = 4.365760$$

The actual air volume flow rate through the fan is

$V_F = m_{av5} / \rho_{av5}$ = 445.8834 / 1.12634 = 395.8676 m^3/s

Since the actual air density and the rotational speed of the fan are not the same as the reference conditions for which fan performance characteristics were specified, the relevant fan laws as given in Kröger [98KR1] are employed.

According to the fan conversion law [98KR1],

$$V_{F/dif} = V_F\left(\frac{N_{F/dif}}{N_F}\right)\left(\frac{d_{Fr}}{d_F}\right)^3 = 395.8676\left(\frac{750}{120}\right)\left(\frac{1.536}{8}\right)^3 = 17.51192 \text{ m}^3/\text{s}$$

At this flow rate the fan static reference pressure drop is given by the specified relation,

$$\Delta p_{F/difs} = 320.85 - 6.9604V_{F/dif} + 0.31373V_{F/dif}^2 - 0.021393V_{F/dif}^3$$

$$= 320.85 - 6.9604(17.51192) + 0.31373(17.51192)^2 - 0.021393(17.51192)^3 = 180.2833 \text{ Pa}$$

The actual change in fan static pressure as expressed by the fan conversion law [98KR1]

$$\Delta p_{Fs} = \Delta p_{F/dif}\left(\frac{N_F}{N_{F/dif}}\right)^2\left(\frac{d_F}{d_{Fr}}\right)^2\left(\frac{\rho_{av6}}{\rho_r}\right) = 180.2833\left(\frac{120}{750}\right)^2\left(\frac{8}{1.536}\right)^2\left(\frac{1.12634}{1.2}\right) = 117.5123 \text{ Pa}$$

At the reference condition the fan shaft power is

$$P_{F/dif} = 4245.1 - 64.134V_{F/dif} + 17.586V_{F/dif}^2 - 0.71079V_{F/dif}^3$$

$$= 4245.1 - 64.134(17.51192) + 17.586(17.51922)^2 - 0.71079(17.51922)^3 = 4697.863 \text{ W}$$

The actual fan shaft power follows from the fan conversion law [98KR1]

$$P_F = P_{F/dif}\left(\frac{N_F}{N_{F/dif}}\right)^3\left(\frac{d_F}{d_{Fr}}\right)^5\left(\frac{\rho_{av6}}{\rho_r}\right) = 4697.863\left(\frac{120}{750}\right)^3\left(\frac{8}{1.536}\right)^5\left(\frac{1.12634}{1.2}\right) = 69222.04 \text{ W}$$

The fan static pressure rise coefficient follows from Kröger [98KR1]

$$K_{F/difs} = \frac{2\Delta p_{Fs}\rho_{av6}}{\left(\frac{4m_{av5}}{\pi d_c^2}\right)^2} = \frac{2\times 117.5123\times 1.12634}{\left(\frac{4\times 445.8834}{\pi\times 8^2}\right)^2} = 3.364199$$

At this stage, it is possible to confirm the value of p_{a5} according to

$$p_{a5} = p_{a1}\left[1-\frac{0.00975\left(H_3+L_{fl}/2\right)}{T_{a1}}\right]^{3.5(1+w_1)\left(1-\frac{w_1}{w_1+0.622}\right)}$$

$$-\left(K_{ilfi}+K_{rzfi}+K_{fsfi}+K_{fl}+K_{spfi}+K_{wdfi}+K_{defi}+K_{ctfi}\right)\frac{\left(\frac{m_{av15}}{Afr}\right)^2}{2\rho_{av15}}$$

$$=101325\left[1-\frac{0.00975(4+1.878/2)}{306.65}\right]^{3.5(1+0.016569)\left(1-\frac{0.016569}{0.016569+0.622}\right)}$$

$$-\begin{pmatrix}5.497609+2.025911+0.4886764+4.487634+0.7069580\\+0.5114949+5.064900+5.212728\end{pmatrix}\frac{\left(\frac{442.1426}{144}\right)^2}{2\times 1.132982} = 101170.6 \text{ Pa}$$

This value is in agreement with that used previously in calculations in this example.

It is assumed that the condition of the air at the inlet of the fan is equal to that at the outlet of the fill, i.e. $T_{a6} = T_{a5}$, $p_{a6} = p_{a5}$ and therefore are $\rho_{av6} = \rho_{av5} = 1.12634$ kg/m^3.

Ignoring pressure differences due to the gravity field, the draft equation can be expressed as

$$\left(K_{ilfi}+K_{rzfi}+K_{fsfi}+K_{fl}+K_{spfi}+K_{wdfi}+K_{defi}+K_{ctfi}+K_{upfi}\right)\frac{\left(\frac{m_{av15}}{Afr}\right)^2}{2\rho_{av15}} - K_{fs}\frac{\left(\frac{m_{av5}}{A_c}\right)^2}{2\rho_{av6}} = 0$$

The terms on the left-hand side of the equation give

$$\left(K_{ilfi}+K_{rzfi}+K_{fsfi}+K_{fl}+K_{spfi}+K_{wdfi}+K_{defi}+K_{ctfi}+K_{upfi}\right)\frac{\left(\frac{m_{av15}}{Afr}\right)^2}{2\rho_{av15}} - K_{fs}\frac{\left(\frac{m_{av5}}{A_c}\right)^2}{2\rho_{av6}}$$

$$=\begin{pmatrix}5.497609+2.025911+0.4886764+4.487634+0.7069580\\+0.5114949+5.064900+5.212728+4.365760\end{pmatrix}\frac{\left(\frac{442.1426}{144}\right)^2}{2\times 1.132982}$$

$$-3.364199\frac{\left(\frac{445.8834\times 4}{\pi\times 8^2}\right)^2}{2\times 1.12634} = -0.00482$$

This value is close to zero and the draft equation is thus satisfied.

The amount of water lost due to evaporation is given by

$$m_{w(evap)} = m_a(w_5 - w_1) = 431.2545(0.033922 - 0.016569) = 7.48343 \text{ kg/s}$$

The path of the air through the counterflow cooling tower, according to the Merkel approach, is shown in figure J.2. Only the inlet and outlet states of the air is known if the Merkel approach is employed. The path of the air according to the more rigorous Poppe approach is also shown in figure J.2. The outlet air is not saturated according to the Poppe approach.

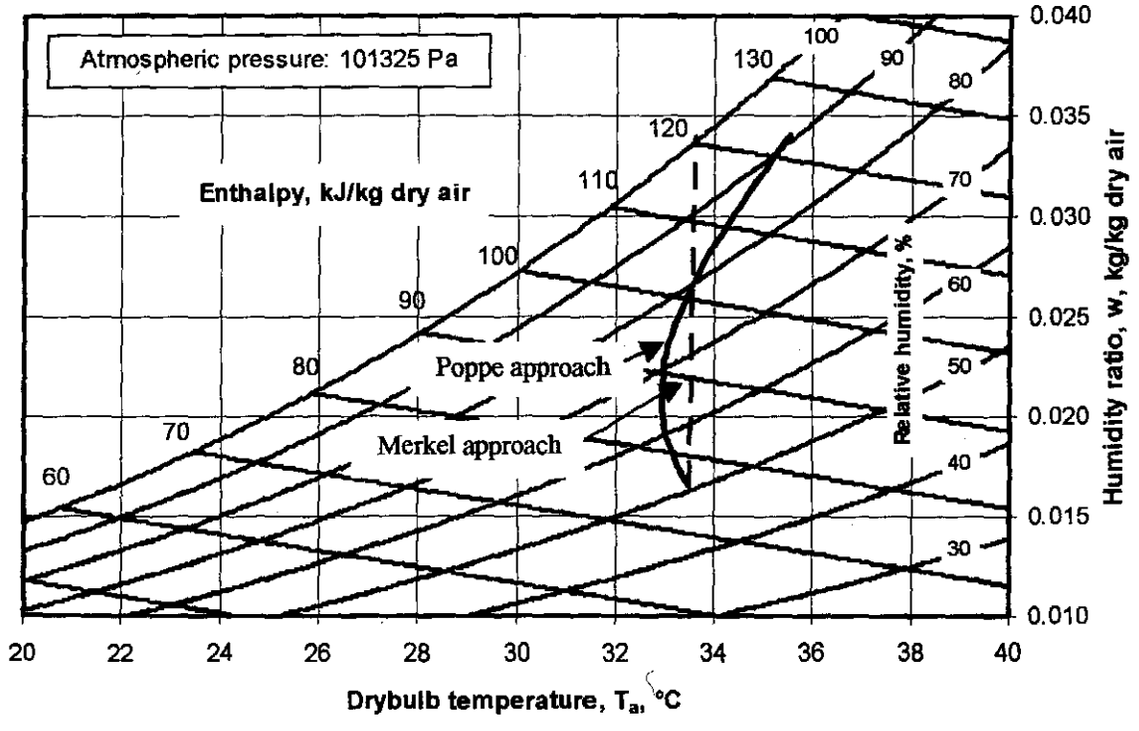

Figure J.2: Psychrometric chart

J.3 COMPARISON BETWEEN DIFFERENT DRAFT EQUATIONS

Table J.1 contains the comparative results of the induced draft cooling tower analyzed in this appendix for two variants of the draft equation. The first variant of the draft equation is equation (J.1), which is used in the analysis in the previous section. The second variant of the draft equation is equation (J.2). Equation (J.2) thus replaces equation (J.1) in the analysis above.

The draft equation for the induced draft wet-cooling tower in the previous section, where the pressure differential between the inside and the outside of the tower is ignored, is according to equation (J.1),

$$\left(K_{ilfi} + K_{rzfi} + K_{fsfi} + K_{fi} + K_{spfi} + K_{wdfi} + K_{defi} + K_{ctfi} + K_{upfi}\right)\frac{\left(\frac{m_{av15}}{Afr}\right)^2}{2\rho_{av15}} - K_{fs}\frac{\left(\frac{m_{av5}}{A_c}\right)^2}{2\rho_{av6}} = 0 \qquad \text{(J.1)}$$

For the case where the pressure differential between the inside and the outside of the tower is taken into account, the draft equation is according to equation (J.2),

$$\left(K_{ilfi}+K_{rzfi}+K_{fsfi}+K_{fi}+K_{spfi}+K_{wdfi}+K_{defi}+K_{ctfi}+K_{upfi}\right)\frac{\left(\frac{m_{av15}}{Afr}\right)^2}{2\rho_{av15}}-K_{fs}\frac{\left(\frac{m_{av5}}{A_c}\right)^2}{2\rho_{av6}} \qquad (J.2)$$
$$=\left(p_{a1}-p_{a9}\right)-\left(p_{a1}-p_{a34}\right)-\left(p_{a34}-p_{a6}\right)-\left(p_{a7}-p_{a8}\right)-\left(p_{a8}-p_{a9}\right)$$

where the pressure differentials are similar to those employed in appendix I.

Table J.1: Differences in results for different draft equations.

Draft equation	(J.1)	(J.2)
Air-vapor mass flow rate, m_{av15}, kg/s	442.1426	443.4894
Air outlet temperature, T_{a5}, K	306.7645	306.7506
Water outlet temperature, T_{wo}, K	303.4677	303.455
Heat rejected, Q, MW	19.243874	19.26578

It can be seen in table J.1 that the differences between the results for equation (J.1) and equation (J.2) for each model are very small. It can therefore be concluded that the pressure differentials due to the pressure gradient in a gravity field can be ignored for mechanical draft cooling towers. This is because the pressure differential due to the fan is the dominating term in equation (J.2).

APPENDIX K

FILL TEST FACILITY AND PROCESSING OF FILL TEST DATA

K.1 INTRODUCTION

The fill test facility where the performance of fill material is tested is described in section K.2. A computer program that is developed to process and analyze the experimental data of a fill test is presented in section K.3. A sample calculation of the processing of the experimental data is presented in section K.4.

K.2 FILL TEST FACILITY

A schematic layout of the wet/dry cooling test facility in the Department of Mechanical Engineering at the University of Stellenbosch is shown in figure K.1. The test facility consists of crossflow and counterflow test sections to test and analyze the performance of cooling tower packing material and spray-cooled heat exchangers. The crossflow section has a height and width of 2.5 m and a depth of 2 m. The counterflow section has a cross sectional area of 1.5 × 1.5 m. The counterflow test section can be extended to any practical height by 750 mm modules which are bolted together.

Hot water is pumped from an underground storage tank to the test sections. The storage tank has a capacity of 45 m^3. The water is heated by recycling it through a 100 kW diesel-fired boiler. During a test, the heated water is pumped from the top of the storage tank to the test section where it is cooled. The cooled water is then fed back to the bottom of the storage tank. This ensures that stratification occurs in the storage tank and that the subsequent supply temperature will remain almost constant for short test runs.

The water flow rate is determined from the pressure drop measured across an orifice plate installed in the supply line according to British Standard 1042 [81BR1]. The water flow rate is varied by a manually operated gate valve.

Air is drawn through the tunnel by a 50 kW centrifugal fan with variable speed control. The mass flow rate of the air is determined by measuring the pressure drop across one or more of the five ASHRAE 51-75 elliptical nozzles mounted in the horizontal section of the windtunnel as shown in figure K.1. The pressure drop is determined by a calibrated electronic pressure transducer.

The temperatures are measured using calibrated copper-constantan thermocouples. Refer to figure K.2 for the location of the thermocouples on the counterflow section.

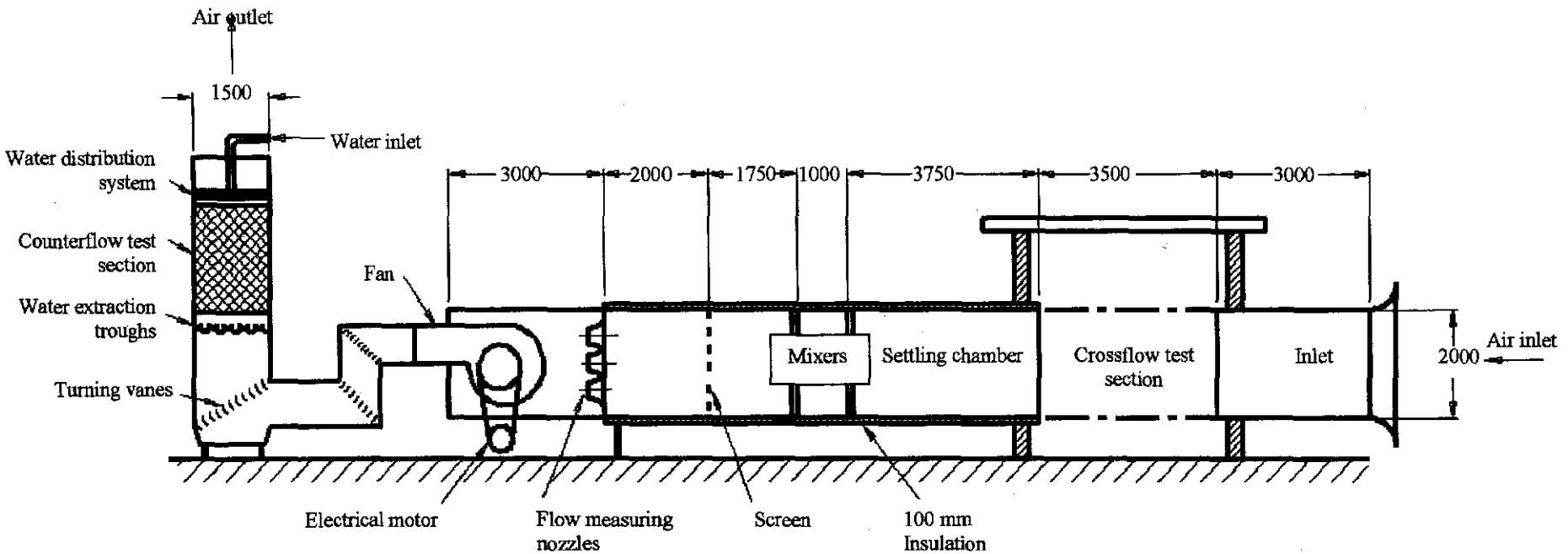

Figure K.1: Schematic layout of wet/dry cooling test facility.

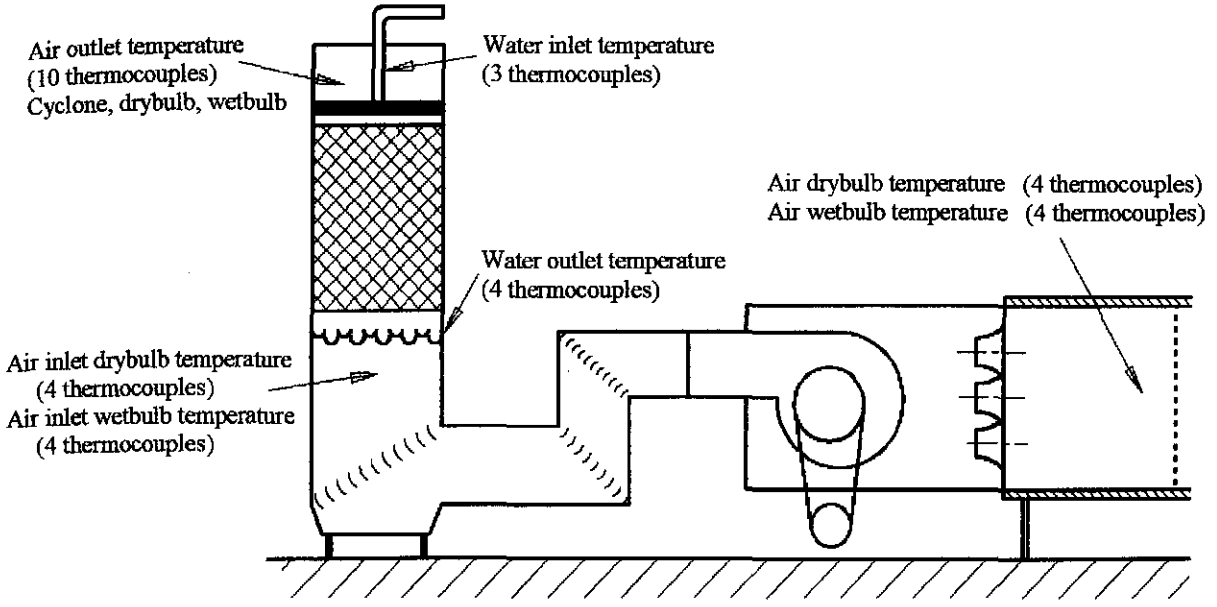

Figure K.2 Thermocouples installed on counterflow section.

The air temperature is measured before the nozzles to accurately predict the density of the air flowing through the nozzles. The drybulb and wetbulb temperatures are the average of four thermocouples each, distributed across a vertical plane.

The air drybulb and wetbulb temperatures are again measured below the water extraction troughs. They are the average of four thermocouples each, distributed across a horizontal plane. The average temperatures of the air below the troughs will be used to determine the inlet properties to the test section. These temperatures may differ from the temperatures measured before the nozzles due to the influence of the fan and the leakage of warm water through the troughs.

The air outlet temperature can be measured by four drybulb/wetbulb measuring probes or in a cyclone in which the water entrained in the air is separated from the air. Ten thermocouples are available to measure the outlet air temperature.

The pressure drop across the fill and troughs is measured by four static pressure probes. Two are installed below the troughs and two are installed above the fill. The pressure drop across the troughs is subtracted from the total pressure drop to obtain the pressure drop across the fill. Refer to Oosthuizen [95OO1] and Baard [98BA1] for a detailed description of the pressure probes, the water distribution system, the water extraction troughs and psychrometric probes.

The data logging system consists of two Isolated Measurement Pods (IMPs). The IMPs are connected to a Pentium Personal Computer (PC) via an S-Net cable and Schlumberger PC card. The data logger has an internal reference point, which eliminates the use of an ice bath needed for temperature measurement purposes. The data logger converts all temperature readings from millivolts to degree Celsius before

transferring them to the PC. The pressure transducers adapt pressure readings to voltage signals, which are transferred to the data logger.

K.3 DEVELOPMENT OF A COMPUTER PROGRAM TO PROCESS AND ANALYZE COOLING TOWER TEST FACILITY DATA.

K.3.1 INTRODUCTION

A Windows 95 computer program, named Natklos, is developed to analyze the experimental data from the approximately forty thermocouples and electronic pressure transducers of the cooling tower test facility. The aim is to process and analyze the data fast and efficiently. Different calculation options can be selected with the press of a button on the user-friendly graphical user interface (GUI). The GUI is developed in Visual C++ 6 while the numerical algorithms are developed in Fortran 77 and Fortran 90.

K.3.2 MAIN PROGRAM DIALOG

The main dialog window of the Natklos program is shown in figure K.3. The three main options that can be accessed from the main dialog window are the processing of the experimental data, the determination of the transfer and loss coefficients according to different analytical models and the determination of empirical relations to represent the transfer and loss coefficients.

K.3.3 PROCESSING OF THE EXPERIMENTAL DATA

As already mentioned, the data logger saves the various temperatures measured by the thermocouples in degrees Celsius while the output from the pressure transducers are saved in volt. The pressures and mean temperatures are calculated with the aid of the dialog window shown in figure K.4. The calibration curves, to convert the voltage signals of the pressure transducers can be supplied in the dialog window shown in figure K.4. There are calibration curves for the pressure transducers that measure the pressure drop over the fill, over the nozzles in the upstream windtunnel and over the orifice plate in the water supply line. The air and water flow rates are determined from these calibration curves. If certain selections are made, some of the functions of the dialog window are disabled. By disabling the non-relevant functions, the dialog window is more user-friendly. The pressure drop over the water troughs are subtracted from the measured pressure drop over both the fill and the troughs.

The data logger writes the data in a file that it receives from the Schlumberger card in forty different channels, twenty channels for each IMP. Due to maintenance or breakdown of thermocouples, it is sometimes necessary to change or disable some the channels on the IMPs. Also, if the discrepancy of one thermocouple is great compared to other ones that are measuring the same quantity, it is sometimes necessary to exclude this temperature from the calculation of the mean temperature. An efficient method is therefore implemented to assign the channels for different quantities on the data processing software.

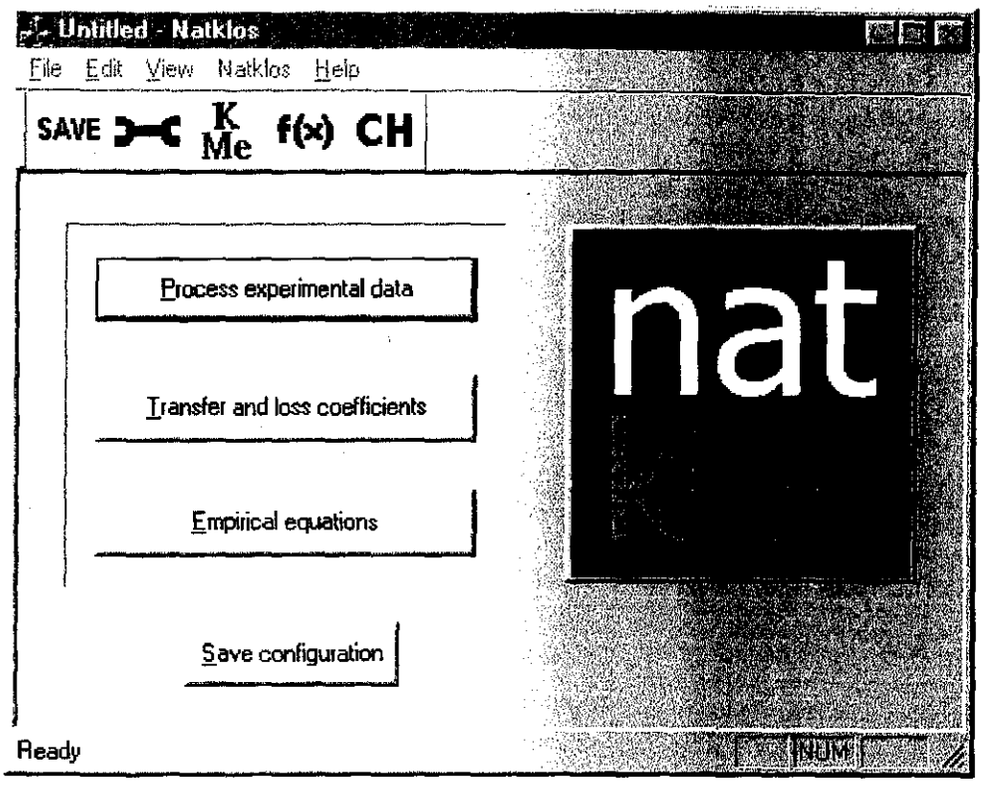

Figure K.3: The main dialog window of the Natklos program.

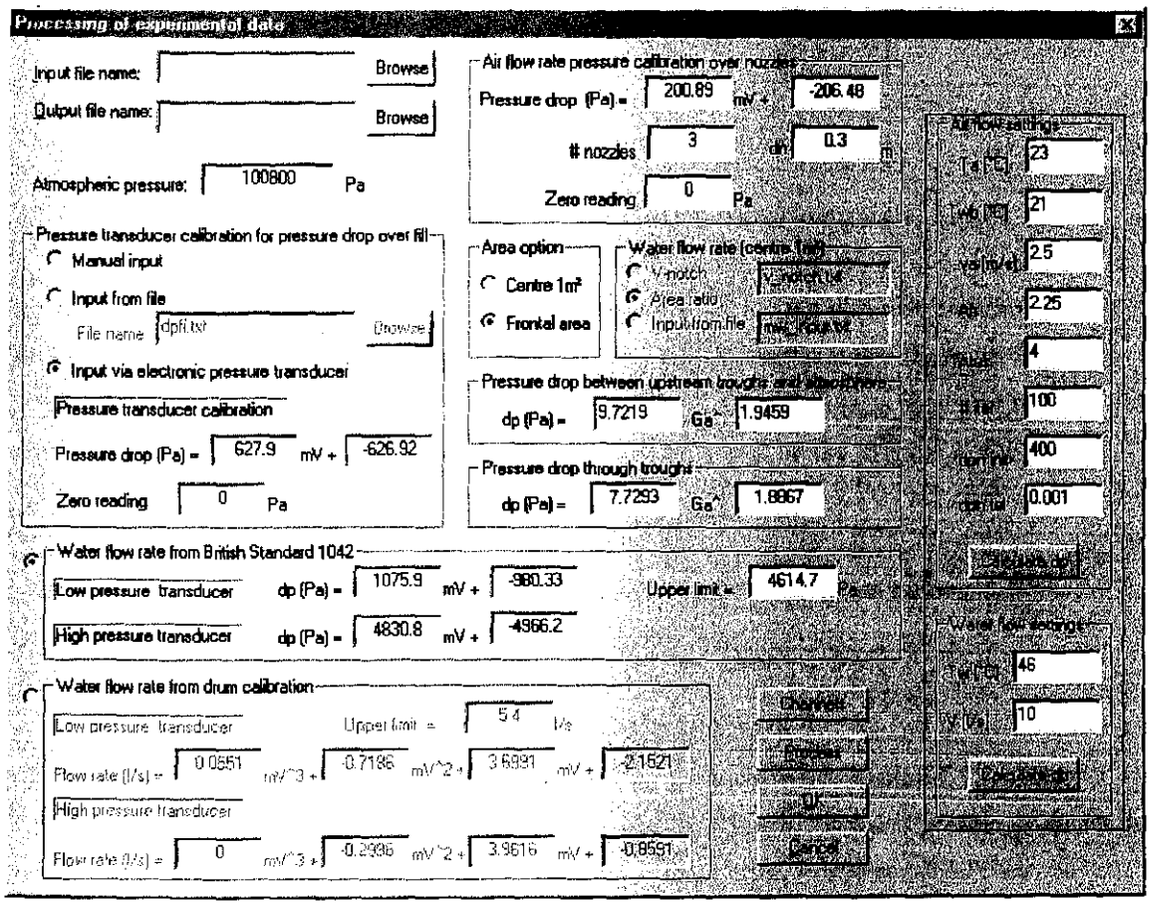

Figure K.4: Dialog window for processing of the experimental results.

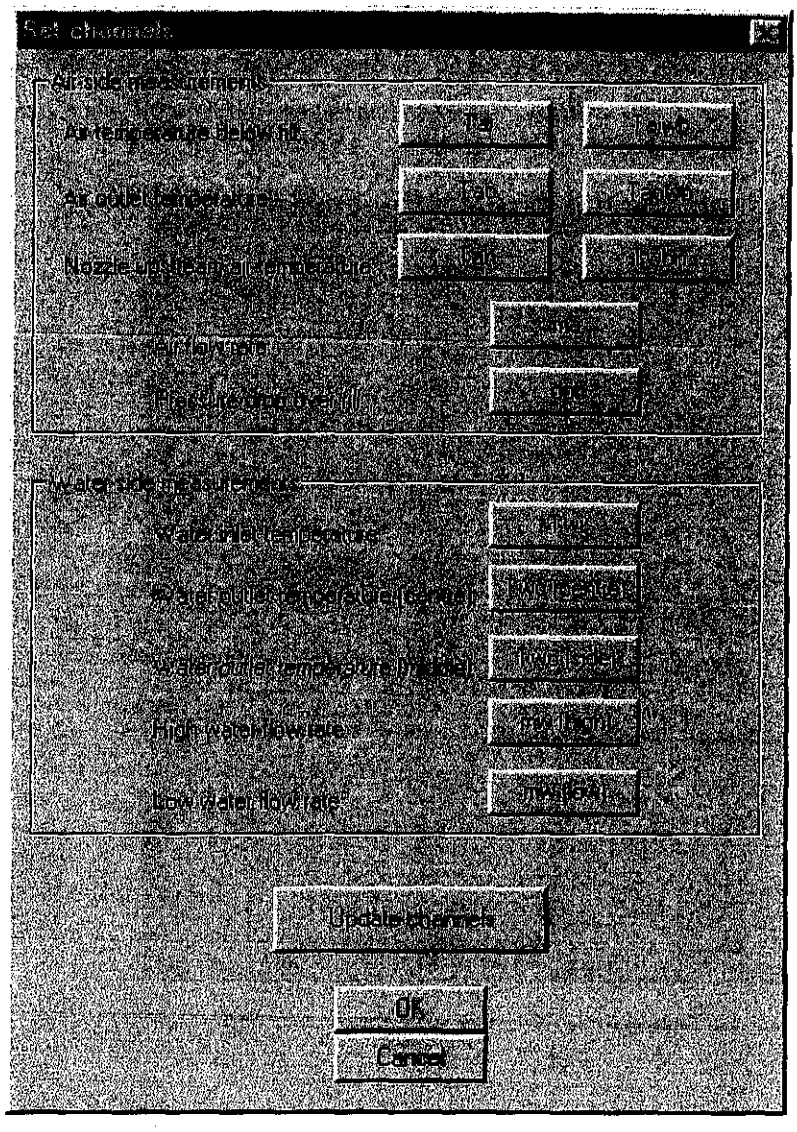

Figure K.5: Dialog window from where the channels are set for the different measurements.

Figure K.5 shows the dialog window from where the channels are set for the different experimental quantities. The dialog shown in figure K.5 is obtained by pressing the 'Channels' button shown in figure K.4. If each of the variable buttons shown in figure K.5 is pressed a dialog window as shown in figure K.6 appears. For example, the air inlet temperature to the test section will be the average of the four selected data logging channels shown in figure K.6.

If the 'Process' button in figure K.4 is pressed, the data of each fill test is written to an output file in following sequence: p_a, T_{ai}, T_{wb}, T_{wo}, m_a, m_w Δp_{fi}.

K.3.4 CALCULATION OF THE TRANSFER AND LOSS COEFFICIENTS

Figure K.7 shows the dialog window where all the transfer and loss coefficients are calculated. The dialog window shown in figure K.7 appears when the 'Transfer and loss coefficients' button is pressed in the dialog window shown in figure K.3. The coefficients according to the Merkel, Poppe and *e-NTU* can be selected. The integration settings for the Merkel and Poppe approaches can be specified. If a rain zone

and/or a spray zone exist, then the effects of these zones can be subtracted from the total measured transfer and loss coefficients. Refer to appendix D for the formulas used to subtract the influences of the rain and spray zones for both the transfer and loss coefficients.

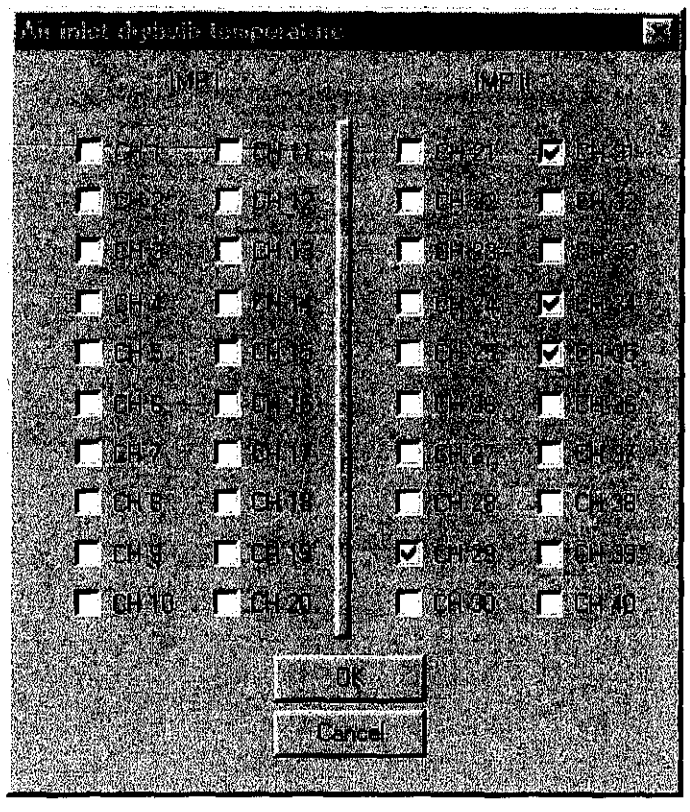

Figure K.6: Dialog window where the channels for a certain measurement are set.

The output file generated by the dialog window shown in figure K.4 is used as the input file in the dialog window shown in figure K.7. An output file with the air and water mass velocities and the transfer and loss coefficients according to the *e-NTU*, Merkel and Poppe approaches is generated when the 'Calculate coefficients' button is pressed in the dialog window shown in figure K.7.

K.3.5 DETERMINATION OF EMPIRICAL EQUATIONS

The dialog window in figure K.8 appears when the 'Empirical equations' button is pressed in the dialog window shown in figure K.3. Empirical equations are generated in this dialog window with a least squares curve fitting method. Conventional linear regression with straight-line transformations can not be used to minimize the objective function, because the empirical equations have generally more than two unknown variables. Therefore, mathematical optimization algorithms are employed to obtain the best possible fit for the empirical equation. The form of the equation can be selected on the dialog window. The coefficients a, b, c and d are obtained to give the best possible fit for the selected form of the equation shown in figure K.8.

As already mentioned, the method of least squares is employed to obtain empirical correlation through the experimentally determined data. The sum of the least squares is given by the function [93BE2],

$$S^2 = \sum_{i=1}^{j} [y_i - y(x_i)]^2 \qquad \text{(K.1)}$$

where y_i are the experimentally determined ordinate for measured values of x_i where x_i is a vector in R^n. j is the number of experimental observations used.

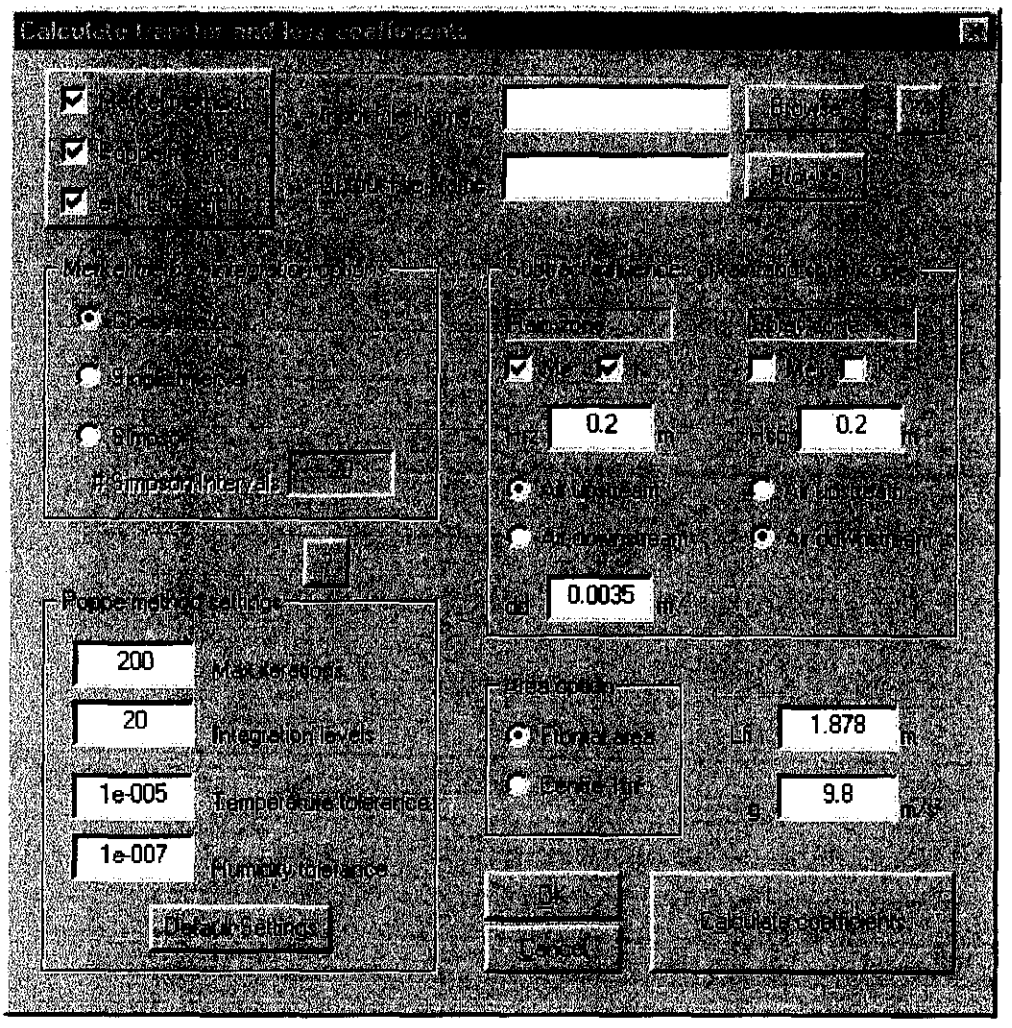

Figure K.7: Dialog window for the calculation of transfer and loss coefficients.

To indicate the reliability of the fit, the correlation coefficient, r, is defined where,

$$r^2 = \frac{\sum [y(x_i) - y_m]^2}{S^2 + \sum [y(x_i) - y_m]^2} \qquad \text{(K.2)}$$

where y_m is the mean of the measured y_i [93BE2].

It can be seen from figure K.8 that the sum of the least squares can be minimized by the LFOPC [82SN1, 83SN1, 85SN1], ETOPC [98SN1, 00SN1] or DYNAMIC-Q [94SN1, 00SN2] optimization algorithms. LFOPC is a gradient method that generates a dynamic trajectory path, from any given stating point to a local optimum. ETOPC is a conjugate gradient method. The DYNAMIC-Q algorithm applies the dynamic

trajectory optimization algorithm LFOPC to successive spherical quadratic approximations of the actual optimization problem.

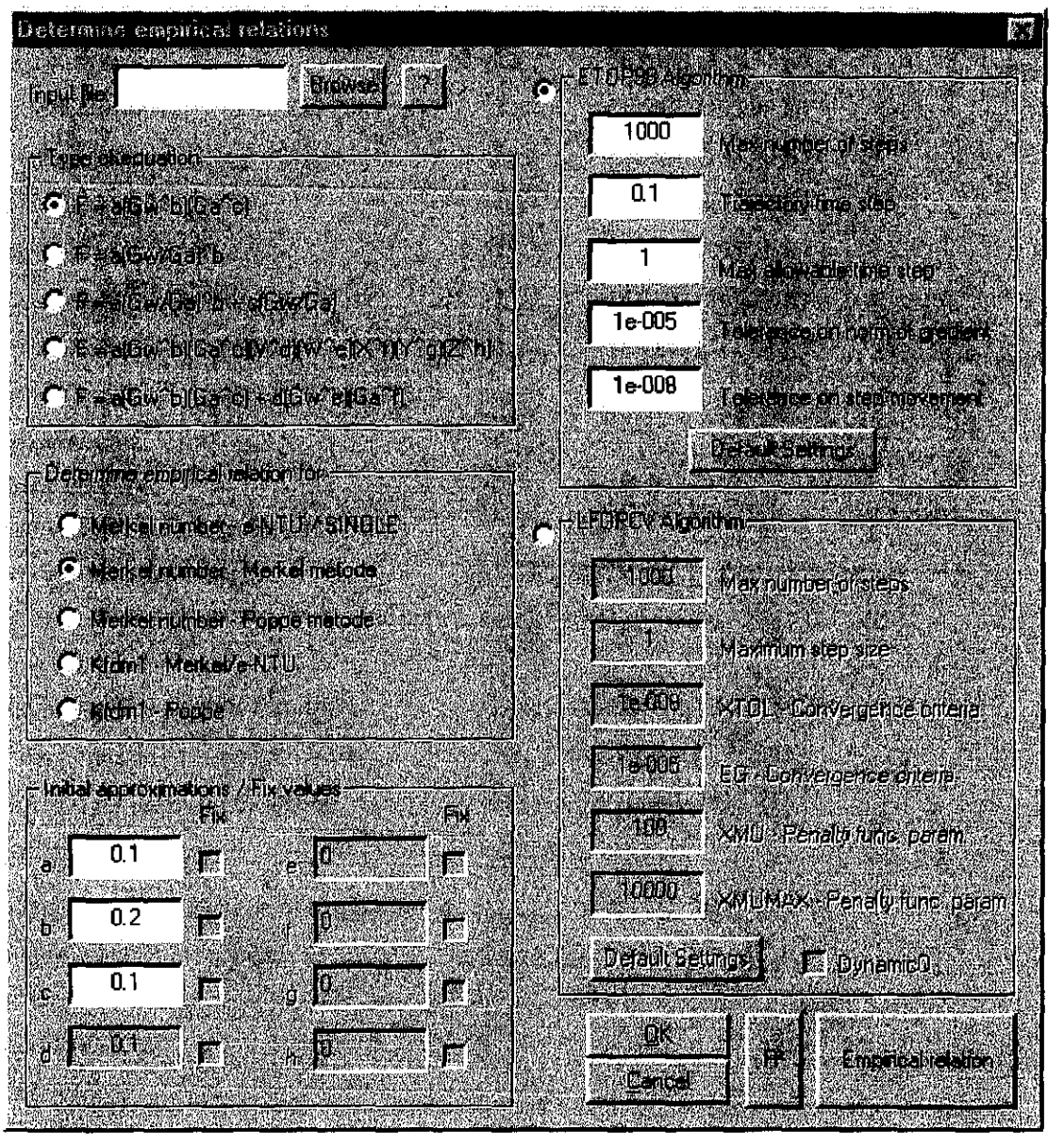

Figure K.8: Dialog window to determine empirical relations.

It can be seen in figure K.8 that the values of the coefficients can be fixed to a certain value. The optimization problem then changes from an unconstrained to a constrained problem. After the first run of the optimization problem is it sometimes useful to round some of the exponents off to less significant digits. The coefficients then can be fixed and the other coefficients can then be optimized to obtain the best fit. The correlation coefficient, r^2, will be an indication how the accuracy of the fit is affected by this procedure.

K.4 SAMPLE CALCULATION OF EXPERIMENTAL DATA PROCESSING

K.4.1 INTRODUCTION

A sample calculation is presented of how the air mass flow rate, the water mass flow rate, the pressure drop over the fill and the energy balance are calculated from experimental measurements.

Temperature measurements:

Water inlet temperature	T_{wi}	= 46.36°C (319.51 K)
Water outlet temperature	T_{wo}	= 31.89°C (305.04 K)
Air temperature below fill	T_{ai}	= 22.35°C (295.50 K)
Wetbulb temperature below fill	T_{wb}	= 20.14°C (293.29 K)
Air temperature (nozzles)	T_{an}	= 22.14°C (295.29 K)
Wetbulb temperature (nozzles)	T_{wbn}	= 19.05°C (292.20 K)
Air temperature in cyclone at air exit	T_{ao}	= 38.31°C (311.46 K)

Other measurements:

Atmospheric pressure	p_a	= 100500 Pa
Pressure drop - orifice plate (voltage)	2.098510 mV	
Pressure drop - nozzles (voltage)	1.377270 mV	

Calibration curves:

Pressure drop - orifice pressure transducer	$\Delta p_{op} = 4830.80\times(\text{mV}) - 4986.20$
Pressure drop - nozzle pressure transducer	$\Delta p_n = 200.89\times(\text{mV}) - 206.48$
Pressure drop – fill pressure transducer	$\Delta p_t = 627.9\times(\text{mV}) - 626.92$
Pressure drop over troughs	$\Delta p_{tr} = 7.72930 G_a^{1.88670}$
Pressure drop (pressure upstream of troughs minus atmospheric pressure)	$\Delta p_{uptr} = 9.7219 G_a^{1.9459}$

Other specifications:

Number of nozzles	$n_n = 3$
Nozzle diameter	$d_n = 0.3$ m
Frontal area of the fill	$A_{fr} = 2.25$ m^2
Wind tunnel area	$A_{tus} = 4$ m^2
Water pipe inside diameter	$d_w = 0.13$ m
Orifice plate diameter	$d_{op} = 0.62$ m

K.4.2 AIR MASS FLOW RATE

The formulas used in this section to obtain the air mass flow rate can be found in [98KR1]. The pressure drop over the nozzles is given, at a pressure transducer voltage of 1.377270mV, by

$\Delta p_n = 200.89\times(\text{mV}) - 206.48 = 200.89\times 1.377270 - 206.48 = 70.19977$ Pa

The discharge area of one nozzle is

$$A_n = \frac{\pi}{4} d_n^2 = \frac{\pi}{4} 0.3^2 = 0.0706858 \text{m}^2$$

Pressure of water vapor from equation (A.2.1) evaluated at T_{wbn}, where T_{wbn} = 292.20K.

z_n = 10.79586(1 – 273.16/292.20) + 5.02808 $\log_{10}$(273.16/292.20) + 1.50474

$\times 10^{-4}[1 - 10^{-8.29692\{(292.20/273.16)-1\}}] + 4.2873 \times 10^{-4}[10^{4.76955(1-273.16/292.20)} - 1] + 2.786118312$

= 3.343007

$p_{vwbn} = 10^{3.343007}$ = 2202.538 Pa

It is assumed that the nozzle upstream pressure is equal to atmospheric pressure. The humidity ratio then follows from equation (A.3.5)

$$w_n = \left(\frac{2501.6 - 2.3263(T_{wbn} - 273.15)}{2501.6 + 1.8577(T_{an} - 273.15) - 4.184(T_{wbn} - 273.15)}\right)\left(\frac{0.62509 p_{vwbn}}{p_a - 1.005 p_{vwbn}}\right)$$

$$- \left(\frac{1.00416(T_{an} - T_{wbn})}{2501.6 + 1.8577(T_{an} - 273.15) - 4.184(T_{wbn} - 273.15)}\right)$$

$$= \left(\frac{2501.6 - 2.3263(292.20 - 273.15)}{2501.6 + 1.8577(295.29 - 273.15) - 4.184(292.20 - 273.15)}\right)\left(\frac{0.62509 \cdot 2202.538}{100500 - 1.005 \cdot 2202.538}\right)$$

$$- \left(\frac{1.00416(295.29 - 292.20)}{2501.6 + 1.8577(295.29 - 273.15) - 4.184(292.20 - 273.15)}\right) = 0.0127123 \text{ kg/kg}$$

At the measured air drybulb temperature of T_{an} = 295.29K, wetbulb temperature of T_{wbn} = 292.20K, find the following thermophysical properties employing the equations given in appendix A.

Density of air-vapor	ρ_{avn} = 1.176541 kg/m3	(A.3.1)
Viscosity of the air vapor mixture	μ_{avn} = 1.811918 × 10^{-5} kg/ms	(A.3.3)

The mass flow rate of air containing water vapor through one nozzle can be given by

$$m_{avn1} = C_n \phi_g Y \pi d_n^2 (2 \rho_{avn} \Delta p_n)^{0.5} / 4$$

where the gas expansion factor is given by

$$\phi_g = 1 - 3\Delta p_n / (4 p_a 1.4) = 1 - (3)(70.19977)/[(4)(100500)(1.4)] = 0.9996258$$

The approach velocity factor is given by

$$Y = 1 + 0.5(A_n / A_{tus})^2 + 2(A_n / A_{tus})^2 \Delta p_n / (1.4 p_a)$$

$$= 1 + 0.5(0.0706858/4)^2 + 2(0.0706858/4)^2\ 70.19977/[(1.4)(100500)] = 1.000156$$

The coefficient of discharge, C_n, is a function of the Reynolds number and is obtained by an iterative procedure. Assume that the Reynolds number, Re_n, for the air vapor mass flow through one nozzle is 210935.1. The coefficient is given by

$$C_n = 0.9758 + 1.08\times10^{-7}\,Re_n - 1.6\times10^{-13}\,Re_n^2$$

$$= 0.9758 + 1.08\times10^{-7}\times210935.1 - 1.6\times10^{-13}\times210935.1^2 = 0.991462$$

The mass flow rate of air containing water vapor through one nozzle can be determined by

$$m_{avn1} = C_n\phi_g Y A_n\left(2\rho_{avn}\Delta p_n\right)^{0.5}$$

$$= (0.991462)(0.9996258)(1.000156)[(2)(1.176541)(70.19977)]^{0.5} = 0.9005343 \text{ kg/s}$$

The corresponding nozzle Reynolds number is:

$$Re_n = \frac{m_{avn1} d_n}{A_n \mu_{avn}} = \frac{(0.9005343)(0.3)}{(0.0706858)(1.8119179\times10^{-5})} = 210936$$

This value is within good agreement with the Reynolds number assumed above. The mass flow rate through all three nozzles is

$m_{avn} = 3m_{avn1} = (3)(0.9005343) = 2.701603$ kg/s

The corresponding dry air mass flow rate through the system is given by

$m_a = m_{avn} / (1 + w_n) = 2.701603 / (1 + 0.0127123) = 2.667697$ kg/s

K.4.3 WATER MASS FLOW RATE

The water mass flow rate is determined with the aid of an orifice plate according to the British Standard 1042 [81BR1, 84BR1]. The upstream pressure tapping is one pipe diameter upstream of the orifice plate while the downstream pressure tapping is half the distance. The method used to determine the water mass flow rate is almost the same as that used to determine the air mass flow rate.

The pressure drop over the orifice plate is given, at a pressure transducer voltage of 2.098510mV, by

$\Delta p_{op} = 4830.80\times(\text{mV}) - 4986.20 = 4830.80\times2.098510 - 4986.20 = 5171.282$ Pa

The density and viscosity of the water is determined at the water inlet temperature, $T_{wi} = 319.51$ K

Density of the water	$\rho_w = 989.6611$ kg/m^3	(A.4.1)
Viscosity of the water	$\mu_w = 5.773254\times10^{-4}$ kg/ms	(A.4.3)

The diameter ratio, σ, of the orifice plate is given by,

$\sigma = d_{op}/d_w = 0.62/0.13 = 0.4769231$

The approach velocity factor is given by

$Y = (1 - \sigma^4)^{-0.5} = (1 - 0.4769231^4)^{-0.5} = 1.026917$

Because the water is incompressible the expansion factor is equal to unity and thus falls away. The coefficient of discharge, C_d, is a function of the Reynolds number and is obtained by an iterative

procedure. Assume that the Reynolds number, Re_{dw}, referred to the inside pipe diameter, is equal to102022. The coefficient of discharge is given by

$$C_d = 0.5959 + 0.0312\beta^{2.1} - 0.1840\beta^8 + 0.0029\beta^{2.5}\left(\frac{1\times10^6}{Re_{dw}}\right)^{0.75} + 0.09L_1 0.0390 - 0.0337L_2\beta^3$$

$$= 0.5959 + 0.0312(0.4769231)^{2.1} - 0.1840(0.4769231)^8 + 0.0029(0.4769231)^{2.5}\left(\frac{1\times10^6}{102002}\right)^{0.75} +$$

$$0.09(1.0)0.0390 - 0.0337(0.47)(0.4769231)^3 = 0.6063129$$

where $L_1 = 1$ and $L_2 = 0.47$ are according to the orifice plate setup.

The mass flow rate of the water can be determined according to

$m_w = C_d Y \pi d_{op}^2 \left(2\rho_w \Delta p_{op}\right)^{0.5}$ =(0.6063129)(1.026917)(π)(0.62)^2[(2)(989.6611)(5171.282)]$^{0.5}$ = 6.014 kg/s

The corresponding velocity of the water in the pipe is given by

$v_w = 4m_w/(\rho_w \pi d_w)$ = (4)(6.014)/[(989.6611)(π)(0.13)] = 0.4578085 m/s

The corresponding nozzle Reynolds number is:

$$Re_{dw} = \frac{\rho_w v_w d_w}{\mu_w} = \frac{(989.6611)(0.4578085)(0.13)}{(5.773254\times10^{-4})} = 102021.8$$

This value is within good agreement with the Reynolds number assumed above.

K.4.4 PRESSURE DROP OVER FILL

The pressure drop over the fill and troughs is given, at a pressure transducer voltage of 1.048190mV, by

Δp_t = 627.9×(mV) – 626.92 = 627.9×1.048190 – 626.92 = 31.23854 Pa

To obtain the pressure drop over the fill, the effect of the troughs must be subtracted from the value determined above. $G_a = m_a/A_{fr}$ = 2.667697/2.25 = 1.185640 kg/m^{2}s.

$\Delta p_{tr} = 7.72930 G_a^{1.88670} = 7.72930(1.185640)^{1.88670} = 10.65779$ Pa

The pressure drop over the fill is

$\Delta p_{fi} = \Delta p_t - \Delta p_{tr}$ = 31.23854 – 10.65779 = 20.58075 Pa

K.4.5 ENERGY BALANCE

The pressure of the air, where the air drybulb and wetbulb temperatures are measured, is higher than atmospheric pressure. This pressure increase is due to the fan. A correlation was obtained by measuring the pressure difference between atmospheric pressure and the pressure below the troughs, were the air inlet temperatures are measured. The properties of the air are then determined at this pressure. The atmospheric pressure is, p_a = 100500 Pa.

The pressure increase, due to the fan, from atmospheric pressure is given by

$\Delta p_{upfr} = 9.7219 G_a^{1.9459} = 9.7219(1.185640)^{1.9459} = 13.5$ Pa

Thus, the pressure upstream of the troughs is given by

$p_{ai} = p_a + \Delta p_{upfr} = 100500 + 13.54116 = 100513.5$ Pa

The enthalpy of the inlet air, i_{mai}, is found according to equation (A.3.6b). At the specified air inlet drybulb temperature of $T_{ai} = 295.50$K and wetbulb temperature of $T_{wb} = 293.29$K find the following:

Pressure of water vapor from equation (A.2.1) evaluated at T_{wb}, where $T_{wb} = 293.29$K.

$z_i = 10.79586(1 - 273.16/293.29) + 5.02808 \log_{10}(273.16/293.29) + 1.50474$

$\times 10^{-4}[1 - 10^{-8.29692\{(293.29/273.16)-1\}}] + 4.2873 \times 10^{-4}[10^{4.76955(1-273.16/293.29)} - 1] + 2.786118312 = 3.37242$

$p_{vwb} = 10^{3.37242} = 2357.34$ Pa

It is assumed that the nozzle upstream pressure is equal to atmospheric pressure. The humidity ratio then follows from equation (A.3.5)

$$w_i = \left(\frac{2501.6 - 2.3263(293.92 - 273.15)}{2501.6 + 1.8577(295.50 - 273.15) - 4.184(293.92 - 273.15)}\right)\left(\frac{0.62509 \cdot 2357.34}{100513.5 - 1.005 \cdot 2357.34}\right)$$

$$-\left(\frac{1.00416(295.29 - 292.20)}{2501.6 + 1.8577(295.50 - 273.15) - 4.184(293.92 - 273.15)}\right) = 0.01439305 \text{ kg/kg}$$

The enthalpy of the inlet air, i_{mai}, is found according to equation (A.3.6b) with $c_{pai} = 1006.508$ J/kgK and $c_{pvi} = 1872.142$ J/kgK being evaluated at $(T_{ai} + 273.15)/2 = (295.50 + 273.15)/2 = 284.325$K according to equations (A.1.2) and (A.2.2) respectively. The latent heat is found to be $i_{fgwo} = 2.5016 \times 10^6$ J/kgK according to equation (A.4.5) at 273.15K. With these values find $i_{mai} = 59225.82$ J/kg dry air.

The pressure downstream of the fill is given by

$p_{ao} = p_{ai} - \Delta p_{fi} = 100513.5 - 20.58075 = 100493.0$ Pa

The outlet air is assumed to be saturated with water vapor. The enthalpy of the outlet air, i_{mao}, is found according to equation (A.3.6b). At the measured saturated outlet temperature of $T_{ao} = 311.46$K find the following:

Pressure of water vapor from equation (A.2.1) evaluated at $T_{ao} = 311.46$ K.

$z_o = 10.79586(1 - 273.16/311.46) + 5.02808 \log_{10}(273.16/311.46) + 1.50474$

$\times 10^{-4}[1 - 10^{-8.29692\{(311.46/273.16)-1\}}] + 4.2873 \times 10^{-4}[10^{4.76955(1-273.16/311.46)} - 1] + 2.786118312 = 3.82852$

$p_{vo} = 10^{3.82852} = 6737.78$ Pa

It is assumed that the nozzle upstream pressure is equal to atmospheric pressure. The humidity ratio then follows from equation (A.3.5)

$$w_o = \left(\frac{0.62509 \cdot 6737.78}{100493.0 - 1.005 \cdot 6737.78} \right) = 0.04969278 \text{ kg/kg dry air}$$

The enthalpy of the outlet air, i_{mao}, is found according to equation (A.3.6b) with c_{pao} = 1006.730 J/kgK and c_{pvo} = 1897.695 J/kgK being evaluated at $(T_{ao} + 273.15)/2 = (311.46 + 273.15)/2 = 292.305$K according to equations (A.1.2) and (A.2.2) respectively. The latent heat is found to be $i_{fgwo} = 2.5016 \times 10^6$ J/kgK according to equation (A.4.5) at 273.15K. With these values find i_{mao} = 168374.7 J/kg dry air.

The enthalpy gained by the air is given by

$$Q_a = m_a (i_{mao} - i_{mai}) = 2.667691(168374.7 - 59225.82) = 291175.5 \text{ W}$$

The heat lost by the water is given by

$$Q_w = m_w c_{pwi} (T_{wi} - 273.15) - (m_w - m_{w(evap)}) c_{pwo} (T_{wo} - 273.15)$$

It is assumed that the outlet air is saturated with water vapor. The amount of water lost due to evaporation is then given by

$$m_{w(evap)} = m_a (w_o - w_i) = 2.667691(0.04969278 - 0.01439305) = 0.094169 \text{ kg/s}$$

c_{pwi} and c_{pwo} are evaluated by equation (A.4.2) at temperatures of T_{wi} = 319.51 K and T_{wo} = 305.04 K respectively to obtain values of 4177.766 and 4177.094 J/kgK respectively.

Thus,

$$Q_w = m_w c_{pwi} (T_{wi} - 273.15) - (m_w - m_{w(evap)}) c_{pwo} (T_{wo} - 273.15)$$

$$=(6.013992)(4177.766)(319.51-273.15)-(6.013992-0.094169)(4177.094)(305.04-273.15) = 298850.5 \text{ W}$$

The energy balance is given by

$$100 \frac{Q_a - Q_w}{Q_a} = 100 \frac{291175.5 - 298850.5}{291175.5} = -2.64\%$$

A difference of 2.64% can be considered as a very good agreement due to the uncertainties associated with experimental measurements.

APPENDIX L

TEMPERATURE DISTRIBUTION DURING NOCTURNAL INVERSIONS

L.1 INTRODUCTION

To determine the effect of nocturnal inversions on the performance of cooling towers it is necessary to have information concerning the vertical temperature and humidity distributions or profiles. Equations are available in the literature that predict the vertical nocturnal temperature profiles from ground-based measurements. It will be shown that these equations are largely incorrect, relatively complex and unsuitable for analytical integration. Existing equations are generally inaccurate in predicting both the height and magnitude of inversions. In this study we rely on a relatively simple empirical relation that predicts inversion temperature profiles throughout the course of a year, with an acceptable degree of accuracy requiring a minimum amount of input data. The proposed empirical relation can be analytically integrated and employed in the analysis of the influence of inversions on cooling tower performance.

L.2 BACKGROUND

The structure of the stable thermal boundary layer is outlined in figure L.1. The temperature inversion itself is contiguous with the earth's surface and exhibits an increase in temperature with height. The inversion region is capped by and isothermal region, which sometimes is accompanied by a "wind jet". Above that the atmosphere exhibits an adiabatic lapse rate. The two most important parameters pertaining to the stability of the inversion are the magnitude of the temperature distribution across the inversion and height of the inversion, which are shown in figure L.1 [90SU1]. The magnitude of the temperature differential, ΔT, is defined as the difference between the maximum temperature and the ground level temperature measured 1 to 2 m above the ground. The height of the inversion top, z_{it}, is defined as the height at which the actual temperature gradient first becomes zero.

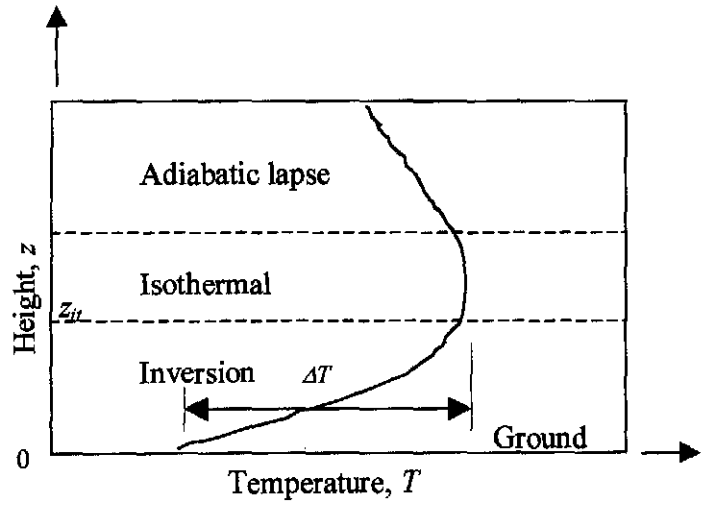

Figure L.1: Structure of the stable boundary layer.

Many theoretical studies have been made to predict the nocturnal atmospheric temperature profile from ground based measurements. The classical method is to assume a semi-infinite medium bounded on one side by the earth's surface, which is considered to radiate a constant heat flux. Under these conditions Anfossi et al. [76AN1] found that the temperature profile $T_{(z,t)}$ takes the form,

$$T_{(z,t)} = T_{(0,0)} - \left[T_{(0,0)} - T_{(0,t)}\right]\left\{\exp\left[\frac{-z^2}{4Kt}\right] - \frac{z}{2}\left[\frac{\pi}{Kt}\right]^{0.5} \operatorname{erfc}\left[\frac{z^2}{4Kt}\right]^{0.5}\right\} \tag{L.1}$$

where z is the height above ground level, t (s) is the elapsed time since the diurnal maximum temperature and K is the thermal eddy diffusivity (assumed to be constant). It will be shown that the thermal eddy diffusivity is not constant, especially in the surface boundary layer. The time origin is taken when the diurnal temperature wave reaches a maximum, i.e. $T_{(0,0)}$ is the maximum daily temperature at ground level.

In order to improve the accuracy of equation (L.1) Anfossi et al. [76AN1] modified the boundary conditions used in the above-mentioned classical solution. Instead of regarding the medium as semi-infinite, an upper boundary z_{it} was introduced. The atmosphere was then bounded by a fixed earth's surface and a time varying inversion "top". This modified solution is given by

$$T_{(z,t)} = T_{(0,0)} - \left[T_{(0,0)} - T_{(0,t)}\right]\left\{\exp\left[\frac{-z^2}{z_{it}}\right] - \left[\frac{z}{z_{it}}\right]\pi^{0.5} \operatorname{erfc}\left[\frac{z}{z_{it}}\right] + 0.278\left[\frac{z}{z_{it}}\right]\right\} \tag{L.2}$$

where z_{it} is defined by Anfossi et al. [76AN1] as

$$z_{it} = (4Kt)^{0.5} \tag{L.3}$$

This new solution showed a marked improvement over the distribution predicted by equation (L.1).

The temperature profile, as predicted by equation (L.2) requires input data of the diurnal surface temperature maximum, $T_{(0,0)}$, the surface temperature at the time of profile extrapolation, $T_{(0,t)}$, and z_{it} which can be computed from the time lapse since the diurnal temperature maximum and a "suitable value" of the thermal eddy diffusivity K from equation (L.3).

By introducing an extra measurement $T_{(z_m,t)}$, being the temperature measured at the height z_m, there would be four data points available to extrapolate the temperature profile from the ground based temperatures $T_{(0,0)}$, $T_{(0,t)}$, $T_{(z_m,0)}$ and $T_{(z_m,t)}$. This is double the amount of information used by Anfossi et al. [76AN1]. Of the four input temperature data available, only three are required. Of all the combinations of the above four temperatures, the difference $T_{(z_m,t)} - T_{(0,t)}$ and $T_{(0,0)} - T_{(0,t)}$ can be determined experimentally to the greatest degree of accuracy. With this information Surridge [86SU1] derives the following equation,

$$\frac{T_{(z_m,t)} - T_{(0,t)}}{T_{(0,0)} - T_{(0,t)}} = 1 - \left\{\exp\left[\frac{-z_m^2}{z_{it}}\right] - \left[\frac{z_m}{z_{it}}\right]\pi^{0.5} \operatorname{erfc}\left[\frac{z_m}{z_{it}}\right] + 0.278\left[\frac{z_m}{z_{it}}\right]\right\} \tag{L.4}$$

This relation describes the ratio of the vertical to temporal temperature difference as a function of the normalized height z_m/z_{it}. The value of z_m/z_{it} can be determined by solving equation (L.4) by successive

approximations. Once the value of z_m/z_{it} is determined, the inversion height z_{it} can be calculated by substituting the value of z_m. Thus the value of z_{it} has been obtained without assuming a value of K or any temporal variation. The value of z_{it} may hence be substituted into equation (L.2), from which the temperature profile may be calculated up to a maximum of z_{it}.

Equation (L.2) does not generally correlate the data well but does give a reasonable indication of the inversion height. The method proposed by Surridge [86SU1] does follow the particular data closely over a part of the inversion but under-predicts the inversion height.

L.3 SIMPLIFIED INVERSION PROFILE

It is obvious that both of the above-mentioned approaches have their limitations. Furthermore, the equations require considerable temperature data, are relatively complex and do not readily allow for further analysis of the influence of inversions on cooling tower performance. In view of these complications, an approximate Kelvin temperature distribution of the form

$$T = (T_r + 273.15)\left(\frac{z}{z_r}\right)^b \tag{L.5}$$

is assumed to be applicable in the stable boundary layer, where T_r and z_r are the reference temperature and reference height respectively. T_r (°C) is measured at z_r which is about 1 m above ground level. The value of the exponent , b, varies throughout the course of the year. An empirical relation for b as a function of the day of the year is developed in section L.4 to section L.6.

L.4 METHOD TO DETERMINE THE EXPONENT OF THE SIMPLIFIED INVERSION PROFILE

An optimization technique is employed to determine optimum values of the exponent, b, of equation (L.5) from experimental data. An objective function, i.e. the function to be minimized, is selected to aid in the determination of b so that equation (L.5) closely represents measured inversion profiles. The objective function is selected to be the modulus of the difference between the area under the proposed curve given by equation (L.5) and the experimentally determined area. The areas referred to are the areas under the temperature versus height curves. Thus, the objective is to minimize the difference in the area between these two curves. The unit of area is mK. As T_r and z_r are known, the only solution variable is the exponent, b. The area under the curve given by equation (L.5) is obtained through integration.

$$A = \int_{z_1}^{z_n} (T_r + 273.15)\left(\frac{z}{z_r}\right)^b dz = \frac{(T_r + 273.15)}{z_r^b}\int_{z_1}^{z_t} (z)^b dz = \frac{(T_r + 273.15)}{z_r^b (b+1)}\left(z_t^{b+1} - z_1^{b+1}\right) \tag{L.6}$$

where z_1 is the height of the measured air temperature closest to the ground (usually 1 to 2 m above ground level) and z_t is the height of the temperature sensor on top of the weather mast.

Since the area under the temperature versus height curve, expressed by equation (L.6), includes the area from the datum of the temperature axis (0 K) to the temperature T_1 at height z_1, it must be subtracted from the area given by equation (L.6). Therefore, the new area is given by

$$A = \frac{(T_r + 273.15)}{z_r^b (b+1)} \left(z_t^{b+1} - z_1^{b+1} \right) - (T_1 + 273.15)(z_t - z_1) \tag{L.7}$$

The areas under the experimentally determined temperature distributions at each time interval are approximated, as shown in figure L.2, through the usage of rectangles and triangles. The approximated area under the experimentally determined temperature-height curve is denoted by A_{ex}. It can be seen that an error is made due to the choice of the triangles, but as the curvature between two adjacent points is not significant, the error is not significant.

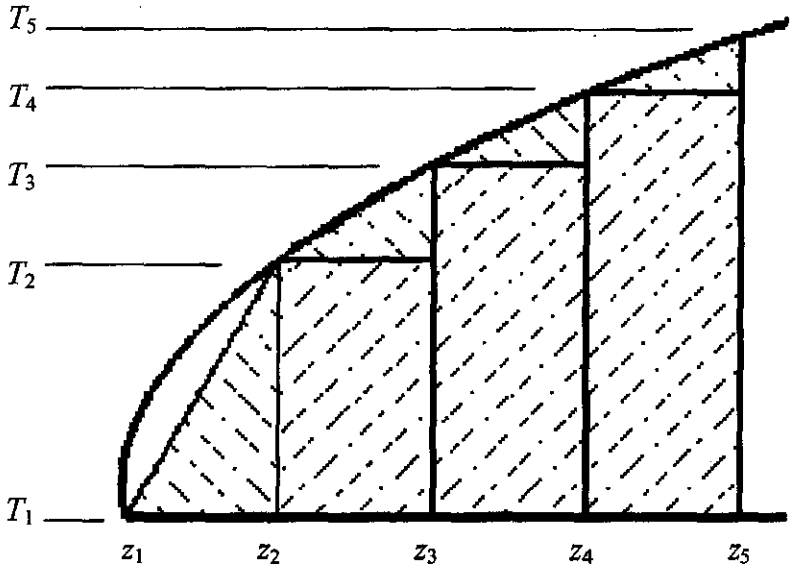

Figure L.2: Area under experimentally determined curve

The objective function, F, is the modulus of the difference between the area determined by equation (L.7) and the area obtained by the method illustrated in figure L.2, i.e.,

$$F = |A - A_{ex}| = \left| \frac{(T_r + 273.15)}{z_r^b (b+1)} \left(z_t^{b+1} - z_1^{b+1} \right) - T_1 (z_t - z_1) - A_{ex} \right| \tag{L.8}$$

where A_{ex} is the is area determined by the graphical method illustrated in figure L.2.

L.5 REFERENCE HEIGHT AND TEMPERATURE

The influence of the reference height, z_r, on the value of the exponent, b, and the accuracy of equation (L.5) are determined in this section. The calculations are performed for reference heights of 1 m, 2 m and 5 m respectively. Reference heights of 1 to 2 m are preferred as the temperature at this height is usually measured by meteorologists.

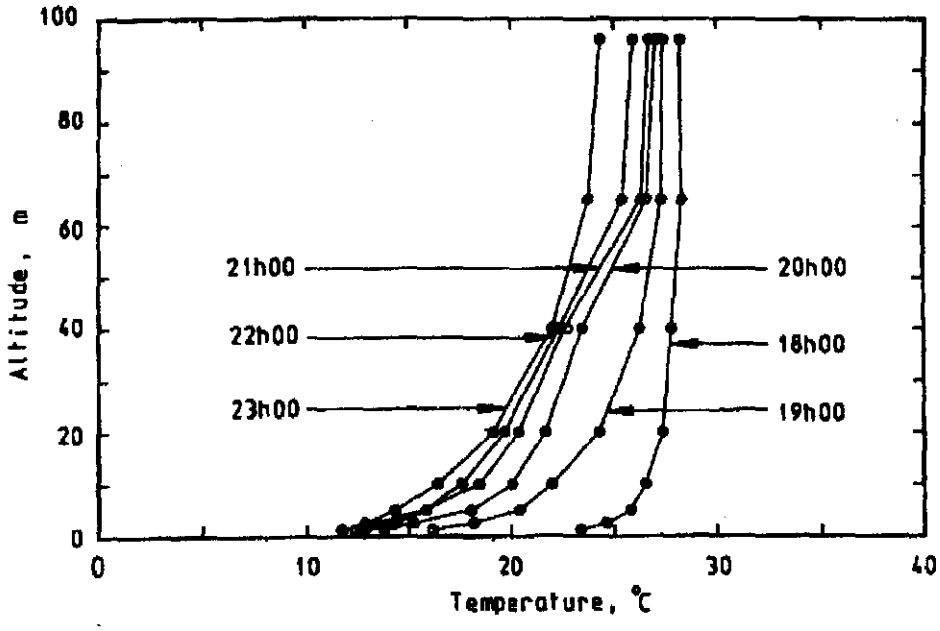

Figure L.3: Temperature inversion profiles during first six hours after inception of an inversion [98KR1].

Kröger [98KR1] presents hourly temperature data measured at eight different heights on a 96 m high weather mast. Figure L.3 shows the temperature inversion profiles, presented by Kröger [98KR1] during the first six hours after the inception of the inversion. The exponent, b, for each hourly interval during the period when nocturnal inversions occur, is determined by the method discussed in the previous section.

Table L.1 gives the optimum values of the exponent b of equation (L.5) at hourly intervals for the different reference heights for the data given in Kröger [98KR1], determined by the method discussed in the previous section. The last row of table L.1 gives the average values of the exponent b during the inversion period for the three different reference heights. It can be seen that the optimal value of the exponent is approximately 0.01 for reference heights of 1 m and 2 m. For a reference height of 5 m, however, the optimum value of the exponent b is approximately 0.013.

Table L.1: The optimum value of the exponent b for reference heights of 1 m, 2 m and 5 m respectively.

Time	b		
	$z_r = 1$m	$z_r = 2$m	$z_r = 5$m
19h00	0.008898	0.008722	0.008734
20h00	0.009632	0.01018	0.010082
21h00	0.01205	0.011314	0.012426
22h00	0.009235	0.009528	0.011352
23h00	0.0093	0.010126	0.012104
00h00	0.011304	0.013027	0.016928
01h00	0.009983	0.011525	0.015631
02h00	0.009359	0.010535	0.012583
03h00	0.008853	0.010051	0.013042
04h00	0.010067	0.011842	0.01589
05h00	0.009796	0.011362	0.014982
06h00	0.009949	0.011317	0.014312
07h00	0.009684	0.010472	0.01239
Average	0.009855	0.010769	0.013112

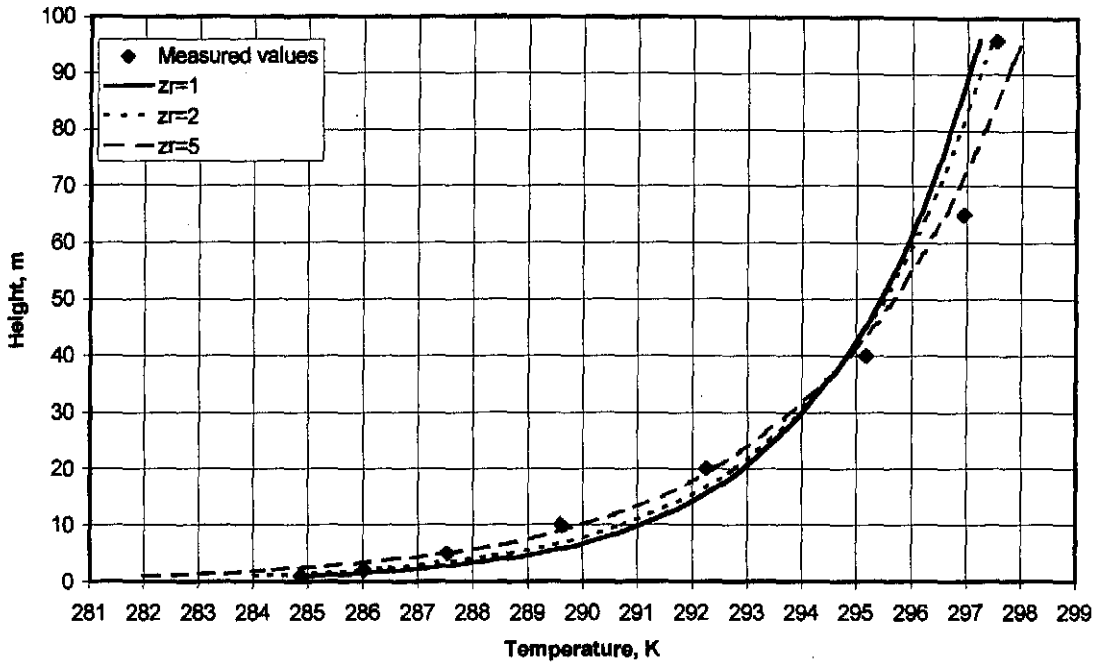

Figure L.4: Height versus temperature profiles of equation (L.5) for three reference heights with the optimum value of the exponent b determined for each reference height.

Figure L.4 illustrates a sample case of the temperature versus height profiles at 23h00 for cases where the different reference heights are employed together with the optimum exponents given in table L.1. The measured data is also shown. It can be seen that nearly all the curves approximated by equation (L.5), at different reference heights, with optimum b values, represent the measured data relatively accurately. If the curve, generated with a reference height of 5 m is extrapolated, it may not represent the real inversion profile as accurately as for reference heights of 1 and 2 m. It is strongly recommended that the same reference height be employed when the value of b is determined as in the subsequent employment of equation (L.5), with b known, to obtain the temperature profile.

L.6 SEASONAL VARIATION OF INVERSIONS

In this section, the seasonal variation of the exponent, b, of equation (L.5) is investigated. The same procedure is followed to obtain the optimum values of the exponent, b, as discussed in section L.4. The reference height, z_r, in equation (L.5) is chosen as 2 m in this investigation.

Data was collected on a 96 m weather mast from 16 March 1994 to 30 January 1995 in a relatively arid area near Lephalale (Ellisras) (23°40'S, 27°47'E). Wind direction, wind speed and drybulb temperatures were measured at heights of 1, 2, 5, 10, 20, 40, 65 and 96 m approximately every six minutes. There were many times during the above-mentioned period where no data was collected. When data was collected, it was done intermittently with the result that continuous data sets, extending over periods where inversions and low wind conditions (less than 2 m/s at all measured heights) were present, are relatively scarce. Table L.2 gives the hourly temperatures at different elevations during the occurrence of nocturnal

inversions throughout the course of a year. Low wind conditions were present during these selected periods of investigation.

Table L.2 (a): Hourly temperatures, wind speed and wind direction at different heights.

	Alt.	21/22 March 1994						
	m	19h00	20h00	21h00	22h00	23h00	00h00	01h00
T, °C	1	21.2	19.9	19.2	19.9	18.5	16.5	17.3
	2	22.5	21	19.8	20.4	19.3	17.3	18
	5	24	22.2	21.1	20.9	19.8	18.4	19.5
	10	25.3	24.7	21.8	21.4	20.9	19.1	20.1
	20	26.2	25.9	25.5	22.6	22.2	20.3	20.7
	40	25.8	25.9	25	23	23.5	20.9	21.6
	65	25.7	25.8	25.2	24	25	21.7	21.9
	96	26.1	26.1	25.7	24.9	25.1	22.7	21.8
v, m/s	10	0.8	0.6	0.6	1.1	0.5	0.9	0.9
	20	0.9	0.4	0.6	1.8	0.4	0.6	1.3
	40	1	0.3	0	1.6	0.7	0	1.9
	65	0.6	0.4	0.1	1.8	2.8	0.9	2.2
	96	0.4	0.4	0	2.2	2.7	2	1.4
Dir, °	10	235	246	181	41	234	215	98
	20	189	175	222	29	241	208	101
	40	184	179	139	44	72	150	99
	65	181	178	166	53	73	83	93
	96	181	159	139	62	57	8	70

Table L.2 (b): Hourly temperatures, wind speed and wind direction at different heights.

	Alt.	23/24 April 1994											
	m	19h00	20h00	21h00	22h00	23h00	00h00	01h00	02h00	03h00	04h00	05h00	06h00	07h00
T, °C	1	18.4	16.4	16	15.6	14.6	12.5	11.1	10.9	10.4	10.1	11.4	11.1	12.6
	2	19.2	17.2	16.6	16.1	15.2	13.6	11.6	11.5	10.8	10.6	11.9	11.3	13
	5	20.2	18.4	17.7	16.9	15.8	14.8	12.7	12.6	11.5	11.8	12.5	12.3	14.2
	10	20.9	19.3	18.3	17.6	16.9	16.7	14.4	13.3	13.2	13.3	13.1	13.1	15
	20	21.9	21.1	19.4	19.3	18.7	18.7	16.1	15.4	17.2	15.9	14	13.9	15.2
	40	24.5	22.2	20.9	21.8	20.1	19.5	17.4	17.8	18	16.8	16.2	15.7	15.9
	65	24.7	23.4	22.3	22.4	21.5	19.8	17.8	18.1	18.5	17.3	18	17.1	16.4
	96	24.8	23.9	23.2	23	23	20.7	19.3	19	20	18.1	18.6	17.1	16.5
v, m/s	10	0.4	0.3	0.3	1.3	0.6	0.7	0.1	0.7	1.1	0.9	1.8	1.9	1.8
	20	0.1	0.3	0.2	1.5	0.7	0.8	0.1	0.8	1.2	0.9	1.6	1.7	1.6
	40	4	4.3	4.2	5	4.3	4.2	3.7	4.3	4.7	4.2	4.6	4.5	4.3
	65	1	1	1	2.2	1.3	0.8	0.1	1.1	1.4	0.9	2	1.9	1.8
	96	1.2	1.1	1.5	2.5	1.4	0.7	0.1	1.1	1.3	0.9	1.5	1.5	1.4
Dir, °	10	18	66	36	129	134	145	120	134	143	149	159	162	164
	20	61	111	116	138	141	141	163	139	142	149	152	156	159
	40	182	181	183	174	179	178	183	177	175	179	176	177	179
	65	209	191	197	161	163	129	172	156	141	127	121	105	103
	96	187	178	181	158	161	128	111	151	138	129	117	102	101

Table L.2 (c): Hourly temperatures, wind speed and wind direction at different heights.

	Alt.	8/9 June 1994												
	m	19h00	20h00	21h00	22h00	23h00	00h00	01h00	02h00	03h00	04h00	05h00	06h00	07h00
T, °C	1	10.4	10.3	11	9.2	7.9	6.6	5.4	4.6	4.3	3.9	4	4.2	2.7
	2	11.4	11	11.3	10	8.6	7.5	6.4	5.6	4.9	4.4	4.7	4.7	3
	5	14.2	12.06	12.1	11.4	9.8	9.9	8.1	7.4	5.7	5.3	5.7	5.2	3.5
	10	16.4	15.6	13.6	12.5	10.6	10.4	9.3	9.4	7.1	6	6.8	8	4.8
	20	17.2	17.4	14.5	13.7	12.2	12	11.8	11.8	11.1	8	9.1	10.2	9.4
	40	16.9	17.8	15.5	14.9	14.7	13.6	12.5	12.8	12.6	11.8	10	11.9	11.5
	65	17.1	17.8	16.8	16	15.7	15.7	14.6	13.9	14	13.5	11.9	12.7	12.3
	96	17.7	17.8	17.2	16.9	16.4	16.7	15.9	14.7	14.4	14	13.3	12.9	12.7
v, m/s	10	1.4	0.7	0.7	1.1	0.6	0.7	0.7	1.1	1	0.6	0.3	0.7	0.9
	20	1.6	2.3	0.7	0.3	1.4	0.5	1.5	1.5	2.2	0.7	0.1	0.3	1.3
	40	1.7	1.9	0.6	1.1	2	2.1	2.3	1.8	1.9	2.6	0.2	0.9	0.1
	65	2.6	2.2	1.8	1.6	1.6	2.6	3.1	0.8	1.4	2.2	0.9	1.4	1
	96	2.2	2.2	2.7	1.6	2.2	2.8	2.7	1	1.2	2.6	1.5	1.3	1.9
Dir, °	10	152	113	279	223	267	175	194	211	195	145	158	301	226
	20	151	109	269	202	249	228	230	212	205	187	303	320	189
	40	139	113	183	184	196	218	204	180	181	186	323	58	157
	65	114	104	110	157	179	209	183	109	138	158	37	87	88
	96	109	101	107	134	156	186	179	109	129	159	65	95	83

Table L.2 (d): Hourly temperatures, wind speed and wind direction at different heights.

	Alt.	23/24 July 1994											
	m	19h00	20h00	21h00	22h00	23h00	00h00	01h00	02h00	03h00	04h00	05h00	06h00
T, °C	1	11.6	8.9	8.6	7.7	7.1	6.7	5.3	4.6	3.7	2.9	2.8	2.6
	2	12.5	9.9	10.1	8.5	7.8	7.6	6.2	5.4	4.6	3.6	3.3	3.3
	5	13.9	12.9	12.6	11	9.9	8.9	8.2	6.6	5.8	5.2	4.2	4.4
	10	17.2	15.1	13.9	13.7	12.7	11	11.6	8.2	9	7.8	6.2	6.2
	20	20.3	16.5	17.3	15.9	16.6	14.3	13.4	11.9	13	10.8	10.4	8.4
	40	20.9	18.9	19.6	17.9	17.7	15.4	15.3	13.4	13.8	12	12.2	10.5
	65	21.5	20.4	19.8	18.2	17.7	16.9	16.1	13.9	14.9	14.2	12.6	12.6
	96	21.9	20.8	20.2	18.8	17.6	17.3	16.6	15	15.2	15	15.8	14.3
v, m/s	10	1.3	0.9	0.1	0.2	0.2	1.5	0.1	1.5	0.9	0.6	1.4	0.4
	20	1.9	1.3	1.4	1.9	2.4	1.2	0.8	2.4	0.9	0.2	2.6	0.3
	40	2.3	1.7	3.2	2.5	2.9	0.8	2.4	2.2	1.1	0.9	2	0.8
	65	2	2.5	3.3	2.4	3.3	2.9	2.6	1.2	3	2.4	0.6	1.9
	96	2	2.9	2.7	1.9	2.9	2.8	2.5	0.9	2	1.7	1.3	2.1
Dir, °	10	0	114	179	101	91	238	221	2.04	226	239	208	288
	20	356	95	89	98	83	219	105	220	176	120	197	331
	40	359	59	101	99	73	122	98	209	99	97	183	46
	65	349	32	92	86	71	95	74	194	82	64	180	70
	96	341	16	65	52	64	77	58	113	66	27	184	58

Table L.2 (e): Hourly temperatures, wind speed and wind direction at different heights.

	Alt. m	5/6 September 1994						
		19h00	20h00	21h00	22h00	23h00	00h00	01h00
T, °C	1	16.4	15	13.3	11.8	10.2	9.6	9
	2	17.8	17.1	14.6	12.8	11	10.4	9.8
	5	20	20	16.7	14.1	12.3	11.9	11.3
	10	21.7	22.7	19.8	15.8	15.7	15.2	14.2
	20	24.3	23.1	23.1	19.5	19.5	17.4	16.7
	40	25.4	22.7	23.2	21	20.5	18.8	18.3
	65	25.4	23.5	23.4	21.3	21.8	21.5	20.6
	96	25	24.8	24.3	22.7	22.2	21.8	21.2
v, m/s	10	0.8	0.9	1	0.6	0.4	0.4	0.1
	20	2.4	0.9	0.7	1.3	0.7	0.6	1
	40	2.8	0.9	0.5	1.1	2.2	2.4	3.1
	65	2.4	1.4	0.7	0.8	2.7	3.4	3.4
	96	2.5	2.1	1.4	1.1	2.7	2.3	2.8
Dir, °	10	1	251	191	235	6	186	235
	20	348	246	266	176	54	92	78
	40	357	273	286	168	70	94	86
	65	358	305	315	133	66	70	60
	96	358	336	350	66	67	51	44

Table L.2 (f): Hourly temperatures, wind speed and wind direction at different heights.

	Alt. m	19/20 October 1994				
		02h00	03h00	04h00	05h00	06h00
T, °C	1	15.6	15.2	14.9	14.3	13.4
	2	16.5	16	15.7	15.1	14.1
	5	17.6	17.5	17.1	17.2	16
	10	18.9	18.9	18.9	19	17.5
	20	20.7	21.1	20.3	20.5	19.4
	40	22.3	22.1	21.7	21.6	21.3
	65	22.5	22.2	22	22.2	22
	96	22.4	22.3	22.1	22.1	22
v, m/s	10	1.4	1.8	0.5	1.4	1.3
	20	1.5	0.9	0.1	1.5	2
	40	4.2	1.5	1.7	2.9	4.8
	65	3.5	1.7	1.4	1.9	3.8
	96	2.7	2.4	1.6	1.5	2.5
Dir, °	10	98	91	98	95	83
	20	107	91	221	95	85
	40	95	96	96	95	95
	65	89	39	69	70	78
	96	69	7	13	47	59

Table L.2 (g): Hourly temperatures, wind speed and wind direction at different heights.

	Alt.	2/3 December 1994					
	m	00h00	01h00	02h00	03h00	04h00	05h00
T, °C	1	21.8	20.4	18.5	18	18.1	18.2
	2	22.4	21.1	19.2	18.7	19	18.9
	5	22.5	21.7	20	20	19.8	19.8
	10	23.2	23.4	20.4	20.9	20.5	20.4
	20	24.3	24.1	22.6	23.2	21.9	20.8
	40	24.9	24.7	24.2	24.1	24.2	21.7
	65	25.4	25.2	24.5	24.3	24.6	22.3
	96	25.7	25.7	24.6	24.3	25.2	22.8
v, m/s	10	0.4	0.4	0.7	0.8	0.9	1.4
	20	0.9	0.3	1.7	1.6	1.2	2.1
	40	0.7	0.2	0.7	0.7	2.3	4.6
	65	1.9	1.1	0.9	1.5	2.9	3.9
	96	2.8	2	0.8	1.1	2.7	2.5
Dir, °	10	96	48	276	274	166	95
	20	179	265	339	341	253	99
	40	276	274	282	286	278	100
	65	218	226	304	337	256	87
	96	212	227	270	303	236	81

Table L.2 (h): Hourly temperatures, wind speed and wind direction at different heights.

	Alt.	20/21 December 1994										
	m	19h00	20h00	21h00	22h00	23h00	00h00	01h00	02h00	03h00	04h00	05h00
T, °C	1	30.8	28.2	26.4	24.7	23.7	24.2	22.8	21.1	19.6	19.9	20.2
	2	31.3	28.9	27.2	25.4	24.5	24.8	23.4	21.7	20.1	20.6	20.9
	5	31.7	29.6	28.5	26.6	25.6	25.1	24.1	22.6	20.8	22	22.4
	10	32.3	30.7	29.1	27.8	26.5	25.5	24.9	24	22.9	23.1	23.4
	20	32.9	31.8	29.7	28.3	27.8	26.2	25.9	24.6	24.8	24.6	24.4
	40	32.8	32.2	30.7	28.9	28.3	26.7	26.4	25.8	25.7	25.7	25.4
	65	32.7	32.2	31.7	30.3	30	28	27	26.6	26.2	26.4	26
	96	32.5	32	31.8	31.4	31.4	28.5	27.4	26.9	26.6	26.5	26
v, m/s	10	1.1	0.4	0.6	0.6	1.1	1.9	1.9	1.1	0.3	1.8	1.9
	20	0.9	0.3	0.4	0.5	0.9	1.5	1.5	0.9	0.3	1.4	1.5
	40	1	0.3	0.5	0.6	1.1	1.8	1.8	1	0.3	1.7	1.8
	65	1.1	0.7	0.8	0.8	1	2.2	2	1.2	0.7	2	1.9
	96	0.9	0.4	0.7	0.7	0.8	1.8	1.7	1	0.5	1.7	1.6
Dir, °	10	137	136	136	136	136	137	137	137	136	137	137
	20	145	144	145	145	145	145	145	145	146	145	145
	40	139	139	140	139	139	139	139	139	140	139	139
	65	108	61	65	68	100	113	117	108	81	115	114
	96	115	52	48	42	88	115	118	110	71	117	116

Table L.3 shows the optimum values of the exponent b for each hourly interval shown in table L.2 with average values of the exponent for each inversion period.

Table L.3: Values of the exponent, b, at hourly intervals.

Time	1	2	3	4	5	6	7	8
	Mrt 21/22	Apr 23/24	June 8/9	July 23/24	Sept 5/6	Oct 19/20	Dec 2/3	Dec 20/21
19h00	(0.0037)	0.0051	(0.0065)	0.0093	(0.0077)			(0.0015)
20h00	(0.0052)	0.0058	(0.0073)	0.0102	(0.0070)			(0.0033)
21h00	(0.0057)	0.0052	0.0051	0.0099	(0.0094)			0.0040
22h00	0.0033	0.0059	0.0059	0.0101	0.0088			0.0045
23h00	0.0049	0.0059	0.0067	(0.0116)	0.0107			0.0050
00h00	0.0043	0.0065	0.0077	0.0091	0.0103		(0.0027)	0.0026
01h00	0.0038	0.0065	0.0079	0.0102	0.0102		0.0040	0.0034
02h00		0.0065	0.0085	0.0088		0.0056	0.0050	0.0045
03h00		0.0080	0.0088	0.0105		0.0063	0.0056	0.0060
04h00		0.0069	0.0082	0.0104		0.0063	0.0052	0.0055
05h00		0.0052	0.0069	0.0101		0.0071	0.0032	0.0049
06h00		0.0051	0.0080	0.0089		0.0077		
07h00		0.0034	0.0092					
Ave.		0.0058	0.0075	0.0098	0.0100	0.0069	0.0050	0.0044
n_d	81	113	159	204	248	293	337	354
$T_{(0,0)}$	33.1	30		27.7	30.9	35.1	38.8	37.8
Time	14h44	14h46		15h20	15h50	15h04	15h59	16h20

The values in table L.3 that are printed in brackets are omitted in the calculation of average values of b. This is because the vertical inversion profiles were not monotonic functions, or significant winds were present at one or more of the heights where measurements were made. Generally values of b were also ignored for a few hours immediately after sunset.

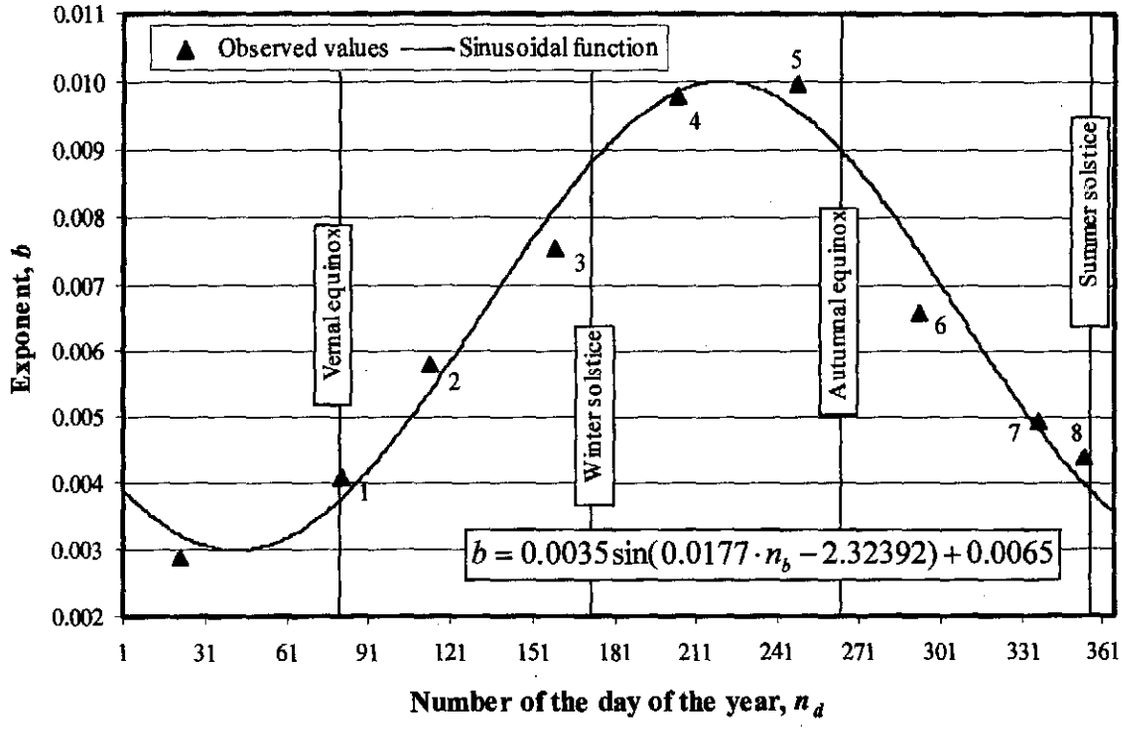

Figure L.5: Summary of annual variation of the exponent b.

Figure L.5 shows the average values of b for a particular inversion period, given in table L.3 as it varies throughout the course of a calendar year.

The tilt in the earth's axis of rotation is the cause of the seasons. The earth's axis of rotation is tilted 23.5° with respect to the plane of its orbit around the sun. Hoffmann [97HO1] presents a summary of important dates during earth's orbit around the sun. When it is winter in the southern hemisphere, the south end of the axis of rotation is tilted away from the sun, while in summer, it is tilted towards the sun. The day when the axis is tilted exactly towards the sun is called the summer solstice, i.e. 23 December in the southern hemisphere. On 21 June, the axis of rotation is tilted directly away from the sun and is called the winter solstice. On 22 March and 22 September, the tilt is in a plane tangential to the earth's orbit around the sun. These days are called the autumn and spring equinoxes, respectively. These dates are shown in figure L.5 and indicate the relation of these dates to the sinusoidal function variation of the exponent, b. Due to the eccentricity of the sun with respect to the earth's orbit, the earth is closer to the sun when it is summer in the southern hemisphere, and there is a tendency for seasonal differences in temperature to be greater in the southern hemisphere than in the northern hemisphere.

The average values of b presented in table L.3 can be correlated by

$$b = 0.0035\sin(0.0177 \cdot n_b - 2.32392) + 0.0065 \qquad \text{(L.9)}$$

where n_b is the number of the day of the year (1 January is the first day of the year). It can be seen from figure L.5 that equation (L.9) correlates the observed values of b relatively well.

Figure M.5 shows the annual variation of relative humidity measured at 08h00 and 14h00 at Pretoria, Germiston and Pietersburg. Figure M.6 shows the average monthly minimum and maximum temperatures at these locations. It can be seen that the annual relative humidity and temperature distributions can also be correlated by sinusoidal functions. It would therefore appear that the exponent, b, at a particular location, is a function of humidity. The exponent b may also be dependent on other variables such as wind speed, heat flux, evapotranspiration and the albedo of vegetation or surface cover.

At other locations the exponent, b, determined by equation (L.9), is not known and can be approximated by equation (L.5). This is done by taking temperature measurements at two different heights and solving for b in equation (L.5). The value of b for the 23/24 July inversion period in table L.3, determined by the method described in section L.4, is 0.0098. If the highest elevation temperature measurements are made at 2, 5 and 10 m, the average value of b is 0.0057, 0.0067 and 0.0091 respectively. It can therefore be concluded that the one temperature measurement be made at as high elevation as possible (typically 10 m) and the second measurement at 1 or 2 m above ground elevation.

L.7 COMPARISON OF SIMPLE INVERSION PROFILE TO OTHER MODELS

Equation (L.1), (L.2), (L.4) and (L.5) are plotted to compare the accuracy of these equations to the measured data presented in table L.2. K is taken constant at 0.3 m^2/s for equations (L.1) and (L.3). Surridge [86SU1] states that T_m must be measured at the top of a low mast, therefore z_m is taken as 10 m

in equation (L.4). Lower heights of z_m generally lead to less accurate results in this investigation. In equation (L.5) z_r is taken as 2 m and b is determined by equation (L.9).

Figures L.6 to L.8 show sample cases of inversion profiles extrapolated from ground based measurements for one inversion period at 22h00, 02h00 and 04h00 during the night of 20 and 21 December.

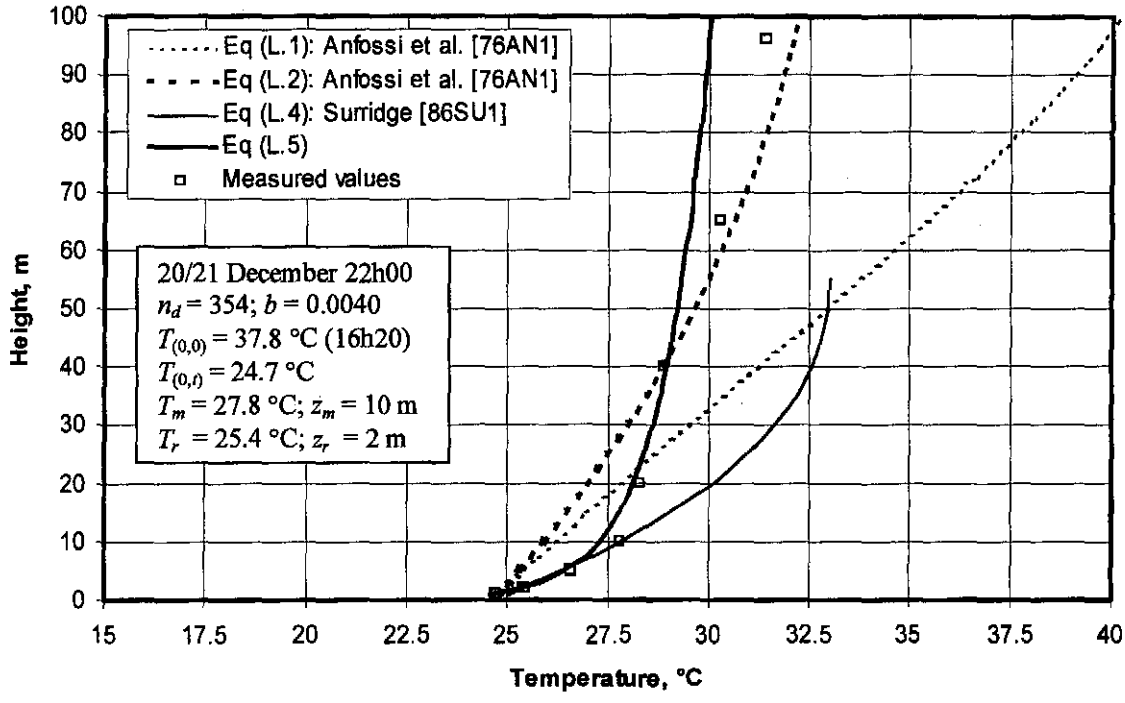

Figure L.6: Comparison between temperature inversion profiles.

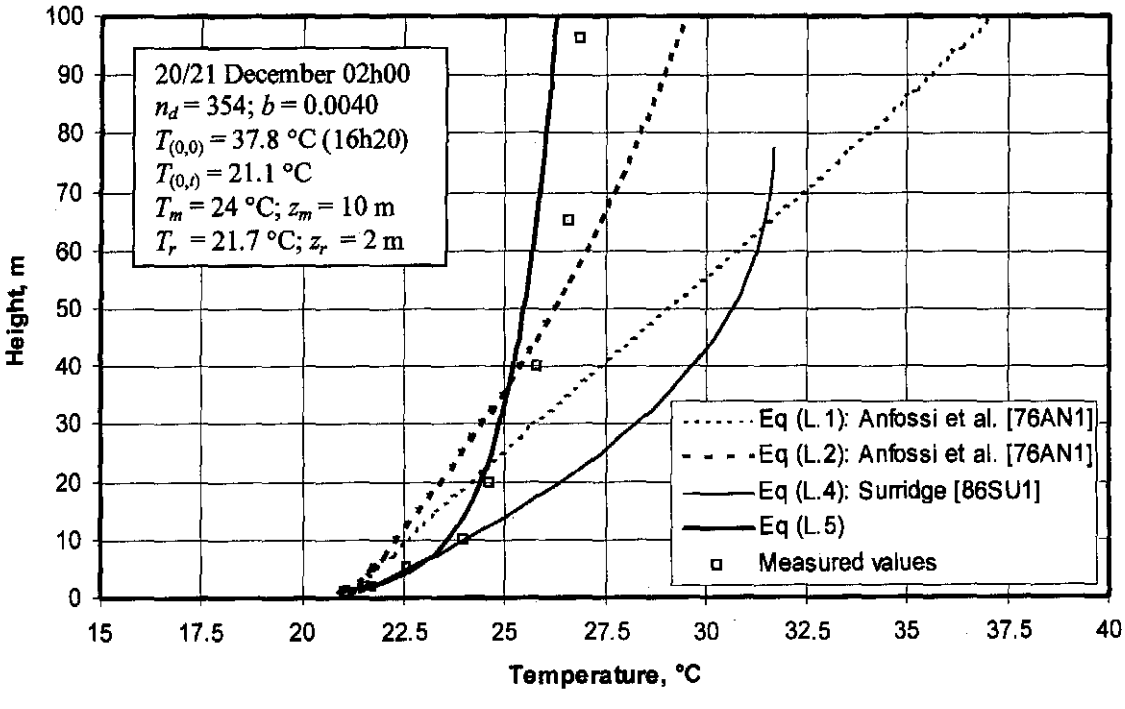

Figure L.7: Comparison between temperature inversion profiles.

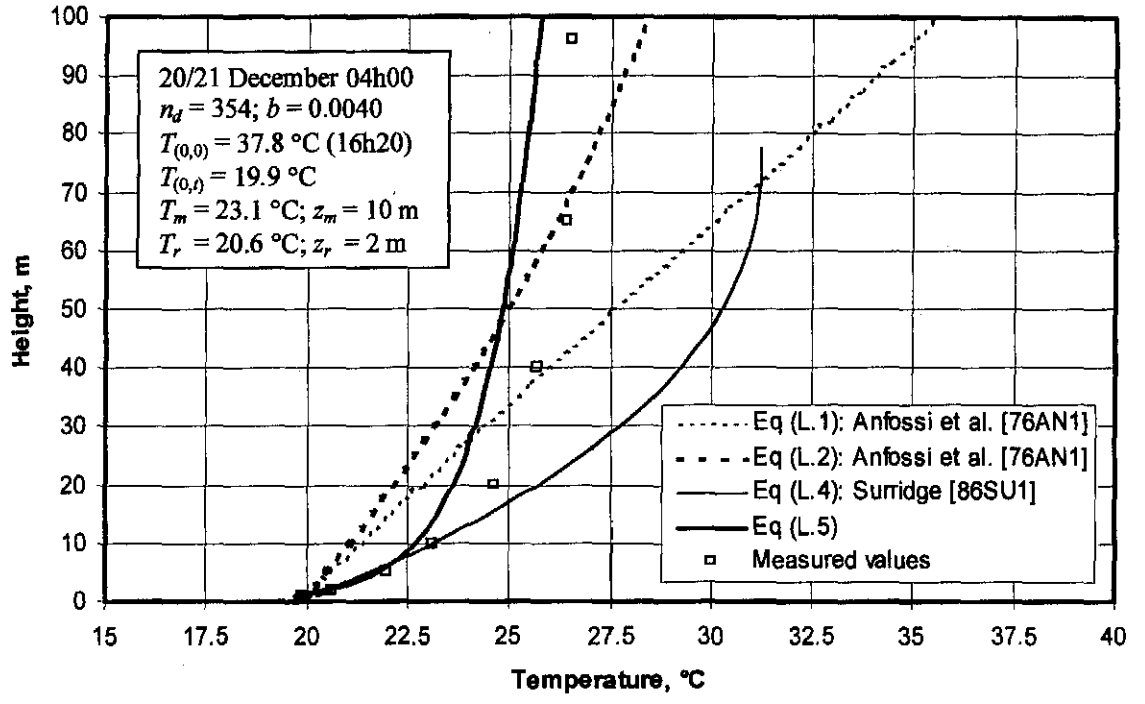

Figure L.8: Comparison between temperature inversion profiles.

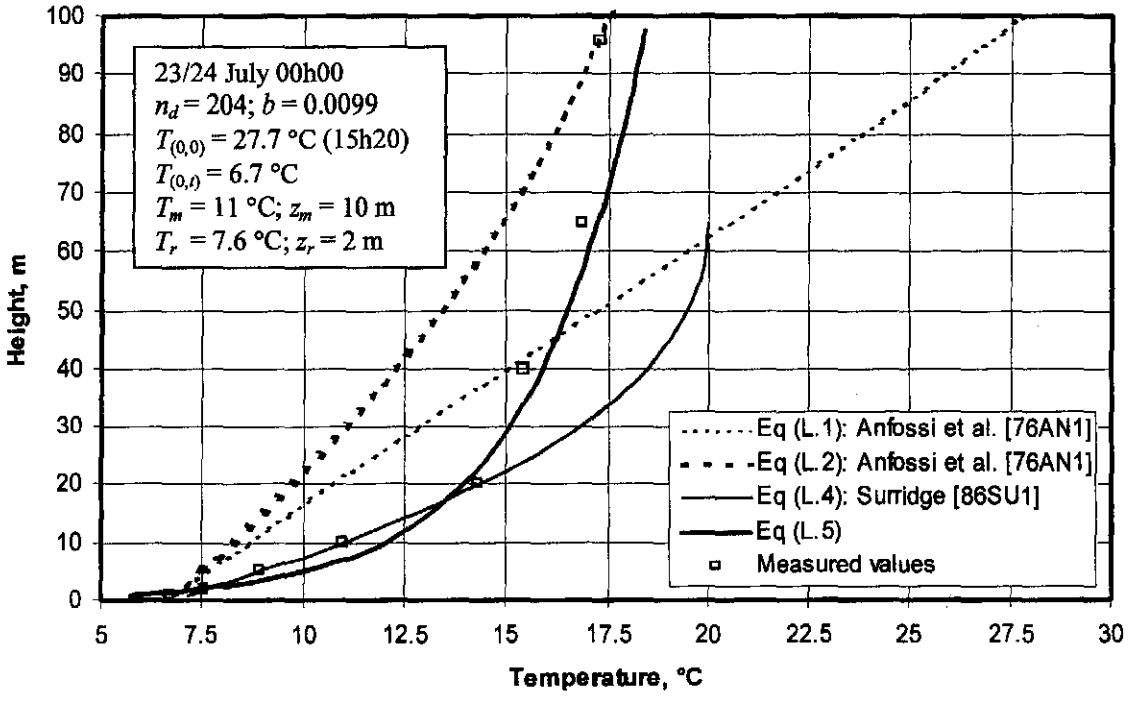

Figure L.9: Comparison between temperature inversion profiles.

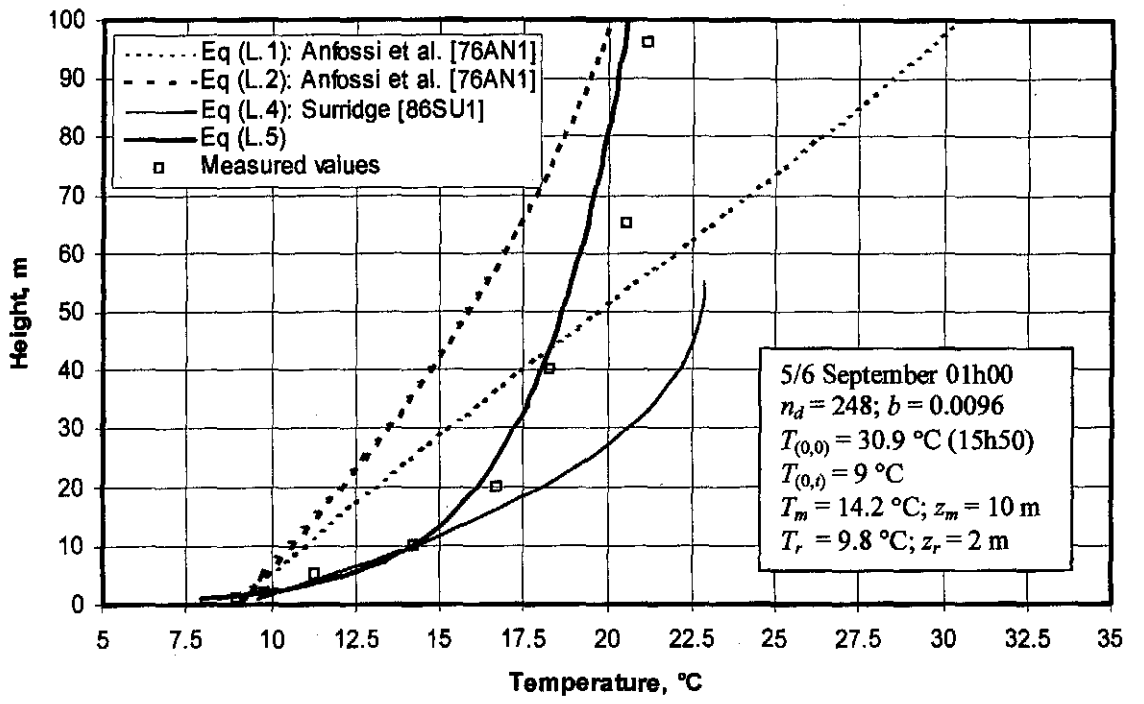

Figure L.10: Comparison between temperature inversion profiles.

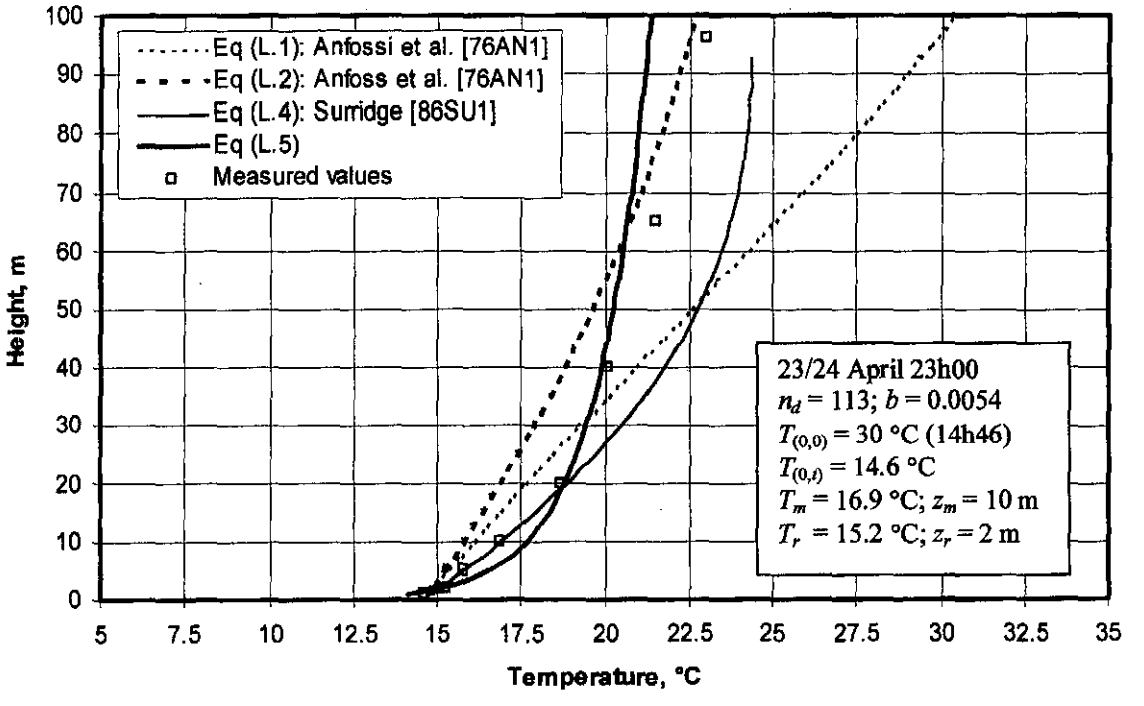

Figure L.11: Comparison between temperature inversion profiles.

Figures L.9 to L.11 show sample cases of inversion profiles at other periods. It can be seen that equation (L.5), proposed in this investigation, correlates the measured data very well during a particular inversion period and throughout the year.

L.8 AVERAGE TEMPERATURE AND PRESSURE DISTRIBUTION

For the proposed further analysis of the influence of inversions on cooling tower performance, it is necessary to validate the accuracy of equation (L.5) and equation (L.9). This is done by comparing the average temperature in the stable boundary layer obtained by measurement to that determined by the integration of equation (L.5), The approximate pressure difference over an altitude of 96 m is also determined from the measured temperatures where the stable boundary layer is 96 m or thicker. This pressure difference is compared to the pressure difference obtained by manipulation of equations (L.5) and (E.3).

At every hourly interval during all the inversion periods given in table L.2, the average difference between the average temperature in the stable boundary layer (between z = 1 m and 96 m) obtained experimentally and empirically is 0.76 K. The maximum difference is 2.68 K. For the pressure distribution, the difference is only 0.50 % with a corresponding maximum difference of 1.35 %.

The empirical relation for the exponent, b, as given by equation (L.9) substituted into equation (L.5) gives very satisfactory results for both the mean temperature and pressure differences in the stable boundary layer.

L.9 THERMAL EDDY DIFFUSIVITY

In the analyses of Anfossi et al. [76AN1] and Surridge [86SU1] the value of the thermal eddy diffusivity is assumed to be constant. It can be seen from figures L.6 to L.11 that these equations with this assumption do not predict the temperature profile accurately. It will be shown that the reason for this inaccuracy of the equations is in part due to the fact that the thermal eddy diffusivity is not constant.

At the present location, the temperature at ground level during an inversion varies approximately linearly as a function of time. Figure L.12 shows the temperatures at ground level, given in table L.2, for the different periods of the year. It can be seen the gradient of all the lines in figure L.12 is approximately the same. The temperature at 1 m above the ground can be approximated by

$$T_1 = c_1 t + c_2 \tag{L.10}$$

where T_1 is in °C and c_1 and c_2 are constants.

From equation (L.5), with a reference height of 1 m, the vertical inversion profile is given by

$$T = (T_1 + 273.15) z^b \tag{L.11}$$

Substitute equation (L.10) into equation (L.11) and find

$$T = (c_1 t + c_2 + 273.15) z^b \tag{L.12}$$

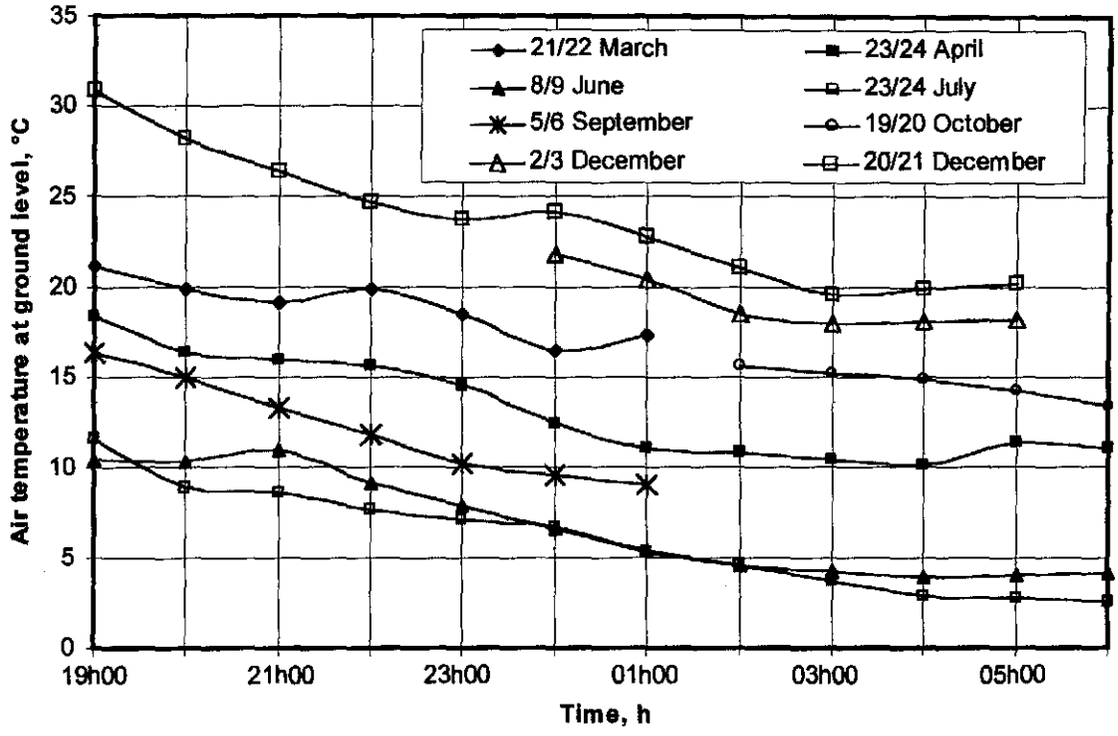

Figure L.12: Nocturnal air temperatures 1m above ground level at different periods.

From Fourier's one-dimensional heat conduction equation it follows that

$$\frac{\partial}{\partial z}\left(k_z \frac{\partial T}{\partial z}\right) = \rho c_p \left(\frac{\partial T}{\partial t}\right) \tag{L.13}$$

Differentiate equation (L.12) with respect to t and find

$$\frac{\partial T}{\partial t} = c_1 z^b \tag{L.14}$$

Differentiate equation (L.12) with respect to z and find

$$\frac{\partial T}{\partial z} = b\left(c_1 t + c_2 + 273.15\right) z^{b-1} \tag{L.15}$$

Substitute equations (L.14) and (L.15) into equation (L.13) and find

$$\frac{\partial}{\partial z}\left[k_z b\left(c_1 t + c_2 + 273.15\right) z^{b-1}\right] = \rho c_1 c_p z^b \tag{L.16}$$

Integrate (L.16) with respect to z to find after rearrangement

$$k_z = \frac{\rho c_p c_1 z^2}{\left(b^2 + b\right)\left[c_1 t + c_2 + 273.15\right]} + \frac{c_3}{\left[c_1 t + c_2 + 273.15\right] b z^{b-1}} \tag{L.17}$$

where c_3 is a constant introduced due to indefinite integration which will later be shown to be $q_{z=0}$.

From Fourier's equation of heat conduction it follows that

$$q = k_z \frac{\partial T}{\partial z} \tag{L.18}$$

Substitute equations (L.15) and (L.17) into (L.18) to find

$$q = \frac{\rho c_p c_1 z^{b+1}}{b+1} + c_3 \qquad \text{(L.19)}$$

From equation (L.19) with $z = 1 \approx 0$ find $c_3 = q_{z=0} \approx q_{z=1}$ where $q_{z=0}$ is the heat flux conducted from the air to the ground due to radiation from the ground into the night sky.

Figure L.13 shows the temperature vs. time gradients of the data given in table L.2 of the atmospheric air during nocturnal inversions for various times during the course of the year. It can be seen that the temperature gradients are relatively constant throughout the year at ground level and at a height of 96 m. The average temperature gradient at ground level, from figure L.13 is approximately –0.7787 K/h or -2.163×10^{-4} K/s, thus from equation (L.10),

$$c_1 \approx -2.163\times10^{-4}\,\text{K/s} \qquad \text{(L.20)}$$

For the inversion period of 23/24 July in table L.2, the number of the day of the year is, n_d = 204 with a corresponding value of b = 0.0099 from equation (L.9).

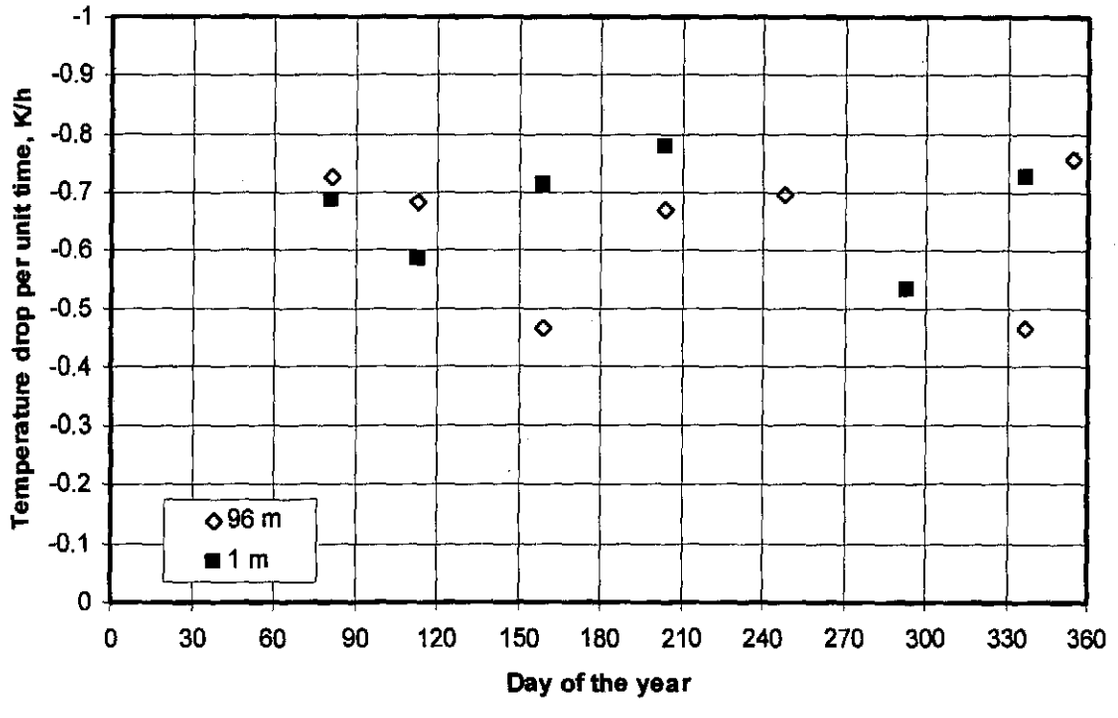

Figure L.13: Temperature drop per unit time at 1 m and 96 m.

The value of c_2, for the inversion period, from equation (L.10) is 11.103 °C, i.e. the temperature above the ground at the beginning of the inversion period under consideration. This is the temperature 1 m above the ground at 19h00 as can be seen from table L.2. If it is assumed that c_p = 1006.5 J/kgK and ρ = 1.2 kg/m^3 k can be determined as a function of $q_{z=0}$ from equation (L.17). Figure L.14 shows the conductivity, k, as a function of the $q_{z=0}$, the heat flux at ground level. The thermal eddy diffusivity is equal to the effective thermal conductivity divided by the product of the density and specific heat. The thermal eddy diffusivity is thus not constant as Anfossi et al. [76AN1] and Surridge [86SU1] assumed.

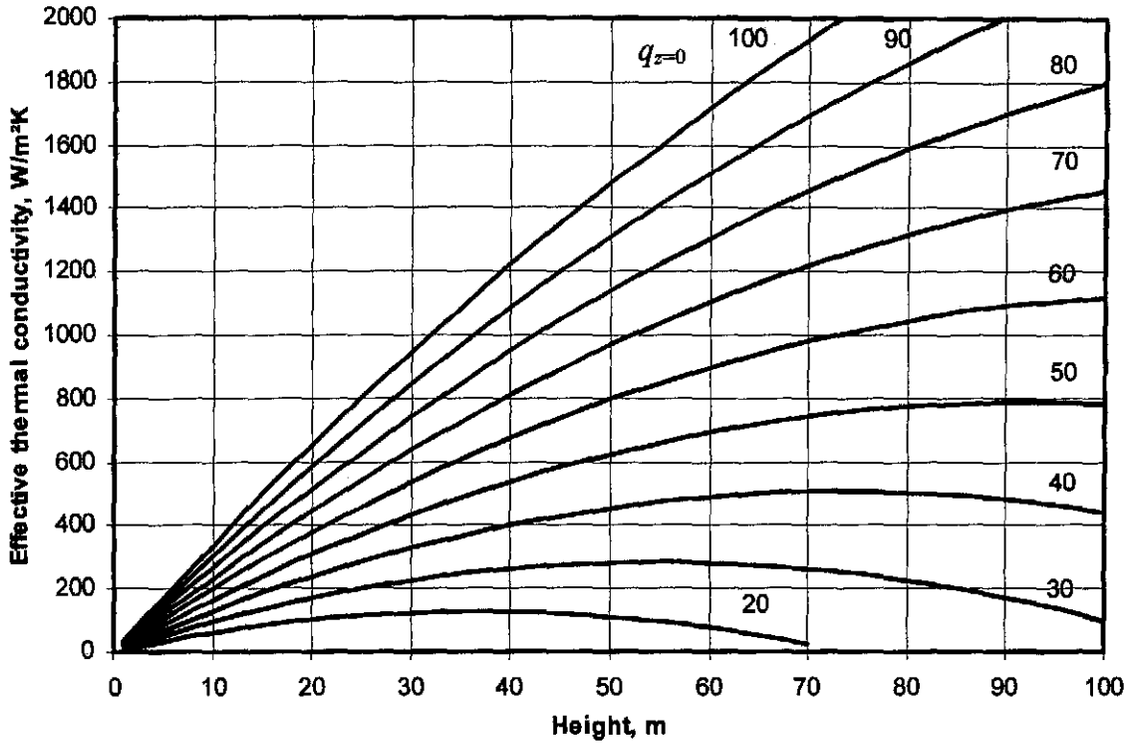

Figure L.14: Atmospheric conductivity for different values of $q_{z=0}$.

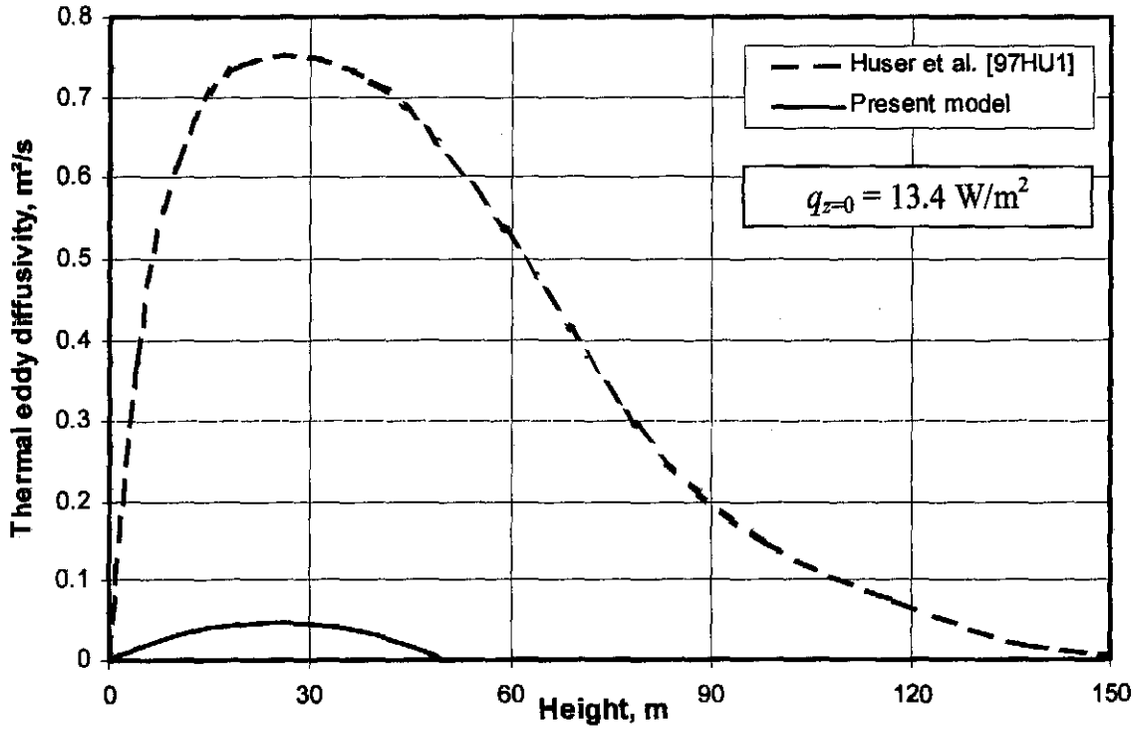

Figure L.15: Comparison between present model and the results of Huser et al. [97HU1].

Huser et al. [97HU1] employed the similarity theory of Monin and Obukhov [54MO1] in conjunction with a commercially available computational fluid dynamics software to find the vertical distribution of the thermal eddy viscosity in the atmospheric boundary layer. The inlet profiles of the computational

domain, which extends 5000 m in the downwind direction, is approximated by Huser et al. [97HU1]. These inlet profiles include the velocity, temperature, and the k and ε turbulence parameters of the k-ε turbulence model of Launder and Spalding [74LA1]. Figure L.15 shows the thermal eddy viscosity profiles of the present model and the results of Huser et al. [97HU1] for a smooth surface where the surface heat flux, $q_{z=0}$ = 13.4 W/m^2. The surface roughness, scaling velocity, scaling temperature, Obukhov length, the height at which velocity shear vanishes and the wind speed at 10 m are 0.01 m, 0.23 m/s, 0.029 K, 130 m, 196 m and 4 m/s respectively in the calculations of Huser et al. [97HU1].

The present model is developed from temperature measurements in a relatively arid area near Lephalale (Ellisras) (23°40'S, 27°47'E) while the model of Huser et al. [97HU1] is applied to Drammen in Norway (59°42'N, 10°12'E). It is therefore not very meaningful to critically compare the results, but it is nevertheless interesting to note the respective trends. It can be seen in figure L.15 that the maximum thermal diffusivities of the present model and the model of Huser et al. [97HU1] occur at approximately the same height. Huser et al. [97HU1] also states that their model over-predicts the thermal eddy diffusivity. Therefore, the results of Huser et al. [97HU1] also concludes that the thermal eddy diffusivity is not constant as Anfossi et al. [76AN1] and Surridge [86SU1] assumed. It should also be noted that the temperature distribution as given by equation (L.12) is a good approximation at lower elevation but becomes less meaningful near the top of the inversion. This means that the effective conductivity given by equation (L.17) is correspondingly less accurate near the top of the inversion.

L.10 INVERSION HEIGHT CALCULATION

As mentioned above, the stable boundary layer is generally accepted to evolve as the square root of time as shown in equation (L.3) [86SU1]. However, faster development of the stable boundary layer has been observed [87SU1]. Values of the thermal eddy diffusivity, K, in equation (L.3) may differ measurably depending on site and ambient conditions. Values of K = 0.3 to 0.5 m^2/s have been observed. K is also assumed to be constant in the analyses of Anfossi et al. [76AN1] and Surridge [86SU1].

Due to the uncertainties associated with equation (L.3) to determine the inversion height, the following procedure can also be employed to determine the inversion height:

The DALR temperature distribution immediately prior to the development of an inversion is given by

$$T = T_{max} - 0.00975z \qquad \text{(L.21)}$$

where T_{max} is the diurnal surface temperature maximum.

Experimental evidence indicates that the mean temporal temperature gradient at elevations above the top of the inversion is approximately 0.43 K/h [90SU1]. Once the stable boundary layer or inversion begins to evolve, the temperature distribution above the inversion can thus be approximated by

$$T = T_{max} - 0.00975z - 0.43t \qquad \text{(L.22)}$$

where t is the time measured in hours.

At the top of the inversion, z_{it}, the temperature as given by equation (L.21) is equal to the temperature given by equation (L.22) i.e.

$$(T_r + 273.15)\left(\frac{z_{it}}{z_r}\right)^b = T_{max} - 0.00975 z_{it} - 0.43t \qquad \text{(L.23)}$$

For a given initial temperature, T_{max}, the value of z_{it} can be determined by an iterative procedure for different ground temperatures at different times.

The procedure presented above is still relatively complex, as it requires the maximum daily temperature as well as the time since the inception of the inversion. The aim is to develop a theoretical model with the minimum amount of input.

Equation (L.5) correlates measured inversion temperature data well for heights of about 1 m above ground elevation and greater heights. Since the temperature gradient of this equation can never be equal to zero it is inadequate at the top of the inversion layer. In this region a more realistic empirical equation for the temperature distribution would be

$$T = (T_r + 273.15)\left(\frac{z}{z_r}\right)^b - 0.00975z \qquad \text{(L.24)}$$

This equation effectively represents the region of transition from the inversion layer to the adiabatic lapse above it. Although this equation could also have been applied at lower elevations in the inversion layer, the simpler equation (L.5) is adequate and makes possible the solution of problems that would otherwise be less amenable to analysis.

An approximate average value for the inversion height can be obtained by differentiating equation (L.24) and equating it to zero, i.e.

$$\frac{dT}{dz} = b(T_r + 273.15)\left(\frac{z_{it}}{z_r}\right)^{b-1} - 0.00975 = 0 \qquad \text{(L.25)}$$

Rearrange equation (L.25) to find

$$z_{it} = \left[\frac{0.00975}{b(T_r + 273.15)}\right]^{\frac{1}{b-1}} \qquad \text{(L.26)}$$

Equation (L.26) will predict, in conjunction with equation (L.9), inversion heights of approximately 300 m in the winter months and approximately 90 m in high summer. These heights are typically observed in nature. The inversion heights predicted by equation (L.26) will remain constant for a particular inversion period. In reality, the inversion will grow throughout the night. The growth rate of the inversion is relatively slow after the first few hours after the inception of the inversion. Equation (L.26) therefore predicts an average value of the inversion height but is not valid during the first few hours after the inception of the inversion.

After a certain time, t, the enthalpy of the air up to the inversion height of z_{it}, for a 1 m^2 column of air, is

$$\int_0^{z_{it}} \rho c_p T dz = \rho c_p \int_0^{z_{it}} (c_1 t + c_2 + 273.15) z^b dz \tag{L.27}$$

The heat flux, $q_{z=0}$, into this 1 m^2 of air is

$$q_{z=0} = \frac{\partial}{\partial t} \int_0^{z_{it}} \rho c_p T dz = \rho c_p \int_0^{z_{it}} c_1 z^b dz = \frac{\rho c_p c_1 z_{it}^{b+1}}{b+1} \tag{L.28}$$

z_{it} is approximately 300 m from equation (L.26) if b = 0.01. From equation (L.28), with c_1 = –2.163 × 10^{-4} K/s, ρ = 1.1 kg/m^3 and c_p = 1000 J/kgK find from equation (L.28) that $q_{z=0}$ = 74.8 W/m^2. This is not unreasonable.

By employing equation (L.24) in equation (L.13) a more realistic value for the effective thermal conductivity will be obtained near the top of the inversion. Figure L.16 shows the effective thermal conductivity predicted by employing equation (L.24) in the analysis. Compare figure L.16 to figure L.14 and see that the effective thermal conductivity is less in figure L.16 than in figure L.14.

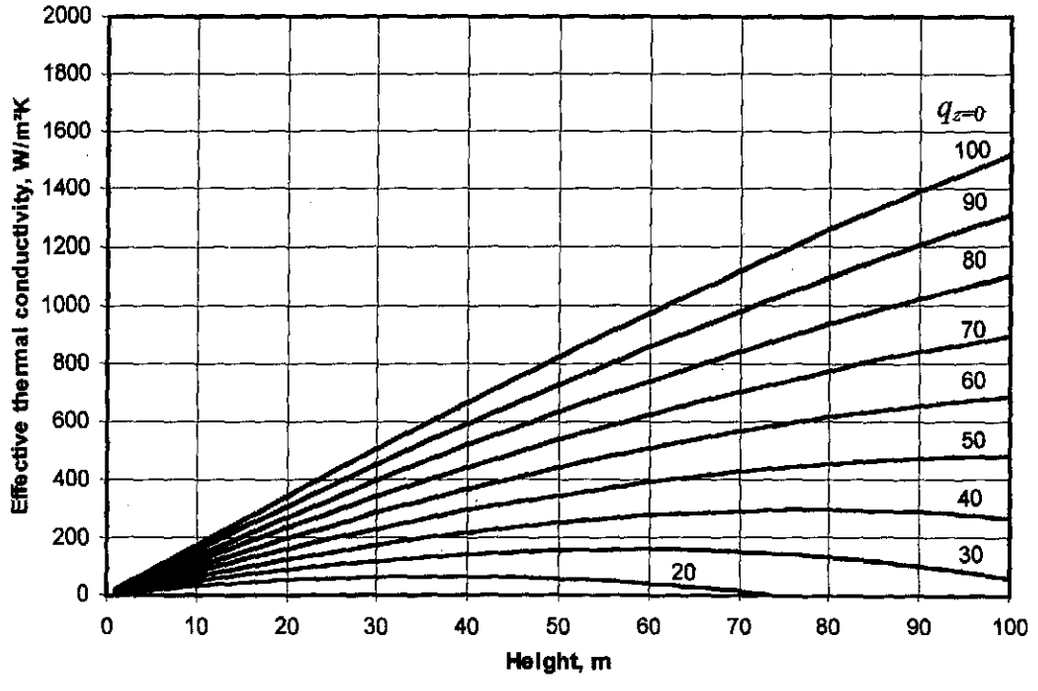

Figure L.16: Atmospheric conductivity for different values of $q_{z=0}$.

L.11 CONCLUSION

Further investigation is necessary to validate the results obtained in this appendix, as limited experimental data was available for analysis. It is anticipated that the value of the exponent b in equation (L.5), given by equation (L.9), will differ depending on the geographical location of the place of interest. Nevertheless, a simple empirical relation is obtained that predicts the vertical temperature profiles during stable conditions relatively accurately and that can be analytically integrated.

APPENDIX M

ATMOSPHERIC HUMIDITY

M.1 INTRODUCTION

To accurately predict the performance of wet cooling towers, humidity profiles in the atmosphere have to be known. The atmospheric humidity influences the heat and mass transfer as well as the draft through the towers. It is found that humidity inversions occur during the same period that temperature inversions occur. The formulas that are employed in the analysis of cooling tower performance, to determine the effect of atmospheric humidity on tower draft, are presented in section E.2.

M.2 MEASUREMENT OF HUMIDITY

Most of the literature devoted to the measurement of the vertical humidity profiles in the atmosphere, focuses on the lower atmosphere. The lower atmosphere extends to the top of the stratosphere, which is approximately 50 km above the surface of the earth [98SE1]. Meteorological weather balloons (radiosondes) or remote sensing techniques are generally employed to obtain the humidity profiles [96HA1]. There are a variety of remote sensing techniques, which employ ground-based instruments and satellites. Empirical models are developed that predict humidity profiles as a function of the altitude and the humidity at ground level. Some of these models are according to Hann [08HA1], Yoshino [75YO1] and Gorchakov [81GO1].

Only the humidity profile in the lower parts of the planetary boundary layer is of importance in the performance analysis of cooling towers. The planetary boundary layer is approximately the first 1 km to 2 km of the atmosphere. The empirical models of Hann [08HA1, Yoshino [75YO1] and Gorchakov [81GO1] are unable to predict the diurnal variations of atmospheric humidity in the planetary boundary layer, but are relatively accurate above the planetary boundary layer, where diurnal changes are small according to McGee [72MC1].

M.3 DIURNAL VARIATION OF ATMOSPHERIC HUMIDITY

After sunrise, water vapor is added to the lower atmosphere by evapotranspiration. This causes a sharp increase in the humidity of the air. The resulting lapse condition becomes most pronounced at the time of maximum surface heating due to convective mixing and subsequent dilution of the vapor concentration. By late afternoon, however, convection wanes as the air near the ground becomes stable. Evaporation continues to supply water vapor to the air above the surface, but the rate of dilution due to mixing slows down and the lapse rate tends toward isothermal. At night, radiative cooling of the air below the dew-point temperature causes dew to form on the ground. The extraction of water vapor from the overlying air causes an inversion to form in the water vapor profile. The depth and strength of this inversion is determined by the downward flux of water vapor in a suitably turbulent environment. The level of turbulence is critical. If it is too low, dew ceases to form since the ground cannot be replenished by water

vapor from above. If it is too high, mixing inhibits surface radiative cooling to below dew-point temperature. Near the surface in the early afternoon, even with strong evapotranspiration, turbulence transfers moisture away from the surface so rapidly that specific humidity usually falls to an early-afternoon minimum. The vertically-transported water vapor then produces a maximum at the same time in the upper boundary layer [88PR1]. Moistening of the atmosphere by evaporation from the underlying surface proceeds quickly and invisibly every day when energy and water are available. The moistening process goes forward at daily rates up to 3-4 kg/m^2. The surface is the source of the water vapor that is mixed through the earth's atmosphere [77MI1]. Vapor moving upward from the source at the earth's surface would, in time, diffuse evenly through the entire atmosphere but it is intermittently removed by condensation in the middle levels of the atmosphere. The interplay between the surface as sole source of vapor and the vapor sinks represented by ascending columns or sheets of air in the atmosphere produces a more or less equilibrium balance that is represented by a vertical decrease in vapor concentration [77MI1].

Case study by Oke [78OK1]

Refer to figure M.1. By day, the profile of vapor concentration lapses with height away from the surface moisture source in the same manner as the temperature profile. Vapor is transported upwards by eddy diffusion in a process analogous to that for sensible heat. In the morning hours the evapotranspiration of surface water (dew, soil water and plant water) into a moderately unstable atmosphere adds moisture to the lower layers and the humidity increases quite sharply. By early afternoon, although vapor flux is at a peak, the humidity concentration drops slightly. This is a result of convective activity having penetrated to such heights in the boundary layer that the vapor concentration becomes diluted by mixture with descending masses of drier air from above. In the late afternoon surface cooling is strong and the lower layers becomes stable. Thus, the ability to transport vapor to higher layers is less than the rate at which it continues to be added from the surface. Moisture converges into the lowest layers and a second humidity maximum is observed. Thereafter evapotranspiration declines into the night period. Under certain conditions the vapor profile may become inverted near the surface so that the vapor is transferred downwards as a dewfall. This depletes the moisture in the lowest layers and humidity decrease, until after sunrise when the cycle recommences. Oke [78OK1] also found that the humidity profile above non-vegetated surfaces, characterized by low absolute moisture content, is far from saturation and has a very weak lapse rate in most occasions.

Case studies by Geiger [65GE1]

Figure M.2 shows average water vapor pressure profiles in the lowest 100 m of the atmosphere for 19 clear summer days measured in Rye, England. Before sunrise there is a flow of water vapor from a height of about 40 m toward the ground, to form dew. Vigorous evaporation is initiated by heating after sunrise, as may be seen from the increase in water vapor pressure in the layer nearest the ground until 06h00. Since eddy diffusion is still restricted, this supply of water vapor is trapped near the ground, and the daily maximum of vapor pressure is reached about 08h00 with powerful humidity gradients (full line). Without any marked change of the gradient, the profiles (broken) then become displaced toward the region of

lower vapor pressure, because of increasing eddy diffusion. This transport out of the layer close to the ground brings about a minimum value at 14h00. At 18h00 the decrease of water vapor pressure with height is still normal, but by 20h00 the decreasing eddy diffusion and increasing water vapor content of the air have reestablished the humidity inversion at the ground, and as time goes on it gradually increases in height, in a similar way to the temperature inversion.

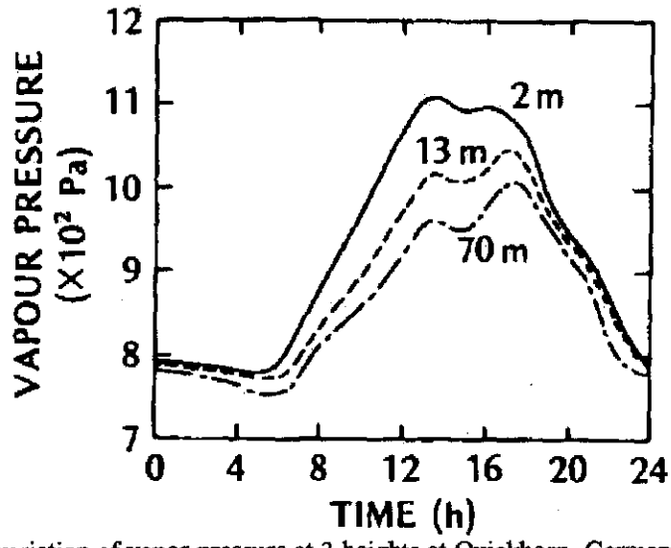

Figure M.1: Diurnal variation of vapor pressure at 3 heights at Quickborn, Germany on cloudless days in May [78OK1].

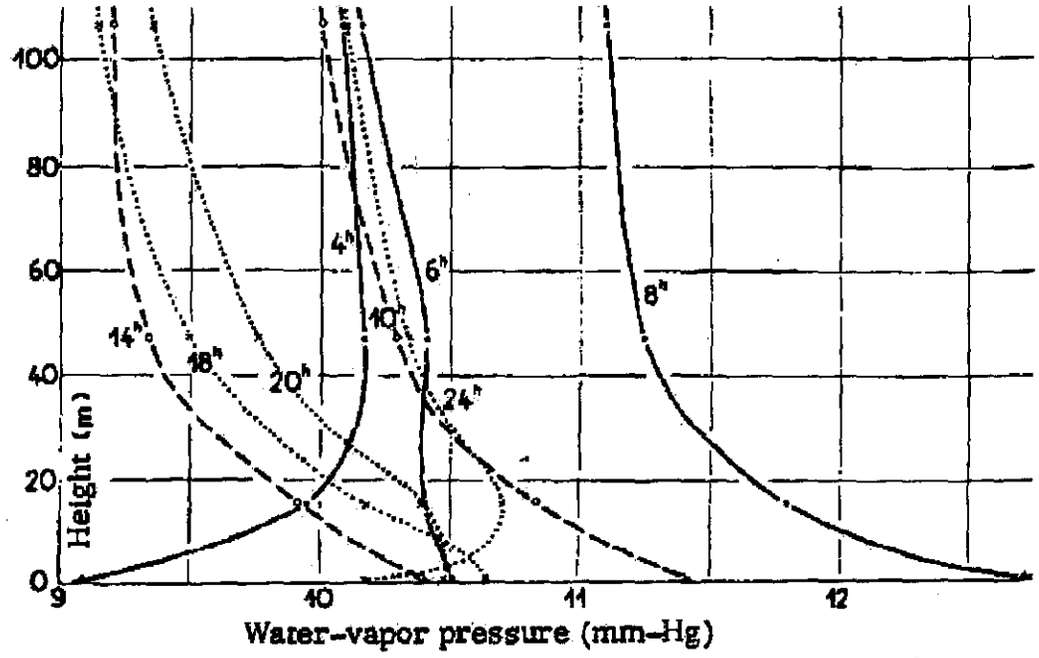

Figure M.2: Profiles of water vapor stratification in the lowest 100 m on clear summer days measured in Rye, England [65GE1].

Figure M.3 shows the data of the water vapor pressure in the first seventy meters of the atmosphere measured at Quickborn, Germany. Here, too, the flow of water vapor is directed downward at night toward the ground surface (covered with dew), and the fall is remarkably large in the hours before

sunrise. During the forenoon, vapor pressure rises close to the ground, and falls at the 70 m level. The transition from day to night conditions can be recognized easily in the average values for the period 20h00 to 22h00.

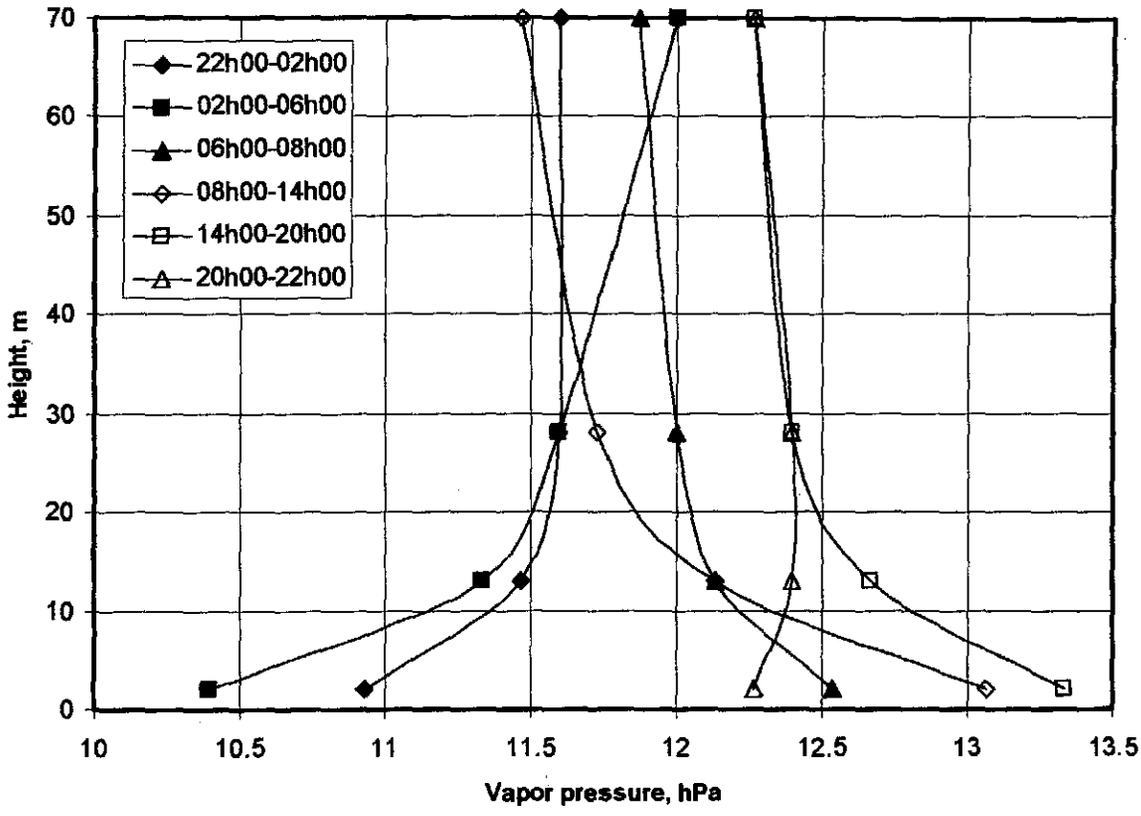

Figure M.3: Water vapor pressure profiles of the first 70 m of the atmosphere, measured at Quickborn, Germany.

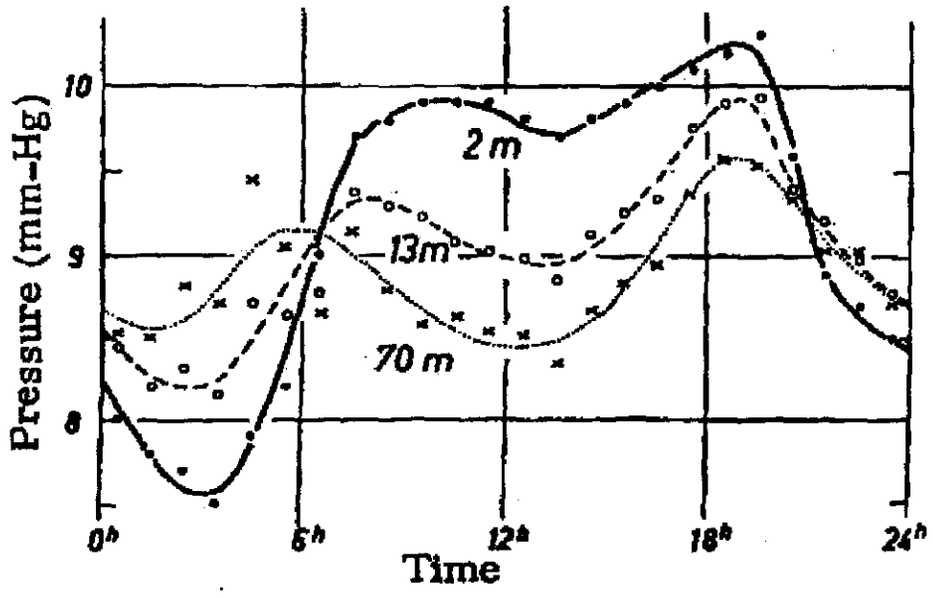

Figure M.4: Diurnal variation of water vapor at Quickborn, Germany on clear July days.

The daily pattern is shown in figure M.4 for heights of 2, 13 and 70m. The well known double wave of vapor pressure is easily recognized. This appears at all levels, but the amplitude of fluctuation increases with approach to the ground. In all these layers, the evening maximum is higher than the morning value. Figure M.4 is, as we might expect, dependant on the season of the year, the weather situation, and the geographic location of the place of observation. If the average of all days is taken, the picture obtained of the layered structure of water vapor distribution is similar, but a rather deflated version of the picture of a clear day.

If conditions in the 100 m layer show a clear cut relation, the same cannot be said for the first few meters close to the ground. In the majority of cases, there is a repetition, on a small scale, of what we found for the first 100 m. This is true particularly in regions of dry climate, rich in radiation.

M.4 ANNUAL VARIATION OF ATMOSPHERIC HUMIDITY

Figure M.5 depicts the average annual variation of the relative humidity measured at three different weather stations on the South African Highveld at 08h00 and 14h00. The data in figure M.5 for Germiston were obtained during a period from 1932 to 1950, for Pretoria during a period from 1938 to 1950 and for Pietersburg from 1904 to 1950 [58ME1]. Figure M.6 shows the corresponding minimum and maximum monthly temperatures.

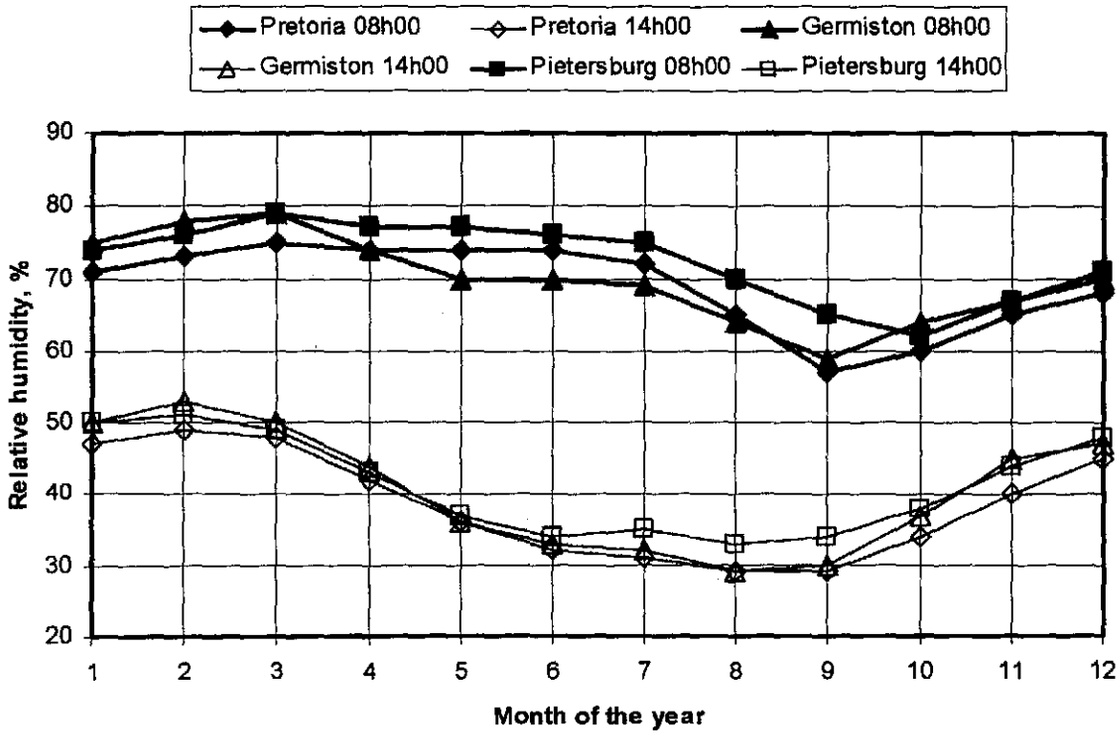

Figure M.5: Average annual variation of relative humidity at 8h00 and 14h00 measured at Pretoria, Germiston and Pietersburg.

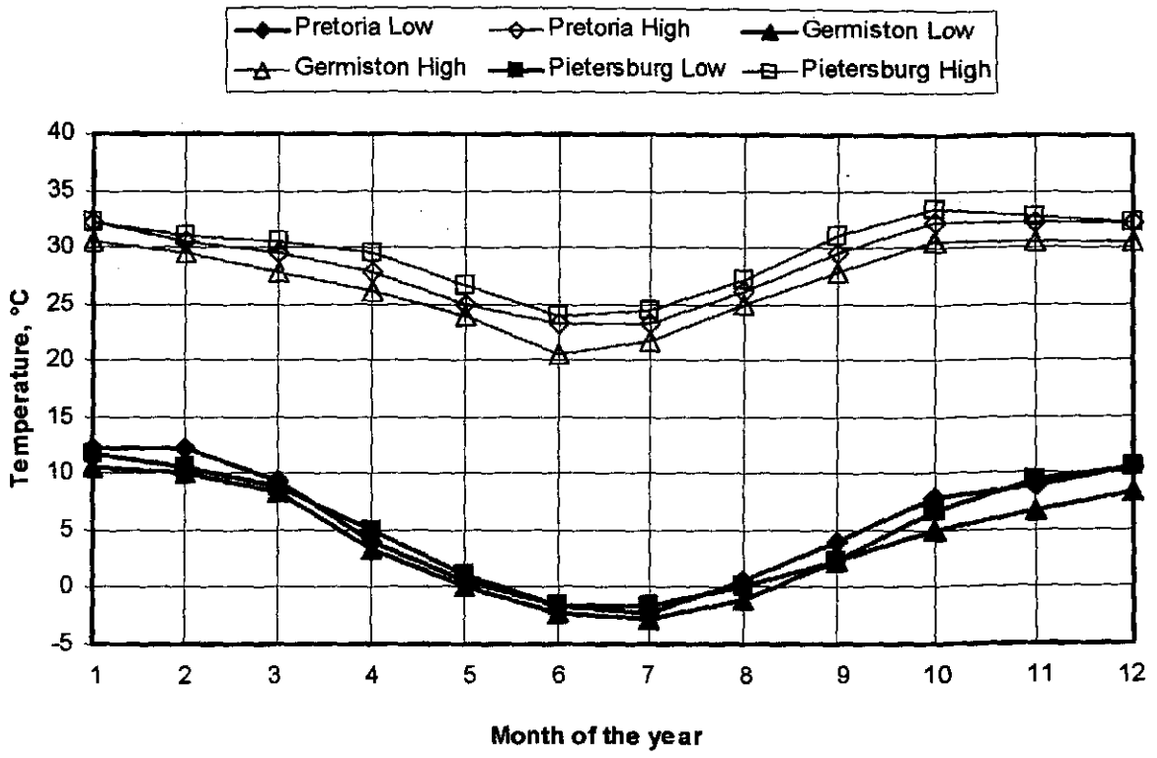

Figure M.6: Average monthly variation of minimum and maximum temperatures measured at Pretoria, Germiston and Pietersburg.

M.5 CONCLUSION

Humidity inversions occur in a similar way as temperature inversions during the night. Oke [78OK1] found that the vertical humidity profile is approximately constant above non-vegetated surfaces during the sunshine hours of the day. Geiger [65GE1] found that the water vapor flows to the ground, from approximately 40m above the ground, to form dew during the night. From these conclusions and the general trends of the humidity profiles shown in figures M.1 to M.4, the effect of humidity profiles on cooling tower performance can be determined.

APPENDIX N

MODELLING OF A COOLING TOWER AS A CIRCULAR JET AND A POINT SINK

N.1 INTRODUCTION

In this study, the height at which a cooling tower draws in air from the atmosphere is determined for different mass flow rates through the cooling tower. The cooling tower is modelled as a turbulent circular jet and a point sink. The inlet of the cooling tower is modelled as point sink while the exit is modelled as a turbulent circular jet. A solution of the flow field for the turbulent circular jet is obtained with an analytical method derived from boundary layer theory. The computational domain in two-dimensional cylindrical coordinates, at which a solution is sought, extends 3000 m in the axial (vertical) direction and 5000 m in the radial direction.

N.2 TURBULENT CIRCULAR JET

The investigation of the flow field far away from a jet is determined in this section by an analytical solution. There are presently three techniques used to study external flows i.e. numerical (digital-computer) solutions, experimentation, and boundary layer theory [94WH1]. Prandtl first formulated the boundary layer theory by making certain order-of-magnitude assumptions to greatly simplify the Navier-Stokes equations into the boundary layer equations. White [91WH1] gives a summary of strong inequalities at large Reynolds numbers:

$$\mathrm{Re}_x >> 1: \qquad \delta << x \qquad v << u \qquad \frac{\partial u}{\partial x} << \frac{\partial u}{\partial y} \qquad \frac{\partial v}{\partial x} << \frac{\partial v}{\partial y} \tag{N.1}$$

where δ is the thickness of the boundary layer. These strong inequalities are used to simplify the Navier-Stokes equations to obtain the boundary layer equations.

Jet velocity profiles are unstable and undergo transition to turbulence early, at a Reynolds number of about 30, based on exit slot width and mean slot velocity [91WH1]. This is the reason why only the turbulent circular jet is investigated in this study and not the laminar turbulent jet. Problems in free turbulent flow are of a boundary layer nature. Schlichting [60SC1] gives the analytical solution for the boundary layer flow of a turbulent jet. The boundary layer equations for a two-dimensional incompressible flow are:

$$\frac{\partial u}{\partial t} + u\frac{\partial u}{\partial x} + v\frac{\partial u}{\partial y} = \frac{1}{\rho}\frac{\partial \tau}{\partial y} \tag{N.2}$$

$$\frac{\partial u}{\partial x} + \frac{\partial v}{\partial y} = 0 \tag{N.3}$$

where τ is the turbulent shear stress. Prandtl's mixing length theory states that:

$$\tau_t = \rho L^2 \left|\frac{\partial u}{\partial y}\right| \frac{\partial u}{\partial y} \tag{N.4}$$

where L is the turbulent mixing length. This equation for shear stress in turbulent flow is unsatisfactory in that the apparent, kinematic velocity ε, vanishes at points of maximum velocity. A hypothesis by Prandtl circumvents this problem by defining a virtual kinematic viscosity which is formed by multiplying the maximum difference in the time-mean flow velocity with a length which is assumed to be proportional to the width, b, of the mixing zone. Thus

$$\varepsilon_t = \chi b(u_{\max} - u_{\min}) \tag{N.5}$$

where χ donates a dimensional number to be determined experimentally. The width of a circular turbulent jet is proportional to x such that the centreline velocity $U \propto x^{-1}$. Thus, the virtual kinematic viscosity becomes:

$$\varepsilon_t = \chi b U \propto x^0 = const = \varepsilon_0 \tag{N.6}$$

which means that it remains constant over the whole of the jet. The differential equations for the velocity distribution are identical to the laminar circular jet, with the only difference in the viscosity, where ε_0 replaces υ in the laminar equations. J is the kinematic momentum flux, which is a measure of the strength of the jet. The velocity distribution of a turbulent jet is

$$u = \frac{3}{8\pi}\frac{J}{\varepsilon_0 x}\frac{1}{\left(1+\frac{1}{4}\eta^2\right)^2} \tag{N.7}$$

$$v = \frac{1}{4}\sqrt{\frac{3}{\pi}}\frac{\sqrt{J}}{x}\frac{\eta - \frac{1}{4}\eta^3}{\left(1+\frac{1}{4}\eta^2\right)^2} \tag{N.8}$$

where

$$\eta = \sqrt{\frac{3}{16\pi}}\frac{\sqrt{J}}{\varepsilon_0}\frac{y}{x} \tag{N.9}$$

According to measurement, the virtual kinematic viscosity is

$$\varepsilon_0 = 0.0161\sqrt{J} \tag{N.10}$$

The flow rate of the jet can be expressed as:

$$V = 0.414\sqrt{J}x \tag{N.11}$$

N.3 POINT SINK

The equation of continuity for incompressible flow in polar coordinates is:

$$\frac{\partial}{\partial r}\left(r^2 v_r \sin\theta\right) + \frac{\partial}{\partial \theta}\left(r v_\theta \sin\theta\right) = 0 \tag{N.12}$$

There exists a stream function such that

$$v_r = -\frac{1}{r^2 \sin\theta}\frac{\partial \varphi}{\partial \theta} \tag{N.13}$$

$$v_\theta = \frac{1}{r\sin\theta}\frac{\partial\varphi}{\partial r} \tag{N.14}$$

The tangential velocity, v_θ, is zero for a point sink. Integrating equation (N.14) gives the radial velocity:

$$\int_\varphi^\varphi d\varphi = -\int_\theta^\theta v_r r^2 \sin\theta d\theta \tag{N.15}$$

$$\varphi = v_r r^2 \cos\theta \tag{N.16}$$

where:

$$v_r = \frac{V}{A} = \frac{V}{4\pi r^2} \tag{N.17}$$

N.4 EXAMPLE CALCULATION AND RESULTS

The outlet of the cooling tower is modelled as a circular jet. The mass flow rate through an arbitrarily chosen cooling tower is assumed to be 15213.68 kg/s, while the outlet diameter of the cooling tower is 58 m. The density of the air, ρ, is 1.204 kg/m^3 and the dynamic viscosity, μ, is 1.8 x 10^{-5} kg/ms. The momentum of the jet is given by

$$J = mv \tag{N.18}$$

where

$$m = \rho A v \tag{N.19}$$

$$A = \frac{\pi}{4}d^2 = \frac{\pi}{4}\left(58^2\right) = 2642.08\ \text{m}^2 \tag{N.20}$$

From equation (N.19) find

$$v = \frac{m}{\rho A} = \frac{15213.68}{(1.204)(2642.08)} = 4.782576\ \text{m/s}$$

From equation (N.18), the momentum flux is

$$J = mv = (15213.68)(4.782576) = 72760.6\ \text{kg m/s}^2$$

The exact solution for the flow field of a turbulent jet, approximated by the boundary layer equations, is given by equation (N.7) to (N.10). The results for the turbulent circular jet can be seen in the first column of table N.1. The streamlines, axial velocity distribution, radial velocity distribution, and the velocity magnitude distribution are illustrated in table N.1. The range of the contour levels for the axial and velocity magnitude distributions is from 0 to 1 m/s. The pitch black contour level represents velocities greater than or equal to 1 m/s. The negative sign in the table for the radial velocity distribution indicates a flow in the negative radial direction.

To solve equation (N.16) and equation (N.17) for the point sink, the volume flow rate, V, must first be determined.

$$\frac{V}{2} = \frac{m}{\rho} = \frac{15213.68}{1.205} = 12625.5\ \text{m}^3/\text{s} \tag{N.21}$$

To maintain the desired flow rate, the strength of the sink must be doubled. For a sink, the volume flux, V, is negative. The results for the point sink in cylindrical coordinates are illustrated in the second column of

Table N.1: Results of circular jet, point sink and superposition of the two flows.

	Turbulent Jet	Sink	Superposition
Stream function	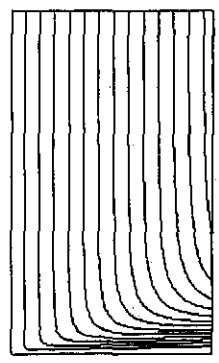	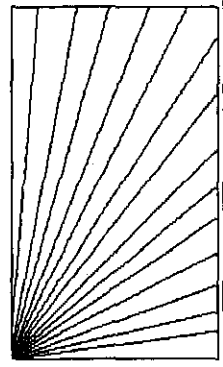	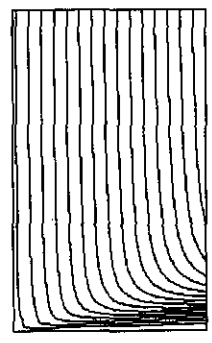
Axial velocity	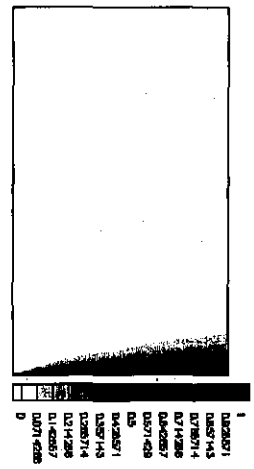	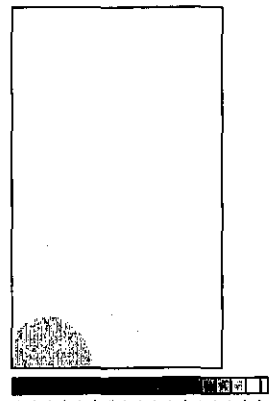	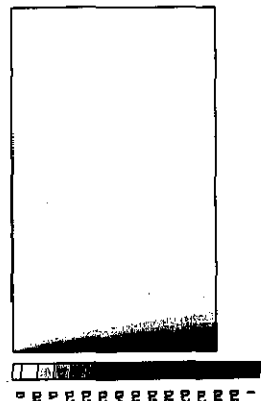
Radial velocity	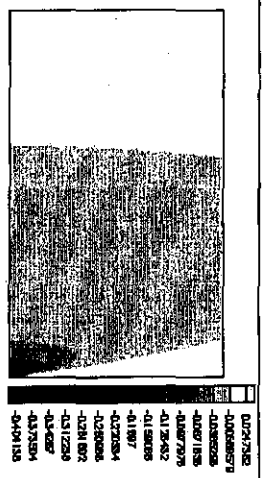	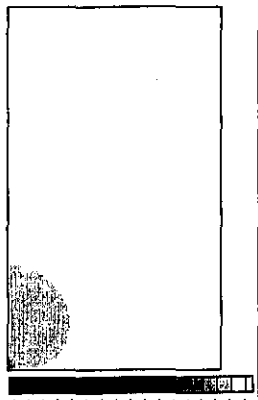	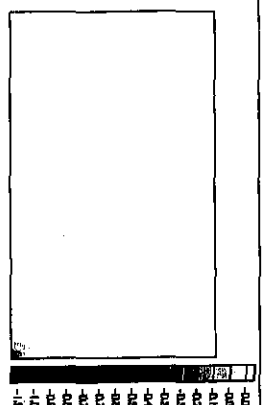
Velocity magnitude	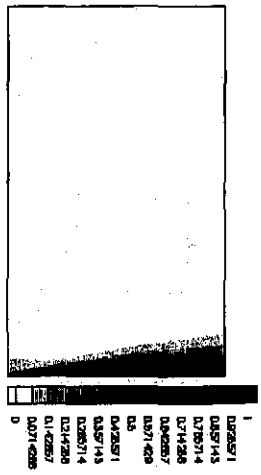	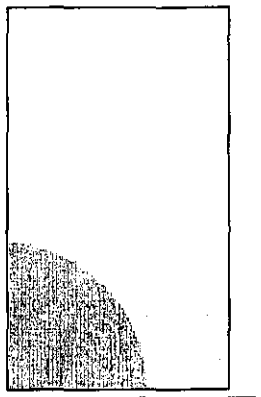	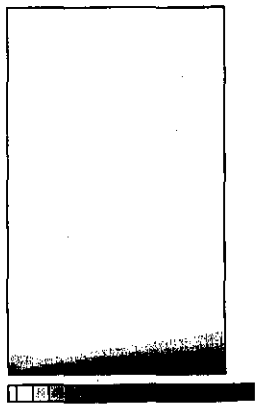

table N.1. Once again the stream function, axial velocity distribution, radial velocity distribution and velocity magnitude distribution are presented.

To combine the results of the turbulent circular jet and the point sink, the principle of superposition is used. Superposition, however, can only be used in potential flows, i.e. when the flow is irrotational and incompressible. Due to the fact that viscous flow is present in the turbulent jet, superposition can not be applied in the region of high velocity gradients. If it is assumed that the flow is laminar and irrotational in the farfield, which is a very reasonable approximation, superposition can be applied.

As the farfield characteristics are required in this study, the assumption of superposition is sufficient. The last column in table N.1 illustrates the results for the superposition of the turbulent jet and the point sink. It can be seen that the influence of the point sink is almost negligible.

Different radial velocity distributions with height are illustrated in figure N.1. Six different distributions are presented. Radial distances from the cooling tower, modelled as a circular jet, of 3000, 4000 and 5000 m are considered. At each distance, the effect of the jet and the combined effect of the jet and sink are presented.

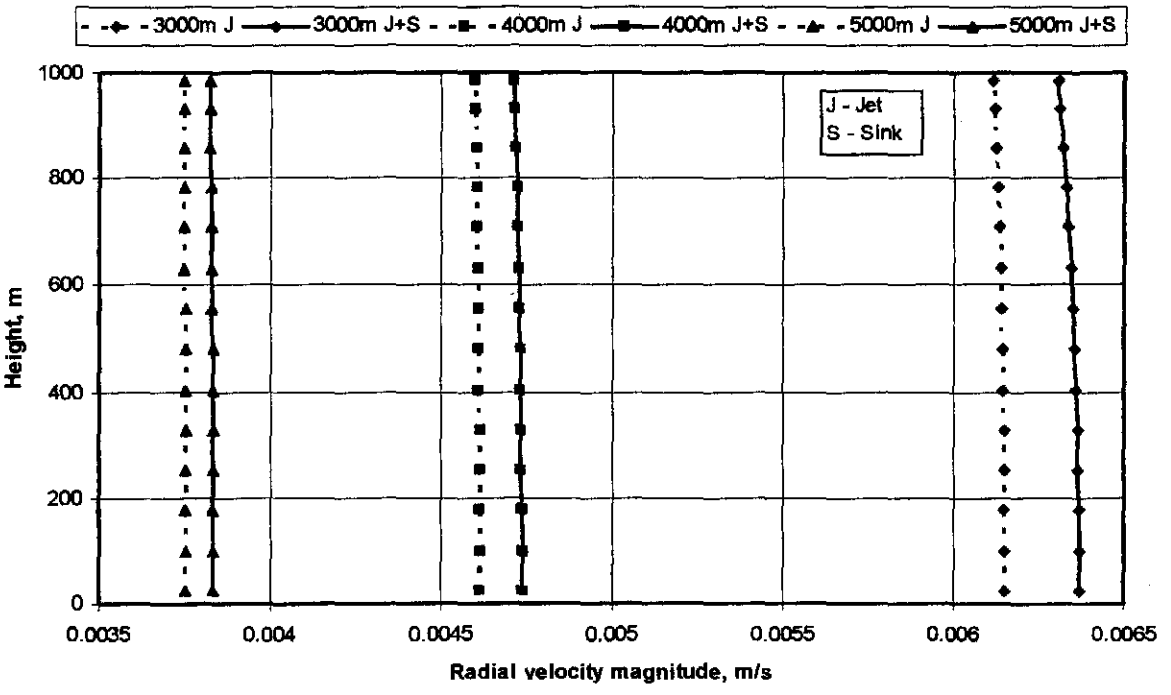

Figure N.1: Radial velocity distribution at different radial distances from the cooling tower.

As expected, the velocity magnitude of the combined effect of the jet and sink is greater that that of the jet alone. This is because the sink extracts flow from the flow field and thus increases the velocity of the air, which is drawn towards the centre axis of the jet, due to the effect of the turbulent jet. It can be seen that the velocity remains constant with altitude for the different cases at the various radial distances from the cooling tower.

The determination of the height, at which the tower draws in air from the surroundings, is presented next. Refer to figure N.2 for the illustration of the variables used in the calculation. The mass flow rate in the atmosphere towards both the jet and the sink can be expressed as

$$m_r = \rho A_r v_r \tag{N.22}$$

where $A_r = P_e H_r$ and P_e is the perimeter. Thus

$$H_r = \frac{m_r}{\rho P_e v_r} \tag{N.23}$$

where $P_e = 2\pi r$. Find

$$H_r = \frac{15213.68}{(1.204)2\pi r v_r} \tag{N.24}$$

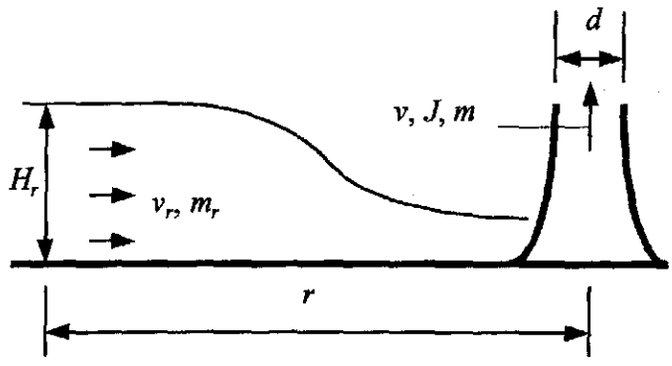

Figure N.2: Illustration of variables

The value of H_r for the example calculation is contained in table N.2 for different air flow rates at various radial distances from the cooling tower. It can be seen that the height, H_r, is approximately 123 m for the analysis with the jet and sink and 127 m for the analysis with the only the jet. The influence of the mass flow rate on the height, H_r, is investigated. Table N.2 and table N.3 contain the results where mass flow rates of respectively 10000 kg/s and 5000 kg/s are used in the calculations. Although the velocity of the air drawn towards the cooling tower is different for each mass flow rate, the height, H_r, remains unchanged for each case at the different radial distances from the cooling tower. This is consistent with the numerical results of Thiart [02TH1].

Table N.2: Altitude, H_r, at different radial distances for two different flow cases with m = 15213.68 kg/s and d = 58 m.

m = 15213.68 kg/s, d = 58 m, v = 4.783 m/s, J = 72760.6 kg m/s^2			
r, m	Flow Case	v_r, m/s	H_r, m
3000 m	Jet	0.0052331	127.032
3000 m	Jet + Sink	0.0054528	121.915
4000 m	Jet	0.0039248	127.031
4000 m	Jet + Sink	0.0040484	123.154
5000 m	Jet	0.0031931	127.031
5000 m	Jet + Sink	0.0032749	123.858

Table N.3: Altitude, H_r, at different radial distances for two different flow cases with m = 10000 kg/s and d = 58 m.

m = 10000 kg/s, d = 58 m, v = 3.143603 m/s, J = 31436.03 kg m/s2			
r, m	Flow Case	v, m/s	H_r, m
3000 m	Jet	0.00344	127.032
3000 m	Jet + Sink	0.003584	121.915
4000 m	Jet	0.00258	127.031
4000 m	Jet + Sink	0.002661	123.154
5000 m	Jet	0.002099	127.031
5000 m	Jet + Sink	0.002153	123.858

Table N.4: Altitude, H_r, at different radial distances for two different flow cases with m = 5000 kg/s and d = 58 m.

m = 5000 kg/s, d = 58 m, v = 1.57180 m/s, J = 7859.01 kg m/s^2			
r, m	Flow Case	v, m/s	H_r, m
3000 m	Jet	0.00172	127.032
3000 m	Jet + Sink	0.001792	121.915
4000 m	Jet	0.00129	127.031
4000 m	Jet + Sink	0.001331	123.154
5000 m	Jet	0.001049	127.031
5000 m	Jet + Sink	0.001076	123.858

Table N.5: Altitude, H_r, at different radial distances for two different flow cases with m = 15213.68 kg/s and d = 100 m.

m = 15213.68 kg/s, d = 100 m, v = 1.608859 m/s, J = 24476.66 kg m/s^2			
r, m	Flow Case	v, m/s	H_r, m
3000 m	Jet	0.003035	219.0209
3000 m	Jet + Sink	0.003255	204.2403
4000 m	Jet	0.002276	219.0195
4000 m	Jet + Sink	0.0024	207.742
5000 m	Jet	0.001852	219.0189
5000 m	Jet + Sink	0.001934	209.7544

Table N.6: Altitude, H_r, at different radial distances for two different flow cases with m = 10000 kg/s and d = 100 m.

m = 10000 kg/s, d = 100 m, v = 1.057508 m/s, J = 10575.08 kg m/s^2			
r, m	Flow Case	v, m/s	H_r, m
3000 m	Jet	0.001995	219.0209
3000 m	Jet + Sink	0.002139	204.2403
4000 m	Jet	0.001496	219.0195
4000 m	Jet + Sink	0.001578	207.742
5000 m	Jet	0.001217	219.0189
5000 m	Jet + Sink	0.001271	209.7544

Table N.7: Altitude, H_r, at different radial distances for two different flow cases with m = 5000 kg/s and d = 100 m.

m = 5000 kg/s, d = 100 m, v = 0.5287539 m/s, J = 2643.770 kg m/s^2			
r, m	Flow Case	v, m/s	H_r, m
3000 m	Jet	0.000998	219.0209
3000 m	Jet + Sink	0.00107	204.2403
4000 m	Jet	0.000748	219.0195
4000 m	Jet + Sink	0.000789	207.742
5000 m	Jet	0.000609	219.0189
5000 m	Jet + Sink	0.000636	209.7544

Table N.5, N.6 and N.7 contain the results where the outlet diameter is changed to 100 m with flow rates of 15213.68, 10000 and 5000 kg/s respectively. It can be seen that the values of H_r are the same for the different mass flow rates, but is substantially larger than the case where the diameter was 58 m.

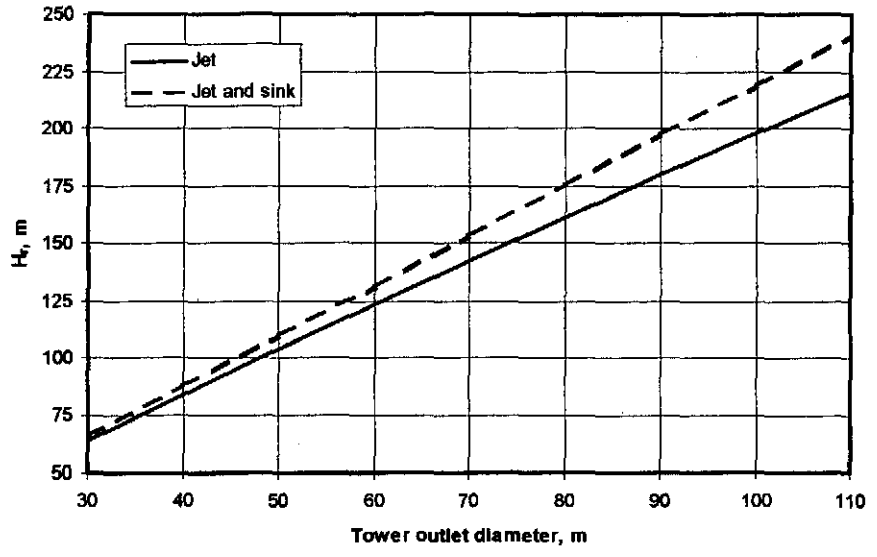

Figure N.3: Height at which tower draws in air from the surroundings versus the outlet diameter of the tower.

Figure N.3 shows the height at which air is drawn in from the surroundings as the outlet diameter of the tower changes. It can be seen that there is a linear relationship between the outlet diameter of the tower and the height, H_r.

N.5 CONCLUSION

It can be seen from the tables N.2 to N.7 that the height, H_r, at different mass flow rates, remains the same for a given outlet diameter of the cooling tower. It is shown in figure N.3 that as the diameter of the tower increases, the height, H_r, increases. Thus, the height from which air is drawn into the cooling tower is only a function of the diameter of the tower and not of the air mass flow rate through the tower. The influence of the height of the tower on the height from which air is drawn into the cooling tower can not be determined by analytical approaches but only by numerical analysis. It is therefore recommended that these results and the effect of the height of the tower be validated by numerical analysis.

APPENDIX O

A CRITICAL COOLING TOWER PERFORMANCE EVALUATION

The performance of natural and mechanical draft cooling towers is critically evaluated in chapter 4 by employing the Merkel, Poppe and *e-NTU* methods of analysis at different operating and ambient conditions respectively. The figures pertaining to the discussion in chapter 4 are presented in this appendix.

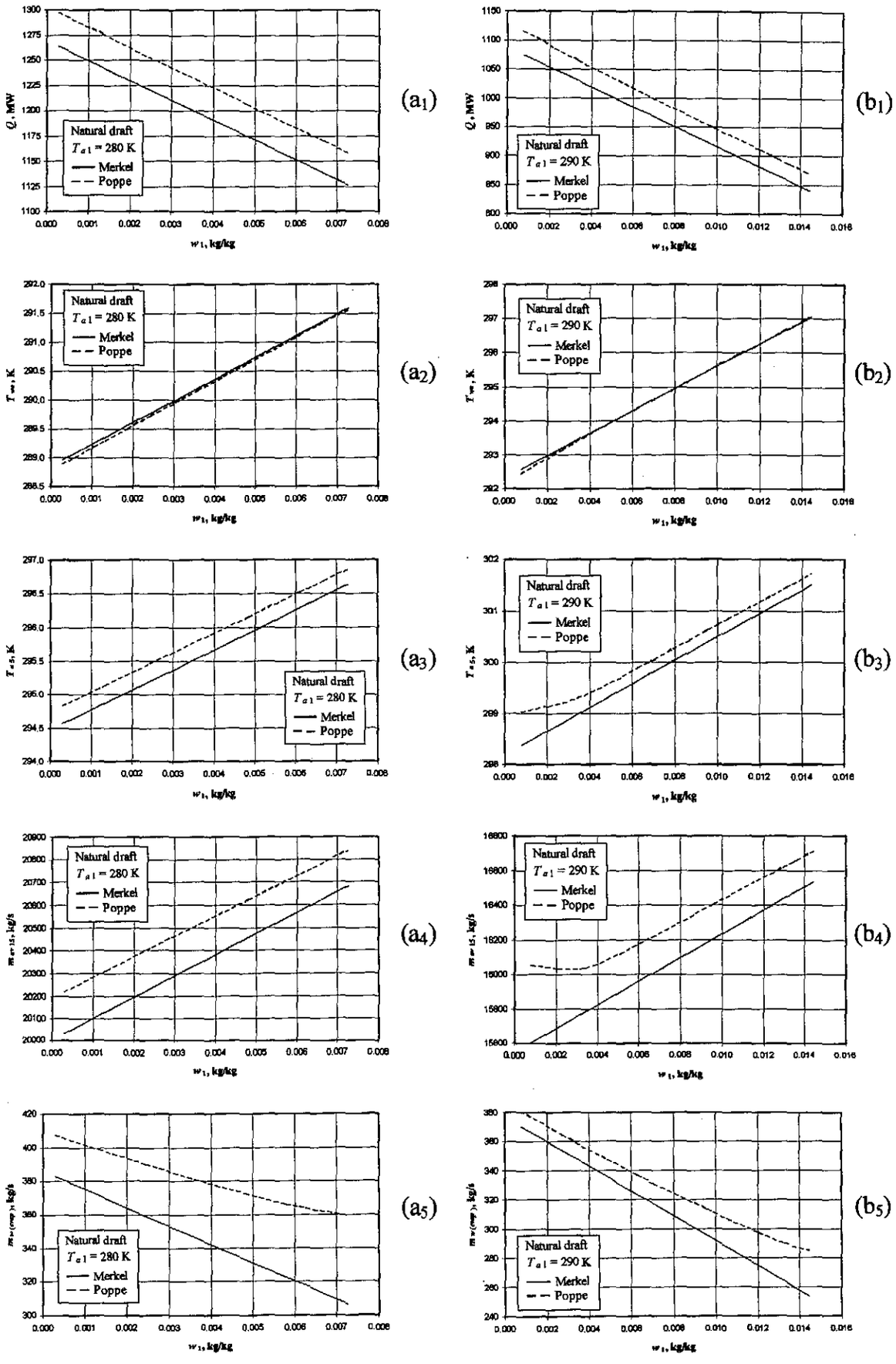

Figure O.1: Performance curves of a natural draft cooling tower.

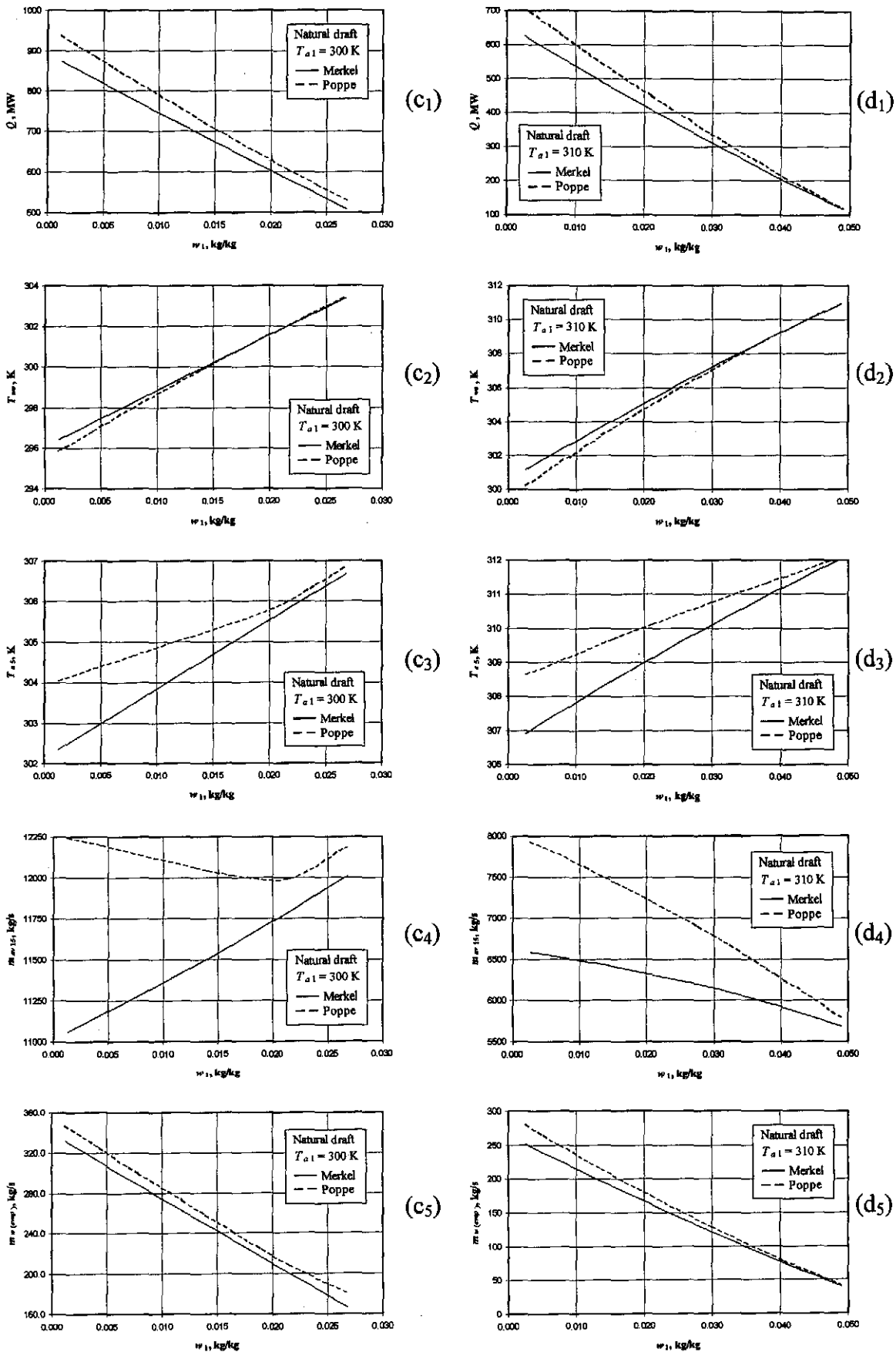

Figure O.1: Performance curves of a natural draft cooling tower.

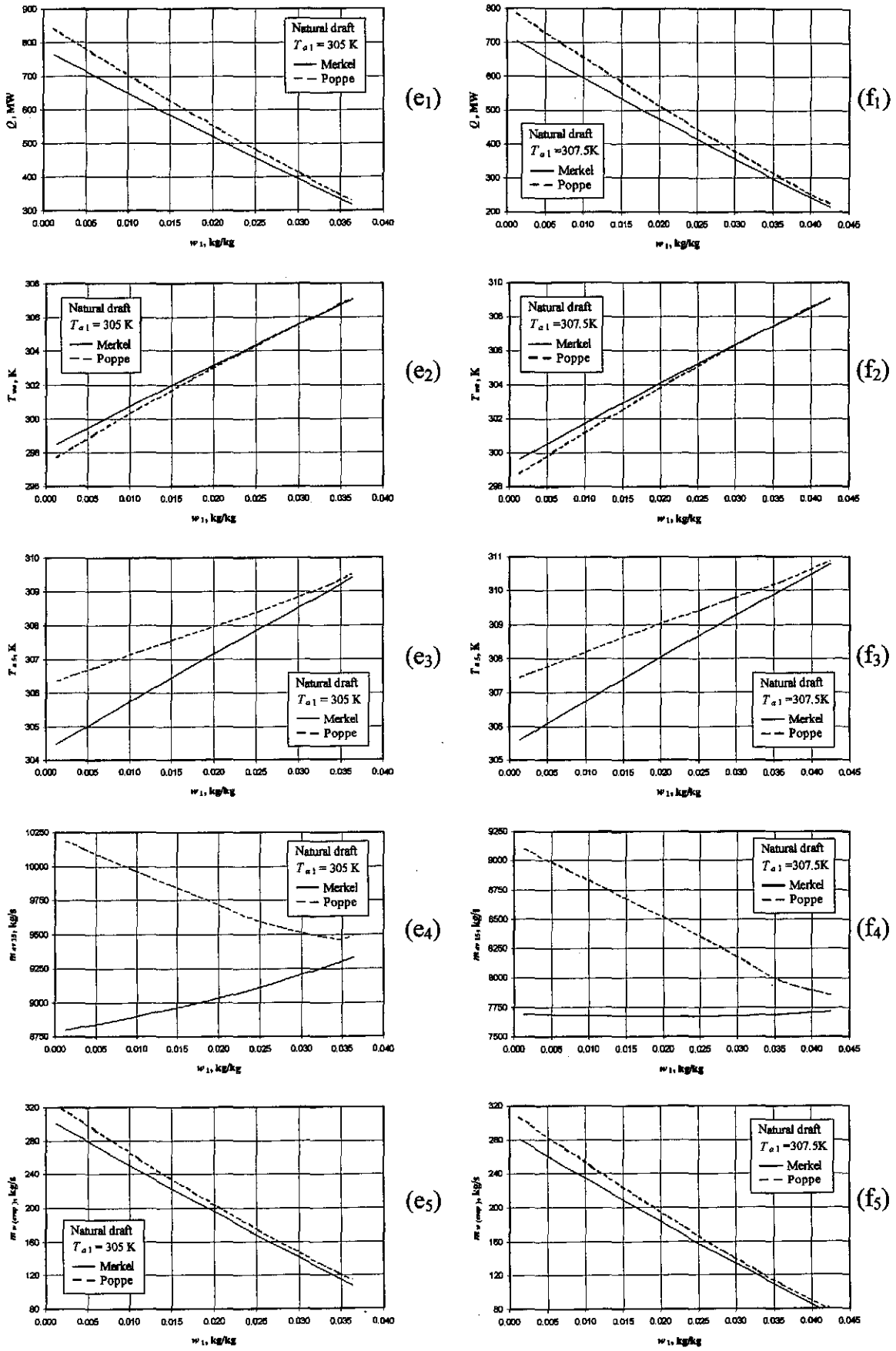

Figure O.1: Performance curves of a natural draft cooling tower.

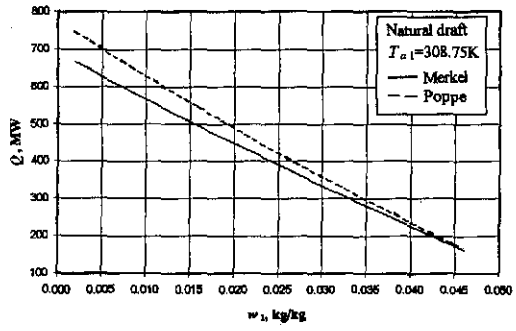

(g1)

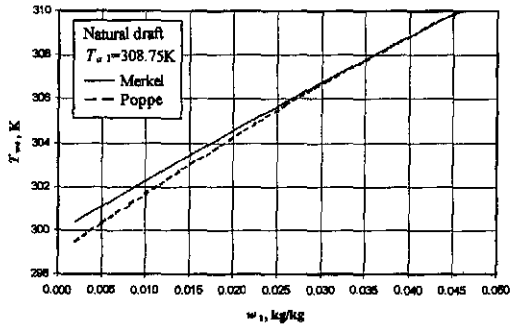

(g2)

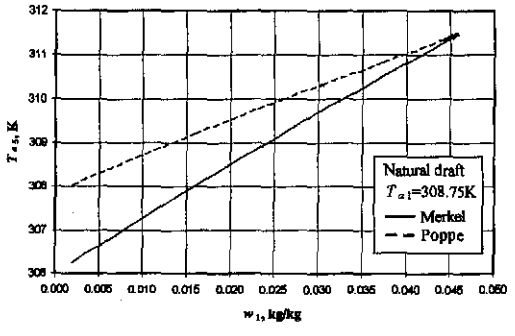

(g3)

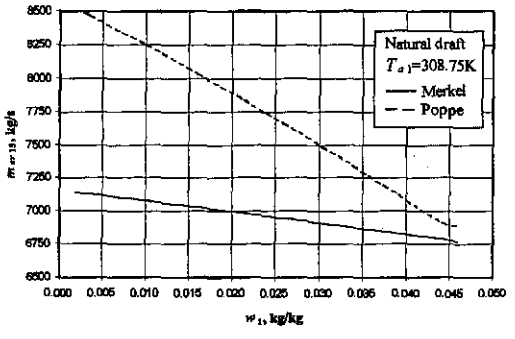

(g4)

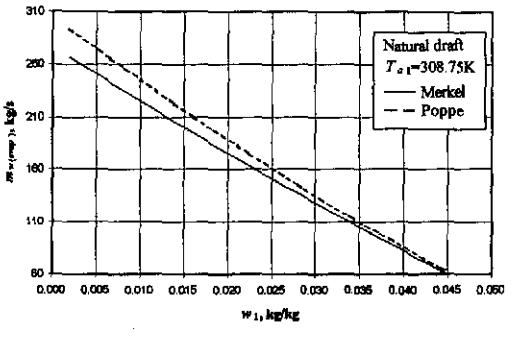

(g5)

Figure O.1: Performance curves of a natural draft cooling tower.

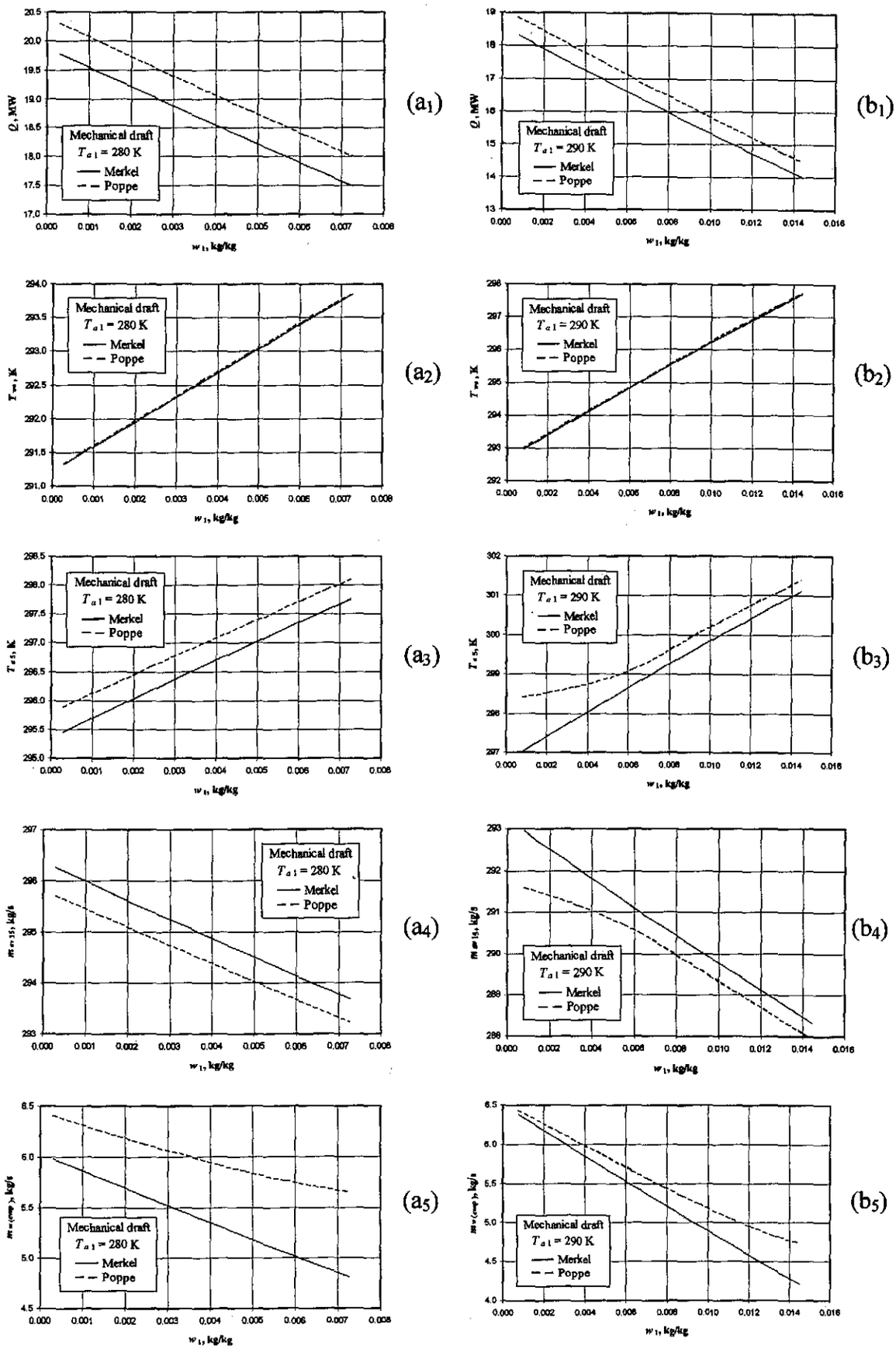

Figure O.2: Performance curves of a mechanical draft cooling tower.

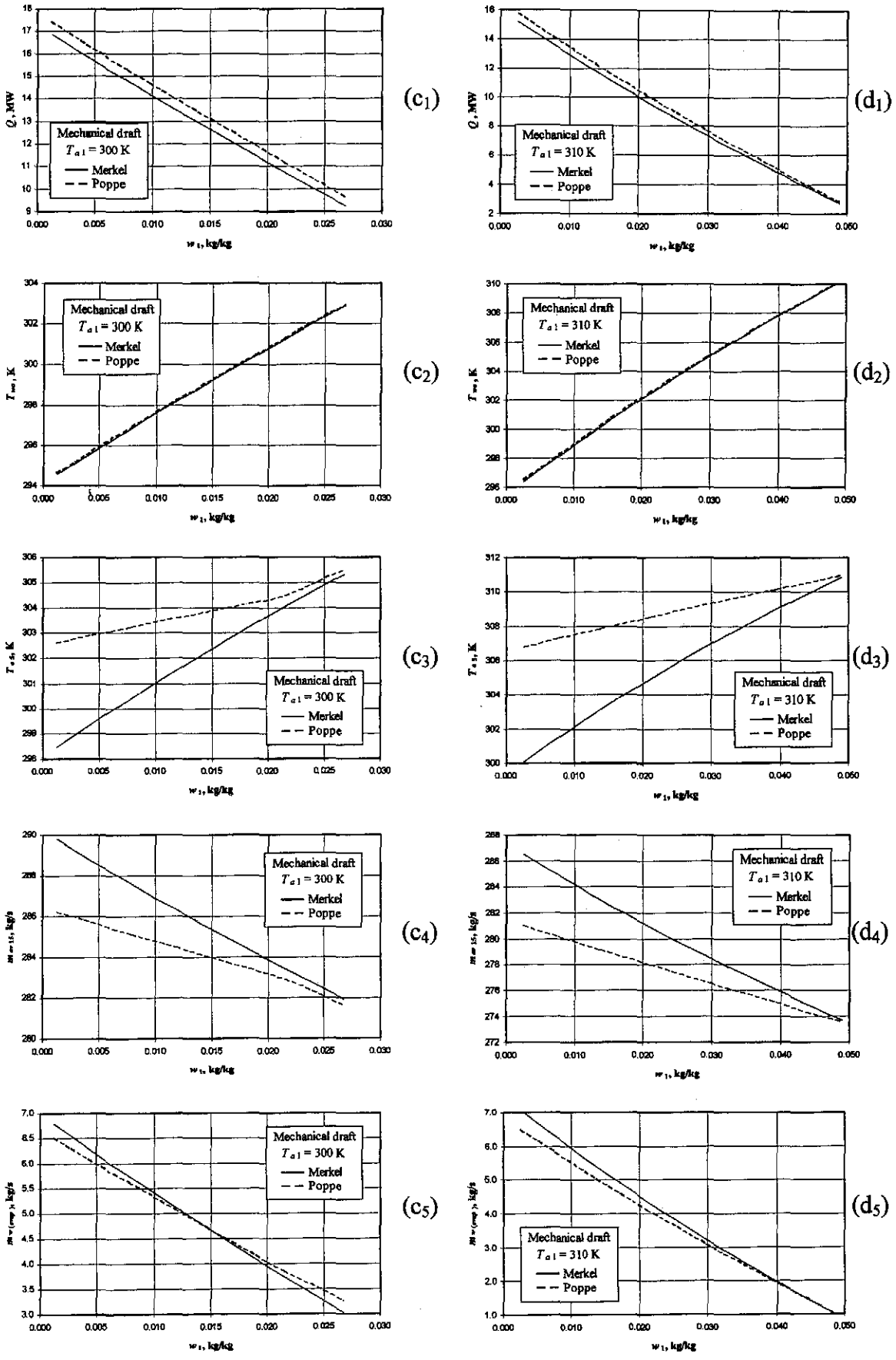

Figure O.2: Performance curves of a mechanical draft cooling tower.

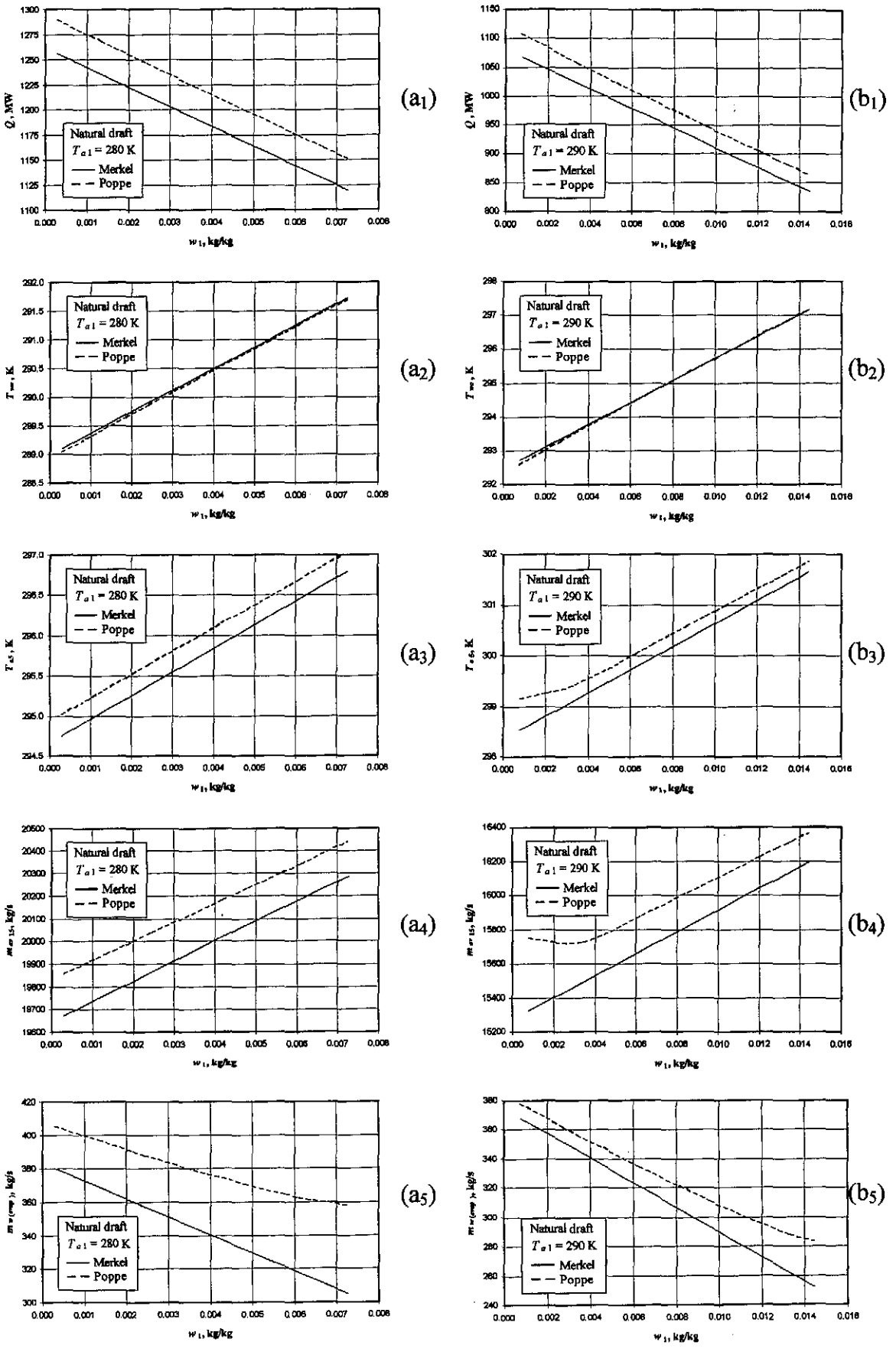

Figure O.3: Performance curves of a natural draft cooling tower with a simplified draft equation.

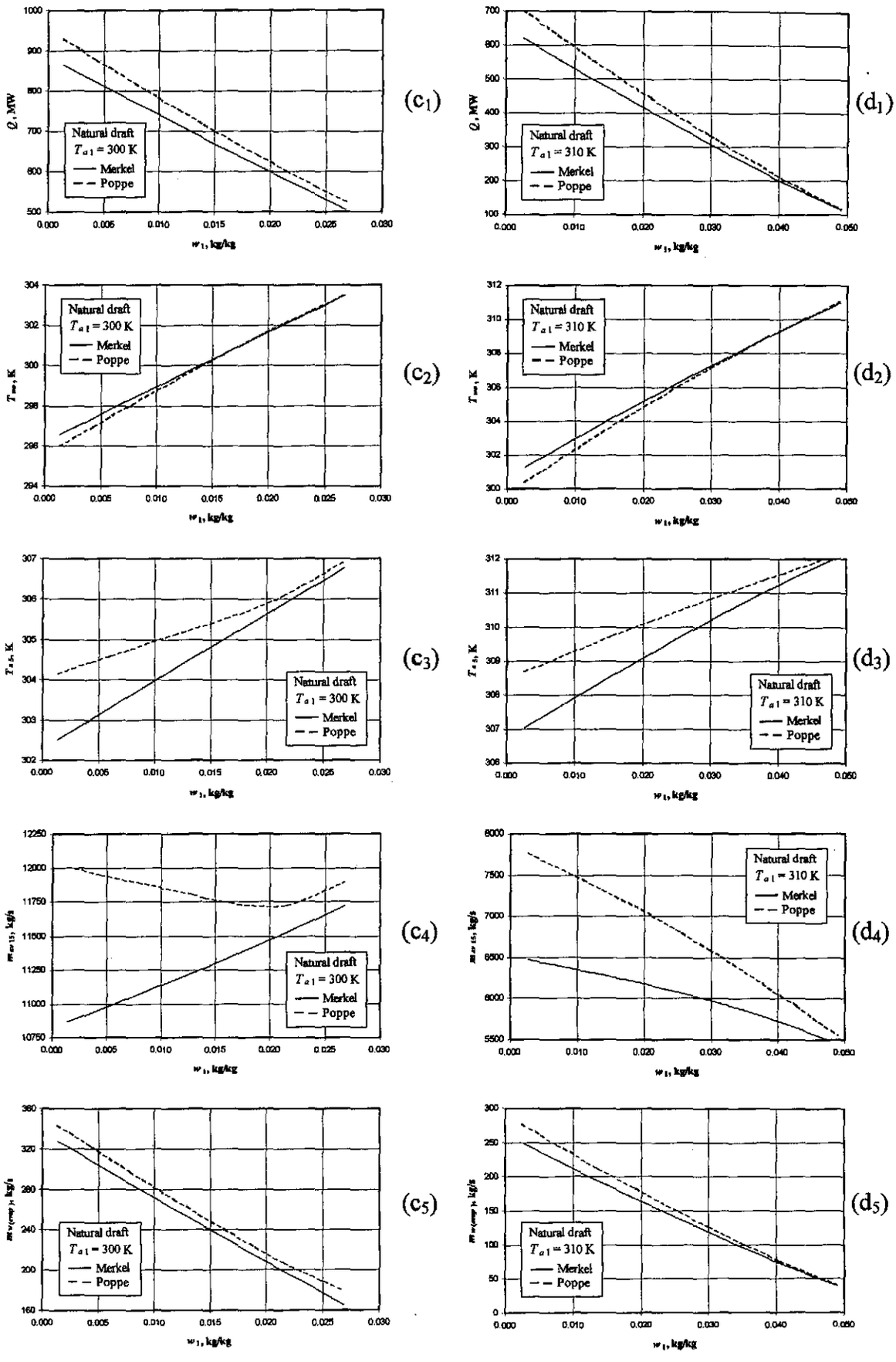

Figure O.3: Performance curves of a natural draft cooling tower with a simplified draft equation.

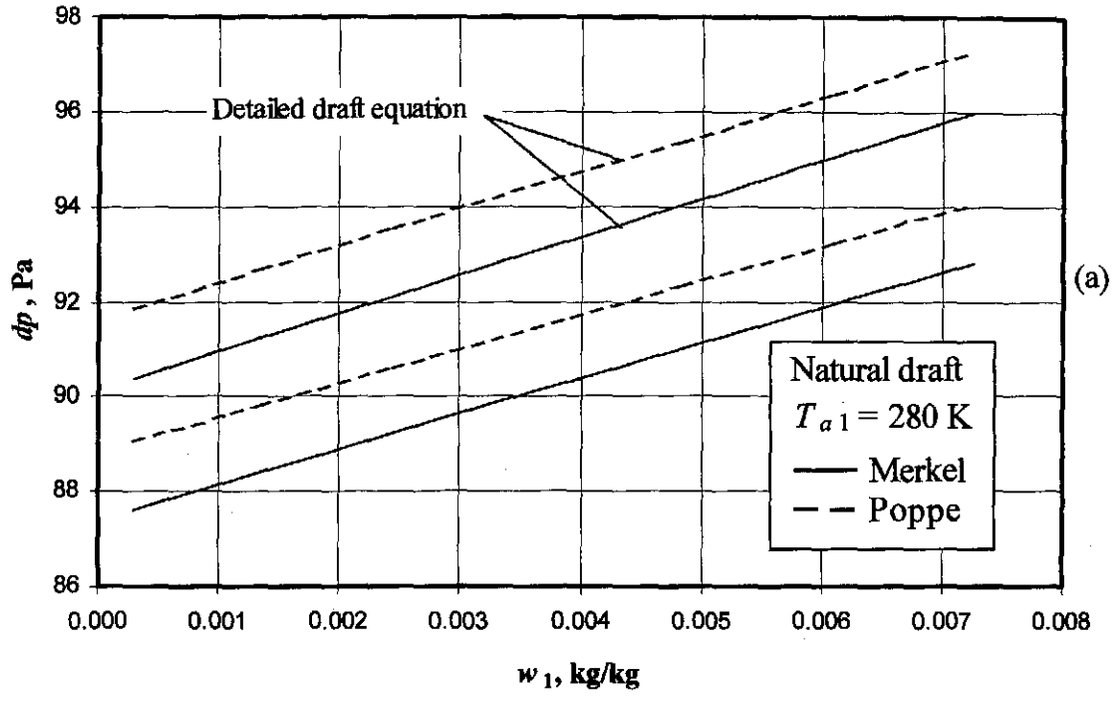

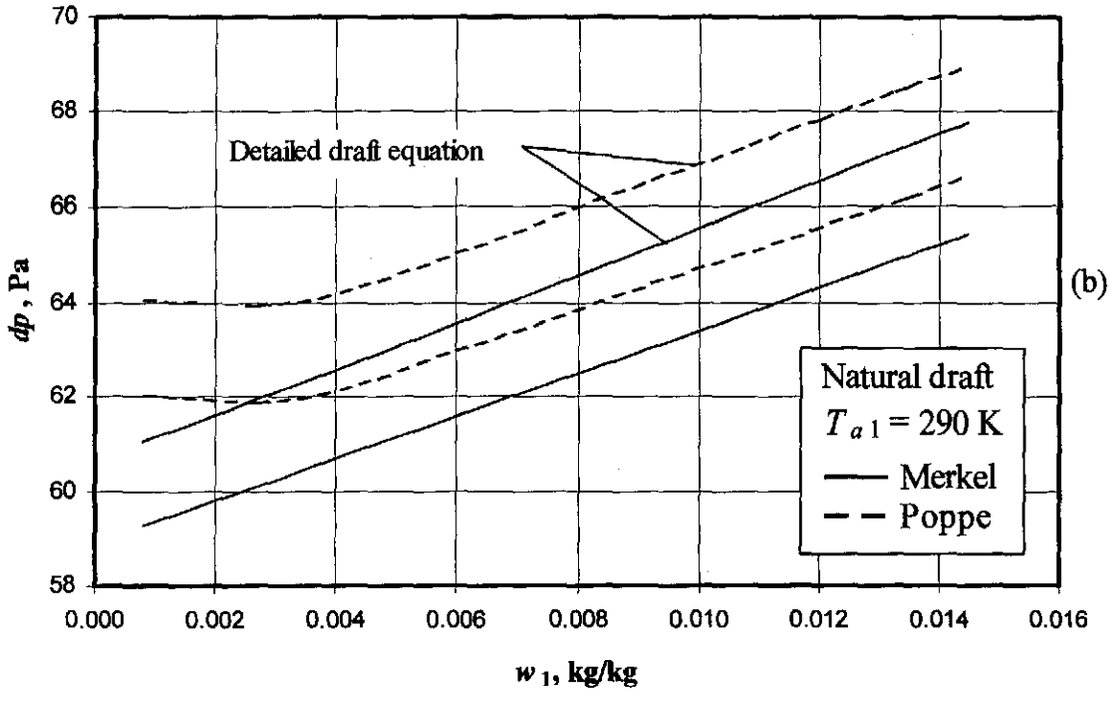

Figure O.4: The difference in the pressure differential between the simplified and detailed draft equations for both the Merkel and Poppe approaches.

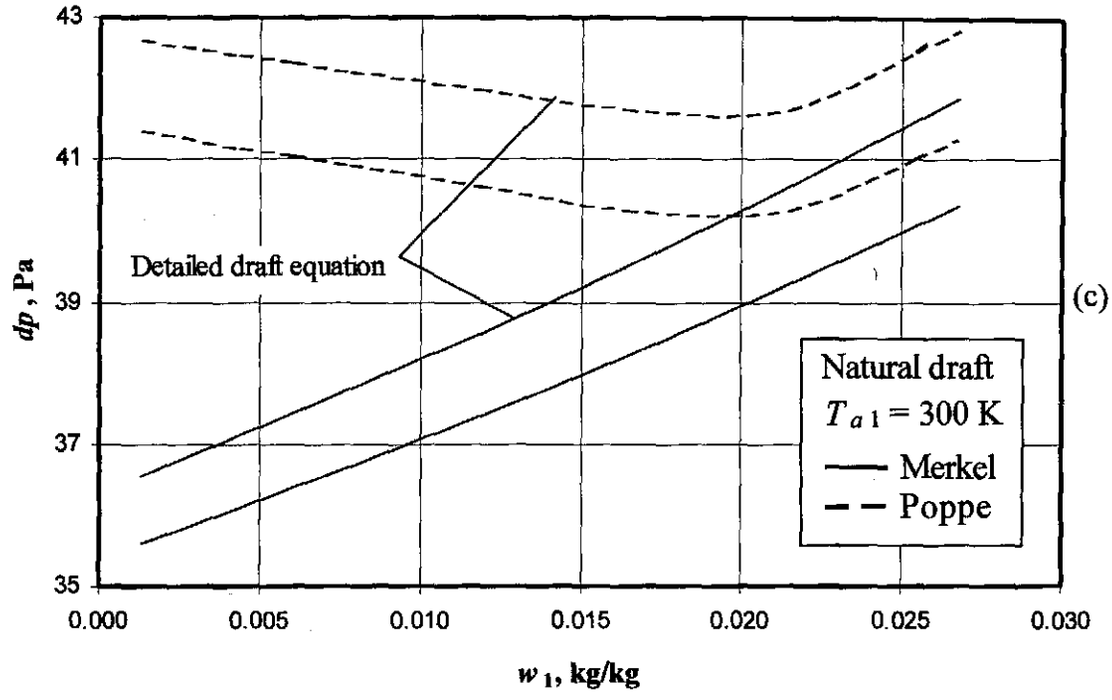

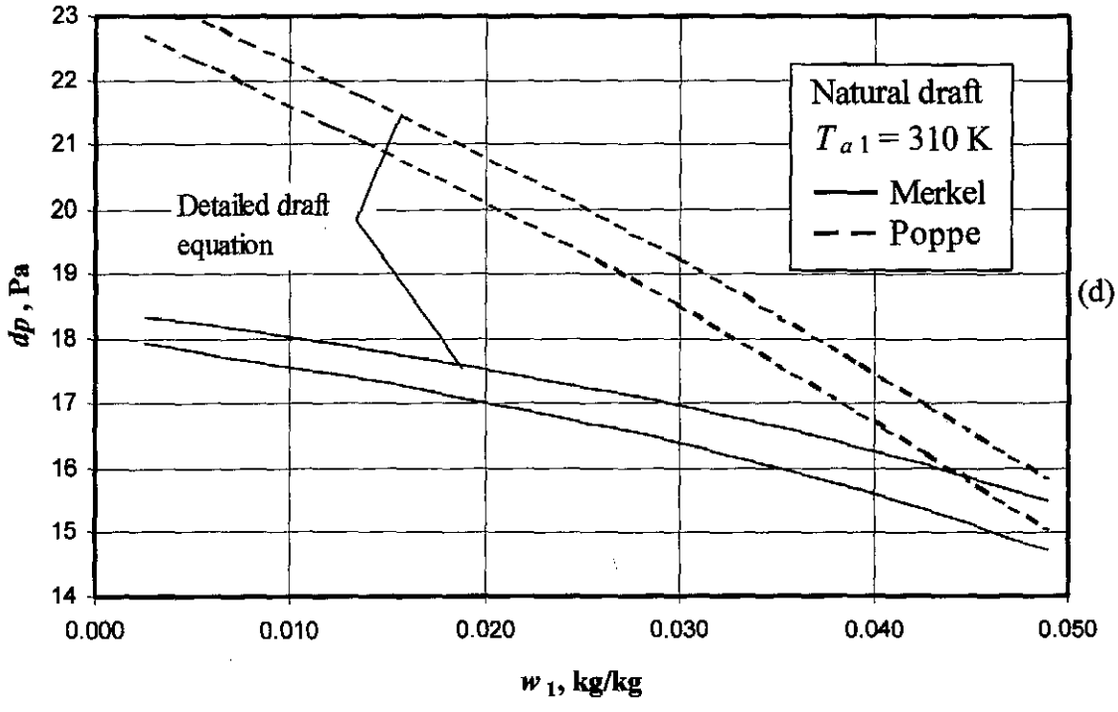

Figure O.4: The difference in the pressure differential between the simplified and detailed draft equations for both the Merkel and Poppe approaches.

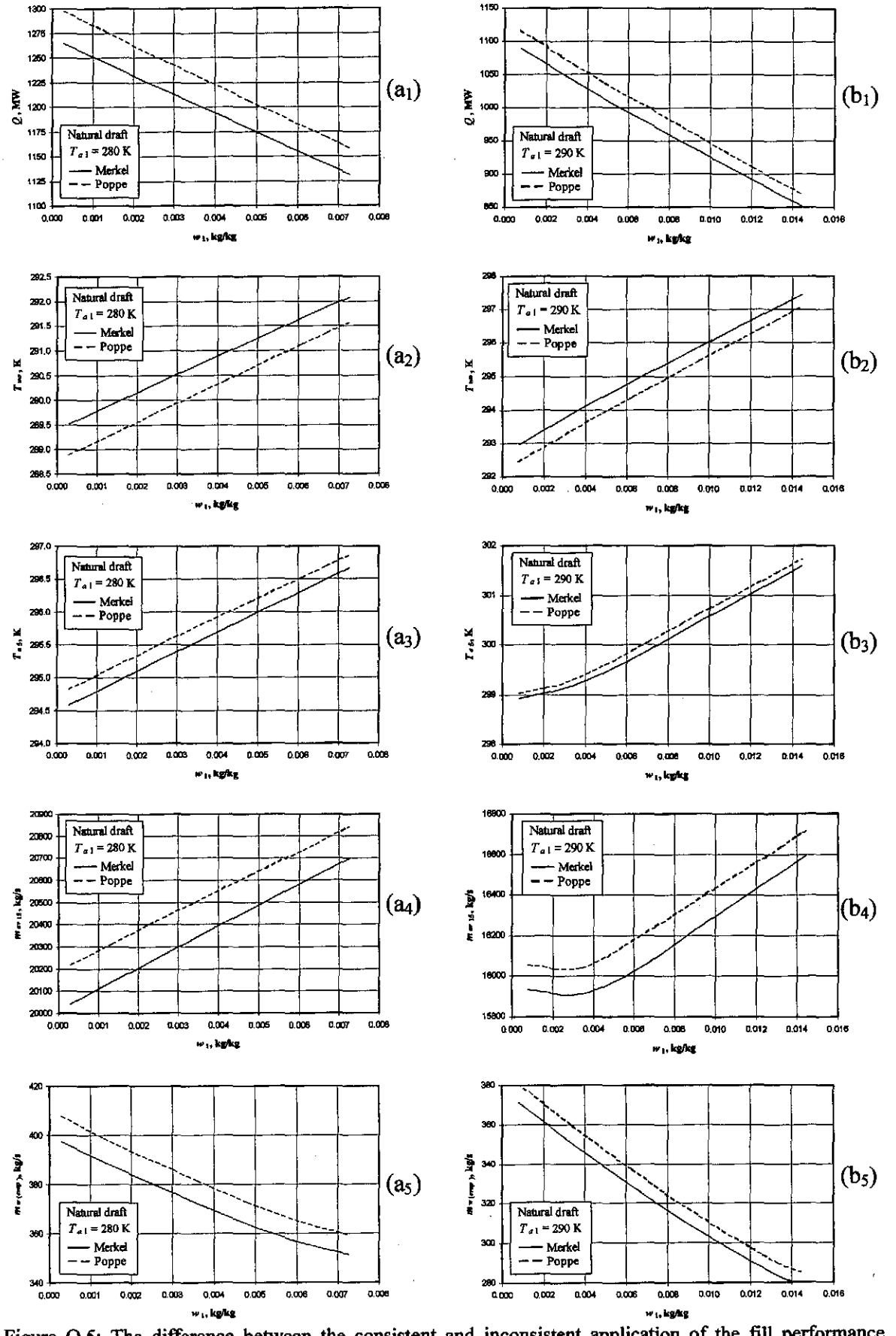

Figure O.5: The difference between the consistent and inconsistent application of the fill performance characteristics while employing the Poppe approach to determine the performance of a natural draft cooling tower.

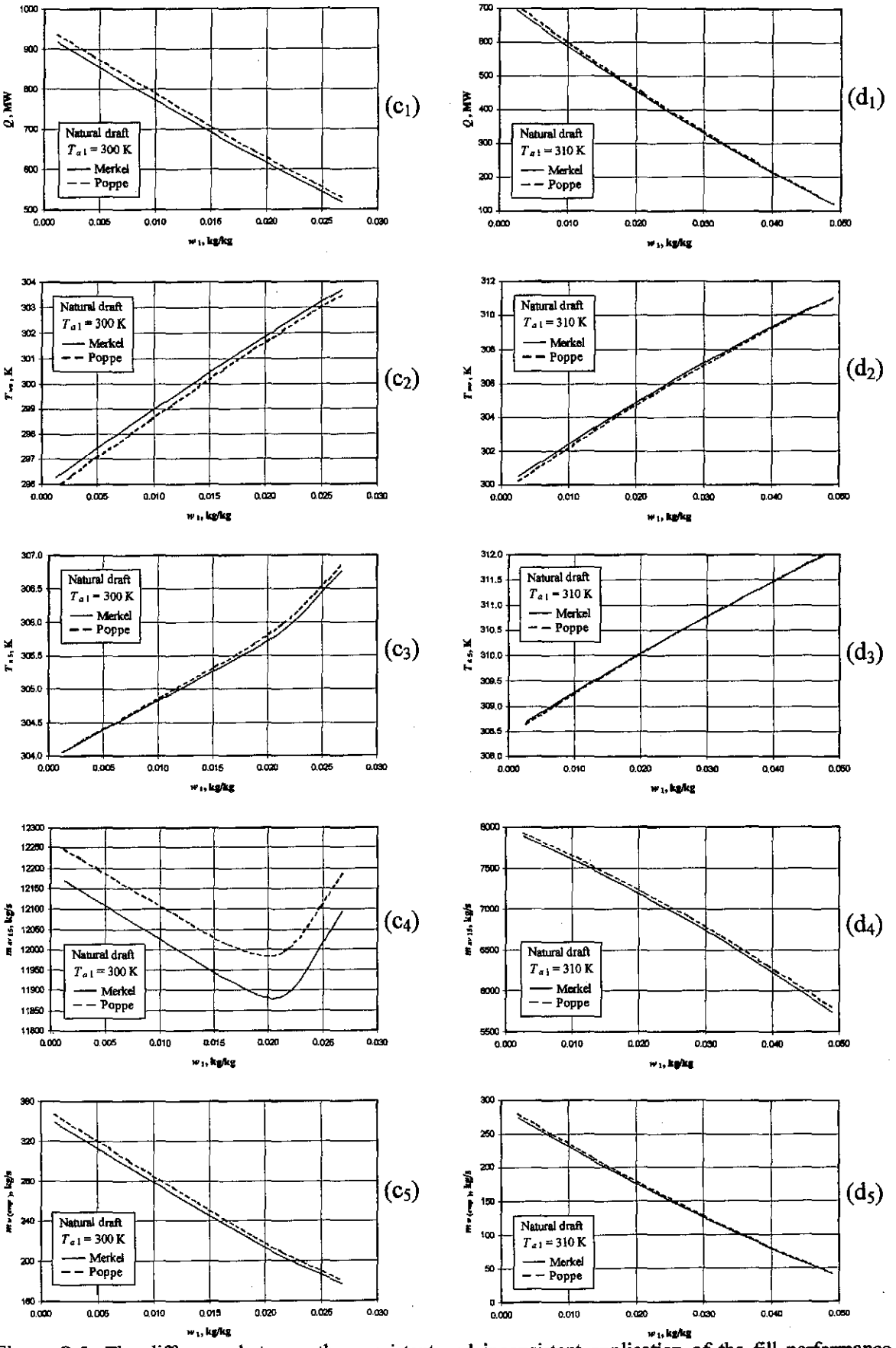

Figure O.5: The difference between the consistent and inconsistent application of the fill performance characteristics while employing the Poppe approach to determine the performance of a natural draft cooling tower.

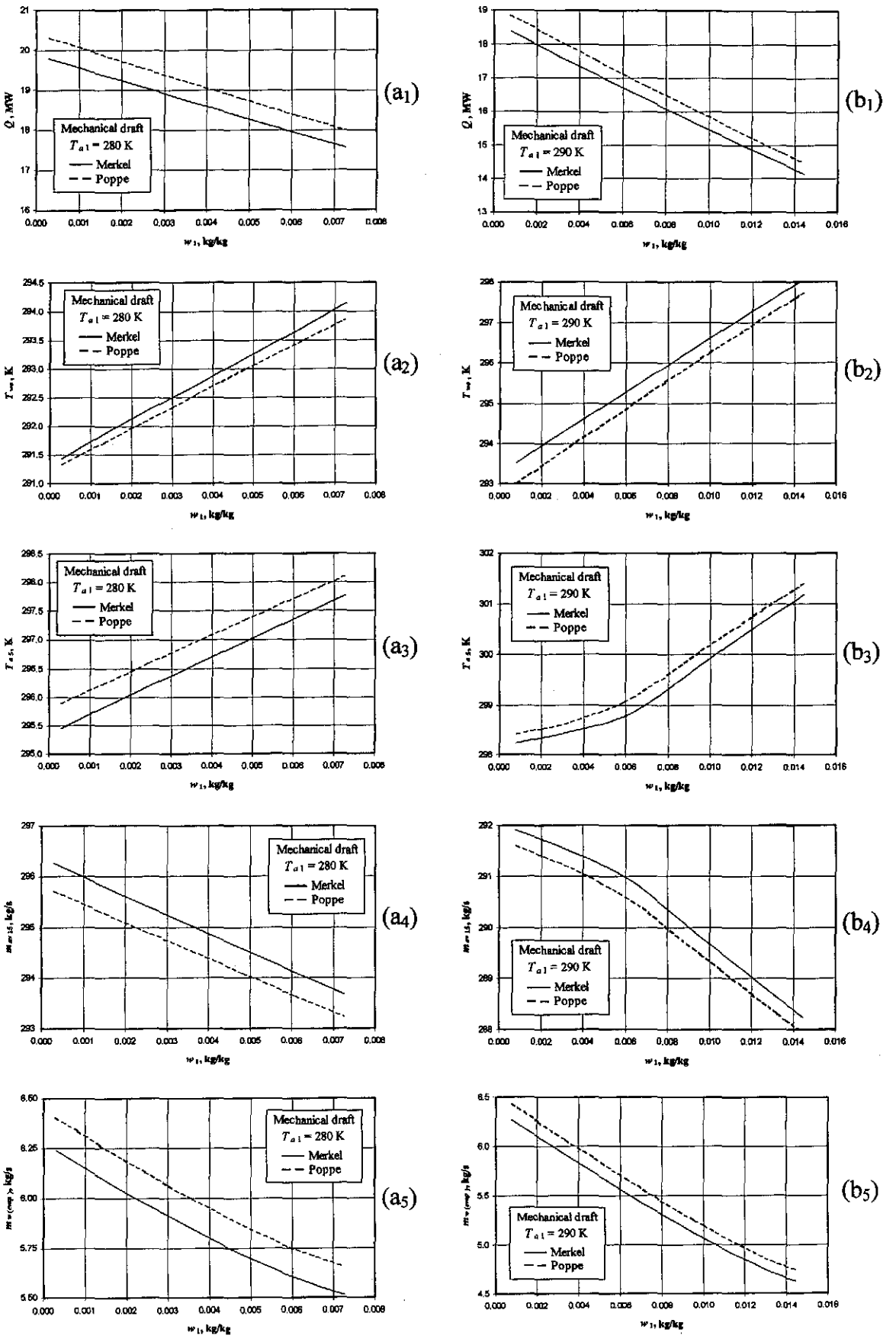

Figure O.6: The difference between the consistent and inconsistent application of the fill performance characteristics while employing the Poppe approach to determine the performance of a mechanical draft cooling tower.

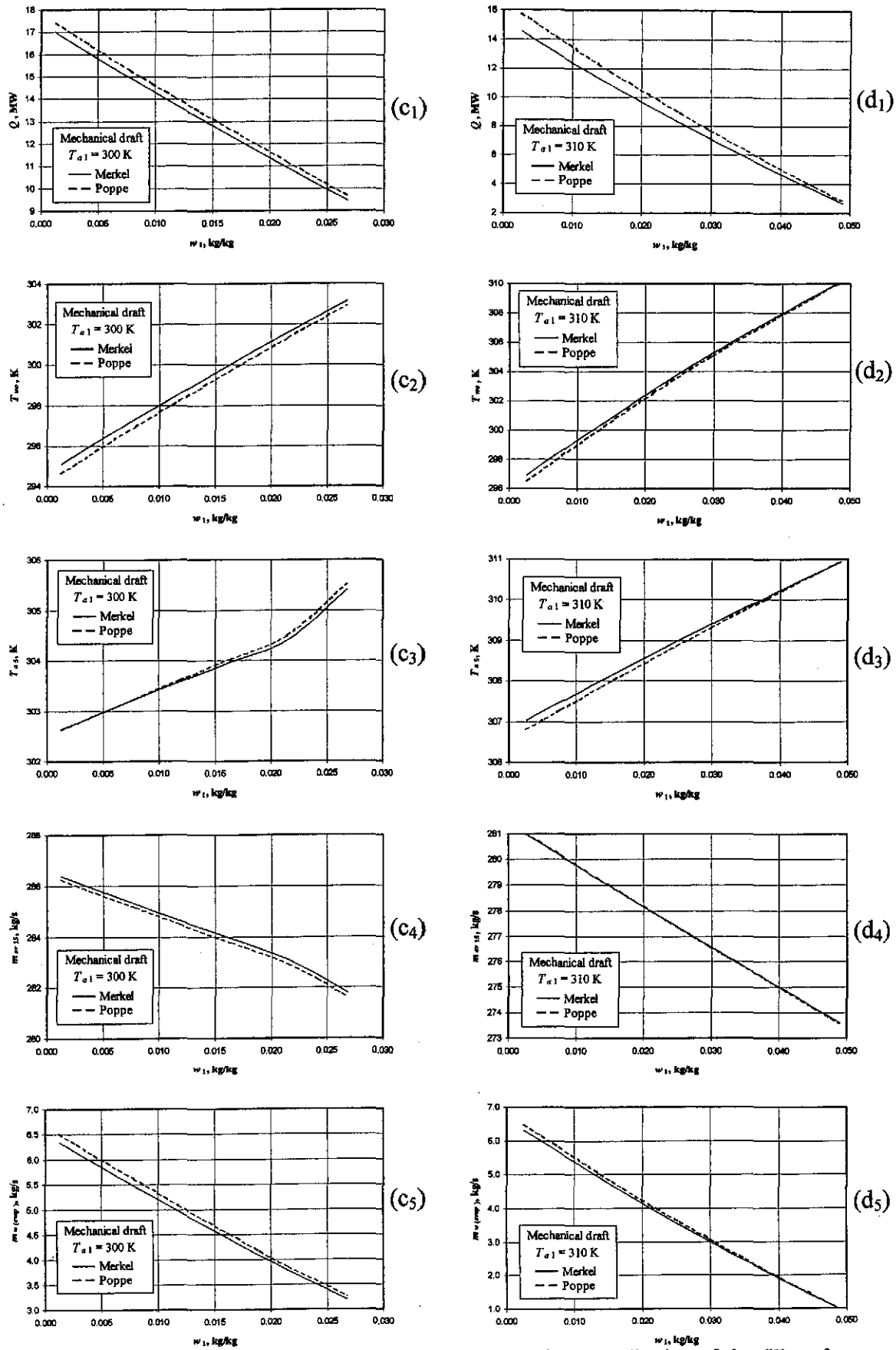

Figure O.6: The difference between the consistent and inconsistent application of the fill performance characteristics while employing the Poppe approach to determine the performance of a mechanical draft cooling tower.

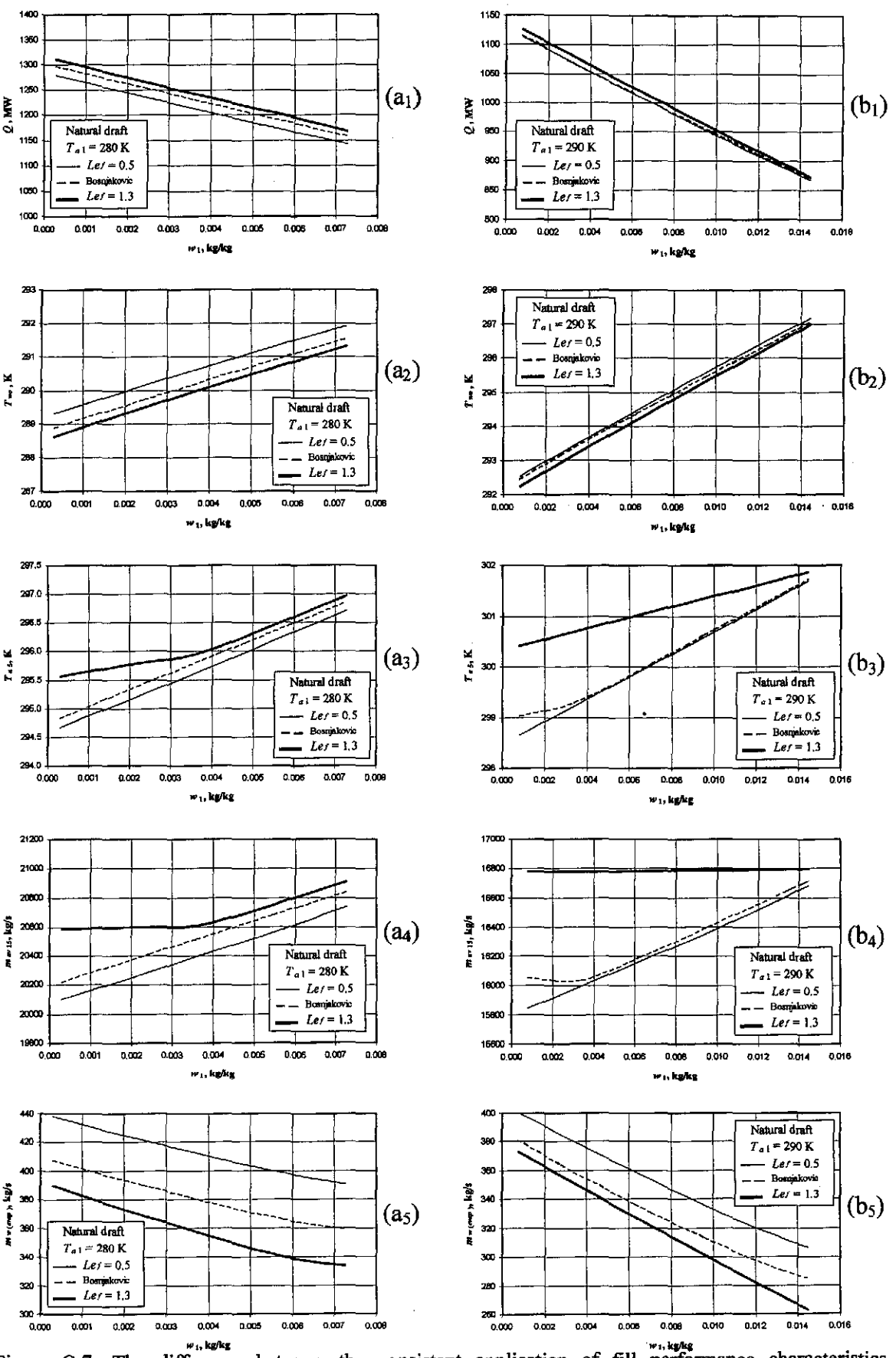

Figure O.7: The difference between the consistent application of fill performance characteristics, determined for different Lewis numbers, while employing the Poppe approach to determine the performance of a natural draft cooling tower.

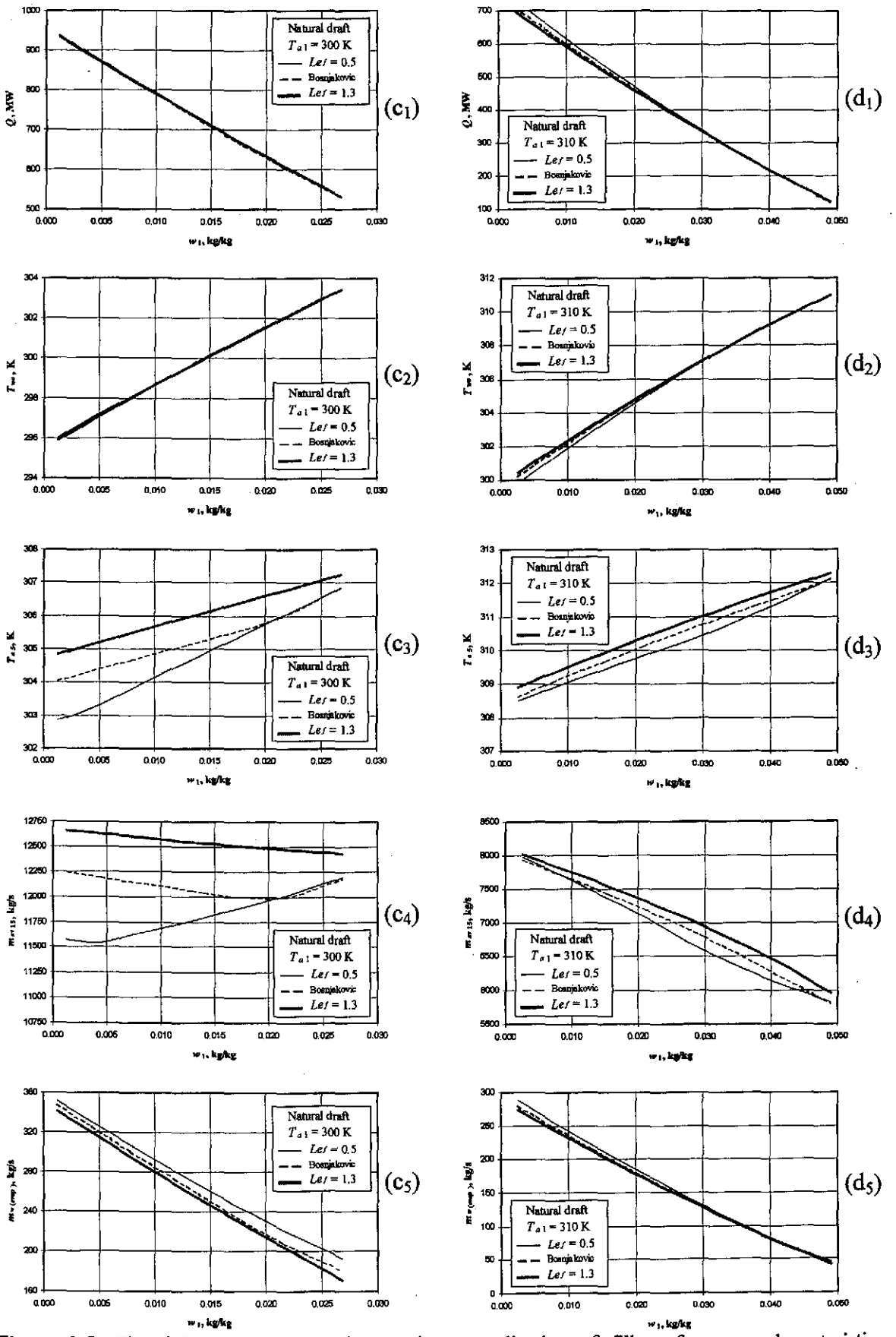

Figure O.7: The difference between the consistent application of fill performance characteristics, determined for different Lewis numbers, while employing the Poppe approach to determine the performance of a natural draft cooling tower.

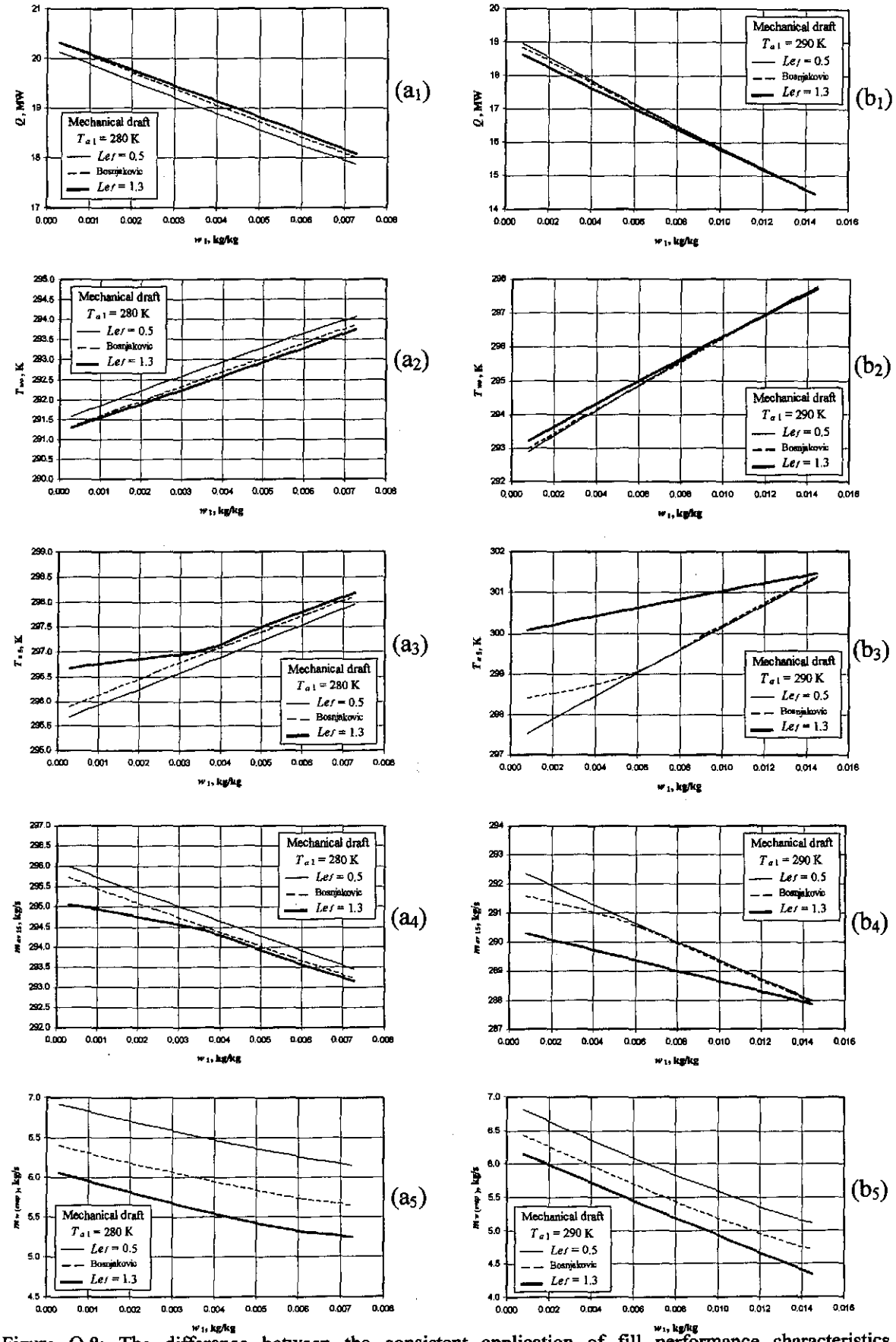

Figure O.8: The difference between the consistent application of fill performance characteristics, determined for different Lewis numbers, while employing the Poppe approach to determine the performance of a mechanical draft cooling tower.

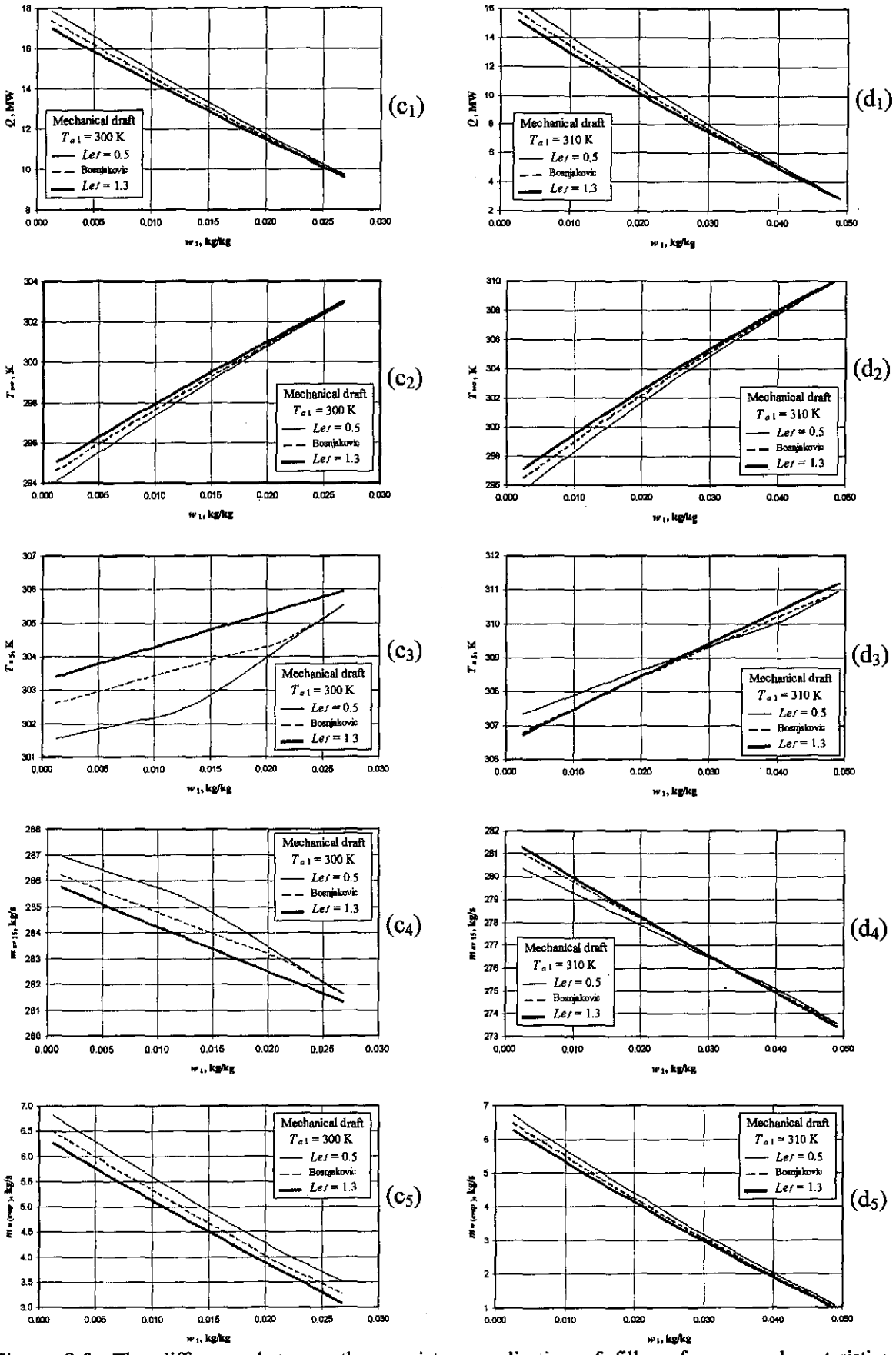

Figure O.8: The difference between the consistent application of fill performance characteristics, determined for different Lewis numbers, while employing the Poppe approach to determine the performance of a mechanical draft cooling tower.

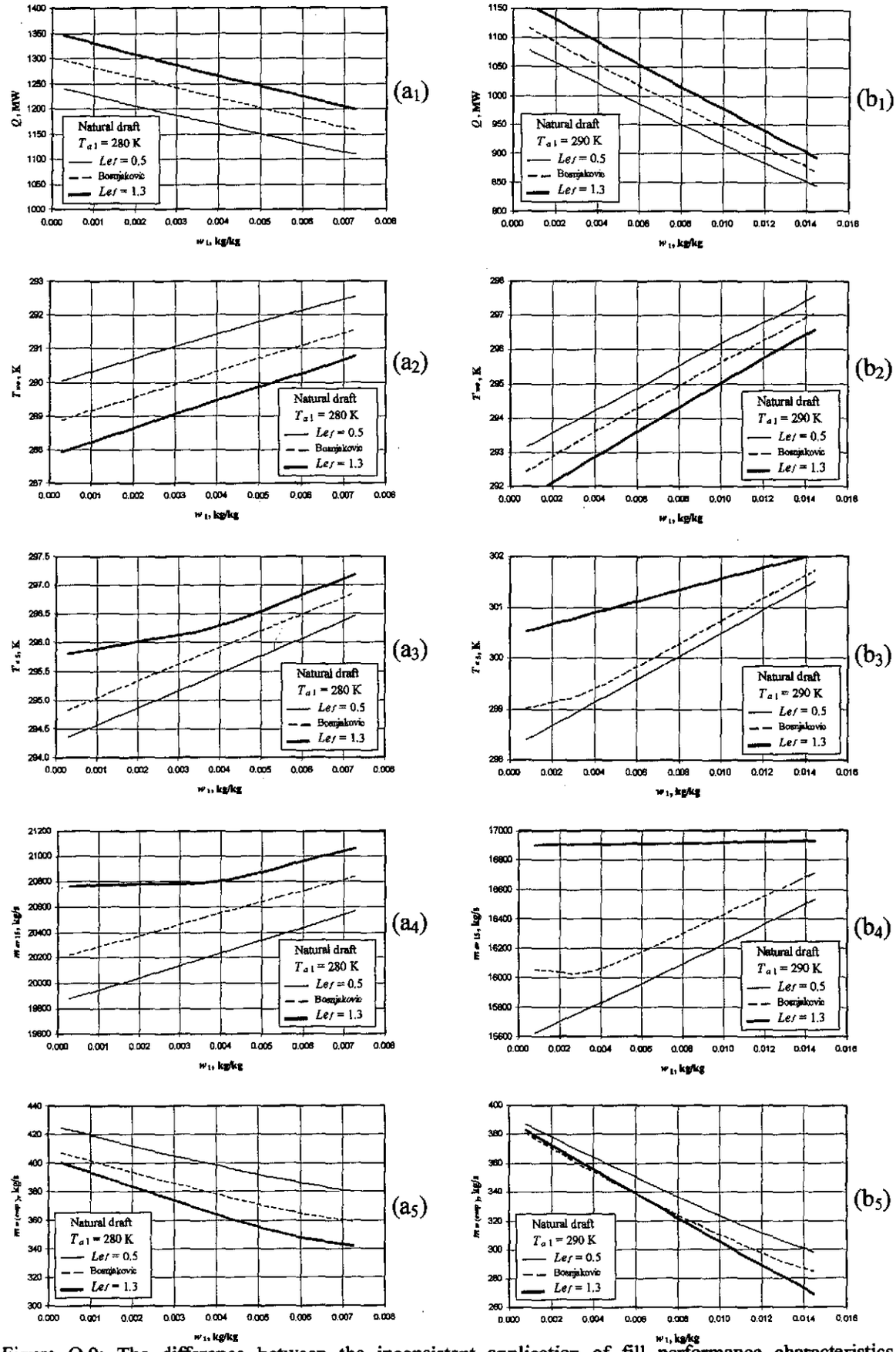

Figure O.9: The difference between the inconsistent application of fill performance characteristics, determined for different Lewis numbers, while employing the Poppe approach to determine the performance of a natural draft cooling tower.

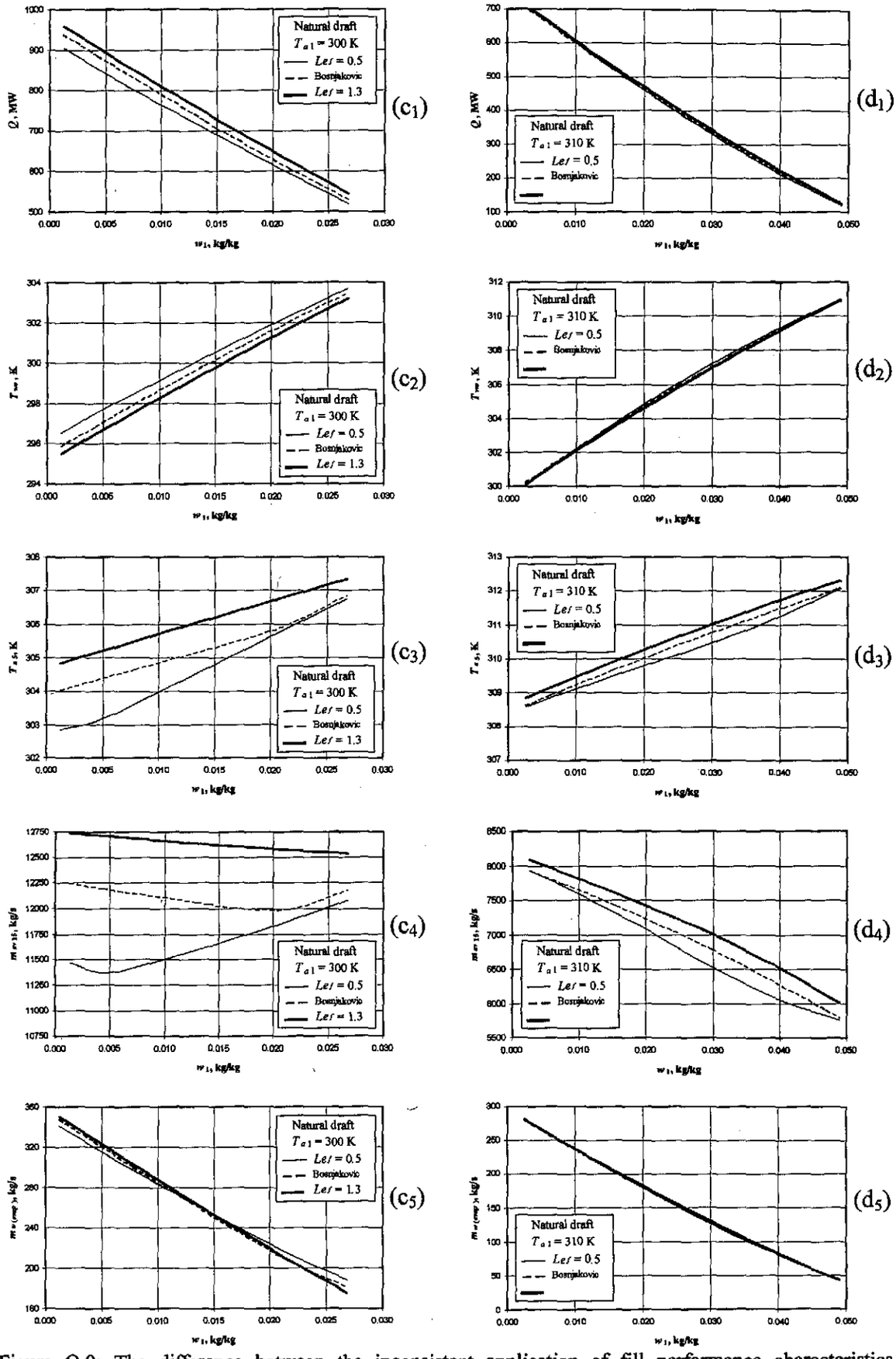

Figure O.9: The difference between the inconsistent application of fill performance characteristics, determined for different Lewis numbers, while employing the Poppe approach to determine the performance of a natural draft cooling tower.

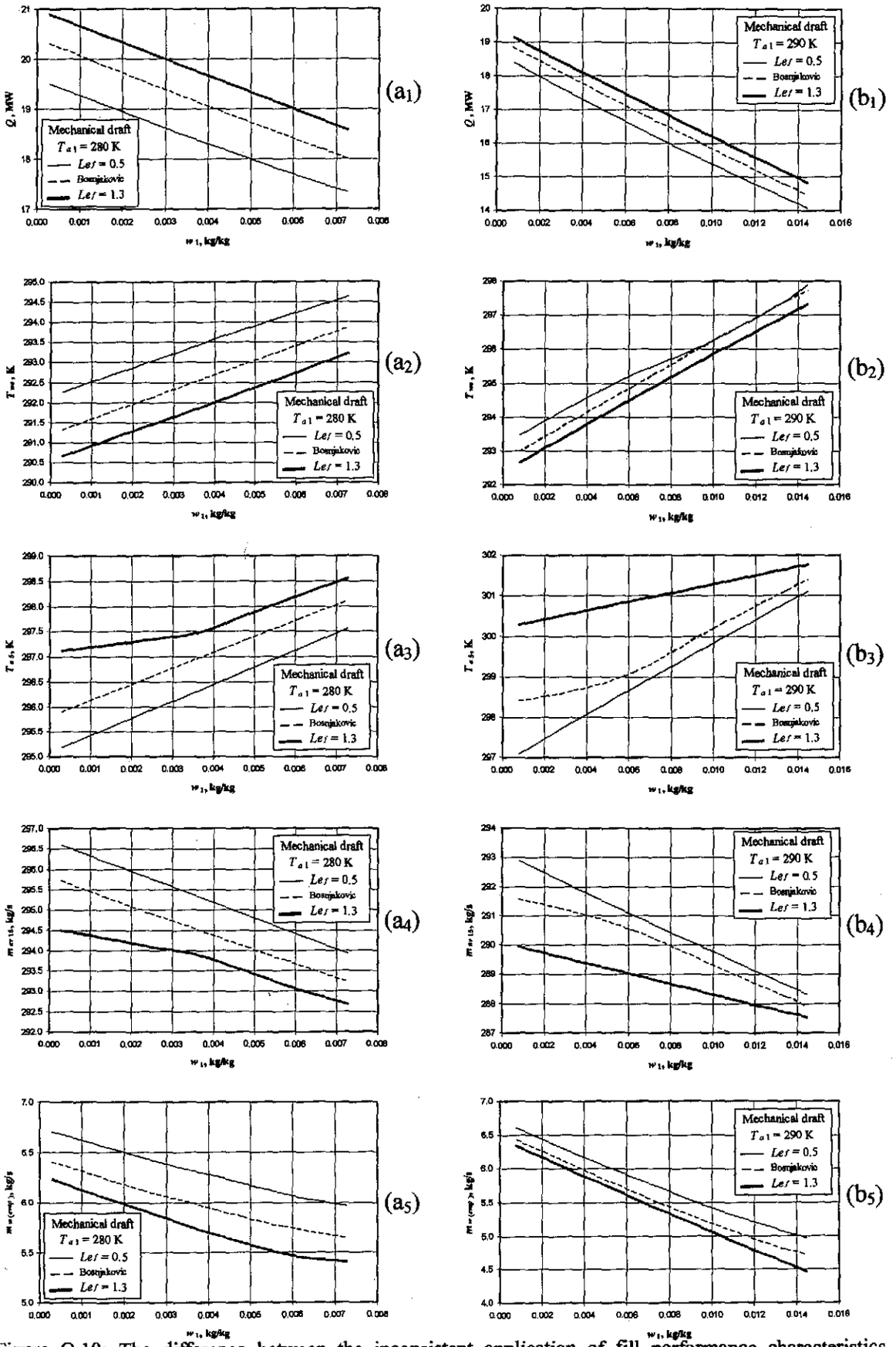

Figure O.10: The difference between the inconsistent application of fill performance characteristics, determined for different Lewis numbers, while employing the Poppe approach to determine the performance of a mechanical draft cooling tower.

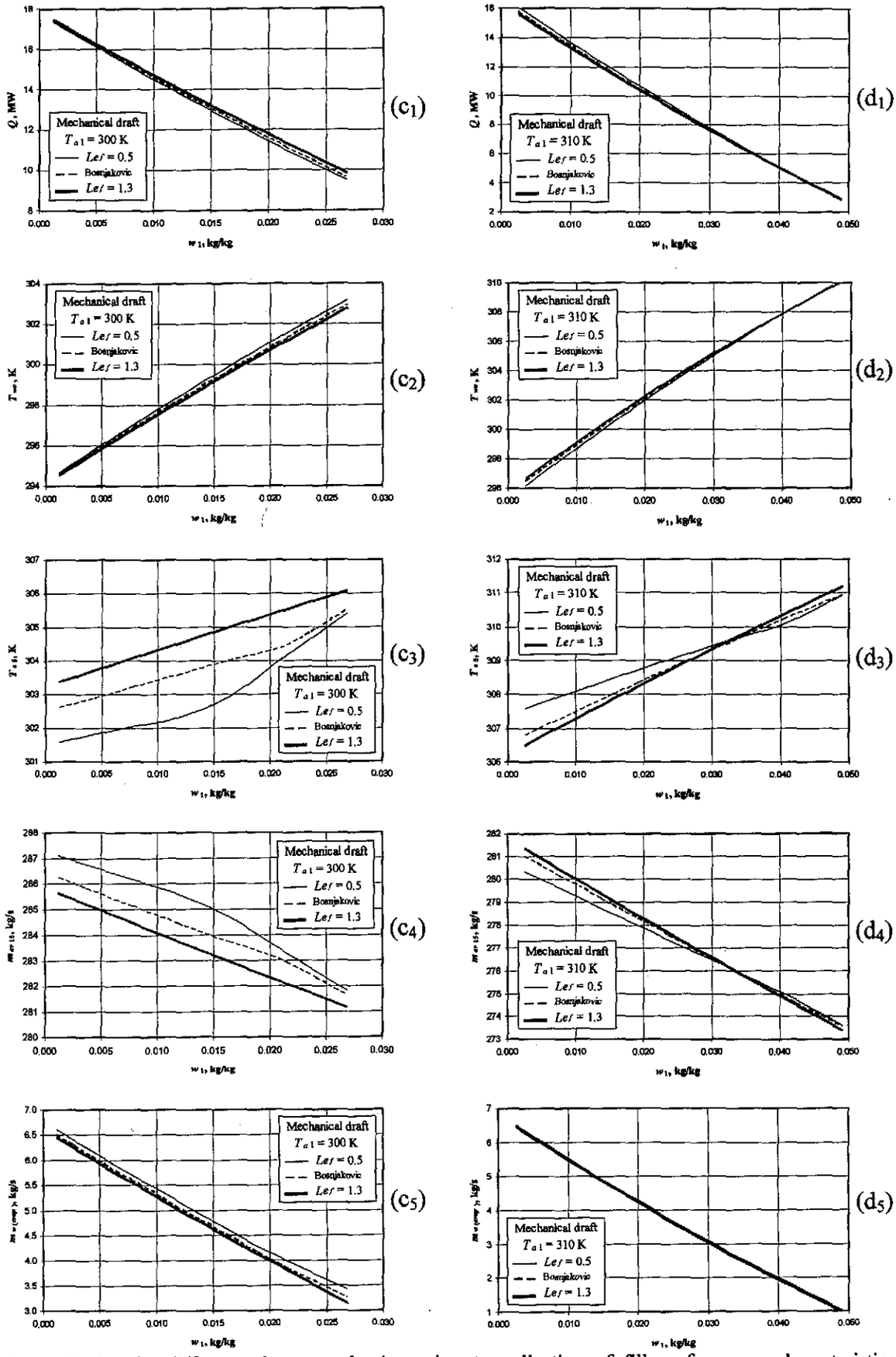

Figure O.10: The difference between the inconsistent application of fill performance characteristics, determined for different Lewis numbers, while employing the Poppe approach to determine the performance of a mechanical draft cooling tower.

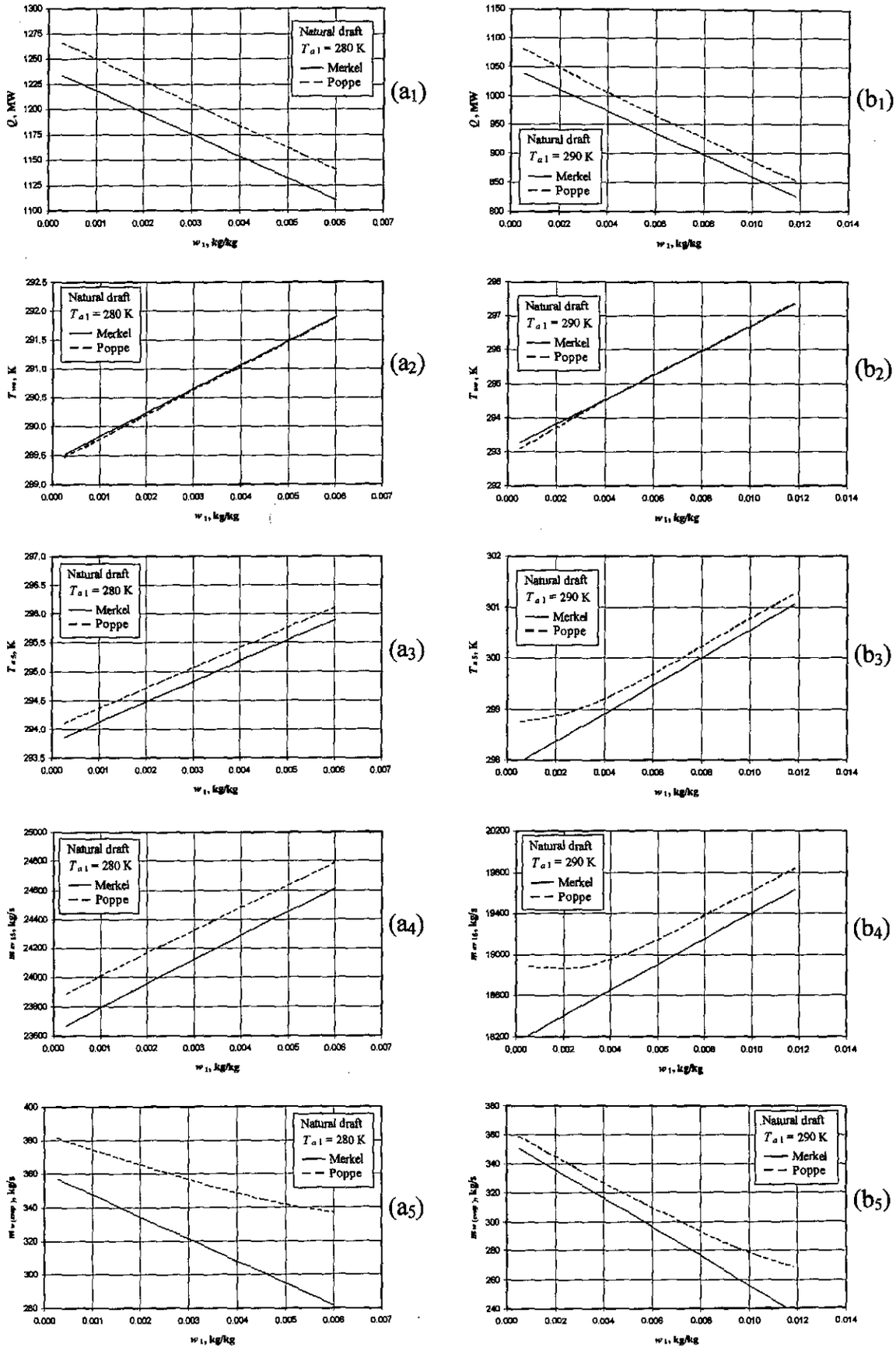

Figure O.11: Performance curves of a natural draft cooling tower at an atmospheric pressure of 101325 Pa.

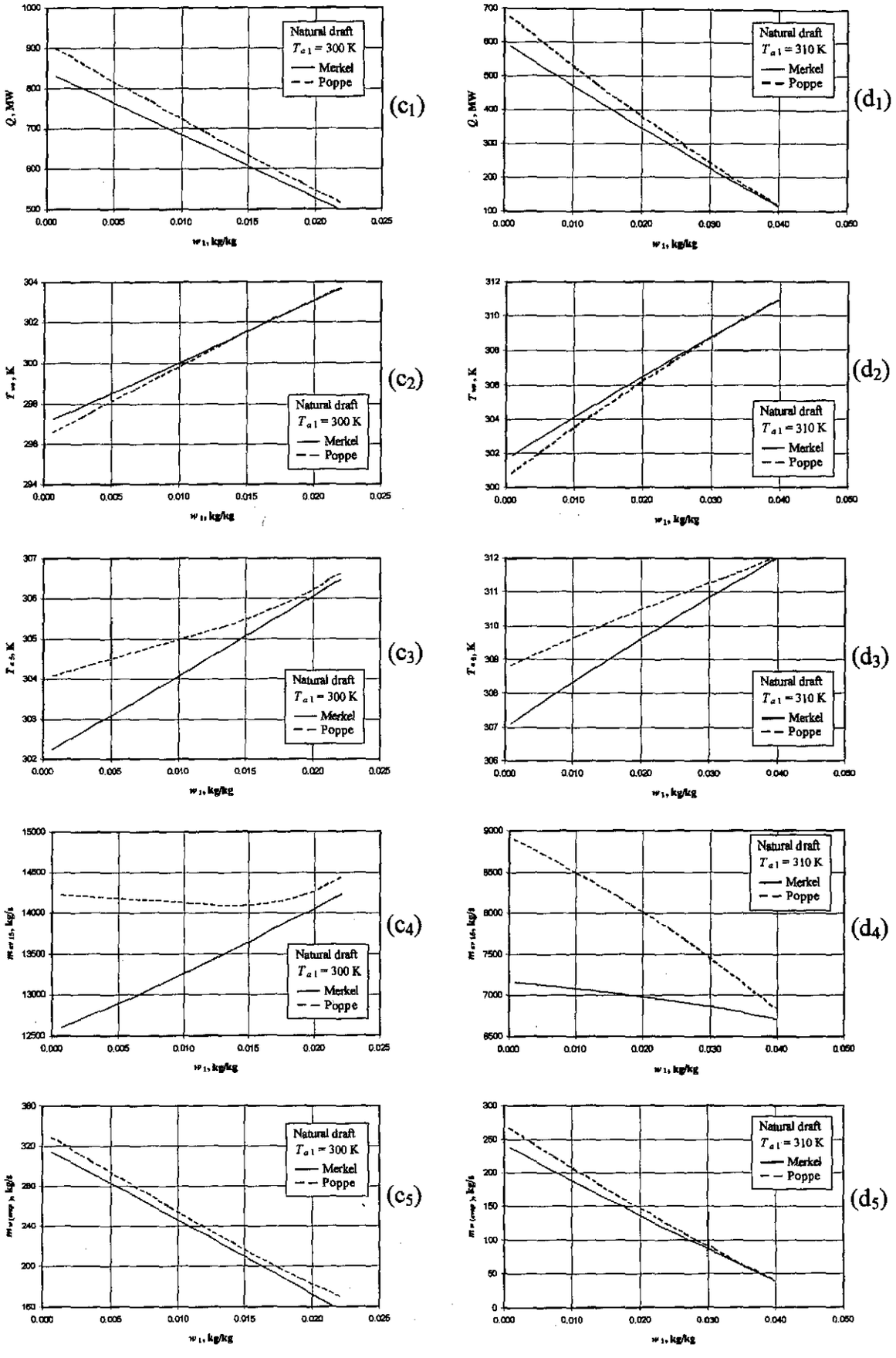

Figure O.11: Performance curves of a natural draft cooling tower at an atmospheric pressure of 101325 Pa.

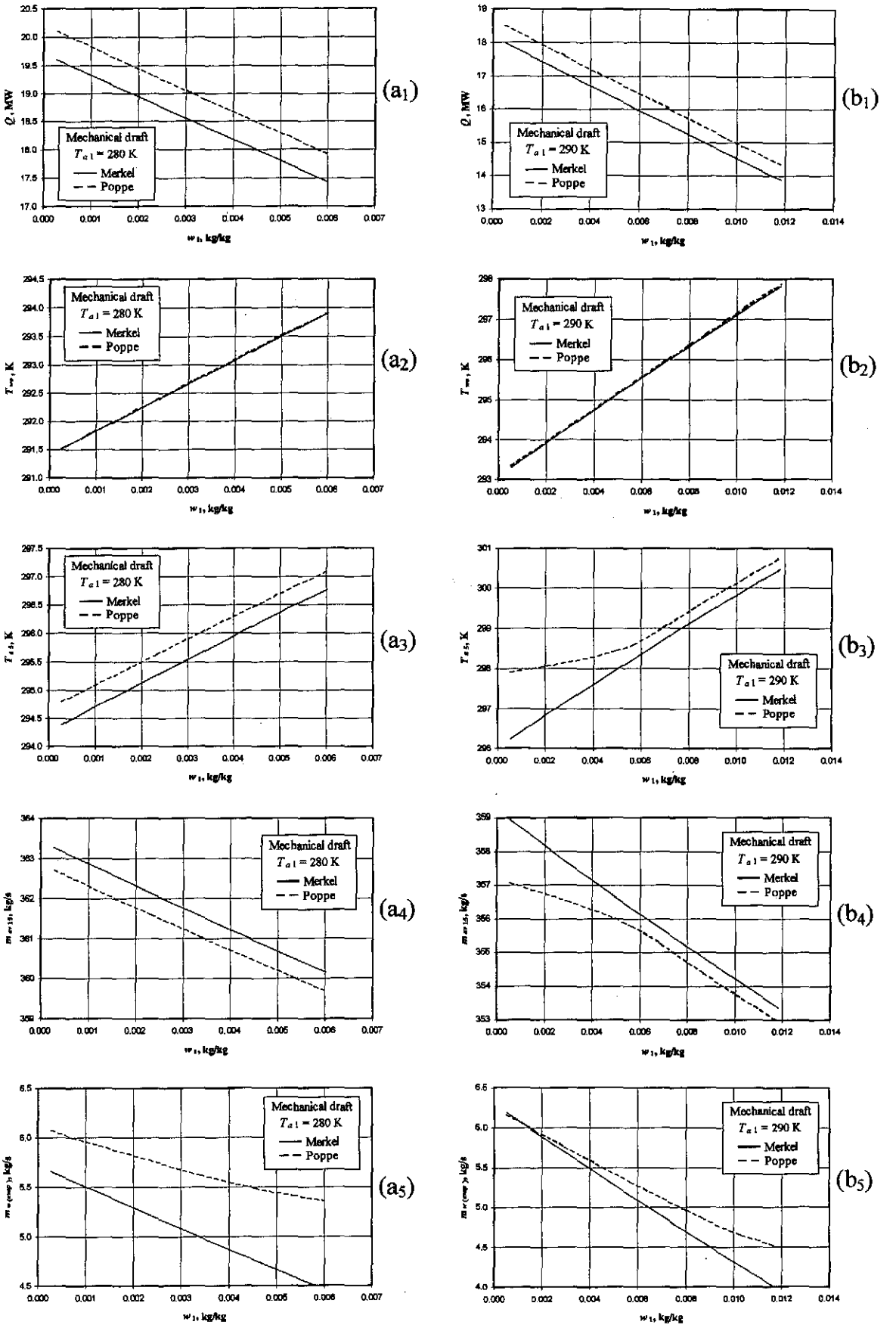

Figure O.12: Performance curves of a mechanical draft cooling tower at an atmospheric pressure of 101325 Pa.

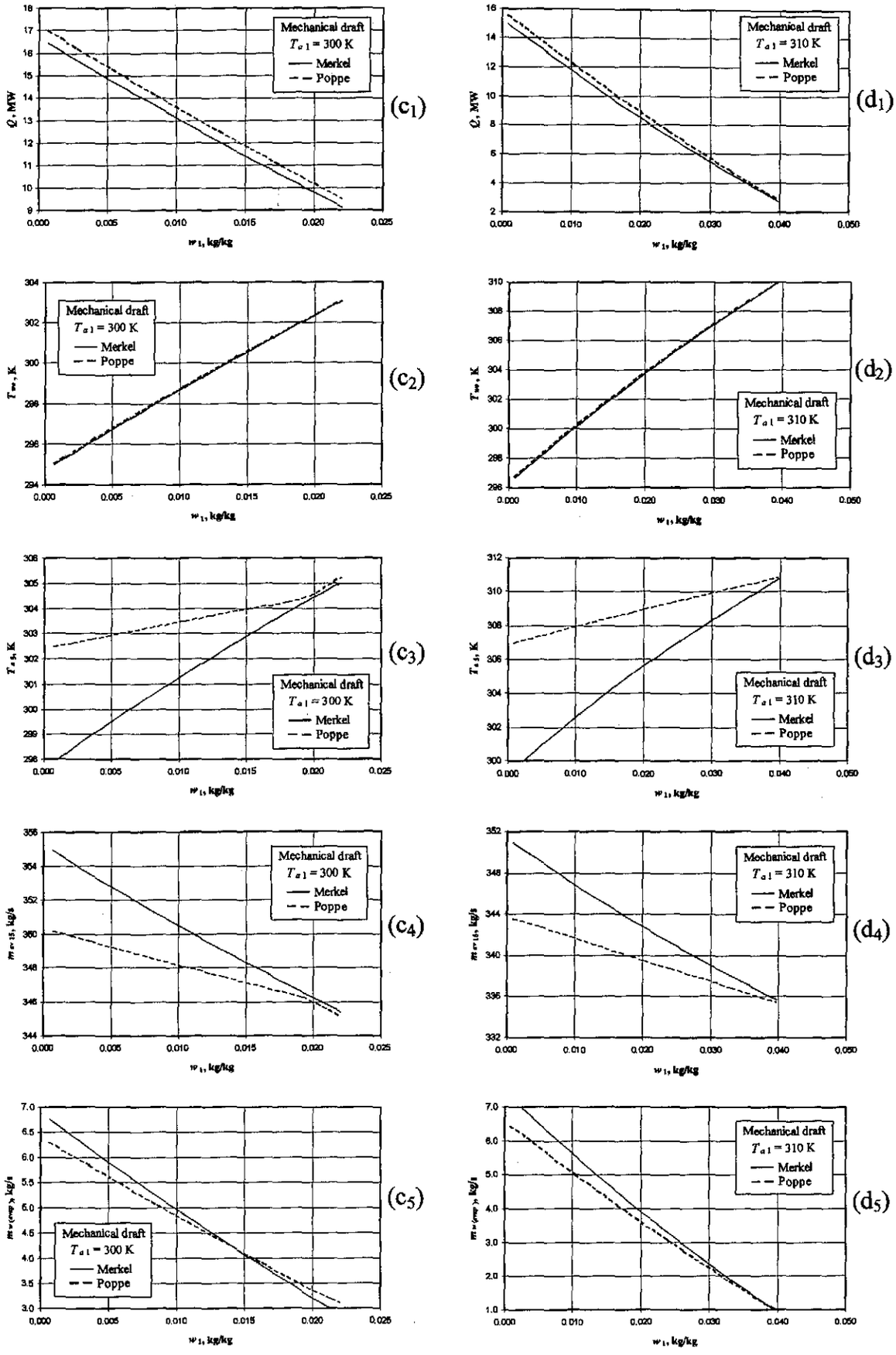

Figure O.12: Performance curves of a mechanical draft cooling tower at an atmospheric pressure of 101325 Pa.

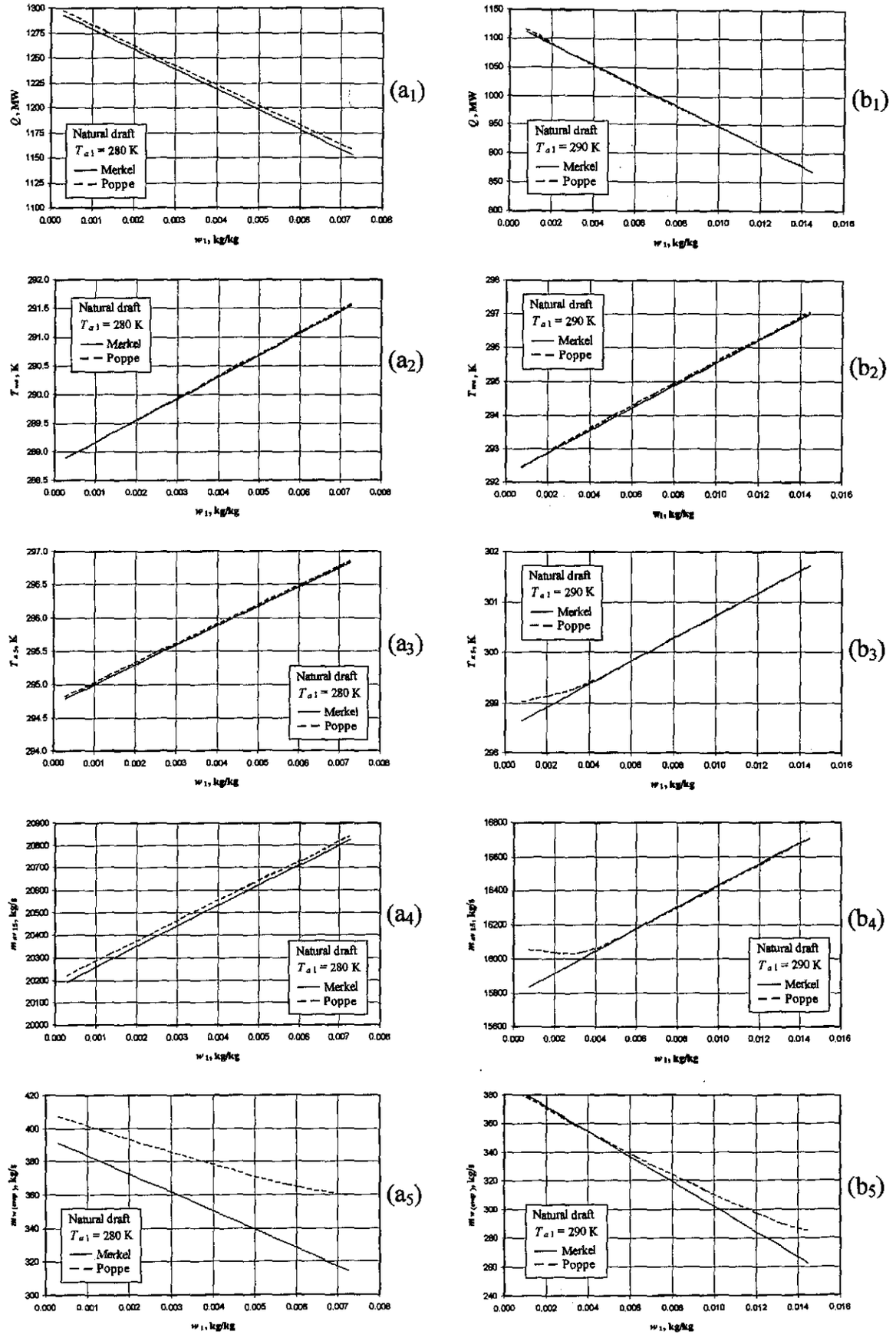

Figure O.13: Performance curves of a natural draft cooling tower determined with an improved energy equation in the Merkel approach.

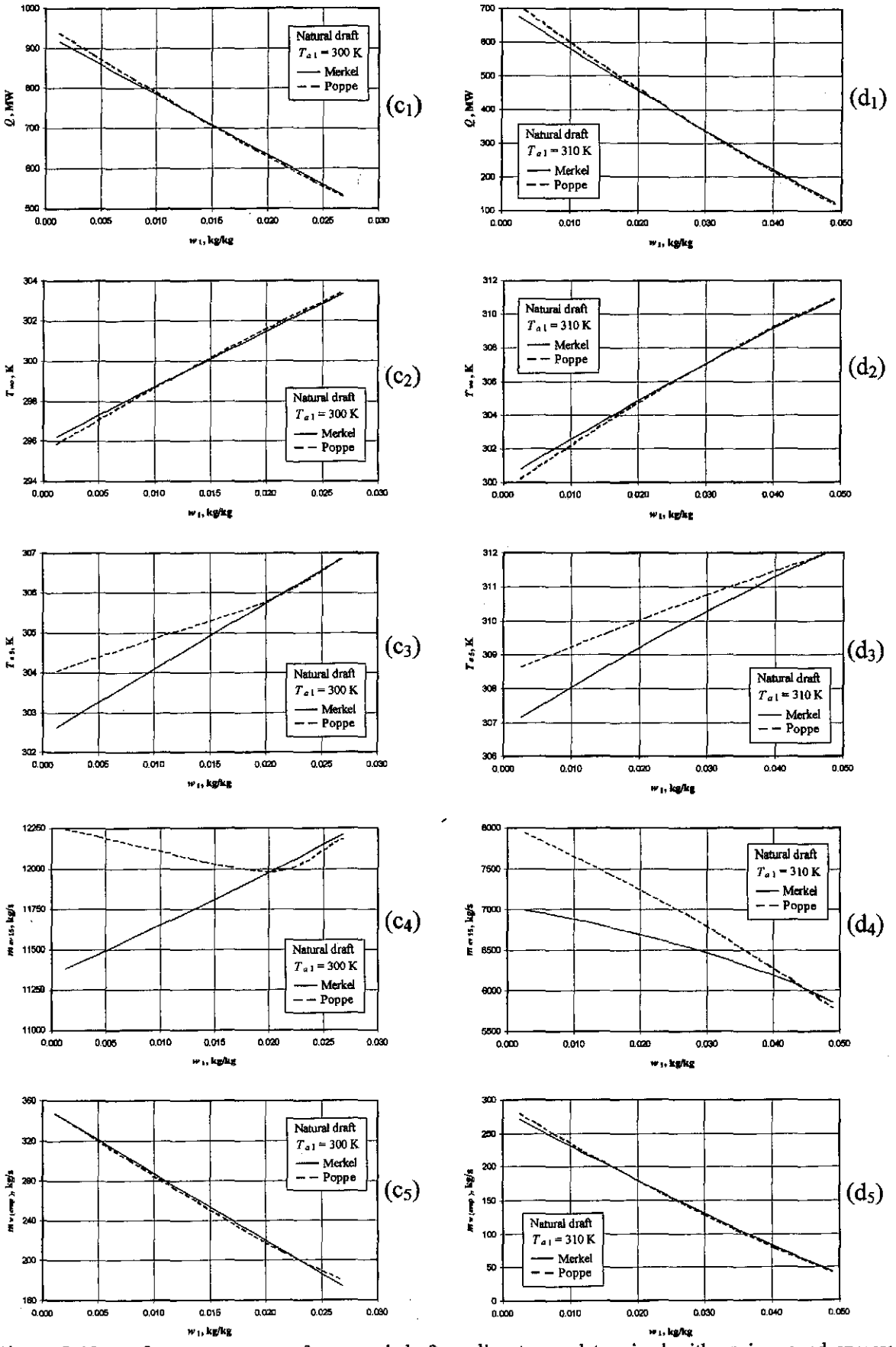

Figure O.13: Performance curves of a natural draft cooling tower determined with an improved energy equation in the Merkel approach.

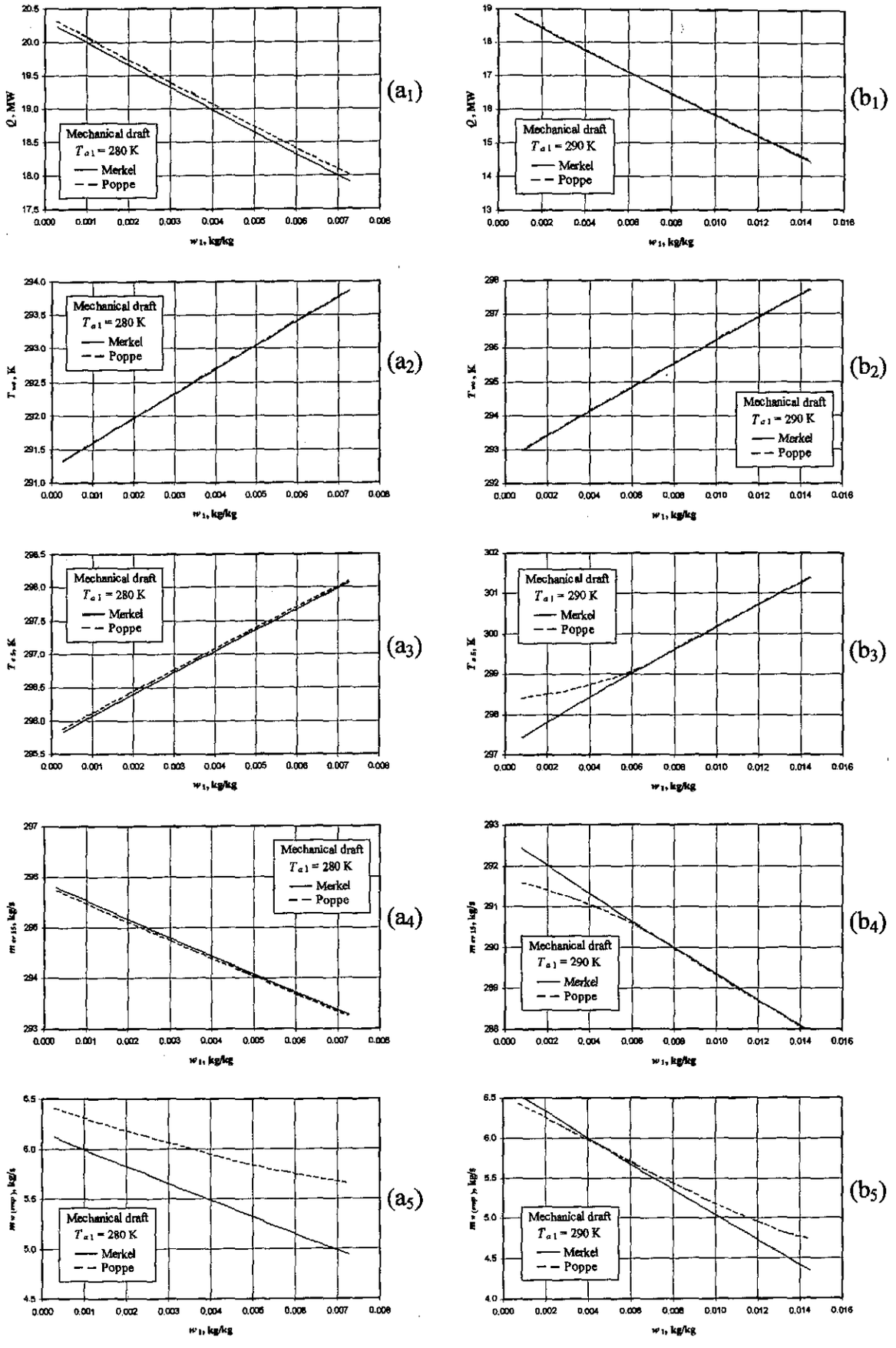

Figure O.14: Performance curves of a mechanical draft cooling tower determined with an improved energy equation in the Merkel approach.

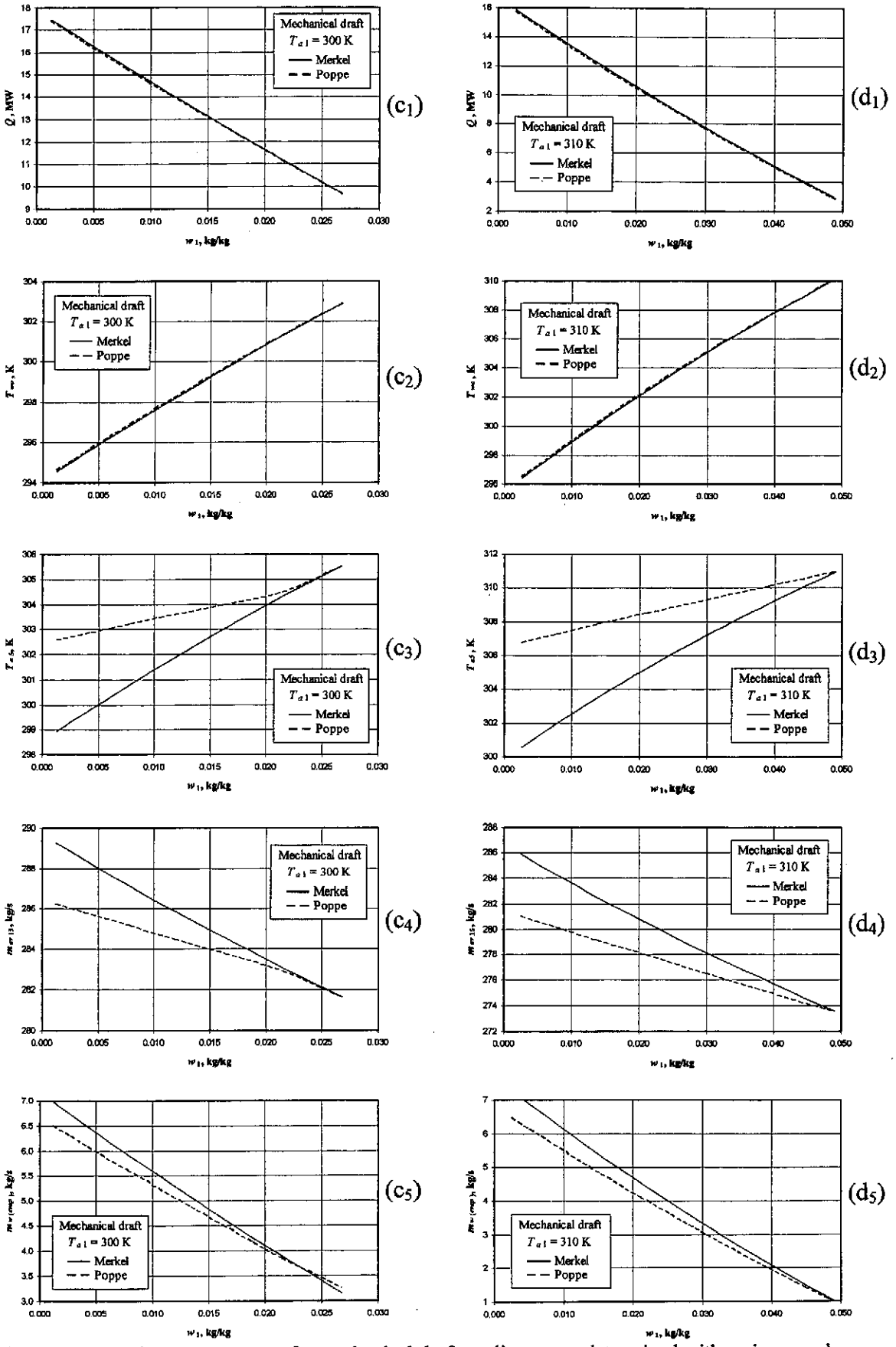

Figure O.14: Performance curves of a mechanical draft cooling tower determined with an improved energy equation in the Merkel approach.

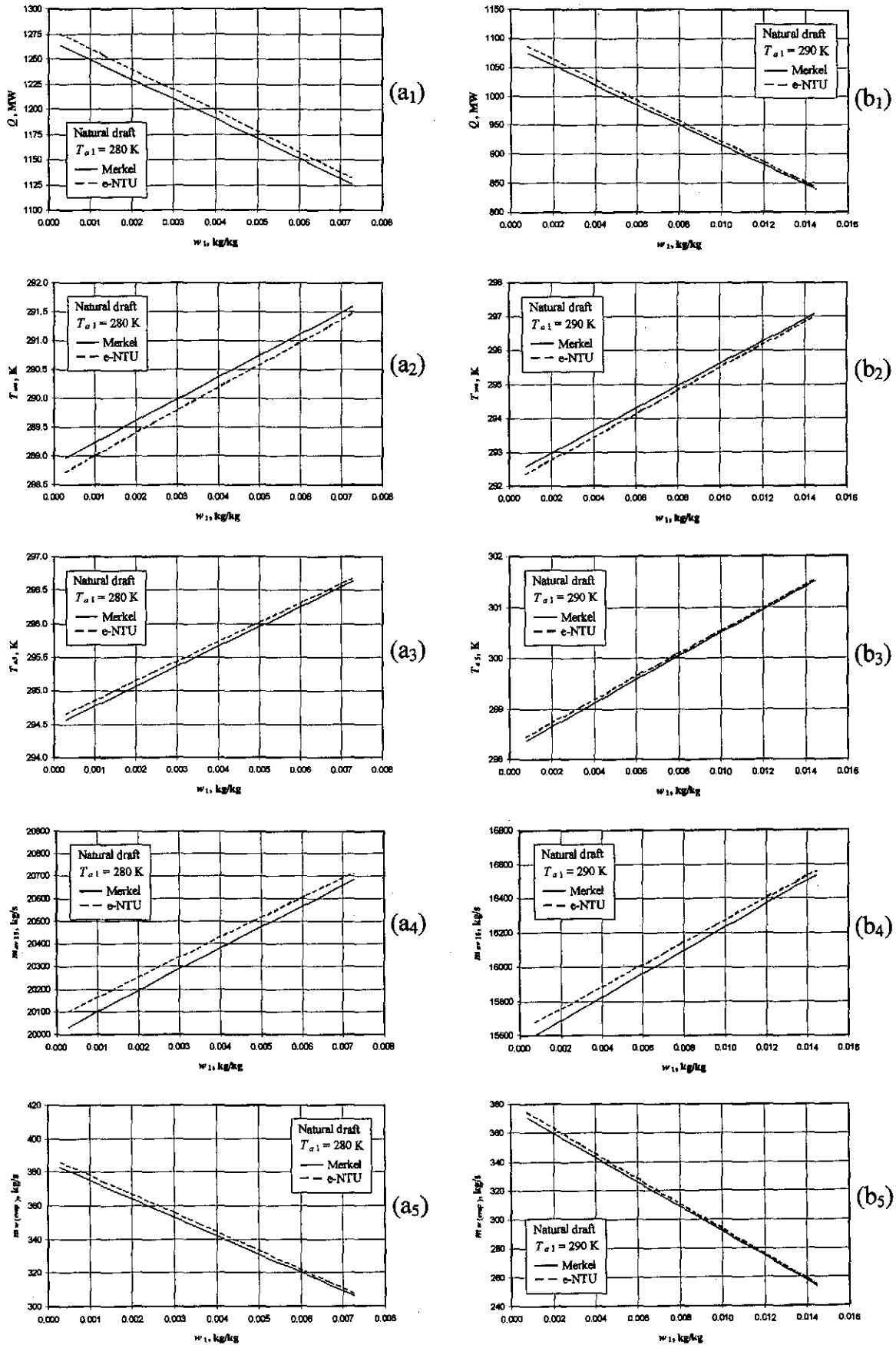

Figure O.15: Performance curves of a natural draft cooling tower while employing the Merkel approach and *e-NTU* approach.

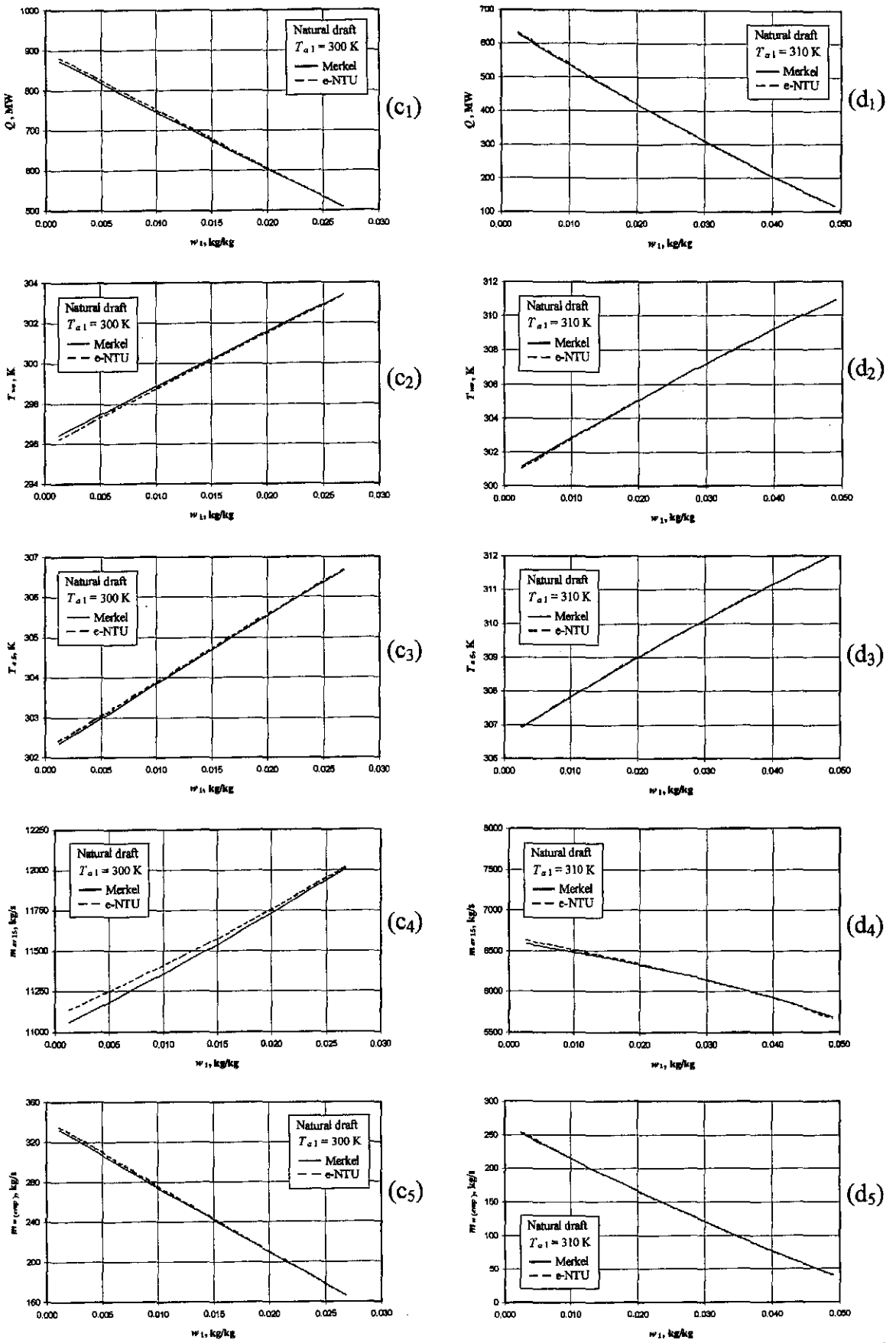

Figure O.15: Performance curves of a natural draft cooling tower while employing the Merkel approach and *e-NTU* approach.

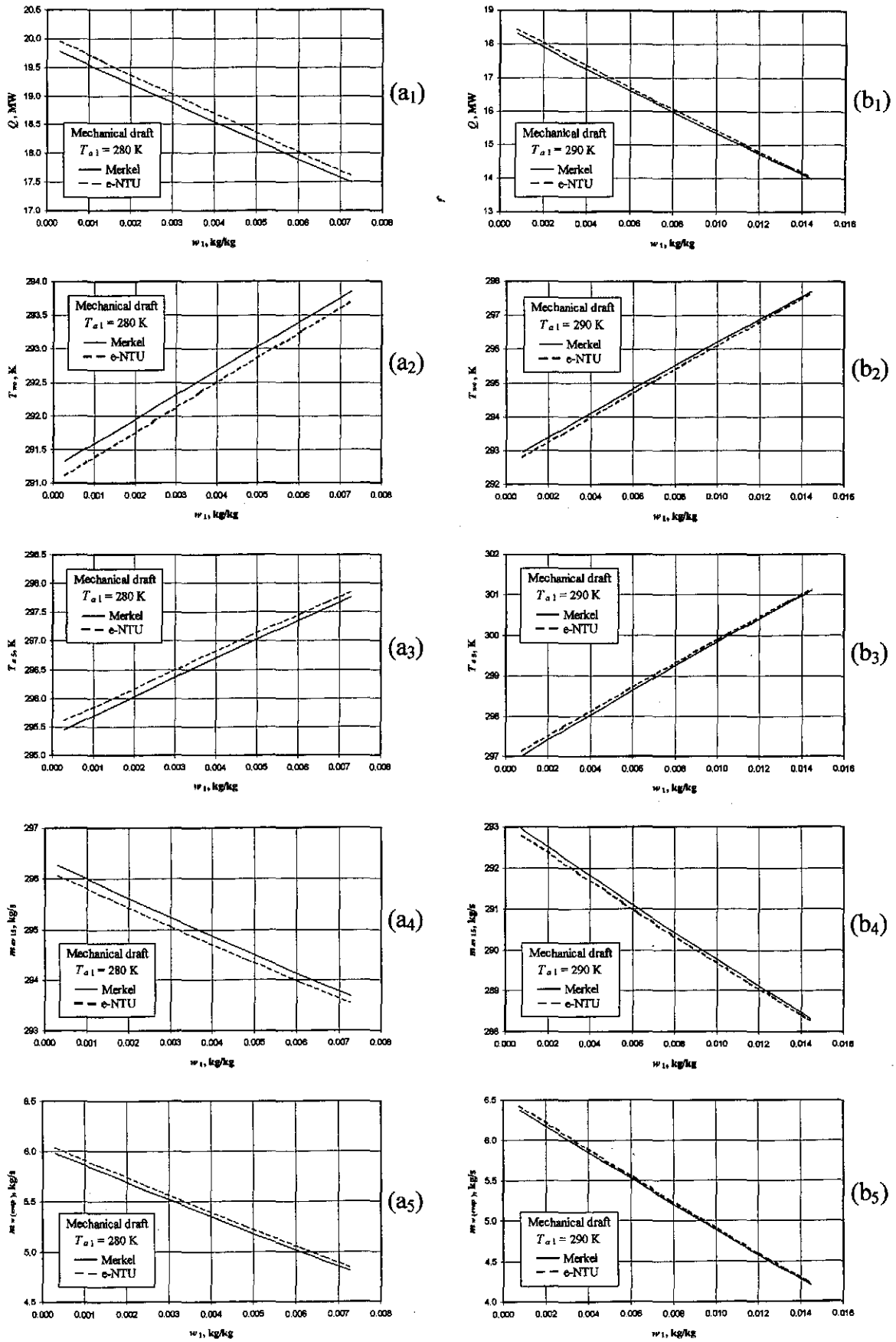

Figure O.16: Performance curves of a mechanical draft cooling tower while employing the Merkel approach and *e-NTU* approach.

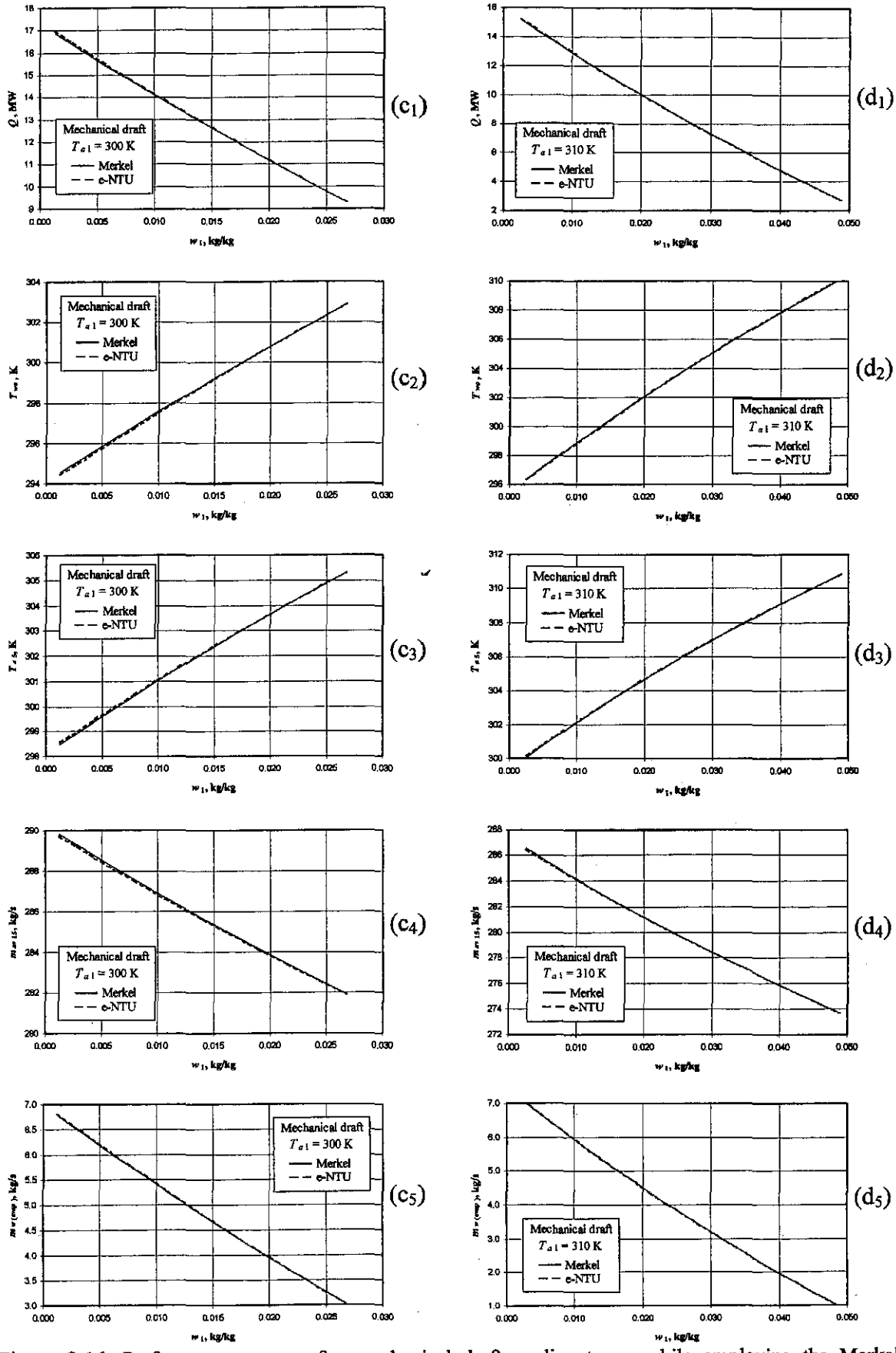

Figure O.16: Performance curves of a mechanical draft cooling tower while employing the Merkel approach and *e-NTU* approach.

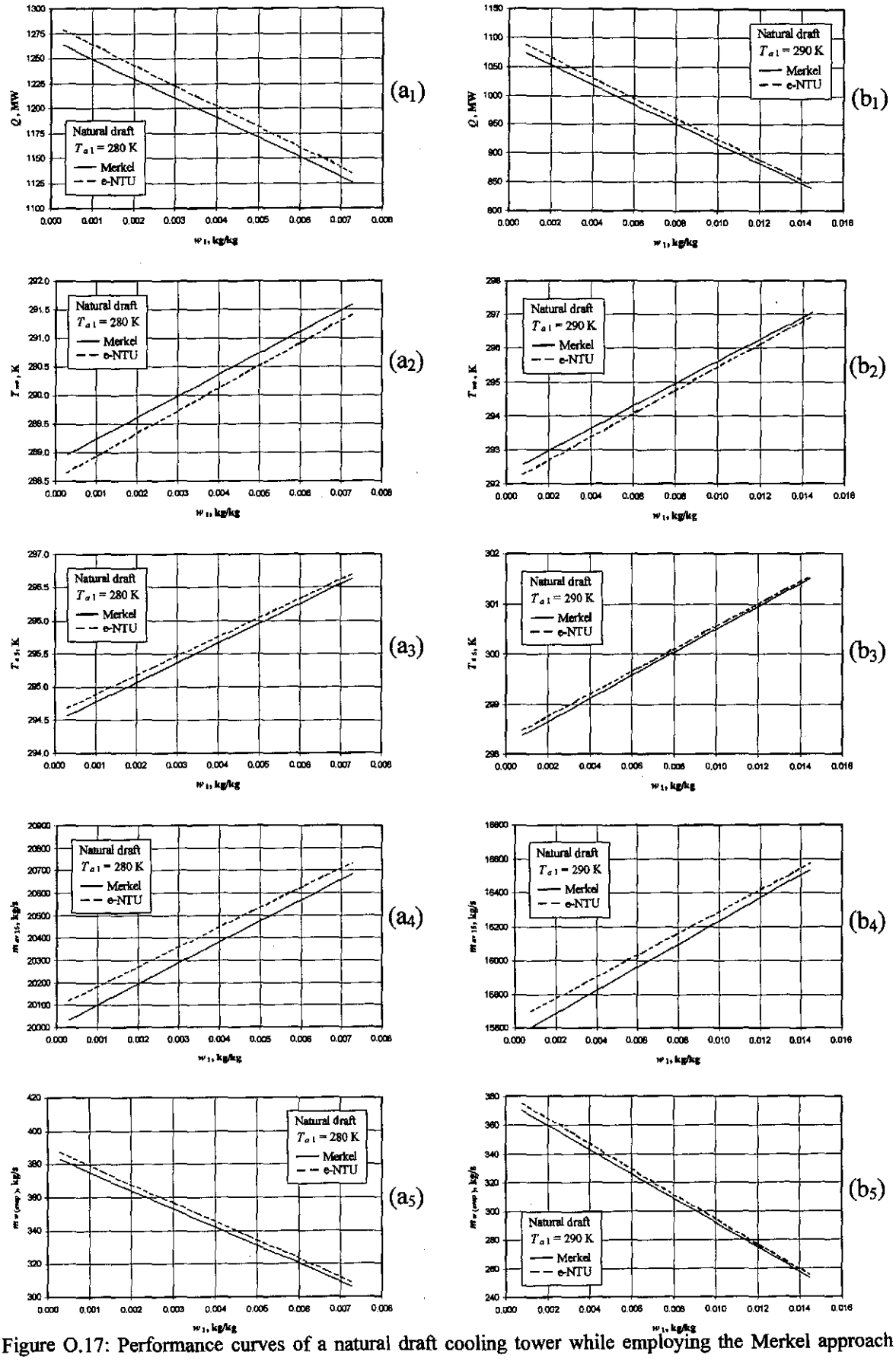

Figure O.17: Performance curves of a natural draft cooling tower while employing the Merkel approach and *e-NTU* approach. The application of the fill characteristics for the *e-NTU* approach is applied inconsistently.

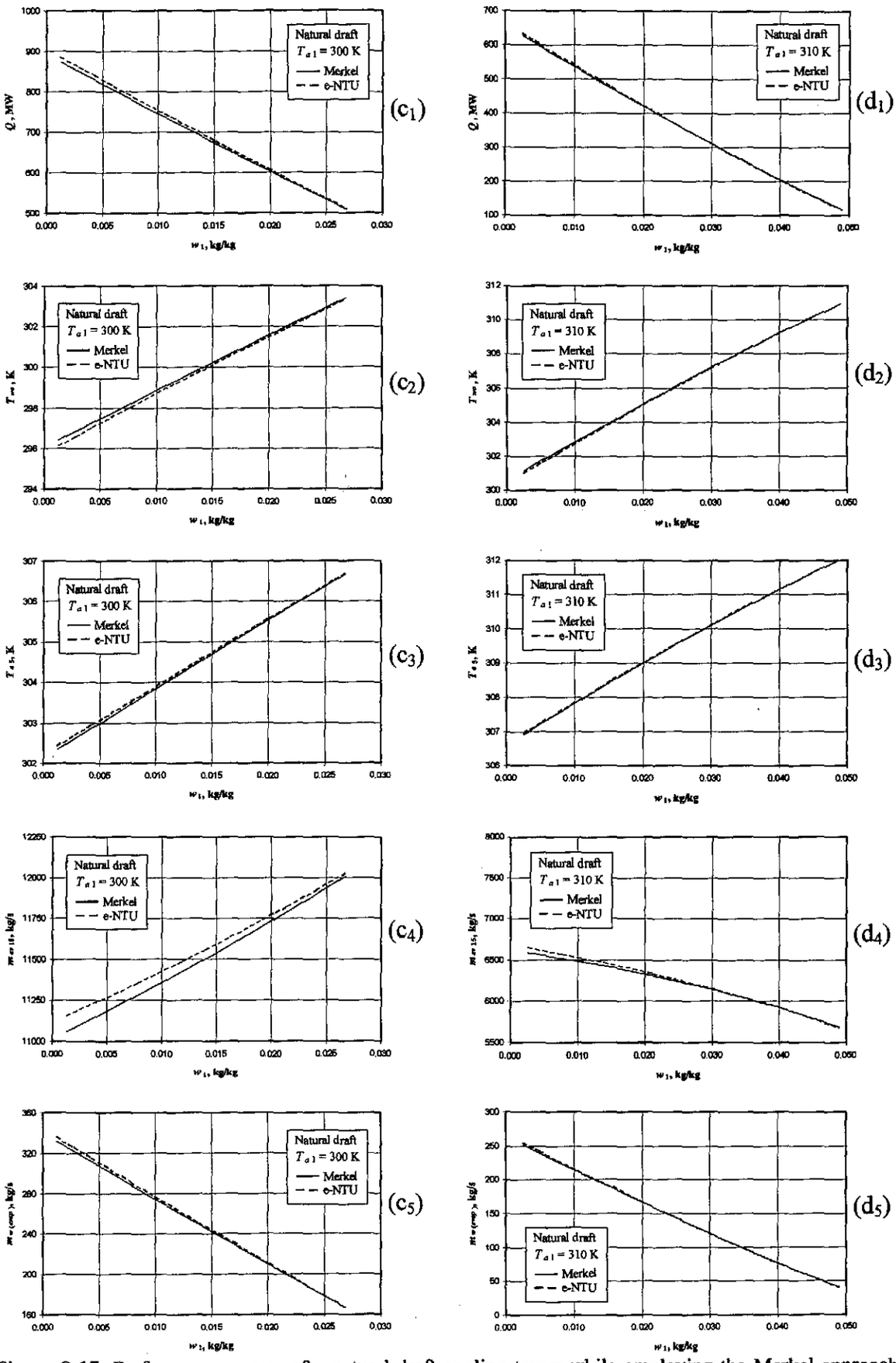

Figure O.17: Performance curves of a natural draft cooling tower while employing the Merkel approach and *e-NTU* approach. The application of the fill characteristics for the *e-NTU* approach is applied inconsistently.

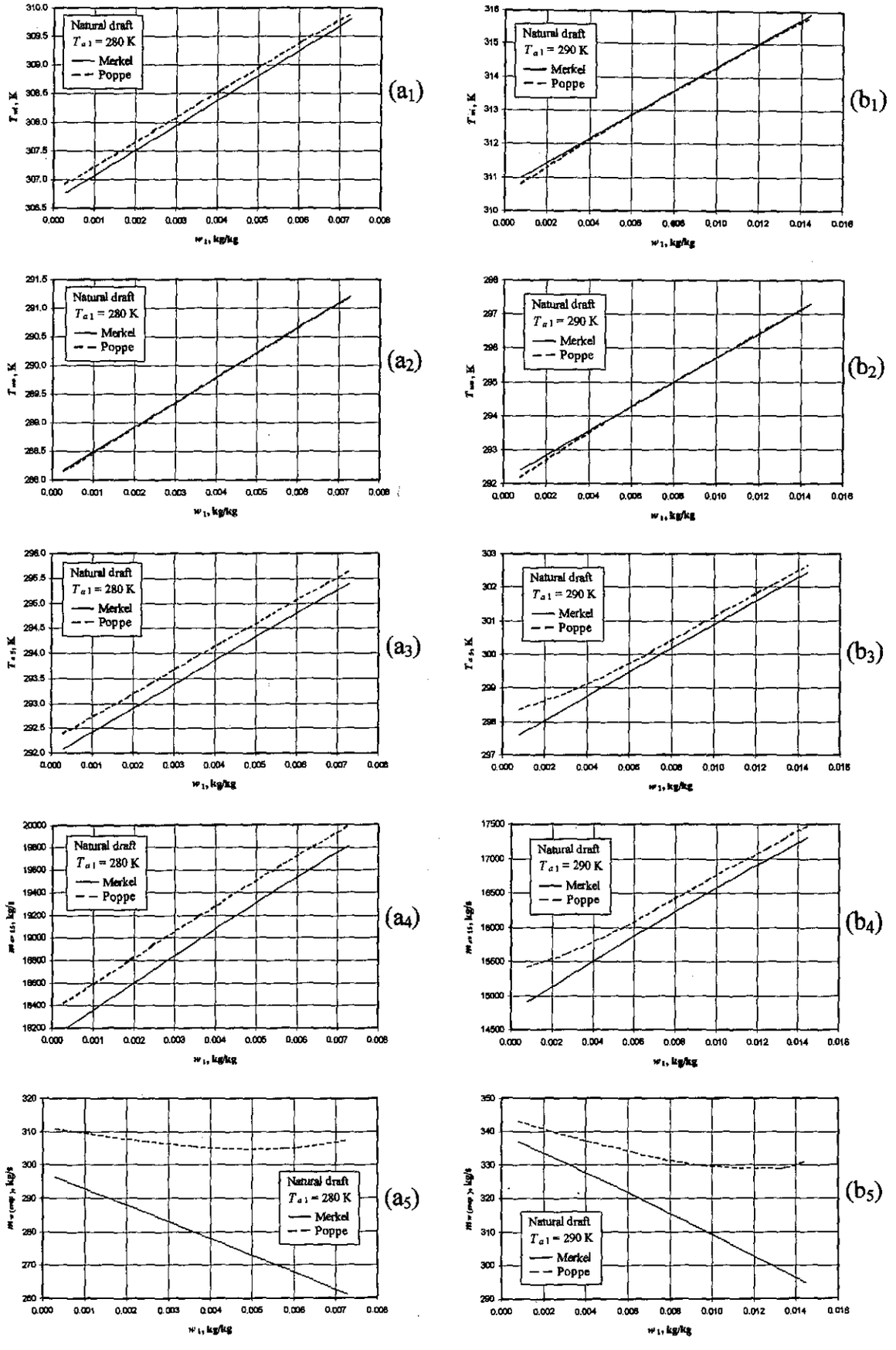

Figure O.18: Performance curves of a natural draft cooling tower where the heat rejection rate is constant.

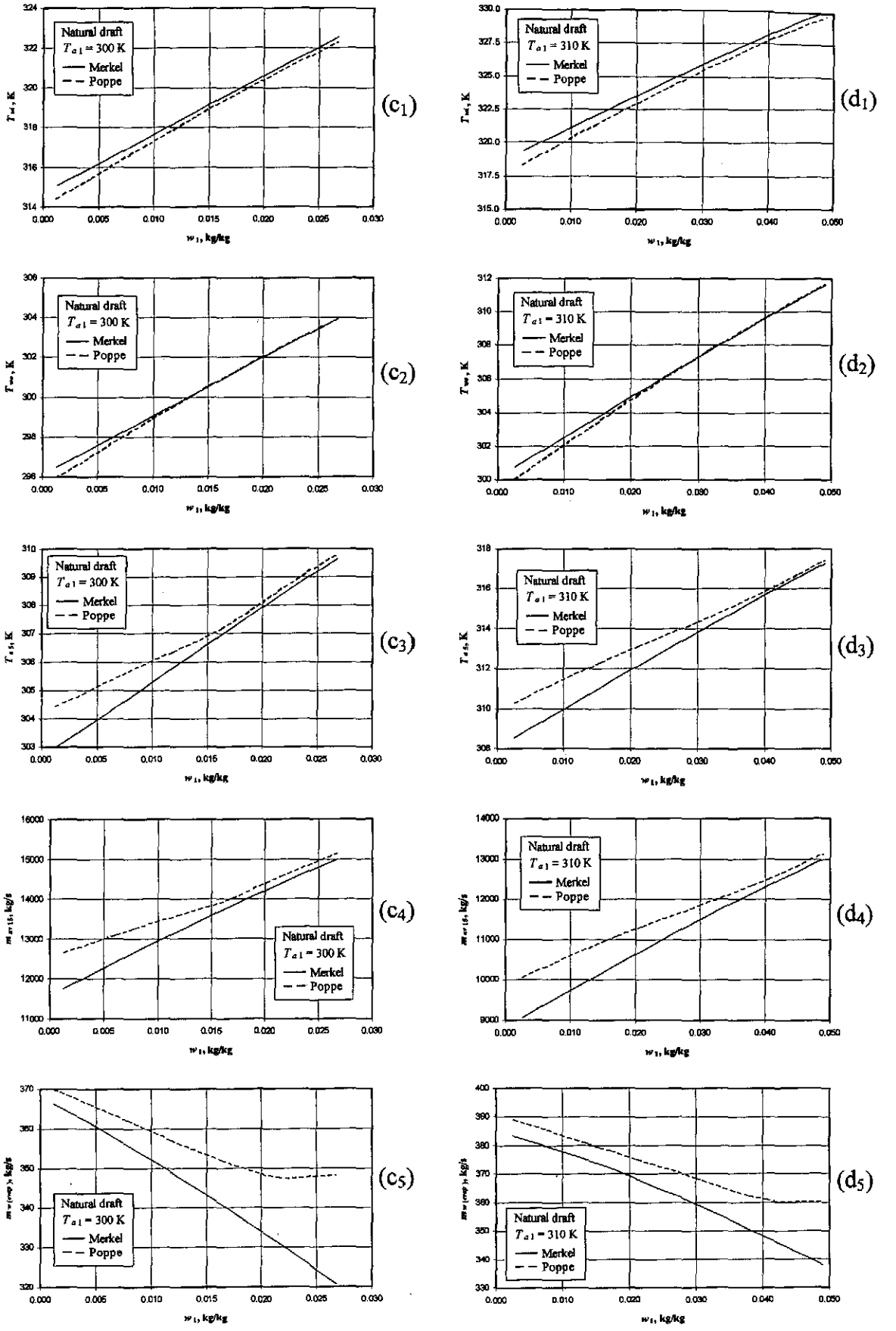

Figure O.18: Performance curves of a natural draft cooling tower where the heat rejection rate is constant.

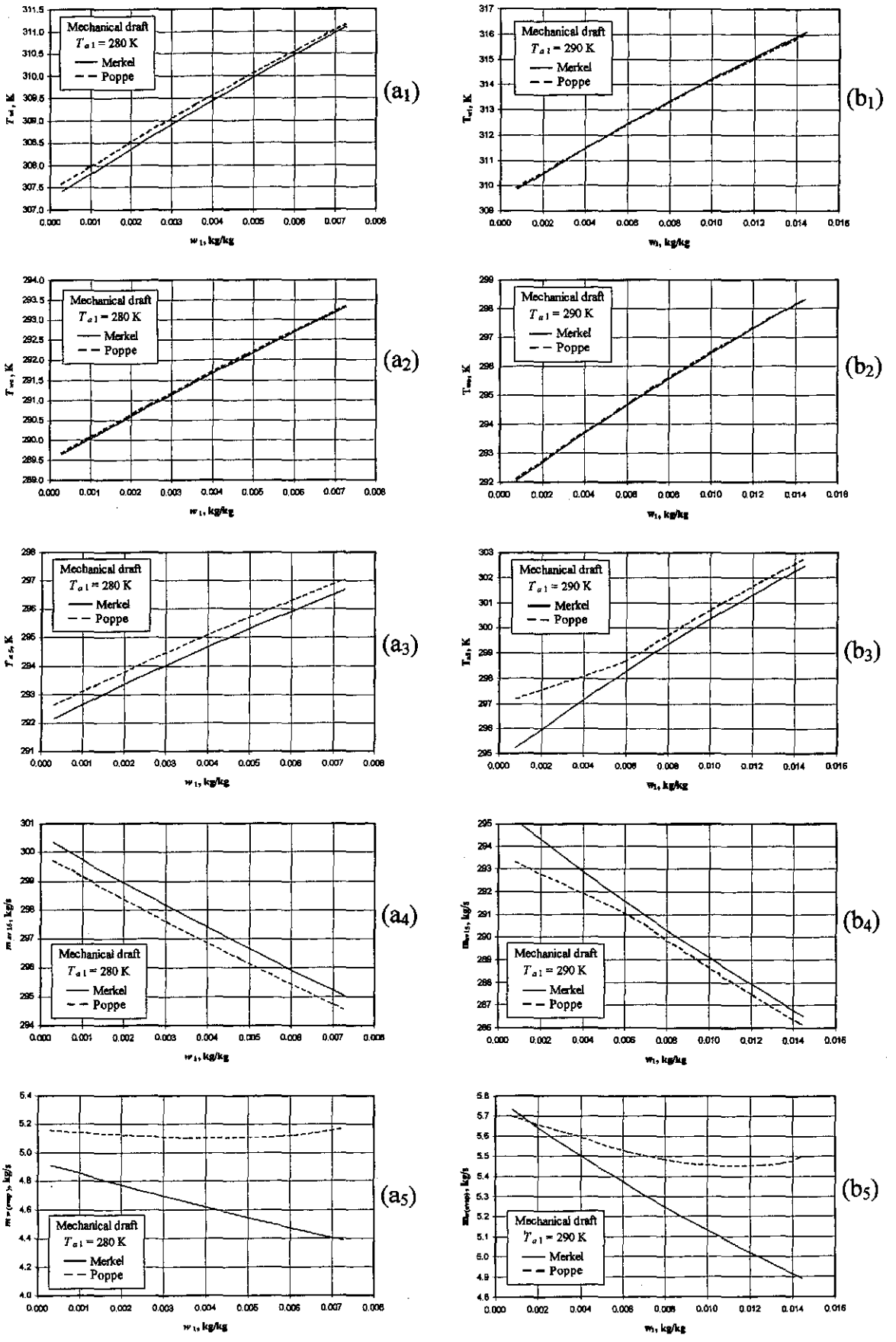

Figure O.19: Performance curves of a mechanical draft cooling tower where the heat rejection rate is constant.

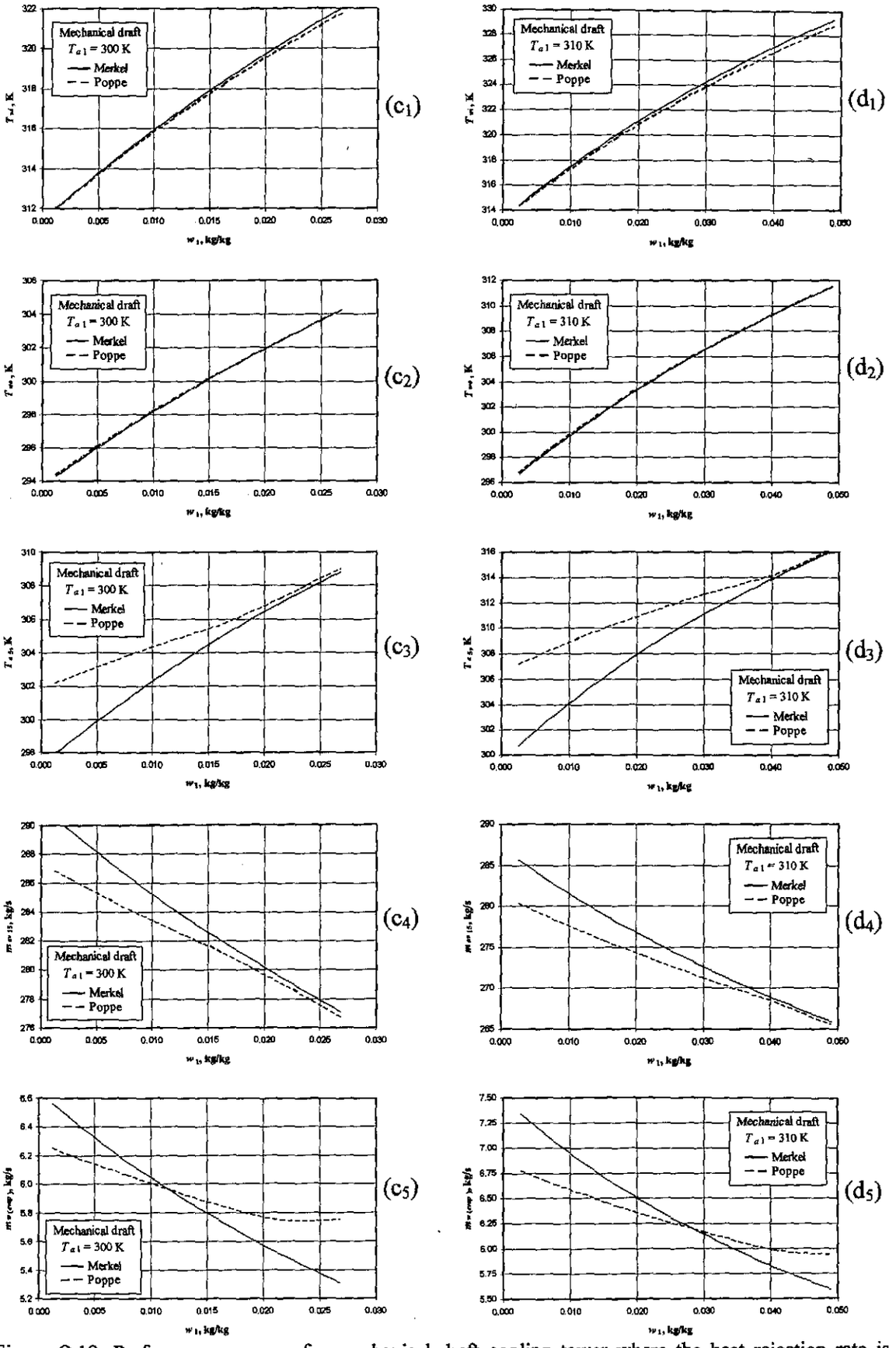

Figure O.19: Performance curves of a mechanical draft cooling tower where the heat rejection rate is constant.

APPENDIX P

WET-COOLING TOWER PERFORMANCE EVALUATION SOFTWARE

P.1 INTRODUCTION

A computer software program, Wet-Cooling Tower Performance Evaluation (WCTPE), is developed to analyze the performance of counterflow and crossflow wet-cooling towers. The graphical user interface of the software is developed in Visual C++ 6 while the program algorithm is developed in the Fortran computer language. All the models and equations cited and derived in this thesis pertaining to wet-cooling towers are included in the software program. For counterflow cooling towers the program is essentially a one-dimensional approach, that yields results orders of magnitude faster than full-blown two-, or three dimensional computational models involving the continuity, momentum and energy equations. However, the two- and three dimensional nature of the problem is accounted for in some of the semi-empirical relations, such as those presented in appendix D for the loss and transfer coefficients of the rain zone.

The sample calculations presented in appendices I and J for the natural draft and mechanical draft wet-cooling towers respectively are examples of the solution process of the software program. Due to the iterative processes involved throughout the solution of the program, mathematical control measures are applied to prevent numerical instability and hence divergence of the solution.

Warnings that occur during the solution process are written to an output file. Some of these warnings occur when empirical relations are employed outside their range of applicability according to one or more variables. Warnings also occur when convergence of iterative processes is not attained in a specified maximum number of iterations within the specified solution tolerances. There are more than fifty different warnings and a possible remedy or remedies are given for each warning that is written to the warnings output file.

Some functions and variable inputs of the program are disabled for certain choices made in the program. This is done to make the software user friendly and to prevent confusion, as only the active parts of the program requires input from the user. This appendix is not intended to be a detailed user manual of the program, but it rather gives an overview of the basic architecture, functions and capabilities of the program.

P.2 ASSUMPTIONS AND SIMPLIFICATIONS

It is mentioned in the section above that the program is virtually a one-dimensional model of cooling tower operation. This can only be achieved by introducing assumptions and simplifications such as,

- The cooling tower operates under steady-state conditions without wind.

- Miscellaneous thermal loads such as make-up water additions, pump head gain and the net heat exchange with the ambient surroundings are negligible.
- Uniform air and water flow rates over the tower cross sectional area.
- For counterflow towers, the thermodynamic properties of the upward airflow and downward water flow vary vertically, but are constant across any cross-section inside the tower.

P.3 PROGRAM AND SOFTWARE DEVELOPMENT

Figure P.1 shows the main dialog window of the computer program after the program is executed from the Windows™ environment.

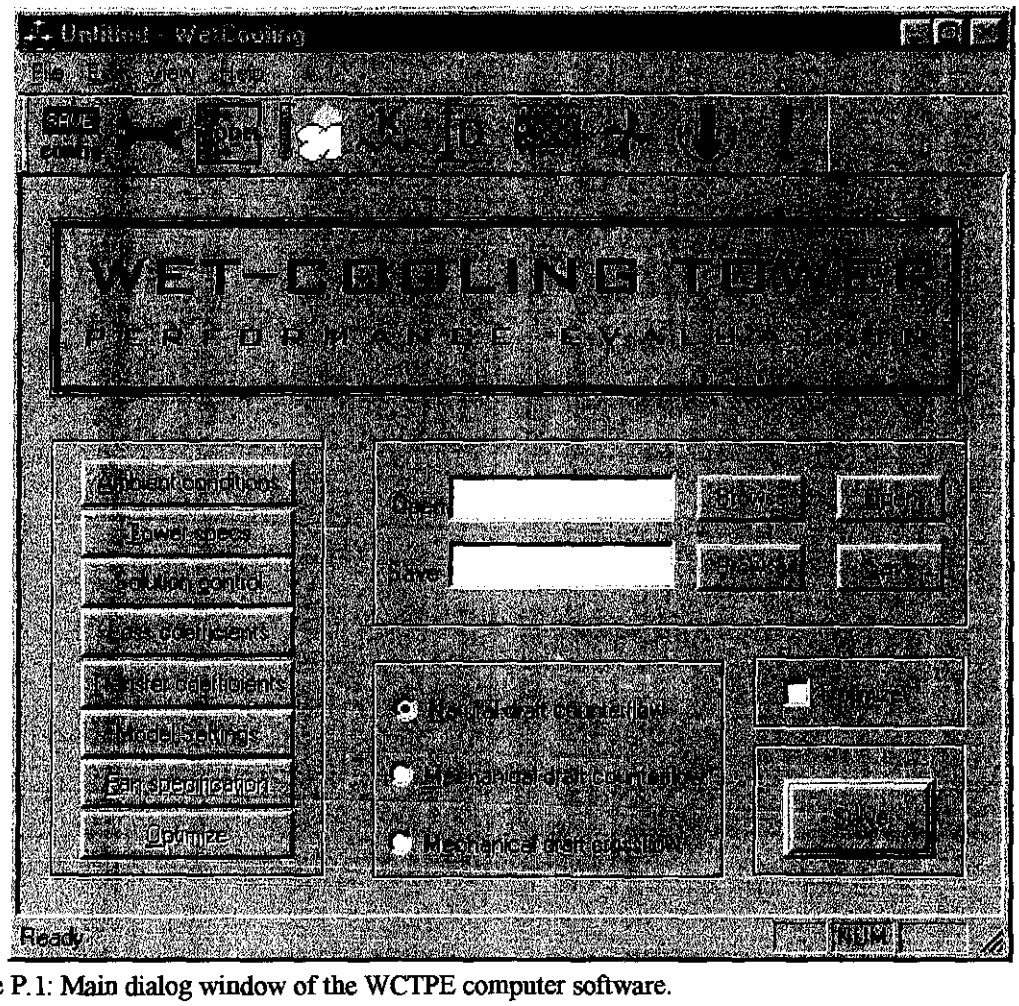

Figure P.1: Main dialog window of the WCTPE computer software.

The toolbar on top of the dialog box consists of nine different buttons. These functions on the toolbar can also be accessed from the buttons presented in the bottom part of the dialog window. Dialog windows for the specification of the atmospheric conditions, tower specifications, solution control, loss coefficients, transfer characteristics, heat and mass transfer model settings and fan specification are accessed from the main dialog window by clicking the appropriate buttons with a computer mouse. All the data entered into the program can be saved in files with user specified file names.

P.3.1 AMBIENT CONDITIONS

The dialog window where the ambient conditions are specified is shown in figure P.2. The ambient air temperature, pressure and temperature lapse rate are entered in the top left hand side of the dialog window. The atmospheric humidity can either be specified by supplying the wetbulb temperature, relative humidity or humidity ratio.

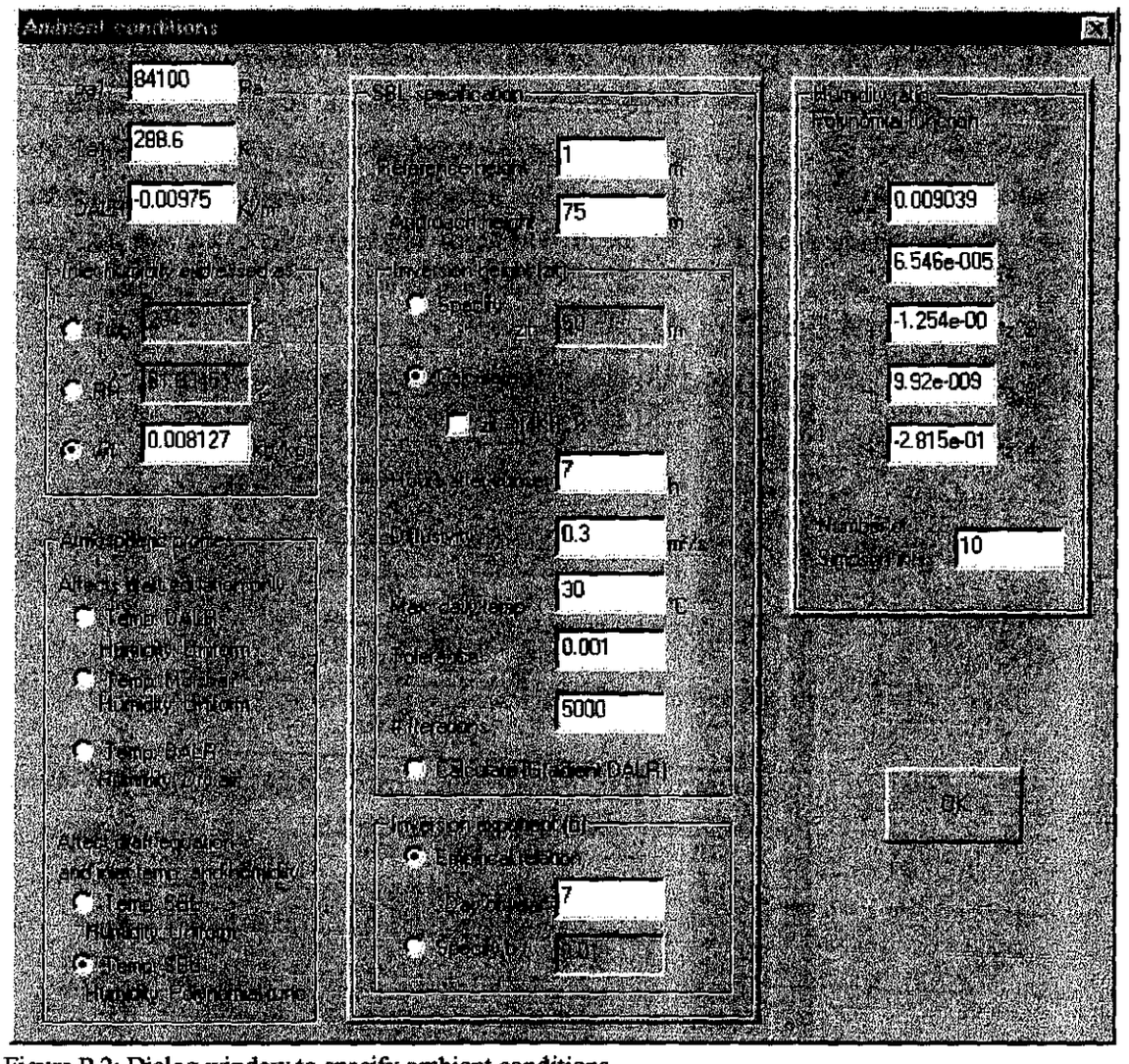

Figure P.2: Dialog window to specify ambient conditions.

Different options of the vertical atmospheric profiles of temperature and humidity can be specified. The characteristics of a stable boundary layer, i.e. when a temperature inversion is present, are specified on the right hand side of figure P.2. The characteristics include the height of the ground-based temperature from which the temperature profile is extrapolated. The height of the inversion can either be specified or iteratively determined by the program. The height of the iteratively determined inversion height is a function of the time elapsed since sunset, the thermal eddy diffusivity of the atmosphere and the maximum daily temperature. The maximum number of iterations and tolerance for the iterative process are also specified. Refer to appendix L for a detailed discussion on the stable boundary layer and the variables associated with it.

P.3.2 SOLUTION CONTROL

The dialog window for the control of the solution is presented in figure P.3. Five variables, i.e., the water outlet temperature, the air temperature and pressure above the drift eliminator, the internal pressure at the top of the cooling tower and the mean air-vapor mass flow rate, are chosen as the primary solution variables of the primary iteration loop of the program and are solved by the Jacobi iterative method. All the other so-called secondary solution variables are either explicitly, or iteratively solved from these arbitrarily chosen primary solution variables. The iterative method utilized for the solution of the secondary variables is the Secant iterative method. Refer to numerical analysis textbooks such as Mathews [92MA1] and Burden and Faires [97BU1] for detailed descussions of the above mentioned iterative schemes. Thus, convergence of the program will be reached when all five variables mentioned above change less than the specified tolerance, specified in figure P.3, from one program iteration to the other within the specified maximum number of iterations.

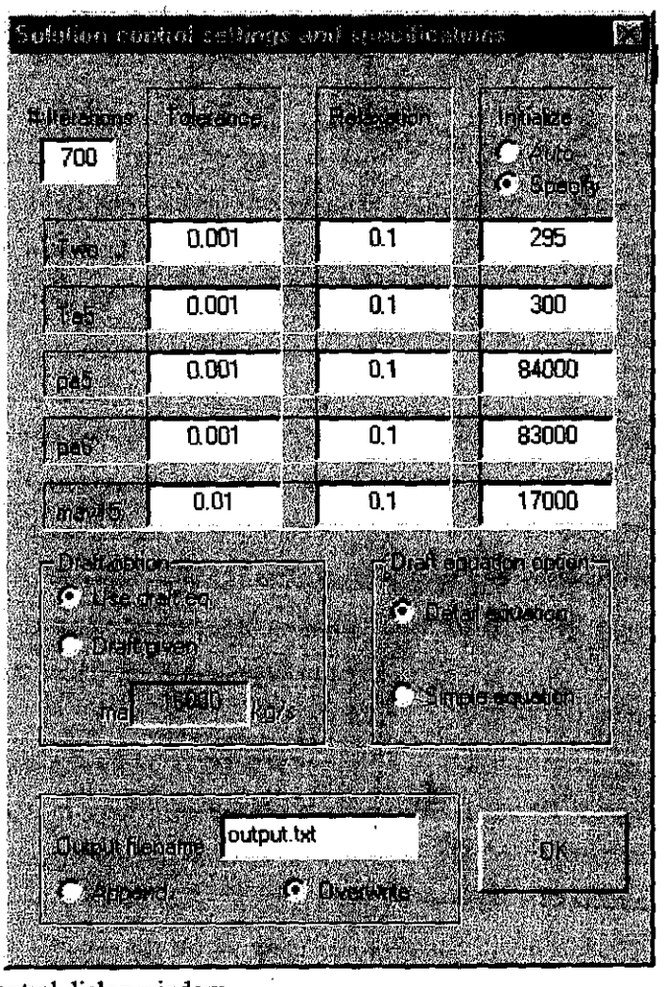

Figure P.3: Solution control dialog window.

In order for the program to start the iterative process successfully, practical initial estimates must be supplied for the five chosen solution variables. Either these initial values can be supplied by the user, or they can be automatically estimated by the program. Refer to appendix I.2 for the procedure followed to initialize the variables.

As already mentioned in the introduction of this appendix, mathematical control measures must be implemented to prevent instability of the iterative process. One way of preventing instability is the implementation of relaxation.

In the iterative solution of the algebraic equations, it is often desirable to slow down the changes, from iteration to iteration, in the values of the dependent variables [80PA1]. This process is called underrelaxation. Underrelaxation is often employed to avoid divergence in the iterative solution of strongly nonlinear equations. In the following discussion A is an arbitrarily chosen variable and B is an arbitrarily chosen function where $A = B$.

If A^* is added to the right hand side and subtracted find,

$$A = A^* + \left(B - A^*\right)$$

A^* is the value of A from the previous iteration. The contents in the parentheses represents the change in A produced by the current iteration. This change can be modified by the introduction of a relaxation parameter, α, so that

$$A = A^* + \alpha\left(B - A^*\right)$$

When the iterations converge, A becomes equal to A^*. There are no general rules for choosing the best value of the underrelaxation factor. The optimum value depends upon a number of factors, such as the nature of the problem and the iterative procedure used. For this program, it was found that relaxation factors of 0.1 for all the selected solution variables prevented divergence for all the sample cases investigated.

Another principle to prevent solution divergence is implemented in the program algorithm. No control from the user, however, is necessary. For Jacobi-type iterative schemes to converge to unique solutions, the arbitrarily chosen matrix C in the linear system $Cx = D$ must be strictly diagonally dominant [92MA1, 97BU1]. Patankar [80PA1] refers to this condition applicable to numerical heat transfer and fluid flow problems as the Scarborough criterion. Thus, the applicable equations in the program algorithm are manipulated to satisfy the Scarborough criterion.

P.3.3 TRANSFER CHARACTERISTICS

The dialog window to specify the transfer characteristics in the fill, spray zone and rain zone is shown in figure P.4. The transfer coefficients can be specified either by constant values or by empirical relations. The empirical relation for the spray zone is given by equation (D.23). The empirical relation for the rain zone is given by equation (D.20) for circular towers and by equation (D.22) for rectangular towers. In addition, the transfer coefficient of a purely counterflow rain zone can also be specified. The empirical relation for the purely counterflow rain zone can be found in Kröger [98KR1]. The empirical relations for the spray and rain zones are not applicable to the crossflow cooling tower.

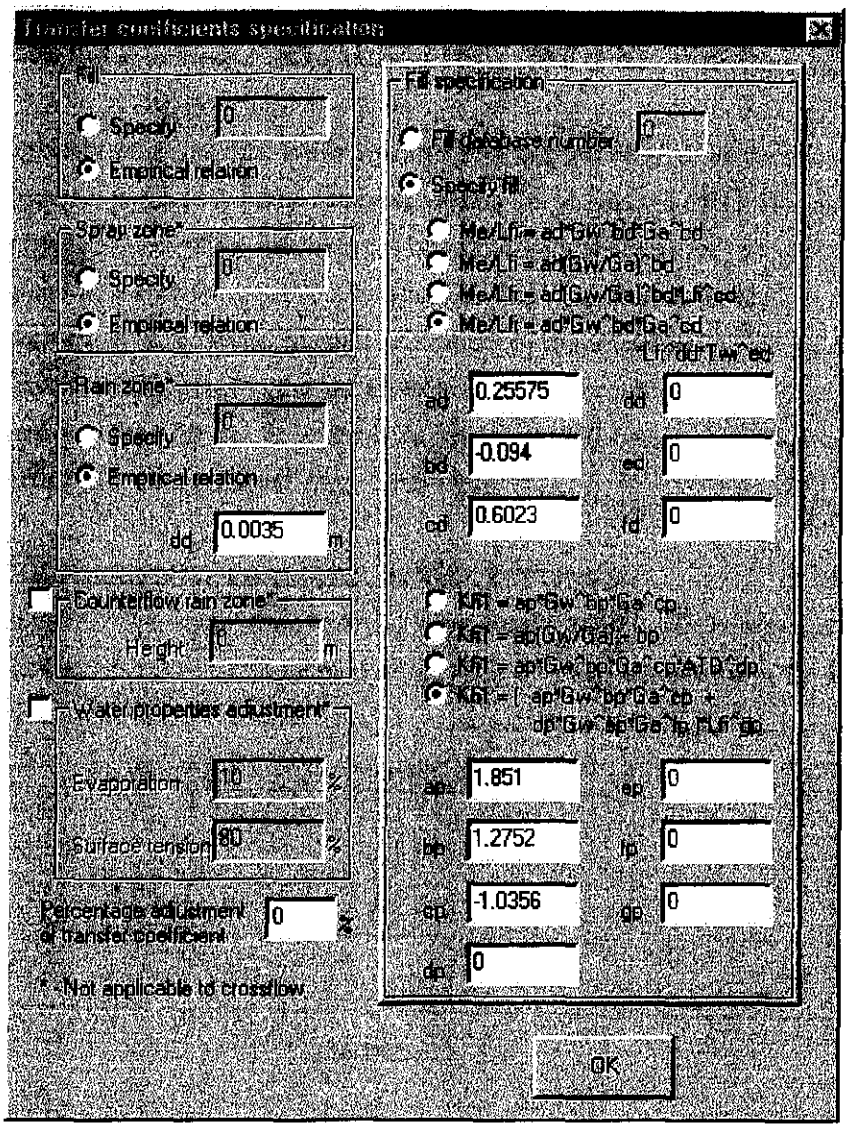

Figure P.4: Dialog window to transfer coefficients.

The empirical relations for all the transfer characteristics are determined by assuming that the cooling water is distilled. In practice, however, the cooling water can be contaminated by various kinds of minerals and impurities. If the evaporation rate and surface tension of a sample of the actual cooling water is determined, the corrected transfer coefficients can be determined.

The properties of the actual cooling water, compared to distilled water, can be entered in the bottom left-hand side of figure P.4 as percentages. The percentages for the evaporation rate and surface tension are the percentages of the cooling water to that of distilled water. Equation (D.20) for the transfer characteristic of the rain zone in circular towers and equation (D.22) for rectangular towers are functions of the surface tension, σ_w, through the a_μ, a_ν and a_L coefficients specified under equation (D.8). The correction of all the transfer coefficients for the surface tension is implemented as follows. The transfer characteristic for the rain zone is calculated with the surface tension of distilled water. The calculation of the transfer coefficient of the rain zone is repeated with the corrected surface tension of the actual cooling water. The percentage change of these two rain zone transfer coefficients are then applied to the fill and

spray zones. The total transfer coefficient is multiplied by the specified evaporation percentage, to account for higher or lower evaporation rates, of the actual cooling water compared to distilled water.

The empirical relation for the transfer characteristic of the fill is given on the right-hand side of the dialog window shown in figure P.4. The empirical relation can be selected either from a database of 49 different counterflow and 7 crossflow fills, or it can be specified by choosing the appropriate form of the empirical relation and then specifying the coefficients. The empirical relation for the loss coefficient of the fill is also specified in this dialog window. The transfer characteristics in the database and the transfer characteristics of fills given in the literature are generally according to the Merkel approach. The transfer characteristic of the fill can be adjusted in the bottom left hand side of figure P.4 to be suitable for employment with the *e-NTU* and Poppe approaches.

P.3.4 COUNTERFLOW TRANSFER MODEL SETTINGS

The settings for the counterflow heat and mass transfer models can be selected in the dialog window shown in figure P.5. The particular model of analysis is specified at the top of the dialog window.

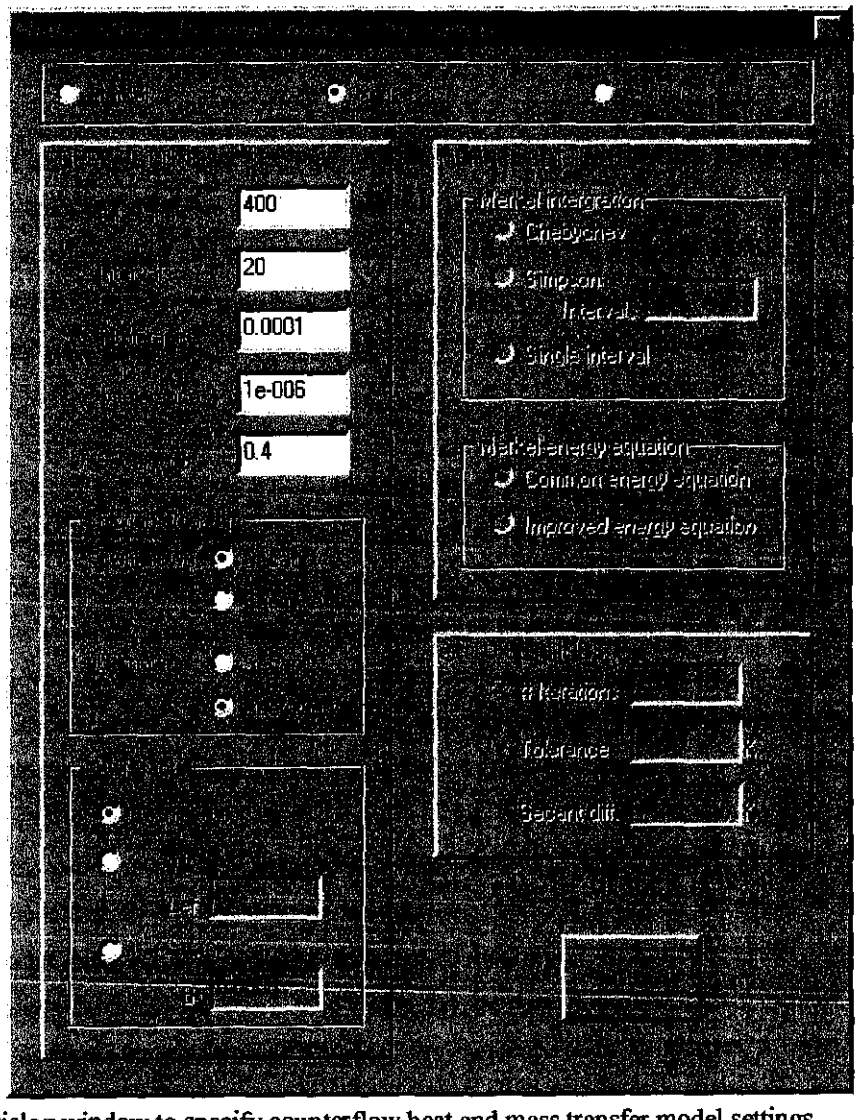

Figure P.5: Dialog window to specify counterflow heat and mass transfer model settings.

For the Merkel approach, the numerical integration algorithm can be selected. The four point Chebyshev numerical integration method is the preferred algorithm for cooling tower analyses [88BR1, 90CO1, 97CO1], but the Simpson algorithm is also included in the program for comparative purposes as the number of intervals can be specified for the Simpson integration algorithm, to obtain very accurate approximations of the integral.

The energy equation applied in the Merkel approach, to calculate the air temperature above the spray zone, can also be chosen. The common energy equation does not account for the change in the water mass flow rate due to evaporation, while the detailed energy equation does. This consideration has far reaching implications for especially natural draft towers, where the draft through the tower is a function of the air temperature above the spray zone.

The *e-NTU* approach is employed in a secondary iterative scheme inside the main program algorithm. The variables specified for the *e-NTU* approach are parameters to control the Secant iterative procedure. The Secant differential in figure P.5 is a parameter to determine two initial approximations for the Secant iterative scheme. Similar Secant differentials will be required for the counterflow Poppe approach as well as the crossflow Merkel and Poppe approaches.

The Poppe approach is also employed in a secondary iterative scheme inside the main program algorithm. Iterative control parameters are specified which include the maximum number of iterations and solution tolerances for the water temperature and outlet humidity ratio. The number of integration levels can also be specified. For example, 2 levels are chosen for the Poppe approach employed in the fill analysis in appendix G, and 5 levels are chosen for the Poppe approach in the analysis of the natural draft cooling tower in appendix I.

The governing equation of the Poppe approach can be solved by different solution algorithms. The governing equations presented in appendix B can be solved by an iterative Secant algorithm, or the governing equations can be manipulated and solved explicitly. The different approaches can be used for comparative studies to evaluate the accuracy of one algorithm compared the other. If the water inlet temperature, T_{wi}, is known and the heat rejected, Q, is unknown, the governing equations are in a different form than when Q is known and T_{wi} is unknown. That is why the explicit or iterative algorithms can be separately specified, in figure P.5, for each instant where T_{wi} is known or unknown.

The Lewis factor, discussed in appendix F, must be specified when the Poppe approach is employed. The Lewis factor can be specified by the equation of Bosnjakovic [65BO1] given by equation (F.16). The Lewis factor can also be specified as a constant, or it can be determined by equation (F.14), where the exponent given in equation (F.14) as 2/3 = 0.667 can also be specified. The Lewis number, *Le*, in equation (F.14) is determined by equation (F.6) where the thermophysical properties, k, ρ and c_p are solved according to the equations in appendix A and the diffusion coefficient is solved by equation (F.7).

It is highly recommended that the same definition of the Lewis factor be employed as was the case when the transfer characteristic of the fill was determined.

P.3.5 CROSSFLOW TRANSFER MODEL SETTINGS

Figure P.6 shows the dialog window for the crossflow model settings. Due to the two-dimensional nature of the crossflow problem as seen in appendix C, the implementation of the transfer models in the program differs from the counterflow problem.

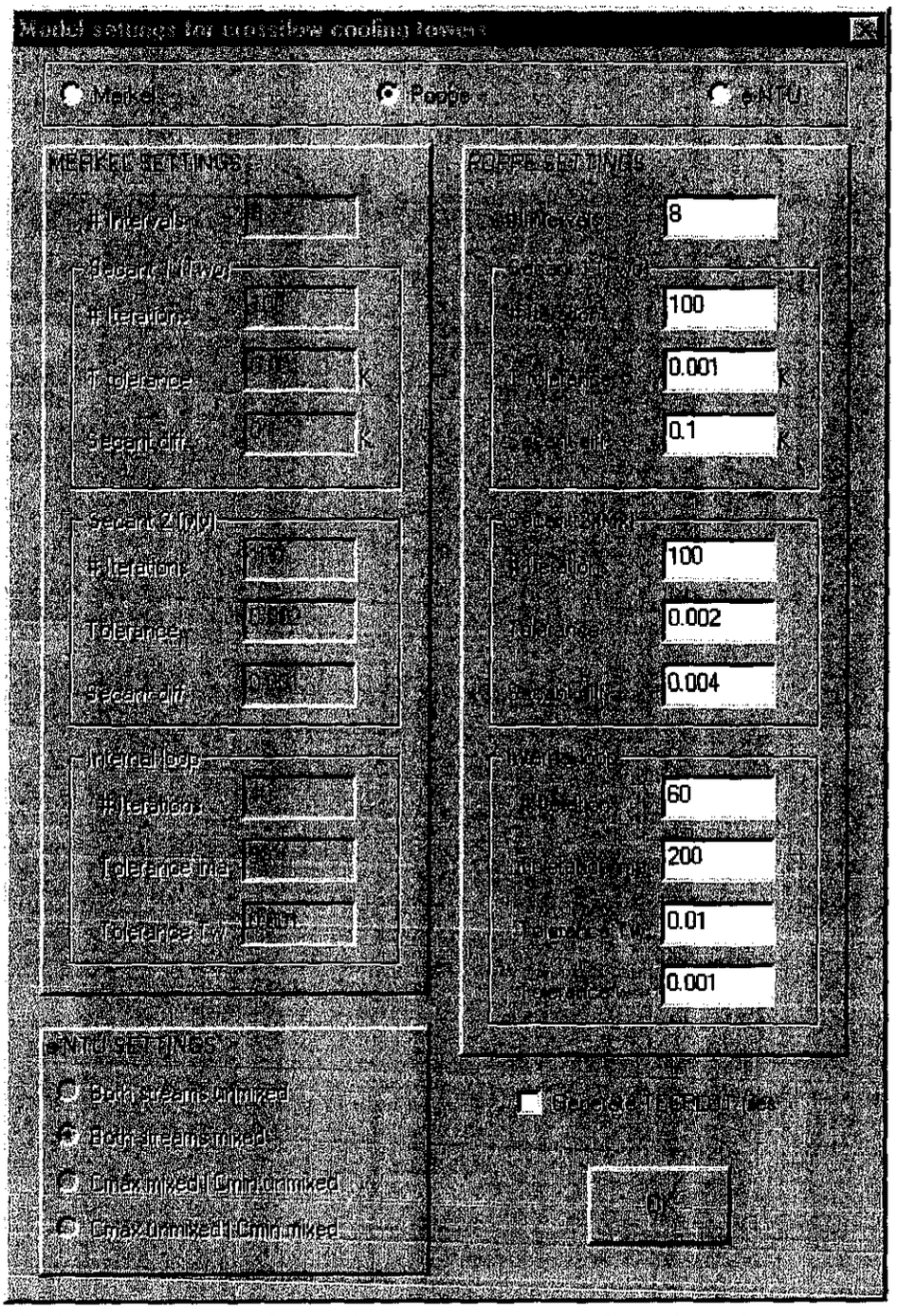

Figure P.6: Dialog window to specify crossflow heat and mass transfer model settings.

The settings for the Merkel and Poppe models in figure P.6 are parameters to control the internal Secant and Jacobi iterative schemes associated with these models. The iterative method employed is discussed in the last paragraph of appendix C. The number of intervals specified are equal in the horizontal and vertical directions. Refer to figure C.2 for an example where the number of intervals is chosen as four.

P.3.6 COOLING TOWER DIMENSIONS

Figures P.7, P.8 and P.9 show the dialog windows where the cooling tower dimensions of mechanical and natural draft towers of counterflow and crossflow configuration are specified. In addition to the dimensions of the cooling towers, it is also specified in each of these dialog windows whether the heat rejected or inlet water temperature is known. The water mass flow rate is also specified on the dialog windows shown in figures P.7 to P.9.

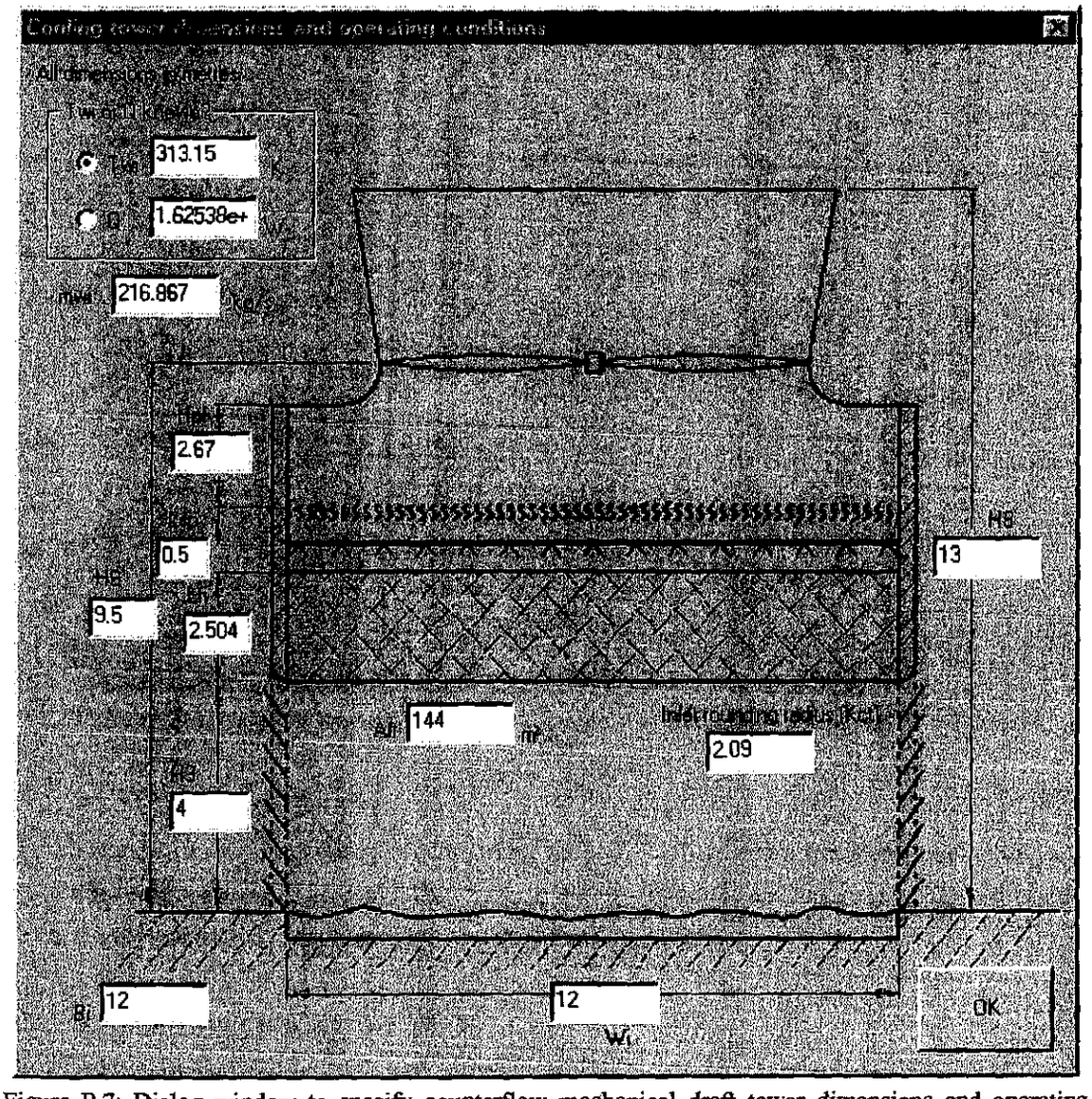

Figure P.7: Dialog window to specify counterflow mechanical draft tower dimensions and operating conditions.

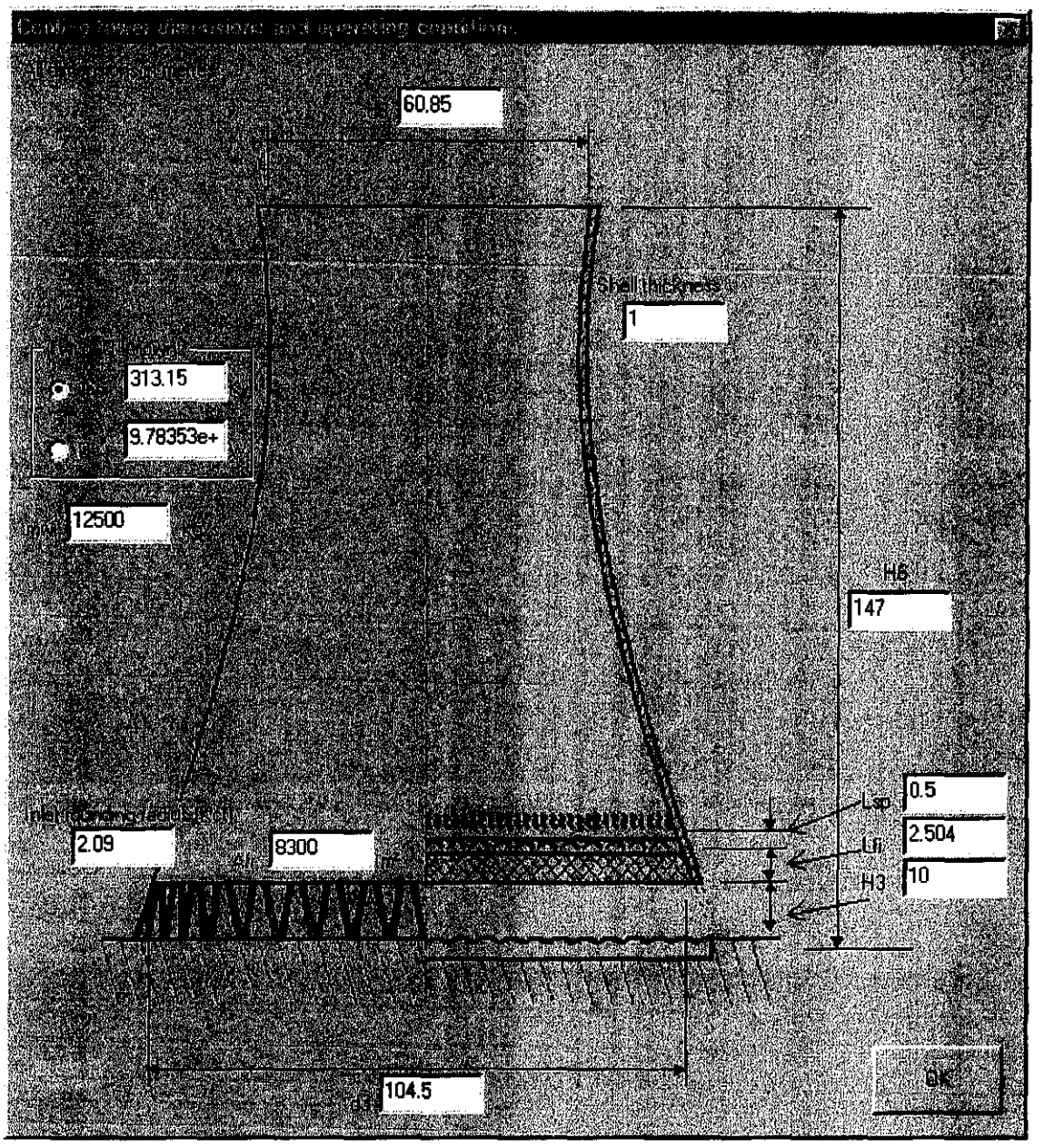

Figure P.8: Dialog window to specify natural draft tower dimensions and operating conditions.

P.3.7 LOSS COEFFICIENTS

Figure P.10 shows the dialog window where the loss coefficients are specified. Loss coefficients can be explicitly specified or be determined by an empirical relation if one is available. The loss coefficient of the fill is specified in the dialog window shown in figure P.4.

P.3.8 FAN SPECIFICATION

For mechanical draft cooling towers the fan can be specified using the dialog window shown in figure P.11. The fan static pressure, fan power and fan efficiency can be specified by sixth order polynomials.

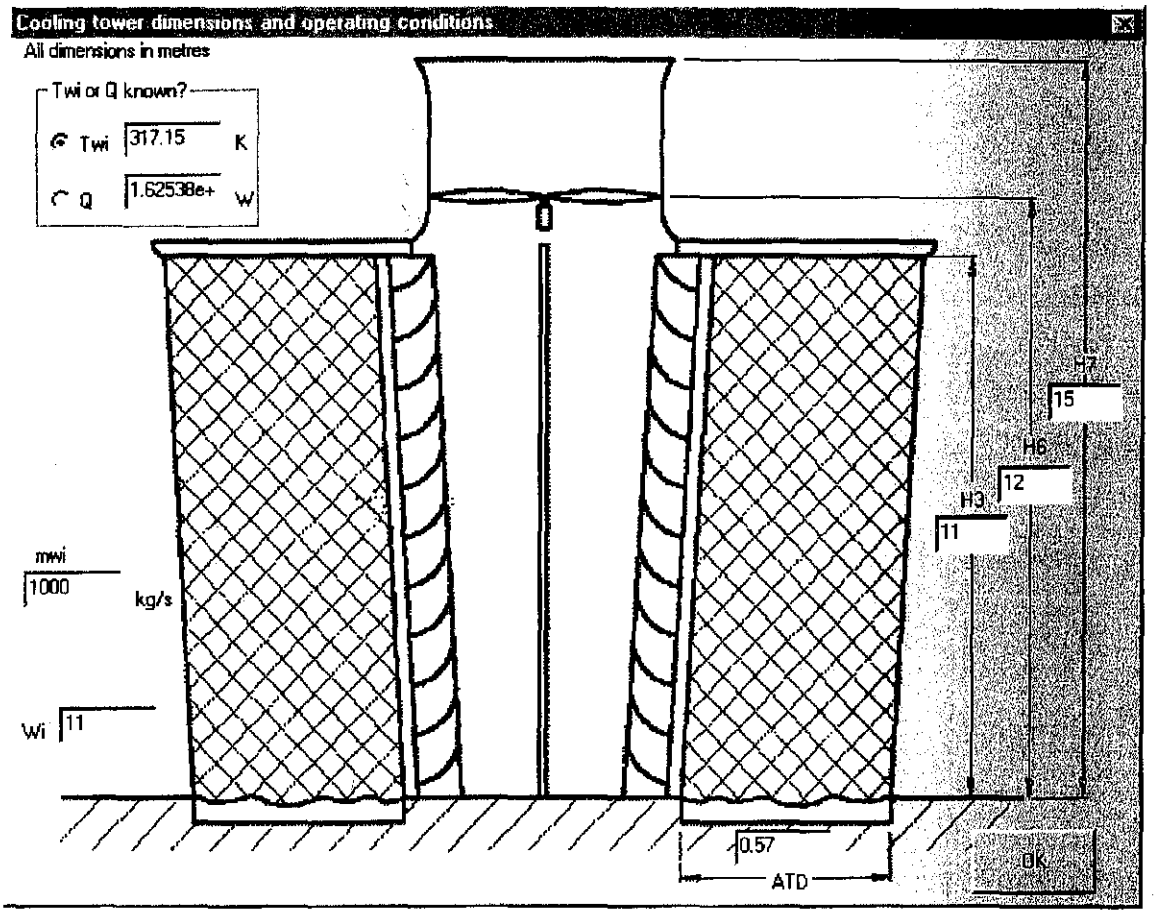

Figure P.9: Dialog window to specify crossflow mechanical draft tower dimensions and operating conditions.

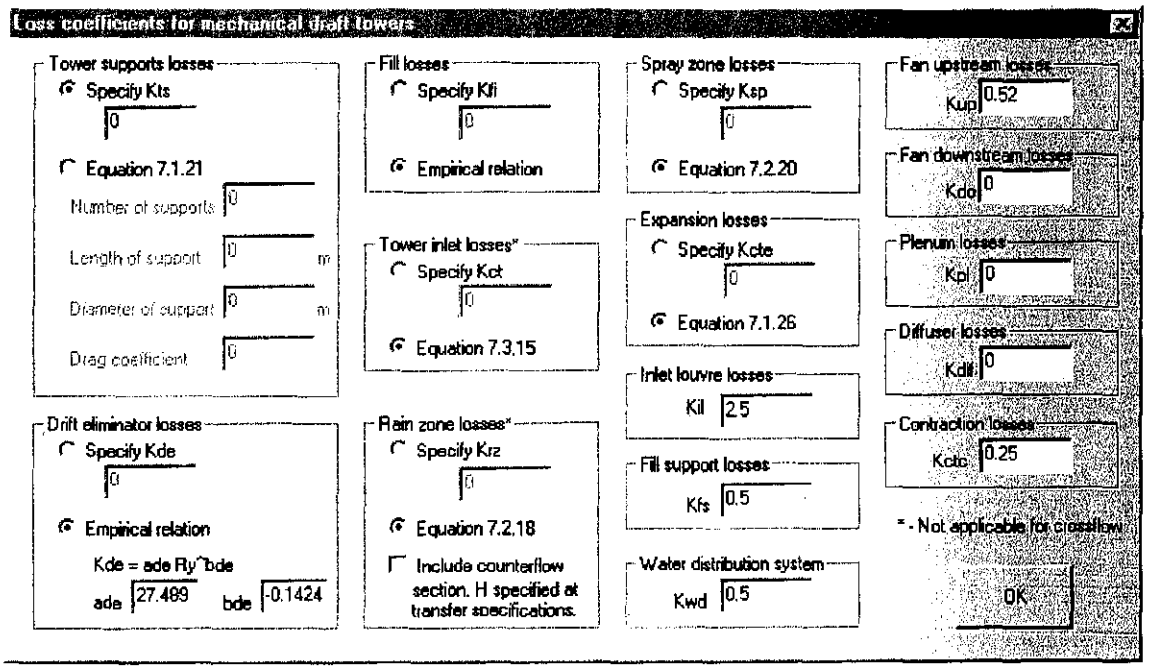

Figure P.10: Dialog window to specify loss coefficients.

The fan and fan casing dimensions are specified as well as the fan model and reference conditions. The fan operating conditions are automatically corrected by the appropriate fan laws. A database of fans can be built by saving the fan specifications entered in the dialog window shown in figure P.11.

P.3.9 COOLING SYSTEM OPTIMIZATION

The geometrical dimensions of natural draft cooling towers can be optimized for the minimum combined operational and capital cost over a selected project period. Refer to appendix U for a detailed discussion of this procedure. In addition, the optimum fill height can be determined for all three types of cooling towers presented above. This simple optimization procedure has only the fill height as a solution variable. At the optimum fill depth the maximum amount of air will flow through the tower while the water is cooled to the minimum temperature for the specific fill height.

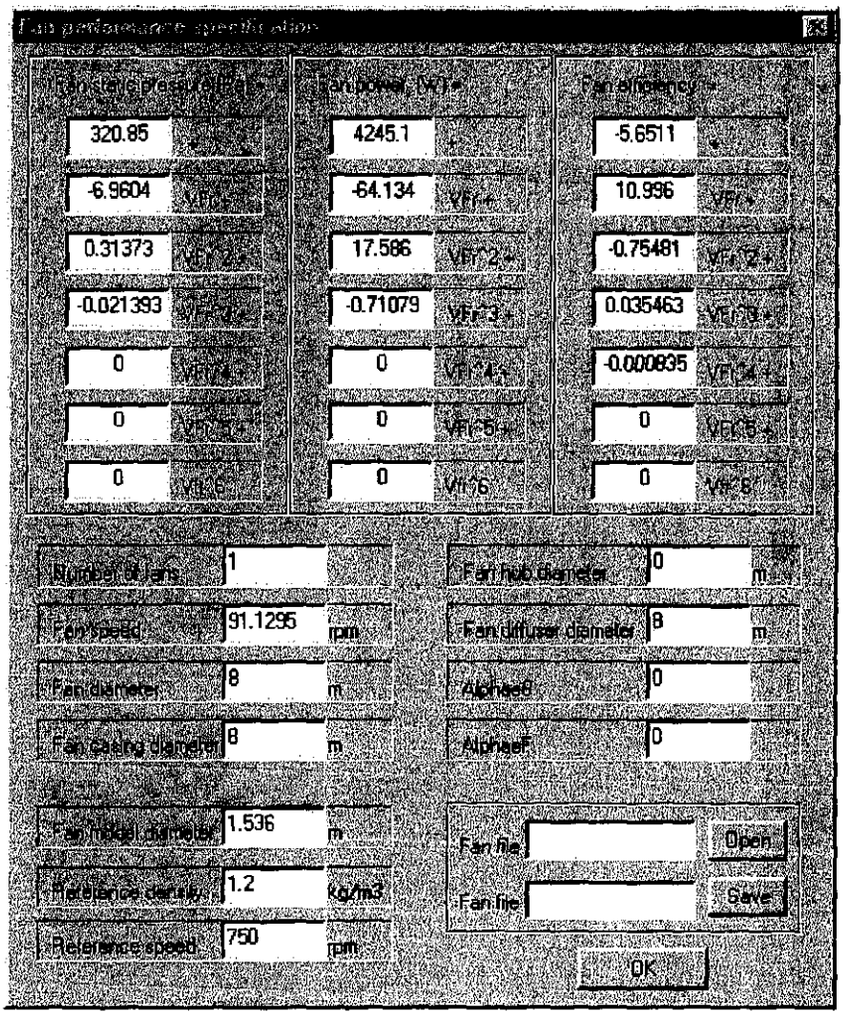

Figure P.11: Dialog window to specify fan.

P.4 CONCLUSION

Due to the simplifications and assumptions made in the development of the software, the program has its limitations. However, it is a very useful tool to predict cooling tower performance. It is also a very useful tool to conduct parametric studies of cooling tower performance and behaviour. Parametric studies can be conducted quickly and efficiently with the maximum control on the solution process.

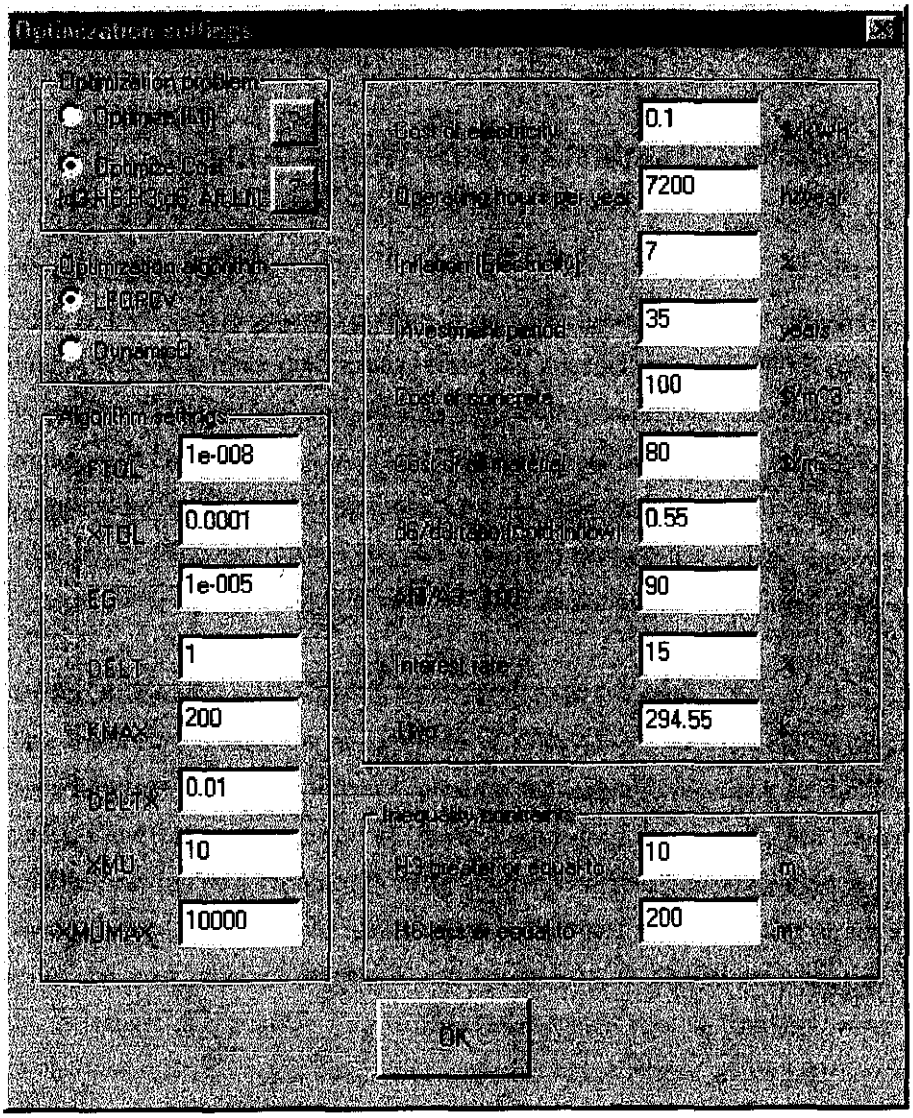

Figure P.12: Dialog window to specify optimization settings.

APPENDIX Q

COOLING TOWER PERFORMANCE CURVES

Q.1 INTRODUCTION

Software is developed to generate cooling tower performance curves for different operating and ambient conditions. A cooling tower performance curve is a graphical tool with which cooling tower performance can be predicted. The performance, i.e., the water outlet temperature or cooling range, can be graphically determined as a function of the ambient temperature, relative humidity, water mass flow rate and water inlet temperature. Cooling tower performance curves can be generated for any cooling tower that can be specified by the WCTPE software program presented in appendix P. This appendix does not serve as a user manual of the software, but illustrates the basic functions and capabilities of the software.

Q.2 PERFORMANCE CURVES GENERATOR SOFTWARE

Cooling Tower Performance Curves Generator (CTPCG) is software that aids in the generation of cooling tower performance curves for different operating and ambient conditions. In addition to the water outlet temperature and cooling range the air outlet temperature, tower draft, heat rejection rate and water evaporatrion rate can be determined from the cooling tower performance curves generated by the CTPCG software. Figure Q.1 shows the graphical user interface of the cooling tower performance curves generator computer program developed with Visual C++ 6. The program consists of four basic steps. Firstly, the ranges of the ambient air temperature, ambient relative humidity, water mass flow rate and inlet water temperature are specified with the number of increments across each variable range. The water outlet temperature is then automatically calculated for each specified operating condition using the WCTPE computer program discussed in appendix P. For the 28 increments of the ambient air temperature, the 9 increments of the relative humidity, the 6 increments of the water flow rate and the 28 increments of the water inlet temperature, 58870 operating points are calculated by the WCTPE computer program.

Step 2 of the computer program defines and calculates the global x-axis and y-axis coordinates of the 58870 cooling tower operating points. The straight lines of the relative humidity and water mass flow rates are also defined in this program step. The operating points must be converted into a structured grid format to reduce the number of data points and to preprocess it for the contour plot generator. The Gnuplot [99WI1] software program is used to generate the contour plots. The density of the structured grid can be defined as seen under step 3 in figure Q.1.

The contour data points of the water outlet temperature and the cooling range are generated in step 4 of the cooling tower performance curve generator. Contour curve smoothing can be obtained by selecting the Bezier smoothing option. The global x-axis and y-axis ranges for the performance curves are defined in this program step. The global y-axis coordinates are expressed in terms of the water inlet temperature.

The global x-axis coordinates are expressed in terms of the ambient air temperature. The data points of the performance curves are written to output files that can be imported into Microsoft Excel, Gnuplot and Tecplot. The variables to plot, in addition to the ambient air temperature, relative humidity, water mass flow rate and inlet water temperature, can be selected under step 4 of the program. The heat rejection rate, Q, the tower draft, m_{av15} and water evaporation rate, $m_{w(evap)}$, must be plotted on a different graph than the water outlet temperature, cooling range and air outlet temperature. The reason for this will be discussed in the next section

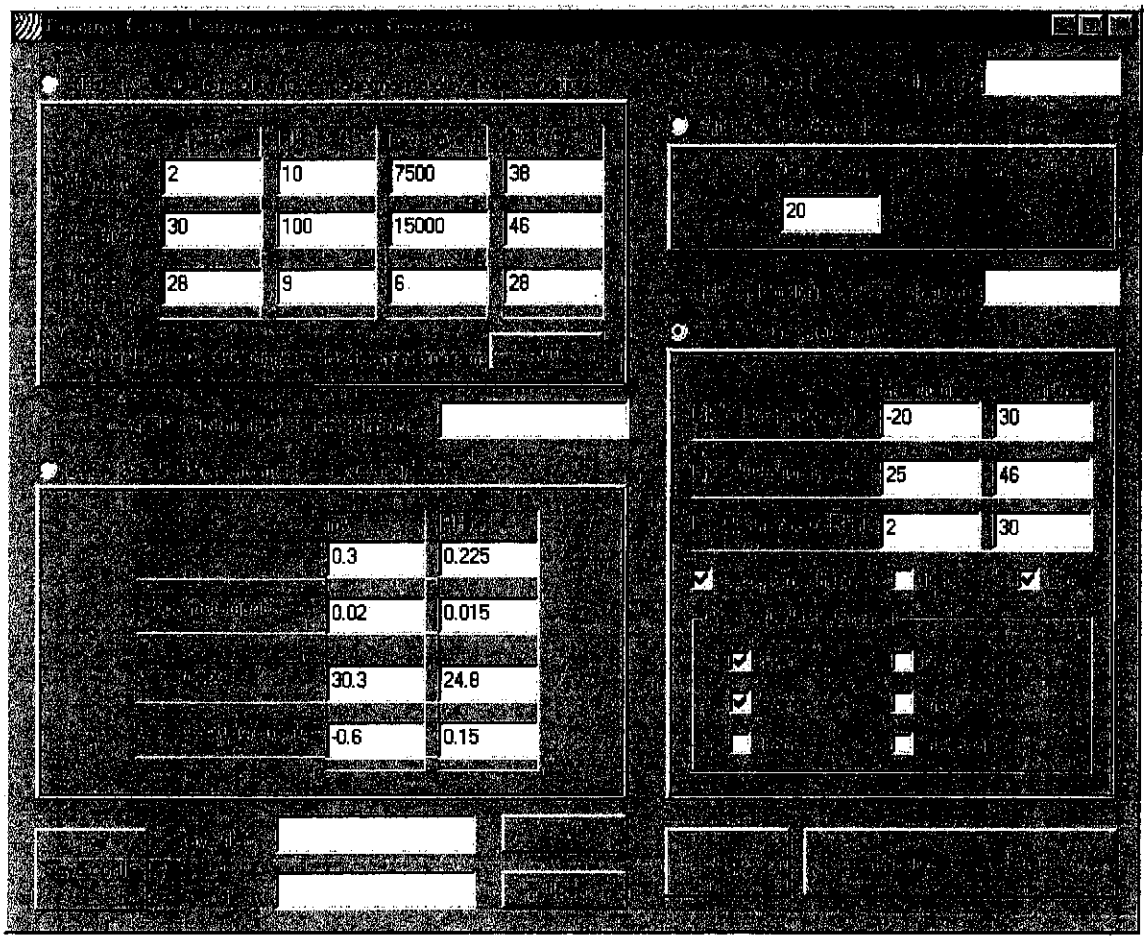

Figure Q.1: Graphical user interface for cooling tower performance curves generator program.

Q.3 COOLING TOWER PERFORMANCE CURVES

Figure Q.2 and figure Q.3 show the cooling tower performance curves generated by the CTPCG computer program for the natural draft cooling tower specified in appendix I. However, the Merkel approach is employed in the generation of the performance curves instead of the Poppe approach. The sample calculation of the performance evaluation of the natural draft tower according to the Merkel approach is given by Kröger [98KR1].

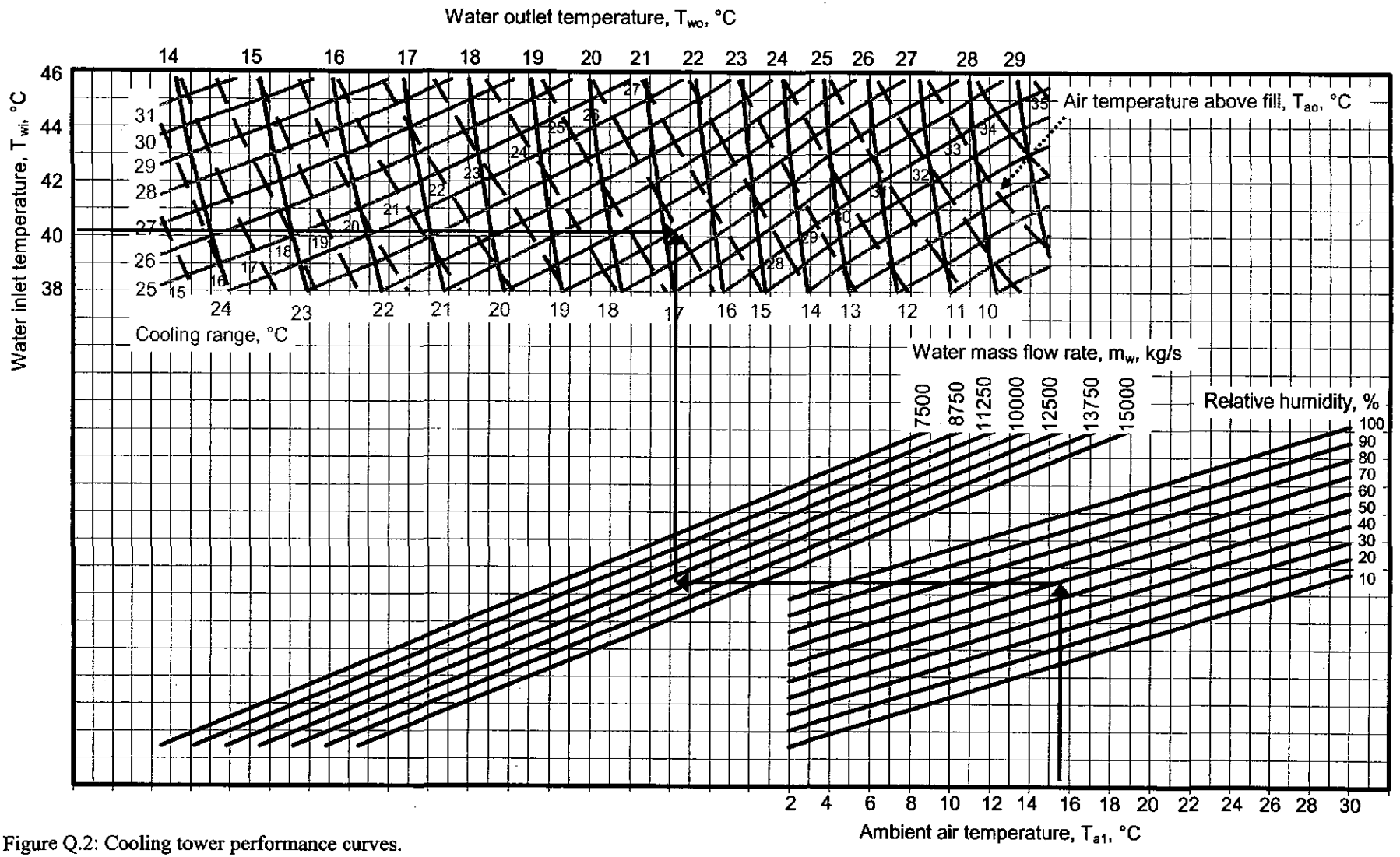

Figure Q.2: Cooling tower performance curves.

Q.3

Q.4

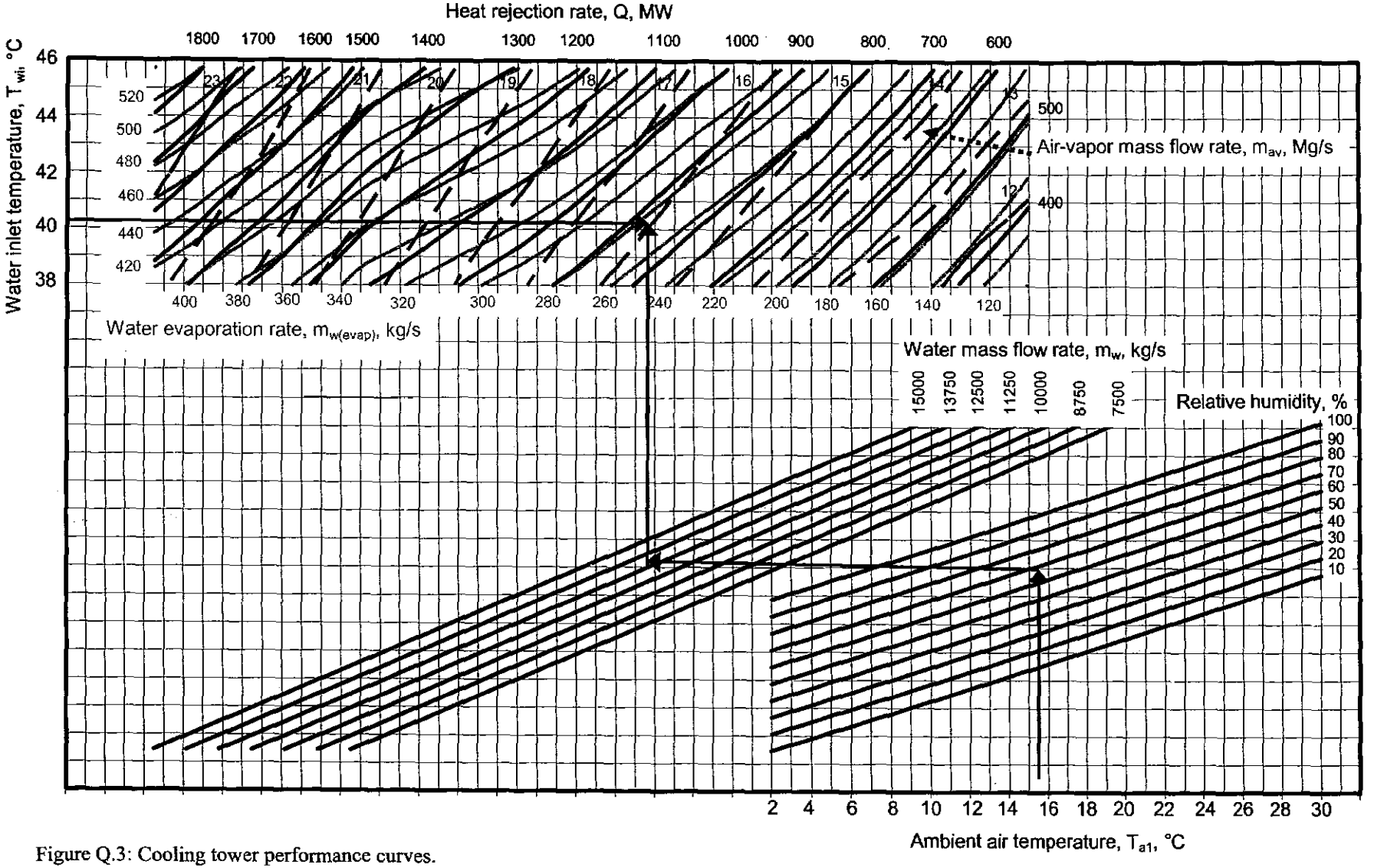

Figure Q.3: Cooling tower performance curves.

Figure Q.2 shows how the water outlet temperature, cooling range and air outlet temperature are obtained when the ambient air temperature, relative humidity, water mass flow rate and water inlet temperature are known. Figure Q.3 shows the how the water evaporation rate, air-vapor mass flow rate and heat rejection rate are obtained when the ambient air temperature, relative humidity, water mass flow rate and water inlet temperature are known. Note that the water mass flow rate lines in figure Q.3 are inverted from those presented in figure Q.2. This is the reason why it is necessary to present the performance curves on two different graphs.

Table Q.1: Comparison of performance curves and Kröger [98KR1]

Variable	Performance curve	Kröger [98KR1]
T_{wo}, °C	21.2	21.376
Range, °C	18.8	18.624
T_{a5}, °C	26.0	26.4219
Q, MW	910	972.713
m_{av15}, kg/s	16500	16845.4
$m_{w(evap)}$, kg/s	285	308.5173

Table Q.1 shows the results, using figure Q.2 and figure Q.3, of the tower specified in appendix I while employing the Merkel approach. These graphically obtained results are compared to the results of a sample calculation of the same tower given by Kröger [98KR1]. It can be seen from table I that the outlet water temperature predicted by the performance curves in figure Q.2 is less than 0.2 °C from the value determined by Kröger [98KR1]. The heat rejection rate and water evaporation rate is approximately 7% less than the values determined by Kröger. The reason for this discrepancy is that the cooling tower performance curves are generated from averaged data. The WCTPE program practically gives identical results to those presented by Kröger [98KR1]. The performance curves are nevertheless a useful tool to predict the approximate cooling tower performance.

Another application for the CTPCG program is to generate performance curves of cooling towers for comparison to the original performance curves supplied by the cooling tower manufacturer. If these two sets of curves compare very well, then the WCTPE program can be employed with confidence in other studies of the cooling tower.

Q.4 CONCLUSION

Cooling tower performance curves are useful tools to predict cooling tower performance for various operating and ambient conditions. However, it is recommended that the WCTPE program presented in appendix P be employed when greater accuracy is required, as the curves generated by the CTPCG program are averaged curves.

APPENDIX R

TRICKLE FILL PERFORMANCE TEST RESULTS

R.1 INTRODUCTION

The performance characteristics of trickle fills of three different heights are determined experimentally. The results are critically evaluated and presented by extended empirical equations. The trickle fills consist of horizontally stacked cylinders as shown in figure R.1. The cylinders have an outside diameter of 90 mm. The height of the spray zones above the fill for all the tests is 150 mm.

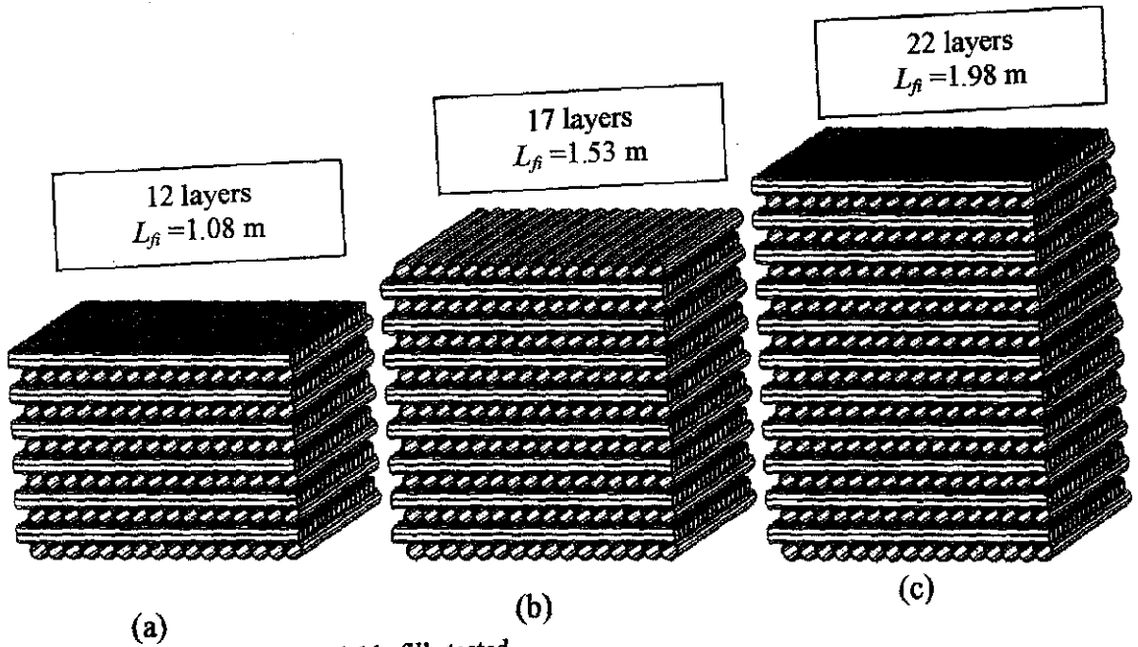

Figure R.1: Three heights of trickle fills tested.

Each fill in figure R.1 is tested at different air and water mass flow rates The results of the tests for the fills shown in figure R.1(a), R.1(b) and R.1(c) are shown in sections R.2, R.3 and R.4 respectively. The test of the 1.53 m high fill, shown in figure R.1(b), is repeated at colder water inlet temperatures to investigate the effect of the inlet water temperature on the transfer coefficient. The results of this test are shown in section R.6. The 1.08 m and 1.98 m fills are then tested at constant water and air mass flow rates to further investigate the effect of the inlet water temperature on fill performance.

R.2 FILL HEIGHT: 1.08 m

Table R.1: Experimental measurements (p_a = 100060 Pa).

	T_{ai} °C	T_{wb} °C	T_{wi} °C	T_{wo} °C	m_a kg/s	m_w kg/s	dp_{fi} Pa	T_{ao} °C
1	12.943	11.905	41.150	31.565	2.677	6.219	12.789	35.954
2	12.592	11.397	41.221	28.916	4.101	6.203	28.033	32.398
3	11.837	10.304	41.252	26.834	5.382	6.174	44.656	29.339
4	11.877	9.939	41.255	25.137	6.743	6.156	70.993	27.893
5	12.524	10.155	41.258	23.825	8.149	6.139	112.324	26.580
6	13.063	10.427	41.248	22.650	9.488	6.145	164.570	25.902
7	14.011	12.867	41.535	34.332	2.779	10.250	19.323	36.862
8	13.868	12.564	41.520	32.437	3.884	10.272	32.459	34.974
9	12.847	11.285	41.479	30.094	5.438	10.262	58.188	33.233
10	12.836	10.870	41.420	28.502	6.806	10.194	90.245	31.650
11	13.468	11.025	41.128	27.242	8.120	10.225	136.201	30.194
12	14.510	11.480	40.121	25.728	9.460	10.237	206.566	28.649
13	15.727	14.427	37.939	34.118	2.688	15.259	32.095	34.461
14	15.375	13.989	36.444	31.508	4.025	15.253	49.694	33.636
15	14.640	12.813	34.672	28.908	5.444	15.265	79.608	31.410
16	14.730	12.428	33.867	27.485	6.650	15.264	114.150	29.945
17	15.189	12.251	33.184	26.160	8.012	15.268	174.013	28.335
18	15.985	12.571	32.817	25.248	9.234	15.268	257.127	27.533

Table R.2: Transfer coefficients, loss coefficients and outlet temperatures according to the different methods (L_{fi} = 1.08 m).

	G_w	G_a	Me_e/L_{fi}	Me_M/L_{fi}	Me_P/L_{fi}	K_{fdm1M}	K_{fdm1P}	T_{aoP}	T_{aoM}
1	2.764	1.190	0.612	0.618	0.684	19.107	19.068	35.091	34.456
2	2.757	1.823	0.763	0.775	0.845	17.627	17.588	32.309	31.757
3	2.744	2.392	0.888	0.906	0.981	16.354	16.321	30.197	29.695
4	2.736	2.997	1.012	1.035	1.115	16.625	16.594	28.467	28.012
5	2.729	3.622	1.134	1.161	1.247	18.064	18.034	27.131	26.719
6	2.731	4.217	1.273	1.303	1.396	19.569	19.540	26.229	25.851
7	4.556	1.235	0.494	0.497	0.568	26.113	26.036	38.102	37.381
8	4.565	1.726	0.597	0.603	0.673	22.306	22.239	36.461	35.796
9	4.561	2.417	0.720	0.731	0.803	20.475	20.417	34.313	33.704
10	4.531	3.025	0.810	0.824	0.899	20.369	20.317	32.628	32.065
11	4.545	3.609	0.893	0.911	0.990	21.675	21.625	31.274	30.754
12	4.550	4.204	1.017	1.040	1.126	24.316	24.268	29.936	29.466
13	6.782	1.194	0.331	0.332	0.385	46.237	46.117	35.746	35.098
14	6.779	1.789	0.459	0.461	0.522	31.997	31.921	33.529	32.960
15	6.784	2.419	0.577	0.580	0.645	28.242	28.184	31.070	30.568
16	6.784	2.956	0.656	0.660	0.728	27.246	27.195	29.644	29.181
17	6.786	3.561	0.752	0.757	0.831	28.715	28.667	28.458	28.029
18	6.786	4.104	0.853	0.860	0.941	31.976	31.926	27.844	27.440

Table R.3: Empirical relations for the Merkel number according to the various methods (L_{fi} = 1.08 m).

Approach	Eq. type	Empirical relation	Correlation coefficient
e-NTU	1	$Me_e / L_{fi} = 0.834905\ G_w^{-0.465726} G_a^{0.615841}$	0.9911
	2	$Me_e / L_{fi} = 1.000951 (G_w / G_a)^{-0.539946}$	0.9749
	3	$Me_e / L_{fi} = 0.008168\ G_w^{0.271388} G_a^{1.950352} + 0.992732\ G_w^{-0.578730} G_a^{0.468523}$	0.9954
Merkel	1	$Me_M / L_{fi} = 0.857501\ G_w^{-0.480158} G_a^{0.624824}$	0.9918
	2	$Me_M / L_{fi} = 1.021224 (G_w / G_a)^{-0.551502}$	0.9774
	3	$Me_M / L_{fi} = 0.008028\ G_w^{0.225358} G_a^{1.996205} + 1.007228\ G_w^{-0.582859} G_a^{0.482056}$	0.9955
Poppe	1	$Me_P / L_{fi} = 0.932891\ G_w^{-0.453190} G_a^{0.592728}$	0.9911
	2	$Me_P / L_{fi} = 1.104216 (G_w / G_a)^{-0.522373}$	0.9760
	3	$Me_P / L_{fi} = 0.008383\ G_w^{0.158542} G_a^{2.070185} + 1.073837\ G_w^{-0.536574} G_a^{0.451302}$	0.9950

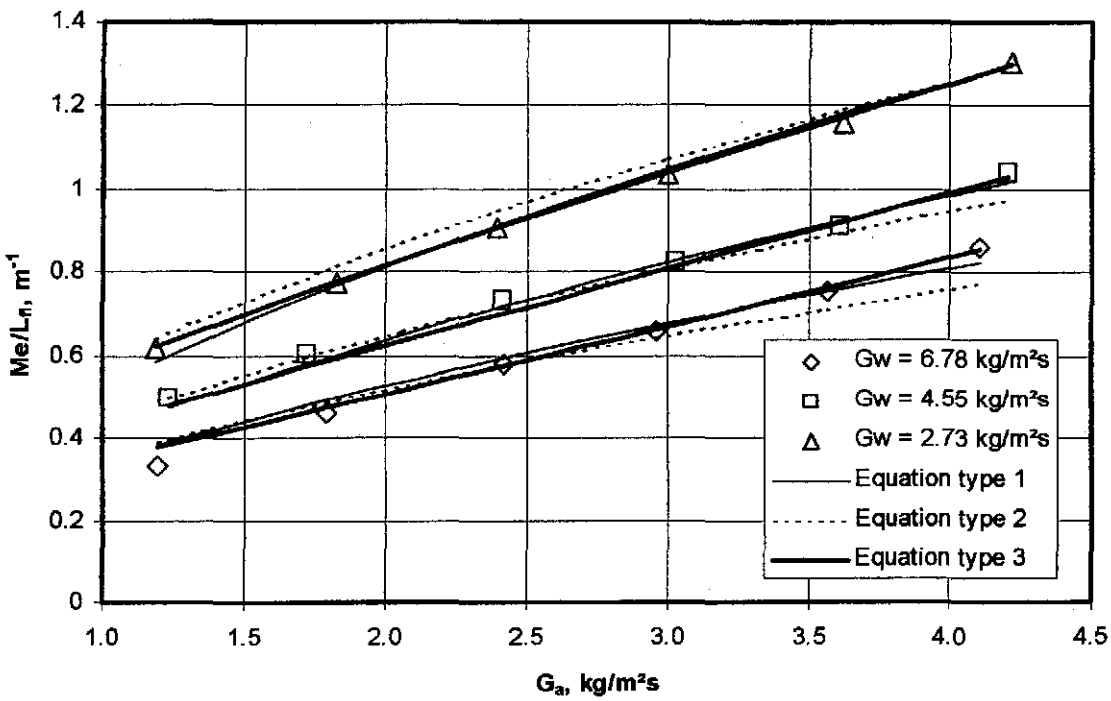

Figure R.2: Comparison of experimental data and empirical equations (L_{fi} = 1.08 m).

Table R.4: Empirical relations for the loss coefficient according to the various methods (L_{fl} = 1.08 m).

Approach	Eq. type	Empirical relation	Correlation coefficient
Merkel and *e-NTU*	1	$K_{fdm1} = 10.054991\ G_w^{0.712342} G_a^{-0.237116}$	0.8043
	2	$K_{fdm1} = 18.517679 (G_w / G_a)^{0.419331}$	0.6199
	3	$K_{fdm1} = 2.330647\ G_w^{1.551011} G_a^{-2.065135} + 5.720996\ G_w^{-0.432653} G_a^{0.521191}$	0.9752
Poppe	1	$K_{fdm1} = 10.026815\ G_w^{0.712256} G_a^{-0.236243}$	0.8039
	2	$K_{fdm1} = 18.484530 (G_w / G_a)^{0.418775}$	0.6187
	3	$K_{fdm1} = 2.331334\ G_w^{1.549666} G_a^{-2.062807} + 5.695113\ G_w^{-0.432545} G_a^{0.523194}$	0.9750

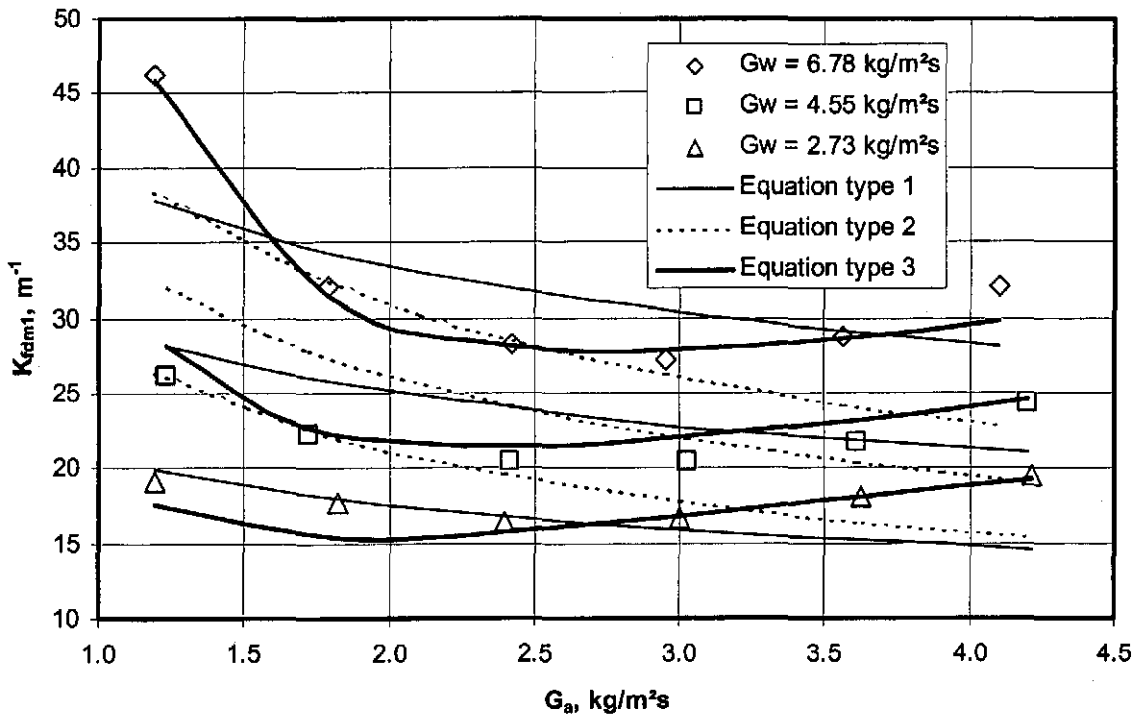

Figure R.3: Comparison of experimental data and empirical relations for the loss coefficient (L_{fl} = 1.08 m).

R.3 FILL HEIGHT: 1.53 m

Table R.5: Experimental measurements (p_a = 101340 Pa).

	T_{ai} °C	T_{wb} °C	T_{wi} °C $_i$	T_{wo} °C	m_a kg/s	m_w kg/s	dp_{fi} Pa	T_{ao} °C
1	16.351	14.451	48.781	34.326	2.701	6.213	18.695	43.753
2	15.951	13.769	48.451	30.551	4.097	6.166	39.393	40.658
3	15.448	12.893	48.432	27.886	5.398	6.171	63.944	38.397
4	15.457	12.414	48.088	25.820	6.707	6.189	99.235	36.304
5	15.912	12.438	47.651	24.149	8.093	6.204	154.657	34.526
6	16.420	12.627	47.113	22.664	9.450	6.149	227.564	32.952
7	16.963	15.303	45.966	36.997	2.727	10.338	25.337	43.310
8	16.448	14.416	45.487	33.794	4.070	10.370	47.584	41.036
9	15.562	13.119	45.067	31.083	5.415	10.330	78.553	38.787
10	15.371	12.390	44.528	28.987	6.753	10.351	120.953	36.848
11	15.886	12.431	44.254	27.363	8.118	10.340	186.495	35.487
12	16.455	12.640	44.013	25.921	9.372	10.342	274.940	34.491
13	17.260	15.430	43.845	38.091	2.730	15.183	37.761	42.136
14	16.971	15.077	43.765	35.800	4.049	15.188	61.901	40.920
15	15.948	13.783	43.665	33.538	5.425	15.093	100.334	39.515
16	15.355	12.789	43.585	31.780	6.760	15.055	151.818	38.414
17	15.365	12.577	43.364	30.349	8.097	15.122	231.878	37.226
18	15.763	12.606	43.228	28.678	9.445	15.069	375.143	36.357

Table R.6: Transfer coefficients, loss coefficients and outlet temperatures according to the different methods (L_{fi} = 1.53 m).

	G_w	G_a	Me_e/L_{fi}	Me_M/L_{fi}	Me_P/L_{fi}	K_{fdm1M}	K_{fdm1P}	T_{aoP}	T_{aoM}
1	2.761	1.201	0.518	0.533	0.597	18.984	18.923	42.240	41.458
2	2.740	1.821	0.660	0.684	0.751	17.228	17.174	38.728	38.060
3	2.743	2.399	0.786	0.816	0.886	16.168	16.122	36.340	35.743
4	2.751	2.981	0.902	0.932	1.007	16.350	16.310	34.205	33.669
5	2.757	3.597	1.028	1.052	1.131	17.601	17.564	32.385	31.904
6	2.733	4.200	1.180	1.189	1.273	19.088	19.053	30.827	30.395
7	4.595	1.212	0.388	0.392	0.458	24.871	24.776	42.894	42.068
8	4.609	1.809	0.502	0.511	0.577	20.842	20.765	40.518	39.776
9	4.591	2.407	0.604	0.620	0.688	19.542	19.475	38.362	37.686
10	4.601	3.001	0.688	0.708	0.778	19.482	19.423	36.378	35.758
11	4.596	3.608	0.775	0.801	0.874	20.881	20.825	34.885	34.316
12	4.597	4.165	0.883	0.914	0.993	23.169	23.113	33.894	33.366
13	6.748	1.213	0.281	0.282	0.342	36.777	36.631	42.012	41.184
14	6.750	1.799	0.382	0.385	0.447	27.272	27.164	40.811	40.040
15	6.708	2.411	0.474	0.481	0.546	24.705	24.612	39.455	38.728
16	6.691	3.005	0.538	0.547	0.612	24.214	24.129	38.040	37.353
17	6.721	3.599	0.596	0.609	0.675	25.908	25.825	36.766	36.121
18	6.697	4.198	0.708	0.727	0.801	30.886	30.796	36.071	35.465

Table R.7: Empirical relations for the Merkel number according to the various methods (L_{fi} = 1.53 m).

Approach	Eq. type	Empirical relation	Correlation coefficient
e-NTU	1	$Me_e / L_{fi} = 0.793101\ G_w^{-0.580211} G_a^{0.674521}$	0.9955
	2	$Me_e / L_{fi} = 0.888688 (G_w / G_a)^{-0.625857}$	0.9905
	3	$Me_e / L_{fi} = 1.267026\ G_w^{-0.182591} G_a^{0.631993} - 0.576009\ G_w^{0.056750} G_a^{0.605960}$	0.9968
Merkel	1	$Me_M / L_{fi} = 0.817071\ G_w^{-0.581055} G_a^{0.670746}$	0.9948
	2	$Me_M / L_{fi} = 0.910464 (G_w / G_a)^{-0.624555}$	0.9903
	3	$Me_M / L_{fi} = 1.299681\ G_w^{-0.121555} G_a^{0.572612} - 0.593218\ G_w^{0.146139} G_a^{0.515254}$	0.9978
Poppe	1	$Me_P / L_{fi} = 0.893319\ G_w^{-0.542378} G_a^{0.625433}$	0.9947
	2	$Me_P / L_{fi} = 0.987536 (G_w / G_a)^{-0.582992}$	0.9901
	3	$Me_P / L_{fi} = 1.321142\ G_w^{-0.111803} G_a^{0.571051} - 0.557590\ G_w^{0.166192} G_a^{0.535537}$	0.9970

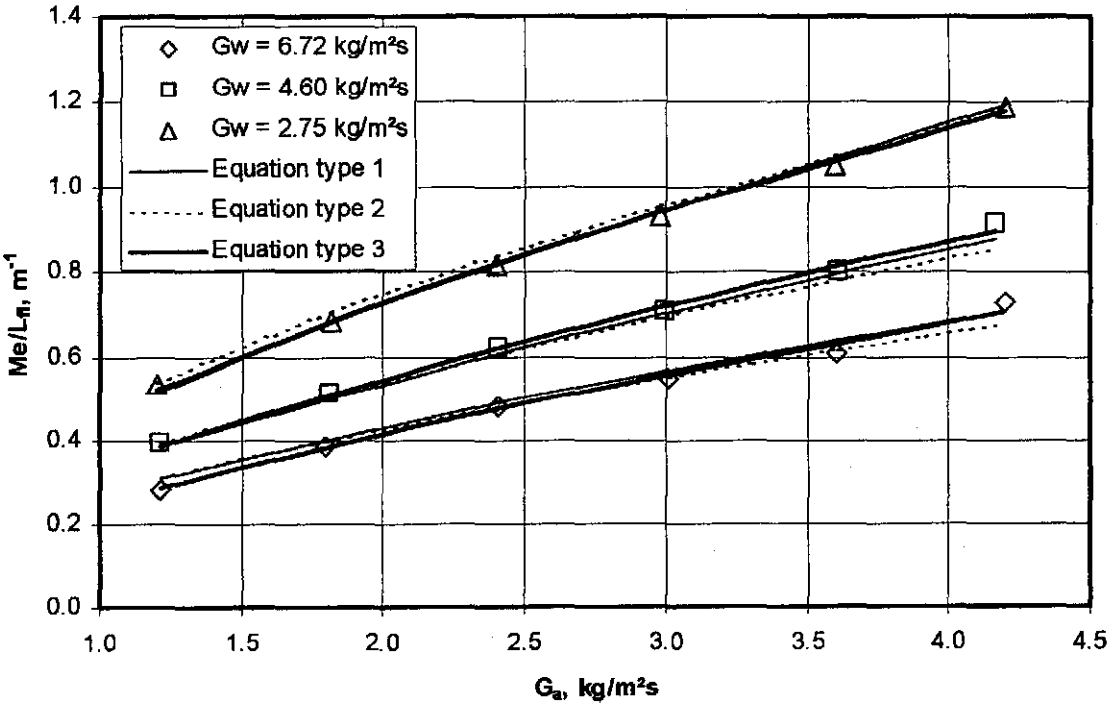

Figure R.4: Comparison of experimental data and empirical equations (L_{fi} = 1.53 m).

Table R.8: Empirical relations for the loss coefficient according to the various methods (L_{fi} = 1.53 m).

Approach	Eq. type	Empirical relation	Correlation coefficient
Merkel and *e-NTU*	1	$K_{fdm1} = 10.855787\ G_w^{0.558271} G_a^{-0.135404}$	0.7562
	2	$K_{fdm1} = 18.587998 (G_w / G_a)^{0.304217}$	0.5234
	3	$K_{fdm1} = 8.885917\ G_w^{0.772070} G_a^{-1.102970} + 1.716322\ G_w^{0.330658} G_a^{1.298676}$	0.9587
Poppe	1	$K_{fdm1} = 10.829610\ G_w^{0.557081} G_a^{-0.134185}$	0.7548
	2	$K_{fdm1} = 18.542800 (G_w / G_a)^{0.303088}$	0.5212
	3	$K_{fdm1} = 8.859530\ G_w^{0.771492} G_a^{-1.104103} + 1.716283\ G_w^{0.329653} G_a^{1.298721}$	0.9585

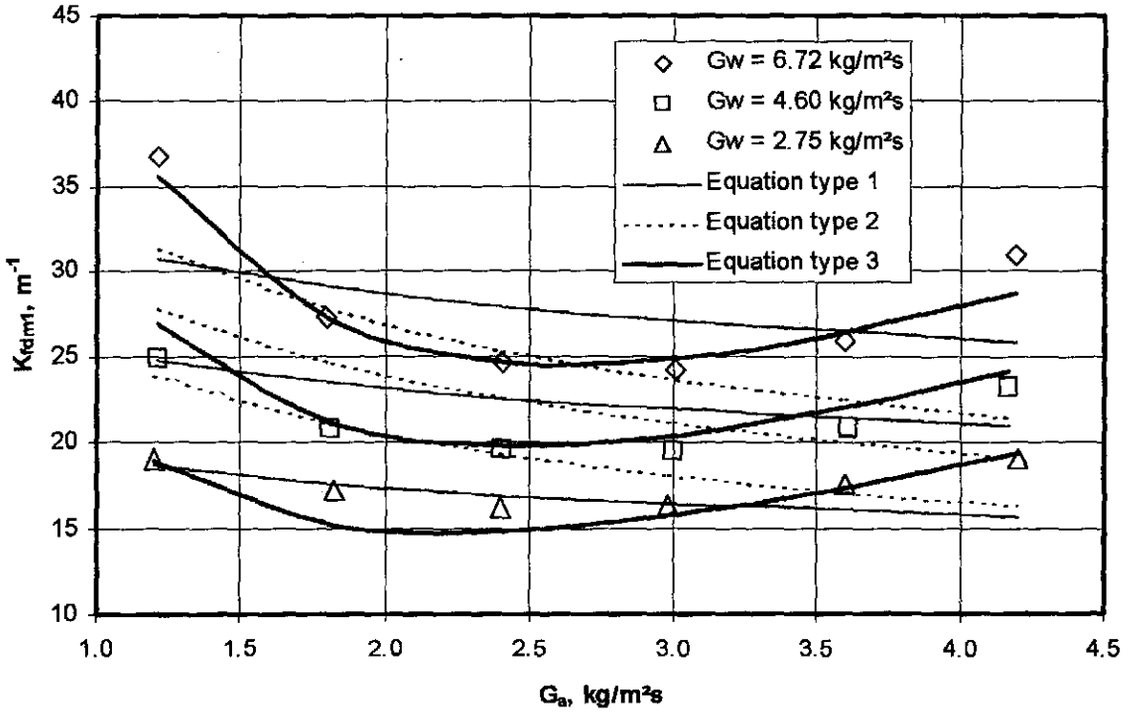

Figure R.5: Comparison of experimental data and empirical relations for the loss coefficient (L_{fi} = 1.53 m).

R.4 FILL HEIGHT: 1.98 m

Table R.9: Experimental measurements (p_a = 100970 Pa).

	T_{ai} °C	T_{wb} °C	T_{wi} °C	T_{wo} °C	m_a kg/s	m_w kg/s	dp_{fi} Pa	T_{ao} °C
1	18.001	14.143	52.856	34.858	2.665	6.343	22.559	47.974
2	17.891	14.057	52.126	30.604	4.002	6.388	48.068	44.435
3	17.354	13.202	51.514	27.266	5.397	6.332	82.355	41.350
4	17.295	12.712	51.104	24.928	6.744	6.322	129.508	38.902
5	17.609	12.616	50.562	23.137	8.056	6.319	195.649	36.829
6	18.271	12.898	49.961	21.782	9.395	6.304	286.882	35.047
7	18.283	15.088	49.252	37.985	2.699	10.183	30.269	46.458
8	17.824	14.502	48.325	33.927	4.083	10.124	59.634	43.560
9	16.947	13.244	47.600	30.937	5.362	10.129	96.806	41.015
10	16.868	12.594	47.016	28.598	6.695	10.095	150.050	38.875
11	17.344	12.720	46.296	26.681	8.086	10.081	231.043	37.009
12	18.016	13.014	45.637	25.154	9.343	10.117	341.255	35.723
13	18.525	15.950	44.656	38.312	2.717	15.149	44.267	43.077
14	17.853	15.028	44.307	35.597	4.040	15.080	75.603	41.655
15	16.903	13.540	43.914	33.052	5.397	15.077	122.481	40.044
16	16.631	12.725	43.587	31.128	6.736	15.114	187.688	38.731
17	17.095	12.628	43.669	29.629	8.106	15.073	288.946	37.665
18	17.738	12.915	43.571	28.382	9.250	15.044	426.801	37.244

Table R.10: Transfer coefficients, loss coefficients and outlet temperatures according to the different methods (L_{fi} = 1.98 m).

	G_w	G_a	Me_e/L_{fi}	Me_M/L_{fi}	Me_P/L_{fi}	K_{fdm1M}	K_{fdm1P}	T_{aoP}	T_{aoM}
1	2.819	1.184	0.451	0.473	0.534	17.862	17.789	46.212	45.350
2	2.839	1.779	0.588	0.621	0.684	16.655	16.591	42.524	41.794
3	2.814	2.399	0.722	0.754	0.821	15.805	15.754	39.258	38.627
4	2.810	2.997	0.851	0.870	0.939	16.043	15.999	36.821	36.259
5	2.808	3.580	0.995	0.985	1.058	17.104	17.064	34.847	34.341
6	2.802	4.176	1.169	1.101	1.176	18.541	18.503	33.154	32.697
7	4.526	1.200	0.346	0.352	0.419	23.013	22.904	46.370	45.459
8	4.500	1.815	0.453	0.468	0.532	19.705	19.619	43.324	42.529
9	4.502	2.383	0.541	0.563	0.627	18.679	18.607	40.907	40.189
10	4.487	2.976	0.618	0.645	0.711	18.716	18.654	38.713	38.060
11	4.481	3.594	0.705	0.736	0.804	19.884	19.826	36.803	36.213
12	4.496	4.152	0.802	0.837	0.910	22.098	22.042	35.468	34.928
13	6.733	1.208	0.270	0.270	0.352	33.240	33.098	43.670	42.812
14	6.702	1.796	0.349	0.352	0.419	25.613	25.506	42.036	41.242
15	6.701	2.399	0.427	0.434	0.499	23.366	23.274	40.462	39.719
16	6.718	2.994	0.481	0.492	0.554	23.120	23.037	38.901	38.205
17	6.699	3.602	0.537	0.552	0.615	24.661	24.580	37.800	37.143
18	6.686	4.111	0.603	0.623	0.689	28.028	27.942	37.052	36.432

Table R.11: Empirical relations for the Merkel number according to the various methods (L_{fi} = 1.98 m).

Approach	Eq. type	Empirical relation	Correlation coefficient
e-NTU	1	$Me_e / L_{fi} = 0.809060\ G_w^{-0.689841} G_a^{0.724050}$	0.9934
	2	$Me_e / L_{fi} = 0.843326 (G_w / G_a)^{-0.706997}$	0.9928
	3	$Me_e / L_{fi} = 1.534059\ G_w^{-0.862216} G_a^{0.630953} - 1.024374\ G_w^{-1.377900} G_a^{0.393037}$	0.9956
Merkel	1	$Me_M / L_{fi} = 0.817647\ G_w^{-0.644301} G_a^{0.672908}$	0.9984
	2	$Me_M / L_{fi} = 0.846533 (G_w / G_a)^{-0.658826}$	0.9980
	3	$Me_M / L_{fi} = 1.262879\ G_w^{-0.298056} G_a^{0.658548} - 0.543287\ G_w^{-0.064423} G_a^{0.648236}$	0.9990
Poppe	1	$Me_P / L_{fi} = 0.892753\ G_w^{-0.589301} G_a^{0.611772}$	0.9969
	2	$Me_P / L_{fi} = 0.917453 (G_w / G_a)^{-0.600831}$	0.9662
	3	$Me_P / L_{fi} = 1.808451\ G_w^{-0.809397} G_a^{0.558907} - 1.270136\ G_w^{-1.371907} G_a^{0.439482}$	0.9976

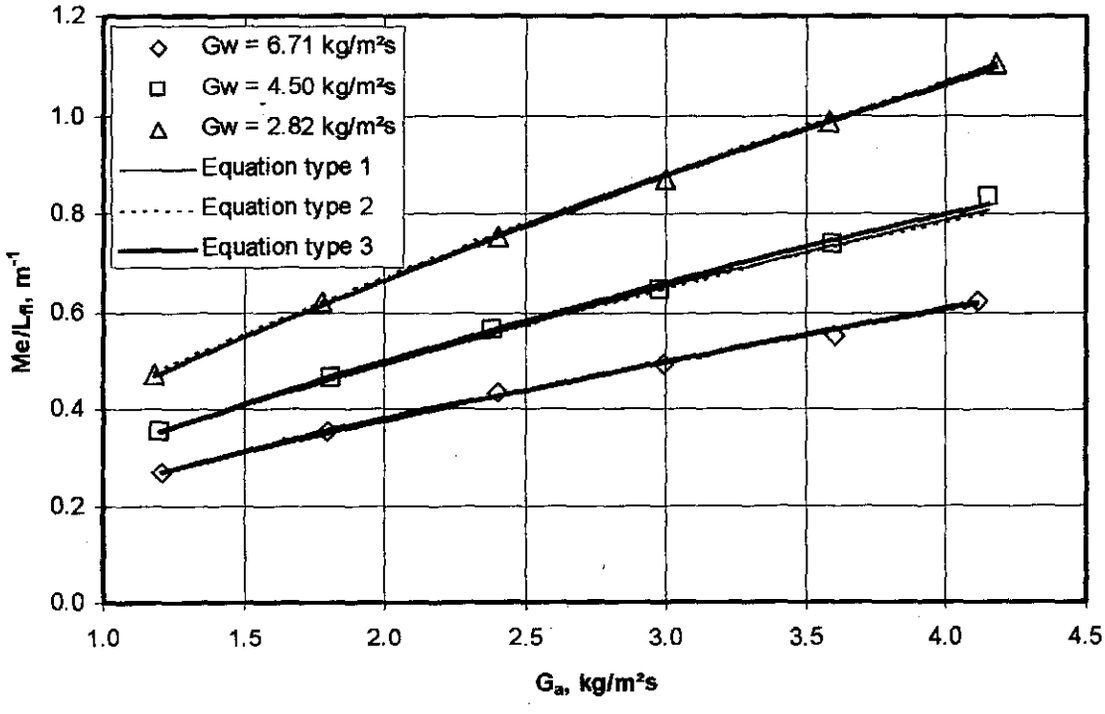

Figure R.6: Comparison of experimental data and empirical equations (L_{fi} = 1.98 m).

Table R.12: Empirical relations for the loss coefficient according to the various methods (L_{fi} = 1.98 m).

Approach	Eq. type	Empirical relation	Correlation coefficient
Merkel and *e-NTU*	1	$K_{fdm1} = 10.539809\ G_w^{0.525842} G_a^{-0.107452}$	0.7779
	2	$K_{fdm1} = 17.952891 (G_w / G_a)^{0.270809}$	0.4998
	3	$K_{fdm1} = 7.047319\ G_w^{0.812454} G_a^{-1.143846} + 2.677231\ G_w^{0.294827} G_a^{1.018498}$	0.9684
Poppe	1	$K_{fdm1} = 10.501559\ G_w^{0.524991} G_a^{-0.105825}$	0.7765
	2	$K_{fdm1} = 17.904821 (G_w / G_a)^{0.269548}$	0.4965
	3	$K_{fdm1} = 6.993131\ G_w^{0.813936} G_a^{-1.147400} + 2.686735\ G_w^{0.294068} G_a^{1.016412}$	0.9682

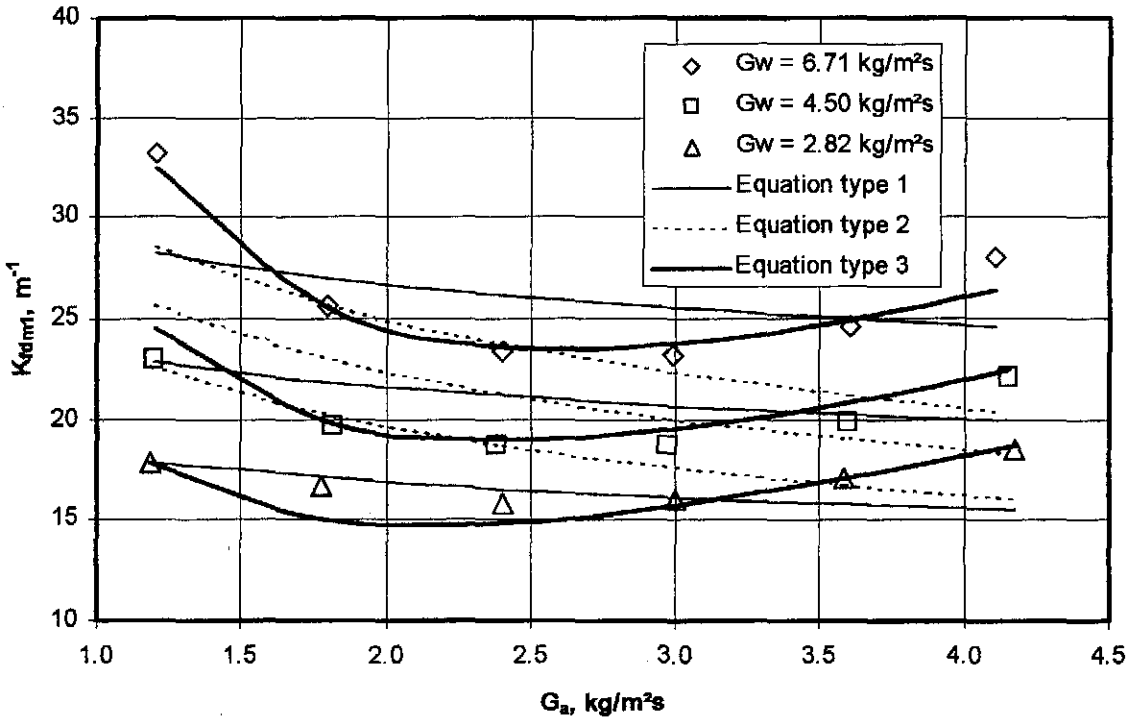

Figure R.7: Comparison of experimental data and empirical relations for the loss coefficient (L_{fi} = 1.98 m).

R.5 SUMMARY AND COMBINED RESULTS

A summary of the equations for the transfer coefficient, according to the Merkel approach, is shown in table R.13. It can be seen from figures R.2, R.4 and R.6 that all three types of equations give accurate representations of the measured data. This is also shown in table R.13 where all the correlation coefficients, r^2, are close to unity.

Table R.13: Summary of the transfer coefficients according to the Merkel approach.

L_{fi}, m	Equation type 1	r^2
1.08	$Me_M / L_{fi} = 0.857501\ G_w^{-0.480158} G_a^{0.624824}$	0.9918
1.53	$Me_M / L_{fi} = 0.817071\ G_w^{-0.581055} G_a^{0.670746}$	0.9948
1.98	$Me_M / L_{fi} = 0.817647\ G_w^{-0.644301} G_a^{0.672908}$	0.9984
L_{fi}, m	**Equation type 2**	r^2
1.08	$Me_M / L_{fi} = 1.021224 (G_w / G_a)^{-0.551502}$	0.9774
1.53	$Me_M / L_{fi} = 0.910464 (G_w / G_a)^{-0.624555}$	0.9903
1.98	$Me_M / L_{fi} = 0.846533 (G_w / G_a)^{-0.658826}$	0.9980
L_{fi}, m	**Equation type 3**	r^2
1.08	$Me_M / L_{fi} = 0.008028\ G_w^{0.225358} G_a^{1.996205} + 1.007228\ G_w^{-0.582859} G_a^{0.482056}$	0.9955
1.53	$Me_M / L_{fi} = 1.299681\ G_w^{-0.121555} G_a^{0.572612} - 0.593218\ G_w^{0.146139} G_a^{0.515254}$	0.9979
1.98	$Me_M / L_{fi} = 1.262879\ G_w^{-0.298056} G_a^{0.658548} - 0.543287\ G_w^{-0.064423} G_a^{0.648236}$	0.9905

The experimental data for the transfer coefficient for all the different fill heights can be represented by

$$Me_M / L_{fi} = 0.932886\ G_w^{-0.541807} G_a^{0.648385} L_{fi}^{-0.361078} \qquad \text{(R.1)}$$

with a correlation coefficient $r^2 = 0.986328$.

Figure R.8 shows the results from equation (R.1) compared to the transfer characteristics obtained from experimental measurements. Tests 1 to 18 in figure R.8 represent the tests for the 1.08 m thick fill. Tests 19 to 36 represent the fill test results of the 1.53 m thick fill and tests 37 to 54 represent the measurements of the 1.98 m thick fill.

Due to the limitations of the fill test facility, it is impossible to conduct the fill tests at a constant water temperature. If the effect of the changing water temperature is included in the correlation, the Merkel number can then be presented by

$$Me_M / L_{fi} = 1.930306\ G_w^{-0.568230} G_a^{0.641400} L_{fi}^{-0.352733} T_{wi}^{-0.178670} \qquad \text{(R.2)}$$

with a correlation coefficient $r^2 = 0.986224$.

A summary of the equations for the loss coefficient according to the Merkel approach is shown in table R.14. It can be seen from the correlation coefficients, r^2, in table R.14 that equation type 3 gives the most accurate representation of the measured data. Equation type 1 and equation type 2 do not correlate the measured data well. This is seen in figures R.3, R.5 and R.6.

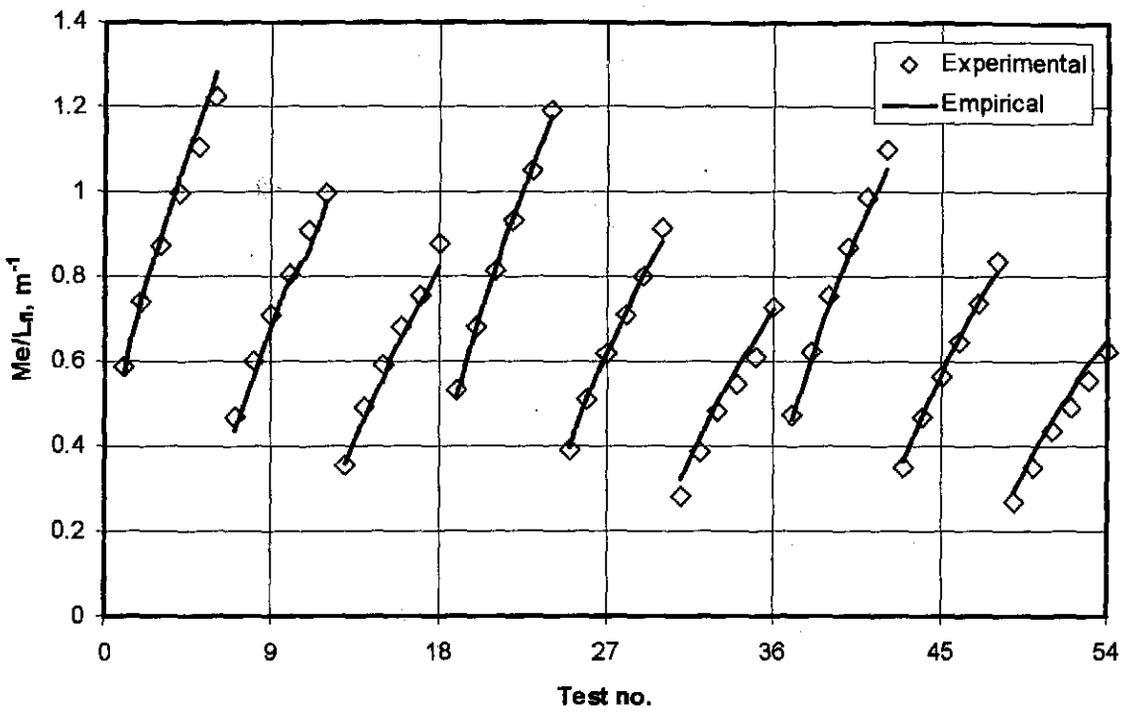

Figure R.8: Transfer characteristic given by equation (R.1) compared to experiemtal results.

Table R.14: Summary of the loss coefficients.

L_{fi}, m	Equation type 1	r^2
1.08	$K_{fdm1} = 10.054991\ G_w^{0.712342} G_a^{-0.237116}$	0.8043
1.53	$K_{fdm1} = 10.855787\ G_w^{0.558271} G_a^{-0.135404}$	0.7548
1.98	$K_{fdm1} = 10.539809\ G_w^{0.525842} G_a^{-0.107452}$	0.7779
L_{fi}, m	**Equation type 2**	r^2
1.08	$K_{fdm1} = 18.517679 (G_w / G_a)^{0.419331}$	0.6199
1.53	$K_{fdm1} = 18.587998 (G_w / G_a)^{0.304217}$	0.5212
1.98	$K_{fdm1} = 17.952891 (G_w / G_a)^{0.270809}$	0.4998
L_{fi}, m	**Equation type 3**	r^2
1.08	$K_{fdm1} = 2.330647\ G_w^{1.551011} G_a^{-2.065135} + 5.720996\ G_w^{-0.432653} G_a^{0.521191}$	0.9752
1.53	$K_{fdm1} = 8.885917\ G_w^{0.772070} G_a^{-1.102970} + 1.716322\ G_w^{0.330658} G_a^{1.298676}$	0.9585
1.98	$K_{fdm1} = 7.047319\ G_w^{0.812454} G_a^{-1.143846} + 2.677231\ G_w^{0.294827} G_a^{1.018498}$	0.9684

The experimental data for the loss coefficient for all the different fill heights can be represented by

$$K_{fdm1} = 11.093641\ G_w^{0.603252} G_a^{-0.148620} L_{fi}^{-0.203976} \qquad \text{(R.3)}$$

with a correlation coefficient r^2 = 0.769823. Equation (R.3) and the test data of the three different fill heights are shown in figure R.9. The correlation coefficient suggested that equation (R.3) does not correlate the data well and this is evident from figure R.9.

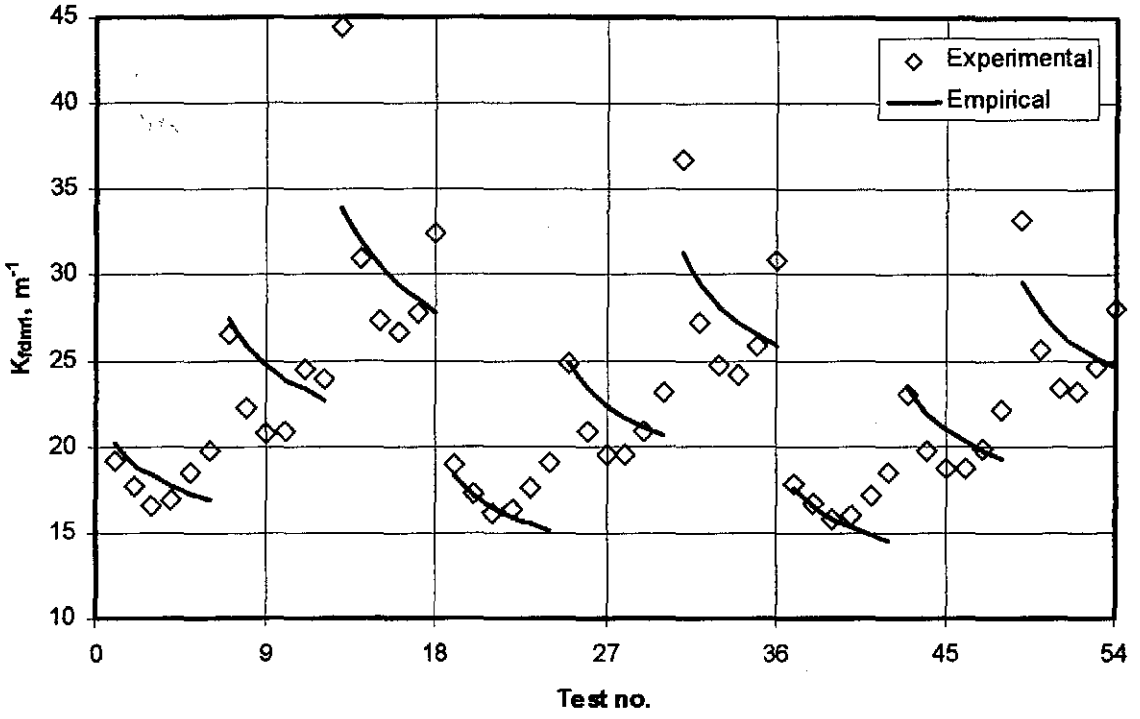

Figure R.9: Loss coefficients given by equation (R.3) compared to experiemtal results.

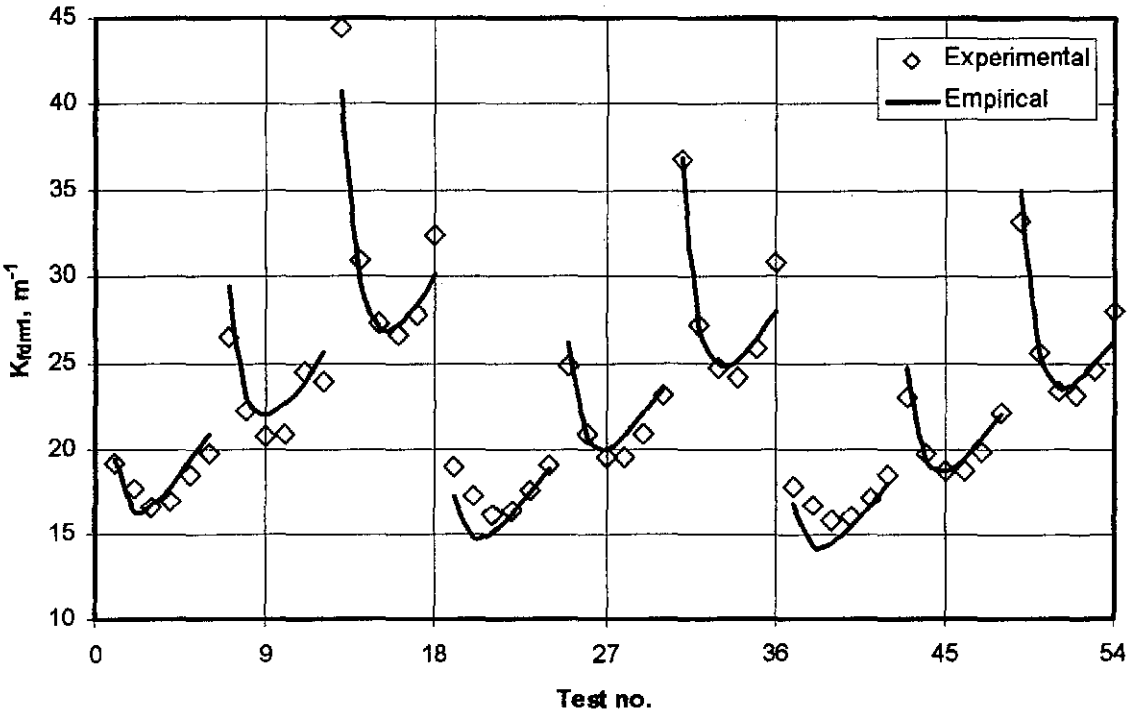

Figure R.10: Loss coefficients given by equation (R.4) compared to experiemtal results.

The data for the tests of all three fill heights can also be correlated by

$$K_{fdm1} = \left(4.547149\, G_w^{1.37677} G_a^{-1.770200} + 5.058140\, G_w^{0.381274} G_a^{0.673116}\right) L_{fi}^{-0.207834} \qquad \text{(R.4)}$$

with a correlation coefficient $r^2 = 0.950862$. It can be seen from figure R.10 that equation (R.4) correlates the data accurately.

As a function of the inlet water temperature, expressed in °C, the loss coefficient is correlated by

$$K_{fdm1} = \left(3.8163\ G_w^{1.149219} G_a^{-1.773193} + 4.296632\ G_w^{0.387023} G_a^{0.673487}\right) L_{fi}^{-0.209736} T_{wi}^{0.040794} \qquad \text{(R.5)}$$

with a correlation coefficient $r^2 = 0.9508$. It can be seen that the loss coefficient is a very weak function of the inlet water temperature as the exponent of T_{wi} in equation (R.5) is very close to zero.

R.6 FILL HEIGHT: 1.53 m TESTED AT COLDER WATER TEMPERATURES.

The fill test presented in section R.3 is repeated in this section at colder water temperatures. The fill test measurements are shown in table R.15 with the corresponding transfer and loss coefficients shown in table R.16. The empirical equations are not plotted for this fill test, as they are essentially the same as those in figures R.4 and R.5.

Table R.15: Experimental measurements (p_a = 101340 Pa).

	T_{ai} °C	T_{wb} °C	T_{wi} °C	T_{wo} °C	m_a kg/s	m_w kg/s	dp_{fi} Pa	T_{ao} °C
1	15.686	14.377	42.329	31.718	2.729	6.250	18.812	38.485
2	15.137	13.606	42.027	28.489	4.115	6.220	38.954	36.116
3	14.605	12.763	41.845	26.122	5.403	6.228	63.052	34.109
4	14.414	12.195	41.630	24.255	6.789	6.240	100.579	32.375
5	14.795	12.104	41.387	22.826	8.115	6.218	153.825	30.922
6	15.246	12.312	41.018	21.548	9.534	6.240	230.210	29.691
7	15.763	14.573	40.578	33.771	2.713	10.250	24.190	38.116
8	15.059	13.716	39.926	30.970	4.049	10.270	45.720	36.358
9	14.315	12.813	39.400	28.597	5.450	10.223	77.528	34.691
10	13.956	12.086	38.956	26.819	6.759	10.253	118.283	33.108
11	14.115	11.862	38.574	25.269	8.166	10.120	184.456	31.787
12	14.462	11.950	38.452	24.132	9.365	10.256	266.665	31.027
13	15.414	14.503	38.178	34.002	2.717	15.050	35.886	36.756
14	15.016	14.084	37.595	31.826	4.069	15.020	59.857	35.566
15	14.351	12.973	37.145	29.873	5.433	14.971	97.078	34.237
16	14.029	12.152	36.672	28.221	6.769	15.002	148.028	32.912
17	14.112	11.934	35.909	26.804	8.157	14.981	226.963	31.625
18	14.445	11.981	35.411	25.663	9.304	14.945	332.053	30.901

If is curve is fitted through the data of this fill test and the fill test presented in section R.3 for the same fill, with the hotter inlet water temperatures, then find

$$Me_M / L_{fi} = 1.907410\ G_w^{-0.599957} G_a^{0.649337} T_{wi}^{-0.209468} \qquad \text{(R.6)}$$

with a correlation coefficient, $r^2 = 0.9951$ and T_{wi} is in °C. The exponents for G_w and G_a are within close tolerance of those presented in table R.7 or table R.13. The exponent of T_{wi} in equation (R.6) is within close tolerance of the exponent of T_{wi} in equation (R.2)

The influence of the inlet water temperature on the performance of a fill is investigated where all other test parameters are held approximately constant.

Table R.16: Transfer coefficients, loss coefficients and outlet temperatures according to the different methods (L_{fi} = 1.53 m).

	G_w	G_a	Me_e/L_{fi}	Me_M/L_{fi}	Me_P/L_{fi}	K_{fdm1M}	K_{fdm1P}	T_{aoP}	T_{aoM}
1	2.778	1.213	0.536	0.545	0.610	19.059	19.019	37.438	36.793
2	2.765	1.829	0.688	0.704	0.772	17.198	17.160	34.667	34.112
3	2.768	2.402	0.817	0.840	0.913	16.186	16.153	32.627	32.131
4	2.773	3.017	0.926	0.954	1.030	16.439	16.409	30.691	30.246
5	2.763	3.607	1.036	1.066	1.146	17.667	17.639	29.180	28.777
6	2.773	4.237	1.173	1.202	1.288	19.218	19.191	27.971	27.609
7	4.555	1.206	0.412	0.415	0.485	24.554	24.491	38.366	37.676
8	4.564	1.800	0.532	0.537	0.606	20.699	20.645	36.207	35.590
9	4.544	2.422	0.638	0.648	0.718	19.440	19.394	34.204	33.648
10	4.557	3.004	0.721	0.735	0.806	19.381	19.339	32.554	32.043
11	4.498	3.629	0.805	0.823	0.896	20.810	20.769	30.963	30.497
12	4.558	4.162	0.908	0.932	1.011	22.910	22.869	30.340	29.902
13	6.689	1.207	0.293	0.293	0.354	36.258	36.165	36.814	36.153
14	6.676	1.808	0.407	0.409	0.474	26.859	26.790	35.457	34.852
15	6.654	2.415	0.505	0.508	0.575	24.495	24.435	34.133	33.564
16	6.667	3.009	0.584	0.590	0.658	24.160	24.105	32.834	32.300
17	6.658	3.625	0.637	0.644	0.710	25.657	25.605	31.201	30.712
18	6.642	4.135	0.716	0.725	0.796	28.926	28.872	30.355	29.898

R.7 FILL HEIGHT: 1.08 m, G_a AND G_w CONSTANT

The 1.08 m fill is tested at approximately constant air and water mass flow rates. Only the inlet water mass flow rate is varied during the duration of the fill test. This is done to investigate the dependence of the transfer coefficient on the inlet water temperature. Table R.17 contains the experimental measurements of the fill test and table R.18 contains the corresponding transfer and loss coefficients.

Table R.17: Experimental measurements (p_a = 100060 Pa)

	T_{ai} °C	T_{wb} °C	T_{wi} °C	T_{wo} °C	m_a kg/s	m_w kg/s	dp_{fi} Pa	T_{ao} °C
1	16.656	11.693	56.252	33.671	6.734	10.137	91.434	
2	16.673	11.705	56.053	33.585	6.735	9.984	91.366	
3	16.631	11.645	55.726	33.499	6.735	10.068	91.131	
4	16.626	11.641	55.453	33.399	6.736	10.088	91.178	
5	16.583	11.570	54.930	33.269	6.734	9.860	91.053	
6	16.536	11.479	54.706	33.118	6.743	10.039	90.700	
7	16.510	11.501	53.758	32.900	6.742	10.012	90.711	
8	16.466	11.512	53.389	32.778	6.748	10.028	90.745	
9	16.414	11.448	53.141	32.657	6.748	9.999	90.437	
10	16.398	11.405	52.811	32.568	6.751	9.992	90.297	
11	16.395	11.388	52.429	32.435	6.745	9.987	89.879	
12	16.400	11.397	52.300	32.387	6.746	9.970	89.883	
13	16.393	11.407	51.882	32.278	6.747	9.954	89.944	
14	16.359	11.362	51.535	32.107	6.749	9.964	89.655	

Table R.17 (continue): Experimental measurements (p_a = 100060 Pa)

	T_{ai} °C	T_{wb} °C	T_{wi} °C	T_{wo} °C	m_a kg/s	m_w kg/s	dp_{fi} Pa	T_{ao} °C
15	16.345	11.347	51.440	32.084	6.749	9.925	89.709	
16	16.336	11.352	51.013	31.968	6.754	9.927	89.766	
17	16.293	11.323	50.702	31.842	6.754	9.937	89.540	
18	16.299	11.339	50.344	31.721	6.749	9.813	89.536	
19	16.336	11.436	49.655	31.486	6.759	9.874	88.673	
20	16.329	11.453	49.495	31.429	6.751	9.855	88.987	
21	16.339	11.495	49.539	31.420	6.756	9.837	89.064	
22	16.297	11.472	49.211	31.340	6.759	9.815	89.077	
23	16.226	11.439	48.506	31.077	6.758	9.809	88.911	
24	16.253	11.537	48.393	31.005	6.757	9.727	88.617	
25	16.270	11.584	48.172	30.975	6.753	9.716	88.521	
26	16.219	11.545	47.783	30.838	6.762	9.842	88.812	
27	16.179	11.516	47.637	30.804	6.760	9.883	88.884	
28	16.128	11.513	47.445	30.718	6.756	9.833	88.716	
29	16.073	11.481	47.287	30.650	6.764	9.880	88.839	
30	16.029	11.469	46.841	30.523	6.756	9.848	88.393	
31	15.869	11.457	46.064	30.199	6.742	9.676	87.983	
32	15.853	11.431	46.069	30.159	6.769	9.701	88.225	
33	15.823	11.435	46.037	30.120	6.768	9.702	88.161	
34	15.806	11.427	45.805	30.053	6.769	9.698	87.868	
35	15.763	11.406	45.351	29.874	6.785	9.581	88.247	
36	15.704	11.382	45.189	29.761	6.783	9.634	88.136	
37	15.661	11.391	45.089	29.719	6.781	9.659	87.919	
38	15.633	11.373	44.906	29.648	6.779	9.588	87.806	
39	15.631	11.393	44.716	29.556	6.781	9.612	87.672	
40	15.570	11.370	44.577	29.483	6.782	9.662	87.747	
41	15.519	11.342	44.337	29.391	6.787	9.621	87.553	
42	15.494	11.326	44.166	29.312	6.784	9.575	87.531	
43	15.485	11.332	43.996	29.247	6.787	9.646	87.561	
44	15.435	11.329	43.826	29.165	6.782	9.599	87.601	
45	15.300	11.239	43.268	29.299	6.763	10.004	89.561	
46	15.267	11.200	43.115	29.254	6.770	10.187	89.534	
47	15.245	11.178	42.770	29.122	6.774	10.196	89.394	
48	15.182	11.159	42.093	28.755	6.781	10.152	89.094	33.414
49	15.119	11.128	42.024	28.717	6.783	10.168	89.311	33.301
50	15.098	11.088	41.861	28.653	6.782	10.184	89.045	33.255
51	15.095	11.078	41.774	28.603	6.783	10.138	89.071	33.190
52	15.073	11.093	41.541	28.527	6.776	10.179	88.867	33.039
53	15.035	11.087	41.479	28.471	6.779	10.121	88.756	32.976
54	15.015	11.070	41.334	28.428	6.785	10.142	88.899	32.898
55	14.996	11.053	41.097	28.321	6.782	10.166	88.796	32.754
56	14.973	11.038	40.902	28.229	6.788	10.147	88.864	32.622
57	14.928	11.032	40.899	28.182	6.790	10.120	88.659	32.564
58	14.906	11.042	40.806	28.172	6.782	10.140	88.488	32.514
59	14.910	11.050	40.565	28.073	6.787	10.125	88.535	32.405
60	14.880	11.047	40.486	27.997	6.788	10.107	88.529	32.343
61	14.851	11.050	40.425	27.976	6.786	10.096	88.515	32.261
62	14.769	11.025	40.388	27.935	6.790	9.965	88.673	32.250
63	14.740	11.021	40.308	27.912	6.790	10.044	88.540	32.188
64	14.698	11.004	40.205	27.863	6.791	10.091	88.350	32.142

Table R.17 (continue): Experimental measurements (p_a = 100060 Pa)

	T_{ai} °C	T_{wb} °C	T_{wi} °C	T_{wo} °C	m_a kg/s	m_w kg/s	dp_{fi} Pa	T_{ao} °C
65	14.675	10.999	40.133	27.821	6.790	10.073	88.282	32.119
66	14.664	11.013	40.174	27.818	6.793	9.986	88.427	32.076
67	14.643	10.990	40.156	27.805	6.794	10.021	88.140	32.042
68	14.615	10.955	40.078	27.766	6.794	10.043	88.212	32.019
69	14.603	10.925	40.009	27.727	6.790	10.022	88.033	31.949
70	14.599	10.909	39.994	27.708	6.796	9.995	88.148	31.891
71	14.572	10.907	39.975	27.708	6.788	10.016	88.000	31.853
72	14.505	10.878	39.915	27.677	6.797	10.026	88.196	31.840
73	14.506	10.881	39.877	27.652	6.789	9.982	87.817	31.839
74	14.481	10.854	39.817	27.613	6.791	9.960	87.904	31.762
75	14.405	10.801	39.743	27.585	6.784	10.020	87.731	31.686
76	14.340	10.769	39.711	27.534	6.791	9.986	87.847	31.627
77	14.295	10.746	39.674	27.523	6.786	9.986	87.538	31.635
78	14.236	10.709	39.573	27.645	6.780	10.329	89.057	31.669
79	14.206	10.710	39.525	27.633	6.781	10.205	88.774	31.633
80	14.172	10.710	39.516	27.604	6.790	10.288	88.852	31.618
81	14.119	10.715	39.451	27.603	6.788	10.214	89.148	31.638
82	14.105	10.715	39.289	27.529	6.788	10.298	89.080	31.530
83	14.119	10.741	39.131	27.477	6.791	10.223	89.169	31.396
84	14.101	10.697	38.998	27.380	6.793	10.142	89.185	31.303
85	14.075	10.656	38.893	27.307	6.795	10.278	89.269	31.205
86	14.056	10.637	38.771	27.246	6.802	10.138	89.013	31.109
87	14.025	10.627	38.551	27.183	6.791	10.260	89.118	31.003
88	13.951	10.631	38.389	27.096	6.798	10.240	88.891	30.881
89	13.919	10.686	38.268	27.058	6.800	10.251	89.076	30.798
90	13.900	10.746	38.123	27.015	6.790	10.233	88.571	30.761
91	13.872	10.741	37.973	26.953	6.802	10.257	88.592	30.669
92	13.835	10.765	37.830	26.876	6.797	10.182	88.835	30.527
93	13.809	10.789	37.645	26.821	6.789	10.219	88.367	30.418
94	13.698	10.705	37.224	26.575	6.795	10.267	88.151	30.047
95	13.631	10.656	37.069	26.498	6.795	10.256	88.375	29.963
96	13.558	10.615	36.890	26.411	6.792	10.259	87.843	29.836
97	13.523	10.622	36.697	26.315	6.790	10.260	87.851	29.699
98	13.484	10.629	36.526	26.245	6.771	10.214	87.475	29.596
99	13.470	10.642	36.357	26.178	6.771	10.207	87.414	29.457
100	13.421	10.642	36.147	26.091	6.778	10.181	87.270	29.360
101	13.411	10.666	35.850	25.959	6.784	10.178	87.470	29.105
102	13.385	10.676	35.661	25.850	6.790	10.136	87.597	28.939
103	13.340	10.656	35.339	25.693	6.804	10.127	88.006	28.739
104	13.322	10.660	35.155	25.584	6.813	10.180	87.962	28.568
105	14.483	11.601	34.882	25.747	6.740	10.416	88.866	28.570
106	14.404	11.592	34.849	25.740	6.734	10.331	88.680	28.531
107	14.308	11.571	34.745	25.683	6.742	10.422	88.809	28.440
108	14.273	11.576	34.676	25.653	6.747	10.411	88.749	28.351
109	14.303	11.678	34.513	25.606	6.742	10.368	88.775	28.286
110	14.264	11.617	34.326	25.475	6.741	10.347	88.509	28.159
111	14.173	11.481	34.221	25.382	6.748	10.268	88.562	28.060
112	14.171	11.405	34.119	25.318	6.748	10.331	88.387	27.967
113	14.200	11.338	33.933	25.216	6.740	10.194	88.666	27.847
114	14.190	11.286	33.857	25.139	6.741	10.356	88.731	27.742

Table R.17 (continue): Experimental measurements (p_a = 100060 Pa)

	T_{ai} °C	T_{wb} °C	T_{wi} °C	T_{wo} °C	m_a kg/s	m_w kg/s	dp_{fi} Pa	T_{ao} °C
115	14.178	11.286	33.688	25.073	6.745	10.349	88.557	27.619
116	14.182	11.302	33.443	24.949	6.743	10.316	88.633	27.492
117	14.145	11.306	33.278	24.852	6.748	10.305	88.694	27.375
118	14.114	11.275	32.923	24.649	6.746	10.290	88.348	27.075
119	14.125	11.349	32.795	24.629	6.745	10.303	88.298	27.056
120	14.202	11.385	32.570	24.524	6.740	10.283	88.212	26.915
121	14.196	11.467	32.319	24.423	6.738	10.224	88.149	26.771
122	14.163	11.417	32.147	24.286	6.748	10.227	88.235	26.645
123	14.143	11.359	31.853	24.122	6.749	10.247	88.009	26.387
124	14.122	11.351	31.580	23.980	6.746	10.227	88.076	26.185
125	14.117	11.334	31.388	23.841	6.749	10.139	87.812	26.027
126	14.100	11.361	31.226	23.790	6.751	10.075	87.775	25.916
127	14.283	11.260	30.378	23.328	6.743	10.352	88.304	25.340
128	14.299	11.330	30.120	23.234	6.742	10.364	88.155	25.188
129	14.372	11.324	29.895	23.107	6.738	10.357	88.028	25.003
130	14.403	11.266	29.673	22.951	6.737	10.358	87.893	24.827
131	14.435	11.221	29.440	22.805	6.739	10.327	87.934	24.601
132	14.432	11.244	29.214	22.688	6.740	10.329	87.746	24.454
133	14.438	11.241	28.969	22.558	6.738	10.303	87.853	24.276
134	14.384	11.299	28.706	22.426	6.740	10.322	87.552	24.089
135	14.341	11.268	28.505	22.292	6.741	10.311	87.671	23.903
136	14.286	11.258	28.309	22.178	6.746	10.301	87.649	23.773
137	14.246	11.255	28.139	22.083	6.745	10.342	87.540	23.644
138	14.225	11.224	27.981	21.971	6.747	10.310	87.453	23.490
139	14.246	11.170	27.795	21.865	6.744	10.307	87.404	23.357
140	14.234	11.198	27.640	21.766	6.752	10.290	87.293	23.215
141	14.228	11.155	27.538	21.702	6.751	10.294	87.379	23.134
142	14.187	11.039	27.347	21.540	6.752	10.313	87.293	22.940

Table R. 18: Transfer coefficients, loss coefficients and outlet temperatures according to the different methods (L_{fi} = 1.08 m).

	G_w	G_a	Me_e/L_{fi}	Me_M/L_{fi}	Me_P/L_{fi}	K_{fdm1M}	K_{fdm1P}	T_{aoP}	T_{aoM}
1	4.506	2.993	0.737	0.767	0.840	20.256	20.152	41.798	40.975
2	4.437	2.993	0.736	0.765	0.838	20.274	20.172	41.466	40.649
3	4.475	2.993	0.739	0.768	0.842	20.232	20.131	41.407	40.593
4	4.483	2.994	0.743	0.772	0.847	20.247	20.147	41.306	40.496
5	4.382	2.993	0.736	0.764	0.836	20.311	20.214	40.625	39.826
6	4.462	2.997	0.749	0.778	0.852	20.160	20.063	40.811	40.012
7	4.450	2.997	0.749	0.777	0.851	20.235	20.142	40.215	39.430
8	4.457	2.999	0.752	0.780	0.855	20.228	20.136	40.034	39.255
9	4.444	2.999	0.756	0.784	0.859	20.180	20.089	39.868	39.092
10	4.441	3.000	0.756	0.783	0.858	20.159	20.070	39.646	38.875
11	4.439	2.998	0.760	0.787	0.862	20.122	20.035	39.446	38.680
12	4.431	2.998	0.761	0.788	0.863	20.128	20.041	39.355	38.592
13	4.424	2.999	0.761	0.788	0.863	20.167	20.081	39.079	38.324
14	4.428	2.999	0.768	0.795	0.871	20.107	20.022	38.928	38.178
15	4.411	3.000	0.767	0.793	0.868	20.130	20.046	38.801	38.053
16	4.412	3.002	0.767	0.793	0.869	20.142	20.059	38.538	37.796

Table R.18: (continue) Transfer coefficients, loss coefficients and outlet temperatures according to the different methods (L_{fi} = 1.08 m).

	G_w	G_a	Me_e/L_{fi}	Me_M/L_{fi}	Me_P/L_{fi}	K_{fdm1M}	K_{fdm1P}	T_{aoP}	T_{aoM}
17	4.416	3.002	0.772	0.798	0.873	20.109	20.027	38.386	37.650
18	4.361	2.999	0.770	0.795	0.871	20.180	20.100	38.008	37.280
19	4.388	3.004	0.780	0.804	0.881	19.950	19.873	37.723	37.006
20	4.380	3.000	0.781	0.806	0.882	20.079	20.003	37.627	36.913
21	4.372	3.003	0.783	0.808	0.884	20.060	19.984	37.648	36.934
22	4.362	3.004	0.781	0.805	0.881	20.077	20.002	37.384	36.675
23	4.359	3.004	0.787	0.811	0.887	20.087	20.013	36.975	36.278
24	4.323	3.003	0.790	0.814	0.890	20.038	19.966	36.847	36.155
25	4.318	3.001	0.788	0.811	0.887	20.056	19.985	36.686	35.999
26	4.374	3.005	0.795	0.818	0.895	20.077	20.006	36.620	35.936
27	4.393	3.005	0.795	0.818	0.895	20.106	20.036	36.576	35.893
28	4.370	3.003	0.796	0.819	0.896	20.112	20.042	36.409	35.732
29	4.391	3.006	0.800	0.822	0.900	20.100	20.031	36.370	35.694
30	4.377	3.003	0.798	0.820	0.897	20.079	20.011	36.041	35.373
31	4.300	2.996	0.801	0.822	0.899	20.137	20.072	35.377	34.727
32	4.311	3.008	0.805	0.826	0.903	20.032	19.968	35.388	34.738
33	4.312	3.008	0.808	0.829	0.907	20.019	19.955	35.398	34.750
34	4.310	3.008	0.808	0.828	0.905	19.965	19.901	35.232	34.588
35	4.258	3.016	0.805	0.825	0.901	20.001	19.940	34.748	34.114
36	4.282	3.015	0.814	0.835	0.912	19.990	19.929	34.776	34.144
37	4.293	3.014	0.817	0.837	0.915	19.952	19.891	34.764	34.134
38	4.262	3.013	0.815	0.835	0.912	19.959	19.899	34.547	33.921
39	4.272	3.014	0.821	0.840	0.918	19.925	19.865	34.491	33.869
40	4.294	3.014	0.826	0.846	0.924	19.937	19.878	34.490	33.870
41	4.276	3.016	0.825	0.844	0.922	19.885	19.826	34.261	33.646
42	4.256	3.015	0.825	0.844	0.922	19.915	19.857	34.102	33.491
43	4.287	3.016	0.830	0.849	0.927	19.900	19.843	34.100	33.490
44	4.266	3.014	0.831	0.850	0.928	19.954	19.897	33.950	33.345
45	4.446	3.006	0.808	0.825	0.902	20.533	20.475	33.856	33.249
46	4.527	3.009	0.814	0.831	0.909	20.478	20.419	33.976	33.368
47	4.532	3.011	0.815	0.832	0.910	20.440	20.382	33.744	33.142
48	4.512	3.014	0.829	0.846	0.925	20.368	20.313	33.323	32.736
49	4.519	3.015	0.831	0.847	0.926	20.411	20.356	33.296	32.709
50	4.526	3.014	0.831	0.847	0.927	20.370	20.315	33.197	32.612
51	4.506	3.015	0.831	0.847	0.926	20.376	20.322	33.085	32.503
52	4.524	3.011	0.833	0.849	0.928	20.384	20.330	32.992	32.414
53	4.498	3.013	0.834	0.850	0.929	20.347	20.294	32.894	32.318
54	4.508	3.015	0.833	0.848	0.927	20.355	20.302	32.793	32.220
55	4.518	3.014	0.836	0.852	0.931	20.359	20.306	32.679	32.110
56	4.510	3.017	0.837	0.852	0.932	20.353	20.301	32.519	31.954
57	4.498	3.018	0.842	0.858	0.938	20.294	20.243	32.523	31.959
58	4.507	3.014	0.841	0.856	0.936	20.308	20.256	32.479	31.916
59	4.500	3.016	0.841	0.856	0.935	20.308	20.257	32.293	31.735
60	4.492	3.017	0.847	0.862	0.942	20.300	20.250	32.258	31.702
61	4.487	3.016	0.846	0.861	0.941	20.314	20.264	32.205	31.651
62	4.429	3.018	0.842	0.857	0.936	20.347	20.298	32.009	31.459
63	4.464	3.018	0.845	0.860	0.939	20.315	20.266	32.052	31.502
64	4.485	3.018	0.849	0.863	0.943	20.264	20.215	32.046	31.496
65	4.477	3.018	0.850	0.865	0.944	20.261	20.212	31.987	31.439
66	4.438	3.019	0.848	0.863	0.942	20.282	20.233	31.917	31.370

Table R.18: (continue) Transfer coefficients, loss coefficients and outlet temperatures according to the different methods (L_{fi} = 1,08 m).

	G_w	G_a	Me_e/L_{fi}	Me_M/L_{fi}	Me_P/L_{fi}	K_{fdmIM}	K_{fdmIP}	T_{aoP}	T_{aoM}
67	4.454	3.019	0.850	0.865	0.945	20.212	20.163	31.948	31.402
68	4.464	3.020	0.852	0.866	0.946	20.230	20.181	31.918	31.372
69	4.454	3.018	0.852	0.866	0.946	20.220	20.171	31.849	31.304
70	4.442	3.020	0.851	0.866	0.945	20.218	20.169	31.799	31.255
71	4.452	3.017	0.852	0.866	0.946	20.225	20.177	31.821	31.277
72	4.456	3.021	0.852	0.866	0.946	20.223	20.175	31.770	31.227
73	4.436	3.017	0.852	0.866	0.946	20.190	20.142	31.712	31.171
74	4.427	3.018	0.852	0.866	0.946	20.206	20.159	31.642	31.102
75	4.453	3.015	0.854	0.868	0.948	20.211	20.163	31.664	31.123
76	4.438	3.018	0.856	0.871	0.950	20.199	20.151	31.607	31.069
77	4.438	3.016	0.855	0.870	0.949	20.165	20.117	31.581	31.043
78	4.591	3.013	0.848	0.862	0.942	20.540	20.491	31.789	31.245
79	4.535	3.014	0.840	0.853	0.932	20.485	20.436	31.579	31.039
80	4.573	3.018	0.848	0.862	0.942	20.440	20.392	31.695	31.155
81	4.539	3.017	0.840	0.854	0.932	20.536	20.488	31.527	30.989
82	4.577	3.017	0.846	0.860	0.940	20.520	20.472	31.536	31.000
83	4.544	3.018	0.841	0.854	0.933	20.540	20.493	31.315	30.784
84	4.507	3.019	0.842	0.855	0.933	20.546	20.500	31.139	30.611
85	4.568	3.020	0.853	0.866	0.946	20.547	20.500	31.261	30.733
86	4.506	3.023	0.845	0.858	0.937	20.467	20.421	30.976	30.453
87	4.560	3.018	0.849	0.861	0.940	20.560	20.514	30.969	30.448
88	4.551	3.021	0.851	0.863	0.942	20.479	20.434	30.840	30.322
89	4.556	3.022	0.851	0.864	0.943	20.513	20.468	30.773	30.259
90	4.548	3.018	0.850	0.863	0.942	20.465	20.420	30.671	30.161
91	4.559	3.023	0.851	0.863	0.942	20.409	20.365	30.570	30.063
92	4.526	3.021	0.851	0.863	0.941	20.506	20.463	30.411	29.909
93	4.542	3.017	0.851	0.862	0.941	20.454	20.412	30.325	29.826
94	4.563	3.020	0.862	0.873	0.953	20.391	20.349	30.116	29.624
95	4.558	3.020	0.861	0.872	0.952	20.454	20.413	29.982	29.493
96	4.560	3.019	0.862	0.873	0.952	20.363	20.322	29.856	29.371
97	4.560	3.018	0.864	0.875	0.955	20.384	20.344	29.738	29.257
98	4.540	3.009	0.863	0.874	0.953	20.429	20.389	29.592	29.115
99	4.536	3.010	0.862	0.872	0.951	20.421	20.382	29.457	28.983
100	4.525	3.012	0.859	0.869	0.947	20.365	20.326	29.252	28.784
101	4.524	3.015	0.859	0.869	0.947	20.390	20.352	29.034	28.572
102	4.505	3.018	0.861	0.871	0.949	20.398	20.360	28.869	28.413
103	4.501	3.024	0.861	0.871	0.948	20.436	20.399	28.605	28.156
104	4.524	3.028	0.869	0.878	0.957	20.374	20.338	28.556	28.110
105	4.629	2.996	0.870	0.879	0.960	20.808	20.771	28.797	28.356
106	4.592	2.993	0.863	0.872	0.951	20.815	20.778	28.668	28.230
107	4.632	2.996	0.869	0.878	0.958	20.795	20.759	28.685	28.248
108	4.627	2.999	0.868	0.877	0.956	20.756	20.720	28.614	28.179
109	4.608	2.996	0.864	0.873	0.952	20.804	20.768	28.466	28.037
110	4.599	2.996	0.870	0.878	0.958	20.760	20.725	28.335	27.909
111	4.564	2.999	0.866	0.875	0.954	20.752	20.718	28.144	27.720
112	4.592	2.999	0.870	0.878	0.958	20.710	20.676	28.125	27.702
113	4.531	2.996	0.861	0.869	0.947	20.849	20.815	27.829	27.411
114	4.603	2.996	0.878	0.887	0.967	20.850	20.815	27.991	27.570
115	4.599	2.998	0.874	0.883	0.962	20.796	20.762	27.831	27.413
116	4.585	2.997	0.875	0.883	0.963	20.840	20.806	27.636	27.225

Table R.18: (continue) Transfer coefficients, loss coefficients and outlet temperatures according to the different methods (L_{fi} = 1.08 m).

	G_w	G_a	Me_e/L_{fi}	Me_M/L_{fi}	Me_P/L_{fi}	K_{fdm1M}	K_{fdm1P}	T_{aoP}	T_{aoM}
117	4.580	2.999	0.878	0.887	0.966	20.837	20.804	27.521	27.113
118	4.573	2.998	0.884	0.892	0.972	20.787	20.755	27.274	26.874
119	4.579	2.998	0.879	0.886	0.966	20.785	20.753	27.175	26.779
120	4.570	2.996	0.879	0.887	0.966	20.804	20.773	27.009	26.617
121	4.544	2.994	0.875	0.882	0.961	20.822	20.792	26.776	26.392
122	4.545	2.999	0.884	0.891	0.971	20.785	20.756	26.681	26.300
123	4.554	3.000	0.887	0.894	0.973	20.744	20.715	26.481	26.105
124	4.545	2.998	0.887	0.894	0.973	20.798	20.770	26.267	25.897
125	4.506	3.000	0.891	0.897	0.976	20.728	20.700	26.076	25.711
126	4.478	3.000	0.880	0.886	0.964	20.725	20.698	25.856	25.496
127	4.601	2.997	0.902	0.908	0.989	20.924	20.897	25.524	25.174
128	4.606	2.996	0.896	0.902	0.982	20.906	20.880	25.323	24.978
129	4.603	2.995	0.899	0.905	0.985	20.907	20.882	25.166	24.825
130	4.603	2.994	0.907	0.913	0.994	20.896	20.870	25.031	24.694
131	4.590	2.995	0.908	0.914	0.994	20.904	20.879	24.830	24.496
132	4.591	2.995	0.909	0.915	0.996	20.868	20.843	24.671	24.343
133	4.579	2.995	0.907	0.913	0.993	20.922	20.898	24.464	24.141
134	4.587	2.995	0.911	0.916	0.997	20.848	20.825	24.303	23.987
135	4.583	2.996	0.916	0.921	1.002	20.880	20.857	24.163	23.850
136	4.578	2.998	0.916	0.922	1.002	20.860	20.837	24.004	23.696
137	4.596	2.998	0.921	0.926	1.007	20.844	20.822	23.920	23.615
138	4.582	2.999	0.925	0.930	1.011	20.823	20.801	23.790	23.488
139	4.581	2.997	0.922	0.927	1.008	20.844	20.822	23.629	23.330
140	4.573	3.001	0.927	0.932	1.013	20.773	20.751	23.524	23.229
141	4.575	3.001	0.927	0.931	1.012	20.804	20.782	23.439	23.146
142	4.583	3.001	0.938	0.943	1.025	20.793	20.772	23.334	23.041

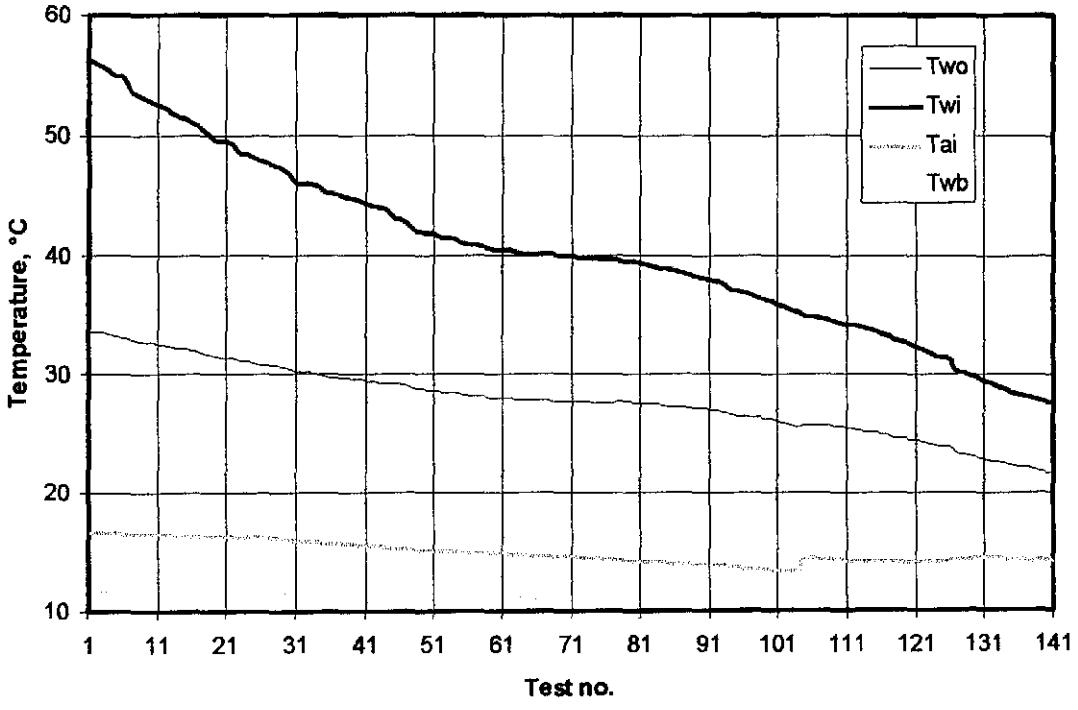

Figure R.11: Variation of air and water temperatures.

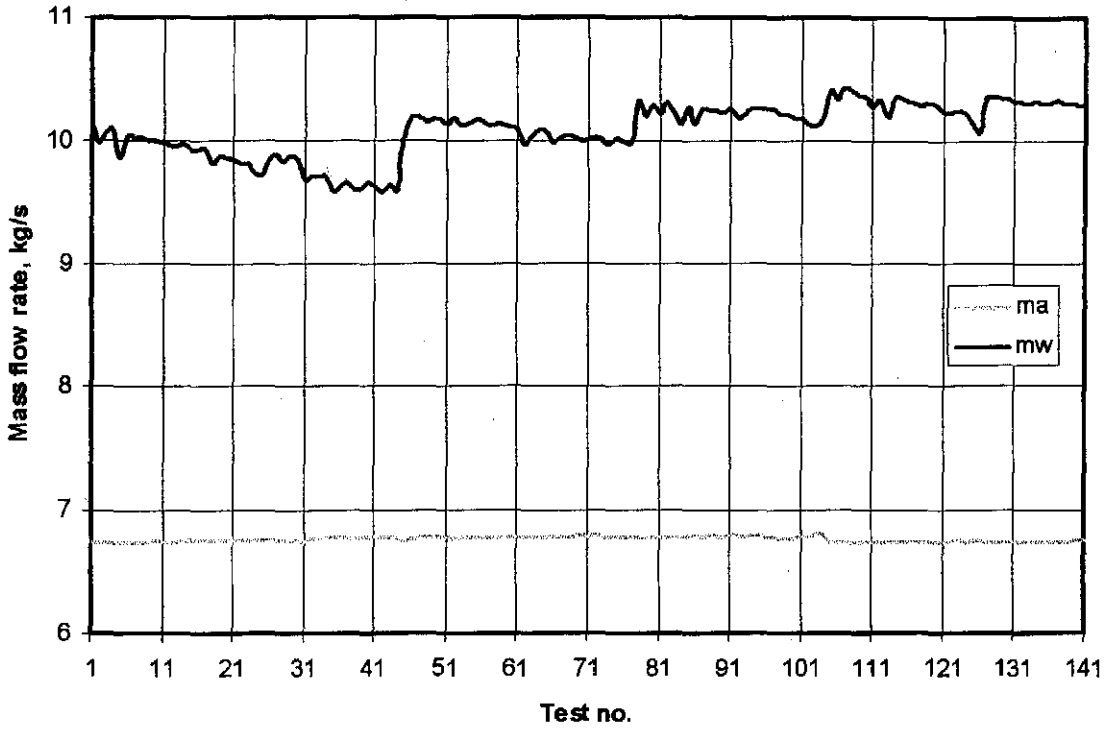

Figure R.12: Air and water mass flow rates during the fill test.

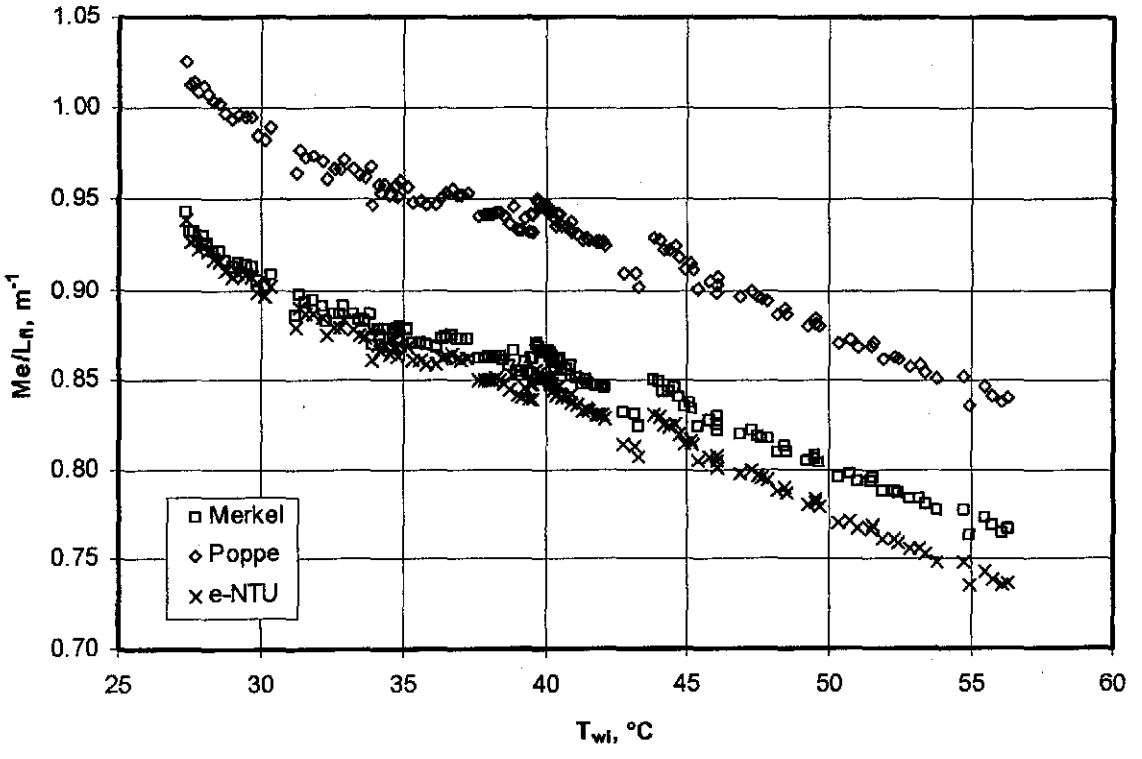

Figure R.13: Transfer coefficients according the *e-NTU*, Merkel and Poppe approaches.

The variation of the air inlet drybulb and wetbulb temperatures and water inlet and outlet temperatures are shown in figure R.11. The air and water mass flow during the fill test is shown in figure R.12. The transfer coefficients according to the *e-NTU*, Merkel and Poppe approaches are plotted against the inlet water temperature in figure R.13. The transfer coefficients according to all the approaches decreases as the water inlet temperature increases. The absolute difference between the transfer coefficients of the Merkel and Poppe approaches remains approximately constant as the water inlet temperature changes.

The transfer coefficients of the e-NTU and Merkel approaches is within close tolerance at colder water inlet temperstures, but as the water increases the difference increases. If a curve is fitted to the data of the Merkel approach in figure R.13 then find

$$Me_M / L_{fi} = cT_{wi}^{-0.2471} \tag{R.7}$$

where c is a constant and the correlation coefficient, $r^2 = 0.9500$.

Figure R.14 shows the measured air outlet temperatures compared to those predicted by the Merkel and Poppe approaches over a wide range of water inlet temperatures. It can be seen that the Poppe approach predicts the water outlet temperatures very accurately over the entire range of water inlet temperatures. This is expected, as the Poppe approach is the more rigorous approach of the two approaches. At lower water inlet temperatures, however, the Merkel approach predicts the outlet air temperatures accurately. This is because supersaturation of the outlet air is not as dominant when the water inlet temperature is colder. The assumption of the Merkel approach that the air is saturated at the air outlet is close to reality, although the air is supersaturated.

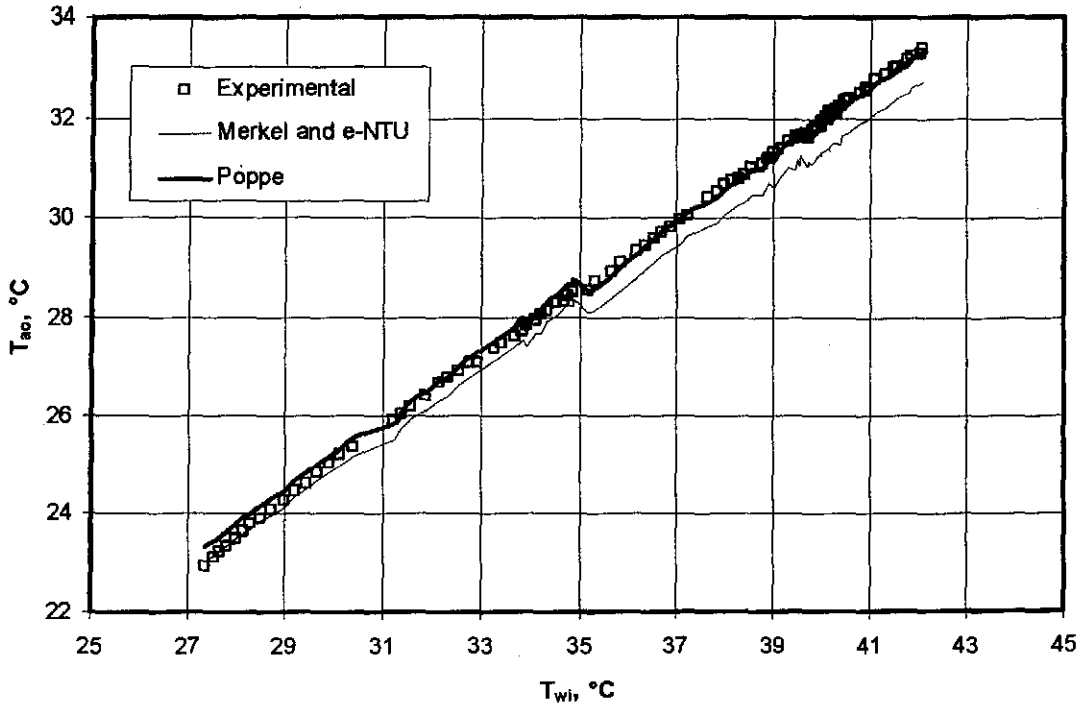

Figure R.14: Measured air outlet temperatures compared to air outlet temperatures predicted by the *e-NTU*, Merkel and Poppe approaches.

R.8 FILL HEIGHT: 1.98 m, G_a AND G_w CONSTANT

The 1.98 m fill is tested at approximately constant air and water mass flow rates. Only the inlet water mass flow rate is varied during the duration of the fill test. Table R.19 contains the experimental measurements of the fill test and table R.20 contains the corresponding transfer and loss coefficients.

Table R.19: Experimental measurements (p_a = 101340 Pa)

	T_{ai} °C	T_{wb} °C	T_{wi} °C	T_{wo} °C	m_a kg/s	m_w kg/s	dp_{fi} Pa	T_{ao} °C
1	14.769	12.323	53.548	30.124	6.732	10.406	153.695	42.867
2	14.709	12.004	53.392	30.048	6.727	10.393	153.050	42.756
3	14.729	11.866	53.268	30.026	6.727	10.357	152.906	42.656
4	14.719	11.836	52.666	29.913	6.727	10.397	153.123	42.378
5	14.650	11.709	52.576	29.820	6.728	10.389	152.812	42.226
6	14.639	11.668	52.104	29.731	6.728	10.379	152.577	41.954
7	14.642	11.678	51.537	29.667	6.728	10.410	152.325	41.626
8	14.631	11.673	51.197	29.535	6.731	10.400	152.155	41.405
9	14.604	11.624	50.746	29.452	6.729	10.387	151.791	41.175
10	14.615	11.634	50.223	29.312	6.728	10.400	151.536	40.903
11	14.609	11.615	49.955	29.243	6.732	10.384	151.518	40.742
12	14.603	11.576	49.391	29.136	6.730	10.386	151.341	40.410
13	14.580	11.548	48.844	28.975	6.733	10.383	151.551	40.019
14	14.549	11.501	48.611	28.846	6.740	10.359	151.256	39.821
15	14.560	11.491	48.177	28.769	6.737	10.334	151.072	39.580
16	14.525	11.459	47.787	28.663	6.736	10.309	150.984	39.333
17	14.503	11.443	47.512	28.579	6.739	10.331	151.013	39.117
18	14.478	11.443	47.077	28.493	6.743	10.329	151.094	38.919
19	14.486	11.447	46.805	28.383	6.740	10.347	150.605	38.695
20	14.539	11.486	46.497	28.300	6.737	10.355	150.447	38.563
21	14.525	11.460	46.116	28.201	6.739	10.314	150.324	38.262
22	14.586	11.514	45.727	28.098	6.739	10.323	150.185	37.982
23	14.650	11.590	45.433	28.023	6.742	10.306	150.212	37.847
24	14.648	11.584	45.279	27.979	6.739	10.303	150.180	37.684
25	14.697	11.649	45.054	27.929	6.739	10.298	149.907	37.542
26	14.660	11.621	44.840	27.845	6.745	10.309	150.146	37.440
27	14.610	11.620	44.638	27.772	6.748	10.266	150.123	37.289
28	14.590	11.568	44.439	27.680	6.749	10.293	149.960	37.071
29	14.525	11.527	44.032	27.655	6.746	10.436	150.565	36.894
30	14.529	11.534	43.869	27.618	6.748	10.427	150.597	36.767
31	14.534	11.545	43.703	27.575	6.750	10.356	150.631	36.723
32	14.518	11.600	43.693	27.567	6.752	10.358	150.663	36.683
33	14.476	11.499	43.560	27.497	6.752	10.411	150.254	36.501
34	14.471	11.517	43.479	27.476	6.755	10.429	150.415	36.479
35	14.419	11.459	43.360	27.416	6.755	10.387	150.606	36.307
36	14.424	11.430	43.281	27.370	6.752	10.392	150.452	36.258
37	14.398	11.408	43.160	27.316	6.758	10.387	150.473	36.197
38	14.424	11.493	43.112	27.332	6.752	10.356	150.468	36.196
39	14.406	11.481	43.086	27.310	6.751	10.386	150.366	36.151
40	14.365	11.409	43.029	27.273	6.752	10.392	150.398	36.073
41	14.369	11.382	42.877	27.221	6.759	10.388	150.509	36.009
42	14.334	11.333	42.716	27.122	6.766	10.360	150.540	35.878

Table R.19 (continue): Experimental measurements (p_a = 101340 Pa)

	T_{ai} °C	T_{wb} °C	T_{wi} °C	T_{wo} °C	m_a kg/s	m_w kg/s	dp_{fi} Pa	T_{ao} °C
43	14.312	11.317	42.533	27.093	6.758	10.348	149.944	35.828
44	14.337	11.287	42.294	27.016	6.757	10.393	150.007	35.603
45	14.368	11.264	42.119	26.916	6.762	10.375	150.194	35.504
46	14.297	11.210	41.823	26.818	6.769	10.256	150.268	35.273
47	14.266	11.197	41.607	26.719	6.766	10.382	150.257	35.079
48	14.259	11.184	41.371	26.654	6.765	10.386	150.050	34.953
49	14.237	11.138	41.095	26.553	6.765	10.369	149.961	34.760
50	14.271	11.149	40.873	26.474	6.766	10.324	149.942	34.576
51	14.220	11.130	40.649	26.345	6.768	10.361	149.531	34.435
52	14.207	11.111	40.436	26.295	6.767	10.348	149.626	34.300
53	14.212	11.088	40.058	26.167	6.764	10.320	149.360	34.009
54	14.202	11.052	39.878	26.046	6.770	10.336	149.420	33.885
55	14.255	11.072	39.566	25.983	6.771	10.341	149.307	33.732
56	14.250	11.035	39.207	25.822	6.774	10.322	149.420	33.427
57	14.210	10.962	38.883	25.682	6.767	10.331	149.181	33.163
58	14.138	10.916	38.449	25.514	6.778	10.310	149.044	32.818
59	14.100	10.849	38.041	25.346	6.780	10.331	148.966	32.556
60	14.101	10.824	37.591	25.171	6.780	10.346	148.914	32.266
61	14.106	10.769	37.137	24.999	6.782	10.345	148.451	31.939
62	14.130	10.775	36.798	24.864	6.779	10.354	148.335	31.690
63	14.182	10.828	36.262	24.693	6.785	10.295	148.349	31.352
64	14.172	10.826	35.830	24.506	6.783	10.344	148.370	30.980
65	14.159	10.737	35.343	24.279	6.786	10.326	148.079	30.579
66	14.074	10.649	34.817	24.008	6.787	10.316	147.977	30.162
67	14.089	10.666	34.404	23.865	6.788	10.313	147.927	29.836
68	14.050	10.623	33.907	23.623	6.791	10.230	147.537	29.485
69	13.988	10.537	33.521	23.405	6.793	10.303	147.307	29.157
70	13.958	10.522	33.174	23.263	6.792	10.289	147.289	28.908
71	14.028	10.568	32.770	23.105	6.793	10.284	147.248	28.626
72	14.025	10.567	32.431	22.954	6.791	10.283	146.831	28.349
73	14.043	10.573	32.112	22.818	6.789	10.303	146.941	28.092
74	14.024	10.559	31.854	22.683	6.798	10.240	147.095	27.869
75	13.997	10.521	31.585	22.533	6.797	10.320	146.893	27.604
76	13.958	10.484	31.228	22.359	6.793	10.295	146.561	27.312
77	13.944	10.468	30.940	22.218	6.794	10.294	146.458	27.078
78	13.930	10.470	30.715	22.116	6.801	10.299	146.741	26.920
79	13.877	10.446	30.502	21.991	6.804	10.272	146.619	26.730
80	13.823	10.403	30.307	21.892	6.805	10.291	146.528	26.584
81	13.845	10.394	30.055	21.769	6.802	10.285	146.310	26.393
82	13.876	10.412	29.944	21.712	6.806	10.221	146.426	26.322
83	13.869	10.398	29.737	21.621	6.806	10.277	146.360	26.169
84	13.876	10.394	29.546	21.533	6.803	10.282	146.105	26.024
85	13.894	10.459	29.375	21.472	6.801	10.262	146.034	25.918

Table R. 20: Transfer coefficients, loss coefficients and outlet temperatures according to the different methods (L_{fi} = 1.98 m).

	G_w	G_a	Me_e/L_{fi}	Me_M/L_{fi}	Me_P/L_{fi}	K_{fdm1M}	K_{fdm1P}	T_{aoP}	T_{aoM}
1	4.625	2.992	0.599	0.634	0.696	18.662	18.579	42.937	42.197
2	4.619	2.990	0.597	0.631	0.693	18.641	18.558	42.788	42.047
3	4.603	2.990	0.593	0.627	0.688	18.640	18.558	42.620	41.880
4	4.621	2.990	0.595	0.629	0.691	18.700	18.620	42.323	41.590
5	4.617	2.990	0.598	0.632	0.695	18.667	18.586	42.274	41.541
6	4.613	2.990	0.598	0.631	0.694	18.672	18.594	41.968	41.241
7	4.627	2.990	0.596	0.629	0.691	18.674	18.597	41.644	40.923
8	4.622	2.992	0.602	0.634	0.697	18.655	18.579	41.459	40.744
9	4.616	2.991	0.600	0.632	0.695	18.653	18.579	41.150	40.440
10	4.622	2.990	0.605	0.637	0.700	18.657	18.584	40.879	40.176
11	4.615	2.992	0.605	0.636	0.700	18.650	18.578	40.681	39.982
12	4.616	2.991	0.604	0.635	0.698	18.681	18.610	40.317	39.625
13	4.615	2.992	0.608	0.638	0.701	18.721	18.652	39.983	39.298
14	4.604	2.996	0.613	0.642	0.707	18.662	18.594	39.829	39.148
15	4.593	2.994	0.610	0.639	0.703	18.689	18.623	39.504	38.829
16	4.582	2.994	0.611	0.639	0.703	18.713	18.648	39.220	38.552
17	4.592	2.995	0.614	0.642	0.706	18.714	18.649	39.080	38.416
18	4.591	2.997	0.612	0.640	0.704	18.728	18.664	38.770	38.112
19	4.599	2.995	0.618	0.646	0.711	18.696	18.633	38.667	38.013
20	4.602	2.994	0.621	0.648	0.714	18.703	18.641	38.502	37.853
21	4.584	2.995	0.620	0.646	0.711	18.707	18.646	38.181	37.538
22	4.588	2.995	0.623	0.649	0.714	18.711	18.651	37.961	37.324
23	4.581	2.997	0.624	0.649	0.715	18.708	18.649	37.757	37.125
24	4.579	2.995	0.625	0.650	0.715	18.730	18.672	37.659	37.030
25	4.577	2.995	0.626	0.651	0.716	18.705	18.648	37.514	36.888
26	4.582	2.998	0.629	0.653	0.719	18.719	18.662	37.391	36.768
27	4.563	2.999	0.628	0.653	0.718	18.713	18.656	37.200	36.582
28	4.575	2.999	0.633	0.657	0.724	18.699	18.643	37.123	36.508
29	4.638	2.998	0.631	0.655	0.721	18.803	18.747	36.970	36.357
30	4.634	2.999	0.631	0.654	0.720	18.809	18.754	36.838	36.228
31	4.603	3.000	0.627	0.649	0.715	18.823	18.768	36.618	36.013
32	4.604	3.001	0.629	0.651	0.717	18.811	18.757	36.632	36.027
33	4.627	3.001	0.633	0.655	0.722	18.766	18.712	36.614	36.010
34	4.635	3.002	0.634	0.657	0.724	18.774	18.720	36.584	35.981
35	4.616	3.002	0.633	0.655	0.722	18.808	18.754	36.443	35.843
36	4.619	3.001	0.636	0.658	0.725	18.812	18.758	36.417	35.817
37	4.617	3.004	0.637	0.659	0.726	18.787	18.734	36.322	35.725
38	4.603	3.001	0.635	0.657	0.723	18.823	18.770	36.260	35.664
39	4.616	3.001	0.638	0.660	0.727	18.813	18.760	36.297	35.701
40	4.619	3.001	0.639	0.661	0.728	18.819	18.766	36.258	35.663
41	4.617	3.004	0.638	0.660	0.727	18.807	18.754	36.132	35.539
42	4.604	3.007	0.641	0.663	0.730	18.782	18.731	35.995	35.406
43	4.599	3.004	0.638	0.659	0.726	18.765	18.714	35.839	35.252
44	4.619	3.003	0.641	0.662	0.729	18.792	18.741	35.738	35.154
45	4.611	3.005	0.645	0.666	0.734	18.795	18.745	35.616	35.035
46	4.558	3.009	0.637	0.657	0.723	18.801	18.752	35.212	34.638
47	4.614	3.007	0.649	0.669	0.738	18.812	18.763	35.276	34.703
48	4.616	3.007	0.649	0.669	0.737	18.806	18.758	35.107	34.538
49	4.609	3.007	0.649	0.668	0.736	18.814	18.766	34.887	34.322
50	4.588	3.007	0.648	0.667	0.735	18.824	18.777	34.678	34.118

Table R. 20 (continue): Transfer coefficients, loss coefficients and outlet temperatures according to the different methods (L_{fi} = 1.98 m).

	G_w	G_a	Me_e/L_{fi}	Me_M/L_{fi}	Me_P/L_{fi}	K_{fdm1M}	K_{fdm1P}	T_{aoP}	T_{aoM}
51	4.605	3.008	0.658	0.677	0.746	18.766	18.719	34.619	34.063
52	4.599	3.008	0.654	0.673	0.742	18.800	18.754	34.426	33.873
53	4.587	3.006	0.654	0.672	0.740	18.807	18.762	34.120	33.574
54	4.594	3.009	0.662	0.680	0.749	18.792	18.747	34.054	33.511
55	4.596	3.009	0.658	0.676	0.744	18.787	18.743	33.801	33.263
56	4.588	3.011	0.662	0.679	0.748	18.804	18.761	33.539	33.007
57	4.592	3.008	0.665	0.682	0.752	18.834	18.791	33.336	32.809
58	4.582	3.012	0.665	0.681	0.750	18.789	18.748	32.973	32.455
59	4.592	3.013	0.668	0.684	0.754	18.790	18.749	32.701	32.189
60	4.598	3.013	0.672	0.687	0.757	18.806	18.767	32.399	31.895
61	4.598	3.014	0.672	0.686	0.756	18.763	18.725	32.045	31.548
62	4.602	3.013	0.676	0.690	0.760	18.783	18.745	31.829	31.338
63	4.576	3.015	0.670	0.683	0.752	18.786	18.750	31.332	30.852
64	4.597	3.015	0.678	0.691	0.762	18.816	18.780	31.103	30.630
65	4.589	3.016	0.681	0.693	0.764	18.789	18.755	30.716	30.252
66	4.585	3.017	0.688	0.701	0.772	18.800	18.767	30.345	29.890
67	4.583	3.017	0.686	0.698	0.769	18.814	18.782	30.008	29.561
68	4.546	3.018	0.686	0.697	0.767	18.780	18.749	29.551	29.115
69	4.579	3.019	0.700	0.711	0.783	18.757	18.726	29.383	28.952
70	4.573	3.019	0.699	0.709	0.781	18.780	18.750	29.093	28.669
71	4.571	3.019	0.700	0.710	0.782	18.788	18.759	28.782	28.366
72	4.570	3.018	0.702	0.712	0.785	18.764	18.736	28.532	28.123
73	4.579	3.017	0.706	0.715	0.788	18.803	18.775	28.317	27.913
74	4.551	3.021	0.704	0.713	0.785	18.790	18.763	28.048	27.651
75	4.587	3.021	0.717	0.726	0.801	18.778	18.751	27.964	27.570
76	4.576	3.019	0.718	0.727	0.801	18.779	18.752	27.668	27.280
77	4.575	3.020	0.721	0.730	0.804	18.771	18.746	27.451	27.069
78	4.577	3.023	0.722	0.730	0.805	18.781	18.756	27.270	26.892
79	4.565	3.024	0.725	0.733	0.808	18.760	18.736	27.094	26.721
80	4.574	3.024	0.727	0.736	0.810	18.758	18.734	26.957	26.588
81	4.571	3.023	0.729	0.738	0.813	18.758	18.734	26.764	26.399
82	4.543	3.025	0.726	0.734	0.808	18.760	18.736	26.615	26.253
83	4.568	3.025	0.730	0.738	0.813	18.760	18.736	26.504	26.145
84	4.570	3.024	0.731	0.739	0.814	18.748	18.725	26.360	26.004
85	4.561	3.023	0.730	0.738	0.812	18.757	18.735	26.213	25.862

It can be seen from figures R.17 and R.18 that the 1.98 m high fill has the same trends as the 1.08 m high fill presented in section R.7.

If a curve is fitted to the data of the Merkel approach in figure R.17 then find

$$Me_M / L_{fi} = cT_{wi}^{-0.2774} \tag{R.8}$$

where c is a constant and the correlation coefficient, r^2 = 0.9831.

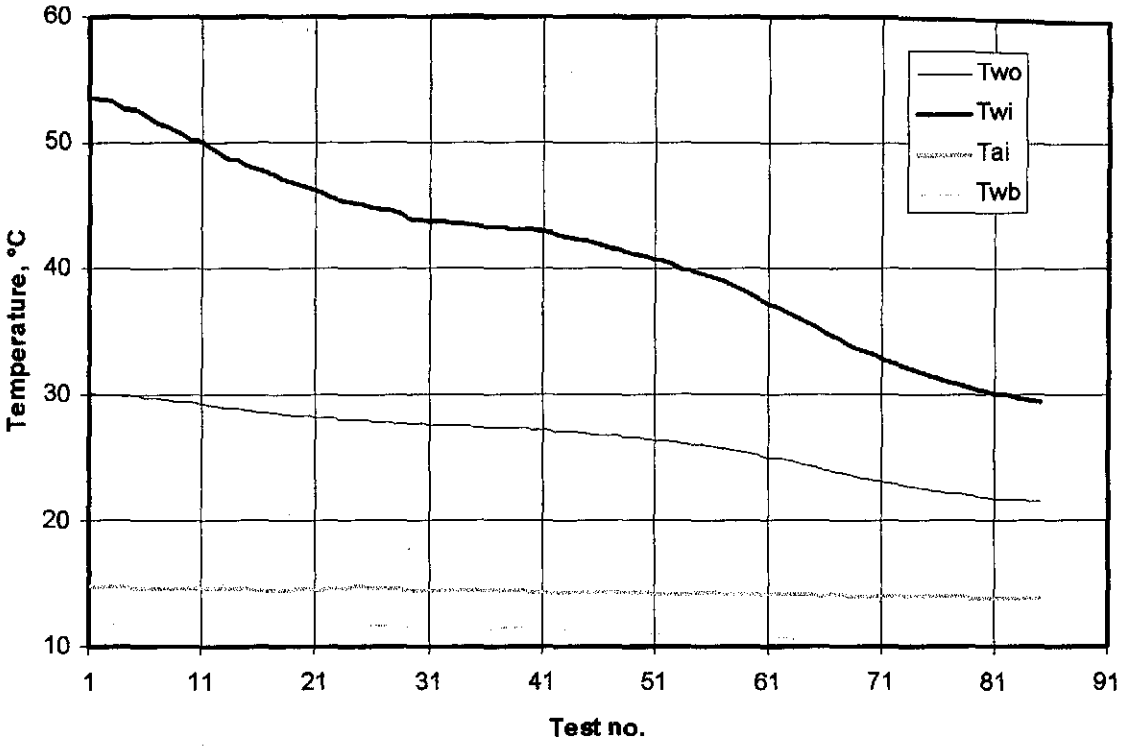

Figure R.15: Variation of air and water temperatures.

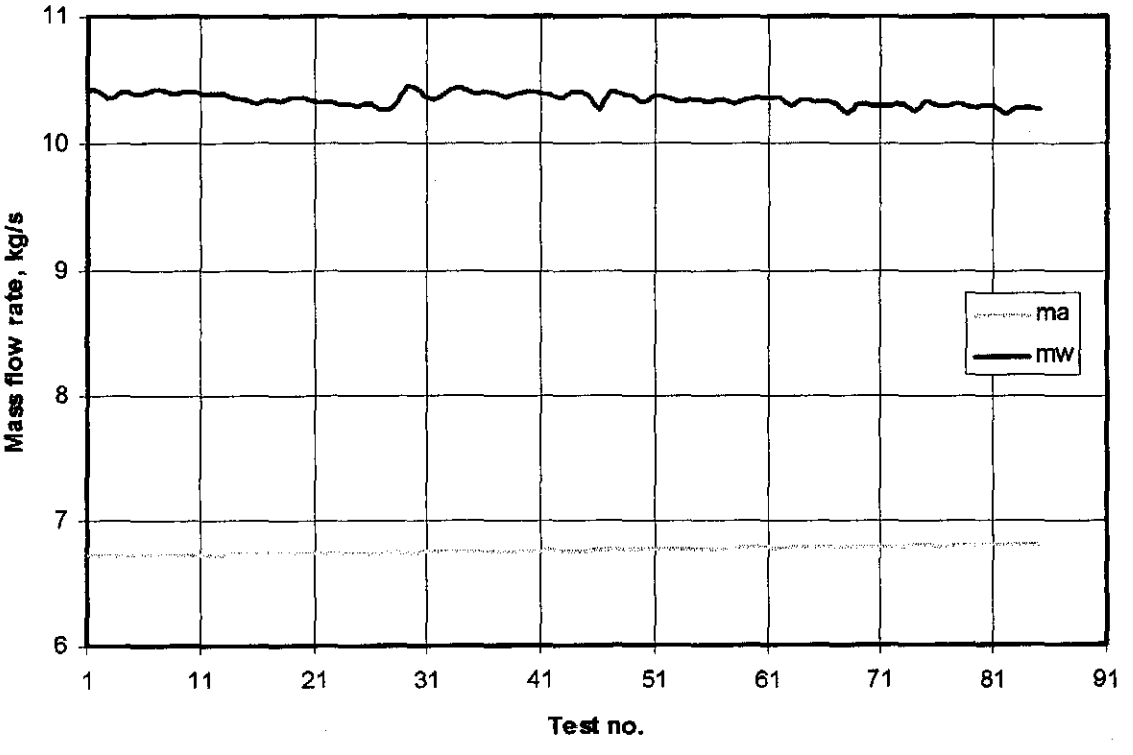

Figure R.16: Air and water mass flow rates during the fill test.

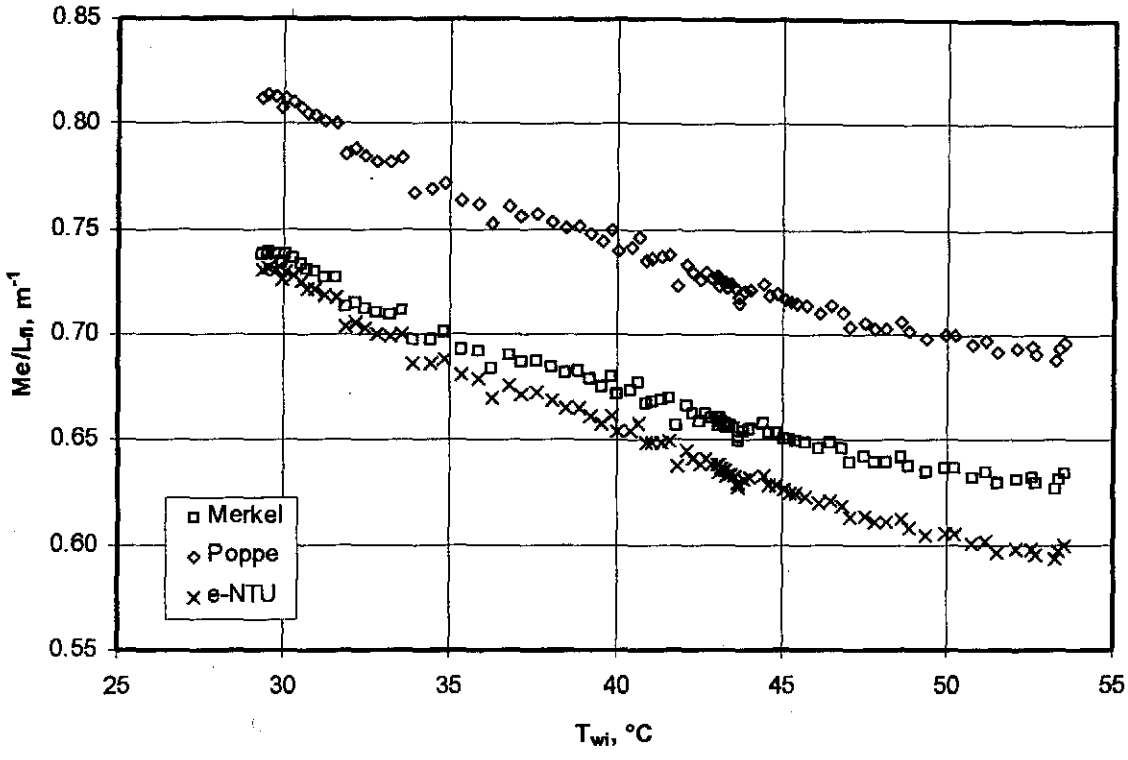

Figure R.17: Transfer coefficients according the *e-NTU*, Merkel and Poppe approaches.

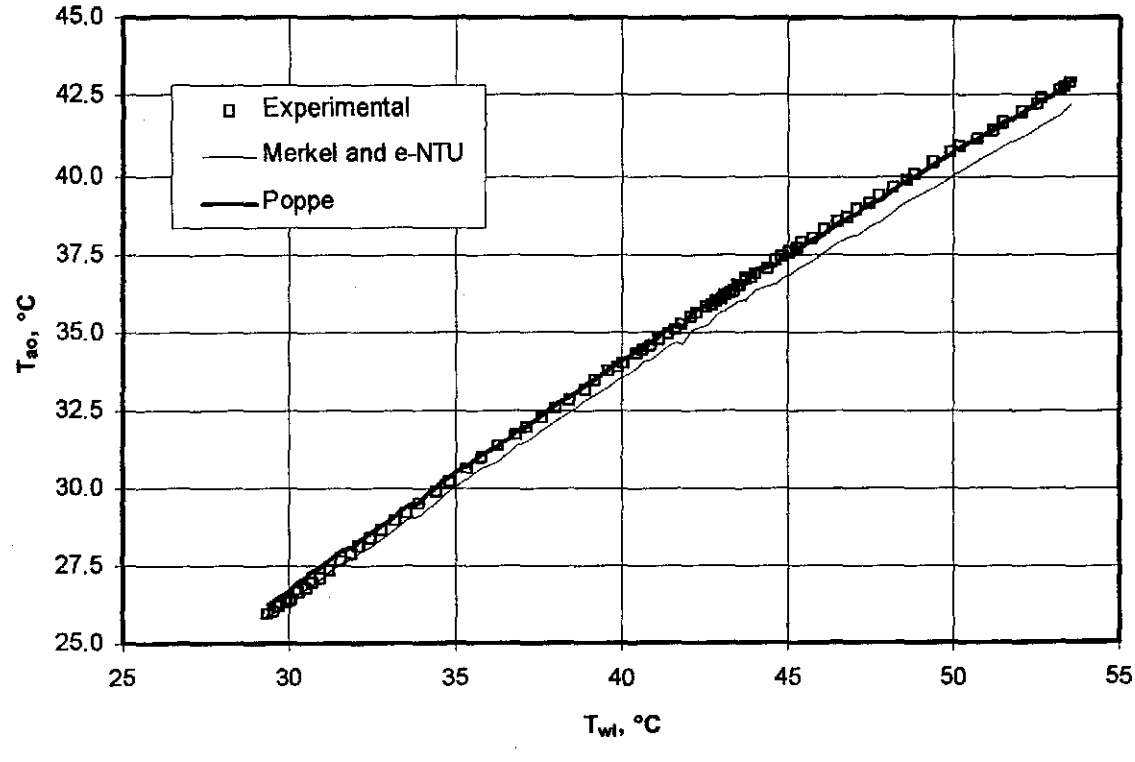

Figure R.18: Measured air outlet temperatures compared to air outlet temperatures predicted by the *e-NTU*, Merkel and Poppe approaches.

R.9 FILL HEIGHT: 1.53 m, TEST REPEATED (24 °C < T_{ai} < 27 °C)

Table R.21: Experimental measurements (p_a = 101340 Pa).

	T_{ai} °C	T_{wb} °C	T_{wi} °C	T_{wo} °C	m_a kg/s	m_w kg/s	dp_{fi} Pa	T_{ao} °C
1	26.841	23.023	47.799	36.311	2.634	6.294	19.064	43.201
2	26.154	22.388	47.778	33.573	3.879	6.184	37.211	40.895
3	25.763	21.767	47.614	31.349	5.191	6.293	61.082	38.808
4	25.850	21.525	47.267	29.635	6.593	6.299	99.143	37.042
5	26.289	21.647	47.052	28.433	7.911	6.275	152.017	35.656
6	26.702	21.824	46.874	27.869	8.591	6.320	184.965	34.913
7	26.418	23.135	46.190	38.569	2.690	10.400	26.429	42.987
8	25.785	22.500	45.673	36.038	3.896	10.434	45.773	40.804
9	25.398	21.853	45.369	33.791	5.266	10.308	76.815	38.900
10	25.363	21.590	44.935	32.258	6.485	10.395	115.712	37.406
11	25.733	21.603	44.569	30.930	7.858	10.400	177.934	36.533
12	26.111	21.711	44.201	30.186	8.609	10.351	223.670	35.744
13	26.256	23.495	43.573	38.989	2.646	15.260	37.792	41.623
14	25.670	22.864	43.369	37.073	3.882	15.237	59.495	40.668
15	25.074	21.986	42.926	35.125	5.217	15.152	94.270	39.142
16	24.837	21.468	42.715	33.722	6.534	15.182	142.662	37.943
17	25.236	21.475	42.479	32.564	7.931	15.156	219.553	37.149
18	25.546	21.586	42.212	31.935	8.650	15.202	275.353	36.587

Table R.22: Transfer coefficients, loss coefficients and outlet temperatures according to the different methods (L_{fi} = 1.53 m).

	G_w	G_a	Me_e/L_{fi}	Me_M/L_{fi}	Me_P/L_{fi}	K_{fdm1M}	K_{fdm1P}	T_{aoP}	T_{aoM}
1	2.797	1.171	0.490	0.501	0.566	19.301	19.244	42.448	41.753
2	2.748	1.724	0.604	0.620	0.686	17.355	17.304	39.756	39.151
3	2.797	2.307	0.728	0.750	0.821	15.981	15.938	37.815	37.274
4	2.800	2.930	0.844	0.866	0.940	16.185	16.147	35.941	35.460
5	2.789	3.516	0.967	0.982	1.061	17.315	17.279	34.649	34.215
6	2.809	3.818	1.054	1.061	1.144	17.879	17.844	34.211	33.796
7	4.622	1.196	0.368	0.371	0.436	25.391	25.299	43.441	42.692
8	4.637	1.732	0.465	0.473	0.538	20.975	20.902	41.439	40.764
9	4.581	2.341	0.563	0.575	0.642	19.376	19.314	39.523	38.912
10	4.620	2.882	0.640	0.655	0.726	19.351	19.295	38.087	37.526
11	4.622	3.492	0.721	0.740	0.813	20.371	20.318	36.743	36.230
12	4.600	3.826	0.780	0.801	0.877	21.382	21.331	36.048	35.562
13	6.782	1.176	0.275	0.276	0.341	37.556	37.425	42.209	41.495
14	6.772	1.725	0.367	0.369	0.435	27.472	27.377	41.074	40.403
15	6.734	2.319	0.448	0.453	0.518	24.238	24.159	39.599	38.973
16	6.747	2.904	0.508	0.514	0.580	23.501	23.430	38.375	37.787
17	6.736	3.525	0.565	0.574	0.641	24.654	24.586	37.238	36.691
18	6.756	3.844	0.608	0.619	0.688	26.035	25.967	36.755	36.229

Table R.23: Empirical relations for the Merkel number according to the various methods (L_{fi} = 1.53 m).

Approach	Eq. type	Empirical relation	Correlation coefficient
e-NTU	1	$Me_e / L_{fi} = 0.786327\ G_w^{-0.590474} G_a^{0.653933}$	0.9965
	2	$Me_e / L_{fi} = 0.847612 (G_w / G_a)^{-0.620771}$	0.9941
	3	$Me_e / L_{fi} = 1.831727\ G_w^{-0.231365} G_a^{0.709589} - 1.149633\ G_w^{-0.115990} G_a^{0.728367}$	0.9971
Merkel	1	$Me_M / L_{fi} = 0.805764\ G_w^{-0.592389} G_a^{0.650846}$	0.9972
	2	$Me_M / L_{fi} = 0.863446 (G_w / G_a)^{-0.620337}$	0.9952
	3	$Me_M / L_{fi} = 1.836449\ G_w^{-0.168045} G_a^{0.645385} - 1.145760\ G_w^{-0.032776} G_a^{0.643715}$	0.9983
Poppe	1	$Me_P / L_{fi} = 0.884005\ G_w^{-0.547641} G_a^{0.599196}$	0.9966
	2	$Me_P / L_{fi} = 0.939648 (G_w / G_a)^{-0.572564}$	0.9947
	3	$Me_P / L_{fi} = 1.863314\ G_w^{-0.147917} G_a^{0.657350} - 1.118364\ G_w^{-0.012514} G_a^{0.677998}$	0.9977

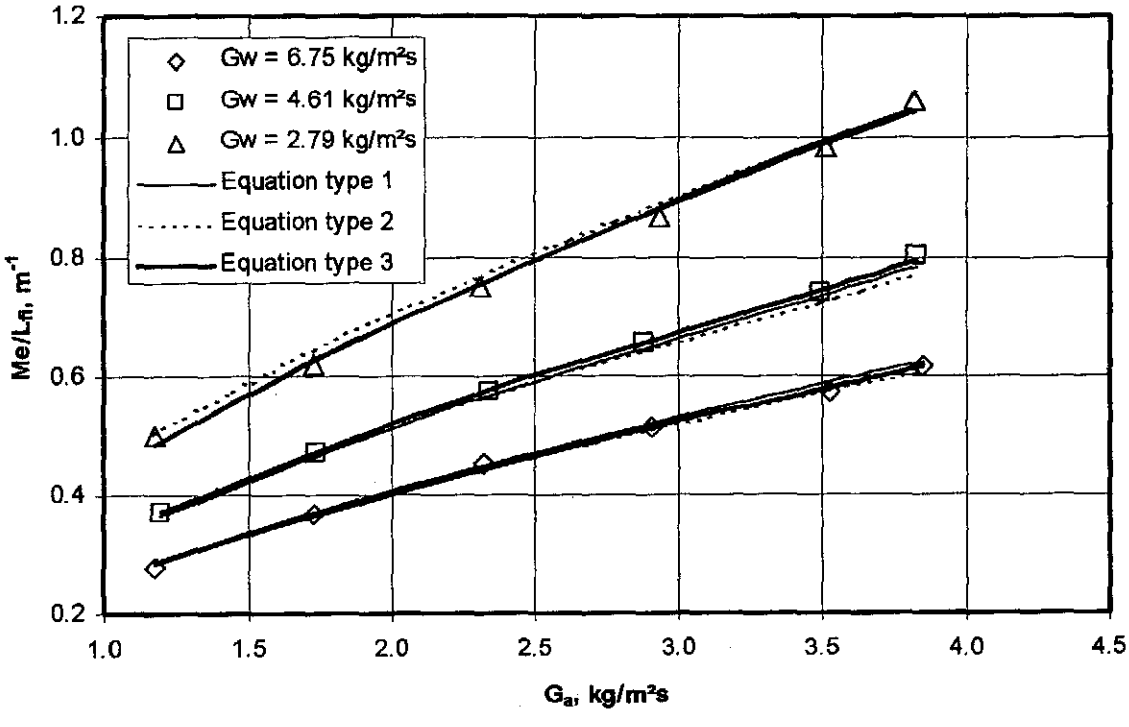

Figure R.19: Comparison of experimental data and empirical equations (L_{fi} = 1.53 m).

Table R.24: Empirical relations for the loss coefficient according to the various methods (L_{fi} = 1.53 m).

Approach	Eq. type	Empirical relation	Correlation coefficient
Merkel and *e-NTU*	1	$K_{fdm1} = 11.804507\ G_w^{0.541354} G_a^{-0.244939}$	0.8282
	2	$K_{fdm1} = 17.144755 (G_w / G_a)^{0.362046}$	0.7133
	3	$K_{fdm1} = 3.699802\ G_w^{1.139958} G_a^{-1.923973} + 6.599771\ G_w^{0.320485} G_a^{0.454993}$	0.9833
Poppe	1	$K_{fdm1} = 11.774221\ G_w^{0.540593} G_a^{-0.243942}$	0.8272
	2	$K_{fdm1} = 17.105425 (G_w / G_a)^{0.361175}$	0.7118
	3	$K_{fdm1} = 3.695143\ G_w^{1.139140} G_a^{-1.923604} + 6.575536\ G_w^{0.319665} G_a^{0.456907}$	0.9832

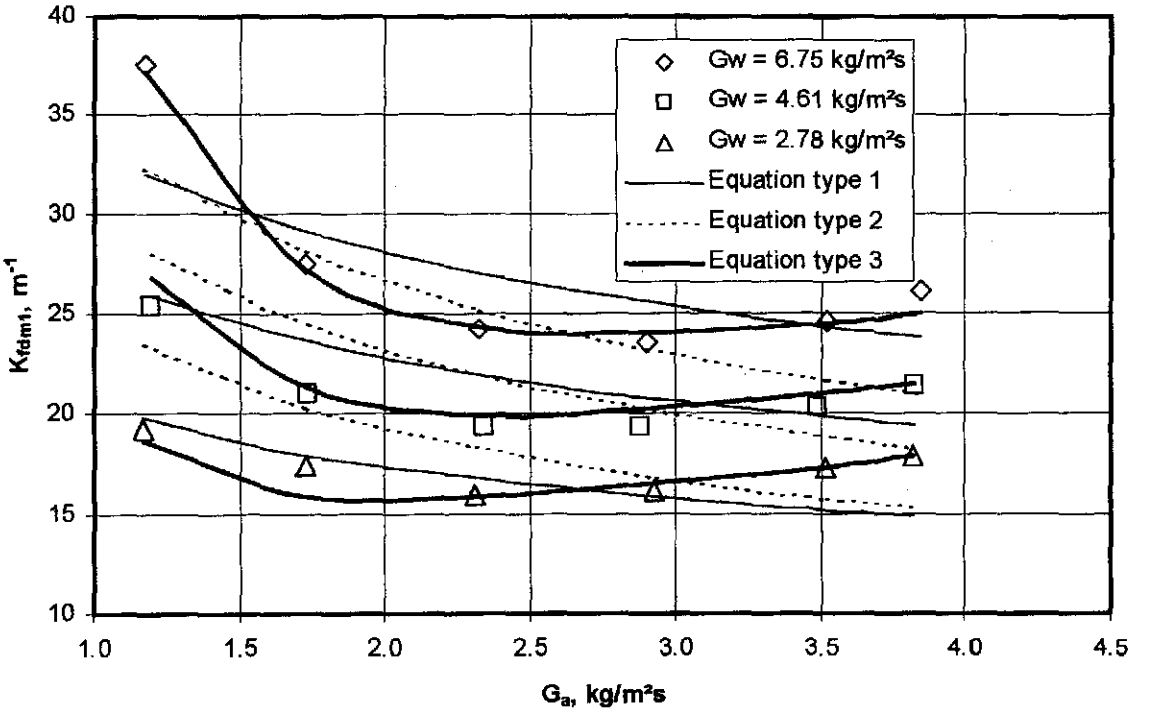

Figure R.20: Comparison of experimental data and empirical relations for the loss coefficient (L_{fi} = 1.53 m).

R.10 FILL HEIGHT: 1.53 m, TEST REPEATED (32 °C < T_{ai} < 35 °C)

Table R.25: Experimental measurements (p_a = 99780 Pa).

	T_{ai} °C	T_{wb} °C	T_{wi} °C$_i$	T_{wo} °C	m_a kg/s	m_w kg/s	dp_{fi} Pa	T_{ao} °C
1	33.007	25.247	48.274	37.108	2.536	6.260	19.140	44.346
2	32.755	24.599	48.231	34.175	3.903	6.283	39.523	41.939
3	32.744	24.084	48.075	32.139	5.135	6.276	63.230	40.081
4	33.312	23.912	47.844	30.614	6.406	6.279	98.328	38.554
5	34.129	24.172	47.650	29.629	7.534	6.264	143.074	37.549
6	34.687	24.333	47.413	29.031	8.261	6.101	177.376	36.865
7	33.015	25.417	46.486	39.200	2.555	10.299	25.532	44.121
8	32.807	24.734	46.105	36.614	3.831	10.293	46.271	42.157
9	32.755	24.117	45.869	34.658	5.061	10.311	74.017	40.623
10	33.069	23.768	45.428	32.930	6.401	10.295	117.304	39.091
11	33.946	24.012	45.131	31.651	7.808	10.266	182.734	37.803
12	34.785	24.289	44.706	30.744	8.797	10.231	250.738	36.903
13	32.842	25.418	43.936	39.522	2.625	15.336	38.913	42.569
14	32.724	24.904	43.687	37.671	3.841	15.299	61.385	41.476
15	32.561	24.103	43.327	35.800	5.178	15.295	99.067	40.180
16	32.827	23.682	43.127	34.499	6.430	15.300	146.638	39.133
17	33.649	23.944	42.877	33.416	7.731	15.203	219.963	38.237
18	34.614	24.169	42.674	32.192	9.064	15.116	347.512	37.745

Table R.26: Transfer coefficients, loss coefficients and outlet temperatures according to the different methods (L_{fi} = 1.53 m).

	G_w	G_a	Me_e/L_{fi}	Me_M/L_{fi}	Me_P/L_{fi}	$K_{fdm\,IM}$	$K_{fdm\,IP}$	T_{aoP}	T_{aoM}
1	2.782	1.127	0.496	0.507	0.578	20.289	20.225	43.383	42.675
2	2.793	1.735	0.632	0.651	0.723	17.721	17.665	40.778	40.112
3	2.789	2.282	0.753	0.775	0.851	16.494	16.442	39.145	38.242
4	2.791	2.847	0.876	0.896	0.975	16.574	16.519	37.991	36.709
5	2.784	3.348	1.009	1.017	1.101	17.494	17.432	37.348	35.735
6	2.711	3.671	1.107	1.100	1.185	18.088	18.021	36.888	34.966
7	4.577	1.136	0.381	0.384	0.463	26.448	26.348	44.270	43.512
8	4.575	1.703	0.483	0.491	0.565	21.371	21.292	42.216	41.530
9	4.583	2.249	0.573	0.585	0.660	19.708	19.639	40.697	39.981
10	4.576	2.845	0.663	0.680	0.757	19.659	19.591	39.339	38.407
11	4.563	3.470	0.763	0.784	0.865	20.664	20.592	38.444	37.236
12	4.547	3.910	0.865	0.888	0.976	22.386	22.308	37.915	36.541
13	6.816	1.167	0.274	0.275	0.346	38.321	38.182	42.699	41.974
14	6.799	1.707	0.364	0.367	0.439	28.280	28.178	41.582	40.899
15	6.798	2.301	0.453	0.458	0.532	25.253	25.164	40.401	39.674
16	6.800	2.858	0.512	0.519	0.591	24.356	24.270	39.466	38.591
17	6.757	3.436	0.581	0.590	0.665	25.342	25.254	38.757	37.689
18	6.718	4.028	0.702	0.717	0.803	29.169	29.069	38.324	37.183

Table R.27: Empirical relations for the Merkel number according to the various methods (L_{fi} = 1.53 m).

Approach	Eq. type	Empirical relation	Correlation coefficient
e-NTU	1	$Me_e / L_{fi} = 0.802686\ G_w^{-0.596023} G_a^{0.693986}$	0.9943
	2	$Me_e / L_{fi} = 0.900275 (G_w / G_a)^{-0.641703}$	0.9889
	3	$Me_e / L_{fi} = 1.271927\ G_w^{-0.263657} G_a^{0.667591} - 0.554315\ G_w^{-0.036227} G_a^{0.650214}$	0.9950
Merkel	1	$Me_M / L_{fi} = 0.814045\ G_w^{-0.588025} G_a^{0.685956}$	0.9939
	2	$Me_M / L_{fi} = 0.913014 (G_w / G_a)^{-0.633821}$	0.9883
	3	$Me_M / L_{fi} = 1.292572\ G_w^{-0.145482} G_a^{0.599911} - 0.589198\ G_w^{0.113166} G_a^{0.550082}$	0.9963
Poppe	1	$Me_P / L_{fi} = 0.894579\ G_w^{-0.533702} G_a^{0.624663}$	0.9924
	2	$Me_P / L_{fi} = 0.995347 (G_w / G_a)^{-0.576918}$	0.9865
	3	$Me_P / L_{fi} = 1.325635\ G_w^{-0.126711} G_a^{0.585201} - 0.558443\ G_w^{0.139244} G_a^{0.559401}$	0.9943

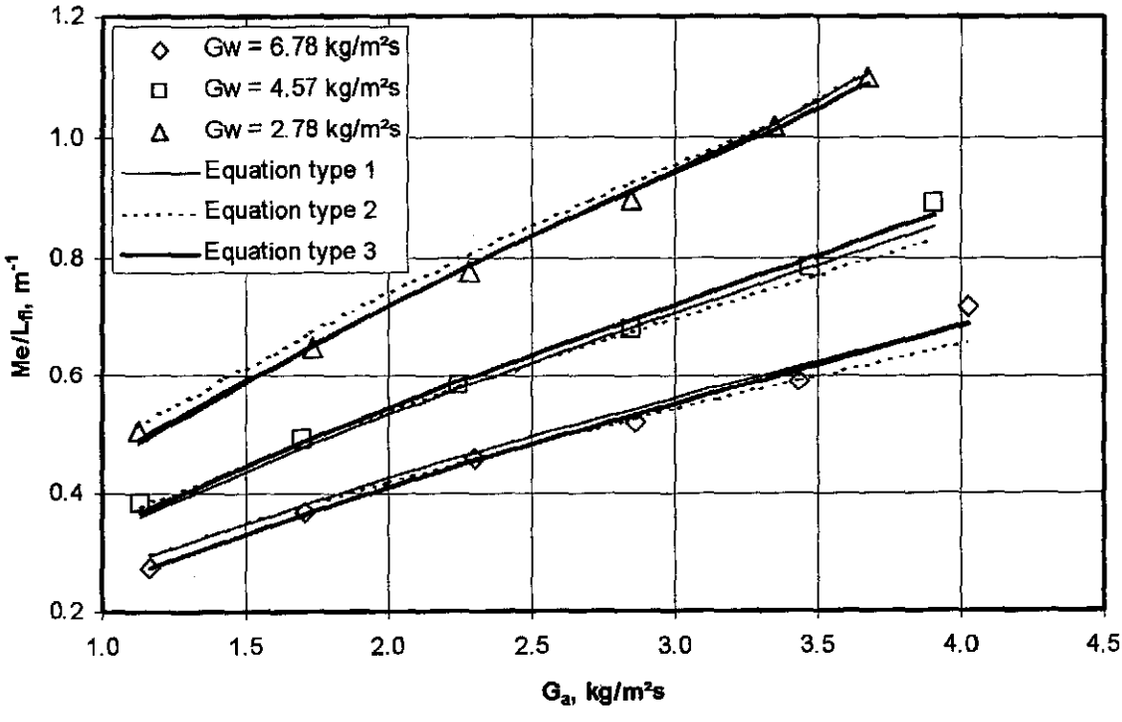

Figure R.21: Comparison of experimental data and empirical equations (L_{fi} = 1.53 m).

Table R.28: Empirical relations for the loss coefficient according to the various methods (L_{fi} = 1.53 m).

Approach	Eq. type	Empirical relation	Correlation coefficient
Merkel and *e-NTU*	1	$K_{fdm1} = 11.636035\ G_w^{0.556388} G_a^{-0.217645}$	0.8282
	2	$K_{fdm1} = 17.781634 (G_w/G_a)^{0.351490}$	0.7133
	3	$K_{fdm1} = 7.807807\ G_w^{0.832091} G_a^{-1.194010} + 2.698714\ G_w^{0.254849} G_a^{1.093894}$	0.9833
Poppe	1	$K_{fdm1} = 11.598391\ G_w^{0.556158} G_a^{-0.217526}$	0.8272
	2	$K_{fdm1} = 17.721574 (G_w/G_a)^{0.351331}$	0.7118
	3	$K_{fdm1} = 7.781392\ G_w^{0.831737} G_a^{-1.194921} + 2.694334\ G_w^{0.255441} G_a^{1.092209}$	0.9832

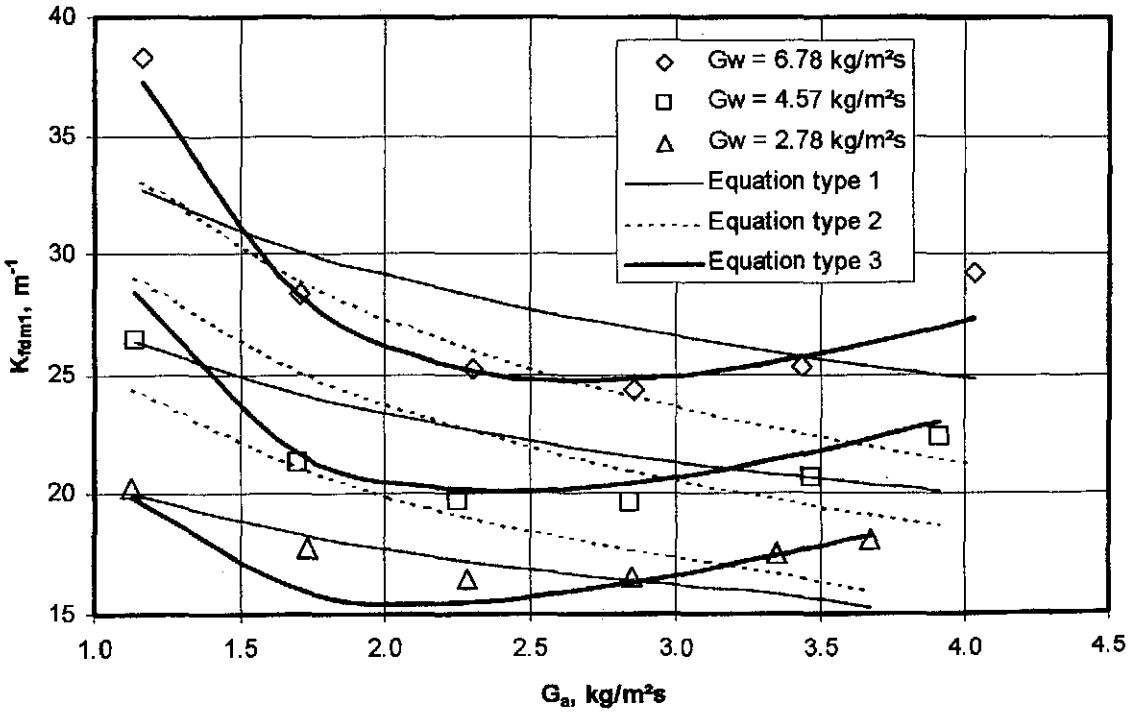

Figure R.22: Comparison of experimental data and empirical relations for the loss coefficient (L_{fi} = 1.53 m).

R.11 THE EFFECT OF AIR TEMPERATURE ON FILL PERFORMANCE

Fill test results of the 1.53 m high trickle fill are presented in sections R.3, R.9 and R.10 respectively for low, intermediate and high temperatures. The test results are combined into one set of data and he effect of the air temperature on fill performance can subsequently be evaluated. Table 29 summarizes the empirical equations of the Merkel numbers according to the Merkel approach of the 1.53 m high trickle grid fill for cool, mils and hot ambient conditions presented in sections R.3, R.9 and R.10 respectively. The empirical equations generated from the combined set of data are also presented in table R.29.

Table R.29: Summary of the transfer coefficients according to the Merkel approach.

T_{ab} °C	Equation type 1	r^2
16.0	$Me_M / L_{fi} = 0.817071\ G_w^{-0.581055} G_a^{0.670746}$	0.9948
25.8	$Me_M / L_{fi} = 0.805764\ G_w^{-0.592389} G_a^{0.650846}$	0.9972
33.3	$Me_M / L_{fi} = 0.814045\ G_w^{-0.588025} G_a^{0.685956}$	0.9939
Comb.	$Me_M / L_{fi} = 0.811211\ G_w^{-0.587437} G_a^{0.671265}$	0.9896
T_{ab} °C	Equation type 2	r^2
16.0	$Me_M / L_{fi} = 0.910464(G_w / G_a)^{-0.624555}$	0.9903
25.8	$Me_M / L_{fi} = 0.863446(G_w / G_a)^{-0.620337}$	0.9952
33.3	$Me_M / L_{fi} = 0.913014(G_w / G_a)^{-0.633821}$	0.9883
Comb.	$Me_M / L_{fi} = 0.896180(G_w / G_a)^{-0.627585}$	0.9855
T_{ab} °C	Equation type 3	r^2
16.0	$Me_M / L_{fi} = 1.299681\ G_w^{-0.121555} G_a^{0.572612} - 0.593218\ G_w^{0.146139} G_a^{0.515254}$	0.9979
25.8	$Me_M / L_{fi} = 1.836449\ G_w^{-0.168045} G_a^{0.645385} - 1.145760\ G_w^{-0.032776} G_a^{0.643715}$	0.9983
33.3	$Me_M / L_{fi} = 1.292572\ G_w^{-0.145482} G_a^{0.599911} - 0.589198\ G_w^{0.113166} G_a^{0.550082}$	0.9963
Comb.	$Me_M / L_{fi} = 1.281200\ G_w^{-0.165354} G_a^{0.600120} - 0.576672\ G_w^{0.08993} G_a^{0.556793}$	0.9916

It is evident from table R.29 that the experiments are repeatable as the respective coefficients of each type of empirical equations are numerically within close tolerance of one another. The correlation coefficients for the empirical equations obtained from the combined data set is of the same order of accuracy as the other empirical equations obtained separately for the cool, mild and hot air temperatures. This suggests, as a first approximation, that the air temperature does not influence the Merkel number or transfer characteristic significantly.

The combined data set, as a function of the inlet air drybulb temperature, is correlated by the relation

$$Me_M / L_{fi} = 0.835550\ G_w^{-0.587470} G_a^{0.670643} T_{ai}^{-0.009106} \qquad \text{(R.9)}$$

where the correlation coefficient, r^2, is 0.9897 and T_{ai} is expressed in °C.

When the effects of the water inlet temperature and inlet air drybulb are included then find the empirical relation

$$Me_M / L_{fi} = 1.952087\ G_w^{-0.611513} G_a^{0.664630} T_{ai}^{-0.010111} T_{wi}^{-0.210834} \quad \text{(R.10)}$$

where the correlation coefficient, r^2, is 0.9894. T_{ai} and T_{wi} are expressed in °C.

As a function of the inlet air wetbulb temperature, the combined data set is correlated by the relation

$$Me_M / L_{fi} = 0.881611\ G_w^{-0.586797} G_a^{0.667188} T_{wb}^{-0.027211} \quad \text{(R.11)}$$

where the correlation coefficient, r^2, is 0.9901 and T_{wb} is expressed in °C.

When the effects of the water inlet temperature and inlet air wetbulb are included then find the empirical relation

$$Me_M / L_{fi} = 1.954254\ G_w^{-0.609244} G_a^{0.661410} T_{wb}^{-0.028767} T_{wi}^{-0.197365} \quad \text{(R.12)}$$

where the correlation coefficient, r^2, is 0.9899. T_{wb} and T_{wi} are expressed in °C.

It is evident from equations (R.9) to (R.12) that the Merkel number, according to the Merkel theory, is a relatively weak function of the inlet air drybulb and wetbulb temperatures. This is because the exponents of T_{ai} and T_{wi} in equations (R.9) to (R.12) are relatively small. Similar trends are observed for the Poppe and *e-NTU* theories. The exponents of T_{wi} in equations (R.10) and (R.12) are approximately equal to the exponent of T_{wi} in equation (R.6), where the effect of the inlet water temperature on the Merkel number is determined explicitly.

The measured Merkel number or transfer characteristic per unit length of fill versus the right hand side of equation (R.10), where the effect of the air temperature is omitted is shown in figure R.23. Figure R.24 shows the measured Merkel number versus equation (R.10). Figures R.23 and R.24 are virtually identical and there is no temperature effect visible in figure R.23. Therefore, the inlet air drybulb temperature has no significant effect on the Merkel number.

The loss coefficient, for the combined data set, can be correlated by the relation

$$K_{fdm1} = 4.587403\ G_w^{1.052197} G_a^{-1.745426} + 5.513909\ G_w^{0.322716} G_a^{0.579324} \quad \text{(R.13)}$$

with a correlation coefficient $r^2 = 0.9721$.

As a function of the inlet air drybulb temperature, the loss coefficient can be correlated by the relation

$$K_{fdm1} = \left(4.84878\ G_w^{1.036998} G_a^{-1.808134} + 5.489596\ G_w^{0.347548} G_a^{0.595861}\right) T_{ai}^{-0.00066} \quad \text{(R.14)}$$

with a correlation coefficient $r^2 = 0.9623$.

It can be seen that the loss coefficient is a very weak function of the inlet air drybulb temperature, as the exponent of T_{ai} in equation (R.5) is very close to zero. The loss coefficients presented in figures R.5, R.20 and R.22 for air inlet drybulb temperatures of 16, 25.8 and 33.3 °C respectively are shown, together with equation (R.13), in figure R.25. It can be seen in figure R.25 that the air inlet temperature has no significant effect on the loss coefficient.

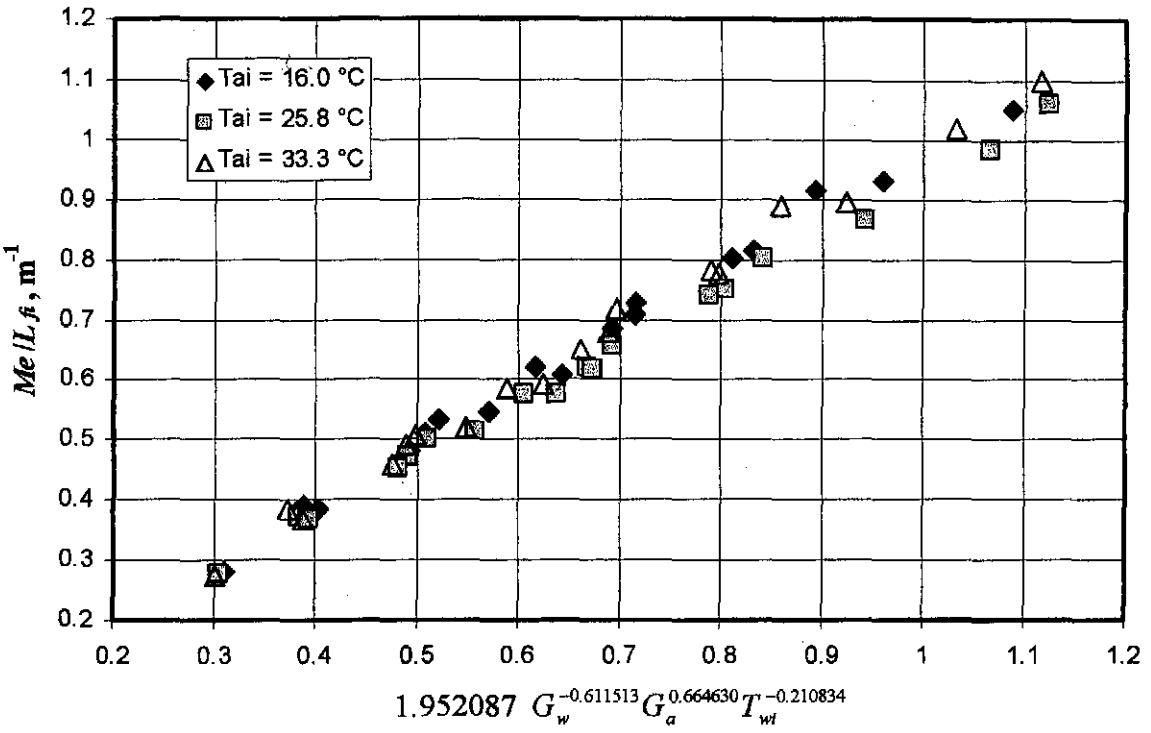

Figure R.23: The measured Merkel number per unit length of fill versus right hand side of equation (R.10) where the temperature of the air is omitted.

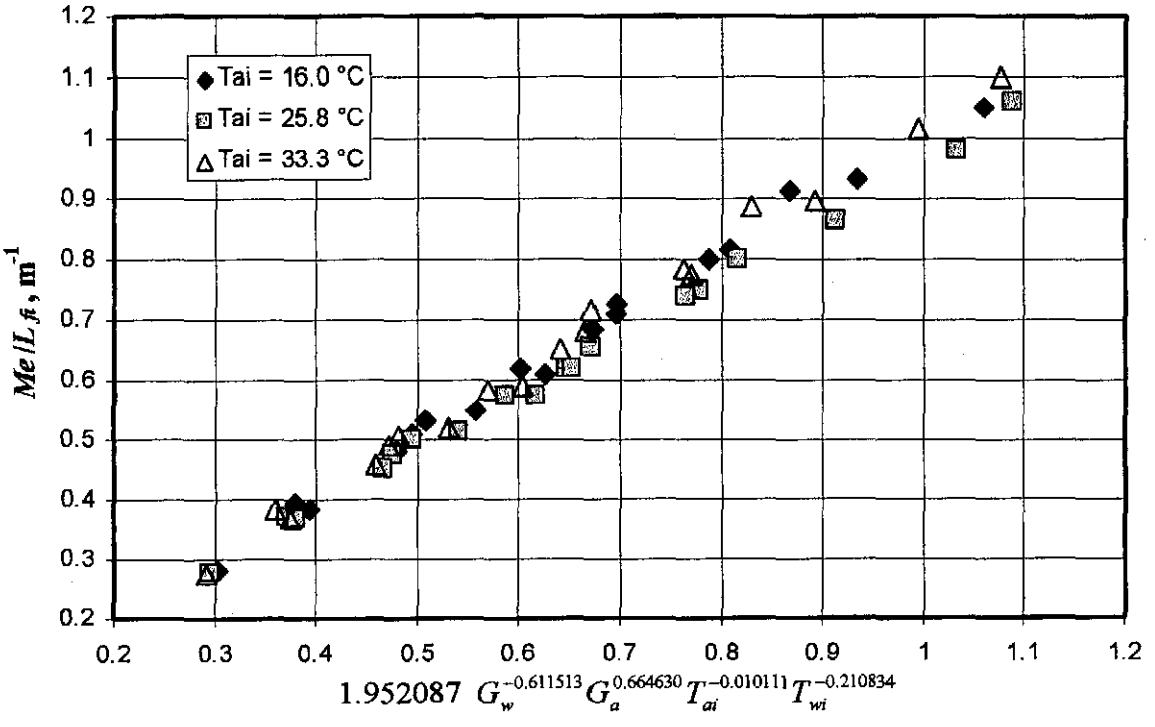

Figure R.24: The measured Merkel number per unit length of fill versus right-hand side of equation (R.10).

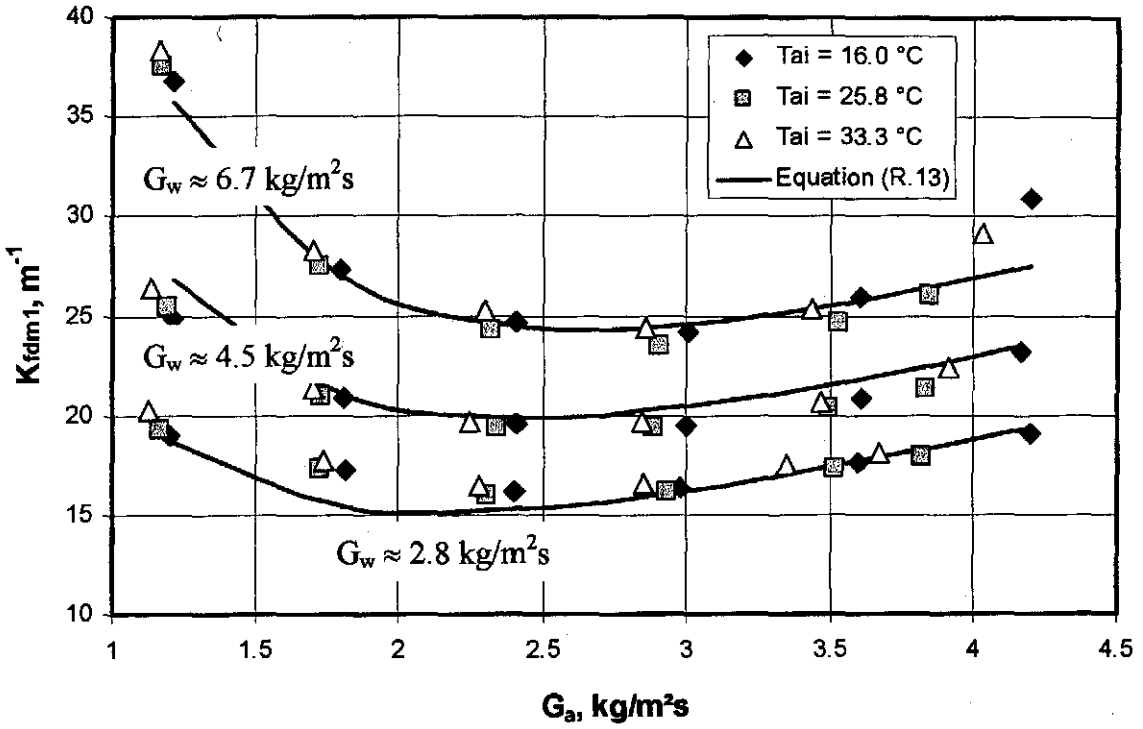

Figure R.25: The loss coefficients at different air inlet temperatures.

APPENDIX S

SPLASH FILL PERFORMANCE TEST RESULTS

S.1 INTRODUCTION

The performance characteristics of a splash fill are determined experimentally for four different fill spacings as shown in figure S.1. The results are critically evaluated and presented by extended empirical equations. The height of the spray zone above the fills is 0.15 m.

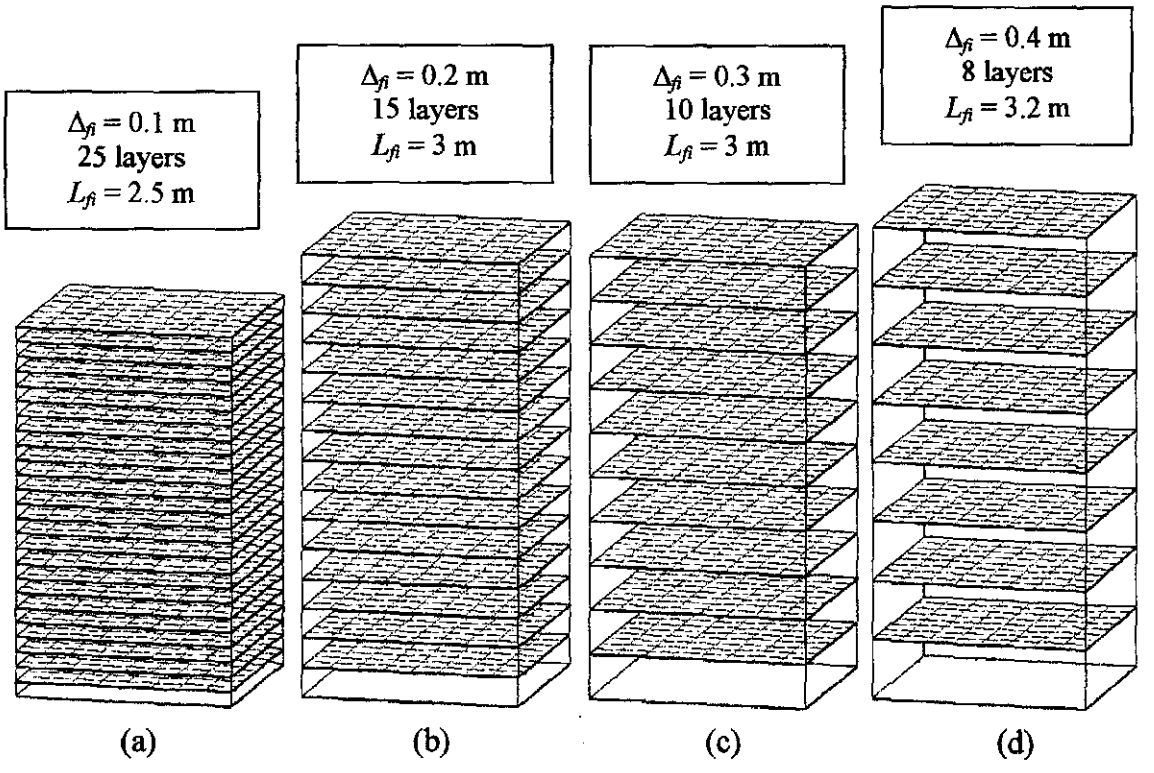

Figure S.1: Four different fill spacings for splash pack fill.

The test results, for the fills shown in figure S.1(a), (b), (c) and (d), are given in sections S.2, S.3, S.4 and S.5 respectively. The measured data are shown in a table for each test with another table showing the corresponding transfer and loss coefficients. The empirical relations for the transfer and loss coefficients for each test are given in separate tables. The empirical relations of the transfer and loss coefficients for the Merkel approach are compared to the measured data and shown in separate figures for each test.

S.2 FILL SPACING: 0.1 m

Table S.1: Experimental measurements (p_a = 100490 Pa).

	T_{ai} °C	T_{wb} °C	T_{wi} °C	T_{wo} °C	m_a kg/s	m_w kg/s	dp_{fi} Pa	T_{ao} °C
1	17.547	15.807	43.409	33.007	2.694	6.171	15.103	37.487
2	17.389	15.480	43.126	30.372	4.104	6.208	29.613	34.651
3	17.361	14.719	42.733	28.239	5.492	6.179	45.373	31.971
4	17.635	14.716	42.600	26.934	6.694	6.121	68.038	30.184
5	18.015	14.785	42.312	25.678	8.074	6.100	100.366	28.959
6	18.367	14.889	42.034	24.894	9.223	6.068	122.673	28.323
7	18.607	17.408	40.973	35.663	2.588	11.860	30.137	36.967
8	18.224	16.550	40.705	33.340	3.929	11.719	47.731	36.630
9	17.740	15.700	40.327	31.198	5.392	11.695	73.401	34.939
10	17.715	15.104	39.708	29.451	6.716	11.566	114.345	33.060
11	17.950	14.940	39.440	28.147	8.003	11.435	159.105	32.011
12	18.274	14.943	39.134	27.217	9.242	11.309	193.437	30.990
13	18.587	17.619	38.257	34.511	2.636	14.546	43.420	35.228
14	17.766	16.844	38.265	32.721	4.015	14.389	65.086	35.181
15	17.296	15.907	38.124	31.037	5.376	14.201	93.659	34.607
16	17.224	15.377	37.843	29.525	6.748	13.975	137.129	33.581
17	17.509	14.896	37.475	28.107	8.173	13.574	183.570	31.404
18	17.706	14.622	37.009	26.946	9.502	13.363	233.049	30.828

Table S.2: Transfer coefficients, loss coefficients and outlet temperatures according to the different methods (Δ_{fi} = 0.1 m).

	G_w kg/m²s	G_a kg/m²s	Me_e/L_{fi} m^{-1}	Me_M/L_{fi} m^{-1}	Me_P/L_f m^{-1}	K_{fdm1M} m^{-1}	K_{fdm1P} m^{-1}	T_{aoP} °C	T_{aoM} °C
1	2.743	1.197	0.284	0.288	0.321	9.805	9.795	37.633	36.979
2	2.759	1.824	0.345	0.351	0.385	8.045	8.031	34.622	34.061
3	2.746	2.441	0.398	0.407	0.442	6.859	6.847	32.131	31.635
4	2.721	2.975	0.442	0.452	0.488	6.917	6.905	30.576	30.127
5	2.711	3.589	0.492	0.503	0.541	7.022	7.011	29.139	28.736
6	2.697	4.099	0.525	0.536	0.576	6.590	6.580	28.062	27.691
7	5.271	1.150	0.182	0.183	0.213	20.361	20.317	38.584	37.901
8	5.208	1.746	0.243	0.245	0.276	13.881	13.848	36.825	36.197
9	5.198	2.396	0.299	0.303	0.336	11.330	11.303	35.067	34.491
10	5.140	2.985	0.342	0.347	0.382	11.414	11.389	33.316	32.789
11	5.082	3.557	0.385	0.391	0.428	11.211	11.188	32.105	31.616
12	5.026	4.107	0.412	0.419	0.456	10.251	10.231	30.898	30.443
13	6.465	1.172	0.158	0.158	0.186	28.177	28.119	36.504	35.892
14	6.395	1.784	0.226	0.227	0.259	18.141	18.100	35.633	35.054
15	6.312	2.389	0.278	0.280	0.314	14.567	14.534	34.434	33.885
16	6.211	2.999	0.323	0.326	0.361	13.571	13.542	33.129	32.617
17	6.033	3.633	0.362	0.366	0.402	12.432	12.408	31.644	31.168
18	5.939	4.223	0.396	0.401	0.438	11.722	11.701	30.384	29.941

Table S.3: Empirical relations for the transfer characteristic according to the various methods (Δ_{fi} = 0.1 m).

Approach	Eq. type	Empirical relation	Correlation coefficient
e-NTU	1	$Me_e / L_{fi} = 0.364409\ G_w^{-0.422824} G_a^{0.571346}$	0.9900
	2	$Me_e / L_{fi} = 0.436402 (G_w / G_a)^{-0.496508}$	0.9713
	3	$Me_e / L_{fi} = 1.127969\ G_w^{-0.071776} G_a^{0.255178} - 0.752887\ G_w^{0.063469} G_a^{0.145449}$	0.9981
Merkel	1	$Me_M / L_{fi} = 0.374457\ G_w^{-0.435520} G_a^{0.577461}$	0.9900
	2	$Me_M / L_{fi} = 0.444827 (G_w / G_a)^{-0.505736}$	0.9735
	3	$Me_M / L_{fi} = 1.134627\ G_w^{-0.086398} G_a^{0.254250} - 0.747394\ G_w^{0.054082} G_a^{0.139992}$	0.9979
Poppe	1	$Me_P / L_{fi} = 0.409266\ G_w^{-0.404903} G_a^{0.540131}$	0.9913
	2	$Me_P / L_{fi} = 0.482331 (G_w / G_a)^{-0.472575}$	0.9741
	3	$Me_P / L_{fi} = 1.152103\ G_w^{-0.077899} G_a^{0.255908} - 0.733838\ G_w^{0.065651} G_a^{0.142894}$	0.9980

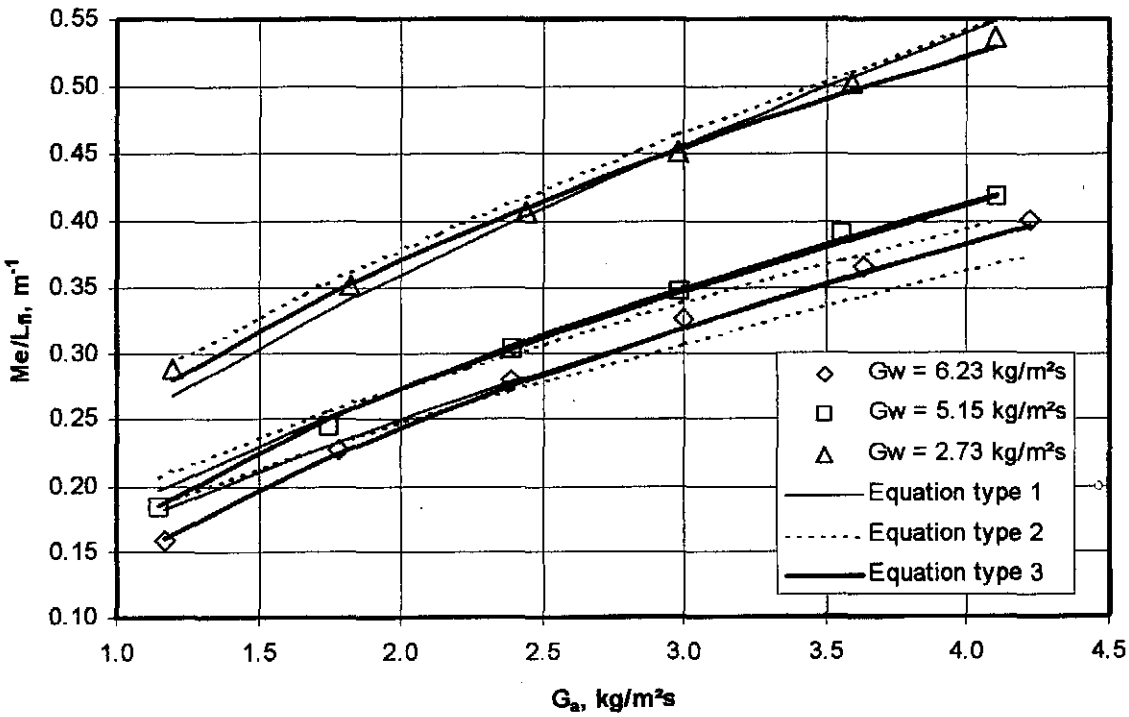

Figure S.2: Comparison of experimental data and empirical equations (Δ_{fi} = 0.1 m).

Table S.4: Empirical relations for the loss coefficient according to the various methods (Δ_{fi} = 0.1 m).

Approach	Eq. type	Empirical relation	Correlation coefficient
Merkel and *e-NTU*	1	$K_{fdm1M} = 4.292617\ G_w^{0.997973} G_a^{-0.593524}$	0.9446
	2	$K_{fdm1M} = 7.439312 (G_w / G_a)^{0.710454}$	0.8975
	3	$K_{fdm1M} = 0.257516\ G_w^{2.388300} G_a^{-2.303946} + 3.729301\ G_w^{0.646977} G_a^{-0.041177}$	0.9947
Poppe	1	$K_{fdm1P} = 4.289381\ G_w^{0.997176} G_a^{-0.5934961}$	0.9445
	2	$K_{fdm1P} = 7.425689 (G_w / G_a)^{0.710230}$	0.8974
	3	$K_{fdm1P} = 0.173797\ G_w^{2.576711} G_a^{-2.444194} + 3.881804\ G_w^{0.668754} G_a^{-0.093127}$	0.9948

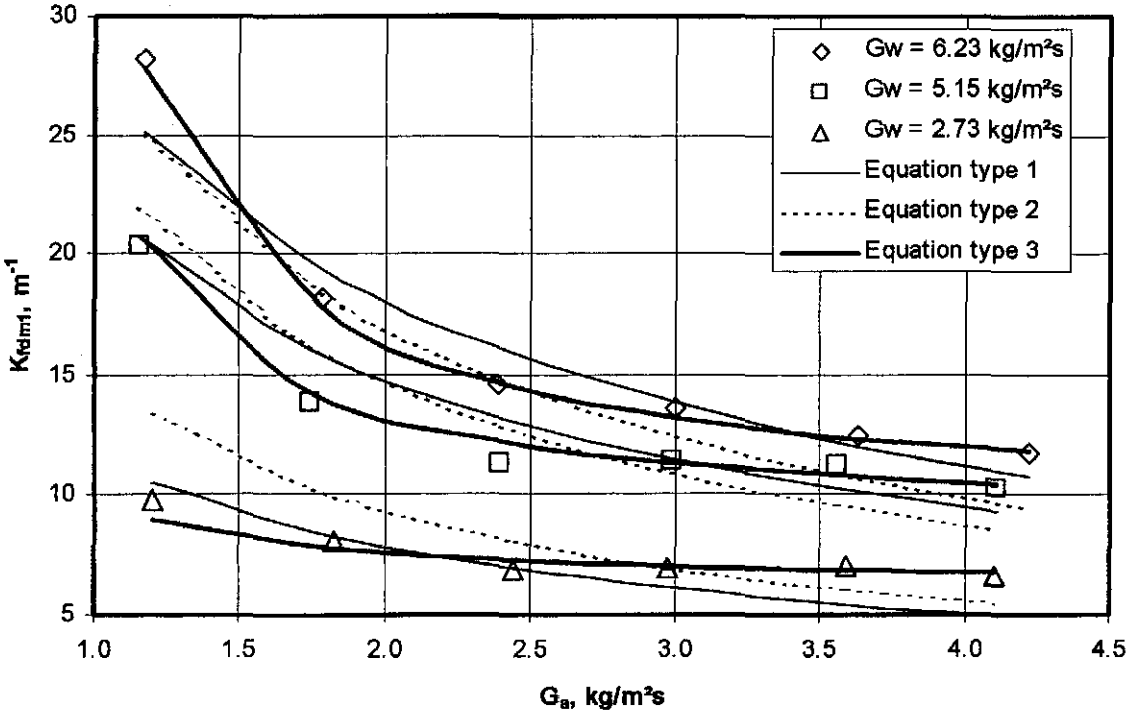

Figure S.3: Comparison of experimental data and empirical equations (Δ_{fi} = 0.1 m).

S.3 FILL SPACING: 0.2 m

Table S.5: Experimental measurements (p_a = 100480 Pa).

	T_{ai} °C	T_{wb} °C	T_{wi} °C	T_{wo} °C	m_a kg/s	m_w kg/s	dp_{fi} Pa	T_{ao} °C
1	14.808	12.959	46.443	34.233	2.866	6.553	16.735	39.922
2	14.476	12.504	46.526	31.783	4.103	6.510	23.930	37.014
3	14.780	11.980	46.610	29.816	5.404	6.525	29.827	34.819
4	14.926	11.724	46.594	28.285	6.727	6.521	43.791	32.964
5	15.439	11.917	46.575	26.968	8.171	6.516	71.501	31.778
6	15.977	12.262	46.610	26.080	9.487	6.515	91.641	31.027
7	15.816	14.085	46.847	38.104	2.921	10.636	25.780	41.861
8	15.712	13.715	46.821	35.948	4.024	10.574	34.316	40.383
9	15.299	12.465	46.824	33.603	5.413	10.631	44.740	38.976
10	15.393	12.268	46.812	31.844	6.765	10.620	66.140	37.537
11	15.819	12.282	46.772	30.322	8.165	10.559	102.194	36.438
12	16.254	12.537	46.669	29.082	9.522	10.575	131.165	35.218
13	17.439	17.101	46.623	40.502	2.769	15.177	40.278	43.617
14	16.415	16.103	45.735	37.730	4.130	15.203	51.796	41.755
15	15.515	13.849	43.883	34.693	5.455	15.204	67.582	39.370
16	15.558	13.317	42.794	32.741	6.764	15.211	94.772	38.324
17	15.936	12.662	40.830	30.500	8.128	15.222	134.642	36.361
18	16.314	12.861	38.592	28.323	9.456	15.226	172.635	33.841

Table S.6: Transfer coefficients, loss coefficients and outlet temperatures according to the different methods (Δ_{fi} = 0.2 m).

	G_w kg/m²s	G_a kg/m²s	Me_e/L_{fi} m^{-1}	Me_M/L_{fi} m^{-1}	Me_P/L_f m^{-1}	K_{fdm1M} m^{-1}	K_{fdm1P} m^{-1}	T_{aoP} °C	T_{aoM} °C
1	2.912	1.274	0.216	0.220	0.244	8.239	8.231	39.040	38.293
2	2.893	1.824	0.255	0.261	0.285	5.596	5.587	36.182	35.518
3	2.900	2.402	0.291	0.298	0.324	3.972	3.965	33.894	33.290
4	2.898	2.990	0.322	0.330	0.357	3.732	3.724	31.921	31.370
5	2.896	3.632	0.356	0.365	0.394	4.115	4.107	30.326	29.825
6	2.896	4.217	0.385	0.394	0.423	3.910	3.902	29.194	28.732
7	4.727	1.298	0.147	0.148	0.168	11.717	11.687	41.499	40.655
8	4.700	1.788	0.181	0.184	0.205	8.101	8.078	39.676	38.895
9	4.725	2.406	0.220	0.224	0.247	5.799	5.781	37.762	37.033
10	4.720	3.007	0.253	0.259	0.283	5.456	5.440	36.167	35.492
11	4.693	3.629	0.285	0.292	0.318	5.782	5.766	34.704	34.078
12	4.700	4.232	0.316	0.324	0.352	5.459	5.444	33.587	33.004
13	6.745	1.231	0.112	0.113	0.131	19.640	19.569	43.270	42.403
14	6.757	1.836	0.150	0.151	0.171	11.345	11.305	40.955	40.167
15	6.757	2.424	0.184	0.186	0.208	8.542	8.514	38.051	37.330
16	6.761	3.006	0.211	0.213	0.236	7.803	7.780	36.006	35.345
17	6.765	3.613	0.240	0.243	0.267	7.725	7.705	33.523	32.930
18	6.767	4.203	0.281	0.285	0.312	7.355	7.339	31.492	30.975

Table S.7: Empirical relations for the transfer characteristic according to the various methods (Δ_{fi} = 0.2 m).

Approach	Eq. type	Empirical relation	Correlation coefficient
e-NTU	1	$Me_e / L_{fi} = 0.289737\ G_w^{-0.496763} G_a^{0.583785}$	0.9876
	2	$Me_e / L_{fi} = 0.322738 (G_w / G_a)^{-0.541922}$	0.9640
	3	$Me_e / L_{fi} = 1.072707\ G_w^{-0.081663} G_a^{0.243658} - 0.782625\ G_w^{0.031122} G_a^{0.156002}$	0.9909
Merkel	1	$Me_M / L_{fi} = 0.298810\ G_w^{-0.509221} G_a^{0.590240}$	0.9872
	2	$Me_M / L_{fi} = 0.330365 (G_w / G_a)^{-0.551192}$	0.9653
	3	$Me_M / L_{fi} = 1.077103\ G_w^{-0.078787} G_a^{0.246703} - 0.779099\ G_w^{0.039566} G_a^{0.157085}$	0.9920
Poppe	1	$Me_P / L_{fi} = 0.325359\ G_w^{-0.483128} G_a^{0.560198}$	0.9871
	2	$Me_P / L_{fi} = 0.357981 (G_w / G_a)^{-0.523260}$	0.9640
	3	$Me_P / L_{fi} = 1.092143\ G_w^{-0.077113} G_a^{0.241133} - 0.767756\ G_w^{0.046927} G_a^{0.150183}$	0.9905

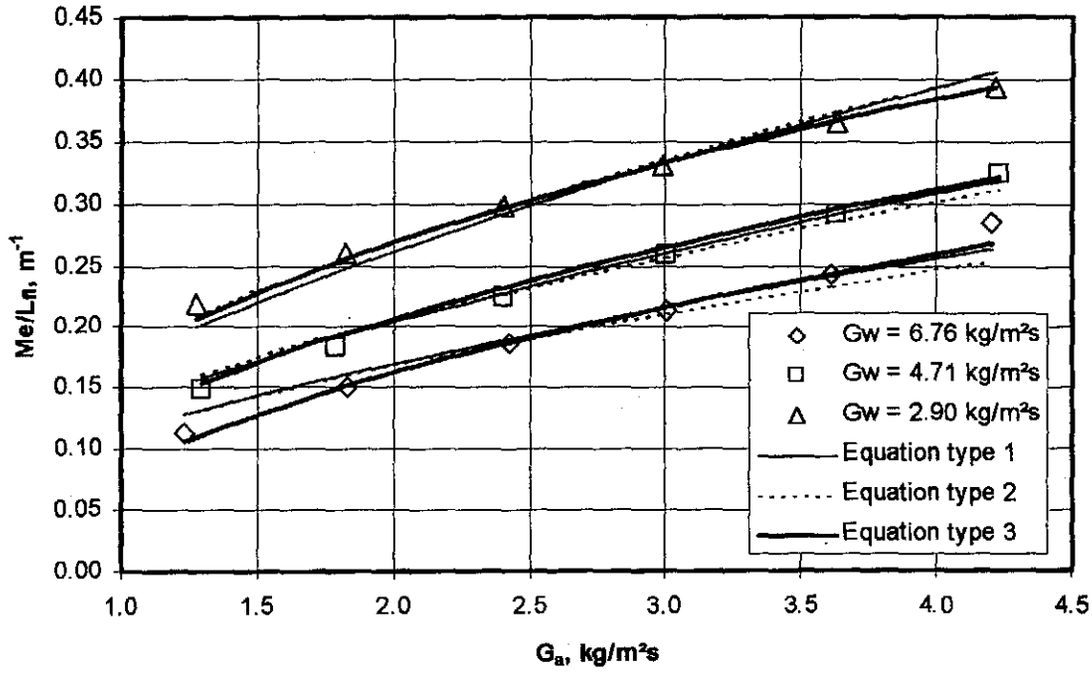

Figure S.4: Comparison of experimental data and empirical equations (Δ_{fi} = 0.2 m).

Table S.8: Empirical relations for the loss coefficient according to the various methods (Δ_{fi} = 0.2 m).

Approach	Eq. type	Empirical relation	Correlation coefficient
Merkel and *e-NTU*	1	$K_{fdm1M} = 4.30145\ G_w^{0.921207} G_a^{-0.87201}$	0.9543
	2	$K_{fdm1M} = 4.23192 (G_w / G_a)^{0.900392}$	0.9518
	3	$K_{fdm1M} = 3.179688\ G_w^{1.083916} G_a^{-1.965418} + 0.639088\ G_w^{0.684936} G_a^{0.642767}$	0.9932
Poppe	1	$K_{fdm1P} = 4.30017\ G_w^{0.93230} G_a^{-0.87192}$	0.9548
	2	$K_{fdm1P} = 4.22661 (G_w / G_a)^{0.89931}$	0.9590
	3	$K_{fdm1P} = 3.196078\ G_w^{1.079447} G_a^{-1.964637} + 0.633738\ G_w^{0.685777} G_a^{0.645903}$	0.9932

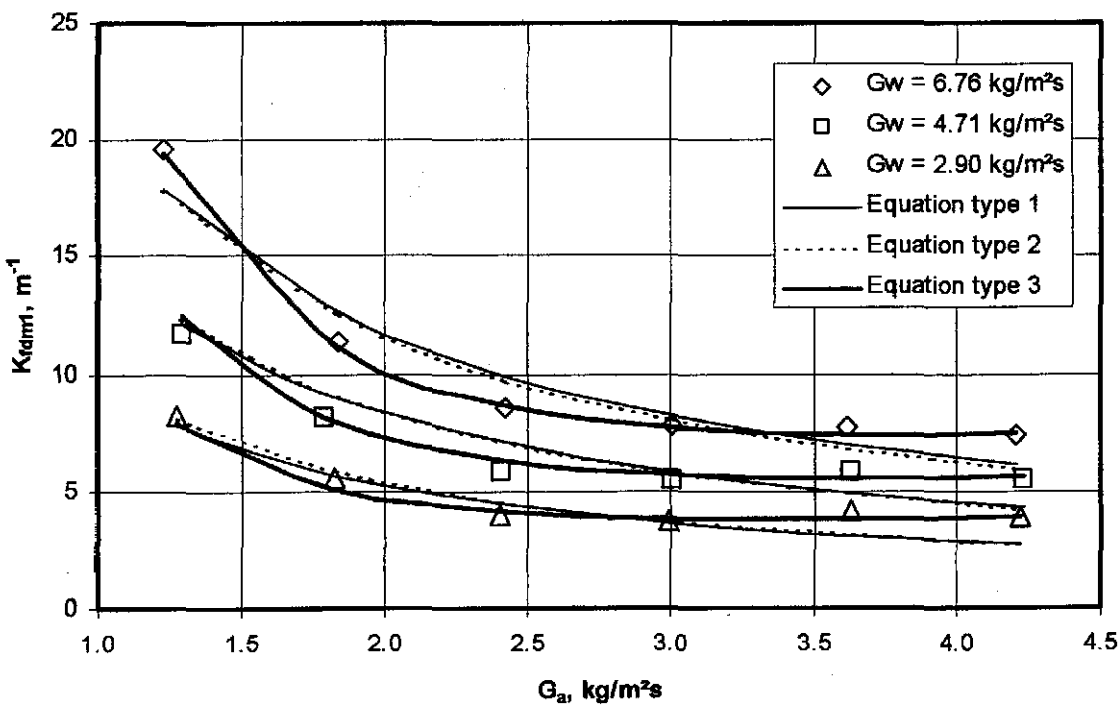

Figure S.5: Comparison of experimental data and empirical equations (Δ_{fi} = 0.2 m).

S.4 FILL SPACING: 0.3 m

Table S.9: Experimental measurements (p_a = 101560 Pa).

	T_{ai} °C	T_{wb} °C	T_{wi} °C	T_{wo} °C	m_a kg/s	m_w kg/s	dp_{fi} Pa	T_{ao} °C
1	13.827	11.929	45.383	33.375	2.949	6.027	17.571	38.346
2	13.725	11.536	45.289	31.337	4.074	6.031	23.192	34.870
3	13.901	11.064	44.919	29.214	5.485	6.027	28.215	31.875
4	14.079	10.934	44.929	27.691	6.850	6.035	40.289	30.083
5	14.506	11.153	44.628	26.332	8.159	6.034	68.247	28.881
6	14.994	11.344	44.224	24.988	9.592	6.036	92.966	28.248
7	14.997	13.496	43.782	36.839	2.825	10.657	28.216	39.245
8	14.652	12.835	43.471	34.368	4.110	10.631	35.996	37.757
9	14.186	11.609	43.004	31.979	5.516	10.632	47.188	35.561
10	14.032	11.067	42.770	30.243	6.753	10.637	67.561	34.352
11	14.386	11.054	42.706	28.758	8.126	10.659	99.516	33.176
12	14.851	11.273	42.528	27.597	9.494	10.624	127.475	32.257
13	16.460	16.053	42.371	37.547	2.858	15.228	42.361	38.753
14	15.459	14.793	42.324	35.762	4.114	15.205	53.616	38.233
15	14.653	12.668	42.220	33.941	5.457	15.214	69.178	37.491
16	14.035	11.648	41.950	32.333	6.754	15.220	96.462	36.543
17	14.166	11.268	41.666	30.722	8.237	15.199	136.104	35.288
18	14.478	11.315	41.455	29.307	9.527	15.213	170.933	34.642

Table S.10: Transfer coefficients, loss coefficients and outlet temperatures according to the different methods (Δ_{fi} = 0.3 m).

	G_w kg/m²s	G_a kg/m²s	Me_e/L_{fi} m^{-1}	Me_M/L_{fi} m^{-1}	Me_P/L_f m^{-1}	K_{fdm1M} m^{-1}	K_{fdm1P} m^{-1}	T_{aoP} °C	T_{aoM} °C
1	2.679	1.310	0.210	0.213	0.235	8.241	8.235	36.765	36.058
2	2.680	1.811	0.240	0.245	0.267	5.581	5.574	34.043	33.410
3	2.679	2.438	0.277	0.282	0.306	3.706	3.700	31.308	30.747
4	2.682	3.045	0.311	0.318	0.343	3.361	3.356	29.535	29.025
5	2.682	3.626	0.347	0.355	0.382	3.997	3.990	28.174	27.713
6	2.683	4.263	0.389	0.398	0.427	3.939	3.932	26.936	26.519
7	4.737	1.256	0.129	0.130	0.146	13.880	13.852	38.345	37.576
8	4.725	1.827	0.172	0.174	0.193	8.282	8.264	36.487	35.784
9	4.725	2.451	0.214	0.216	0.238	6.000	5.986	34.492	33.843
10	4.727	3.001	0.250	0.254	0.277	5.709	5.695	33.185	32.578
11	4.737	3.611	0.287	0.293	0.318	5.793	5.780	32.094	31.528
12	4.722	4.220	0.317	0.323	0.350	5.437	5.425	30.937	30.412
13	6.768	1.270	0.108	0.109	0.125	19.824	19.773	38.991	38.248
14	6.758	1.828	0.142	0.142	0.160	12.085	12.052	37.662	36.953
15	6.762	2.425	0.171	0.172	0.192	8.869	8.844	36.126	35.435
16	6.764	3.002	0.199	0.201	0.222	8.076	8.053	34.796	34.139
17	6.755	3.661	0.233	0.236	0.259	7.663	7.642	33.602	32.985
18	6.761	4.234	0.273	0.278	0.304	7.187	7.169	33.025	32.441

Table S.11: Empirical relations for the transfer characteristic according to the different methods (Δ_{fi} = 0.3 m).

Approach	Eq. type	Empirical relation	Correlation coefficient
e-NTU	1	$Me_e / L_{fi} = 0.243744\ G_w^{-0.454727} G_a^{0.645462}$	0.9799
	2	$Me_e / L_{fi} = 0.306690 (G_w / G_a)^{-0.542662}$	0.9536
	3	$Me_e / L_{fi} = 1.035456\ G_w^{0.085019} G_a^{0.361755} - 0.805507\ G_w^{0.181184} G_a^{0.313734}$	0.9916
Merkel	1	$Me_M / L_{fi} = 0.249013\ G_w^{-0.464089} G_a^{0.653578}$	0.9794
	2	$Me_M / L_{fi} = 0.312837 (G_w / G_a)^{-0.551295}$	0.9543
	3	$Me_M / L_{fi} = 1.026925\ G_w^{0.04034} G_a^{0.366635} - 0.792561\ G_w^{0.184318} G_a^{0.316749}$	0.9915
Poppe	1	$Me_P / L_{fi} = 0.270391\ G_w^{-0.441671} G_a^{0.628913}$	0.9788
	2	$Me_P / L_{fi} = 0.338802 (G_w / G_a)^{-0.528249}$	0.9521
	3	$Me_P / L_{fi} = 1.051589\ G_w^{0.088689} G_a^{0.356080} - 0.797118\ G_w^{0.1936080} G_a^{0.304773}$	0.9904

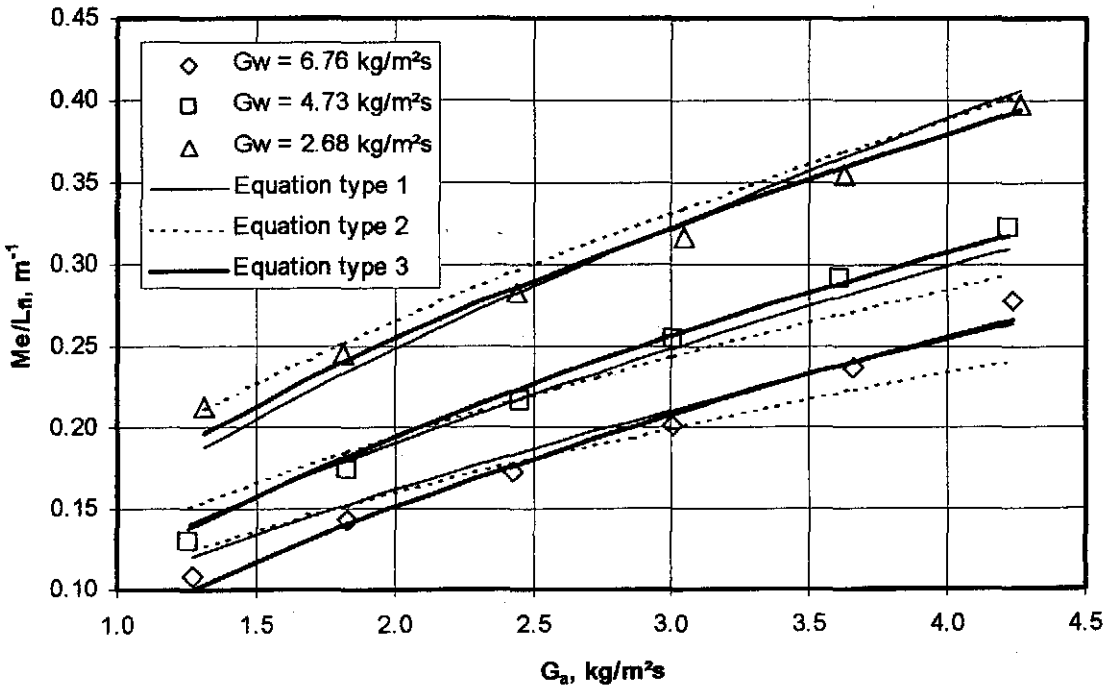

Figure S.6: Comparison of experimental data and empirical equations (Δ_{fi} = 0.3 m).

Table S.12: Empirical relations for the loss coefficient according to the various methods (Δ_{fi} = 0.3 m).

Approach	Eq. type	Empirical relation	Correlation coefficient
Merkel and *e-NTU*	1	$K_{fdm1M} = 4.163824\ G_w^{0.897218} G_a^{-0.931478}$	0.9518
	2	$K_{fdm1M} = 3.982891 (G_w / G_a)^{0.918727}$	0.9516
	3	$K_{fdm1M} = 4.276605\ G_w^{0.971935} G_a^{-1.699623} + 0.319932\ G_w^{0.642241} G_a^{1.066190}$	0.9947
Poppe	1	$K_{fdm1P} = 4.166137\ G_w^{0.895630} G_a^{-0.931793}$	0.9517
	2	$K_{fdm1P} = 3.975401 (G_w / G_a)^{0.918329}$	0.9515
	3	$K_{fdm1P} = 4.283539\ G_w^{0.969848} G_a^{-1.699905} + 0.318727\ G_w^{0.641672} G_a^{1.067842}$	0.9947

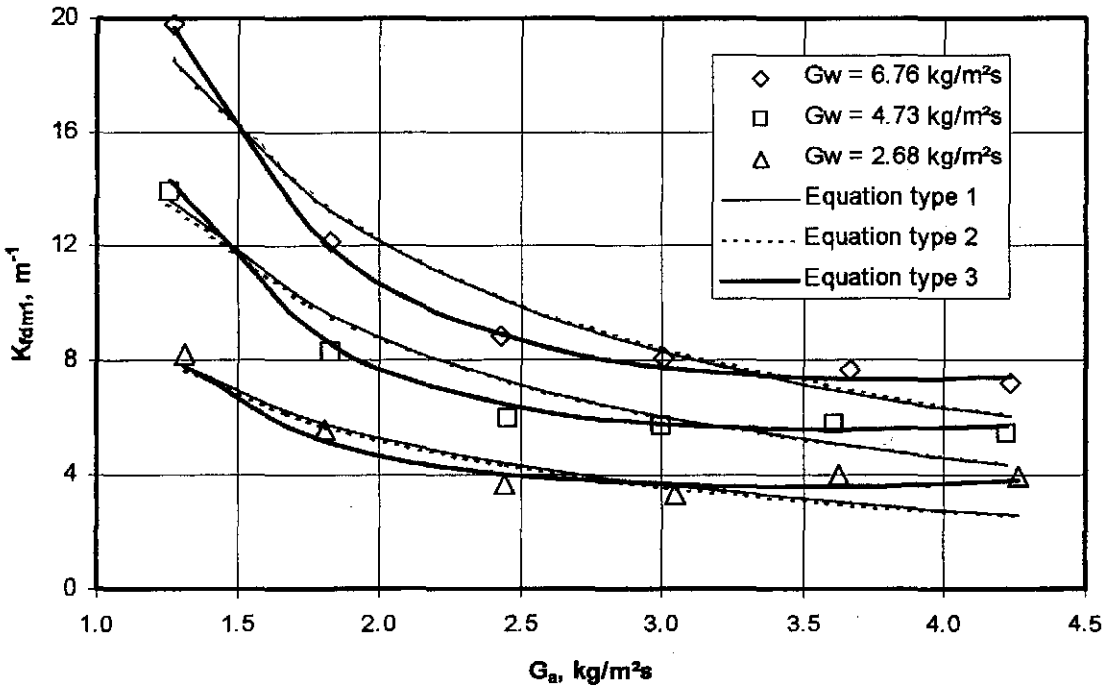

Figure S.7: Comparison of experimental data and empirical equations (Δ_{fi} = 0.3 m).

S.5 FILL SPACING: 0.4 m

Table S.13: Experimental measurements (p_a = 100950 Pa).

	T_{ai} °C	T_{wb} °C	T_{wi} °C	T_{wo} °C	m_a kg/s	m_w kg/s	dp_{fi} Pa	T_{ao} °C
1	18.799	18.523	49.280	37.710	2.740	6.722	23.267	28.300
2	18.634	18.428	49.755	35.738	3.972	6.745	29.186	30.171
3	18.451	17.944	49.883	33.870	5.311	6.743	34.041	32.958
4	18.718	17.939	49.883	32.427	6.622	6.666	45.814	34.502
5	19.105	17.982	49.818	30.827	8.014	6.695	75.265	34.240
6	19.651	18.214	49.866	29.536	9.379	6.700	99.317	33.388
7	19.873	19.873	49.933	41.803	2.660	10.760	32.021	44.269
8	19.590	19.590	49.956	39.025	4.118	10.783	40.890	42.657
9	18.910	18.687	49.930	36.926	5.380	10.718	50.302	41.343
10	18.799	18.799	49.803	35.090	6.651	10.652	70.643	39.187
11	19.173	18.016	49.552	33.381	8.044	10.687	106.767	37.418
12	19.682	18.184	48.472	31.454	9.411	10.653	135.553	36.772
13	23.036	23.036	43.582	39.557	2.663	15.122	45.347	40.836
14	20.700	20.700	42.113	36.975	3.881	15.128	53.115	38.998
15	19.412	19.412	40.768	34.376	5.410	15.129	70.267	37.126
16	18.418	18.418	39.895	32.619	6.668	15.051	95.215	35.883
17	18.536	18.080	39.364	31.133	8.060	15.129	129.654	35.111
18	18.996	18.144	38.956	29.957	9.364	15.107	167.915	34.302

Table S.14: Transfer coefficients, loss coefficients and outlet temperatures according to the different methods (Δ_{fi} = 0.1 m).

	G_w kg/m²s	G_a kg/m²s	Me_e/L_{fi} m^{-1}	Me_M/L_{fi} m^{-1}	Me_P/L_f m^{-1}	K_{fdm1M} m^{-1}	K_{fdm1P} m^{-1}	T_{aoP} °C	T_{aoM} °C
1	2.987	1.218	0.165	0.168	0.187	11.170	11.149	41.241	40.481
2	2.998	1.765	0.194	0.198	0.217	6.588	6.574	38.769	38.090
3	2.997	2.360	0.223	0.228	0.248	4.276	4.267	36.497	35.885
4	2.963	2.943	0.250	0.256	0.277	3.678	3.670	34.694	34.143
5	2.976	3.562	0.290	0.297	0.321	4.109	4.100	33.516	33.013
6	2.978	4.168	0.332	0.338	0.365	3.954	3.946	32.651	32.190
7	4.782	1.182	0.108	0.109	0.123	15.810	15.760	43.945	43.088
8	4.793	1.830	0.147	0.149	0.166	8.353	8.326	41.835	41.064
9	4.763	2.391	0.177	0.180	0.199	6.012	5.993	40.027	39.307
10	4.734	2.956	0.205	0.210	0.230	5.515	5.498	38.451	37.778
11	4.750	3.575	0.240	0.246	0.269	5.691	5.674	37.222	36.601
12	4.735	4.183	0.285	0.293	0.319	5.287	5.273	35.897	35.338
13	6.721	1.183	0.092	0.093	0.107	21.955	21.902	40.646	39.996
14	6.724	1.725	0.122	0.122	0.138	12.234	12.207	38.210	37.624
15	6.724	2.405	0.160	0.160	0.178	8.379	8.361	35.977	35.440
16	6.689	2.963	0.182	0.183	0.202	7.521	7.505	34.148	33.638
17	6.724	3.582	0.219	0.221	0.243	7.010	6.996	33.258	32.779
18	6.714	4.162	0.256	0.258	0.283	6.725	6.712	32.601	32.152

Table S.15: Empirical relations for the transfer characteristic according to the various methods (Δ_{fi} = 0.4 m).

Approach	Eq. type	Empirical relation	Correlation coefficient
e-NTU	1	$Me_e / L_{fi} = 0.189421\ G_w^{-0.406131} G_a^{0.702488}$	0.9753
	2	$Me_e / L_{fi} = 0.274704 (G_w / G_a)^{-0.563612}$	0.9207
	3	$Me_e / L_{fi} = 0.292061\ G_w^{-0.075223} G_a^{0.460930} - 0.099761\ G_w^{0.301183} G_a^{0.244985}$	0.9783
Merkel	1	$Me_M / L_{fi} = 0.195062\ G_w^{-0.418215} G_a^{0.707961}$	0.9759
	2	$Me_M / L_{fi} = 0.280500 (G_w / G_a)^{-0.571781}$	0.9251
	3	$Me_M / L_{fi} = 0.305797\ G_w^{-0.050807} G_a^{0.455455} - 0.110328\ G_w^{0.319306} G_a^{0.252678}$	0.9770
Poppe	1	$Me_P / L_{fi} = 0.213383\ G_w^{-0.396999} G_a^{0.680197}$	0.9742
	2	$Me_P / L_{fi} = 0.304395 (G_w / G_a)^{-0.547953}$	0.9212
	3	$Me_P / L_{fi} = 0.327906\ G_w^{-0.041972} G_a^{0.439712} - 0.114295\ G_w^{0.333573} G_a^{0.238620}$	0.9774

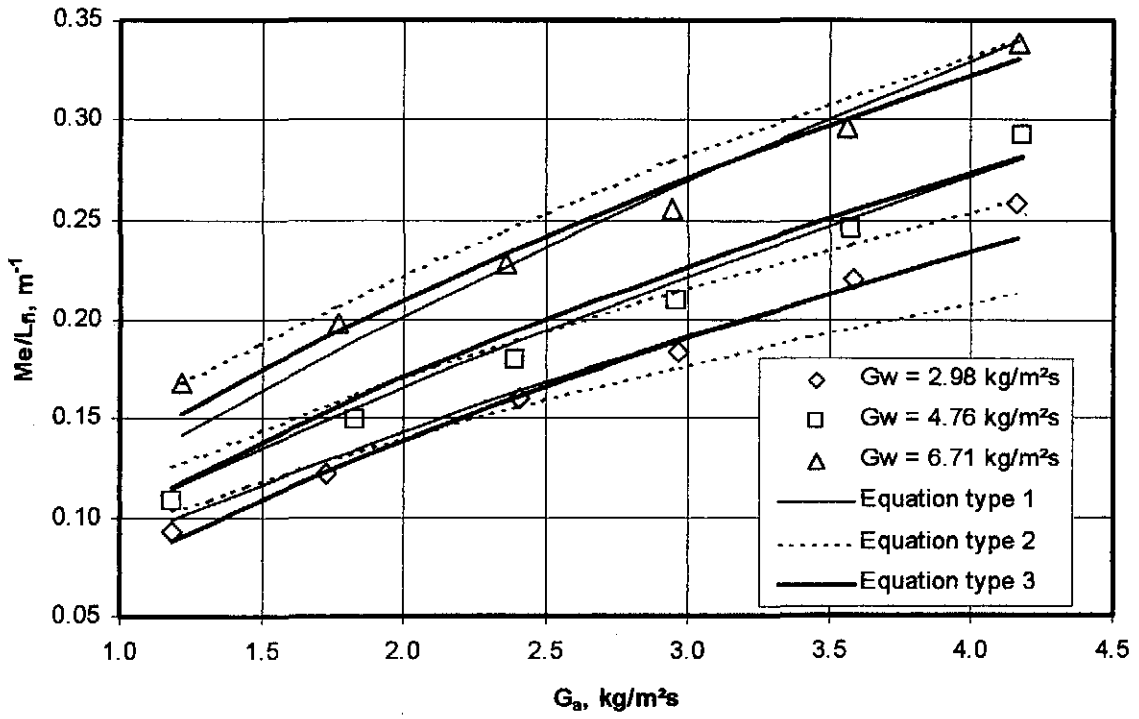

Figure S.8: Comparison of experimental data and empirical equations (Δ_{fi} = 0.4 m).

Table S.16: Empirical relations for the loss coefficient according to the various methods (Δ_{fi} = 0.4 m).

Approach	Eq. type	Empirical relation	Correlation coefficient
Merkel and *e-NTU*	1	$K_{fdm1M} = 3.478872\ G_w^{0.939791} G_a^{-0.968447}$	0.9416
	2	$K_{fdm1M} = 3.349466 (G_w / G_a)^{0.959075}$	0.9415
	3	$K_{fdm1M} = 6.010822\ G_w^{0.800143} G_a^{-1.886076} + 0.353521\ G_w^{0.695382} G_a^{0.942744}$	0.9955
Poppe	1	$K_{fdm1P} = 3.472315\ G_w^{0.939584} G_a^{-0.968594}$	0.9416
	2	$K_{fdm1P} = 3.341588 (G_w / G_a)^{0.959107}$	0.9414
	3	$K_{fdm1P} = 6.003348\ G_w^{0.799475} G_a^{-1.885029} + 0.350371\ G_w^{0.696669} G_a^{0.945598}$	0.9955

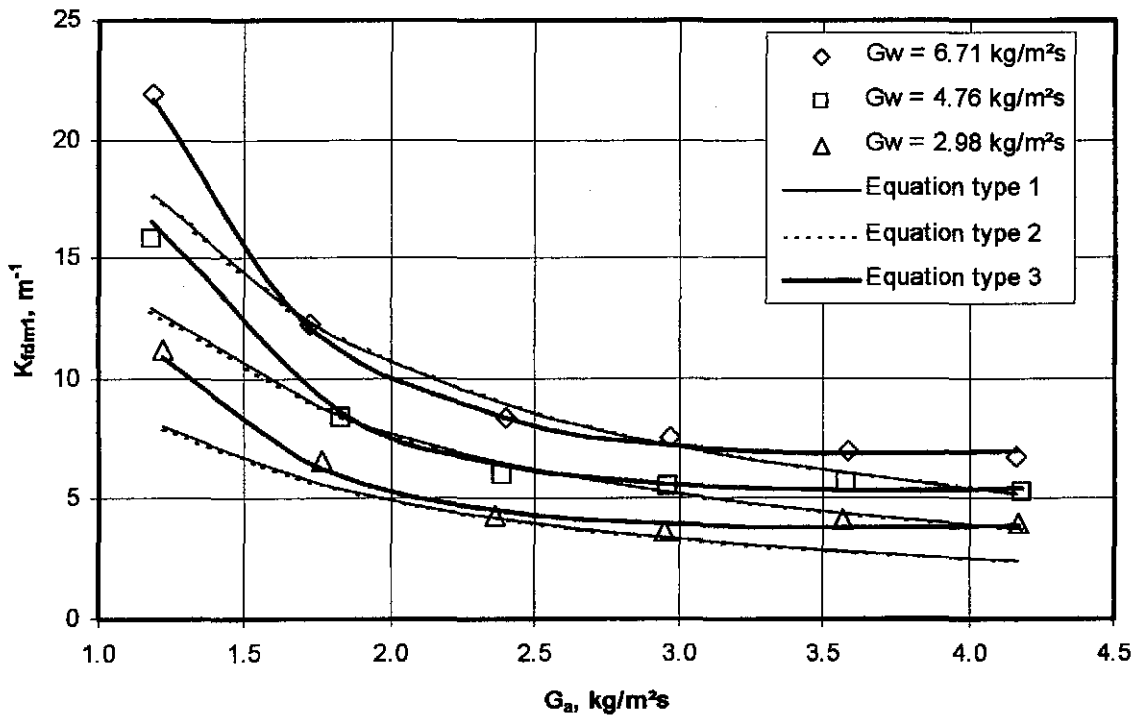

Figure S.9: Comparison of experimental data and empirical equations (Δ_{fi} = 0.4 m).

S.6 SUMMARY OF SPLASH PACK RESULTS

Table S.17 presents a summary of the three types of empirical equations of the transfer characteristic according to the Merkel approach, for each of the four fill heights tested. Equation type 3 gives the best correlation for all the fills tested followed by equation type 1 and equation type 2. Although equation type 3 gives the best accuracy, as can be seen from the values of the correlation coefficients in table S.17, equation type 1 gives correlations of the same order of accuracy. This can be seen from figures S.2, S.4, S.6 and S.8 for fill spacings of 0.1, 0.2, 0.3 and 0.4 m respectively.

Table S.17: Summary of the transfer coefficients according to the Merkel approach.

Δ_{fi}, m	Equation type 1	r^2
0.1	$Me_M / L_{fi} = 0.374457\ G_w^{-0.435520} G_a^{0.577461}$	0.9900
0.2	$Me_M / L_{fi} = 0.298810\ G_w^{-0.509221} G_a^{0.590240}$	0.9872
0.3	$Me_M / L_{fi} = 0.249013\ G_w^{-0.464089} G_a^{0.653578}$	0.9794
0.4	$Me_M / L_{fi} = 0.195062\ G_w^{-0.418215} G_a^{0.707961}$	0.9759
Δ_{fi}, m	**Equation type 2**	r^2
0.1	$Me_M / L_{fi} = 0.444827(G_w / G_a)^{-0.505736}$	0.9735
0.2	$Me_M / L_{fi} = 0.330365(G_w / G_a)^{-0.551192}$	0.9653
0.3	$Me_M / L_{fi} = 0.312837(G_w / G_a)^{-0.551295}$	0.9543
0.4	$Me_M / L_{fi} = 0.280500(G_w / G_a)^{-0.571781}$	0.9251
Δ_{fi}, m	**Equation type 3**	r^2
0.1	$Me_M / L_{fi} = 1.134627 G_w^{-0.086398} G_a^{0.254250} - 0.747394 G_w^{0.054082} G_a^{0.139992}$	0.9979
0.2	$Me_M / L_{fi} = 1.077103 G_w^{-0.078787} G_a^{0.246703} - 0.779099 G_w^{0.039566} G_a^{0.157085}$	0.9920
0.3	$Me_M / L_{fi} = 1.026925 G_w^{0.040340} G_a^{0.366635} - 0.792561 G_w^{0.184318} G_a^{0.316749}$	0.9915
0.4	$Me_M / L_{fi} = 0.305797 G_w^{-0.050807} G_a^{0.455455} - 0.110328 G_w^{0.319306} G_a^{0.252678}$	0.9770

The data of the coefficients in tables S.2, S.6, S.10 and S.14 are evaluated together to obtain the following general empirical relations, applicable to all the fills tested. Neglecting the effect of the fill height, the experimental data for the transfer coefficient for all the different fill spacings can be presented by

$$Me_M / L_{fi} = 0.164488\ G_w^{-0.459352} G_a^{0.614346} \Delta_{fi}^{-0.347798} \quad \text{(S.1)}$$

with a correlation coefficient $r^2 = 0.9748$ and where Δ_{fi} is the fill spacing in metres.

If the effect of the fill height is included in the correlation then find

$$Me_M / L_{fi} = 1.021213\ G_w^{-0.45510} G_a^{0.615114} \Delta_{fi}^{-0.103487} L_{fi}^{-1.369334} \quad \text{(S.2)}$$

with a correlation coefficient $r^2 = 0.9845$.

If the effect of the water inlet temperature, expressed in °C, is included in the correlation then find

$$Me_M / L_{fi} = 2.011515\ G_w^{-0.493143} G_a^{0.604637} \Delta_{fi}^{-0.154237} L_{fi}^{-0.913309} T_{wi}^{-0.311016} \quad \text{(S.3)}$$

with a correlation coefficient $r^2 = 0.9858$.

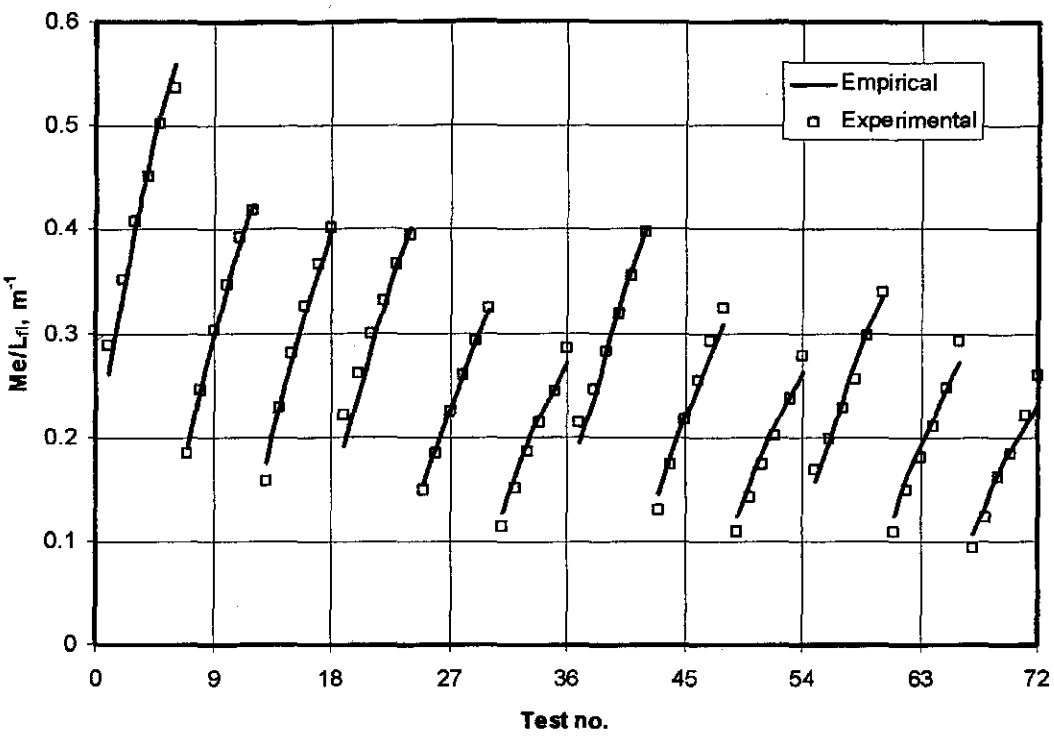

Figure S.10: Comparison between measured data and equation (S.2).

Figure S.10 shows the comparison between the measured data and equation (S.2) for the Merkel approach. Test numbers 1 to 18, 19 to 36, 37 to 54 and 55 to 72 in figure S.10 respectively refer to the 0.1, 0.2, 0.3 and 0.4 m spacing fill tests.

It is important to note that the equations given above are only accurate for the specific fills tested. It is not intended to extrapolate the equations for other fills heights and fill spacings. For example, if Δ_{fi} is chosen as 0.4 m then L_{fi} in the equations must be 3.2 m as can be seen in figure S.1(d).

Table S.18 presents a summary of the three types of empirical equations of the loss coefficients according to the Merkel approach, for each of the four fill spacings tested. Equation type 1 gives a very accurate correlation of the experimental data as the correlation coefficients in table S.18 is very close to 1. Equation type 1 and equation type 2 are less accurate and give curve fits of approximately the same accuracy. This is because the modulus of the exponents of G_a and G_w are approximately equal for equation type 1.

If the effect of the fill height is neglected then a correlation through the measurements of all four of the tested fills is given by

$$K_{fdm1M} = \left(1.655585 G_w^{1.83200} G_a^{-1.919182} + 0.805749 G_w^{0.596214} G_a^{0.381360}\right) \Delta_{fi}^{-0.310972} \qquad \text{(S.4)}$$

with a correlation coefficient $r^2 = 0.9212$.

If the fill height is included in the correlation then find

$$K_{fdm1M} = \left(10.05368 G_w^{1.297029} G_a^{-1.992125} + 7.76125 G_w^{0.595059} G_a^{0.251349}\right) \Delta_{fi}^{-0.042869} L_{fi}^{-1.542947} \qquad \text{(S.5)}$$

with a correlation coefficient $r^2 = 0.9419$. Figure S.11 shows the comparison between the measured data and equation (S.5) for the Merkel approach.

Table S.18: Summary of the transfer coefficients according to the Merkel approach.

Δ_{fi}, m	Equation type 1	r^2
0.1	$K_{fdm1M} = 4.292617\ G_w^{0.997973} G_a^{-0.593524}$	0.9446
0.2	$K_{fdm1M} = 4.30145\ G_w^{0.921207} G_a^{-0.87201}$	0.9543
0.3	$K_{fdm1M} = 4.163824\ G_w^{0.897218} G_a^{-0.931478}$	0.9518
0.4	$K_{fdm1M} = 3.478872\ G_w^{0.939791} G_a^{-0.968447}$	0.9416
Δ_{fi}, m	Equation type 2	r^2
0.1	$K_{fdm1M} = 7.439312 (G_w / G_a)^{0.710454}$	0.8975
0.2	$K_{fdm1M} = 4.23192 (G_w / G_a)^{0.900392}$	0.9518
0.3	$K_{fdm1M} = 3.982891 (G_w / G_a)^{0.918727}$	0.9516
0.4	$K_{fdm1M} = 3.349466 (G_w / G_a)^{0.959075}$	0.9415
Δ_{fi}, m	Equation type 3	r^2
0.1	$K_{fdm1M} = 0.257516 G_w^{2.388300} G_a^{-2.303946} + 3.729301 G_w^{0.646977} G_a^{-0.041177}$	0.9947
0.2	$K_{fdm1M} = 3.179688 G_w^{1.083916} G_a^{-1.965418} + 0.639088 G_w^{0.684936} G_a^{0.642767}$	0.9932
0.3	$K_{fdm1M} = 4.276605 G_w^{0.971935} G_a^{-1.699623} + 0.319932 G_w^{0.642241} G_a^{1.066190}$	0.9947
0.4	$K_{fdm1M} = 6.010822 G_w^{0.800143} G_a^{-1.886076} + 0.353521 G_w^{0.695382} G_a^{0.942744}$	0.9955

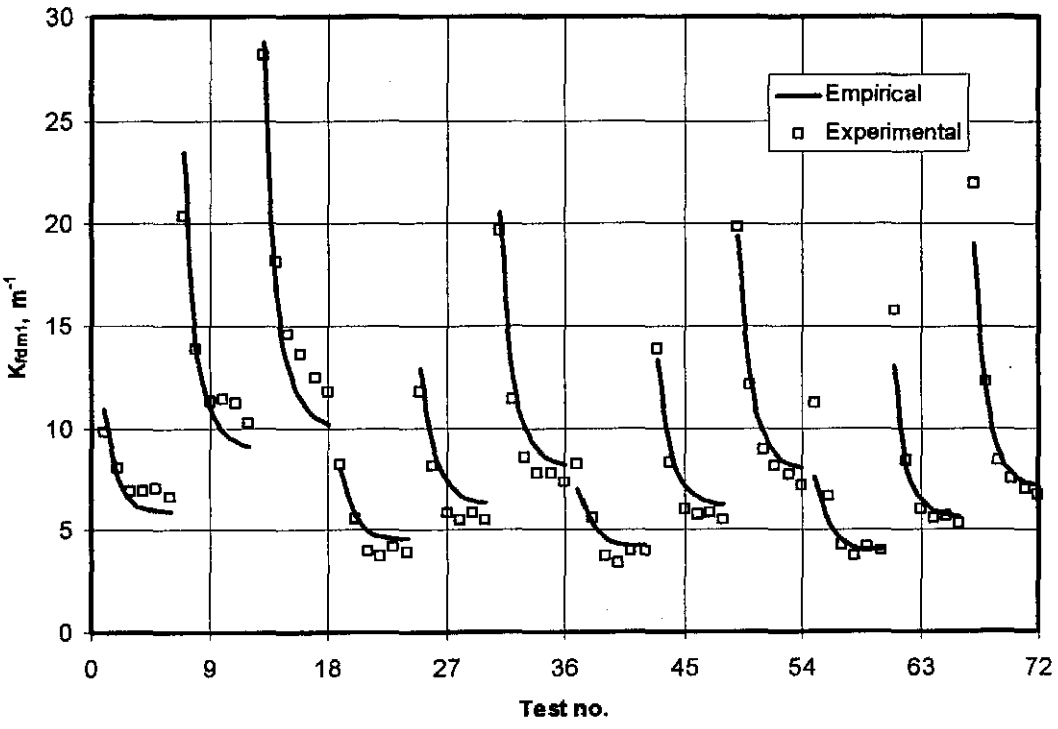

Figure S.11: Comparison between measured data and equation (S.5).

APPENDIX T

FILM FILL PERFORMANCE TEST RESULTS

T.1 INTRODUCTION

The performance characteristics of cross-corrugated film fills of three different heights are determined experimentally. The results are critically evaluated and presented by empirical equations. The film fills are stacked in layers consisting of horizontally stacked rectangular parallelepipeds. A schematic diagram of the film fills is shown in figure T.1. Each layer is stacked 90° relative to the layer below. The parallelepipeds are 0.3 m high, 0.3 m wide and 1.2 m long. The height of the spray zones above the fill for all the tests is 15 cm.

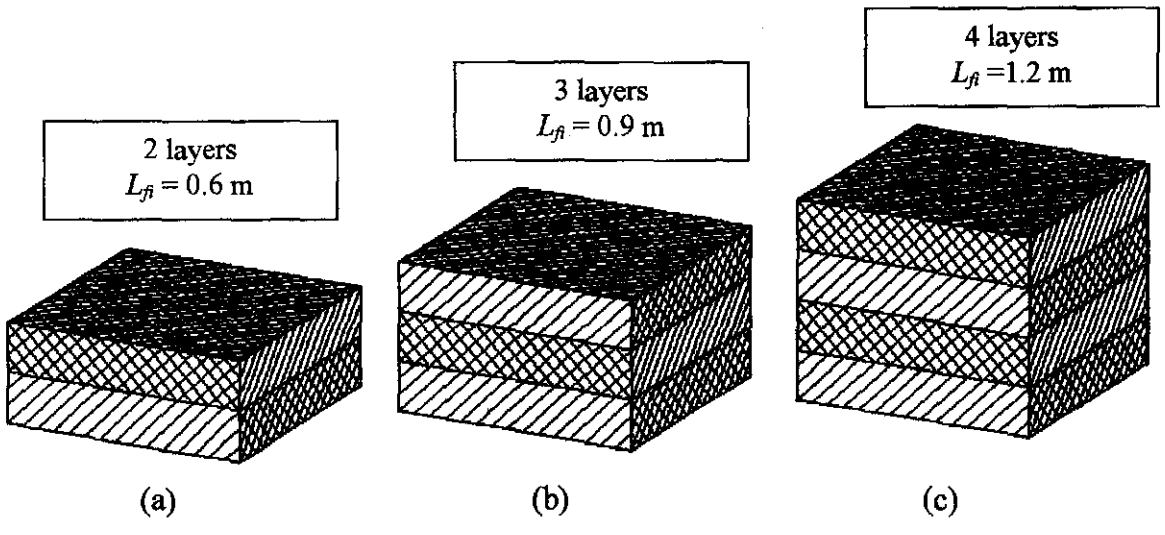

Figure T.1: Three heights of cross-corrugated film fills tested.

Each fill in figure T.1 is tested at different air and water mass flow rates The results of the tests for the fills shown in figure T.1(a), T.1(b) and T.1(c) are shown in sections T.2, T.3 and T.4 respectively.

T.2 FILL HEIGHT: 0.6 m

Table T.1: Experimental measurements (p_a = 100620 Pa).

	T_{ai} °C	T_{wb} °C	T_{wi} °C	T_{wo} °C	m_a kg/s	m_w kg/s	dp_{fi} Pa	T_{ao} °C
1	23.941	19.912	47.597	37.007	2.685	6.297	11.138	40.376
2	23.145	19.006	47.428	34.222	3.989	6.390	22.665	38.435
3	22.347	17.941	47.253	31.801	5.291	6.375	36.567	36.651
4	22.290	17.475	47.301	29.932	6.628	6.300	56.427	35.329
5	22.642	17.491	47.124	28.374	7.960	6.358	83.519	33.802
6	23.312	17.782	46.959	27.036	9.299	6.358	113.950	32.579
7	23.201	19.562	46.662	38.826	2.700	10.449	12.659	42.646
8	22.793	19.122	46.346	36.137	4.028	10.413	25.276	40.424
9	22.007	17.935	46.199	33.905	5.286	10.462	42.241	38.906
10	21.629	17.294	46.045	31.998	6.621	10.384	65.216	37.675
11	22.082	17.316	45.908	30.437	7.990	10.438	96.722	36.153
12	22.726	17.579	45.522	28.966	9.349	10.453	132.885	35.260
13	23.508	20.565	45.175	40.185	2.658	15.343	19.844	42.287
14	22.963	19.943	44.988	38.013	3.953	15.358	32.182	40.841
15	21.995	18.594	44.761	35.808	5.326	15.370	54.915	39.659
16	21.374	17.639	44.200	33.907	6.624	15.354	82.540	38.226
17	21.728	17.520	44.044	32.470	7.980	15.295	122.097	37.193
18	22.252	17.872	43.680	31.110	9.298	15.337	160.147	36.519

Table T.2: Transfer coefficients, loss coefficients and outlet temperatures according to the different methods (L_{fi} = 0.6 m).

	G_w kg/m²s	G_a kg/m²s	Me_e/L_{fi} m^{-1}	Me_M/L_{fi} m^{-1}	Me_P/L_f m^{-1}	K_{fdm1M} m^{-1}	K_{fdm1P} m^{-1}	T_{aoP} °C	T_{aoM} °C
1	2.799	1.193	0.896	0.908	1.011	27.908	27.809	39.922	39.206
2	2.840	1.773	1.148	1.170	1.286	25.805	25.719	37.439	36.805
3	2.833	2.351	1.397	1.430	1.559	23.864	23.792	35.345	34.771
4	2.800	2.946	1.636	1.676	1.817	23.629	23.566	33.669	33.149
5	2.826	3.538	1.905	1.948	2.104	24.357	24.299	32.555	32.079
6	2.826	4.133	2.217	2.255	2.425	24.411	24.359	31.677	31.243
7	4.644	1.200	0.759	0.765	0.879	30.982	30.844	42.529	41.725
8	4.628	1.790	0.999	1.013	1.137	27.795	27.677	40.397	39.675
9	4.650	2.349	1.217	1.241	1.377	27.169	27.062	38.796	38.121
10	4.615	2.943	1.419	1.453	1.598	26.939	26.844	37.180	36.556
11	4.639	3.551	1.643	1.687	1.847	27.567	27.479	36.053	35.475
12	4.646	4.155	1.907	1.963	2.139	27.762	27.683	35.058	34.526
13	6.819	1.181	0.523	0.525	0.614	50.026	49.808	42.204	41.407
14	6.826	1.757	0.747	0.752	0.862	36.629	36.469	41.102	40.354
15	6.831	2.367	0.974	0.984	1.112	34.625	34.481	39.897	39.184
16	6.824	2.944	1.149	1.166	1.303	33.924	33.795	38.410	37.742
17	6.798	3.547	1.325	1.349	1.497	34.736	34.615	37.372	36.743
18	6.817	4.132	1.549	1.583	1.750	33.628	33.521	36.631	36.045

Table T.3: Empirical relations for the transfer characteristic according to the various methods (L_{fi} = 0.6 m).

Approach	Eq. type	Empirical relation	Correlation coefficient
e-NTU	1	$Me_e / L_{fi} = 1.115805\ G_w^{-0.400945} G_a^{0.773647}$	0.9878
	2	$Me_e / L_{fi} = 1.757441 (G_w / G_a)^{-0.582890}$	0.9047
	3	$Me_e / L_{fi} = 1.453563\ G_w^{0.043374} G_a^{0.655501} - 0.500908 \cdot G_w^{0.422441} G_a^{0.552463}$	0.9940
Merkel	1	$Me_M / L_{fi} = 1.131871\ G_w^{-0.403632} G_a^{0.782625}$	0.9869
	2	$Me_M / L_{fi} = 1.796447 (G_w / G_a)^{-0.588290}$	0.9029
	3	$Me_M / L_{fi} = 1.638988\ G_w^{0.282648} G_a^{0.682887} - 0.802755\ G_w^{0.560711} G_a^{0.644229}$	0.9970
Poppe	1	$Me_P / L_{fi} = 1.232608\ G_w^{-0.370925} G_a^{0.748191}$	0.9859
	2	$Me_P / L_{fi} = 1.952821 (G_w / G_a)^{-0.556132}$	0.8931
	3	$Me_P / L_{fi} = 1.497125\ G_w^{0.276216} G_a^{0.665735} - 0.589942\ G_w^{0.634757} G_a^{0.622408}$	0.9962

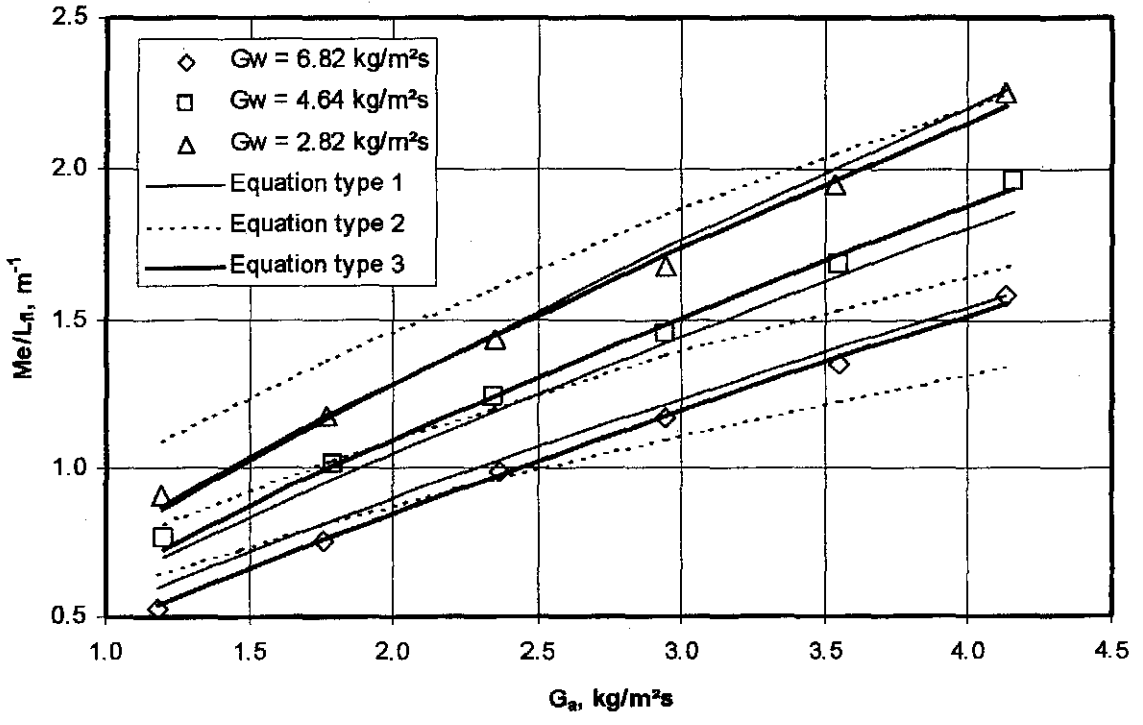

Figure T.2: Comparison of experimental data and empirical equations (L_{fi} = 0.6 m).

Table T.4: Empirical relations for the loss coefficient according to the various methods (L_{fi} = 0.6 m).

Approach	Eq. type	Empirical relation	Correlation coefficient
Merkel and *e-NTU*	1	$K_{fdm1M} = 17.162976\ G_w^{0.485379} G_a^{-0.206927}$	0.8152
	2	$K_{fdm1M} = 24.528308\ (G_w/G_a)^{0.313113}$	0.6858
	3	$K_{fdm1M} = 0.00819\ G_w^{5.465533} G_a^{-3.666315} + 17.545503\ G_w^{0.345860} G_a^{-0.036969}$	0.9613
Poppe	1	$K_{fdm1P} = 17.118512\ G_w^{0.484076} G_a^{-0.205697}$	0.8136
	2	$K_{fdm1P} = 24.461621 (G_w/G_a)^{0.311897}$	0.6836
	3	$K_{fdm1P} = 0.003132\ G_w^{4.755218} G_a^{-3.631669} + 17.238242 G_w^{0.349702} G_a^{-0.030826}$	0.9591

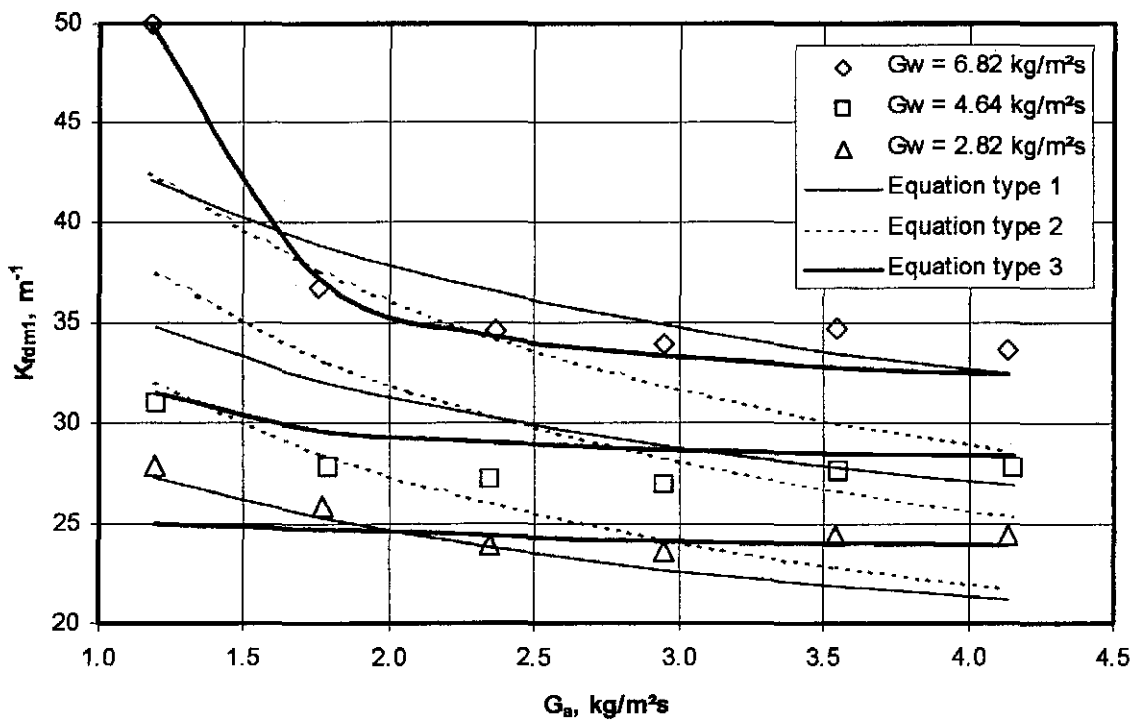

Figure T.3: Comparison of experimental data and empirical equations (L_{fi} = 0.6 m).

T.3 FILL HEIGHT: 0.9 m

Table T.5: Experimental measurements (p_a = 100950 Pa).

	T_{ai} °C	T_{wb} °C	T_{wi} °C	T_{wo} °C	m_a kg/s	m_w kg/s	dp_{fi} Pa	T_{ao} °C
1	21.490	17.574	46.252	34.169	2.745	6.201	16.052	40.742
2	21.060	17.028	46.057	31.212	3.985	6.180	31.042	38.582
3	20.546	16.110	45.922	28.443	5.359	6.144	51.440	36.455
4	20.504	15.632	45.674	26.476	6.634	6.123	76.526	34.904
5	21.078	15.810	45.308	24.831	8.021	6.098	114.345	33.192
6	21.719	16.124	45.070	23.618	9.303	6.047	154.239	32.032
7	21.609	18.573	43.850	36.198	2.716	10.043	16.995	40.954
8	21.003	17.749	43.444	33.401	3.948	9.962	32.715	39.213
9	20.247	16.421	42.934	30.606	5.402	9.869	58.232	37.360
10	20.171	15.825	42.483	28.639	6.669	9.877	86.515	36.065
11	20.566	15.709	42.161	26.965	8.013	9.795	125.962	34.741
12	21.264	15.932	41.707	25.398	9.379	9.851	175.598	33.409
13	21.724	18.619	41.287	36.431	2.754	14.695	22.724	39.454
14	21.212	17.940	41.165	34.443	3.996	14.595	39.174	38.594
15	20.282	16.572	40.882	32.243	5.368	14.470	67.710	37.363
16	19.965	15.884	40.728	30.610	6.627	14.422	102.540	36.334
17	20.179	15.755	40.734	29.198	8.025	14.333	153.822	35.656
18	20.954	15.891	40.784	27.762	9.338	14.343	204.969	35.070

Table T.6: Transfer coefficients, loss coefficients and outlet temperatures according to the different methods (L_{fi} = 0.9 m).

	G_w kg/m²s	G_a kg/m²s	Me_e/L_{fi} m^{-1}	Me_M/L_{fi} m^{-1}	Me_P/L_f m^{-1}	K_{fdm1M} m^{-1}	K_{fdm1P} m^{-1}	T_{aoP} °C	T_{aoM} °C
1	2.756	1.220	0.849	0.866	0.972	26.062	25.977	40.284	39.572
2	2.747	1.771	1.066	1.096	1.207	23.931	23.858	37.679	37.056
3	2.731	2.382	1.317	1.360	1.482	22.078	22.018	35.415	34.864
4	2.721	2.949	1.533	1.580	1.711	21.574	21.523	33.606	33.109
5	2.710	3.565	1.802	1.843	1.984	22.165	22.119	32.108	31.664
6	2.687	4.135	2.087	2.104	2.254	22.294	22.253	31.005	30.602
7	4.463	1.207	0.675	0.681	0.797	28.004	27.904	41.186	40.445
8	4.427	1.755	0.887	0.900	1.021	25.474	25.385	39.299	38.628
9	4.386	2.401	1.098	1.122	1.248	24.406	24.330	37.122	36.515
10	4.390	2.964	1.283	1.318	1.452	23.932	23.864	35.589	35.031
11	4.353	3.561	1.482	1.528	1.671	24.260	24.199	34.240	33.728
12	4.378	4.169	1.763	1.822	1.984	24.751	24.696	33.314	32.844
13	6.531	1.224	0.534	0.535	0.660	36.491	36.367	39.992	39.273
14	6.487	1.776	0.714	0.719	0.844	29.805	29.702	38.961	38.284
15	6.431	2.386	0.898	0.908	1.038	28.684	28.590	37.660	37.020
16	6.410	2.945	1.045	1.061	1.195	28.630	28.542	36.597	35.991
17	6.370	3.567	1.194	1.218	1.357	29.394	29.311	35.633	35.064
18	6.375	4.150	1.441	1.481	1.642	28.929	28.851	35.282	34.742

Table T.7: Empirical relations for the transfer characteristic according to the different methods (L_{fi} = 0.9 m).

Approach	Eq. type	Empirical relation	Correlation coefficient
e-NTU	1	$Me_e / L_{fi} = 1.073109\ G_w^{-0.444337} G_a^{0.770970}$	0.9921
	2	$Me_e / L_{fi} = 1.588654 \left(G_w / G_a\right)^{-0.606334}$	0.9340
	3	$Me_e / L_{fi} = 1.382687\ G_w^{0.001953} G_a^{0.739225} - 0.492783\ G_w^{0.344143} G_a^{0.714955}$	0.9944
Merkel	1	$Me_M / L_{fi} = 1.092357\ G_w^{-0.443876} G_a^{0.774531}$	0.9910
	2	$Me_M / L_{fi} = 1.625041 \left(G_w / G_a\right)^{-0.607805}$	0.9321
	3	$Me_M / L_{fi} = 1.625618\ G_w^{0.091940} G_a^{0.702913} - 0.735958\ G_w^{0.376496} G_a^{0.665399}$	0.9951
Poppe	1	$Me_P / L_{fi} = 1.193519\ G_w^{-0.397740} G_a^{0.724438}$	0.9900
	2	$Me_P / L_{fi} = 1.767607 \left(G_w / G_a\right)^{-0.561449}$	0.9225
	3	$Me_P / L_{fi} = 1.526182\ G_w^{0.078237} G_a^{0.695680} - 0.556982\ G_w^{0.419584} G_a^{0.675151}$	0.9933

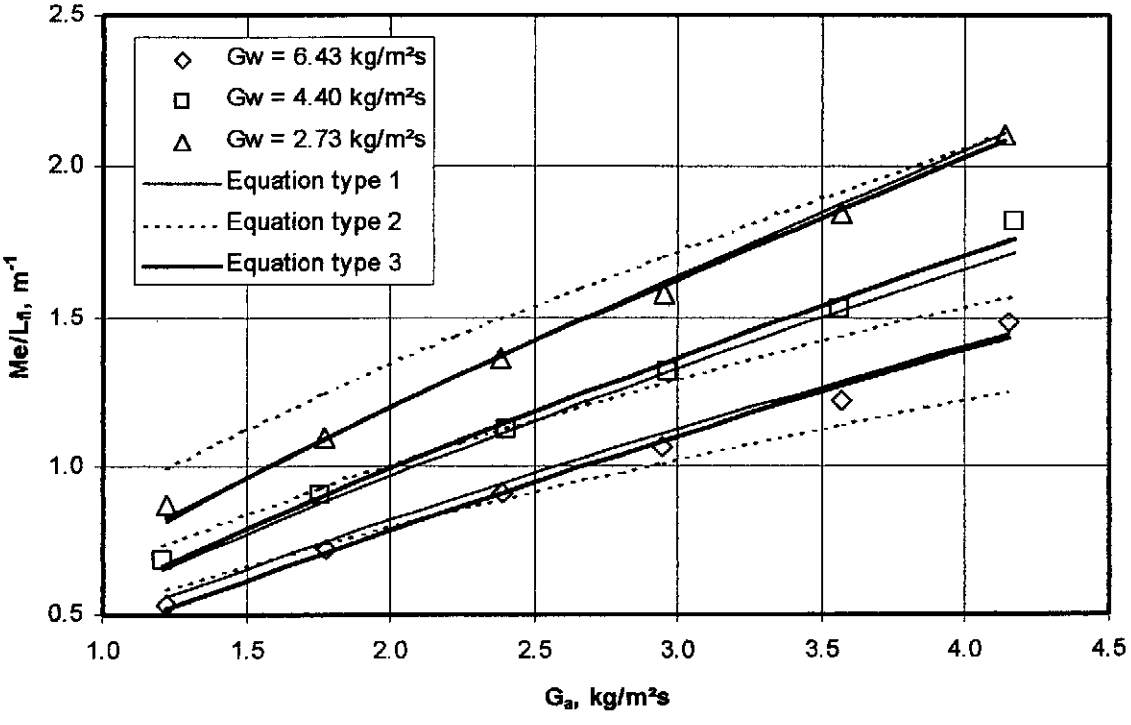

Figure T.4: Comparison of experimental data and empirical equations (L_{fi} = 0.9 m).

Table T.8: Empirical relations for the loss coefficient according to the various methods (L_{fi} = 0.9 m).

Approach	Eq. type	Empirical relation	Correlation coefficient
Merkel and *e-NTU*	1	$K_{fdm1M} = 18.216653\ G_w^{0.330968} G_a^{-0.140105}$	0.8506
	2	$K_{fdm1M} = 23.089652 (G_w/G_a)^{0.215184}$	0.7223
	3	$K_{fdm1M} = 1.633204\ G_w^{1.250268} G_a^{-3.873083} + 16.170094\ G_w^{0.288861} G_a^{0.012429}$	0.9304
Poppe	1	$K_{fdm1P} = 18.166799\ G_w^{0.330291} G_a^{-0.139161}$	0.8493
	2	$K_{fdm1P} = 23.033881 (G_w/G_a)^{0.214362}$	0.7200
	3	$K_{fdm1P} = 1.561219\ G_w^{1.276792} G_a^{-3.931459} + 16.173258 G_w^{0.287875} G_a^{0.011599}$	0.9300

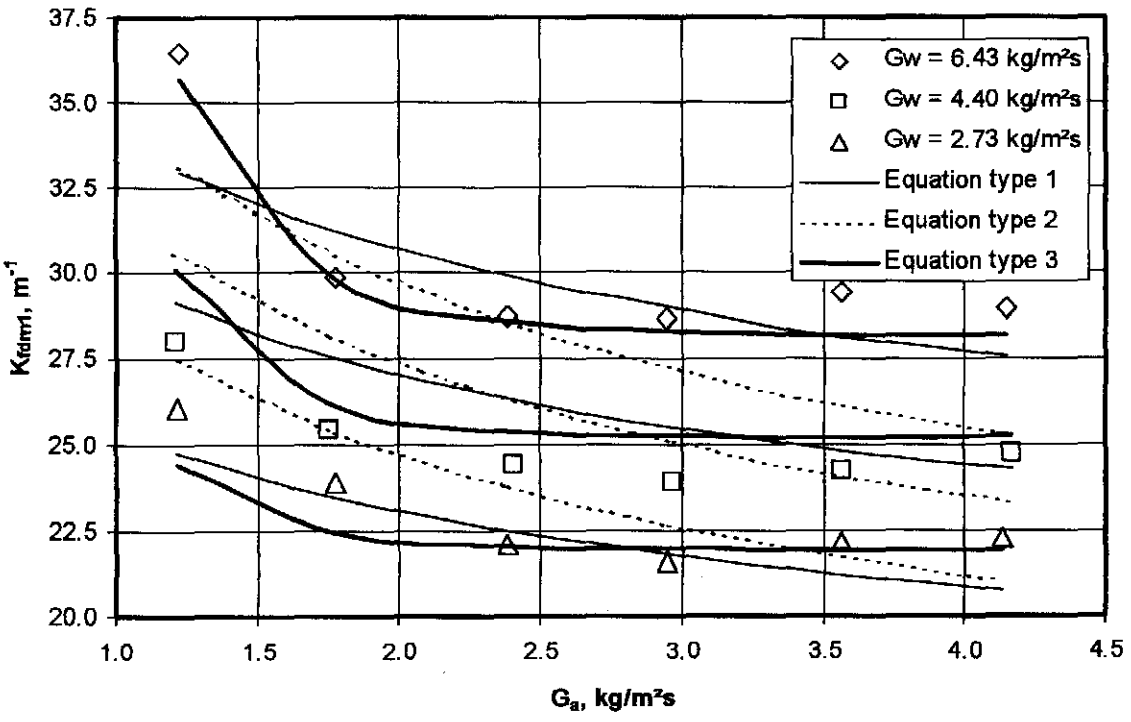

Figure T.5: Comparison of experimental data and empirical equations (L_{fi} = 0.9 m).

T.4 FILL HEIGHT: 1.2 m

Table T.9: Experimental measurements (p_a = 101020 Pa).

	T_{ai} °C	T_{wb} °C	T_{wi} °C	T_{wo} °C	m_a kg/s	m_w kg/s	dp_{fi} Pa	T_{ao} °C
1	22.787	17.282	44.500	32.906	2.715	6.372	21.090	40.502
2	22.468	16.739	44.154	29.703	3.988	6.354	40.996	38.385
3	22.374	16.079	43.971	27.221	5.285	6.331	66.197	36.410
4	22.736	15.866	43.568	25.164	6.684	6.275	102.465	34.632
5	23.405	16.100	43.159	23.607	8.006	6.236	149.358	33.225
6	24.076	16.435	42.750	22.319	9.420	6.191	208.263	31.938
7	23.591	18.493	41.830	34.844	2.661	9.997	22.022	39.505
8	23.077	17.833	41.347	31.968	3.935	9.928	42.702	38.096
9	22.553	16.686	40.875	29.321	5.329	9.804	73.625	36.294
10	22.636	16.286	40.504	27.399	6.615	9.700	110.577	35.052
11	23.465	16.504	40.095	25.746	7.959	9.569	161.016	33.828
12	24.156	16.689	39.754	24.257	9.342	9.528	224.387	32.390
13	24.155	19.208	38.740	34.553	2.673	13.895	27.143	37.470
14	23.690	18.461	38.459	32.348	4.031	13.643	50.272	36.594
15	22.961	17.227	38.260	30.377	5.298	13.512	81.935	35.818
16	22.914	16.543	38.004	28.700	6.597	13.276	124.537	34.805
17	23.117	16.445	37.632	27.082	7.992	13.100	183.626	33.579
18	23.952	16.772	37.295	25.726	9.341	12.972	241.428	32.655

Table T.10: Transfer coefficients, loss coefficients and outlet temperatures according to the different methods (L_{fi} = 1.2 m).

	G_w kg/m²s	G_a kg/m²s	Me_e/L_{fi} m^{-1}	Me_M/L_{fi} m^{-1}	Me_P/L_f m^{-1}	K_{fdm1M} m^{-1}	K_{fdm1P} m^{-1}	T_{aoP} °C	T_{aoM} °C
1	2.832	1.207	0.753	0.769	0.873	26.321	26.241	40.118	39.420
2	2.824	1.773	0.960	0.990	1.098	23.719	23.652	37.543	36.937
3	2.814	2.349	1.151	1.192	1.304	21.941	21.886	35.407	34.866
4	2.789	2.971	1.358	1.403	1.521	21.369	21.323	33.395	32.916
5	2.771	3.558	1.607	1.647	1.774	21.801	21.760	31.991	31.561
6	2.752	4.186	1.914	1.925	2.058	22.038	22.002	30.757	30.370
7	4.443	1.183	0.584	0.588	0.710	28.509	28.422	40.104	39.395
8	4.412	1.749	0.790	0.801	0.924	25.221	25.144	38.391	37.751
9	4.357	2.368	0.968	0.990	1.112	23.872	23.805	36.454	35.873
10	4.311	2.940	1.131	1.163	1.289	23.386	23.327	34.946	34.415
11	4.253	3.537	1.338	1.382	1.517	23.607	23.554	33.690	33.207
12	4.235	4.152	1.594	1.651	1.802	23.938	23.890	32.725	32.282
13	6.176	1.188	0.454	0.453	0.581	34.961	34.868	37.928	37.282
14	6.063	1.792	0.652	0.655	0.785	28.414	28.335	36.921	36.316
15	6.005	2.355	0.824	0.833	0.967	26.905	26.832	35.986	35.407
16	5.900	2.932	0.946	0.960	1.088	26.502	26.435	34.757	34.212
17	5.822	3.552	1.124	1.146	1.283	26.720	26.658	33.709	33.206
18	5.766	4.151	1.345	1.380	1.534	25.750	25.696	32.980	32.513

Table T.11: Empirical relations for the transfer characteristic according to the different methods (L_{fi} = 1.2 m).

Approach	Eq. type	Empirical relation	Correlation coefficient
e-NTU	1	$Me_e / L_{fi} = 0.974989\ G_w^{-0.468433} G_a^{0.788223}$	0.9909
	2	$Me_e / L_{fi} = 0.1438010 (G_w / G_a)^{-0.644151}$	0.9454
	3	$Me_e / L_{fi} = 1.370484\ G_w^{-0.249137} G_a^{0.748290} - 0.441297\ G_w^{0.028141} G_a^{0.703293}$	0.9915
Merkel	1	$Me_M / L_{fi} = 0.996604\ G_w^{-0.469512} G_a^{0.790386}$	0.9905
	2	$Me_M / L_{fi} = 1.471826 (G_w / G_a)^{-0.645730}$	0.9451
	3	$Me_M / L_{fi} = 1.357391\ G_w^{0.110577} G_a^{0.712196} - 0.567207\ G_w^{0.443165} G_a^{0.669846}$	0.9942
Poppe	1	$Me_P / L_{fi} = 1.090362\ G_w^{-0.408136} G_a^{0.725775}$	0.9891
	2	$Me_P / L_{fi} = 1.604656 (G_w / G_a)^{-0.585132}$	0.9349
	3	$Me_P / L_{fi} = 1.380517\ G_w^{0.112753} G_a^{0.698206} - 0.517075\ G_w^{0.461071} G_a^{0.681271}$	0.9917

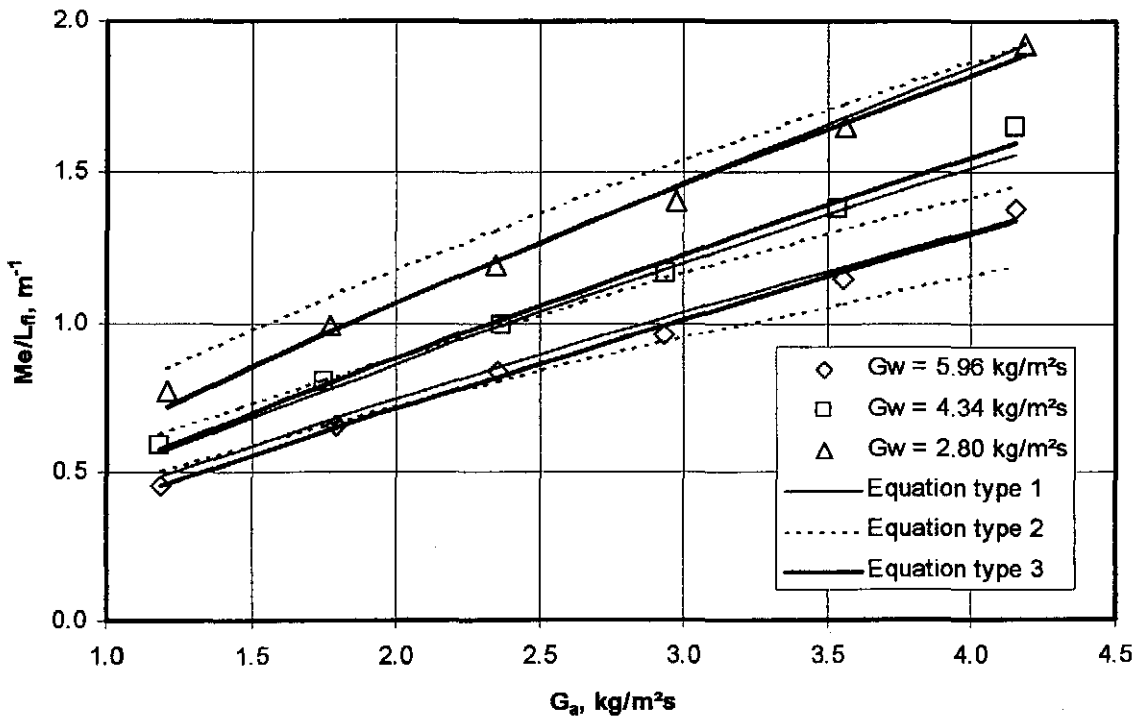

Figure T.6: Comparison of experimental data and empirical equations (L_{fi} = 1.2 m).

Table T.12: Empirical relations for the loss coefficient according to the various methods (L_{fi} = 1.2 m).

Approach	Eq. type	Empirical relation	Correlation coefficient
Merkel and *e-NTU*	1	$K_{fdm1M} = 19.658921\ G_w^{0.281255} G_a^{-0.175177}$	0.8561
	2	$K_{fdm1M} = 22.448599 (G_w / G_a)^{0.211132}$	0.8154
	3	$K_{fdm1M} = 3.897830\ G_w^{0.777271} G_a^{-2.114727} + 15.327472\ G_w^{0.215975} G_a^{0.079696}$	0.9562
Poppe	1	$K_{fdm1P} = 19.601207\ G_w^{0.281090} G_a^{-0.174400}$	0.8546
	2	$K_{fdm1P} = 22.399835 (G_w / G_a)^{0.210566}$	0.8133
	3	$K_{fdm1P} = 3.859490\ G_w^{0.782298} G_a^{-2.119420} + 15.295976\ G_w^{0.215311} G_a^{0.080546}$	0.9559

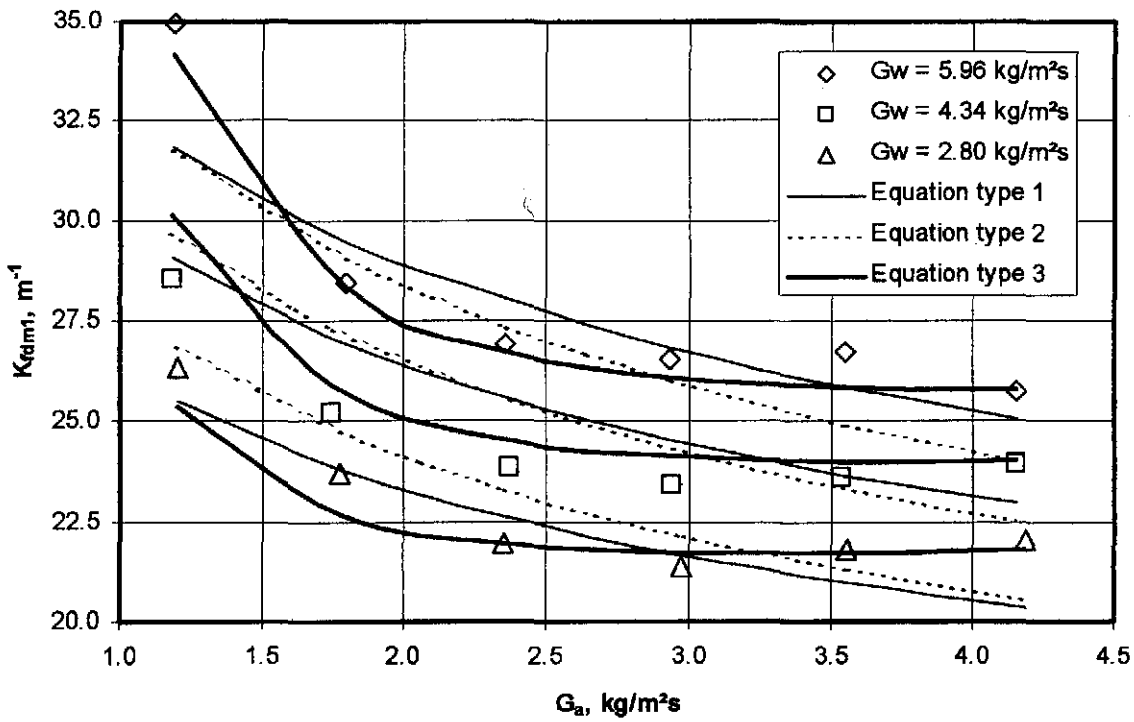

Figure T.7: Comparison of experimental data and empirical equations (L_{fi} = 1.2 m).

T.5 SUMMARY AND COMBINED RESULTS

A summary of the equations for the transfer coefficient, according to the Merkel approach, is shown in table T.13. It can be seen from figures T.2, T.4 and T.6 that equation types 1 and 3 give accurate representations of the measured data. This is also shown in table T.13 where all the correlation coefficients, r^2, for these equation types are close to unity.

Table T.13: Summary of the transfer coefficients according to the Merkel approach.

L_{fi}, m	Equation type 1	r^2
0.6	$Me_M / L_{fi} = 1.131871\ G_w^{-0.403632} G_a^{0.782625}$	0.9869
0.9	$Me_M / L_{fi} = 1.092357\ G_w^{-0.443876} G_a^{0.774531}$	0.9910
1.2	$Me_M / L_{fi} = 0.996604\ G_w^{-0.469512} G_a^{0.790386}$	0.9905
L_{fi}, m	**Equation type 2**	r^2
0.6	$Me_M / L_{fi} = 1.796447 (G_w / G_a)^{-0.588290}$	0.9029
0.9	$Me_M / L_{fi} = 1.625041 (G_w / G_a)^{-0.607805}$	0.9321
1.2	$Me_M / L_{fi} = 1.471826 (G_w / G_a)^{-0.645730}$	0.9451
L_{fi}, m	**Equation type 3**	r^2
0.6	$Me_M / L_{fi} = 1.638988\ G_w^{0.282648} G_a^{0.682887} - 0.802755\ G_w^{0.560711} G_a^{0.644229}$	0.9970
0.9	$Me_M / L_{fi} = 1.625618\ G_w^{0.091940} G_a^{0.702913} - 0.735958\ G_w^{0.376496} G_a^{0.665399}$	0.9951
1.2	$Me_M / L_{fi} = 1.357391\ G_w^{0.110577} G_a^{0.712196} - 0.567207\ G_w^{0.443165} G_a^{0.669846}$	0.9942

The experimental data for the transfer coefficient for all the different fill heights can be represented by

$$Me_M / L_{fi} = 1.019766\ G_w^{-0.432896} G_a^{0.782744} L_{fi}^{-0.292870} \qquad \text{(T.1)}$$

with a correlation coefficient $r^2 = 0.9880$.

Figure T.8 shows the results from equation (T.1) compared to the transfer characteristics obtained from experimental measurements. Tests 1 to 18 in figure T.8 represent the tests for the 0.6 m thick fill. Tests 19 to 36 represent the fill test results of the 0.6 m thick fill and tests 37 to 54 represent the measurements of the 1.2 m thick fill.

Due to the limitations of the fill test facility, it is impossible to conduct the fill tests at a constant water temperature. If the effect of the changing water temperature is included in the correlation, the Merkel number can then be presented by

$$Me_M / L_{fi} = 1.722176\ G_w^{-0.448804} G_a^{0.778434} L_{fi}^{-0.315937} T_{wi}^{-0.132799} \qquad \text{(T.2)}$$

with a correlation coefficient $r^2 = 0.9876$. T_{wi} is expressed in °C.

A summary of the equations for the loss coefficient according to the Merkel approach is shown in table T.14. It can be seen from the correlation coefficients, r^2, in table T.14 that equation type 3 gives the most

accurate representation of the measured data. Equation type 1 and equation type 2 do not correlate the measured data well. This is seen in figures T.3, T.5 and T.6.

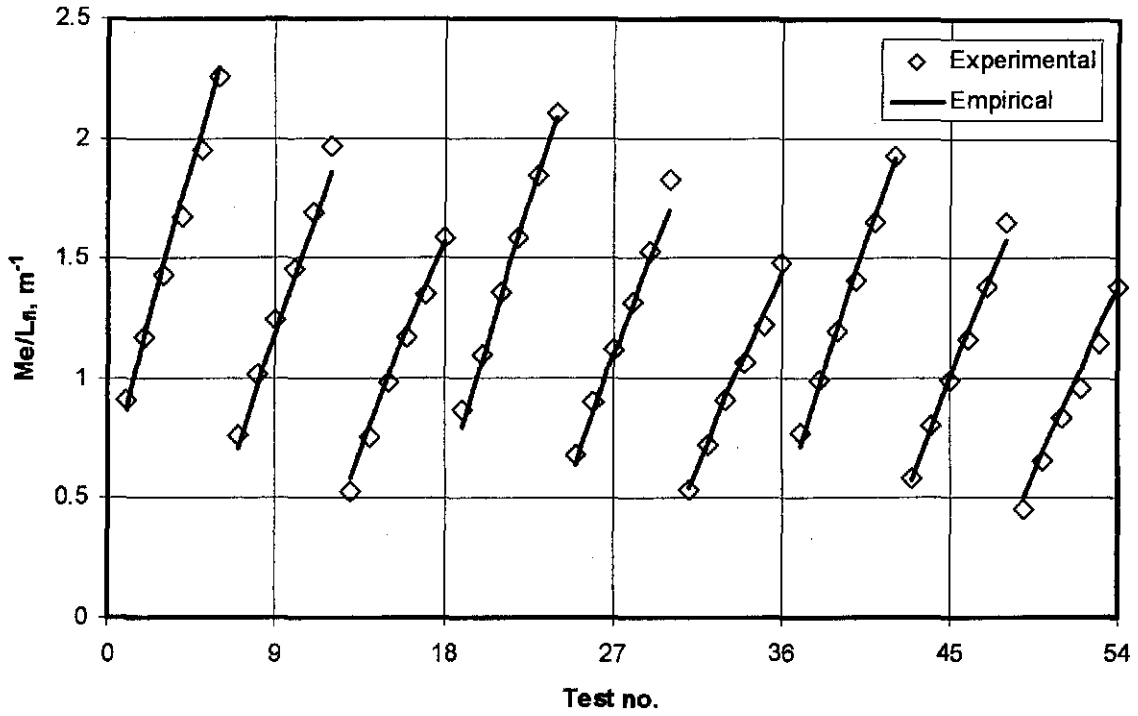

Figure T.8: Transfer characteristic given by equation (T.1) compared to experiemtal results.

Table T.14: Summary of the loss coefficients.

L_{fi}, m	Equation type 1	r^2
0.6	$K_{fdm1M} = 17.162976\ G_w^{0.485379} G_a^{-0.206927}$	0.8152
0.9	$K_{fdm1M} = 18.216653\ G_w^{0.330968} G_a^{-0.140105}$	0.8506
1.2	$K_{fdm1M} = 19.658921\ G_w^{0.281255} G_a^{-0.175177}$	0.8561
L_{fi}, m	**Equation type 2**	r^2
0.6	$K_{fdm1M} = 24.528308\ (G_w/G_a)^{0.313113}$	0.6858
0.9	$K_{fdm1M} = 23.089652(G_w/G_a)^{0.215184}$	0.7223
1.2	$K_{fdm1M} = 22.448599(G_w/G_a)^{0.211132}$	0.8154
L_{fi}, m	**Equation type 3**	r^2
0.6	$K_{fdm1M} = 0.00819\ G_w^{5.465533} G_a^{-3.666315} + 17.545503\ G_w^{0.345860} G_a^{-0.036969}$	0.9613
0.9	$K_{fdm1M} = 1.633204\ G_w^{1.250268} G_a^{-3.873083} + 16.170094\ G_w^{0.288861} G_a^{0.012429}$	0.9304
1.2	$K_{fdm1M} = 3.897830\ G_w^{0.777271} G_a^{-2.114727} + 15.327472\ G_w^{0.215975} G_a^{0.079696}$	0.9562

The experimental data for the loss coefficient for all the different fill heights can be represented by

$$K_{fdm1} = 16.753566\ G_w^{0.401127} G_a^{-0.170454} L_{fi}^{-0.235370} \qquad \text{(T.3)}$$

with a correlation coefficient $r^2 = 0.8276$. Equation (T.3) and the test data of the three different fill heights are shown in figure T.9. The correlation coefficient suggests that equation (T.3) does not correlate the data well and this is evident from figure T.9.

The data for the tests of all three fill heights can also be correlated by

$$K_{fdm1} = \left(5.154914\ G_w^{0.877646} G_a^{-1.462034} + 10.806728\ G_w^{0.226578} G_a^{0.293222}\right) L_{fl}^{-0.236292} \qquad \text{(T.4)}$$

with a correlation coefficient $r^2 = 0.904013$. It can be seen from figure T.10 that equation (T.4) correlates the data relatively accurately.

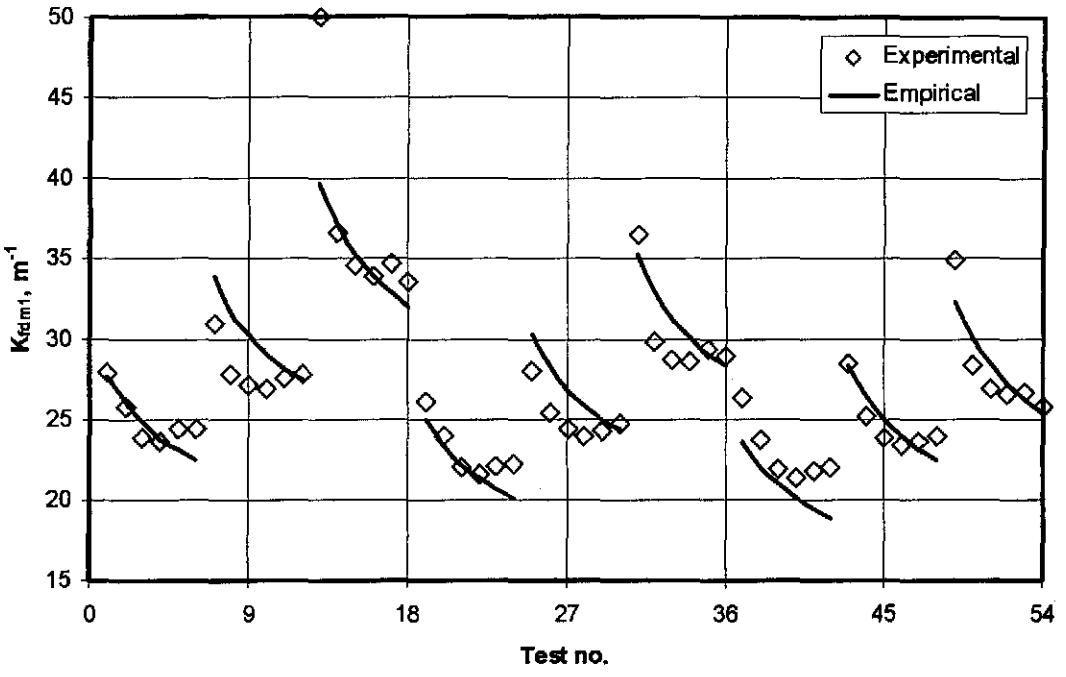

Figure T.9: Loss coefficients given by equation (T.3) compared to experiemtal results.

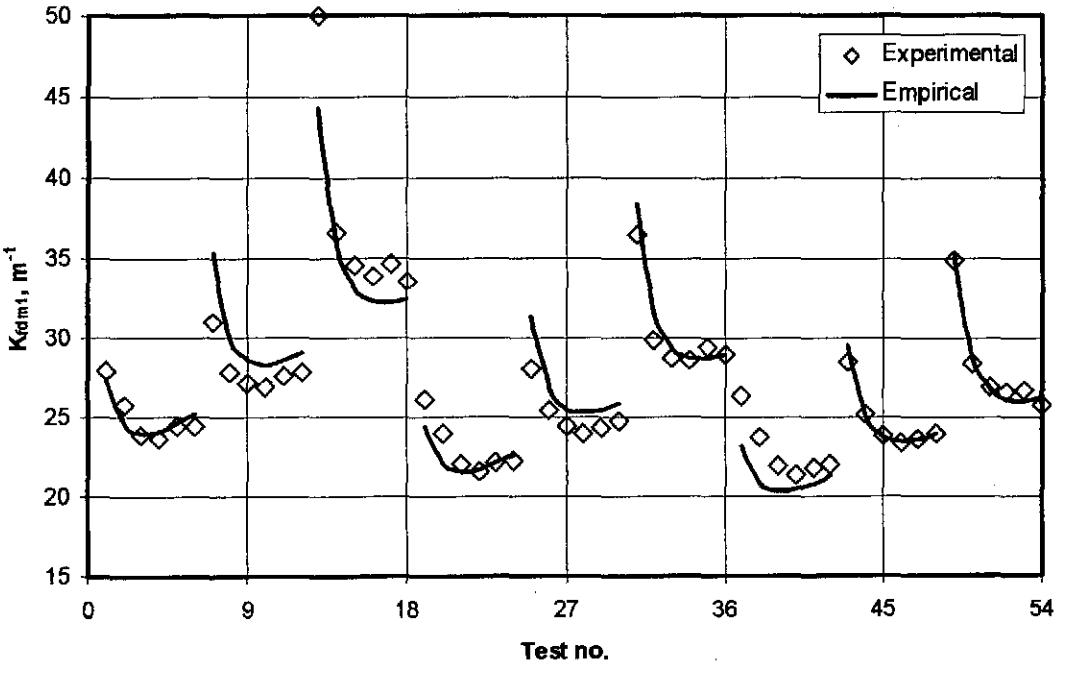

Figure T.10: Loss coefficients given by equation (T.4) compared to experiemtal results.

APPENDIX U

COOLING SYSTEM OPTIMIZATION

U.1 INTRODUCTION

The dimensions of a counterflow natural draft wet-cooling tower are optimized to obtain the minimum combined operational and capital cost compounded over a specified economic life of the cooling tower. The performance characteristics of a typical turbo-generator system are shown in figure U.1. It can be seen that the system performs optimally at a certain recooled water temperature, T_{wo}. The cooling tower therefore needs to supply the condenser water at a certain temperature at the base load to obtain maximum power output. The cooling tower outlet temperature is therefore fixed in a cooling tower optimization analysis.

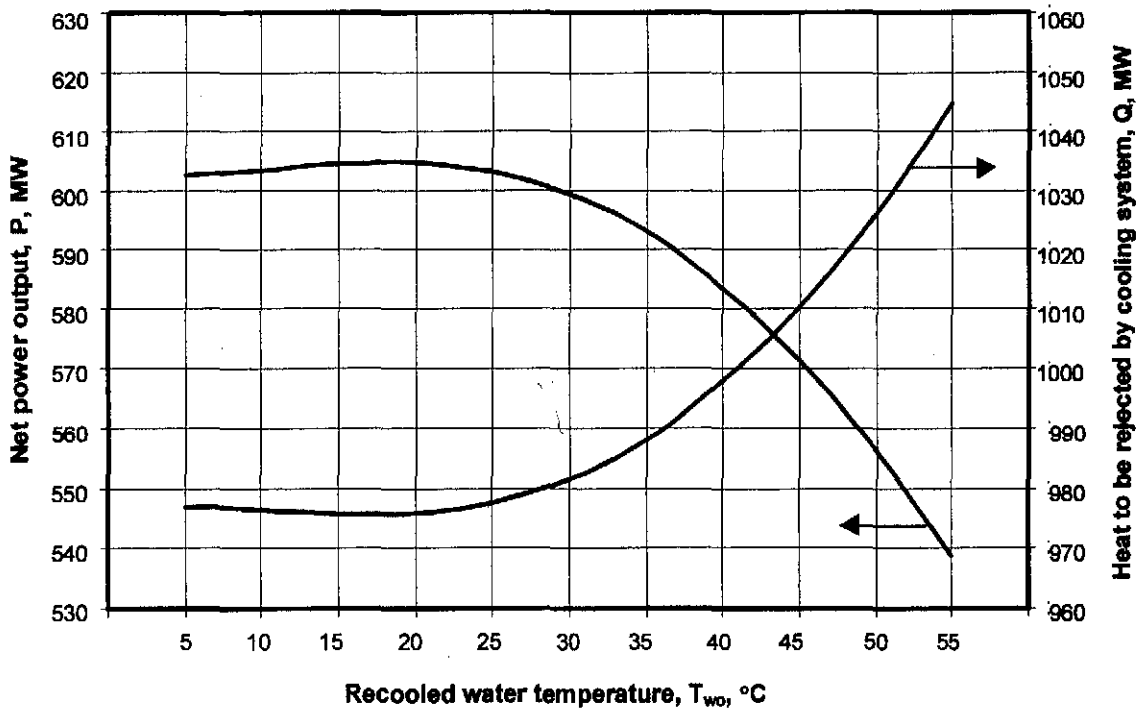

Figure U.1: Performance characteristics of turbo-generator-condenser system.

The analysis that follows is very basic but it can be readily expanded to include more detailed cost approximations. However, the present analysis shows the powerful capabilities of the WCTPE computer program, described in appendix P, when it is employed in conjunction with the LFOPC [82SN1, 83SN1, 85SN1] and DYNAMIC-Q [94SN1, 00SN2] mathematical optimization algorithms. More detailed optimization analyses applied to cooling systems are according to Li and Priddy [85LI1], Conradie [95CO1], Kintner-Meyer et al. [95KI1], Conradie et al. [98CO1], Kröger [98KR1] and Castro et al. [00CA1].

U.2 THE OPTIMIZATION PROBLEM

The optimization problem can generally be given in the following form:

Minimize $f(\boldsymbol{x})$, $\boldsymbol{x} = (x_1, x_2, \ldots, x_n)^T$

such that $h_i(\boldsymbol{x}) = 0$, $i = 1,2,\ldots,m \leq n$ (equality constraints) (U.1)

and $g_j(\boldsymbol{x}) \leq 0$ $j = 1,2,\ldots,r$ (inequality constraints)

The solution, which may or may not be unique, is given by

$$\boldsymbol{x}^* = \left[x_1^*, x_2^*, \ldots, x_n^*\right]^T$$

f is the objective function and h_i and g_j are equality and inequality constraint functions respectively that define a feasible region.

U.3 OPTIMIZATION VARIABLES

There are only three primary geometrical solution variables in the optimization analysis presented here, i.e., H_3, H_6 and d_3. Refer to figure I.1 for a description of the variables. Three more geometrical variables are functions of these primary geometrical variables, i.e., A_{fr}, L_{fi} and d_6 where d_6 is a function of d_3. Kröger [98KR1] states that to prevent cold inflow at the top of natural draft cooling towers the ratio of the tower outlet to tower base diameters must be approximately 0.6.

The area at the tower lip is given by

$$A_3 = \frac{\pi}{4} d_3^2 \tag{U.2}$$

A_{fr} is less than A_3 to make provision for the fill support structure and water distribution system. It is assumed in this analysis that the ratio of A_{fr}/A_3 is constant. A_{fr} is therefore a function of d_3.

L_{fi} is a function of A_{fr}. As the diameter, d_3, changes during the optimization process, and A_{fr} is changing, L_{fi} will change to obtain the desired water outlet temperature, for optimum turbo-generator performance as discussed above, for the given fill frontal area, A_{fr}. The transfer effects of the rain and spray zones are included in the analysis when the height of the fill, L_{fi}, is determined.

U.4 THE OBJECTIVE FUNCTION

The objective function consists of the sum of the operational costs and capital costs compounded over a specified economic life of the project. The simplified operational and capital cost components employed in the optimization analysis are presented below.

U.4.1 TOWER OPERATIONAL COST

The pumping power can be expressed by

$$P_{pump} = m_w g\left(H_3 + L_{fi} + L_{sp}\right) \tag{U.3}$$

The operating cost of the pump for one year is given by

$$C_{pump} = P_{pump} C_{elec} \tau \tag{U.4}$$

where τ is the total hours per year that the pump is working and C_{elec} is the cost of electricity. The effect of the motor-pump efficiency can be included in C_{elec} , for example, multiply C_{elec} by 1.1 if the motor-pump efficiency is 90 %.

The operating cost of the pump compounded over the selected period, expressed in years, is given by

$$C_{pump} = \sum_{n=1}^{years} P_{pump} C_{elec} \tau (1 + f/100)^{n-1} \tag{U.5}$$

where f is the inflation rate to account for the increase in the cost of electricity due to inflation.

U.4.2 TOWER CAPITAL COST

The volume of the concrete in the tower shell can be approximated by

$$V_s = \frac{\pi}{2}(d_3 + d_6) t_s H_6 \tag{U.6}$$

The capital cost of the tower shell is given by

$$C_s = V_s C_{conc} \tag{U.7}$$

where C_{conc} is the cost of concrete per unit volume.

The volume of the fill is given by

$$V_{fi} = A_{fi} L_{fi} \tag{U.8}$$

The cost of the fill is given by

$$C_{fi} = V_{fi} C_{fi} \tag{U.9}$$

where C_{fi} is the cost of the fill material per unit volume.

The total capital cost over the selected period is given by

$$C_{cap} = (C_s + C_{fi})(1 + i/100)^{years} \tag{U.10}$$

where i is the inflation rate.

The objective function for optimization is thus given by

Minimize $(C_{cap} + C_{pump})$ (U.11)

U.5 CONSTRAINTS

It is possible to include equality and inequality constraints into the optimization analysis. Only two inequality constraints are included in this analysis, i.e.,

$$H_3 \geq c_1 \tag{U.12}$$

$H_6 \leq c_2$

where c_1 and c_2 are constants. These inequality constraints are included into the optimization analysis to ensure that physically realistic results are obtained.

U.6 SAMPLE OPTIMIZATION

The dimensions of the cooling tower specified in appendix I are optimized in this analysis to obtain the minimum combined operating and capital cost over the economic life of the cooling tower. However, the Merkel method is employed in the analysis instead of the Poppe method. Kröger [98KR1] presents the performance analysis of the tower presented in appendix I employing the Merkel method. The cost and optimization variables employed in this example optimization analysis are only for illustrative purposes and do not necessarily resemble realistic and practical values. However, the values are chosen to be as realistic as possible. The water outlet temperature determined by Kröger [98KR1], T_{wo} = 294.526 K (21.376 °C), is fixed in the analysis. It is assumed that this is the water outlet temperature for a given base load (Q = 972.3714 MW) for the given water inlet temperature.

The cost and optimization variables:

Cost of electricity, C_{elec}	= 0.03 \$/kWh
Operating hours per year, τ	= 8760 h/year
Inflation rate	= 3 %
Economic life of cooling tower	= 35 years
Cost of concrete	= 200 \$/m^3
Cost of fill	= 25 \$/m^3
Diameter ratio to prevent cold inflow, d_6/d_3	= 0.58 (same as tower in appendix I)
Area ratio to make provision for fill supports etc., A_{fr}/A_3	= 0.9677 (same as tower in appendix I)
Prime interest rate	= 7 %

Table U.1 shows the dimensions of the cooling tower specified both in Kröger [98KR1] and appendix I and the cooling tower dimensions obtained by the cost optimization. The LFOPC [82SN1, 83SN1, 85SN1] optimization algorithm is employed in conjunction with the WCTPE program, described in appendix P, to obtain the tower dimensions for the minimum combined capital and operational cost. It can be seen from table U.1 that the total cost is reduced by 18.7 % for this particular optimization analysis.

Table U.1: Cooling tower dimensions with corresponding total cost

	H_6, m	d_3, m	A_{fr}, m^2	H_3, m	L_{fi}, m	d_6, m	Total cost, m\$
Kröger [98KR1]	147	104.5	8300	10	2.504	60.85	330.459
Optimized	139.218	99.897	7584.64	4.925	4.614	57.94	268.715

Figure U.2 shows the magnitude of the normalized objective function as convergence commences for the optimization analysis.

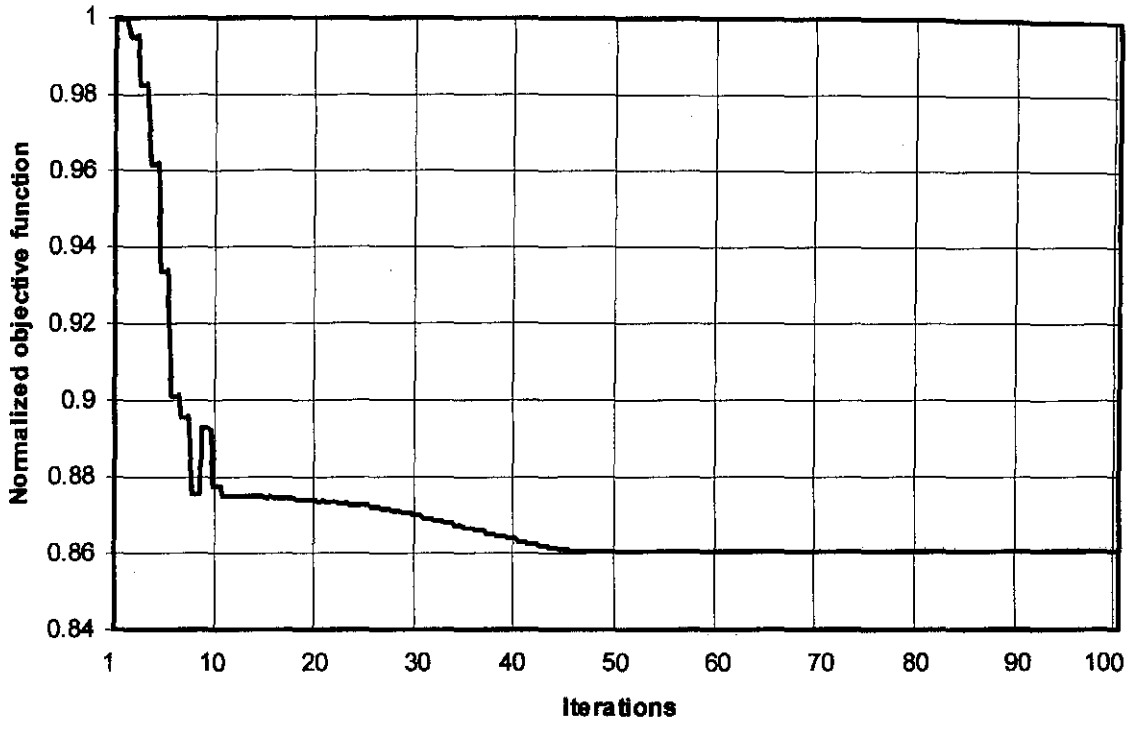

Figure U.2: Normalized objective function obtained by the LFOPC optimization algorithm.

Figure U.3 shows the solution domain for the sample optimization problem where T_{wo} = 294.526 and where H_3 is held constant at 5 m. Figure U.3 is generated manually by employing the WCTPE program without an optimization algorithm. Figure U.4 shows the contour plot of the solution domain shown in figure U.3. The total cost in figures U.3 and U.4 is shown as a function of d_3 and H_6 where H_3 is held constant at 5 m. Only d_3, H_6 and H_3 are presented in figures U.3 and U.4 as these are the primary solution variables of the optimization process, as described in section U.3.

It can be seen from figure U.4 that a minimum value of the total cost does exist for the sample optimization problem defined above. The values for H_6 and d_3 given in table U.1, with $H_3 \approx 5$ m, are shown in figure U.4. It can therefore be concluded that the LFOPC optimization algorithm accurately determines the tower dimensions to obtain the minimum cost over the economic life of the cooling tower. The absolute values for the minimum cost in table U.1 and figure U.4 differ due to the assumption that H_3 = 5 in figure U.4 and H_3 = 4.925 in table U.1.

As can be seen in figure U.3, the total cost is relatively high when the diameter of the tower, d_3, and the height of the tower, H_6, decreases at relatively small values of d_3 and H_6. The increase in cost is due to the fact that the height of the fill increases to achieve the same cooling load to compensate for the reduced draft (H_6 decreases) and reduced fill frontal area (d_3 decreases).

Figure U.5 shows the solution domain where H_3 is 5, 10 and 15 m. Figure U.6 shows the contour plots of the total cost where H_3 is equal to 10 and 15 m.

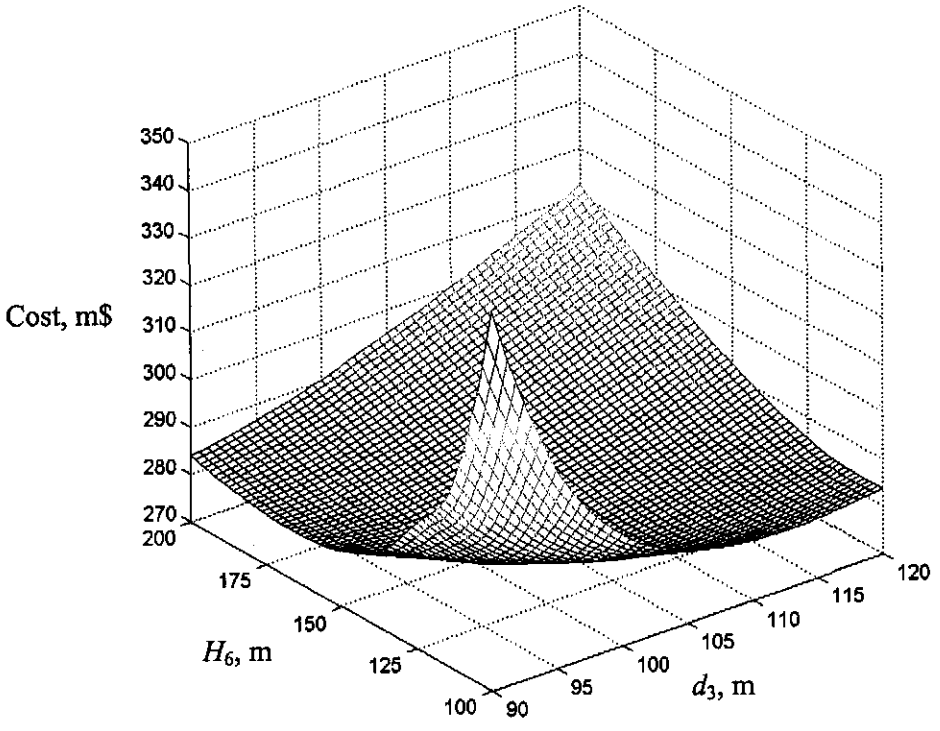

Figure U.3: Solution domain where H_3 = 5 m.

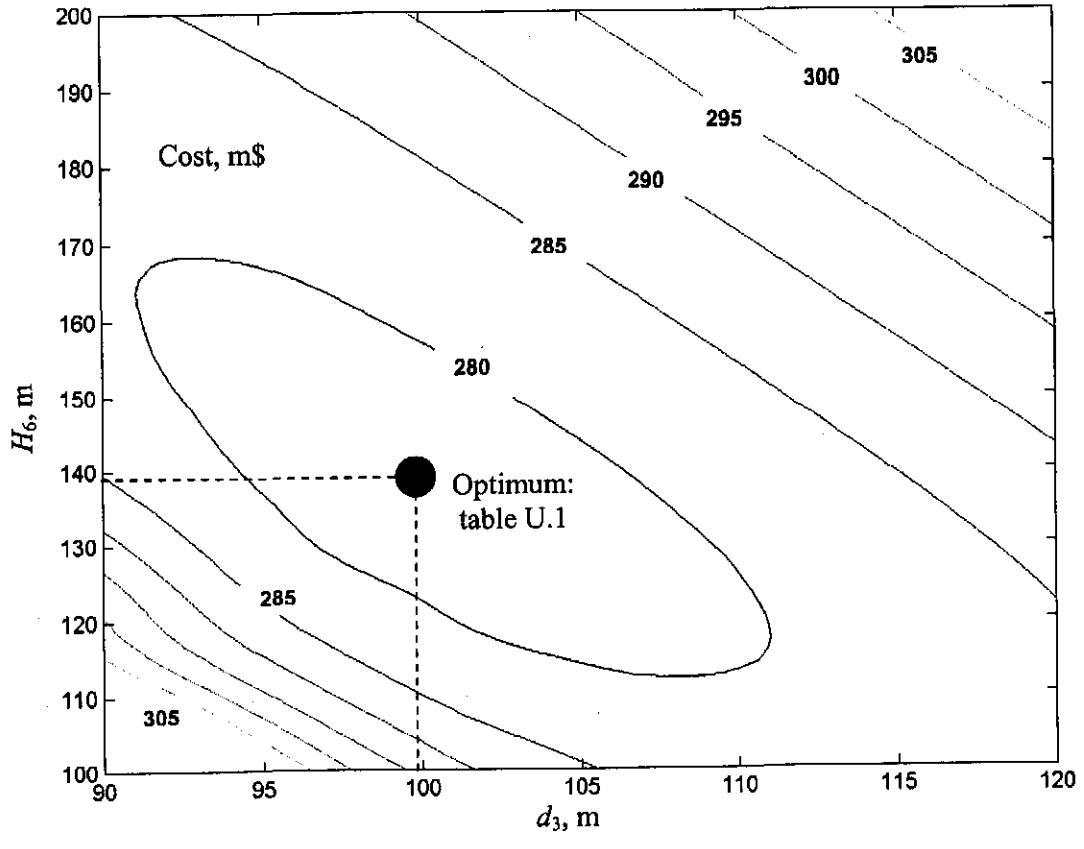

Figure U.4: Contour plot of total cost where H_3 = 5 m.

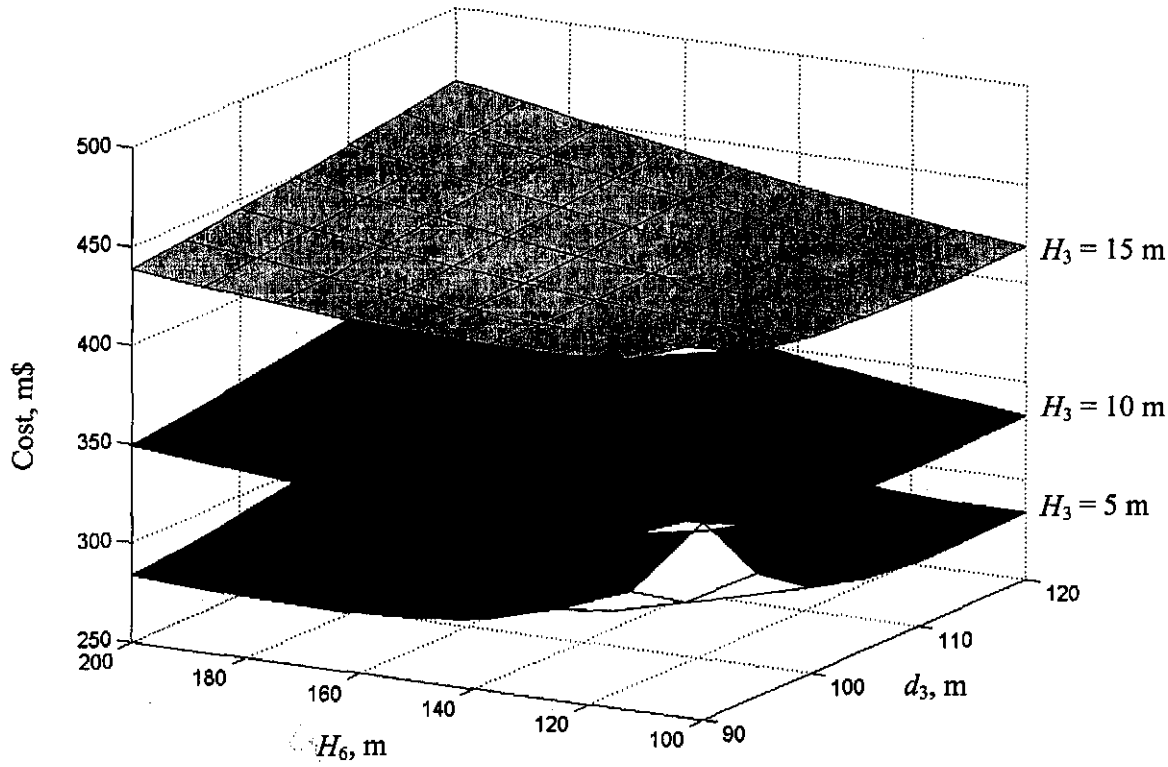

Figure U.5: Comparison between solution domains for H_3 equal to 5, 10 and 15 m.

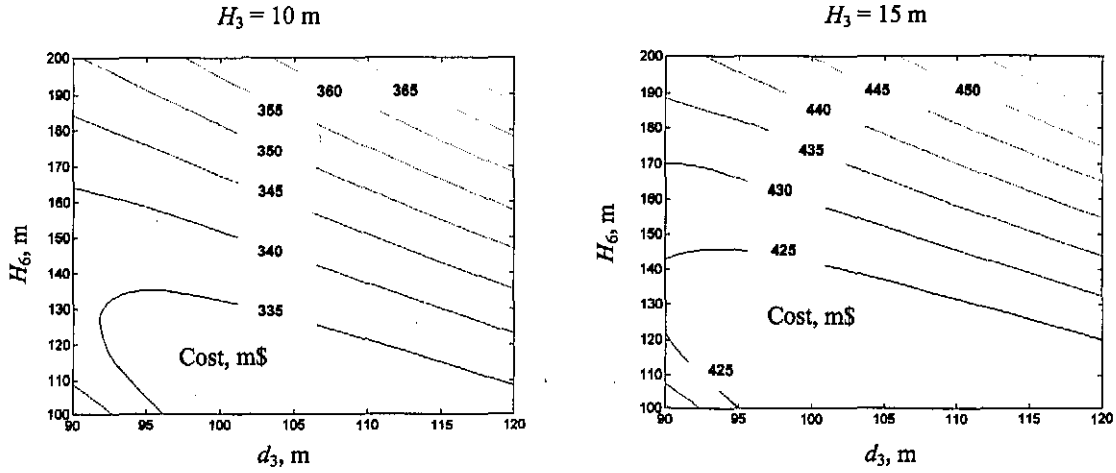

Figure U.6: Contour plot of total cost where H_3 is equal to 10 and 15 m.

U.7 CONCLUSION

The WCTPE computer program, discussed in appendix P, is successfully employed, in conjunction with mathematical optimization algorithms, to obtain the dimensions of a natural draft cooling wet-tower for the minimum operating and capital costs, compounded over the economic life of the cooling tower. The total operating and capital cost in this particular optimization analysis is reduced by 18.7 %. The results of the mathematical optimization algorithm are verified by a manual investigation of the solution domain.

APPENDIX V

SAMPLE CALCULATION OF THE INFLUENCE OF TEMPERATURE AND HUMIDITY PROFILES ON COOLING TOWER PERFORMANCE

V.1 INTRODUCTION

The reduction in the thermal performance of a natural draft cooling tower is investigated during the occurrence of nocturnal temperature and humidity inversions. The natural draft cooling tower, specified in appendix I, is the reference tower employed in this investigation. The heat rejection rate, Q, and cooling range, $T_{wi} - T_{wo}$, from appendix I are 1003.4775 MW and 18.5928 K respectively. It is assumed in appendix I that the vertical temperature distribution follows the dry adiabatic lapse rate (*DALR*) of −0.00975 K/m and that the vertical humidity ratio profile is constant.

The analysis that follows is a comparative investigation where the temperature, specified at ground level during temperature inversions, is not necessarily a practical value. The same temperature is specified at ground level during inversions as was the case where a *DALR* was assumed (see appendix I). The temperature at ground level during an inversion period is generally relatively low. The performance, where temperature and humidity inversions are employed in the analysis, is compared to the case where a *DALR* and a constant humidity ratio are employed. The possible error in tower performance evaluation is determined when no provision is made for the temperature and humidity inversion profiles to determine the effective inlet conditions and the reduction in tower draft.

It is assumed in the following sample calculation that the exponent, b, in equation (L.5) is 0.01. The maximum value of b in figure L.4 is 0.01 during the winter. The magnitude of the temperature inversion, as defined in figure L.1, is the strongest when b is at its maximum value. It is assumed in this investigation that T_{a1} and T_{wb} are measured 1 m above ground level. This is generally referred to as the ground level measurements. T_{a1} in appendix I is 288.6 K. T_r in equation (L.5) is therefore $(T_{a1} - 273.15)$ = (288.6 − 273.15) = 15.45 °C. and z_r in equation (L.5) is 1 m. The effect of b on cooling tower performance is investigated in section V.6.

For this cooling tower with d_6 = 60.85 m, the height from which ambient air is drawn into the cooling tower, H_r, is approximately 135 m from figure N.3. It is assumed that no wind is present in the analysis in appendix N. Wilber et al. [85WI1] found from experience that H_r is between 50 and 100 m for practical natural draft cooling towers while Lauraine et al. [88LA1] estimate H_r to be between 50 and 150 m. It is recommended that the value of H_r be taken as approximately half the height of the cooling tower shell. It is therefore assumed, in the sample calculation that follows, that H_r is 73.5 m. The effect of H_r on the results is investigated in section V.5.

V.2 MEAN INLET AIR TEMPERATURE: SAMPLE CALCULATION

The height of the temperature inversion is given by equation (L.26),

$$z_{it} = \left[\frac{-DALR}{b(T_r + 273.15)}\right]^{\frac{1}{b-1}} = \left[\frac{0.00975}{0.01(15.45+273.15)}\right]^{\frac{1}{0.01-1}} = 313.51 \text{ m}$$

z_{it} is greater than the height from which air is drawn into the cooling tower, H_r. Equation (E.27) can therefore be employed to calculate the mean temperature at the inlet of the cooling tower,

$$T_{aim} = (T_r + 273.15)\left(\frac{H_r}{z_r}\right)^b\left(\frac{1}{b+1}\right) + 0.00975\left(\frac{H_r}{2}\right)\left(1 - \frac{H_3}{H_r}\right)$$

$$= (15.45+273.15)\left(\frac{73.5}{1}\right)^{0.01}\left(\frac{1}{0.01+1}\right) + 0.00975\left(\frac{73.5}{2}\right)\left(1 - \frac{10}{73.5}\right) = 298.60 \text{ K}$$

This is 10 K higher than the measured air drybulb temperature at ground level. The presence of a temperature inversion can therefore have a pronounced effect on the effective inlet temperature compared to the measured value. When b, as shown in figure L.4 is at its minimum value of 0.003 during the summer, then z_{it} = 90 m from equation (L.26) and T_{aim} = 291.8018 K from equation (E.27). This is only 3.2 K higher than the measured air drybulb temperature at ground level.

V.3 MEAN INLET HUMIDITY RATIO: SAMPLE CALCULATION

Figures M.2 and M.3 show examples of inversion vapor pressure profiles that occur during the night. The humidity ratio profiles follow approximately the same trends as the vapor pressure profiles. The humidity at 04h00 in figure M.2 and at 02h00-06h00 in figure M.3 falls by approximately 12 % during the first 40 m. The height of the humidity inversion in figure M.2 is approximately 40 m. It is assumed in this analysis that the height of the humidity inversion profile is 40 m. The humidity is assumed to be approximately constant above 40 m. The humidity ratio at ground level is found to be 0.008127 kg/kg dry air in appendix I for the specified ambient conditions. The following fourth order polynomial gives the humidity ratio to be 0.008127 kg/kg 1 m above ground level and approximately 12 % less at a height of 40 m after which it remains approximately constant,

$$w = c_1 + c_2 z + c_3 z^2 + c_4 z^3 + c_5 z^4 \qquad \text{(V.1)}$$

where c_1 to c_5 are constants where c_1 = 8.0812×10^{-3}, c_2 = 4.6139×10^{-5}, c_3 = -7.0639×10^{-7}, c_4 = 4.6179×10^{-9} and c_5 = -1.0709×10^{-11}. Equation (V.1) is plotted in figure V.1. The humidity profile is expressed by a polynomial since the humidity profile can be specified as constant, linear and non-linear.

The average humidity at the inlet of the cooling tower, w_{im}, is given by the equation

$$w_{im} = \int_0^{H_r} w \, dz \Big/ H_r \qquad \text{(V.2)}$$

Substitute equation (V.1) into equation (V.2) and find after integration

$$w_{im} = c_1 + \frac{c_2 H_r}{2} + \frac{c_3 H_r^2}{3} + \frac{c_4 H_r^3}{4} + \frac{c_5 H_r^4}{5} \qquad \text{(V.3)}$$

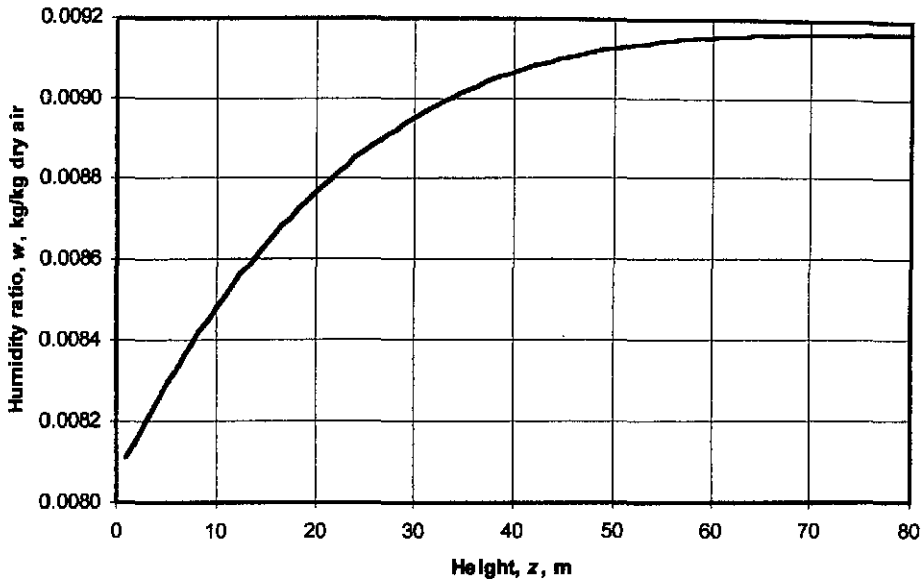

Figure V.1: Inversion humidity profile

Substitute constants c_1 to c_5 given below equation (V.1) and H_r = 75 m into equation (V.3) and find w_{im} = 0.0089 kg/kg dry air. The effective inlet humidity ratio, during this humidity inversion, is approximately 9.6 % higher than when it is assumed that the humidity ratio profile is constant.

V.4 EXTERNAL PRESSURE DISTRIBUTION: SAMPLE CALCULATION

The pressure distribution external to the cooling tower is calculated in this analysis as accurately as possible as both the vertical temperature and humidity profiles are considered. The calculation is relatively complex, due to the inclusion of the humidity profile in the analysis, and can generally not be employed in a simple cooling tower performance analysis. This is because it requires numerical integration to calculate the pressure distribution. It will be shown, however, that the humidity inversion has a negligible effect on tower draft.

As mentioned in appendix E, the temperature and humidity profiles also influence the draft through the tower as the pressure distribution on the outside of the outside of the tower is a function of both the temperature and humidity profiles. The pressure at the top of the tower shell, external to the tower, is given by equation (E.6),

$$p_7 = p_1 \exp\left(-\frac{0.622 \cdot g}{R} \int_0^{H_6} \frac{(w+1)}{(w+0.622)} \frac{dz}{T} \right) \tag{V.4}$$

where w is given by equation (V.1) and T by equation (L.5). Substitute equations (V.1) and (L.5) into equation (V.4). The integral in equation (V.4) is then given by

$$\int_0^{H_6} \frac{(w+1)}{(w+0.622)} \frac{dz}{T} = \int_0^{H_6} \frac{\left(c_1 + c_2 z + c_3 z^2 + c_4 z^3 + c_5 z^4 + 1\right)}{\left(c_1 + c_2 z + c_3 z^2 + c_4 z^3 + c_5 z^4 + 0.622\right)\left(T_r + 273.15\right)\left(\frac{z}{z_r}\right)^b} dz \tag{V.5}$$

The integral in equation (V.5) can only be evaluated by numerical methods like Simpson's composite rule [97BU1]. For H_6 = 147 m, z_r = 1 m, T_r = 15.45 °C, b = 0.01 and c_1 to c_5 given below equation (V.1), the integral in equation (V.5) is determined by Simpson's composite rule with 20 intervals to give 0.7823663.

Thus, from equation (V.4) and numerical integration result of equation (V.5) find

$$p_7 = 84100 \exp\left(-\frac{0.622 \cdot 9.8 \cdot 0.7823663}{287.08}\right) = 82714.47 \text{ Pa}$$

The pressure differential on the outside of the cooling tower is

$p_1 - p_7 = 84100 - 82714.47 = 1385.53$ Pa

This pressure difference is 1445.73 Pa in appendix I. This reduced pressure differential will cause a reduction in draft through the tower.

V.5 REDUCTION IN TOWER PERFORMANCE

As already mentioned, the heat rejection rate, Q, from appendix I is 1003.4775 MW. It is assumed in appendix I that the vertical temperature distribution follows the *DALR* of –0.00975 K/m, the vertical humidity ratio profile is constant, w_i = 0.008127 kg/kg dry air and T_{ai} = 288.6 K.

If it assumed that the vertical humidity profile is constant and the increase in the temperature, as calculated in section V.2 (T_{atm} = 298.67), is employed in performance calculation then Q = 802.4774 MW. This is approximately 20 % less than 1003.4775 MW. The detrimental effect of the temperature inversion on tower draft is also included in this evaluation where the pressure differential on the outside of the cooling tower is calculated by equation (E.18), i.e., $p_1 - p_7$ = 1386.70 Pa.

If it is not assumed that the vertical humidity profile is constant, but given by the value calculated in section V.3 (w_{im} = 0.0089 kg/kg dry air) then Q = 787.9063 MW. This is 21.5 % and 1.8 % less than 1003.4775 MW and 802.4774 MW respectively. The reduction in the draft due to the reduced pressure differential, as calculated in section V.4, is included in the performance evaluation. The effect of the humidity inversion on tower draft is negligible.

Thus, the relatively strong temperature inversion reduces tower performance by approximately 20 % in this particular case. The effect of the humidity ratio inversion on tower performance is less pronounced than the temperature inversion and causes an additional 1.5 % reduction in performance. A weak temperature inversion during the summer, where b = 0.003, reduces tower performance by 7.8 %.

Approximately 20 % of the reduction in performance is due to the reduction in draft and approximately 80 % is due to the increased effective inlet air temperature and humidity, where the effect of the increased effective inlet humidity is essentially negligible.

V.6 INFLUENCE OF H_r ON TOWER PERFORMANCE

The effect of the height from which air is drawn into a cooling tower, H_r, on the performance of the cooling towers is investigated. H_r is varied between 50 m and 150 m. Figure V.2 shows the effect of the variation of H_r on the effective inlet air drybulb temperature and humidity ratios. There is only a 2 K increase in the effective inlet air drybulb temperature when H_r is varied from 50 to 100 m. As already mentioned, Wilber et al. [85WI1] found that the approach height is between 50 and 100 m for practical natural draft cooling towers while Lauraine et al. [88LA1] estimate H_r to be between 50 and 150 m.

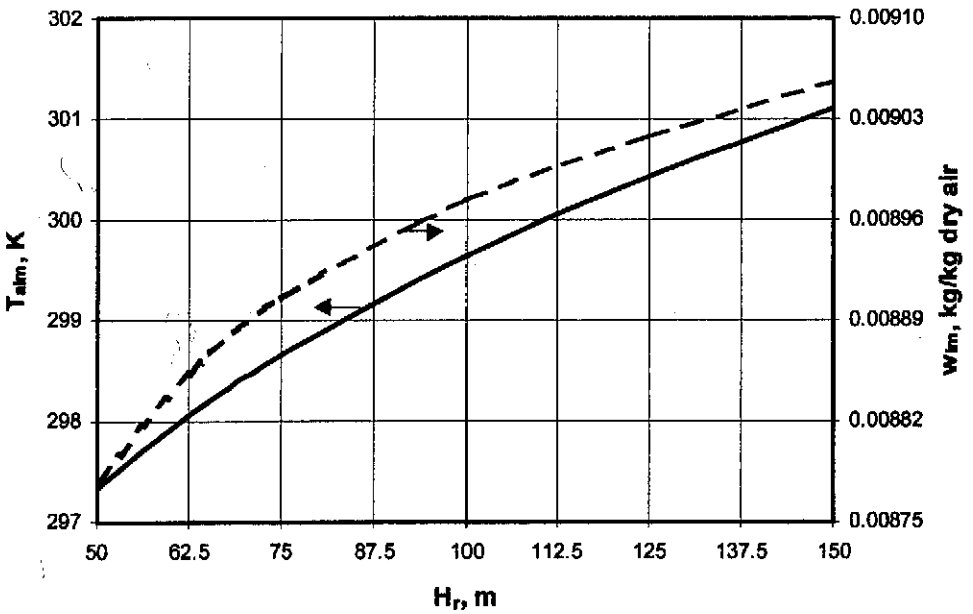

Figure V.2: Effective air inlet temperature and humidity ratio versus H_r.

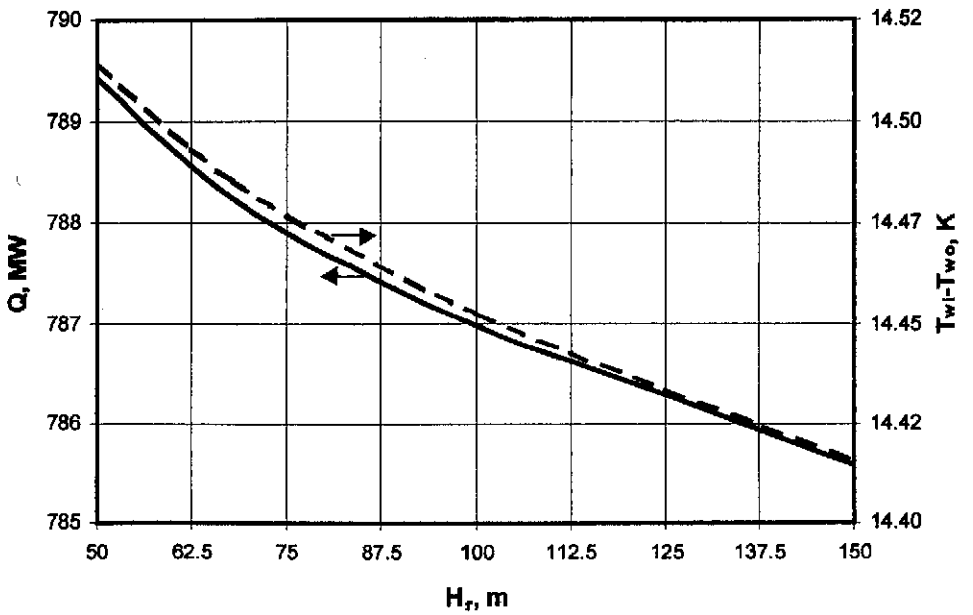

Figure V.3: Heat rejected and cooling range versus H_r.

Figure V.3 shows the heat rejected and cooling range as a function of H_r during the occurrence of temperature and humidity inversions. Q is reduced by only 0.3 % and the cooling range by 0.06 K when

H_r is increased from 50 to 100 m. The performance of natural draft cooling towers is, therefore, relatively insensitive to H_r.

V.7 INFLUENCE OF *b* ON TOWER PERFORMANCE

Figure V.4 shows the effect that the exponent, *b*, in equation (L.5) has on the effective inlet air drybulb temperature and the temperature inversion height from equation (L.26) when H_r = 73.5 m. The minimum and maximum values of *b* in figure L.4 are 0.003 and 0.01 respectively. z_{it} from equation (L.26), with T_r = 15.45 °C, varies between 90 m and 313.51 m for the minimum and maximum values of *b* respectively. The corresponding reduction in the heat rejection rate and cooling range, between the minimum and maximum values of *b*, are shown in figure V.5 and are 15% and 2.6 K respectively.

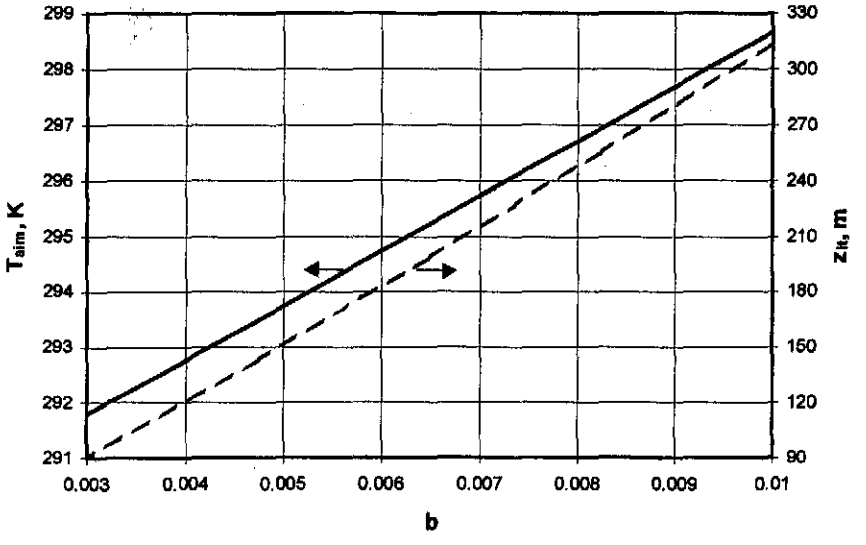

Figure V.4: Effective air inlet temperature and temperature inversion height versus *b*.

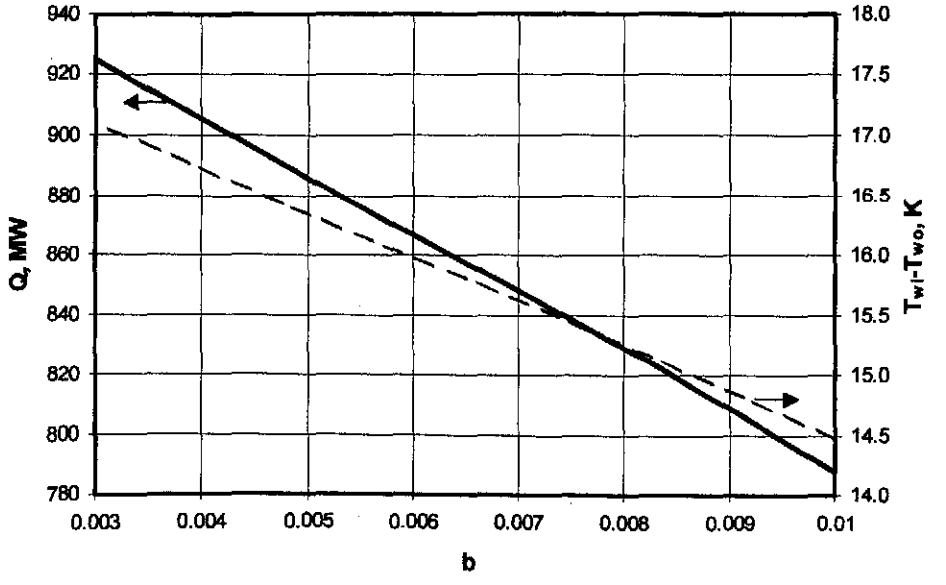

Figure V.5: Heat rejected and cooling range versus *b*.

V.9 CONCLUSION

The presence of a temperature inversion can have a pronounced effect on the effective mean inlet temperature compared to the measured temperature value at or near ground level. It is found in this investigation that a relatively strong temperature inversion reduces a particular tower performance by approximately 20 %. A relatively weak inversion reduces a particular tower performance by approximately 8 %. The effect of the humidity ratio inversion on the same tower performance is less pronounced than the temperature inversion and causes an additional 1.5 % reduction in performance. Approximately 80 % of the reduction in performance is due to the increased mean inlet temperature and 20 % is due to the reduction in draft. The performance of natural draft cooling towers is relatively insensitive to H_r where H_r is practically half the height of the tower shell. The predicted heat rejection rates differ by only 0.3 % when H_r is increased from 50 m to 100 m. It is recommended that H_r is taken as approximately half the height of the tower shell.